

**Synthesis of**  
**Bacterial Protease Inhibitors as new**  
**Antibiotics**

**Dissertation**

zur Erlangung des Grades  
des Doktors der Naturwissenschaften  
der Naturwissenschaftlich-Technischen Fakultät  
der Universität des Saarlandes

von

**Katrin Voos**  
Dipl. Pharm. & Apothekerin

Saarbrücken  
2023

Tag des Kolloquiums: 20. Dezember 2023

Dekan: Prof. Dr. Ludger Santen

Berichterstatter: Prof. Dr. Christian Ducho

Prof. Dr. Anna K. H. Hirsch

Vorsitz: Prof. Dr. Claus Jacob

Akad. Mitarbeiter: Dr. Agnes-Valencia Weiß

Die vorliegende Arbeit wurde unter der Betreuung durch Herrn Prof. Dr. Christian Ducho an der Universität des Saarlandes in der Naturwissenschaftlich-Technischen Fakultät im Fachbereich Pharmazie im Zeitraum von November 2016 bis März 2021 angefertigt.

Erstgutachter: Prof. Dr. Christian Ducho

Zweitgutachter: Prof. Dr. Anna K. H. Hirsch





## ABSTRACT

Antimicrobial resistances are on the rise and so-called “pathoblockers” are one way to overcome the fast development of resistances to new antibiotics. Secreted proteases, such as collagenase H (ColH) of *Clostridium histolyticum*, collagenase Q1 (ColQ1) of *Bacillus cereus*, or elastase B (LasB) from *Pseudomonas aeruginosa* are attractive targets for the development of pathoblockers as they are crucial to establish the bacterial infection without affecting viability.

This work comprises a detailed structure-activity relationship (SAR) study of *N*-aryl acetamides as inhibitors of LasB and ColH. Changes in the side chain and in the zinc-binding moiety led to highly increased activities on either LasB or ColH. Some compounds even showed the potential for dual inhibition.

Moreover, the biological activity of synthesized derivatives was not only tested on purified enzyme, but selectivity was observed towards several human off-targets. Additionally, the potential of the compounds was underlined by more advanced tests such as an *ex vivo* pig skin-, *in vitro* skin- and lung-cell- as well as *in vivo* *Galleria mellonella* larvae infection models.

Taken together, the here presented SAR study with biological evaluation introduces derivatives of *N*-aryl acetamides as highly active compounds with great potential for further drug development towards LasB for local lung treatment with low systemic exposure, or for further optimization regarding the treatment of *Bacillary* or *Clostridial* infections.

## ZUSAMMENFASSUNG

Sogenannte Pathoblocker sind alternative Antibiotika mit deutlich verlangsamer Resistenzentwicklung. Sekretierte Proteasen wie Kollagenase H (ColH) von *Clostridium histolyticum*, Kollagenase Q1 (ColQ1) von *Bacillus cereus* oder Elastase B (LasB) von *Pseudomonas aeruginosa* sind attraktive Ziele für die Entwicklung von solchen Pathoblockern, da sie entscheidend für die Etablierung der bakteriellen Infektion sind, ohne die Überlebensfähigkeit der Bakterien zu beeinträchtigen.

Die hier vorliegende Arbeit umfasst detaillierte Studien zur Struktur-Wirkungs-Beziehung (SAR) von *N*-Arylacetamiden als Inhibitoren von LasB und ColH. Veränderungen in der Seitenkette und in der Zink-bindenden Einheit erhöhten die Aktivitäten gegenüber LasB oder ColH signifikant. Einige der gezeigten Verbindungen zeigten sogar das Potenzial für eine duale Hemmung.

Im Rahmen der biologischen Evaluation wurde die Selektivität gegenüber verschiedenen menschlichen Enzymen bewiesen. Des Weiteren konnte die Aktivität der Substanzen mittels *ex-vivo* Schweinehaut-, *in-vitro* Haut- und Lungenzell- sowie *in-vivo* *Galleria mellonella* Larven-Infektionsmodelle verdeutlicht werden.

Zusammenfassend stellen *N*-Arylacetamidderivate Verbindungen mit großem Potenzial für die weitere Arzneimittelentwicklung dar. Dies gilt insbesondere für die potenzielle lokale Behandlung von Lungeninfektionen mit *P. aeruginosa* oder im Hinblick auf eine mögliche Optimierung der Substanzen in Richtung Bacillus- oder Clostridieninfektionen.

# TABLE OF CONTENTS

<b>Table of Contents</b> .....	<b>I</b>
<b>Publications and Chapters Included in this Thesis</b> .....	<b>III</b>
<b>Contribution Reports</b> .....	<b>V</b>
<b>List of Symbols and Abbreviations</b> .....	<b>VI</b>
<b>I. Introduction</b> .....	<b>1</b>
1. Bacteria and Bacterial Infections .....	1
1.1 About Bacteria and Infectious Diseases .....	1
1.2 The Golden Era of Antibiotics .....	1
1.3 Resistances are on the Rise.....	2
1.4 The Antibiotic Pipeline .....	3
2. Pathoblockers – an Anti-Virulence Approach .....	4
3. Bacterial Proteases as Anti-Virulence Targets.....	5
3.1 Collagenases as Virulence Factors of <i>Clostridia</i> and <i>Bacilli</i> .....	7
3.2 Elastase B as Virulence Factor of <i>Pseudomonas aeruginosa</i> .....	11
<b>II. Aim of the Thesis</b> .....	<b>15</b>
<b>III. Published Results</b> .....	<b>17</b>
Chapter A: Discovery of a Potent Inhibitor Class with High Selectivity toward Clostridial Collagenases.....	17
Chapter B: Phosphonate as a Stable Zinc-Binding Group for “Pathoblocker” Inhibitors of Clostridial Collagenase H (ColH).....	27
Chapter C: Inhibition of Collagenase Q1 of <i>Bacillus cereus</i> as a Novel Antivirulence Strategy for the Treatment of Skin-Wound Infections.....	41
Chapter D: <i>N</i> -Aryl mercaptoacetamides as a Potential Multi-target Inhibitors of Metallo- $\beta$ -lactamases (MBLs) and the Virulence Factor LasB from <i>Pseudomonas aeruginosa</i> .....	55
<b>IV. Unpublished Results</b> .....	<b>68</b>
Chapter E: <i>N</i> -Aryl-2- <i>iso</i> -butylmercaptoacetamides: the discovery of highly potent and selective inhibitors of <i>Pseudomonas aeruginosa</i> virulence factor LasB and <i>Clostridium histolyticum</i> virulence factor ColH.....	68
Chapter F: Optimized Phosphonate Derivatives as Highly Potent Inhibitors of <i>P. aeruginosa</i> Virulence Factor Elastase B (LasB) and <i>Clostridium</i> Virulence Factor Collagenase H (ColH) .....	109

Introduction.....	111
Results and Discussion.....	112
Conclusion .....	119
Experimental Section.....	119
Acknowledgments.....	120
Chapter G: Functionalized $\alpha$ -Side chains as Booster for the Inhibitory Activity of <i>N</i> -Aryl mercaptoacetamides on <i>C. histolyticum</i> Virulence Factor ColH.....	121
Introduction.....	122
Results and Discussion.....	123
Conclusion .....	132
Experimental Section.....	133
Acknowledgments.....	134
<b>V. Final Discussion and Outlook.....</b>	<b>135</b>
1. Summary.....	135
1.1 2-Mercapto- <i>N</i> -(4-acetylphenyl) acetamide as starting point for further optimization towards highly active and selective ColH and LasB inhibitors.....	135
1.2 The SAR of substituted 2-mercapto- <i>N</i> -aryl acetamides toward ColH and LasB.....	136
1.3 Phosphonate as a suitable replacement of thiol function for both ColH and LasB.....	139
2. Outlook .....	141
2.1 Optimized Phosphonates for ColH by the introduction of a functionalized side chain and other aryl moieties .....	141
2.2 Phosphonate prodrugs for better bioavailability with regard to deep tissue infections.....	141
2.3 Combination of phosphonate with peptidic elongation .....	142
2.4 Additional investigations on the structure-activity relationship .....	143
<b>VI. References .....</b>	<b>145</b>
<b>Appendix</b>	

The references in section 5 (“VI. References”) refer to section I, II, IV (Chapter **F** and **G**) and V of this work. References for section III (“III. Published Results”), VI (Chapter **E**) and the appendix are listed in each subchapter, referring to the main text and the supporting information, respectively.

## PUBLICATIONS AND CHAPTERS INCLUDED IN THIS THESIS

The section “III. Published Results” of this thesis contains four chapters, which are referred to in the text by their letters (A – D) and have been published in peer-reviewed journals.

### **Chapter A: Discovery of a Potent Inhibitor Class with High Selectivity toward Clostridial Collagenases**

Esther Schönauer,+ Andreas M. Kany,+ Jörg Haupenthal, Kristina Hüsecken, Isabel J. Hoppe, Katrin Voos, Samir Yahiaoui, Brigitta Elsässer, Christian Ducho, Hans Brandstetter, Rolf W. Hartmann; *J. Am. Chem. Soc.* **2017**, *139*, 12696–12703.

DOI: 10.1021/jacs.7b06935.<sup>1</sup>

### **Chapter B: Phosphonate as a Stable Zinc-Binding Group for “Pathoblocker” Inhibitors of Clostridial Collagenase H (ColH)**

Katrin Voos, Esther Schönauer, Alaa Alhayek, Jörg Haupenthal, Anastasia Andreas, Rolf Müller, Rolf W. Hartmann, Hans Brandstetter, Anna K. H. Hirsch, Christian Ducho; *ChemMedChem* **2021**, *16*, 1257 – 1267.

DOI: 10.1002/cmdc.202000994.<sup>2</sup>

### **Chapter C: Inhibition of Collagenase Q1 of *Bacillus cereus* as a Novel Antivirulence Strategy for the Treatment of Skin-Wound Infections**

Alaa Alhayek, Essak S. Khan, Esther Schönauer, Tobias Däinghaus, Roya Shafiei, Katrin Voos, Mitchell K. L. Han, Christian Ducho, Gernot Posselt, Silja Wessler, Hans Brandstetter, Jörg Haupenthal, Aránzazu del Campo, Anna K. H. Hirsch; *Adv. Ther.*, **2022**, *5* (3), 2100222.

DOI: 10.1002/adtp.202100222.<sup>3</sup>

### **Chapter D: N-Aryl mercaptoacetamides as a Potential Multi-target Inhibitors of Metallo- $\beta$ -lactamases (MBLs) and the Virulence Factor LasB from *Pseudomonas aeruginosa***

Samir Yahiaoui,+ Katrin Voos,+ Jörg Haupenthal, Thomas Wichelhaus, Denia Frank, Lilia Weizel, Marco Rotter, Steffen Brunst, Jan S. Kramer, Ewgenij Proschak, Christian Ducho, Anna K. H. Hirsch; *RSC Med. Chem.* **2021**, Advance Article.

DOI: 10.1039/D1MD00187F.<sup>4</sup>

Further unpublished results are included in the section “IV. Unpublished Results” and will be referred to in the text by the letters E to G, where chapter E can already be found in version 1 on the preprint server ChemRxiv®.

### **Chapter E: N-Aryl-2-iso-butylmercaptoacetamides: the discovery of highly potent and selective inhibitors of *Pseudomonas aeruginosa* virulence factor LasB and *Clostridium histolyticum* virulence factor ColH**

Katrin Voos,+ Samir Yahiaoui,+ Jelena Konstantinović, Esther Schönauer, Alaa Alhayek, Asfandyar Sikandar, Khadidja Si Chaib, Tizian F. Ramspoth, Katharina Rox, Jörg Haupenthal, Jesko Köhnke, Hans Brandstetter, Christian Ducho, Anna K. H. Hirsch; *ChemRxiv*. Cambridge: Cambridge Open Engage; **2022**.

DOI: 10.26434/chemrxiv-2022-fjrqr.<sup>5</sup>

**Chapter F: Optimized Phosphonate Derivatives as Highly Potent Inhibitors of *Pseudomonas aeruginosa* Virulence Factor Elastase B (LasB) and *Clostridium histolyticum* Virulence Factor Collagenase H (ColH)**

**Chapter G: Functionalized  $\alpha$ -Side Chains as Booster for the Inhibitory Activity of *N*-Aryl mercaptoacetamides on *Clostridium histolyticum* Virulence Factor ColH**

Parts of the results from chapters **E**, **F** and **G** are included in the international patent application “Inhibitors of *Pseudomonas aeruginosa* virulence factor LasB”, which was filed on August 25<sup>th</sup>, 2020 to the European Patent Office (EP 20 192 608.6; International application number: PCT/EP2021/073381, International Filing Date 24<sup>th</sup> August 2021).<sup>6</sup>

Parts of the results from chapter **F** are included in the paper manuscript “Inhibitors of the Elastase LasB for the treatment of *Pseudomonas aeruginosa* lung infections”, which was recently submitted and is currently under review. The current version can be found as preprint:

Jelena Konstantinović, Andreas M. Kany, Alaa Alhayek, Ahmed S. Abdelsamie, Asfandyar Sikandar, Katrin Voos, Yiwen Yao, Anastasia Andreas, Roya Shafiei, Brigitta Loretz, Esther Schönauer, Robert Bals, Hans Brandstetter, Rolf W. Hartmann, Christian Ducho, Claus-Michael Lehr, Christoph Beisswenger, Rolf Müller, Katharina Rox, Jörg Hauptenthal, Anna K. H. Hirsch; *ChemRxiv*. Cambridge: Cambridge Open Engage; **2023**.

DOI: 10.26434/chemrxiv-2023-bszcb.<sup>7</sup>

## CONTRIBUTION REPORTS

### **Chapter A: Discovery of a Potent Inhibitor Class with High Selectivity toward Clostridial Collagenases**

The author synthesized and characterized the compounds **1** and **16** and wrote the experimental part for the mentioned compounds.

### **Chapter B: Phosphonate as a Stable Zinc-Binding Group for “Pathoblocker” Inhibitors of Clostridial Collagenase H (ColH)**

The author synthesized and characterized all new compounds. She wrote and conceived the manuscript.

### **Chapter C: Inhibition of Collagenase Q1 of *Bacillus cereus* as a Novel Antivirulence Strategy for the Treatment of Skin-Wound Infections**

The author synthesized compound **1**.

### **Chapter D: *N*-Aryl mercaptoacetamides as a Potential Multi-target Inhibitors of Metallo- $\beta$ -lactamases (MBLs) and the Virulence Factor LasB from *Pseudomonas aeruginosa***

The author synthesized and characterized all new compounds. She wrote and conceived the manuscript together with Samir Yahiaoui who contributed equally.

### **Chapter E: *N*-Aryl-2-*iso*-butylmercaptoacetamides: the discovery of highly potent and selective inhibitors of *Pseudomonas aeruginosa* virulence factor LasB and *Clostridium histolyticum* virulence factor ColH**

The author synthesized and characterized 81 out of the 113 newly synthesized intermediate and final compounds. She wrote and conceived the manuscript together with Samir Yahiaoui who contributed equally.

### **Chapter F: Optimized Phosphonate Derivatives as Highly Potent Inhibitors of *Pseudomonas aeruginosa* Virulence Factor Elastase B (LasB) and *Clostridium histolyticum* Virulence Factor Collagenase H (ColH)**

The author synthesized and characterized 14 new intermediates and 6 (of the 9 tested) new final compounds (additionally to the tested 11 final compounds of which the synthesis is already depicted in Chapter **B**). She wrote and conceived the chapter.

### **Chapter G: Functionalized $\alpha$ -Side chains as Booster for the Inhibitory Activity of *N*-Aryl mercaptoacetamides on *Clostridium histolyticum* Virulence Factor ColH**

The author synthesized and characterized 13 intermediates and 8 (of the 17 tested) final compounds. She wrote and conceived the chapter.

## LIST OF SYMBOLS AND ABBREVIATIONS

$\mu\text{M}$	Micro molar
AA	Amino acid
Ac	Acetyl
ACE	Angiotensin converting enzyme
ACN	Acetonitrile
ADAM17	see TACE
ADME	Absorption, Distribution, Metabolism and Excretion
AMP	Antimicrobial peptide
AMR	Antimicrobial resistance
aq.	Aqueous
AUC	Area under the curve
BALF	Bronchoalveolar lavage fluid
bisPOM	Bis-pivaloyloxymethyl
Boc	<i>tert</i> -butoxycarbonyl
Boc <sub>2</sub> O	Di- <i>tert</i> -butyl dicarbonate
br	Broad signal [NMR]
calc.	Calculated
CDC	Center for Disease Control and Prevention [U.S. Government]
CF	Cystic fibrosis
ChC	<i>Clostridium histolyticum</i> collagenase (e.g. ColH, ColG, ...)
Cit	Citrulline
ColA	Collagenase A (e.g. from <i>C. perfringens</i> or <i>B. cereus</i> )
ColB	Collagenase B (e.g. from <i>B. thuringiensis</i> )
ColG	Collagenase G (e.g. from <i>C. histolyticum</i> )
ColH	Collagenase H (e.g. from <i>C. histolyticum</i> )
ColQ1	Collagenase Q1 (e.g. from <i>B. cereus</i> )
ColT	Collagenase T (e.g. from <i>C. tetani</i> )
COSY	Correlation spectroscopy (NMR)
CU	Collagenase Unit
CYP	Cytochrome P450
d	Days or duplet (NMR)
DCM	Dichloromethane
dd	Duplet of duplet (NMR)
ddd	Duplet of duplet of duplet (NMR)
DIPEA	<i>N,N</i> -diisopropylethylamine
DL-DAB	DL-2,4-diaminobutyric acid
DMAP	4-Dimethylaminopyridine
DMF	<i>N,N</i> -dimethylformamide



DMSO	Dimethyl sulfoxide
dt	Duplet of triplet (NMR)
e.g.	For example [lat. <i>exempli gratia</i> ]
ECFSPR	European cystic fibrosis society patient registry
EDCl	<i>N</i> -(3-dimethylaminopropyl)- <i>N'</i> -ethylcarbodiimide hydrochloride
EDTA	Ethylenediaminetetraacetic acid
ELF	Epithelial lining fluid
eq.	Equivalents
ESI	Electrone spray ionization (MS)
ESRF	European Synchrotron Radiation Facility
Et	Ethyl
et al.	And others [lat. <i>et alii</i> ]
EtOAc	Ethyl acetate
FALGPA	Furylacryloyl-Leu-Gly-Pro-Ala
FBDD	Fragment-based drug discovery
FDA	US Food and Drug Administration
Fmoc	9-Fluorenylmethoxycarbonyl
Fmoc-Cl	9-Fluorenylmethoxycarbonyl chloride
FRET	Förster resonance energy transfer
g	Gram
h	Hour(s)
HATU	<i>N</i> -[(dimethylamino)-1 <i>H</i> -1,2,3-triazolo-[4,5- <i>b</i> ]pyridin-1-ylmethylene]- <i>N</i> -methylmethanaminium hexafluorophosphate <i>N</i> -oxide
HBTU	<i>N,N,N',N'</i> -tetramethyl- <i>O</i> -(1 <i>H</i> -benzotriazol-1-yl)uronium hexafluorophosphate
HCV	Hepatitis C virus
HDAC	Histone deacetylase
HDP	Hexadecyloxypropyl
HEK	Human Embryonic Kidney 293 cells
Hex	Hexane
HIPS	Helmholtz Institute for Pharmaceutical Research Saarland
HIV	Human immunodeficiency viruses
HMBC	Heteronuclear multiple bond coherence (NMR)
HPLC	High performance liquid chromatography
HRMS	High resolution mass spectrometry
HSQC	Heteronuclear single quantum coherence (NMR)
Hyp	Hydroxyproline
Hz	Hertz
HZI	Helmholtz Center for Infectious Diseases, Braunschweig
i.e.	That is [lat. <i>id est</i> ]
<i>i</i> Bu	<i>iso</i> -butyl
IC <sub>50</sub>	Drug concentration required for 50% inhibition

iPr	iso-propyl
IR	Infrared (spectroscopy)
ITC	Isothermal titration calorimetry
J	Scalar coupling constant [Hz] (NMR)
kDa	Kilo dalton
Ki	Inhibitory Constant
Kpg	Lysin-gingipain
LasB	Elastase B
lat.	Latin
LC-MS	Liquid chromatography–mass spectrometry
LT50	Median lethal times
M	Molar $\left[\frac{\text{mol}}{\text{L}}\right]$
m	Multiplet
m.p.	Melting point
max.	Maximum
MBL	Metallo-β-lactamase
Me	Methyl
MeCN	Acetonitrile
MeOH	Methanol
MES	2-( <i>N</i> -morpholino)ethanesulfonic acid (buffer agent)
MIC	Minimum inhibitory concentration
min	Minute(s)
mL	Millilitre
MMP	Matrix metalloprotease
MRSA	Methicillin-resistant <i>Staphylococcus aureus</i>
MS	Mass spectrometry
MTT	3-(4,5-Dimethylthiazol-2-yl)-2,5-diphenyltetrazolium bromide
MW	Molecular weight
n.d.	Not determined
n.i.	No inhibition
nBu	<i>n</i> -butyl
nm	Nanometre
nM	Nano molar
NMR	Nuclear magnetic resonance
<i>n</i> Pr	<i>n</i> -propyl
OECD	Organisation for Economic Co-operation and Development
OIE	<i>Office International des Epizooties</i> = World Organisation for Animal Health (WOAH)
Pbf	2,2,4,6,7-Pentamethylidihydrobenzofuran-5-sulfonyl
PD	Peptidase domain
PDB	Protein data base
PE	Petroleum ether

Ph	Phenyl
Phg	Phenylglycine
PK	Pharmacokinetic
ppm	Parts per million (NMR)
QSAR	Quantitative structure–activity relationship
quant.	Quantitative
$R_f$	Retardation factor (TLC)
RKI	Robert Koch Institute
rpm	Rounds per minute
rt	Room temperature
s	Singlet
SAR	Structure-activity relationship
sBu	<i>sec</i> -butyl
SD	Standard deviation
$S_N2$	Nucleophilic substitution type 2
SPR	Surface plasmon resonance
STIKO	Standing Committee on Vaccination
t	Triplet (NMR)
TACE	TNF- $\alpha$ converting enzyme
td	Triplet of duplet (NMR)
TFA	Trifluoroacetic acid
THF	Tetrahydrofurane
TLC	Thin layer chromatography
TMSBr	Trimethylbromosilane
TNF- $\alpha$	Tumor necrosis factor $\alpha$
$t_R$	Retention time (HPLC)
UK	United Kingdom
UN	United Nations
US	United States
UV	Ultraviolet (spectroscopy)
$\tilde{\nu}$	Wave number [ $\text{cm}^{-1}$ ] (IR)
WHO	World health organization
ZBG	Zinc-binding group
$\delta$	NMR chemical shift [ppm]
$\lambda$	Wavelength [nm] (UV)
$\lambda_{\text{max}}$	Wavelength at maximum of UV absorption [nm]

### **Abbreviation of Amino Acids**

<b>amino acid</b>	<b>single letter code</b>	<b>triple letter code</b>	<b>amino acid</b>	<b>single letter code</b>	<b>triple letter code</b>
alanine	A	Ala	leucine	L	Leu
arginine	R	Arg	lysine	K	Lys
asparagine	N	Asn	methionine	M	Met
aspartic acid	D	Asp	phenylalanine	F	Phe
cysteine	C	Cys	proline	P	Pro
glutamic acid	E	Glu	serine	S	Ser
glutamine	Q	Gln	threonine	T	Thr
glycine	G	Gly	tryptophane	W	Try
histidine	H	His	tyrosine	Y	Tyr
isoleucine	I	Ile	valine	V	Val

# I. INTRODUCTION

## 1. Bacteria and Bacterial Infections

### 1.1 About Bacteria and Infectious Diseases

It was in 1673 that the Dutch scientist Antonie Philips van Leeuwenhoek was the first person ever who observed bacteria as “molds” through a self-made microscope.<sup>8</sup> Three years later he was able to describe these bacteria “molds” more precisely in a letter to the Royal Society of London as “Animaculis” (= little animals).<sup>9</sup> However, it took another 200 years until the German physician and scientist Robert Koch proved bacteria as a cause of infectious diseases. In 1876, he demonstrated the relationship between *Bacillus anthracis* as a pathogen and the development of anthrax.<sup>10</sup>

Even though less than 1% of all known bacteria are pathogenic,<sup>11</sup> in the year 2016, three of the Top 10 globally leading causes of death (together 10% of all deaths) were associated with bacterial infections.<sup>12</sup> Until the discovery of the first antibiotics in the first half of the 20<sup>th</sup> century, infectious diseases even were the primary cause of death all around the globe.<sup>13</sup>

### 1.2 The Golden Era of Antibiotics

It was more or less by chance that Sir Alexander Fleming discovered the antibiotic effect of the mold *Penicillium notatum* in 1928.<sup>14</sup> It took another decade until the team around Sir Howard Walter Florey and Ernst B. Chain developed purification and isolation methods of the active ingredient penicillin in the broths and to evaluate penicillin's properties,<sup>15</sup> before it was used excessively in World War II.<sup>16,17</sup> Penicillin was introduced into the market in 1945.<sup>17</sup> The outcome of bacterial pneumonia and bloodstream infections that before had a survival rate of just 10% was extremely improved and reached levels of 90% survival with penicillin treatment.<sup>18</sup>

Meanwhile, the German pathologist Gerhard Johannes Paul Domagk discovered the antibiotic effect of sulfanilamides.<sup>19</sup> “Prontosil” was the first antibiotic substance that was introduced into the market in 1937. All four scientists – Domagk, Fleming, Florey, and Chain – were awarded The Nobel Prize in Physiology or Medicine for their findings (Domagk in 1939, Fleming, Florey and Chain in 1945).

Most of the antibiotics used today were developed in the 1950s and 1960s, which were later referred to as the golden age of antibiotic discovery.<sup>20</sup> They did not just decrease the mortality of “classic” infectious diseases but are also the reason why we are able to conduct complicated surgeries, such as organ transplantations, joint replacements, and many more.

### 1.3 Resistances are on the Rise

The first penicillin resistance was observed in 1947 just a few years after it had started to be widely used.<sup>21,22</sup> The leading cause of resistance development is the overuse of antibiotics in humans, in agriculture, and in animal health.<sup>23–25</sup>

All kinds of surgeries are critically endangered due to the current rise of resistances and the lack of new antibiotic classes since 1987, as they require additional antibiotic intake to prevent wound infections.<sup>20,26</sup> Additionally, it is twice as likely that resistant bacteria form complications during the infection and the mortality risk is even three times as high as for infections with non-resistant germs.<sup>27</sup>

Today, more than 35,000 people die per year (2019) in the US<sup>28</sup> and more than 33,000 (in 2015) in Europe<sup>29</sup> due to bacteria that have developed or gained antimicrobial resistance (AMR). Though the numbers vary from study to study, scientists agree that AMR will become even more dangerous if we do not fight it. Already in 2014, the UK *Review on Antimicrobial Resistance* reported that in 2050 infectious diseases will be more lethal than cancer is today.<sup>30</sup> This finding was again supported by the final report on *Drug-resistant infections* of The World Bank in 2017.<sup>31</sup>

Since 1987, almost no new classes of antibiotics were developed, while more and more resistances occurred to all existing antibiotics (see Figure 1; it took almost 20 years from discovery to market introduction for Linezolid and Daptomycin, but just 3 years to observe the first resistances).<sup>20,32</sup>

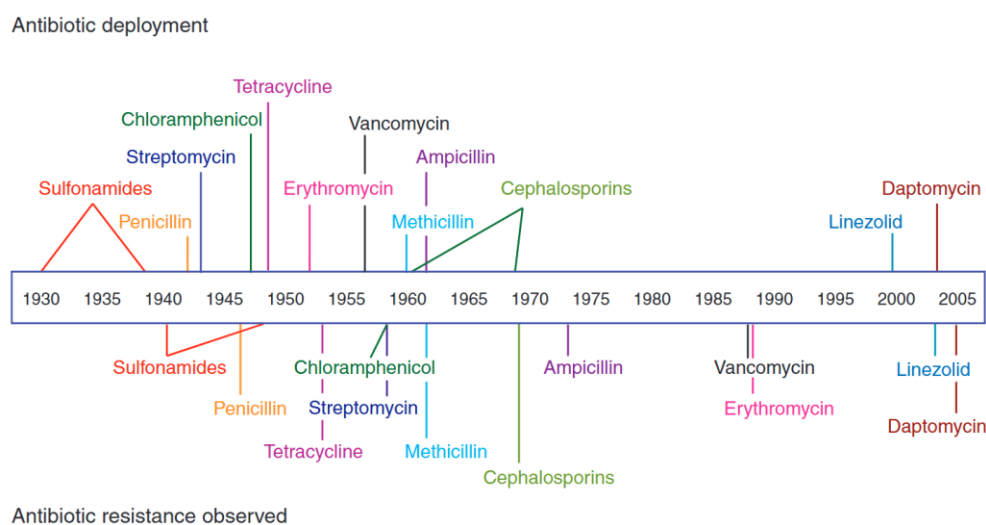


**Figure 1. Timeline of antibiotic deployment and the occurrence of antibiotic resistance.**<sup>32</sup> The year each antibiotic was deployed is depicted above the timeline, and the year resistance to each antibiotic was observed is depicted below the timeline (with the caveat that the appearance of antibiotic resistance does not necessarily imply that a given antibiotic has lost all clinical utility).

(Reprinted by permission from Nature Publishing Group: Springer Nature, *Nat. Chem. Biol.*, Targeting virulence: a new paradigm for antimicrobial therapy. Anne E. Clatworthy *et al.*, Copyright © 2007)

If we do not start to develop new antibiotics and to use both, old and new ones, consciously with more care, we navigate into a post-antibiotic era.

## I. Introduction

One way to decrease the use of antibiotics is to develop sufficient vaccines so that infections can completely be prevented. Consulting the Standing Committee on Vaccination (STIKO) at the Robert Koch Institute (RKI) in Germany, vaccines against nine bacteria are available.<sup>33</sup>

Another way would be the development of rapid and inexpensive diagnostic tools to determine the causative agent for disease in every patient before the use of antibiotics. With that, unnecessary intake of antibiotics could be avoided, and more specific drugs could be prescribed.

Even taking all these strategies into account, we cannot manage without at least some novel antibiotics. Therefore, new alternatives with slower resistance development are urgently needed.<sup>34</sup>

### 1.4 The Antibiotic Pipeline

The number of large pharmaceutical companies conducting research in the field of antibiotics declined from 18 in 1990 to just six in 2015, mostly due to financial reasons. Most antibiotics are inexpensive compared to other drugs, have just short treatment periods (except for anti-tuberculosis drugs), and should be held back for emergency treatment of AMR pathogens.<sup>35,36</sup> This leads to a small profit margin for the companies as the average cost to go through all stages of clinical development is about one billion dollars and the typical success rate from preclinical to market access is just 1.5%.<sup>37-39</sup> Together with the constant threat of resistance development and therefore extremely cautious (and therefore low) use and possible market withdrawal, companies tend to orientate themselves to more promising indications.

Luckily, a lot of research institutions and small to medium-sized companies still conduct research in the field of antibiotics.<sup>40</sup> By the end of 2019, 41 classical antibiotics were listed in clinical trials, with the majority of those still being inhibitors of old targets (31 of 41).<sup>41</sup> Though a lot of companies still focus on old targets, more and more try to find new approaches, such as using phages,<sup>42,43</sup> antibodies,<sup>44-46</sup> or targeting virulence factors.<sup>32,47-49</sup> Additionally to the aforementioned 41 traditional antibiotics, another 30 of these “non-traditional antibiotics” are in clinical development, mainly vaccines, and antibodies, but also two anti-virulence drugs.

As the latter approach is also employed in this work, it will be highlighted in more detail in the following sections.

## 2. Pathoblockers – an Anti-Virulence Approach

Other than traditional antibiotics, that reduce bacterial growth or viability,<sup>50,51</sup> so-called “pathoblockers” aim to decrease the pathogenicity of bacteria by targeting their virulence factors.<sup>32,47-49</sup> Virulence factors are factors or mechanisms that lead to the establishment of disease in the host. As most virulence factors are not essential for bacterial survival, the evolutionary pressure is low.<sup>32</sup> Therefore, it is thought that their inhibitors are less likely to lead to AMR.

Prominent virulence factors include adhesins, factors that facilitate biofilm formation, the bacterial communication system (quorum sensing), toxin secretion systems, and direct toxins, just to name a few of them.<sup>32,47-49</sup>

So far, some antibody solutions that eliminate bacterial toxins are already approved as drugs.<sup>52-54</sup> One example is the human monoclonal antibody BEZLOTOXUMAB which targets the *C. difficile* toxin B. It received approval of the US Food and Drug Administration (FDA) in 2016.<sup>54</sup>

Other pathoblockers are under investigation in fundamental and preclinical research, while only two made it into the clinic so far, one of these being recently approved.<sup>55-58</sup>

One of these clinically tested pathoblockers is the lysin-gingipain (Kgp) inhibitor Atuzaginstat (**COR388**, company: CORTEXIME). Gingipains are secreted cysteine proteases from the periodontal pathogen *Porphyromonas gingivalis*, which also play a role in the progression of Alzheimer’s disease.<sup>56,59-61</sup> These gingipains perturb the human immune response very effectively by hydrolyzing tumor necrosis factor  $\alpha$  (TNF- $\alpha$ ) and a variety of cytokines.<sup>62-65</sup> Hence, Kgp inhibitors reduce the virulence of *P. gingivalis* tremendously and were therefore in a large clinical phase II/III study (GAIN) for the treatment of periodontal disease and Alzheimer’s disease.<sup>56,59-61</sup> Unfortunately, the trial did not reach its primary endpoint and CORTEXIME announced to start a confirmatory trial. Before the registration of this trial, CORTEXIME changed its name to QUINCE THERAPEUTICS and sold the full gingipain inhibitor program to LIGHTHOUSE PHARMACEUTICALS in early 2023.<sup>66,67</sup> It is yet unclear if these molecules will be developed any further.

The other pathoblockers is the liposomal **Cal02** (company: EAGLE PHARMACEUTICALS, early development by COMBIOXIM) which is a broad-spectrum anti-virulence inhibitor being active on both bacterial and viral infections (including SARS-CoV-2).<sup>55,68,69</sup> It acts as a liposomal trap, mimicking cell membranes, and is therefore able to encapsulate and with that neutralize excreted virulence factors. Just recently it was granted FDA approval and Fast-Track Designation as a first-in-class broad-spectrum anti-virulence agent for the adjunct treatment of severe community-acquired bacterial pneumonia.<sup>57</sup>



### 3. Bacterial Proteases as Anti-Virulence Targets

As demonstrated by the example of Atuzaginstat and Cal02, a possible and effective anti-virulence approach can be to target (secreted) bacterial proteases.

Proteases catalyze the cleavage of one of the most important chemical linkages in living matter: the peptide bond. Therefore, they play a crucial role in all organisms from viruses to fungi to animals and humans.<sup>70-72</sup> They are highly important for the homeostasis of the human body,<sup>70,73</sup> but also for the progression of various bacterial and viral infections.<sup>72,74,75</sup>

Proteases can be classified either by the position of the peptide cleavage or more accurately by their catalytic mode of action. If the scissile bond of their substrate is in the middle of the protein sequence, they are called endopeptidases, while the so-called exopeptidases cleave their substrates near the N- or C-terminus.<sup>71</sup>

There are five types of catalytic mechanisms: cysteine-, serine-, threonine-, aspartate-, and metalloproteases. While in the first three, the named amino acids serve as initial nucleophiles for the hydrolysis of the protein, resulting in a covalent bond of substrate and enzyme, an active water molecule is the sole nucleophile in the aspartate- and metalloproteases.<sup>71,76,77</sup>

To understand the binding of a substrate to the protein, it is crucial to understand the nomenclature of proteases by Schechter and Berger.<sup>78</sup> The substrate binding to the protease in its simplified representation (see Figure 2) corresponds to the lock-and-key model of Fischer.<sup>79</sup> The peptide's amino acids (AA) are numbered P1 to Pn from the scissile bond towards the N-terminus, and P1' to Pn' towards the C-terminus. The surface of the protein which forms the corresponding binding pocket for each AA is called a subsite and is numbered S1 to Sn (non-primed sites), or S1' to Sn' (primed sites), respectively.<sup>73,78</sup>

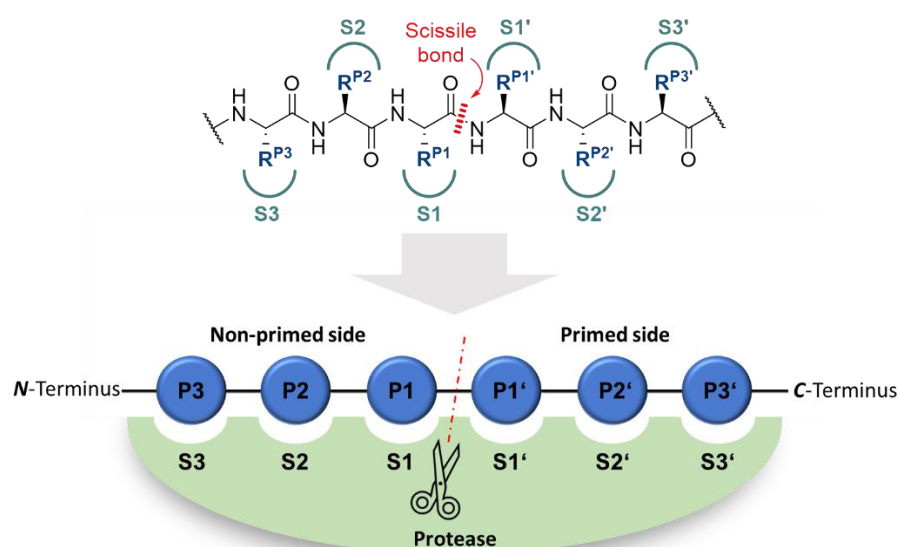


**Figure 2.** Schematic representation of a protein substrate binding to a protease.<sup>73</sup> (Adapted from Boris Turk, *Nat. Rev. Drug Discov.* **2006**, 5 (9), 785–799.)

## I. Introduction

While there are already several inhibitors of human proteases, *e.g.*

- Captopril (see Figure 3) as an inhibitor of the angiotensin-converting enzyme (ACE) for the treatment of hypertension<sup>80</sup>
- Vorinostat (see Figure 3) as a histone deacetylase (HDAC) inhibitor for cancer treatment<sup>81,82</sup>
- Dabigatran (see Figure 3) as a thrombin inhibitor to be used as anticoagulant<sup>83</sup>

and inhibitors of viral proteases, *e.g.*

- Darunavir as a human immunodeficiency viruses (HIV) protease inhibitor<sup>84</sup>
- Simeprevir as a hepatitis C virus (HCV) protease inhibitor<sup>85</sup>

on the market (just to name a few), no inhibitors of bacterial proteases have received market approval so far.

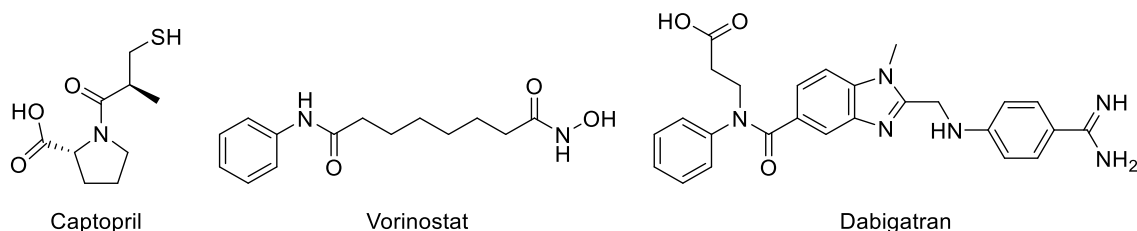


**Figure 3.** Chemical structures of the human protease inhibitors Captopril, Vorinostat and Dabigatran.

As previously mentioned, only one bacterial protease inhibitor was in late-stage clinical development (Atuzaginstat).<sup>56,59-61</sup> However, with the current fast increase in antibiotic resistance, those bacterial proteases represent highly attractive new drug targets.<sup>72,74,77,86</sup>

This work is mainly focused on the zinc- and calcium-dependent metalloproteases collagenase H (ColH) from *Clostridium histolyticum* (*Hathewayia histolytica*) and elastase B (LasB) from *Pseudomonas aeruginosa*, and the selectivity profile of their inhibitors over other zinc-containing human and bacterial metalloproteases, such as human matrix metalloproteases (MMPs) and bacterial metallo- $\beta$ -lactamases (MBLs).

### 3.1 Collagenases as Virulence Factors of *Clostridia* and *Bacilli*

#### 3.1.1 *Clostridia*

*Clostridia* are Gram-positive, anaerobic, spore-forming bacteria. Prominent representatives include the pathogens *C. botulinum*, *C. difficile* (now: *Clostridioides difficile*), *C. histolyticum* (now: *Hathewayia histolytica*), *C. perfringens*, and *C. tetani*. They can cause severe human diseases<sup>87,88</sup> such as tetanus, muscle necrosis (gas gangrene), soft tissue necrosis (wound burn), botulism, and colitis, which are accompanied by high mortality rates in most cases.<sup>89,90</sup> Some representatives of the species even have been cultured to be used as bioweapons.<sup>91,92</sup>

Among all bacteria, *Clostridia* produce the highest number of toxins.<sup>93</sup> Those include neurotoxins, such as tetanus toxin (*C. tetani*) and botulinum toxin (*C. botulinum*), with the latter being the most toxic protein known.<sup>93</sup> Also, enterotoxins such as toxins A and B from *C. difficile* and histotoxins, which include the collagenases G (ColG) and H (ColH) from *C. histolyticum* and collagenase A (ColA) from *C. perfringens*, are widely spread.<sup>87</sup> ColA from *C. perfringens* is closely related to ColH, as they share 36% identity.<sup>94</sup> *Clostridia* can distribute their toxins via horizontal gene transfer between subgroups.<sup>93</sup>

Collagenases as prominent virulence factors will be highlighted in this work in more detail.<sup>95</sup> However, collagenases are not only produced by *Clostridia* but can also be found in *Bacilli*.

#### 3.1.2 *Bacilli*

*Bacilli* are also Gram-positive, facultatively anaerobic, spore-forming bacteria that can be found ubiquitously in the environment. They facilitate their pathogenicity using a high variety of virulence factors, including hemolysins, phospholipase C, enterotoxins, and proteases.<sup>96,97</sup> Prominent members of this species are *B. anthracis*, the causative agent of anthrax,<sup>98</sup> *Bacillus thuringiensis*, a widely used bacterial insecticide,<sup>99</sup> and *Bacillus cereus* which can induce gastrointestinal disorders such as food-poisoning,<sup>100</sup> but also non-gastrointestinal diseases such as periodontal diseases,<sup>101</sup> endophthalmitis<sup>102</sup> and wound infections.<sup>103,104</sup>

For *B. thuringiensis* it was shown that it employs its collagenase B (ColB) for host invasion.<sup>105</sup> *B. cereus* also expresses two collagenases, ColA and ColQ1, and though their activity in food poisoning has not yet been described, Beecher *et al.* observed a progressive degradation of the collagenous lens capsule prior to the full endophthalmitis outbreak.<sup>106</sup> This suggests that the collagenases are responsible for host invasion.<sup>106</sup> Additionally, collagenases have also been found in dental plaques of *B. cereus*-mediated periodontal disease.<sup>107,108</sup>

### 3.1.3 Bacterial Collagenases

The primary function of bacterial collagenases is the degradation of collagen as an amino acid and nitrogen source for nutritional purposes.<sup>109</sup> Collagen is the most abundant protein in mammalian bodies.<sup>110</sup> It is a substantial part of the extracellular matrix: it can be found all over in skin, tendons, and cartilage, and accounts for up to 30% of total protein content in the human body.<sup>111</sup> Collagen contains a right-handed triple helix composed of three left-handed  $\alpha$ -chains. Its amino acid sequence is a repeating motif of Gly-X-Y, whereas X and Y can be any amino acid but are most often proline and hydroxyproline.<sup>111</sup> It is highly resistant to proteolysis due to this structure. Mammalian collagenases such as matrix metalloprotease 1 (MMP-1) cleave collagen at only one site.<sup>112</sup> In contrast to that, bacterial collagenases are most often so-called “true” collagenases meaning that they can cleave the triple helical collagen structure at multiple sites.<sup>87</sup>

The most thoroughly studied bacterial collagenases are ColG and H from *C. histolyticum*, sometimes also referred to as “*Clostridium histolyticum* collagenase”, ChC. ColH and ColG are multi-domain proteins having an N-terminal collagenase unit (CU) that contains the peptidase domain (PD).<sup>113</sup> They are part of the gluzincin family and their peptidase domain contains the catalytic zinc ion that is coordinated in the HEXXH motif by two histidine residues (His415 and His419 for ColH) and a downstream glutamate (Glu447 for ColH).<sup>114</sup> Water (or the hydroxide ion) serves as further zinc coordinator and is the nucleophile for the proteolytic reaction.<sup>115,116</sup>

Additionally, ColH has an aspartate amino acid (Asp421) which also coordinates the zinc ion, while the other clostridial collagenases have a serine in that position.<sup>117</sup> This makes ColH conformationally more rigid than ColG. Therefore, ColG shows a higher collagenolytic activity, making it a Class I collagenase, while ColH has a higher peptidolytic activity and is assigned to the Class II collagenases.<sup>118</sup>

The first X-ray crystal structure of the collagen-binding domain of ColG was published in 2003 by Wilson *et al.*<sup>119</sup> It took until 2011 for the first co-crystal structures of the peptidase domain of ColG being published by Eckhard *et al.*,<sup>120</sup> soon followed by further (co-)crystal structures of the peptidase domains of ColH and ColT.<sup>117</sup> This is now a strong advantage for rational inhibitor development.

As mentioned, secreted collagenases also play a role in the pathogenesis of *B. cereus* and *B. thuringiensis*.<sup>121,122</sup> As the latter is no human pathogen the focus will be on ColQ1 and ColA from *B. cereus*. In contrast to clostridial collagenases, little is known about collagenases from *Bacillus* species and no crystal structures are available as of now. However, ColA of *B. cereus* ATCC 14579 was cloned and purified by Abfalter *et al.* in 2016. It shows 44% identity to both ColG and ColH and a homology model with ColG was obtained.<sup>121</sup> ColQ1 is a close homolog of ColA and was purified and analyzed just recently in 2021 by Hoppe *et al.*<sup>123</sup>. Both have a sequence identity of 72% and a similarity of 84%. Compared to clostridial collagenases they show remarkably high collagenolytic and peptidolytic activities, so they cannot be easily classified as Class I or Class II collagenases.

## I. Introduction

All of these collagenases are considered crucial virulence factors for the respective pathogens. They enable the invasion into the host by the degradation of collagen barriers.<sup>118,124–126</sup> Furthermore, the resultant amino acids can then be used as nitrogen sources for the nutrition of the bacteria, and the toxin diffusion and spread into deep tissue is promoted.<sup>125,127</sup>

### 3.1.4 Inhibitors of Bacterial Collagenases

There is limited precedent for the development of selective bacterial collagenase inhibitors. Most literature-known inhibitors were tested on their activity against “*Clostridium histolyticum* collagenase”, ChC. It is usually not disclosed, whether ChC was purified ColH, ColG, or a mixture of both. As zinc- and calcium-dependent metalloproteases, ChC can – like other metalloproteases – be inhibited by zinc-chelating agents such as phenantroline and EDTA.<sup>117</sup>

In the 1980s, a lot of work on peptide-based ChC inhibitors was published.<sup>128–132</sup> Among those, the unselective inhibitor isoamyl phosphonyl-Gly-Pro-Ala (**1**, Figure 4)<sup>130</sup> might be the most prominent one and was also co-crystallized with ColH, ColG, and ColT by Eckhard *et al.* in 2011 and 2013.<sup>117,120</sup>

Additionally, naturally occurring substances like aloins (from *Aloe* extracts),<sup>133</sup> aranciamycin (antibiotic produced by *Streptomyces griseoflavus*),<sup>134</sup> scoporone (from *Viola yedoensis*),<sup>135</sup> and caffeine (*e.g.* from *Coffea arabica*)<sup>136</sup> were found to be broad spectrum bacterial and human collagenase inhibitors (Figure 4). This is most probably also due to their metal-chelating properties.

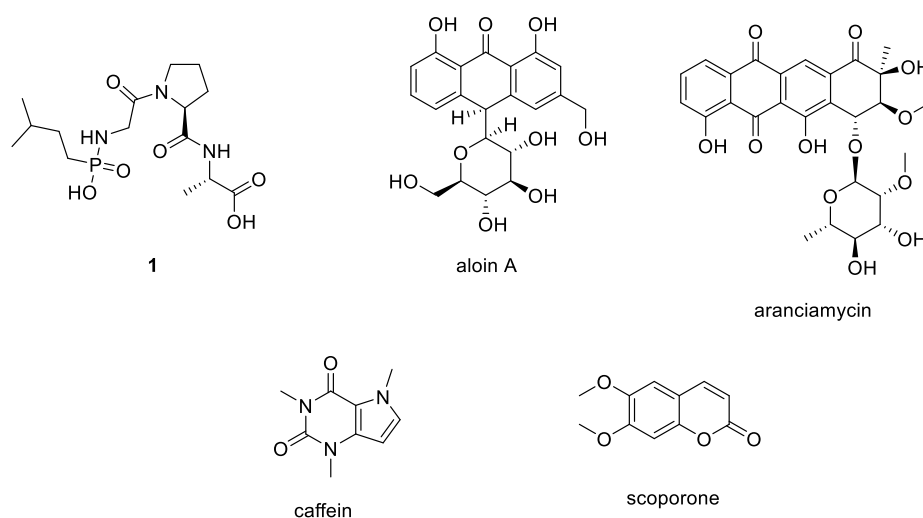


**Figure 4.** A selection of known peptidic and naturally occurring ChC inhibitors.

The only synthetic published collagenase inhibitors are those of the group of Supuran and Scozzafava *et al.*<sup>137–143</sup> Between 2000 – 2003, their group developed a wide variety of *N*-(benzyl)-*N*-(sulfonyl)amino acid hydroxamates and carboxylates as ChC inhibitors. Here, the hydroxamates were by two orders of magnitudes more active than the corresponding carboxylates (*e.g.*, **2** vs. **3**, Figure 5

## I. Introduction

and Table 1),<sup>137</sup> while changing the first amino acid from alanine (**3**) to glycine (**4**) or valine (**5**) did not make much of a difference (**3** – **5** all having a  $K_i < 10$  nM, Figure 5 and Table 1).<sup>137–139</sup> Additionally, the sulfonyl moiety could be exchanged by an ureido or a thioureido moiety with retention of its activity.<sup>140,141</sup> As an example, the thioureido compound **6** is depicted in Figure 5.<sup>140</sup>

As one of their last works about ChC inhibitors, Supuran and Scozzafa's group proposed the introduction of 5-amino-2-mercapto-1,3,4-thiadiazole as zinc-binding group (ZBG) to a very similar sulfonyl scaffold (**7**, Figure 5).<sup>142</sup> Unfortunately, this led to inhibitors with  $K_i$  values increased by three orders of magnitude, while still absolutely no selectivity over MMPs was archived (Table 1).

For a better overview, the  $K_i$  values of some selected synthetic inhibitors by Supuran and Scozzafava *et al.* depicted in Figure 5 are summed up in Table 1.

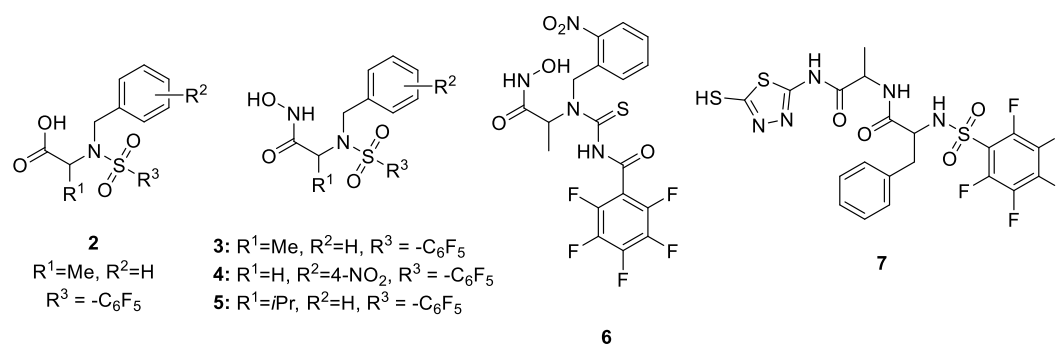


**Figure 5.** Selection of synthetic ChC inhibitors published between 2000 and 2003 by Supuran *et al.*<sup>137–142</sup>

**Table 1.** Inhibition of ChC and MMPs with hydroxamates and thiadiazoles as reported by Supuran *et al.*<sup>137–142</sup>

Compound	$K_i$ (nM)				
	MMP-1 <sup>a</sup>	MMP-2 <sup>a</sup>	MMP-8 <sup>a</sup>	MMP-9 <sup>a</sup>	ChC <sup>b</sup>
<b>2</b>	n.d.	n.d.	n.d.	n.d.	500
<b>3</b>	n.d.	n.d.	n.d.	n.d.	6
<b>4</b>	3.0	0.7	0.1	0.6	5
<b>5</b>	n.d.	n.d.	n.d.	n.d.	5
<b>6</b>	n.d.	n.d.	n.d.	n.d.	8
<b>7</b>	9000	6000	1000	2000	5000

<sup>a</sup>Spectrophotometric assay with Ac-Pro-Leu-Gly-S-Leu-Leu-Gly-OEt  
<sup>b</sup>Spectrophotometric assay with FALGPA  
n.d. = not determined

## I. Introduction

Thus, we propose that this non-selectivity over human off-targets is the reason why no other group tried to develop further ChC inhibitors after Supuran *et al.* until now, despite the attractiveness of ChC and other bacterial collagenases as antivirulence targets, **if** they are inhibited selectively.

### 3.2 Elastase B as Virulence Factor of *Pseudomonas aeruginosa*

#### 3.1.1 *Pseudomonas aeruginosa*

According to the World Health Organization (WHO) priority list published in 2018, *Pseudomonas aeruginosa* is currently one of the most problematic pathogens and listed as priority 1.<sup>144,145</sup> Additionally, the Centers for Disease Control and Prevention (CDC) also listed it as serious threat in 2019.<sup>146</sup> This opportunistic Gram-negative bacillus is a leading cause of nosocomial infections<sup>147-150</sup> causing burn wound infections,<sup>147,148,151</sup> keratitis<sup>152-154</sup>, urinary tract infections, and lung infections (especially in cystic fibrosis patients).<sup>147,155,156</sup> According to the European cystic fibrosis society patient registry (ECFSPR) annual data report (2018), up to 53% of adult cystic fibrosis (CF) patients suffer from chronic lung infections caused by *P. aeruginosa*.<sup>157</sup> Such an infection then causes 2.6-fold higher mortality in CF patients.<sup>158</sup>

*P. aeruginosa* secretes a biofilm that leads to adhesions to surfaces such as in catheters, which might be the reason for its high abundance in hospitals.<sup>159,160</sup> This biofilm, which is also found on mucosal surfaces and in lung fluids, causes the production of exopolysaccharides which reduces the effectiveness of phagocytosis and antibiotic therapy.<sup>160,161</sup> Additionally, *P. aeruginosa* is characterized by high resistance to many classes of antibiotics.<sup>162</sup> This makes *P. aeruginosa* an extremely hard-to-treat pathogen.

It is known that *P. aeruginosa* has a large abundance of virulence factors, a lot of them being cell-associated, *e.g.*, the quorum sensing system.<sup>163-165</sup> Unfortunately, inhibitors of those often suffer from poor *in vivo* performance as they have to cross the Gram-negative cell wall. However, there is also a large variety of secreted virulence factors, such as different proteases, lipases, exotoxins, and pyrocyanins.<sup>166</sup> Addressing these as targets would therefore not require bacterial cellular uptake.

#### 3.1.2 Elastase B (*LasB*)

Elastase B (*LasB*) – also called pseudolysin – is one of the aforementioned secreted virulence factors of *P. aeruginosa*.<sup>167,168</sup> It plays a major role in host colonization and the attenuation of the human immune response.<sup>167-170</sup> *LasB* is a 33 kDa extracellular zinc- and calcium-containing metalloprotease that belongs to the thermolysin (M4) family of zinc-dependent neutral metalloendopeptidases.<sup>171</sup> It is encoded by the gene *lasB*, which is regulated by the quorum sensing system via *las* and *rhl* genes.<sup>172,173</sup> The 53.4 kDa preproenzyme has a 2.4 kDa signal peptide and an 18 kDa propeptide.<sup>174</sup> The signal peptide is cleaved during the passage through the inner membrane, while the propeptide is cleaved by

## I. Introduction

autoproteolysis in the periplasm. It forms an inactive non-covalent complex with the actual elastase (LasB), which is then translocated through the outer membrane as active LasB.<sup>174</sup>

LasB might be the most important virulence factor of *P. aeruginosa* as it not only promotes biofilm formation<sup>175</sup> but also has a large variety of possible substrates. The cleavage of cytokines,<sup>176</sup> natural antimicrobial peptide (AMP) LL-37,<sup>177</sup> and complement factors<sup>178</sup> by LasB leads to a decreased immune response. In parallel, the hydrolysis of surfactant proteins A and D in the lungs reduces phagocytosis.<sup>179–181</sup> With that, *P. aeruginosa* can hardly be attacked by the human immune system. Additionally, LasB also recognized laminin,<sup>182</sup> elastin,<sup>183</sup> and collagen<sup>184</sup> as substrates which help the pathogen in degrading the host's tissue and to facilitate colonization.

LasB's important role in the facilitation of a functional infection was proven by infection models with wild-type *P. aeruginosa* and knock-out mutants. Those mutants induce less severe keratitis in rabbits,<sup>185</sup> less death in *Caenorhabditis elegans*,<sup>186</sup> and less severe pneumonic infections in mice.<sup>187</sup>

Taking all of this together, LasB is a highly attractive drug target and quite some work has been done to find suitable inhibitors of LasB in the past.

### 3.1.3 Inhibitors of LasB

As LasB is a zinc- and calcium-dependent metalloprotease, it can – like ColH – be inhibited by metal-chelating agents such as EDTA and phenanthroline.<sup>171</sup> Also, the broad-spectrum metalloprotease inhibitor phosphoramidon (**8**, Figure 6) is a submicromolar inhibitor of LasB. Phosphoramidon also was used as a ligand to crystallize LasB (protein data base (PDB) reference: 3DBK) and to determine several essential structural motifs of LasB inhibitors.<sup>188–190</sup>

Already in 1992, Yokota *et al.* demonstrated that a monoclonal antibody can inhibit LasB.<sup>191</sup> Recently in 2019, Galdino *et al.* published that the copper complex  $\text{Cu}(\text{phenidione})_3(\text{ClO}_4)_2 \cdot 4\text{H}_2\text{O}$  (**9**, Figure 6) displays high *in vitro* activity against LasB ( $K_i = 90$  nM), low toxicity in mice and mediated enhanced survival in an *in vivo* infection model with *Galleria mellonella* larvae.<sup>172</sup> This is to our best knowledge the only known LasB inhibitor that does not bind to the active site zinc ion.

All other known LasB inhibitors possess prominent zinc-chelating moieties, such as carboxylates, hydroxamates, and thiols. In 2011, Cathcart *et al.* published an *N*-peptidyl mercaptoacetamide compound (**10**) that showed high *in vitro* activity against LasB ( $K_i = 41$  nM) and was able to reduce biofilm formation.<sup>192</sup> Docking experiments with this inhibitor were done and the results were compared to the binding mode of phosphoramidone **8**.<sup>190</sup>

A virtual screening by Zhu *et al.* in 2015 revealed *N*-aryl mercaptoacetamides as possible inhibitors of LasB with low micromolar inhibition values.<sup>193</sup> Unfortunately, they were not active in their *in vivo* infection model with *C. elegans*. They postulated that this might be the case due to the rapid oxidation of the thiol to its inactive disulfide derivative. Indeed, when using a thioacetate prodrug form of the



## I. Introduction

aforementioned thiol (**11**, Figure 6), the median lethal times ( $LT_{50}$ ) of *C. elegans* were restored to the level of an infection with a LasB-knockout mutant strain.<sup>193</sup>

The same inhibitor scaffold was found by Kany *et al.* in 2018 and even co-crystallized with LasB.<sup>194</sup> The *in vitro* activities were comparable to those observed by Zhu *et al.* (**12**, Figure 6). Additionally, a high selectivity of the thiocarbamate prodrug form over human enzymes (MMPs, HDACs, and TACE) was proven, making this scaffold very attractive for further development. However, in the employed *in vivo* infection model using *Galleria mellonella* larvae, a thiocarbamate prodrug was not active, while the parent thiol was.<sup>194</sup> Kany *et al.* also found that the thiol zinc-binding motif can be exchanged by a hydroxamate group (**13**, Figure 6) and that this molecule then can reduce biofilm formation.<sup>195</sup>

In 2022, Kaya *et al.* published a benzylated analog (**14**) of Kany's compound **12**, as well as several other analogs with different aryl substitution patterns and even functionalized aryl moieties.<sup>196,197</sup> These molecules' LasB *in vitro* inhibitory activities (**14**,  $IC_{50} = 2.7 \pm 0.4$  M vs. **12**,  $IC_{50} = 6.6 \pm 0.3$  M), as well as the *in vivo* activity in a *Galleria mellonella* larvae infection model, were increased while selectivity against human off-targets such as TACE and MMPs was retained.

In 2021, Leiris *et al.* published a potent carboxylic acid derived LasB inhibitor (**15**, Figure 6).<sup>189</sup> It possessed the same binding mode as the other LasB inhibitors with its indane ring occupying the lipophilic S1' binding pocket and the benzothiazole binding to the S2' cleft. Its selectivity over three MMPs and ACE was demonstrated, making it interesting for further development regarding the first *in vivo* activity.<sup>189</sup>

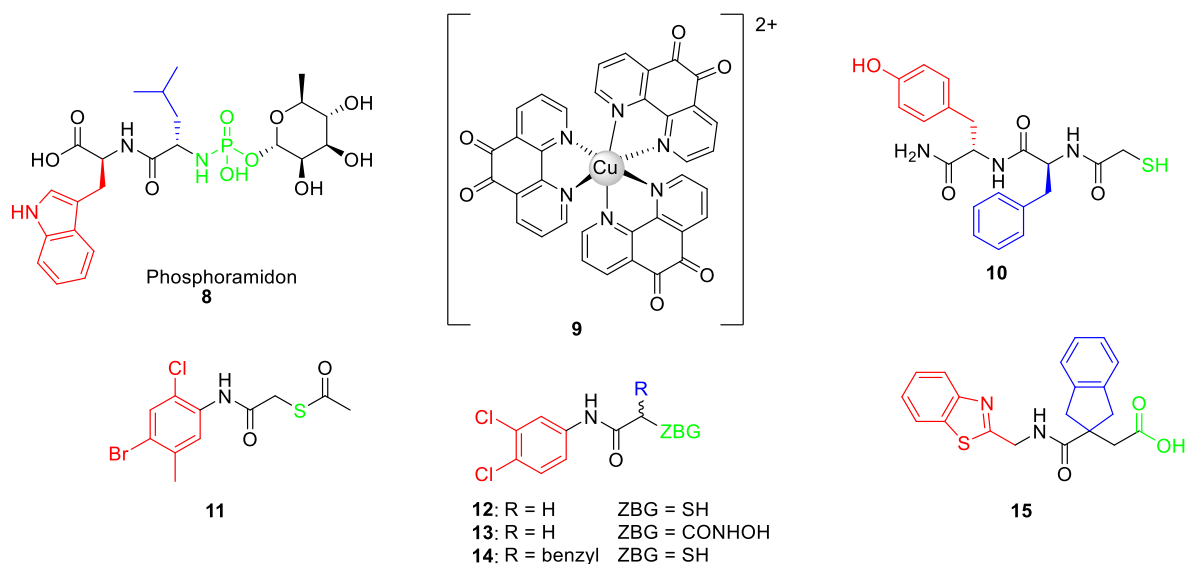


**Figure 6.** Various previously reported inhibitors of LasB.<sup>188–190,194–196</sup> Side chains binding to the S1' binding pocket are highlighted in blue, those in the S2' binding pocket in red and the ZBG is colored green.

Taking all the information about the different co-crystal structures of LasB with varying inhibitors together, it can be seen that a zinc-binding group is needed for good activity, followed by a bulky hydrophobic residue that can occupy the lipophilic S1' binding pocket. Here, no polar substituents seem to be tolerated. For the S2' binding pocket, aromatic side chains are preferred and they can

## I. Introduction

contain a hydrogen bond donor, such as hydroxyl.<sup>188-190,194,195</sup> In Figure 6, the corresponding binding units are color encoded. Residues in the S1' binding pocket are highlighted in blue, those in the S2' binding pocket in red, and the ZBG is colored green.

## II. AIM OF THE THESIS

As AMR expands further and further, research for antibacterial agents with new modes of action is urgently needed. One of the novel approaches is designing so-called “pathoblockers” that disarm bacteria by inhibiting their virulence factors rather than killing them. The attenuated bacteria then will be eliminated by the host’s immune response or can be addressed more efficiently with other “classic” antibiotics.

One anti-virulence approach is the inhibition of secreted bacterial proteases. These usually play a pivotal role in establishing the disease as they facilitate bacterial colonization, nutrition supply, tissue damage, and elusion of the host’s immune system. Also, they are usually easy to target as known permeability issues can be avoided due to their extracellular location. As they are often not crucial for bacterial viability, low selection pressure is exerted, which should result in very low resistance development.

Two prominent bacterial proteases are collagenase H (ColH) from *C. histolyticum* and elastase B (LasB) from *P. aeruginosa*. Both virulence factors are essential for the respective bacteria to induce their often-lethal diseases, such as gas gangrene (*C. histolyticum*) and lung infections –especially in cystic fibrosis patients (*P. aeruginosa*).

Unfortunately, known inhibitors of these enzymes often lack selectivity over human MMPs, as they are designed to bind in the primed region and interact with the metal ion in the catalytic site. Therefore, this work aimed at the design, synthesis, and biological evaluation of inhibitors for both ColH and LasB with high selectivity over the aforementioned off-targets.

This thesis is divided into seven chapters (named chapters **A – G**), each with a specific focus concerning the general topic.

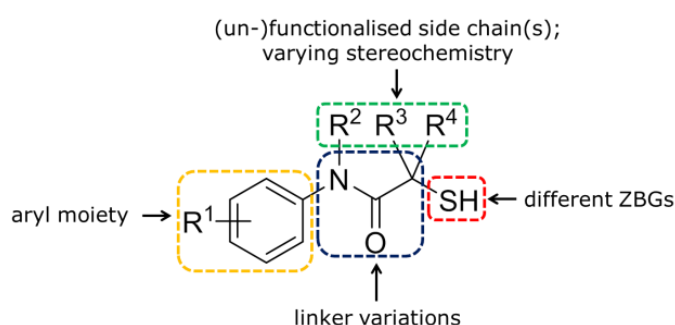


**Figure 7.** General structure of all ColH and LasB inhibitors in this thesis.

Chapter A: A surface plasmon resonance (SPR)-based screening of a protease inhibitor library followed by a Förster resonance energy transfer (FRET)-based inhibition assay on ColH shall identify possible structures able to inhibit ColH, which shall then serve as starting point for further structure-based optimization. This work revealed thiocarbamate based prodrugs of mercaptoacetamides as selective

## II. Aim of the Thesis

inhibitors for ColH. Those mercaptoacetamides can be divided into four segments which can be structurally modified (see Figure 7). Aryl modifications will be discussed in Chapter **A**, while other modifications are part of the following chapters.

Chapter B to Chapter C: As thiols are highly prone to oxidation, these chapters will focus on the search for an alternative zinc-binding group (see in red, Figure 7) for our first hit compound found in chapter **A**. Biological evaluation of the compounds shall prove the efficacy of analogs of our hit compound for the further development to suitable drugs as pathoblocking agents.

Chapter D: Kany *et al.* found that *N*-arylmecapto acetamides can inhibit LasB in the micromolar range.<sup>194,198</sup> But while for ColH only *para*-substitution on the aryl moiety with polar, hydrogen bond accepting moieties is tolerated, the substitution pattern for LasB inhibitors includes lipophilic multi-substitution. One of Kany's inhibitors was also found to inhibit IMP-7, a metallo- $\beta$ -lactamase (MBL). MBLs are also attractive drug targets, as they catalyze the hydrolysis of all kinds of  $\beta$ -lactam antibiotics. Therefore, this part of the thesis aims to the proof of concept that the structural class of *N*-aryl mercaptoacetamides can be used as multi-target inhibitors for virulence and resistance factors.

(However, further synthetic approaches to optimize the multi-target inhibitor activity of these compounds are now under investigation at the Helmholtz Institute for Pharmaceutical Research Saarland (HIPS) and are no more part of this work.)

Chapter E to Chapter G: The largest part of this dissertation will focus on establishing a detailed structure-activity relationship (SAR) for both LasB and ColH inhibition by subsequent variation of our first hit compound found in Chapter **A** and its phosphonate analog found in Chapter **C** (Figure 7). Synthesis of analogs followed by their biological characterization shall lead to optimized structures capable to be used for further (pre-) clinical development.

## III. PUBLISHED RESULTS

### **Chapter A: Discovery of a Potent Inhibitor Class with High Selectivity toward Clostridial Collagenases.**

Esther Schönauer,<sup>±</sup> Andreas M. Kany,<sup>±</sup> Jörg Hauptenthal, Kristina Hüsecken, Isabel J. Hoppe, Katrin Voos, Samir Yahiaoui, Brigitta Elsässer, Christian Ducho, Hans Brandstetter\* and Rolf W. Hartmann\*

<sup>±</sup> these authors contributed equally

\* corresponding authors

Reprinted with permission from *J. Am. Chem. Soc.* **2017**, *139*, 12696–12703.

DOI:10.1021/jacs.7b06935

Copyright (2017) American Chemical Society

*As this chapter comprizes a publication, compound numbers of this chapter are independent from other parts of this thesis.*

### III. Published Results

#### **Full contribution report:**

R. W. H., H. B., C.D., J. H., A. M. K. and E. S. conceived and coordinated the study. E. S. expressed and purified the clostridial collagenases and mutants, performed the functional assays, performed the ColH crystallization experiments and structure determination, comparison of collagenase and MMP structures and wrote parts of the manuscript. A. M. K. selected the compounds for SAR evaluation and contributed to the SAR interpretation, synthesized thiols and selected thiocarbamates, established and performed the LC-MS-based stability assay, performed the ITC measurements, and wrote parts of the manuscript. E. S. and A. M. K. contributed equally. R. W. H., H. B., and C.D. edited the manuscript, supplied funding, and supervised the project. J. H. co-supervised the project, planned MMP and cytotoxicity assays. K. H. performed the SPR screening. I. J. H. expressed and purified ColQ1. K. V. synthesized compounds 1 and 16. S. Y. planned parts of the synthesis of the other compounds. B. E. performed computational pKa calculations. All authors reviewed the results and approved the final version of the manuscript.



## Discovery of a Potent Inhibitor Class with High Selectivity toward Clostridial Collagenases

Esther Schönauer,<sup>†,⊥</sup> Andreas M. Kany,<sup>‡,⊥</sup> Jörg Hauptenthal,<sup>‡,⊥</sup> Kristina Hüsecken,<sup>‡</sup> Isabel J. Hoppe,<sup>†,⊥</sup> Katrin Voos,<sup>§</sup> Samir Yahiaoui,<sup>‡,⊥</sup> Brigitta Elsässer,<sup>†,⊥</sup> Christian Ducho,<sup>§</sup> Hans Brandstetter,<sup>\*,†,⊥</sup> and Rolf W. Hartmann<sup>\*,‡,§,⊥</sup>

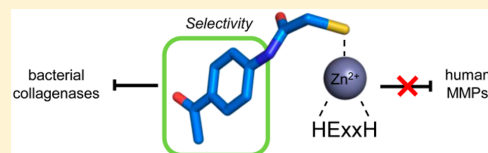
<sup>†</sup>Division of Structural Biology, Department of Molecular Biology, University of Salzburg, Billrothstrasse 11, 5020 Salzburg, Austria

<sup>‡</sup>Department of Drug Design and Optimization, Helmholtz Institute for Pharmaceutical Research Saarland (HIPS), Campus E8.1, 66123 Saarbrücken, Germany

<sup>§</sup>Department of Pharmacy, Pharmaceutical and Medicinal Chemistry, Saarland University, Campus C2.3, 66123 Saarbrücken, Germany

### Supporting Information

**ABSTRACT:** Secreted virulence factors like bacterial collagenases are conceptually attractive targets for fighting microbial infections. However, previous attempts to develop potent compounds against these metalloproteases failed to achieve selectivity against human matrix metalloproteinases (MMPs). Using a surface plasmon resonance-based screening complemented with enzyme inhibition assays, we discovered an *N*-aryl mercaptoacetamide-based inhibitor scaffold that showed sub-micromolar affinities toward collagenase H (ColH) from the human pathogen *Clostridium histolyticum*. Moreover, these inhibitors also efficiently blocked the homologous bacterial collagenases, ColG from *C. histolyticum*, ColT from *C. tetani*, and ColQI from the *Bacillus cereus* strain QI, while showing negligible activity toward human MMPs-1, -2, -3, -7, -8, and -14. The most active compound displayed a more than 1000-fold selectivity over human MMPs. This selectivity can be rationalized by the crystal structure of ColH with this compound, revealing a distinct non-primed binding mode to the active site. The non-primed binding mode presented here paves the way for the development of selective broad-spectrum bacterial collagenase inhibitors with potential therapeutic application in humans.



## INTRODUCTION

Clostridia represent a family of ubiquitously occurring Gram-positive bacteria comprising perilous pathogens that cause diseases such as botulism (*Clostridium botulinum*), gas gangrene (*C. perfringens*), tetanus (*C. tetani*), or pseudomembranous colitis (*C. difficile*).<sup>1,2</sup> These toxigenic clostridia still represent a threat to public health, as tetanus and clostridial myonecrosis have maintained high mortality rates and pseudomembranous colitis is a known severe complication of antibiotic therapy.<sup>3–6</sup> Furthermore, substantial amounts of pathogenic clostridia were cultured in the past 60 years for use as bioweapons.<sup>7</sup> Consequently, massive efforts have been aimed at unraveling the molecular basis of these life-threatening infections. Nevertheless, such infections remain a major challenge, as this knowledge did not yet lead to satisfactory treatment options.

The high lethality of these bacteria is related to collagenases which are crucial for clostridial virulence, given their critical role in colonization and evasion of host immune defense, acquisition of nutrients, facilitation of dissemination, or tissue damage during infection. Additionally, they might potentiate clostridial histotoxicity by facilitating toxin diffusion.<sup>2,8,9</sup>

The physiological substrate of clostridial collagenases is collagen, the main component of the extracellular matrix in mammals (up to 90%).<sup>10,11</sup> Its defining characteristic is the collagen triple-helix, which is perpetuated by the triplet repeat Gly-X-Y (X and Y positions are mostly occupied by proline (28%) and hydroxyproline (38%)).<sup>12</sup> The natively folded triple helix is highly resistant to proteolysis.<sup>13,14</sup> Even the most prominent human collagenases, the matrix metalloproteinases MMP-1, -2, -8, -13, -14, and -18, can cleave the triple helix only at a single site.<sup>15,16</sup> In contrast to that, clostridial collagenases can process collagen triple helices at multiple sites, as the active site displays a remarkable selectivity for the Gly-Pro-Y triplets,<sup>17</sup> and they can decompose collagen completely into small peptides.<sup>18,19</sup>

The inhibition of these extracellular collagenases is conceptually attractive, as it does not attack the pathogen directly but rather blocks the colonization and infiltration of the host by the clostridia. Thereby reducing the Darwinian selection pressure, targeting bacterial virulence is considered a promising approach to combat the emerging threat of drug-

Received: July 4, 2017

Published: August 18, 2017

resistant bacteria.<sup>20–22</sup> To date, several anti-virulence targets have been validated, demonstrating the potential of this approach.<sup>23–28</sup> Kasagne et al. showed, for example, that a collagenase knock-out strain from *Leptospira interrogans* displayed reduced virulence in an *in vivo* model.<sup>28</sup>

Targeting extracellular enzymes provides a substantial benefit because inhibitors do not need to cross the bacterial cell wall, which has turned out to be challenging in many cases.<sup>29–31</sup> Consequently, bacterial collagenases represent prime targets for an effective therapy against clostridial and bacillary infections.<sup>6,9,32,33</sup>

Clostridial collagenases are zinc metalloproteinases of ~115 kDa with a multi-domain organization, homologues of which are also found in many bacilli. The mature protein harbors an N-terminal collagenase unit of ~78 kDa, which is the minimal collagenolytic entity, followed by a varying composition of two to three accessory domains, which are thought to be involved in collagen swelling and binding to fibrillar collagen.<sup>34–38</sup> The collagenase unit is composed of the activator domain and the peptidase domain.<sup>34</sup> The peptidase domain harbors the catalytic zinc ion, which is coordinated by the two histidines of the canonical zinc-binding HEXXH motif, and a downstream glutamate.<sup>4,34,35,39–41</sup> The glutamate residue in the HEXXH motif acts as the general acid/base, which polarizes the catalytic water essential for catalysis. This polarized water molecule performs the nucleophilic attack, while the zinc ion serves as an oxyanion hole to the carbonyl oxygen of the scissile peptide bond.<sup>42</sup>

Several groups have been working on the development of clostridial collagenase inhibitors in the past, focusing on the collagenases G (ColG) and H (ColH) from *C. histolyticum*. In this context, besides the identification of active compounds from *Viola yedoensis*,<sup>43</sup> inhibitors based on sulfonlated derivatives of L-valine hydroxamate<sup>44</sup> have been synthesized as well as sulfonyl aminoacyl hydroxamates.<sup>45</sup> Furthermore, compounds incorporating 5-amino-2-mercapto-1,3,4-thiadiazole zinc binding functions,<sup>46</sup> arylsulfonyl-ureido and 5-dibenzo-suberenyl/suberyl,<sup>47</sup> or succinyl hydroxamate and iminodiacetic acid hydroxamate moieties<sup>48</sup> have been described. These inhibitors follow the classic architecture of metalloprotease inhibitors with a backbone that mimics the natural substrate, which is connected via a linker to a zinc-binding group that chelates the catalytic zinc ion and, thereby, expels the essential catalytic water molecule from the active site.<sup>49,50</sup> These inhibitors were developed as substrate analogues and/or designed on the basis of inhibitors for other metalloproteases that share the HEXXH motif,<sup>51</sup> like thermolysin or MMPs.<sup>44,47,52–58</sup> Unfortunately, the synthetic clostridial collagenase inhibitors are not selective, inhibiting clostridial collagenases and MMPs alike.<sup>44,45,47,48,55–57,59–61</sup> Therefore, they are not suitable for antibacterial therapy in humans. Consequently, novel and more effective drug candidates are urgently needed.

Efforts to design selective inhibitors were hampered by the lack of high-resolution structural data on clostridial collagenases until 2011. The first crystal structures revealed that, although there is no significant sequence homology between the peptidolytic domains of clostridial collagenases and MMPs, their active sites share a similar catalytic zinc ion-binding geometry and the canonical non-prime-site substrate-recognition motif, the edge strand.<sup>17</sup>

In this study, we wanted to capitalize on the recent crystal structures of the peptidase domains of three clostridial

collagenases<sup>34,41</sup> with the aim to rationally develop small organic molecules targeting collagenase ColH from *C. histolyticum*. In the following we describe the discovery of inhibitors which are highly active and selective for clostridial collagenases over MMPs and have the potential to be further optimized for a future therapeutic application in humans. Their selectivity can be rationalized on the basis of a co-crystal structure of the peptidase domain of ColH in complex with an inhibitor, revealing a distinct non-primed mode of binding of the inhibitor to the active site.

## RESULTS AND DISCUSSION

**Discovery of New Inhibitory Scaffold.** To discover new low-molecular-weight inhibitory compounds, a focused protease inhibitor library was screened with a surface plasmon resonance (SPR)-based binding assay using the amine-coupled peptidase domain of ColH (ColH-PD) as ligand. To ensure the integrity of ColH-PD after immobilization, the collagenase-specific peptidic substrate N-(3-[2-furyl]acryloyl)-L-leucyl-glycyl-L-prolyl-L-alanine (FALGPA)<sup>62</sup> was used as positive control (Figure S1a). A total of 1520 structurally diverse small molecules with an average molecular weight (MW) of  $389 \pm 78$  Da were screened at  $100 \mu\text{M}$ . Compounds showing a MW-normalized response higher than that of  $500 \mu\text{M}$  FALGPA (i.e.,  $35 \mu\text{-refractive index units}$ ) were classified as hits. The SPR screen resulted in 202 primary hits. Nineteen compounds were excluded from the subsequent testing as known promiscuous inhibitors,<sup>63</sup> resulting in a hit rate of 12.0% (Figure S2).

The secondary functional screening assessed the potential of the 183 SPR hits to inhibit the peptidolytic activity of ColH-PD using a custom-made fluorescence resonance energy transfer (FRET) substrate. Typically, the FALGPA<sup>62</sup> and Wünsch<sup>64</sup> assays are used to characterize the activity of clostridial collagenases due to their easy setup and commercial availability next to their specificity for these enzymes.<sup>62,65,66</sup> However, the low binding affinity of these peptides together with their low signal-to-noise ratios severely limits the sensitivity of these assays. Consequently, substantial amounts of enzyme and substrate are needed in characterization studies (e.g.,  $K_M$  values for FALGPA are in the mM range<sup>62,67</sup>). To facilitate our screening process, we designed and synthesized a decapeptide (Mca-Ala-Gly-Pro-Pro-Gly-Pro-Dpa-Gly-Arg-NH<sub>2</sub>) to be used as a substrate for a FRET-based assay. Its sequence was based on the detailed profile of the primed and non-primed cleavage site specificity of clostridial collagenases as determined by Proteomic Identification of protease Cleavage Sites (PICS) recently.<sup>17,68</sup> The assay sensitivity was increased by several orders of magnitude compared to the FALGPA assay by the application of the FRET technology.<sup>69,70</sup> The  $K_M$  value of this substrate is  $62 \pm 8 \mu\text{M}$  for ColH-PD. The 183 SPR binders were screened at a final concentration of  $40 \mu\text{M}$ . The inhibitor isoamylphosphonyl-Gly-Pro-Ala (Figure S1b) was used as positive control in the assay.<sup>58</sup> In sum, the SPR-based and activity-based screenings led to six functional hits (>25% inhibition) with MWs ranging from ~210 to ~385 Da (Figure S3). The two most active inhibitors in this assay were mercaptoacetamides 1 and 2 (Table 1). Compound 2 led to an inhibition of ColH-PD *in vitro* similar to that of isoamylphosphonyl-Gly-Pro-Ala, both at  $40 \mu\text{M}$ , i.e.,  $82 \pm 3\%$  and  $81 \pm 1\%$ , respectively.

Dose-response studies revealed an  $\text{IC}_{50}$  value of  $1.9 \pm 0.3 \mu\text{M}$  for this compound, while the non-substituted aniline



Table 1. IC<sub>50</sub> Values of Mercaptoacetamide Compounds for ColH-PD

Compound	R	IC <sub>50</sub> (μM)	Compound	R	IC <sub>50</sub> (μM)
1		25 ± 6	7		0.19 ± 0.02
2		1.9 ± 0.3	8		0.19 ± 0.03
3		0.010 ± 0.002	9		19 ± 3
4		0.044 ± 0.007	10		23 ± 3
5		0.071 ± 0.009	11		26 ± 4
6		0.12 ± 0.01	12		31 ± 7

derivative 1 showed lower activity toward ColH-PD (IC<sub>50</sub> = 25 ± 6 μM). Our further hits showed considerably weaker inhibition and, in one case, proved to be incompatible with the FRET assay at high concentration. The high potency of the *N*-aryl mercaptoacetamides combined with their relatively low molecular weight encouraged us to investigate this promising compound class further in order to improve the inhibitory activity.

**Characterization of Mercaptoacetamide Hits.** A total of 36 derivatives of this compound class were purchased (see Tables 1, 3, and S1). Six derivatives showed improved inhibition compared to 2 (3–8). Generally, the introduction of functional groups in *para*-position to the aniline turned out to be favorable, considering the striking loss of activity of *ortho*-methoxy-substituted compound 11 compared to its *para*-analogue 5 (*ortho*-effect), and *ortho*-chloro-substituted compound 12 compared to its *para*-analogue 7. The superior performance of *para*-derivatives was also evident regarding the 100-fold decrease in IC<sub>50</sub> of 7 compared to its *meta*-chloro-substituted counterpart 9. In comparison to the unsubstituted compound 1, *meta*-substituted compounds 9 and 10 showed no significant improvement in IC<sub>50</sub>. Removal of the 3-methyl-group of compound 2 even led to a 16-fold decreased IC<sub>50</sub> (compound 6), suggesting that the *meta*-substitution is not beneficial for ColH inhibition.

Regarding electronic properties of our hits it becomes apparent that the best compounds 3–5, displaying IC<sub>50</sub> values in the two-digit nanomolar range, bear oxygen-containing groups with hydrogen bond accepting properties.

**Selectivity against MMPs and Broad-Spectrum Inhibition of Other Bacterial Collagenases.** To determine the selectivity of our compounds toward clostridial and bacillial collagenases on the one hand, and MMPs on the other, selected compounds (3 and 7, Figure 1) were tested using *in vitro*

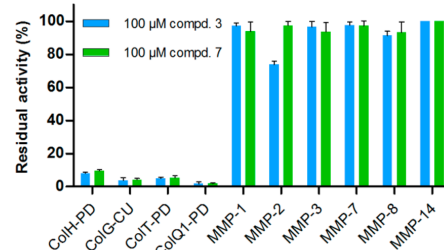
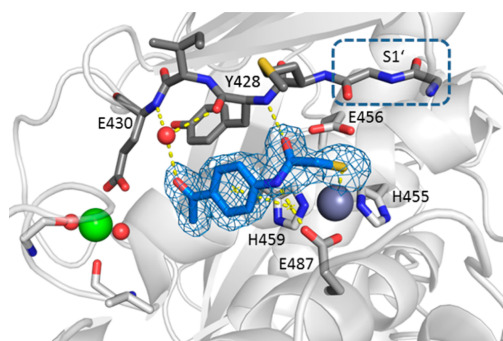


Figure 1. Inhibition of selected MMPs and bacterial collagenases by *N*-aryl mercaptoacetamide compounds 3 and 7.

inhibition assays with ColH-PD and the peptidase domains of ColT (ColT-PD), the collagenase units of ColG (ColG-CU) and of ColQ1 (ColQ1-CU), as well as the catalytic domains of MMP-1, -2, -3, -7, -8, and -14. The hydroxamate-based peptidomimetic batimastat (Figure S1c) is a highly potent and unselective inhibitor of MMPs<sup>71</sup> and was used as a positive control. MMPs are highly similar to each other in their active-site topology, which has made the development of selective active-site directed MMP inhibitors a challenging task.<sup>72,73</sup> The S1' binding site is the major specificity determinant in MMPs. Based on the S1' site, the MMPs are typically divided into deep, intermediate and shallow S1' binding pocket groups (e.g., deep: MMP-3, -12, and -14; intermediate: MMP-2, -8, and -9; shallow: MMP-1 and -7).<sup>74</sup> Therefore, we chose a panel of MMPs to investigate the binding of our compounds to all three S1' pocket types. In line with published results,<sup>71</sup> batimastat displayed IC<sub>50</sub> values below 10 nM for all of these MMPs (Table S2). As expected from this broad-spectrum zinc metalloproteinase inhibitor, batimastat also inhibited ColH-

PD, ColT-PD, ColG-CU and ColQ1-CU (Figure S4). Intriguingly, compounds 3 and 7 resulted in no or negligible inhibition of the tested MMPs (Figure 1 and Figure S5). Only in case of MMP-2, we observed 25% inhibition at 100  $\mu$ M compound 3, while ColH-PD was efficiently inhibited, showing less than 10% residual activity. Thus, we observed a more than 1000-fold selectivity of these two compounds for ColH over MMPs. Strikingly, the clostridial collagenase homologues ColG and ColT, and the bacillial collagenase ColQ1, were even more efficiently inhibited, showing 5% or less residual activity when treated with 100  $\mu$ M compound 3 or 7. A similar compound scaffold had been reported by Zhu et al. to inhibit LasB, an extracellular elastase from *Pseudomonas aeruginosa*.<sup>75</sup> In sum, these findings showed that the *N*-aryl mercaptoacetamide-based inhibitors are not only selective against MMPs, but are also potent broad-spectrum inhibitors of bacterial collagenases.

**Crystal Structure of the Peptidase Domain of ColH in Complex with Compound 3.** To rationalize the binding mode of the *N*-aryl mercaptoacetamide-based inhibitors, we aimed to solve the crystal structure of ColH-PD in complex with compound 3. The structure was determined at 1.87 Å resolution with all residues being defined in the electron density at excellent geometric and crystallographic parameters (Table S3). The overall topology of the peptidase domain showed the expected thermolysin-like fold. The average root-mean-square displacements (RMSDs) of backbone atoms between the structure of the apo-peptidase domain and the peptidase domain in complex with isoamylphosphonyl-Gly-Pro-Ala were 0.133 and 0.123 Å, respectively. The peptidase domain of ColH is divided horizontally by the active-site cleft into an upper N-terminal and a lower C-terminal subdomain (CSD). Substrates can bind to the active-site cleft from the left (non-primed side) to the right (primed side) when viewed in standard orientation.<sup>76</sup> Central elements of the N-terminal subdomain (NSD) are the active-site helix and a mixed five-strand  $\beta$ -sheet. The zinc-binding motif HEXXH, which provides the two zinc-coordinating histidines and the general acid/base glutamate, is located in the active-site helix (Figure 2). The lowermost  $\beta$ -strand of the mixed  $\beta$ -sheet shapes the upper perimeter of the



**Figure 2.** Peptidase domain of ColH in complex with the hydrolysis product of compound 3. Close-up view of the active site in ball-and-stick representation. The inhibitor (blue) is shown in sticks with the maximum likelihood weighted  $2F_o - F_c$  electron density map contoured at  $1\sigma$ . The catalytic zinc ion (dark gray), calcium ion (green), and water molecule (red) are shown as spheres. The S1' site (shown in dashed blue box) formed by Gly425 and Gly426 in the edge strand (shown in dark gray sticks) is indicated.

active-site cleft, the edge strand. The edge strand interacts in an antiparallel manner with the substrate predominantly on the non-primed side.<sup>34,77,78</sup> The third zinc ligand is a glutamate residue, located on the glutamate helix of the CSD. The insertion of 30 residues between the HEXXH motif and this glutamate residue shapes (i) the non-primed side of the active-site cleft and (ii) a calcium-binding site crucial for enzymatic activity.<sup>34,41,77</sup>

A well-defined electron density was observed for the ligand bound in the active site. The structure of compound 3 could be clearly modeled into the density (Figure 2), except for the carbonyl unit of the thiocarbamate moiety. Instead, the electron density showed the sulfur atom coordinating the catalytic zinc ion, suggesting that the thioester group had been hydrolyzed in the co-crystallization process. This result prompted an investigation of our newly discovered class of inhibitors with particular emphasis on the stability of the thiocarbamate function in aqueous buffers such as the buffer system of the functional assay and the crystallization buffer.

**Stability of the Thiocarbamate Unit.** Two inhibitors with major differences in potency (7, 12) were selected and the hydrolytic formation of the corresponding free thiol was analyzed by liquid chromatography–mass spectrometry (LC-MS). Free thiols were synthesized as references for the stability assay. The conversions of compounds 7 and 12 into compounds 14 and 15, respectively, proceeded rapidly in 10 mM HEPES, pH 7.5 at 22.5 °C, with thiocarbamate half-lives of  $26.8 \pm 1.4$  min (7) and  $20.6 \pm 0.9$  min (12, Figure 3). These results corroborated that the inhibition of thiocarbamates 1–12 was predominantly due to the respective free thiols. Considering the preparation time and the pre-incubation time of 1 h for each compound with ColH-PD before the functional assay was started by addition of the substrate the

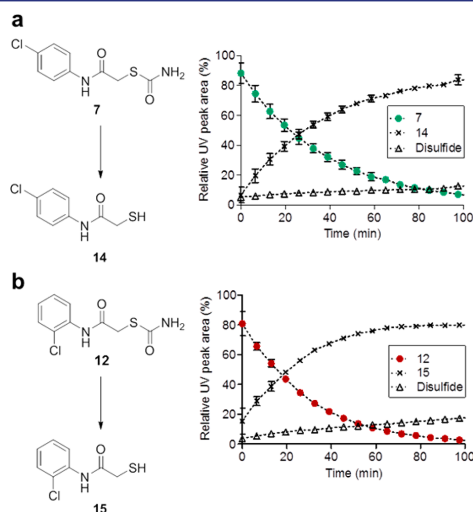


**Figure 3.** Conversion of thiocarbamates 7 and 12 into the respective corresponding free thiols: (a) compound 7 into 14 and (b) compound 12 into 15. Time course of hydrolysis in 10 mM HEPES, pH 7.4 (10% methanol), at 22.5 °C was monitored by LC-MS, showing conversion into corresponding thiol and to minor extent into another compound which is most likely the disulfide oxidation product.<sup>79</sup>

thiocarbamates were quantitatively converted within the time frame of the experiment. Thiol formation was also demonstrated at pH 6.4, corresponding to the buffer used for co-crystallization (Figure S6).

**Confirmation of Thiol as Active Compound.** To further substantiate these findings, we followed two different strategies. First, we studied the inhibitory activities of the free thiols 13–15. Thus, we determined the  $IC_{50}$  values of the free thiols 13–15 with ColH-PD in the presence of the reducing agent TCEP. The resulting  $IC_{50}$  values of 0.017, 0.21, and 40  $\mu\text{M}$  corresponded well with 0.010, 0.19, and 31  $\mu\text{M}$  of the thiocarbamate analogues (Tables 1 and 2).

**Table 2. Inhibition of ColH-PD by Thiol Compounds in the Presence of 5 mM TCEP**

Compound	R	$IC_{50}$ ( $\mu\text{M}$ )
13		0.017 ± 0.002
14		0.21 ± 0.01
15		40 ± 9

The results of the MMP and bacterial collagenase inhibition assays could also be reproduced using the thiol compounds, with 13 and 14 demonstrating a similarly high selectivity against MMPs and a broad-spectrum inhibition of bacterial collagenases (Figure 4).

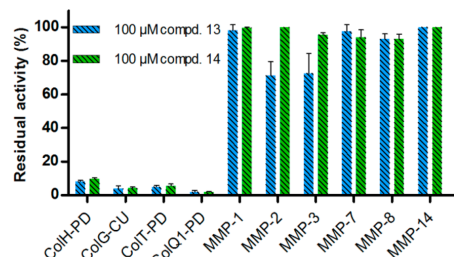
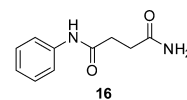


**Figure 4. Inhibition of selected MMPs and bacterial collagenases by thiol compounds 13 and 14.**

As a second strategy, we aimed to synthesize a structural analogue of compound 1 lacking the hydrolytically instable thioester motif. The formal replacement of the sulfur atom with a methylene group led to the carboxamide analogue 16, which was prepared and tested for its inhibitory activity toward ColH-PD (Figure 5). Compound 16 was devoid of any activity even at 1000  $\mu\text{M}$ . This demonstrated that the carbamoyl moiety in 1 does not contribute to target binding, but is just part of a



**16**  
no inhibition (ColH-PD) @ 1000  $\mu\text{M}$

**Figure 5. Structure and inhibitory activity of the non-hydrolyzable carboxamide analogue 16.**

prodrug-like structure which furnishes the corresponding bioactive thiol by chemical hydrolysis.

Further in line with our findings, dithiocarbamates 17–21 (Table 3) were inactive toward ColH-PD. LC-MS experiments

**Table 3. Structure and Activity of Dithiocarbamates**

Compound	R	Inhibition at 100 $\mu\text{M}$ (%)
17		no inhibition
18		no inhibition
19		no inhibition
20		no inhibition
21		12 ± 3

with the dithiocarbamate analogue of our best hit 3 showed no formation of free thiol 13 within the time frame of our assay, explaining the inactivity of these derivatives by stability toward hydrolysis (Figure S7).

In addition, the thermodynamic profile of the interaction between compounds 7 and 14 and ColH-PD was determined. As expected, isothermal titration calorimetry (ITC) measurements resulted in very similar affinities and free energy values, resulting from the hydrolysis of 7 to furnish thiol 14 (Table 4). Compound binding to ColH-PD turned out to be enthalpy-driven. In sum, the findings from the stability assay, the *in vitro* assay and the ITC data confirmed the thiols as active compounds in our enzyme inhibition assay.

**Cytotoxicity Test.** Regarding the potential therapeutic use of our compounds in humans, we investigated the cytotoxic properties of selected *N*-aryl mercaptoacetamides. Cytotoxicity tests using HEP G2 cells showed compounds 13 and 14 to display low cytotoxicity, comparable to that of the marketed antibiotic rifampicin (Table 5), while doxorubicin as control showed the expected cytotoxic effect. These findings underline

**Table 4.** ITC and IC<sub>50</sub> Results of the Thiocarbamate–Thiol Pair 7 and 14

	7	14
IC <sub>50</sub> ( $\mu\text{M}$ ) <sup>a</sup>	0.19 $\pm$ 0.02	0.21 $\pm$ 0.01
K <sub>D</sub> ( $\mu\text{M}$ ) <sup>b</sup>	0.309 $\pm$ 0.045	0.360 $\pm$ 0.038
$\Delta G$ (kcal mol <sup>-1</sup> ) <sup>b</sup>	-8.9 $\pm$ 0.1	-8.8 $\pm$ 0.1
$\Delta H$ (kcal mol <sup>-1</sup> ) <sup>b</sup>	-12.7 $\pm$ 1.2	-15.4 $\pm$ 0.3
-T $\Delta S$ (kcal mol <sup>-1</sup> ) <sup>b</sup>	3.8 $\pm$ 1.3	6.6 $\pm$ 0.4
N <sup>b,c</sup>	0.54 $\pm$ 0.05	0.48 $\pm$ 0.03

<sup>a</sup>IC<sub>50</sub> refers to the functional FRET assay. <sup>b</sup>Results are from at least two independent measurements. <sup>c</sup>The low stoichiometry could be explained by incomplete zinc occupation of the active sites.<sup>41</sup>

the potential of our compounds for the development of novel anti-infectives.

**Table 5.** Cytotoxicity of 13, 14, and Three Reference Compounds in HEP G2 Cells

compound	concn ( $\mu\text{M}$ )	reduction of viability (%)
13	100	17 $\pm$ 12
14	100	28 $\pm$ 12
rifampicin	100	29 $\pm$ 5
doxorubicin	1	50 $\pm$ 5
batimastat	100	13 $\pm$ 7

**Zinc Coordination by a Thiolate.** The identification of the thiol as active compound in our functional assays was in excellent agreement with the crystal structure analysis which demonstrated that only a sulfur atom, to be precise a thiolate, was coordinating the catalytic zinc ion. To validate our conclusions on the protonation state of the sulfur atom, we calculated the pK<sub>a</sub> values for the thiol group resulting from the hydrolysis of thiocarbamate **3** in solution and when bound to the active site using the Molecular Operating Environment (MOE) software.<sup>80</sup> The pK<sub>a</sub> of the thiol group was strongly lowered from 9.0 in the solvent to 3.1 by the direct coordination to the zinc ion. This suggests that the thiol is fully ionized to the thiolate form in both the activity assay and the crystallization experiment upon binding to the active site.

**Binding Mode of the *N*-Aryl Mercaptoacetamide Compound to the Active Site of ColH-PD.** The hydrolysis product of compound **3** binds to the S3 to S1 substrate binding pockets (Figure 2). The thiolate coordinates the zinc ion with a sulfur-to-zinc distance of 2.27 Å. In the S1 pocket, the amide oxygen of compound **3** forms a hydrogen bond with the main-chain amide nitrogen of Tyr428 (3.11 Å) of the NSD, while the amide nitrogen of compound **3** hydrogen-bonds with the carbonyl oxygen (OE2) of Glu487 (2.97 Å) of the CSD. In addition, the benzene ring of the ligand is involved in a  $\pi$ - $\pi$ -stacking interaction with the imidazole ring of His459 (centroid-centroid distance of 3.80 Å). The oxygen of the acetyl group of **3** interacts via a bridging water molecule (3.07 Å) with the main-chain oxygen of Tyr428 in S1 (3.11 Å) and with the main-chain nitrogen of Glu430 in S3 (2.84 Å). Thus, the inhibitor is well-braced in-between the NSD and the CSD of the peptidase domain.

Importantly, the binding mode of the inhibitor is not directed toward the primed substrate-binding sites, but toward the non-primed recognition sites in-between the calcium-binding site and the catalytic zinc ion. Thus, this complex of ColH-PD with the thiol derived from compound **3** is the first to

describe non-primed interactions between a clostridial collagenase and an active site-directed ligand.

**Identification of Selectivity Determinant.** The thiol derived from compound **3** interacts with two central elements of the active site: (i) the zinc ion and its liganding sphere (His455, Glu456, His459, and Glu487), and (ii) the edge strand (Gly425–Glu430). These two central elements are also present in MMPs.<sup>17</sup> A structurally, but not sequentially, homologous edge strand frames the upper rim of the active site in MMPs, and the zinc-liganding sphere composed of the HEXXH motif and a third proteinaceous ligand is nearly identical between the MMPs and the clostridial collagenases. The geometry of the zinc-liganding sphere is almost perfectly superimposable in clostridial collagenases and MMPs (RMSD = 0.060 Å between ColH and MMP-1). Only the third zinc-binding residue differs. While in MMPs, this position is occupied by a histidine; in clostridial collagenases, this ligand is a glutamate provided by the gluzincin-specific glutamate helix. Given this high similarity in the active site between clostridial collagenases and MMPs, this triggered the question of how we can rationalize the observed differences in selectivity of the *N*-aryl mercaptoacetamide compounds toward the two enzyme families. A first *in silico* structural analysis of the active sites of MMP-1, -2, -3, -8, -12, and -13 suggested that (i) these enzymes could accommodate the mercaptoacetamide compounds in their non-primed substrate pockets, and that (ii) the residues on the edge strand and the zinc ion are positioned as such as to allow productive interactions with the thiolate. Yet, the MMPs, lacking the zinc-binding glutamate, cannot provide the hydrogen-bonding partner for the amide nitrogen of the mercaptoacetamide inhibitor. Hence, is the interaction with the gluzincin-specific Glu487 crucial for selectivity? To test this hypothesis, we mimicked the zinc-liganding sphere of MMPs in ColH-PD by mutating Glu487 into a histidine. A comparison of the apparent inhibition constant K<sub>i(app)</sub> of compound **11** toward wild-type ColH-PD and the mutant E487H, 92  $\pm$  8 and 166  $\pm$  23  $\mu\text{M}$ , respectively, showed that the mutation did not result in a drastic change in the inhibitory potency. This suggests that the interaction with the edge strand on the non-primed site, mediated via main-chain contacts, is the main structural selectivity determinant. This hypothesis is further supported by a structural analysis of the edge-strand conformations in MMPs and clostridial collagenases in the ligand-bound state. Within each family, the ligand-bound edge-strand conformation is highly conserved (Figure 6). Compared to the clostridial situation, the edge strand in MMPs is tilted by 27–29°. This tilted orientation could explain the inefficient binding of the *N*-aryl mercaptoacetamide compounds to the MMPs, suggesting that the interactions with the non-primed edge strand (S1–S3) are the crucial selectivity determinants.

It was also interesting to see that related mercaptoacetamide derivatives were shown to inhibit LasB from *P. aeruginosa*.<sup>75</sup> Analysis of our best compound **13** in an *in vitro* LasB inhibition assay revealed a more than 1000-fold lower activity compared to ColH (data not shown). This is likely due to the distinct binding mode of compound **13** to the non-primed binding site of ColH (Figure 2) in contrast to the proposed primed binding mode of the related compounds in LasB by Zhu et al.<sup>75</sup>

With regard to future inhibitor design, these findings suggest that by (i) amplification of the interactions with the edge strand and (ii) extension of the inhibitor scaffold in *para*, i.e., by developing the compound further into the non-primed substrate recognition pockets, even more potent and selective

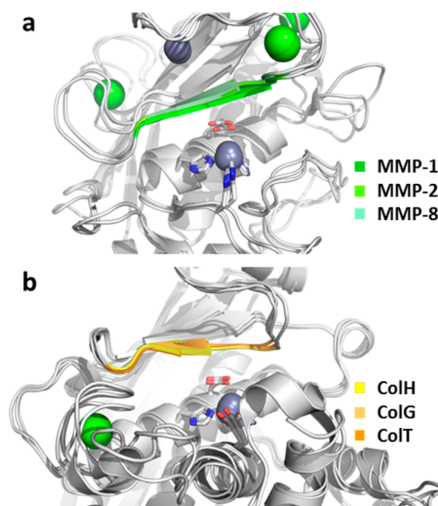


**Figure 6.** Close-up on the superpositioned active sites of three MMPs (a) and of three clostridial collagenases (b) in the ligand-bound state. The ligands have been removed for better visualization. The HEXXH motif is shown in sticks, and the zinc ions (gray) and calcium ions (green) are shown as spheres. The edge strand on top of the catalytic zinc is highlighted in color.

compounds could be developed. In compounds with optimized affinity to the edge strand and the non-primed substrate binding pockets, we plan to investigate the replacement of the thiol moiety by a less reactive ZBG. Such lead compounds hold the promise of higher efficacy and therefore higher safety in potential therapeutic applications in humans.

## CONCLUSION

We identified a novel compound scaffold for the selective inhibition of clostridial collagenases. Starting with an SPR-based primary screening of a focused library, we validated the SPR-hits in a secondary enzyme inhibition assay using a custom-tailored FRET peptide substrate for clostridial collagenases. Two mercaptoacetamide derivatives were the most potent functional hits in this assay. Further derivatization of these initial hits, in particular the introduction of oxygen-containing groups in *para*-position to the aniline, led to the generation of highly potent *N*-aryl mercaptoacetamide-based clostridial collagenase inhibitors with  $IC_{50}$  values in the two-digit nanomolar range. These compounds showed unprecedented selectivity against MMPs, while at the same time they displayed a broad-spectrum inhibition of bacterial collagenases. The selectivity of these compounds could be rationalized on the basis of a co-crystal structure of ColH-PD with the most active compound, revealing a distinct non-primed binding mode of the inhibitor to the active site. The mercaptoacetamides were also shown to display no cytotoxicity toward human cells. These insights pave the way for the development of selective broad-spectrum bacterial collagenase inhibitors with potential therapeutic application in humans.

## ASSOCIATED CONTENT

### Supporting Information

The Supporting Information is available free of charge on the ACS Publications website at DOI: 10.1021/jacs.7b06935.

Supporting Figures S1–S7 and Tables S1–S3, giving molecular structures of positive controls, SPR and functional screening hits, inhibition of the selected MMPs and bacterial collagenases by batimastat, MMP inhibition assay, LC-MS analyses of **3** and **21**, structure and activity of additional thiocarbamates and related compounds, and data collection and refinement statistics (PDF)

## AUTHOR INFORMATION

### Corresponding Authors

\*hans.brandstetter@sbg.ac.at

\*rolf.hartmann@helmholtz-hzi.de

### ORCID

Esther Schönauer: 0000-0002-2625-9446

Andreas M. Kany: 0000-0001-7580-3658

Jörg Haupenthal: 0000-0003-3991-2800

Isabel J. Hoppe: 0000-0001-9050-1260

Samir Yahiaoui: 0000-0001-5134-5007

Brigitta Elsässer: 0000-0002-9087-243X

Hans Brandstetter: 0000-0002-6089-3045

Rolf W. Hartmann: 0000-0002-5871-5231

### Author Contributions

<sup>†</sup>E.S. and A.M.K. contributed equally.

### Notes

The authors declare no competing financial interest.

## ACKNOWLEDGMENTS

This work was supported by grants from the Austrian Science Fund (project W\_01213 & M\_1901). We thank Dr. Elfriede Dall for X-ray data collection, Dr. Werner Tegge for peptide synthesis, and Dr. Christine Maurer and Jeannine Jung for technical support.

## REFERENCES

- (1) Cato, E.; George, W.; Finegold, S. *Bergey's Manual of Systematic Bacteriology*; Williams & Wilkins: Baltimore, 1986; pp 1141–1200.
- (2) Hatheway, C. L. *Clin. Microbiol. Rev.* **1990**, *3*, 66–98.
- (3) Burke, M. P.; Opeskin, K. *Am. J. Forensic Med. Pathol.* **1999**, *20*, 158–162.
- (4) Bruggemann, H.; Baumer, S.; Fricke, W. F.; Wiezer, A.; Liesegang, H.; Decker, I.; Herzberg, C.; Martinez-Arias, R.; Merkl, R.; Henne, A.; Gottschalk, G. *Proc. Natl. Acad. Sci. U. S. A.* **2003**, *100*, 1316–1321.
- (5) Taubes, G. *Science* **2008**, *321*, 360.
- (6) Taubes, G. *Science* **2008**, *321*, 356–361.
- (7) Armon, S. S.; Schechter, R.; Inglesby, T. V.; Henderson, D. A.; Bartlett, J. G.; Ascher, M. S.; Eitzen, E.; Fine, A. D.; Hauer, J.; Layton, M.; Lillibridge, S.; Osterholm, M. T.; O'Toole, T.; Parker, G.; Perl, T. M.; Russell, P. K.; Swerdlow, D. L.; Tonat, K.; Working Group on Civilian Biodefense. *JAMA* **2001**, *285*, 1059–1070.
- (8) Matsushita, O.; Okabe, A. *Toxicol.* **2001**, *39*, 1769–1780.
- (9) Popoff, M. R.; Bouvet, P. *Future Microbiol.* **2009**, *4*, 1021–1064.
- (10) Burgeson, R. E.; Nimni, M. E. *Clin. Orthop. Relat. Res.* **1992**, *282*, 250–272.
- (11) Brozek, J.; Grande, F.; Anderson, J. T.; Keys, A. *Ann. N. Y. Acad. Sci.* **1963**, *110*, 113–140.



- (12) Ramshaw, J. A.; Shah, N. K.; Brodsky, B. J. *Struct. Biol.* **1998**, *122*, 86–91.
- (13) Bruckner, P.; Prockop, D. J. *Anal. Biochem.* **1981**, *110*, 360–368.
- (14) Bächinger, H. P.; Bruckner, P.; Timpl, R.; Prockop, D. J.; Engel, J. *Eur. J. Biochem.* **1980**, *106*, 619–632.
- (15) Nagase, H.; Visse, R.; Murphy, G. *Cardiovasc. Res.* **2006**, *69*, 562–573.
- (16) Fields, G. B. *J. Biol. Chem.* **2013**, *288*, 8785–8793.
- (17) Eckhard, U.; Huesgen, P. F.; Brandstetter, H.; Overall, C. M. *J. Proteomics* **2014**, *100*, 102–114.
- (18) Seifter, S.; Harper, E. In *The Enzymes*; Boyer, P. D.; Academic Press: New York, 1971; pp 649–697.
- (19) Mookhtiar, K. A.; Van Wart, H. E. *Matrix Suppl.* **1992**, *1*, 116–126.
- (20) Rasko, D. A.; Sperandio, V. *Nat. Rev. Drug Discovery* **2010**, *9*, 117–128.
- (21) Heras, B.; Scanlon, M. J.; Martin, J. L. *Br. J. Clin. Pharmacol.* **2015**, *79*, 208–215.
- (22) Clatworthy, A. E.; Pierson, E.; Hung, D. T. *Nat. Chem. Biol.* **2007**, *3*, 541–548.
- (23) Storz, M. P.; Maurer, C. K.; Zimmer, C.; Wagner, N.; Brengel, C.; de Jong, C.; Lucas, S.; Müsken, M.; Häussler, S.; Steinbach, A.; Hartmann, R. W. *J. Am. Chem. Soc.* **2012**, *134*, 16143–16146.
- (24) Lu, C.; Maurer, C. K.; Kirsch, B.; Steinbach, A.; Hartmann, R. W. *Angew. Chem., Int. Ed.* **2014**, *53*, 1109–1112.
- (25) Hung, D. T.; Shakhnovich, E. A.; Pierson, E.; Mekalanos, J. J. *Science* **2005**, *310*, 670–674.
- (26) Wagner, S.; Sommer, R.; Hinsberger, S.; Lu, C.; Hartmann, R. W.; Empting, M.; Titz, A. *J. Med. Chem.* **2016**, *59*, 5929–5969.
- (27) Böttcher, T.; Sieber, S. A. *J. Am. Chem. Soc.* **2008**, *130*, 14400–14401.
- (28) Kasagne, K.; Hu, W.; Ojcius, D. M.; Sun, D.; Ge, Y.; Zhao, J.; Yang, X. F.; Li, L.; Yan, J. *J. Infect. Dis.* **2014**, *209*, 1105–1115.
- (29) Lewis, K. *Nat. Rev. Drug Discovery* **2013**, *12*, 371–387.
- (30) Payne, D. J.; Gwynn, M. N.; Holmes, D. J.; Pompliano, D. L. *Nat. Rev. Drug Discovery* **2007**, *6*, 29–40.
- (31) Graef, F.; Vukosavljevic, B.; Michel, J.-P.; Wirth, M.; Ries, O.; De Rossi, C.; Windbergs, M.; Rosilio, V.; Ducho, C.; Gordon, S.; Lehr, C.-M. *J. Controlled Release* **2016**, *243*, 214–224.
- (32) Peterkofsky, B. *Methods Enzymol.* **1982**, *82*, 453–471.
- (33) Supuran, C. T.; Scozzafava, A.; Mastrolorenzo, A. *Expert Opin. Ther. Pat.* **2001**, *11*, 221–259.
- (34) Eckhard, U.; Schönauer, E.; Nüss, D.; Brandstetter, H. *Nat. Struct. Mol. Biol.* **2011**, *18*, 1109–1114.
- (35) Matsushita, O.; Jung, C. M.; Katayama, S.; Minami, J.; Takahashi, Y.; Okabe, A. *J. Bacteriol.* **1999**, *181*, 923–933.
- (36) Matsushita, O.; Jung, C. M.; Minami, J.; Katayama, S.; Nishi, N.; Okabe, A. *J. Biol. Chem.* **1998**, *273*, 3643–3648.
- (37) Matsushita, O.; Koide, T.; Kobayashi, R.; Nagata, K.; Okabe, A. *J. Biol. Chem.* **2001**, *276*, 8761–8770.
- (38) Wang, Y.-K.; Zhao, G.-Y.; Li, Y.; Chen, X.-L.; Xie, B.-B.; Su, H.-N.; Lv, Y.-H.; He, H.-L.; Liu, H.; Hu, J.; Zhou, B.-C.; Zhang, Y.-Z. *J. Biol. Chem.* **2010**, *285*, 14285–14291.
- (39) Jung, C. M.; Matsushita, O.; Katayama, S.; Minami, J.; Sakurai, J.; Okabe, A. *J. Bacteriol.* **1999**, *181*, 2816–2822.
- (40) Bond, M. D.; Van Wart, H. E. *Biochemistry* **1984**, *23*, 3085–3091.
- (41) Eckhard, U.; Schönauer, E.; Brandstetter, H. *J. Biol. Chem.* **2013**, *288*, 20184–20194.
- (42) Matthews, B. W. *Acc. Chem. Res.* **1988**, *21*, 333–340.
- (43) Oshima, N.; Narukawa, Y.; Takeda, T.; Kiuchi, F. *J. Nat. Med.* **2013**, *67*, 240–245.
- (44) Supuran, C. T.; Scozzafava, A. *Eur. J. Pharm. Sci.* **2000**, *10*, 67–76.
- (45) Clare, B. W.; Scozzafava, A.; Supuran, C. T. *J. Med. Chem.* **2001**, *44*, 2253–2258.
- (46) Scozzafava, A.; Supuran, C. T. *Bioorg. Med. Chem. Lett.* **2002**, *12*, 2667–2672.
- (47) Ilies, M. A. M.; Banciu, M. D.; Scozzafava, A.; Ilies, M. A. M.; Caproiu, M. T.; Supuran, C. T. *Bioorg. Med. Chem.* **2003**, *11*, 2227–2239.
- (48) Santos, M. A.; Marques, S.; Gil, M.; Tegoni, M.; Scozzafava, A.; Supuran, C. T. *J. Enzyme Inhib. Med. Chem.* **2003**, *18*, 233–242.
- (49) Jacobsen, F. E.; Lewis, J. A.; Cohen, S. M. *ChemMedChem* **2007**, *2*, 152–171.
- (50) Rouffet, M.; Cohen, S. M. *Dalton Trans.* **2011**, *40*, 3445–3454.
- (51) Hooper, N. M. *FEBS Lett.* **1994**, *354*, 1–6.
- (52) Grobelny, D.; Galardey, R. E. *Biochemistry* **1985**, *24*, 6145–6152.
- (53) Vencill, C. F.; Rasnick, D.; Crumley, K. V.; Nishino, N.; Powers, J. C. *Biochemistry* **1985**, *24*, 3149–3157.
- (54) Dive, V.; Yiotakis, A.; Nicolaou, A.; Toma, F. *Eur. J. Biochem.* **1990**, *191*, 685–693.
- (55) Scozzafava, A.; Supuran, C. T. *Bioorg. Med. Chem.* **2000**, *8*, 637–645.
- (56) Scozzafava, A.; Ilies, M. A.; Manole, G.; Supuran, C. T. *Eur. J. Pharm. Sci.* **2000**, *11*, 69–79.
- (57) Supuran, C. T.; Briganti, F.; Mincione, G.; Scozzafava, A. *J. Enzyme Inhib.* **2000**, *15*, 111–128.
- (58) Galardey, R. E.; Grobelny, D. *Biochemistry* **1983**, *22*, 4556–4561.
- (59) Scozzafava, A.; Supuran, C. T. *J. Med. Chem.* **2000**, *43*, 3677–3687.
- (60) Scozzafava, A.; Supuran, C. T. *Eur. J. Med. Chem.* **2000**, *35*, 299–307.
- (61) Supuran, C. T. In *Drug Design of Zinc-Enzyme Inhibitors*; Supuran, C. T., Winum, J.-Y., Eds.; John Wiley & Sons, Inc.: Hoboken, NJ, 2009; pp 721–729.
- (62) Van Wart, H. E.; Steinbrink, D. R. *Anal. Biochem.* **1981**, *113*, 356–365.
- (63) Baell, J. B.; Holloway, G. A. *J. Med. Chem.* **2010**, *53*, 2719–2740.
- (64) Wunsch, E.; Heidrich, H. H.-G. *Hoppe-Seyler's Z. Physiol. Chem.* **1963**, *333*, 149–151.
- (65) Komsa-Penkova, R. S.; Rashap, R. K.; Yomtova, V. M. *J. Biochem. Biophys. Methods* **1997**, *34*, 237–249.
- (66) Watanabe, K. *Appl. Microbiol. Biotechnol.* **2004**, *63*, 520–526.
- (67) Eckhard, U.; Schönauer, E.; Ducka, P.; Briza, P.; Nüss, D.; Brandstetter, H. *Biol. Chem.* **2009**, *390*, 11–18.
- (68) Schilling, O.; Overall, C. M. *Nat. Biotechnol.* **2008**, *26*, 685–694.
- (69) Fields, G. B. *Methods Mol. Biol.* **2010**, *622*, 393–433.
- (70) Knight, C. G. *Methods Enzymol.* **1995**, *248*, 18–34.
- (71) Rasmussen, H. S.; McCann, P. P. *Pharmacol. Ther.* **1997**, *75*, 69–75.
- (72) Cathcart, J.; Pulkoski-Gross, A.; Cao, J. *Genes Dis.* **2015**, *2*, 26–34.
- (73) Overall, C. M.; López-Otín, C. *Nat. Rev. Cancer* **2002**, *2*, 657–672.
- (74) Park, H. I.; Jin, Y.; Hurst, D. R.; Monroe, C. A.; Lee, S.; Schwartz, M. A.; Sang, Q.-X. *J. Biol. Chem.* **2003**, *278*, 51646–51653.
- (75) Zhu, J.; Cai, X.; Harris, T. L.; Gooyit, M.; Wood, M.; Lardy, M.; Janda, K. D. *Chem. Biol.* **2015**, *22*, 483–491.
- (76) Gomis-Rüth, F. X.; Botelho, T. O.; Bode, W. *Biochim. Biophys. Acta, Proteins Proteomics* **2012**, *1824*, 157–163.
- (77) Cerdà-Costa, N.; Xavier Gomis-Rüth, F. *Protein Sci.* **2014**, *23*, 123–144.
- (78) Gomis-Rüth, F. X. *J. Biol. Chem.* **2009**, *284*, 15353–15357.
- (79) Prammar, Y.; Das Gupta, V.; Bethea, C. J. *Clin. Pharm. Ther.* **1992**, *17*, 185–189.
- (80) Labute, P. *Proteins: Struct., Funct., Genet.* **2009**, *75*, 187–205.

**Chapter B: Phosphonate as a Stable Zinc-Binding Group for “Pathoblocker”  
Inhibitors of Clostridial Collagenase H (ColH)**

Katrin Voos, Esther Schönauer, Alaa Alhayek, Jörg Haupenthal, Anastasia Andreas, Rolf Müller, Rolf W. Hartmann, Hans Brandstetter, Anna K. H. Hirsch\* and Christian Ducho\*

\* corresponding authors

Reprinted with permission from *ChemMedChem* **2021**, *16*, 1257 – 1267.

DOI: 10.1002/cmdc.202000994

Copyright (2021) Wiley & Chemistry Europe

*As this chapter comprises a publication, compound numbers of this chapter are independent from other parts of this thesis.*

### III. Published Results

#### **Full contribution report:**

C. D., A. K. H. H., and K. V. conceived and coordinated the study. K. V. synthesized compounds 8 – 28, did the SAR interpretation, conceived, and wrote the manuscript. C. D., A. K. H. H. and H. B. edited the manuscript, supplied funding, and supervised the project. E. S. expressed and purified the clostridial collagenases and performed the functional assays. A. Alhayek planned and executed the *ex vivo* pig skin degradation assay. J. H. planned MMP, HDAC, TACE and cytotoxicity assays. A. Andreas planned and executed the *in vivo* zebrafish larvae toxicity assay. R. M. supervised parts of the project. R. W. H. supplied funding, and supervised parts of the project. All authors reviewed the results and approved the final version of the manuscript.





 Very Important Paper


# Phosphonate as a Stable Zinc-Binding Group for “Pathoblocker” Inhibitors of Clostridial Collagenase H (ColH)

Katrin Voos,<sup>[a]</sup> Esther Schönauer,<sup>[b]</sup> Alaa Alhayek,<sup>[c, e]</sup> Jörg Haupenthal,<sup>[c]</sup> Anastasia Andreas,<sup>[d, e]</sup> Rolf Müller,<sup>[d, e]</sup> Rolf W. Hartmann,<sup>[c, e]</sup> Hans Brandstetter,<sup>[b]</sup> Anna K. H. Hirsch,<sup>\*,[c, e]</sup> and Christian Ducho<sup>\*,[a]</sup>

Microbial infections are a significant threat to public health, and resistance is on the rise, so new antibiotics with novel modes of action are urgently needed. The extracellular zinc metalloprotease collagenase H (ColH) from *Clostridium histolyticum* is a virulence factor that catalyses tissue damage, leading to improved host invasion and colonisation. Besides the major role of ColH in pathogenicity, its extracellular localisation makes it a highly attractive target for the development of new antivirulence agents. Previously, we had found that a highly selective and potent thiol prodrug (with a hydrolytically cleavable

thiocarbamate unit) provided efficient ColH inhibition. We now report the synthesis and biological evaluation of a range of zinc-binding group (ZBG) variants of this thiol-derived inhibitor, with the mercapto unit being replaced by other zinc ligands. Among these, an analogue with a phosphonate motif as ZBG showed promising activity against ColH, an improved selectivity profile, and significantly higher stability than the thiol reference compound, thus making it an attractive candidate for future drug development.

## Introduction

Due to emerging resistances against established antibacterial agents, the treatment of bacterial infections might be thrown back to a state similar to the pre-antibiotic era. In an estimated

worst-case scenario, it has been predicted that by 2050, infectious diseases caused by antibiotic-resistant microbes might lead to higher death tolls than cancer does today.<sup>[1]</sup> Hence, there is an urgent need to develop antibiotics with novel modes of action, high efficacy and a reduced tendency to induce the development of resistances.<sup>[2]</sup>

A promising way of overcoming the problem of fast resistance development is the design of so-called “pathoblockers”, that is, compounds that target virulence factors rather than vital factors of bacteria, in contrast to classical antibiotics.<sup>[3]</sup> Bacteria that are thus “disarmed” by pathoblockers should ideally cause either no or at least a strongly attenuated disease. Furthermore, such pathoblocker-induced reduction of pathogenicity should provide the immune system the necessary time to develop a full humoral and cellular immune response to eliminate the bacteria, possibly aided by a low-dose adjunctive treatment with antibiotics.

*Clostridium* (including the prominent species *C. difficile*, *C. histolyticum* (*Hathewayia histolytica*), *C. tetani*, *C. botulinum*, *C. septicum*, and *C. perfringens*) is a genus of Gram-positive anaerobic bacteria that is ubiquitous. They cause severe human diseases such as tetanus, gas gangrene (myonecrosis), botulism, bacterial corneal keratitis, and other dangerous infections<sup>[4]</sup> with high mortality rates.<sup>[5]</sup> Some of these species have even been cultivated and are bioweapons.<sup>[6]</sup>

Collagenase is a prominent virulence factor for the progression of Clostridia-associated diseases.<sup>[7]</sup> It is a calcium- and zinc-dependent metalloprotease that destroys the host's connective tissue and uses it as a carbon source. This leads to improved host invasion and colonisation and hence to breaching of the human immune system. Also, the spread of toxins into the damaged tissue is promoted.<sup>[5b,8]</sup> Collagens, the natural

- [a] K. Voos, Prof. Dr. C. Ducho  
Department of Pharmacy, Pharmaceutical and Medicinal Chemistry  
Saarland University  
Campus C2 3, 66123 Saarbrücken (Germany)  
E-mail: christian.ducho@uni-saarland.de
- [b] Dr. E. Schönauer, Prof. Dr. H. Brandstetter  
Department of Biosciences and  
Christian Doppler Laboratory for Innovative Tools for Biosimilar Characterization  
Division of Structural Biology, University of Salzburg  
Billrothstrasse 11, 5020 Salzburg (Austria)
- [c] A. Alhayek, Dr. J. Haupenthal, Prof. Dr. R. W. Hartmann,  
Prof. Dr. A. K. H. Hirsch  
Department of Drug Design and Optimization  
Helmholtz Institute for Pharmaceutical Research Saarland (HIPS)  
Helmholtz Centre for Infection Research (HZI)  
Campus E8 1, 66123 Saarbrücken (Germany)  
E-mail: anna.hirsch@helmholtz-hips.de
- [d] A. Andreas, Prof. Dr. R. Müller  
Department of Microbial Natural Products  
Helmholtz Institute for Pharmaceutical Research Saarland (HIPS)  
Helmholtz Centre for Infection Research (HZI)  
Campus E8 1, 66123 Saarbrücken (Germany)
- [e] A. Alhayek, A. Andreas, Prof. Dr. R. Müller, Prof. Dr. R. W. Hartmann,  
Prof. Dr. A. K. H. Hirsch  
Department of Pharmacy, Saarland University  
Campus E8 1, 66123 Saarbrücken (Germany)

Supporting information for this article is available on the WWW under <https://doi.org/10.1002/cmdc.202000994>

© 2021 The Authors. ChemMedChem published by Wiley-VCH GmbH. This is an open access article under the terms of the Creative Commons Attribution License, which permits use, distribution and reproduction in any medium, provided the original work is properly cited.

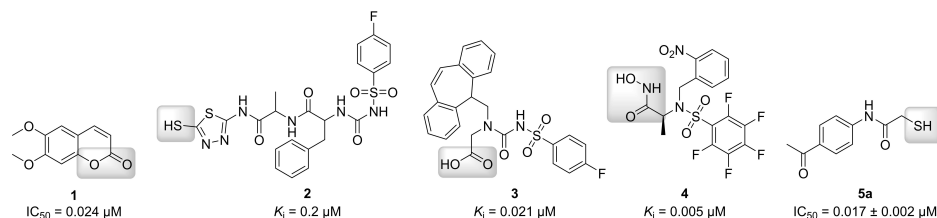


**Figure 1.** Structural diversity of selected previously reported ColH inhibitors with the zinc-binding groups highlighted in grey.<sup>[9]</sup>

substrates of ColH, are the most abundant proteins of the human extracellular matrix and can be found throughout all organs (especially in skin, bones and joints). Their triple-helical structure is formed by three intertwined left-handed helices and is based on a shared repetitive Gly-X<sub>aa</sub>-Y<sub>aa</sub> motif. In this motif, X<sub>aa</sub> and Y<sub>aa</sub> can be nearly any amino acid, but a proline in the X<sub>aa</sub> (28%) and a hydroxyproline in the Y<sub>aa</sub> (38%) position, respectively, occur most frequently.<sup>[10]</sup>

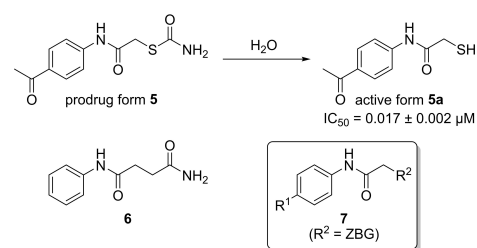
Clostridial collagenases are multidomain proteins whose collagenolytic core is composed of an activator domain and a peptidase domain.<sup>[11]</sup> In the latter, the catalytic zinc ion is coordinated by two histidines in an HEXXH motif and a downstream glutamate.<sup>[5a,11]</sup> Mechanistically, the general acid-base glutamate in the HEXXH motif polarises the nucleophilic water molecule in the active site. This polarisation is further facilitated by the zinc ion acting as a Lewis acid (promoted water mechanism). Additionally, by polarising and stabilising the carbonyl oxygen, the zinc ion simultaneously increases the electrophilicity of the carbonyl carbon atom of the scissile amide bond in the bound collagen substrate.<sup>[12]</sup> Co-crystal structures of collagenase H (ColH) and collagenase G (ColG) from *C. histolyticum* with a selective and an unselective binder, respectively, are available (PDB IDs: ColH with selective inhibitor: 5O7E;<sup>[13]</sup> ColG with unselective inhibitor: 2Y6I<sup>[11]</sup>). Clostridial collagenases represent “true” collagenases, that is, they are collagen-specific and can degrade collagen in its native triple-helical structure. This cleavage can occur at multiple sites, thus generating small peptide fragments.<sup>[7,8a]</sup> In contrast, human matrix metalloproteases (MMPs), that also include “true” collagenases, are only able to cleave collagen at one site.<sup>[14]</sup> After cleavage, the collagen fragments then have to undergo further hydrolytic steps catalysed by different enzymes.

Besides the crucial role of clostridial collagenases in disease development, their extracellular localisation<sup>[7]</sup> makes them highly attractive drug targets. The penetration of the bacterial cell wall often represents a major challenge for antibacterial drug development,<sup>[15]</sup> but can thus be avoided in this case. Naturally occurring collagenase-inhibiting coumarin derivatives (e.g., 1, Figure 1) were found in extracts of *Viola yedoensis*.<sup>[9a]</sup> Supuran and co-workers have made major contributions to the emerging field of synthetic inhibitors of bacterial collagenases. They have prepared and studied a variety of compounds that mimic the natural substrate with an amide backbone and bind

strongly to the active site via a zinc-binding group (ZBG). The latter coordinates to the zinc ion and displaces the essential water molecule from the active site. The inhibitors vary in their different ZBG, including 2-mercapto-substituted 1,3,4-thiadiazole (e.g., 2),<sup>[9b]</sup> carboxylate (e.g., 3),<sup>[9c]</sup> and hydroxamic acid units (e.g., 4;<sup>[9d-f]</sup> Figure 1). However, all of these compounds show one major drawback in that they are also strong inhibitors of human MMPs due to highly homologous motifs in the active sites of both enzyme families. These off-target effects severely limit their potential to become suitable drug candidates.

More recently, we have reported the first selective inhibitor 5 of bacterial collagenases. “Hit” compound 5 contains a thiocarbamate unit as a hydrolytically cleavable prodrug moiety of the thiol 5a, which then strongly binds to the zinc ion and therefore inhibits ColH in the low-nanomolar range (Scheme 1).<sup>[13]</sup> This compound was also co-crystallised with the target enzyme, revealing the exact binding mode in the non-primed binding region. The interactions with the non-primed edge strand, whose conformation is conserved and distinct for clostridial collagenases, provide the high selectivity towards various bacterial collagenases, including ColH and ColG from *C. histolyticum*, ColT from *C. tetani*, and ColQ1 from *Bacillus cereus*, over the unwanted inhibition of human MMPs.<sup>[13]</sup>

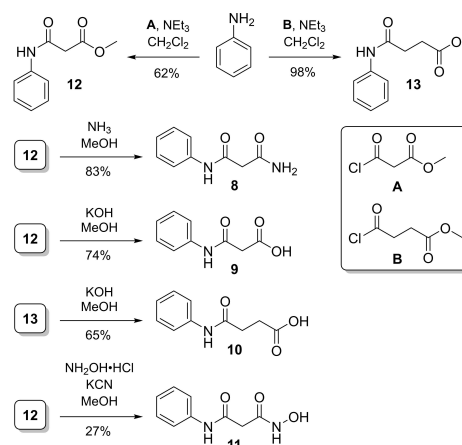
Very recently, we demonstrated that the linker unit in structures of type 5a, that is, the motif connecting the aromatic moiety and the thiol ZBG, can be varied. Thus, cyclisation to a



**Scheme 1.** Structures of the previously identified “hit” ColH inhibitor 5, its active thiol form 5a (after prodrug cleavage) and previously reported amide analogue 6. General structure 7 of the novel potential collagenase inhibitors reported in this work (ZBG = zinc-binding group).

succinimide is tolerated with a moderate loss of activity if the thiol is kept in its relative position.<sup>[16]</sup> This, however, indicated that inhibitor **5a** can be further varied and optimised. One obvious objective of such an optimisation process would be the replacement of the ZBG. Even though there are thiol-containing drugs in clinical use,<sup>[17a,b]</sup> thiols generally suffer from their limited stability, mainly due to oxidative disulfide formation that often leads to rapid inactivation.<sup>[17c]</sup> Therefore, a replacement of the thiol with a different ZBG would be highly useful, even if it might potentially lead to some loss of inhibitory activity. Our goal was to retain the high selectivity of **5a** for the inhibition of bacterial collagenases vs. human off-targets. Hence, the *N*-arylacетamide core structure was kept intact and only the thiol moiety as the metal-binding group was exchanged for various other ZBGs. Among the significant number of zinc-binding units described in the literature,<sup>[18]</sup> we decided to focus on sterically smaller motifs in order to retain the previously identified binding mode.<sup>[13]</sup>

An amide **6** as a stable analogue of the thiocarbamate structure of prodrug **5** (Scheme 1) has already been reported by us.<sup>[13]</sup> Amide **6** had the same length as the thiocarbamate **5**. However, it was more than 400-fold less potent as a ColH inhibitor. This result suggested to us that the overall length of **6** might not fit into the ColH active site, as the (shorter) thiol **5a** (and not thiocarbamate **5**) was the actual zinc-binding inhibitor. This consideration has significantly influenced our design of the novel series **7** of potential ColH inhibitors described herein (Scheme 1). Thus, most of the new target compounds contained only one methylene unit to connect the amide carbonyl of the core structure and the ZBG (in analogy to **5a**). In this work, we therefore report the synthesis and biological evaluation of 16 novel analogues of **5a** with alternative, more stable ZBGs attached to the core structure (general structure **7**, Scheme 1).



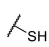
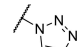
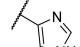
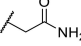
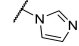
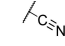
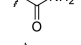
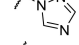
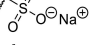
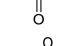
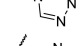
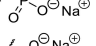
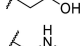
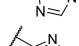
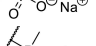
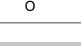
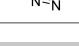

Scheme 2. Synthesis of target compounds 8–11.

## Results and Discussion

### Chemistry

As a first set of target compounds, we prepared new analogues **8–11** with amide (**8**), carboxylate (**9**, **10**) and hydroxamate (**11**) units as potential ZBG (Scheme 2, see also Table 1). Succinic acid derivative **10** is a notable exception to the aforementioned design principle (cf. general structure **7**; Scheme 1) as it was the higher homologue of malonic acid derivative **9** and the acid

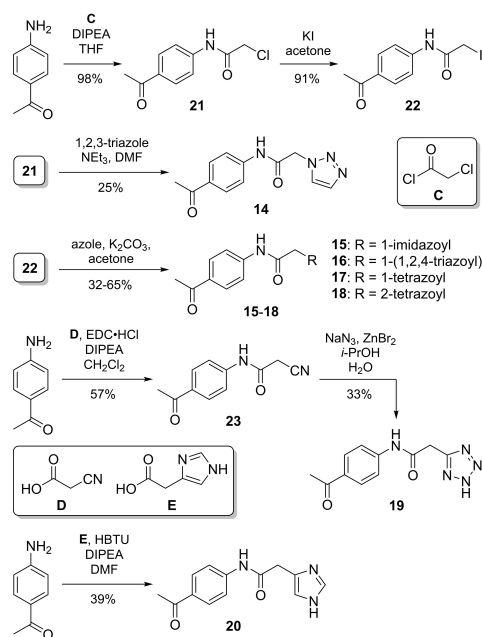
**Table 1.** *In vitro* inhibitory activities of all synthesised target compounds as well as reference compounds **5a** and **6** against ColH.

Cpd.	R <sup>1</sup>	R <sup>2</sup>	IC <sub>50</sub> [μM]	Cpd.	R <sup>1</sup>	R <sup>2</sup>	IC <sub>50</sub> [μM]	Cpd.	R <sup>1</sup>	R <sup>2</sup>	IC <sub>50</sub> [μM]
<b>5a</b>	Ac		0.017 ± 0.002 <sup>[13]</sup>	<b>14</b>	Ac		> 500	<b>20</b>	Ac		> 500
<b>6</b>	H		> 500 <sup>[13]</sup>	<b>15</b>	Ac		448 ± 33	<b>23</b>	Ac		> 500
<b>8</b>	H		> 500	<b>16</b>	Ac		> 500	<b>24</b>	Ac		> 500
<b>9</b>	H		> 500	<b>17</b>	Ac		> 500	<b>25</b>	Ac		> 500
<b>10</b>	H		> 500	<b>18</b>	Ac		> 500	<b>26</b>	Ac		7 ± 1
<b>11</b>	H		~500	<b>19</b>	Ac		22 ± 1	<b>27</b>	Ac		> 500

derivative of amide **6**, thus having one extra methylene unit to connect the ZBG to the core structure.

Target compounds **8–11** were obtained via acylation of aniline to give methyl esters **12** and **13** as intermediates in 62 and 98% yield, respectively. Subsequently, **12** was treated with ammonia, potassium hydroxide or hydroxylamine to furnish **8**, **9** and **11**, respectively, in 27 to 83% yield. Ester saponification of **13** afforded **10** in 65% yield (Scheme 2).

The zinc ion in the active site of ColH is complexed by two histidine residues.<sup>[5a,11,13]</sup> Therefore,azole compounds **14–20** (Scheme 3, see also Table 1) were synthesised to mimic the imidazole moiety of histidine. Triazole derivative **14** was prepared in the following manner. Acylation of *p*-aminoacetophenone with chloroacetyl chloride gave alkyl chloride **21** in 98% yield, and alkylation of 1,2,3-triazole with **21** furnished **14** in 25% yield. In order to obtain an alkylating agent with higher reactivity, **21** was converted into alkyl iodide **22** in a Finkelstein reaction (91% yield). Iodide **22** was then used for the alkylation of other azoles, affording target compounds **15–18** in 32–65% yield. Amide coupling of *p*-aminoacetophenone and cyanoacetic acid gave nitrile intermediate **23** in 57% yield, which was transformed into the target tetrazole **19** by zinc-catalysed cycloaddition with sodium azide (33% yield). Imidazole-derived analogue **20** was synthesised in one step (by amide coupling of *p*-aminoacetophenone) in 39% yield (Scheme 3).



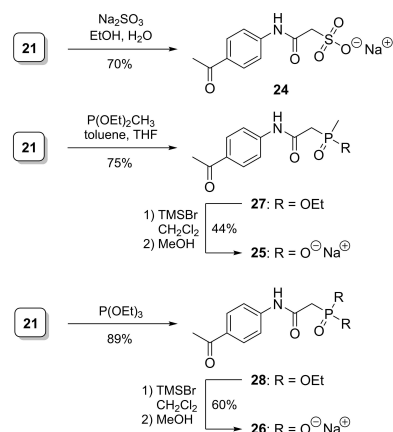
Scheme 3. Synthesis of azole-derived target compounds **14–20**.

In order to exploit the potential of electrostatic interactions, negatively charged ZBGs were also explored. Hence, target compounds **24** (with a sulfonate unit as ZBG), **25** (phosphinate), and **26** (phosphonate) were synthesised using the previously employed alkyl chloride intermediate **21** (Scheme 4). Sulfonate **24** was obtained by alkylation of sulfite in 70% yield. Both phosphinate **25** and phosphonate **26** were prepared in two steps each, with the first step being a Michaelis–Arbuzov reaction to give ethyl esters **27** and **28** in 75 and 89% yield, respectively. This was followed by silyl-mediated cleavage of the ethyl ester to afford (after ion exchange) highly pure sodium salts **25** and **26** in yields of 44 and 60%, respectively.

#### *In vitro* inhibition of ColH

All synthesised target compounds were tested in a previously described FRET-based *in vitro* assay for ColH inhibition, using a custom-made quenched fluorescent peptide as substrate.<sup>[13]</sup> The inhibitory activities ( $IC_{50}$  values) were obtained from steady-state kinetics. Varying concentrations of the compounds were preincubated with the peptidase domain of ColH (10 nM) for 1 h before the reactions were started by the addition of the peptide substrate.  $IC_{50}$  values were determined by nonlinear regression analysis and are listed in Table 1.

Interestingly, only two out of the 16 tested compounds with various zinc-binding groups showed notable inhibitory activity against ColH. These were tetrazole derivative **19** ( $IC_{50}$  = 22  $\mu$ M) and phosphonate **26** ( $IC_{50}$  = 7  $\mu$ M). However, both compounds were considerably weaker inhibitors of ColH than thiol **5a** ( $IC_{50}$  = 17 nM). As **26** was about three times more active than **19**, it was decided to further investigate phosphonate **26** for other biological properties in order to elucidate if it might be a suitable alternative to **5a**, in spite of its decreased inhibitory potency towards the target collagenase ColH.



Scheme 4. Synthesis of anionic target compounds **24–26**.

### Selectivity over potential human off-targets

Inhibitors of bacterial collagenases might potentially also bind to human zinc-dependent enzymes as “off-targets”, even though the results obtained with thiocarbamate **5** had demonstrated that pronounced selectivity can be achieved (see above).<sup>[13]</sup> We have therefore investigated if phosphonate **26** (in comparison to thiol **5a** as the active form of **5**) inhibited a selection of such zinc-dependent human off-targets. Our goal was to at least retain the selectivity of “hit” compound **5** when the ZBG is changed. The human enzymes chosen for this study were six representatives of the MMP family, histone deacetylases 3 (HDAC-3) and 8 (HDAC-8), and the tumour necrosis factor  $\alpha$  (TNF- $\alpha$ ) converting enzyme (TACE, also known as ADAM-17). It should be noted that **5** had previously only been tested for the unwanted inhibition of MMPs.<sup>[13]</sup>

Inhibitory activities of both **5a** and novel ColH inhibitor **26** against this panel of potential human off-targets are provided in Table 2 (as percentage inhibition at a fixed concentration of 100  $\mu\text{M}$ ). Against the six selected MMP enzymes, both ColH inhibitors showed no notable to very moderate inhibition at this rather high concentration. An exception was the inhibition of MMP-8 (36% @100  $\mu\text{M}$ ) and MMP-14 (47% @100  $\mu\text{M}$ ), respectively, by phosphonate **26**. In contrast, both enzymes were not inhibited by thiol **5a**.<sup>[13]</sup> However, this implies that the *in vitro* inhibitory activities of **26** towards these two representatives of the MMP family were still more than one order of magnitude lower than towards ColH as its bacterial target. Overall, the rather limited inhibition of MMPs as human off-targets by **26** confirmed our initial design principle to retain the aromatic anilide core structure that had been shown to be crucial for the selectivity of **5/5a**.<sup>[13]</sup>

As noted, the other potential human off-targets investigated in this context were two representatives of the HDAC family and TACE. Regarding the unwanted inhibition of these three enzymes, phosphonate **26** was superior to thiol **5a** throughout (Table 2). Thus, thiol **5a** showed significantly higher inhibition of the two HDAC tested (~50% inhibition with **5a** vs. maximum ~10% with **26**) and in particular of TACE (~80% with **5a** vs. ~20% with **26**). The unwanted inhibition of TACE would lead to a decreased release of TNF- $\alpha$ , hence causing a reduced immune

response of the host<sup>[19]</sup> and thereby providing the bacteria with a higher chance to establish a critical infection.<sup>[20]</sup> The absence of notable HDAC and TACE inhibition for **26** represents a major advantage of this novel phosphonate-derived ColH inhibitor.

### Cytotoxicity against human cells

The new ColH inhibitor **26** was also investigated for potential cytotoxic effects against three representative human cell lines, that is, HepG2, HEK293, and A549 cells. Within the experimental error, **26** showed a comparable or even slightly lower decrease of cell viability (as an indicator of toxicity) than the previous “hit” compound **5a** in all investigated cell lines at 100  $\mu\text{M}$  compound concentration (Table 3). As a reference compound, the approved antibiotic rifampicin (that is clinically used in the long-term therapy of tuberculosis<sup>[21]</sup>) was also studied. Rifampicin showed a comparable decrease of cell viability as both tested ColH inhibitors **26** and **5a** at an identical concentration (100  $\mu\text{M}$ ). As further references and also as positive controls, the chemotherapeutic agents doxorubicin<sup>[22a]</sup> and epirubicin<sup>[22b]</sup> were employed and were found to be notably toxic at a 100-fold lower concentration (i.e., 1  $\mu\text{M}$ ) in all three cell lines. In turn, it can be concluded that even a 100-fold higher concentration of **26** might be tolerated based on these cytotoxicity studies.

### Toxicity in a zebrafish model

In order to determine the toxicity of ColH inhibitors **26** and **5a** in an *in vivo* setting, a zebrafish larvae toxicity assay was performed. Zebrafish are very small and almost transparent organisms. They can be cultured in small volumes of media, leading to very small amounts of compounds being needed for testing. Furthermore, zebrafish develop their organ systems, which show high similarity to the mammalian cardiovascular, nervous, and digestive systems,<sup>[23a,b]</sup> in less than one week,<sup>[23a,c,d]</sup> thus making the experiments fast and relatively inexpensive. Using this assay, we aimed to determine the maximally tolerated dose (MTD) at which no toxic effects of the compounds were observed. It was found that both phosphonate **26** and thiol reference **5a** showed no toxic effects at concentrations up to 100  $\mu\text{M}$ .

**Table 2.** *In vitro* inhibitory activities of novel ColH inhibitor **26** (ZBG = phosphonate) and reference compound **5a** (ZBG = thiol) against a panel of potential human off-targets.

Human enzyme	Inhibition [%] at 100 $\mu\text{M}$ compound <sup>[a]</sup>	
	<b>5a</b> (thiol)	<b>26</b> (phosphonate)
MMP-1	n.i. <sup>[b]</sup>	19 $\pm$ 4
MMP-2	19 $\pm$ 8	18 $\pm$ 1
MMP-3	n.i.	n.i.
MMP-7	n.i.	n.i.
MMP-8	n.i.	36 $\pm$ 1
MMP-14	n.i.	47 $\pm$ 13
HDAC-3	51 $\pm$ 7	11 $\pm$ 2
HDAC-8	48 $\pm$ 5	n.i.
TACE	79 $\pm$ 7	21 $\pm$ 8

[a] Means of at least two independent measurements, 10 nM enzyme concentration. [b] n.i. = no inhibition (< 10%).

**Table 3.** Cytotoxicity (as decrease of cell viability) of ColH inhibitors **26** (ZBG = phosphonate) and **5a** (ZBG = thiol) as well as of three reference compounds against three human cell lines.

Compound	c [ $\mu\text{M}$ ]	Decrease of viability [%] after 48 h <sup>[a]</sup>		
		HepG2	HEK293	A549
<b>5a</b> (thiol)	100	15 $\pm$ 9	53 $\pm$ 0	18 $\pm$ 12
<b>26</b> (phosphonate)	100	8 $\pm$ 10	32 $\pm$ 4	20 $\pm$ 2
rifampicin	100	33 $\pm$ 13	29 $\pm$ 13	9 $\pm$ 13
doxorubicin	1	57 $\pm$ 14	47 $\pm$ 9	53 $\pm$ 13
epirubicin	1	68 $\pm$ 10	49 $\pm$ 11	56 $\pm$ 12

[a] Means of at least two independent measurements.



### Ex vivo pig skin degradation assay

To investigate the activity of collagenase inhibitors on tissue in a more complex experimental setting, an *ex vivo* pig skin degradation assay using purified ColQ1 from *B. cereus* has recently been developed.<sup>116</sup> The degradation of collagen in this mammalian tissue was measured as a rate of hydroxyproline (Hyp) release. This assay had previously been used to demonstrate the efficacy of succinimide **29** (Figure 2) as an inhibitor of bacterial collagenase activity.<sup>116</sup> Succinimide derivative **29** had an  $IC_{50}$  value of  $0.06 \pm 0.01 \mu\text{M}$  against ColH *in vitro*, which indicates that it is ca. 100-fold more potent than phosphonate **26**. Towards ColQ1 (at a fixed inhibitor concentration of  $100 \mu\text{M}$ ), **29** had shown complete ( $100 \pm 2\%$ ) inhibition, which corresponded to an  $IC_{50}$  value significantly below  $100 \mu\text{M}$ .<sup>116</sup> Using the same *in vitro* assay, novel phosphonate **26** had an  $IC_{50}$  value of  $183 \pm 7 \mu\text{M}$ . However, in the *ex vivo* assay, **26** reduced the formation of Hyp to 75% of the Hyp production of the control at a concentration of  $100 \mu\text{M}$ , which is nearly identical to the potency of **29** (Figure 3).

Overall, succinimide **29** showed a stronger reduction of Hyp formation at elevated concentrations than phosphonate **26**, in particular at 300 and  $400 \mu\text{M}$ , respectively (Figure 3). However, this difference in potency was far less than what was expected based on the significant difference of the aforementioned *in vitro* activities ( $IC_{50}$  values). It should also be noted that succinimide **29** appears to reach a "plateau" in activity between about 300 and  $400 \mu\text{M}$  while phosphonate **26** had a nearly linear correlation of concentration and activity. This "plateau" in the activity of **29** might eventually result from disulfide

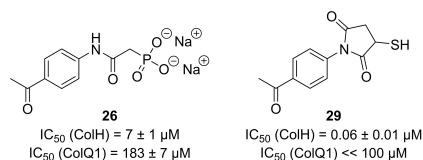


Figure 2. Structures and *in vitro* potencies for collagenase inhibition of compounds **26** and **29**.<sup>116</sup>

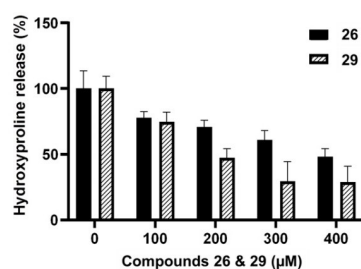


Figure 3. *Ex vivo* pig skin degradation assay: hydroxyproline release after 24 h upon treatment with **26** and **29**<sup>116</sup> (in % relative to the controls).

formation at higher concentrations. This again highlights the benefit of employing an oxidation-resistant ZBG (as in **26**) to provide air-stable alternatives to thiol-derived inhibitors.

### Conclusions

In summary, we herein report the exchange of the thiol ZBG of previously published selective ColH inhibitors with more stable ZBGs, with the selectivity of the thiol-based "hit" compound **5a** being retained. Thus, the structure of **5a** was varied to furnish phosphonate derivative **26**. In contrast to the thiol group in **5a**, the phosphonate as a ZBG in **26** is not prone to oxidation or degradation. Novel inhibitor **26** still showed reasonably potent (i.e., micromolar) inhibition of the clostridial collagenase ColH, while apparently retaining the binding mode of **5a** and therefore its remarkable selectivity over potential human off-targets such as MMPs. In comparison to **5a**, we observed a better selectivity of **26** over other human off-targets (HDAC and TACE), suggesting it might be an improved hit structure for further development. Inhibitor **26** showed no indication of major toxicity in three different human cell lines as well as high tolerance in an *in vivo* zebrafish toxicity assay. Furthermore, we demonstrated the efficacy of **26** not only in an *in vitro* enzyme assay for collagenase activity, but also in a more complex *ex vivo* pig skin degradation assay. The results from this assay highlight the potency of **26** and the relevance of a stable (non-thiol) ZBG for biological activity in a complex biological setting. Overall, **26** should therefore be considered as a new improved hit structure for the development of potent inhibitors of bacterial collagenases that will now undergo further optimisation in our laboratories.

### Experimental Section

**General methods:** All chemicals, starting materials and reagents were purchased from standard suppliers and used without further purification. Air- and/or water-sensitive reactions were carried out under nitrogen atmosphere with anhydrous solvents. Anhydrous solvents were obtained in the following manner: THF, DMF and  $\text{CH}_2\text{Cl}_2$  were dried with a solvent purification system (MBRAUN MB SPS 800). All other solvents were of technical quality and distilled prior to use, and deionised water was used throughout. Reactions were monitored by TLC on aluminium plates precoated with silica gel 60 F254 (VWR). Visualisation of the spots was carried out using UV light (254 nm) and/or staining under heating (V55 stain: 4 g vanillin, 25 mL conc.  $\text{H}_2\text{SO}_4$ , 80 mL AcOH, 680 mL MeOH; CAM stain: 12 g ammonium molybdate, 0.5 g ceric ammonium molybdate, 235 mL  $\text{H}_2\text{O}$ , 15 mL conc.  $\text{H}_2\text{SO}_4$ ; ninhydrin stain: 1.5 g ninhydrin, 100 mL *n*-butanol, 3.0 mL AcOH).  $R_f$  values are given to the nearest 0.05. Column chromatography was carried out on silica gel 60 (40–63  $\mu\text{m}$ , 230–400 mesh ASTM, VWR) under flash conditions. Preparative centrifugal TLC was performed on a Chromatotron<sup>TM</sup> 7924T (T-Squared Technology) using glass plates coated with silica gel 60 PF<sub>254</sub> containing a fluorescent indicator (VWR, thickness depending on the amount of crude material to be separated, for 50–500 mg: 1 mm layer). Ion-exchange chromatography was carried out using DOWEX<sup>TM</sup> 50WX8 resin (200–400 mesh, VWR) in the  $\text{Na}^+$  form. Semipreparative HPLC was performed on a VWR-Hitachi system equipped with an L-2300 pump, an L-2200 autosampler, an L-2455

diode array detector (DAD) and a LichroCart™ Purospher™ RP18e column (5 μm, 10×250 mm, VWR). NMR spectra were recorded using the following Bruker NMR spectrometers: for <sup>1</sup>H NMR spectra at 500 MHz and <sup>13</sup>C NMR spectra at 126 MHz: Avance™ 500; for <sup>31</sup>P NMR spectra at 203 MHz: Avance™ 500. For the assignment of signals, <sup>1</sup>H,<sup>1</sup>H COSY, <sup>1</sup>H,<sup>13</sup>C HSQC and <sup>1</sup>H,<sup>13</sup>C HMBC spectra were used. All <sup>13</sup>C and <sup>31</sup>P NMR spectra are <sup>1</sup>H-decoupled. All spectra were recorded at room temperature if not indicated otherwise and were referenced internally to solvent residual signals wherever possible. Chemical shifts (δ) are quoted in ppm and coupling constants (*J*) are reported in Hz. Low-resolution mass spectra were recorded on a liquid chromatography-coupled mass spectrometer (LC-MS) Surveyor MSQ Plus from Finnigan. For the LC separation prior to detection, a Nucleodur™ 100-5 C<sub>18</sub> column (5 μm, 3×125 mm) was used. High-resolution mass spectra were recorded on a Thermo Scientific Q Exactive Orbitrap mass spectrometer with ESI ionisation mode coupled with an Ultimate 3000 HPLC system by Thermo Scientific, equipped with a Thermo Accucore™ phenyl-X column (2.1 μm, 3×100 mm). Melting points (mp) were measured on a melting point apparatus SMP3 (Stuart Scientific) and were not corrected.

**General procedure (GP1) for the synthesis of azole derivatives:** Alkyl iodide **22** (1.0 equiv), K<sub>2</sub>CO<sub>3</sub> (1.1 equiv), and the respective azole (1.1 equiv) were suspended in acetone (20 mL, ~25 mM) and stirred at 70 °C overnight (15–20 h). EtOAc (200 mL) was added, and the organic layer was washed with water (3×30 mL) and brine (50 mL) and dried over Na<sub>2</sub>SO<sub>4</sub>. The solvent was evaporated under reduced pressure and the resultant crude product was purified by column chromatography to give the respective azole derivative.

**General procedure (GP2) for the cleavage of ethyl esters:** The respective ethyl ester (1.0 equiv) was dissolved in CH<sub>2</sub>Cl<sub>2</sub> (10 mL). TMSBr (5.0 equiv) was added dropwise over 10 min, and the reaction was stirred at RT overnight (15–20 h). MeOH (10 mL) was then added, and the mixture was stirred for 1–2 h. The solvent was evaporated under reduced pressure, the resultant crude product was purified by HPLC and the obtained product was converted into its Na<sup>+</sup> form by ion-exchange column chromatography to give the respective title compound.

**N<sup>1</sup>-Phenylmalonamide (8):** Methyl ester **12** (49 mg, 0.25 mmol) was dissolved in MeOH (6 mL). NH<sub>3</sub> solution (33%, 3 mL) was added, and the reaction mixture was stirred at RT overnight. The solvent was evaporated under reduced pressure and the resultant crude product was purified by column chromatography (CH<sub>2</sub>Cl<sub>2</sub>/MeOH 100:0→95:5) to give **8** as a white solid (37 mg, 83%). <sup>1</sup>H NMR (500 MHz, [D<sub>6</sub>]DMSO): δ = 10.07 (s, 1H, Ph-NH), 7.58 (d, *J* = 7.6 Hz, 2H, 2'-H, 6'-H), 7.51 (br, 1H, NH<sub>2</sub>-a), 7.30 (t, *J* = 7.9 Hz, 2H, 3'-H, 5'-H), 7.11 (br, 1H, NH<sub>2</sub>-b), 7.04 (t, *J* = 7.4 Hz, 1H, 4'-H), 3.21 (s, 2H, 2-H) ppm. <sup>13</sup>C NMR (126 MHz, [D<sub>6</sub>]DMSO): δ = 168.68 (C-1 or C-3), 165.74 (C-1 or C-3), 138.96 (C-1'), 128.71 (C-3', C-5'), 123.27 (C-4'), 119.02 (C-2', C-6'), 44.50 (C-2) ppm. HRMS (ESI): calcd. for C<sub>9</sub>H<sub>11</sub>N<sub>2</sub>O<sub>2</sub> [*M*+*H*]<sup>+</sup> 179.0815, found 179.0813. TLC (petroleum ether/EtOAc 1:1): *R*<sub>f</sub> = 0.10.

**3-Oxo-3-(phenylamino)propanoic acid (9):** Methyl ester **12** (102 mg, 0.528 mmol) was dissolved in MeOH (5 mL). KOH solution (50 g/L, 1.2 mL) was added, and the reaction mixture was stirred at 35 °C for 4 h. It was then acidified with HCl, and EtOAc (200 mL) was added. The organic layer was washed with HCl (2 M, 4×40 mL) and brine (50 mL) and then dried over Na<sub>2</sub>SO<sub>4</sub>. The solvent was evaporated under reduced pressure, and the resultant crude product was purified by column chromatography (CH<sub>2</sub>Cl<sub>2</sub>/MeOH/HCOOH 95:4:1) to give **9** as a white solid (70 mg, 74%). <sup>1</sup>H NMR (500 MHz, [D<sub>6</sub>]DMSO): δ = 12.68 (br, 1H, COOH), 10.13 (s, 1H, NH), 7.57 (d, *J* = 7.6 Hz, 2H, 2'-H, 6'-H), 7.31 (t, *J* = 7.9 Hz, 2H, 3'-H, 5'-H), 7.05 (t, *J* = 7.4 Hz, 1H, 4'-H), 3.34 (s, 2H, 2-H) ppm. <sup>13</sup>C NMR

(126 MHz, [D<sub>6</sub>]DMSO): δ = 169.28 (C-1 or C-3), 164.57 (C-1 or C-3), 138.95 (C-1'), 128.76 (C-3', C-5'), 123.38 (C-4'), 119.01 (C-2', C-6'), 43.99 (C-2) ppm. HRMS (ESI): calcd. for C<sub>9</sub>H<sub>10</sub>NO<sub>3</sub> [*M*+*H*]<sup>+</sup> 180.0655, found 180.0654. TLC (petroleum ether/EtOAc/HCOOH 49:49:2): *R*<sub>f</sub> = 0.20.

**4-Oxo-4-(phenylamino)butanoic acid (10):** Methyl ester **13** (204 mg, 0.985 mmol) was dissolved in MeOH (4 mL). KOH solution (50 g/L, 2.2 mL) was added, and the reaction mixture was stirred at 35 °C for 4 h. It was then acidified with HCl and EtOAc (200 mL) was added. The organic layer was washed with HCl (2 M, 4×40 mL) and brine (50 mL) and then dried over Na<sub>2</sub>SO<sub>4</sub>. The solvent was evaporated under reduced pressure, and the resultant crude product was purified by column chromatography (petroleum ether/EtOAc/HCOOH 70:29:1) to give **10** as a white solid (124 mg, 65%). <sup>1</sup>H NMR (500 MHz, [D<sub>6</sub>]DMSO): δ = 12.20 (br, 1H, COOH), 9.94 (br, 1H, NH), 7.57 (d, *J* = 7.6 Hz, 2H, 2'-H, 6'-H), 7.28 (t, *J* = 7.9 Hz, 2H, 3'-H, 5'-H), 7.01 (t, *J* = 7.4 Hz, 1H, 4'-H), 2.56–2.50 (m, 4H, 2-H, 3-H) ppm. <sup>13</sup>C NMR (126 MHz, [D<sub>6</sub>]DMSO): δ = 173.83 (C-1 or C-4), 170.06 (C-1 or C-4), 139.30 (C-1'), 128.65 (C-3', C-5'), 122.88 (C-4'), 118.87 (C-2', C-6'), 31.04 (C-2 or C-3), 28.82 (C-2 or C-3) ppm. HRMS (ESI): calcd. for C<sub>10</sub>H<sub>12</sub>NO<sub>3</sub> [*M*+*H*]<sup>+</sup> 194.0812, found 194.0810. TLC (petroleum ether/EtOAc/HCOOH 49:49:2): *R*<sub>f</sub> = 0.25.

**N<sup>1</sup>-Hydroxy-N<sup>2</sup>-phenylmalonamide (11):** Hydroxylamine hydrochloride (497 mg, 7.15 mmol), DIPEA (1.50 mL, 8.61 mmol) and KCN (19 mg, 0.29 mmol) were dissolved in MeOH (5 mL), and the mixture was heated to reflux. After 10 min, a solution of methyl ester **12** (91 mg, 0.47 mmol) in MeOH (5 mL) was added, and the reaction mixture was stirred under reflux overnight. It was then concentrated under reduced pressure, acidified with HCl (1 M, 100 mL) and extracted with EtOAc (5×50 mL). The combined organics were dried over Na<sub>2</sub>SO<sub>4</sub>, and the solvent was evaporated under reduced pressure. The resultant crude product was purified by HPLC (water+0.1% TFA, MeCN+0.1% TFA, 95:5→0:100) to give **11** as a slightly orange solid (25 mg, 27%). <sup>1</sup>H NMR (500 MHz, [D<sub>6</sub>]DMSO): δ = 10.61 (s, 1H, NHOH), 10.10 (s, 1H, Ph-NH), 8.96 (br, 1H, NHOH), 7.57 (d, *J* = 7.8 Hz, 2H, 2'-H, 6'-H), 7.30 (t, *J* = 7.8 Hz, 2H, 3'-H, 5'-H), 7.05 (t, *J* = 7.3 Hz, 1H, 4'-H), 3.11 (s, 2H, 2-H) ppm. <sup>13</sup>C NMR (126 MHz, [D<sub>6</sub>]DMSO): δ = 165.27 (C-1 or C-3), 163.48 (C-1 or C-3), 138.93 (C-1'), 128.76 (C-3', C-5'), 123.38 (C-4'), 119.07 (C-2', C-6'), 42.03 (C-2) ppm. HRMS (ESI): calcd. for C<sub>9</sub>H<sub>9</sub>N<sub>2</sub>O<sub>3</sub> [*M*-*H*]<sup>-</sup> 193.0619, found: 193.0609. TLC (CH<sub>2</sub>Cl<sub>2</sub>/MeOH/HCOOH 90:9:1): *R*<sub>f</sub> = 0.15.

**Methyl 3-oxo-3-(phenylamino)propanoate (12):** Aniline (400 μL, 4.39 mmol) and NEt<sub>3</sub> (1.20 mL, 8.61 mmol) were dissolved in CH<sub>2</sub>Cl<sub>2</sub> (10 mL) and cooled to 0 °C. Methyl malonyl chloride (500 μL, 5.24 mmol) was added dropwise over 15 min, and the reaction mixture was stirred at 0 °C for 3 h. The reaction was quenched with cold water (15 mL), and the mixture was diluted with CH<sub>2</sub>Cl<sub>2</sub>. The organic layer was washed with sat. NaHCO<sub>3</sub> solution (5×40 mL) and dried over Na<sub>2</sub>SO<sub>4</sub>. The solvent was evaporated under reduced pressure, and the resultant crude product was purified by column chromatography (CH<sub>2</sub>Cl<sub>2</sub>) to give **12** as a slightly orange solid (523 mg, 62%). <sup>1</sup>H NMR (500 MHz, CDCl<sub>3</sub>): δ = 9.15 (br, 1H, NH), 7.55 (d, *J* = 8.1 Hz, 2H, 2'-H, 6'-H), 7.33 (t, *J* = 7.9 Hz, 2H, 3'-H, 5'-H), 7.13 (t, *J* = 7.4 Hz, 1H, 4'-H), 3.80 (s, 3H, OCH<sub>3</sub>), 3.49 (s, 2H, 2-H) ppm. <sup>13</sup>C NMR (126 MHz, CDCl<sub>3</sub>): δ = 170.58 (C-1 or C-3), 162.82 (C-1 or C-3), 137.54 (C-1'), 129.15 (C-3', C-5'), 124.76 (C-4'), 120.25 (C-2', C-6'), 52.82 (OCH<sub>3</sub>), 41.45 (C-2) ppm. MS (ESI): *m/z* = 216.0 [*M*+Na]<sup>+</sup>. TLC (petroleum ether/EtOAc 7:3): *R*<sub>f</sub> = 0.10.

**Methyl 4-oxo-4-(phenylamino)butanoate (13):** Aniline (100 μL, 1.10 mmol) and NEt<sub>3</sub> (300 μL, 2.15 mmol) were dissolved in CH<sub>2</sub>Cl<sub>2</sub> (5 mL) and cooled to 0 °C. Methyl succinyl chloride (170 μL, 1.38 mmol) was added dropwise over 10 min, and the reaction mixture was stirred at 0 °C for 3.5 h. The reaction was quenched with cold water (15 mL), and the mixture was diluted with CH<sub>2</sub>Cl<sub>2</sub>.



The organic layer was washed with sat. NaHCO<sub>3</sub> solution (4 × 30 mL) and dried over Na<sub>2</sub>SO<sub>4</sub>. The solvent was evaporated under reduced pressure and the resultant crude product was purified by centrifugal TLC (CH<sub>2</sub>Cl<sub>2</sub>) to give **13** as a white solid (222 mg, 98%). <sup>1</sup>H NMR (500 MHz, CDCl<sub>3</sub>): δ = 7.71 (br, 1H, NH), 7.50 (d, *J* = 7.9 Hz, 2H, 2'-H, 6'-H), 7.29 (t, *J* = 7.9 Hz, 2H, 3'-H, 5'-H), 7.09 (t, *J* = 7.4 Hz, 1H, 4'-H), 3.70 (s, 3H, OCH<sub>3</sub>), 2.75 (t, *J* = 6.5 Hz, 2H, 2-H or 3-H), 2.66 (t, *J* = 6.5 Hz, 2H, 2-H or 3-H) ppm. <sup>13</sup>C NMR (126 MHz, CDCl<sub>3</sub>): δ = 173.78 (C-1 or C-4), 169.84 (C-1 or C-4), 137.97 (C-1'), 129.07 (C-3', C-5'), 124.35 (C-4'), 119.90 (C-2', C-6'), 52.12 (OCH<sub>3</sub>), 32.20 (C-2 or C-3), 29.36 (C-2 or C-3) ppm. HRMS (ESI): calcd. for C<sub>11</sub>H<sub>12</sub>N<sub>2</sub>O<sub>2</sub> [M+H]<sup>+</sup> 208.0968, found 208.0961. TLC (petroleum ether/EtOAc 7:3): R<sub>f</sub> = 0.10.

**N-(4-Acetylphenyl)-2-(1H-1,2,3-triazol-1-yl)acetamide (14)**: Alkyl chloride **21** (60 mg, 0.28 mmol), NEt<sub>3</sub> (90 μL, 0.65 mmol) and 1H-1,2,3-triazole (20 μL, 0.34 mmol) were dissolved in DMF (10 mL) and stirred at RT for 8 d. EtOAc (250 mL) was added, and the organic layer was washed with water (5 × 30 mL) and brine (30 mL) and then dried over Na<sub>2</sub>SO<sub>4</sub>. The solvent was evaporated under reduced pressure, and the resultant crude product was purified by column chromatography (CH<sub>2</sub>Cl<sub>2</sub>/MeOH 99:1) to give **14** as a white solid (17 mg, 25%). <sup>1</sup>H NMR (500 MHz, [D<sub>6</sub>]DMSO): δ = 10.83 (s, 1H, NH), 8.17 (d, *J* = 0.9 Hz, 1H, 5'-H), 7.96 (d, *J* = 8.8 Hz, 2H, 3'-H, 5'-H), 7.77 (d, *J* = 0.8 Hz, 1H, 4'-H), 7.72 (d, *J* = 8.8 Hz, 2H, 2'-H, 6'-H), 5.41 (s, 2H, 2-H), 2.53 (s, 3H, acetyl-CH<sub>3</sub>) ppm. <sup>13</sup>C NMR (126 MHz, [D<sub>6</sub>]DMSO): δ = 196.52 (acetyl-C=O), 164.96 (C-1), 142.69 (C-1'), 133.15 (C-4'), 132.15 (C-4), 129.61 (C-3', C-5'), 126.55 (C-5'), 118.53 (C-2', C-6'), 52.04 (C-2), 26.45 (acetyl-CH<sub>3</sub>) ppm. MS (ESI): *m/z* = 245.0 [M+H]<sup>+</sup>. HRMS (ESI): calcd. for C<sub>13</sub>H<sub>12</sub>N<sub>4</sub>O<sub>2</sub> [M+H]<sup>+</sup> 245.1033, found 245.1030. TLC (CH<sub>2</sub>Cl<sub>2</sub>/MeOH 95:5): R<sub>f</sub> = 0.15.

**N-(4-Acetylphenyl)-2-(1H-imidazol-1-yl)acetamide (15)**: General procedure GP1 with 1H-imidazole (41 mg, 0.60 mmol) and alkyl iodide **22** (156 mg, 0.515 mmol) to give **15** as a white solid (47 mg, 38%). <sup>1</sup>H NMR (500 MHz, [D<sub>6</sub>]DMSO): δ = 10.65 (s, 1H, NH), 7.95 (d, *J* = 8.8 Hz, 2H, 3'-H, 5'-H), 7.72 (d, *J* = 8.8 Hz, 2H, 2'-H, 6'-H), 7.64 (s, 1H, 2'-H), 7.17 (t, *J* = 1.9 Hz, 1H, 5'-H), 6.90 (t, *J* = 0.9 Hz, 1H, 4'-H), 4.96 (s, 2H, 2-H), 2.53 (s, 3H, acetyl-CH<sub>3</sub>) ppm. <sup>13</sup>C NMR (126 MHz, [D<sub>6</sub>]DMSO): δ = 196.50 (acetyl-C=O), 166.43 (C-1), 142.93 (C-1'), 138.35 (C-2'), 131.93 (C-4'), 129.59 (C-3', C-5'), 127.92 (C-4'), 120.76 (C-5'), 118.39 (C-2', C-6'), 49.18 (C-2), 26.43 (acetyl-CH<sub>3</sub>) ppm. HRMS (ESI): calcd. for C<sub>13</sub>H<sub>12</sub>N<sub>2</sub>O<sub>2</sub> [M+H]<sup>+</sup> 244.1081, found 244.1078. TLC (CH<sub>2</sub>Cl<sub>2</sub>/MeOH 9:1): R<sub>f</sub> = 0.20.

**N-(4-Acetylphenyl)-2-(1H-1,2,4-triazol-1-yl)acetamide (16)**: General procedure GP1 with 1H-1,2,4-triazol (46 mg, 0.67 mmol) and alkyl iodide **22** (165 mg, 0.545 mmol) to give **16** as a slightly orange solid (87 mg, 65%). <sup>1</sup>H NMR (500 MHz, [D<sub>6</sub>]DMSO): δ = 10.76 (s, 1H, NH), 8.56 (s, 1H, 5'-H), 8.01 (s, 1H, 3'-H), 7.95 (d, *J* = 8.8 Hz, 2H, 3'-H, 5'-H), 7.71 (d, *J* = 8.8 Hz, 2H, 2'-H, 6'-H), 5.19 (s, 2H, 2-H), 2.53 (s, 3H, acetyl-CH<sub>3</sub>) ppm. <sup>13</sup>C NMR (126 MHz, [D<sub>6</sub>]DMSO): δ = 196.58 (acetyl-C=O), 165.26 (C-1), 151.47 (C-3'), 145.69 (C-5'), 142.73 (C-1'), 132.16 (C-4'), 129.66 (C-3', C-5'), 118.55 (C-2', C-6'), 51.85 (C-2), 26.51 (acetyl-CH<sub>3</sub>) ppm. MS (ESI): *m/z* = 245.0 [M+H]<sup>+</sup>. HRMS (ESI): calcd. for C<sub>12</sub>H<sub>10</sub>N<sub>4</sub>O<sub>2</sub> [M+H]<sup>+</sup> 245.1033, found 245.1030. TLC (CH<sub>2</sub>Cl<sub>2</sub>/MeOH 95:5): R<sub>f</sub> = 0.10.

**N-(4-Acetylphenyl)-2-(1H-tetrazol-1-yl)acetamide (17)** and **N-(4-acetylphenyl)-2-(2H-tetrazol-2-yl)acetamide (18)**: General procedure GP1 with 1H-tetrazole (27 mg, 0.39 mmol) and alkyl iodide **22** (101 mg, 0.333 mmol) to give **17** as a white solid (28 mg, 34%) and **18** as a white solid (26 mg, 32%). **17**: <sup>1</sup>H NMR (500 MHz, [D<sub>6</sub>]DMSO): δ = 10.90 (s, 1H, NH), 9.43 (s, 1H, 5'-H), 7.96 (d, *J* = 8.8 Hz, 2H, 3'-H, 5'-H), 7.71 (d, *J* = 8.8 Hz, 2H, 2'-H, 6'-H), 5.54 (s, 2H, 2-H), 2.53 (s, 3H, acetyl-CH<sub>3</sub>) ppm. <sup>13</sup>C NMR (126 MHz, [D<sub>6</sub>]DMSO): δ = 196.55 (acetyl-C=O), 164.14 (C-1), 145.26 (C-5'), 142.50 (C-1'), 132.27 (C-4'), 129.64 (C-3', C-5'), 118.59 (C-2', C-6'), 50.14 (C-2), 26.46 (acetyl-CH<sub>3</sub>) ppm.

MS (ESI): *m/z* = 246.0 [M+H]<sup>+</sup>, 268.0 [M+Na]<sup>+</sup>. HRMS (ESI): calcd. for C<sub>11</sub>H<sub>12</sub>N<sub>2</sub>O<sub>2</sub> [M+H]<sup>+</sup> 246.0986, found 246.0982. TLC (CH<sub>2</sub>Cl<sub>2</sub>/MeOH 95:5): R<sub>f</sub> = 0.25. **18**: <sup>1</sup>H NMR (500 MHz, [D<sub>6</sub>]DMSO): δ = 10.95 (s, 1H, NH), 9.05 (s, 1H, 5'-H), 7.96 (d, *J* = 8.8 Hz, 2H, 3'-H, 5'-H), 7.70 (d, *J* = 8.8 Hz, 2H, 2'-H, 6'-H), 5.78 (s, 2H, 2-H), 2.53 (s, 3H, acetyl-CH<sub>3</sub>) ppm. <sup>13</sup>C NMR (126 MHz, [D<sub>6</sub>]DMSO): δ = 196.53 (acetyl-C=O), 163.52 (C-1), 153.42 (C-5'), 142.40 (C-1'), 132.34 (C-4'), 129.61 (C-3', C-5'), 118.65 (C-2', C-6'), 55.05 (C-2), 26.46 (acetyl-CH<sub>3</sub>) ppm. HRMS (ESI): calcd. for C<sub>11</sub>H<sub>12</sub>N<sub>2</sub>O<sub>2</sub> [M+H]<sup>+</sup> 246.0986, found 246.0984. TLC (CH<sub>2</sub>Cl<sub>2</sub>/MeOH 95:5): R<sub>f</sub> = 0.40.

**N-(4-Acetylphenyl)-2-(2H-tetrazol-5-yl)acetamide (19)**: A suspension of nitrile **23** (102 mg, 0.505 mmol), NaN<sub>3</sub> (159 mg, 2.45 mmol) and ZnBr<sub>2</sub> (100 mg, 0.444 mmol) in *i*PrOH/water (1:3) was stirred under reflux for 2 d. After cooling to RT, EtOAc (200 mL) was added, and the organic layer was washed with HCl (0.2 M, 3 × 50 mL) and brine (50 mL) and then dried over Na<sub>2</sub>SO<sub>4</sub>. The solvent was evaporated under reduced pressure, and the resultant crude product was purified by centrifugal TLC (CH<sub>2</sub>Cl<sub>2</sub>/MeOH 100:0 → 90:10) to give **19** as a white solid (41 mg, 33%). <sup>1</sup>H NMR (500 MHz, [D<sub>6</sub>]DMSO): δ = 16.26 (br, 1H, 2'-NH), 10.78 (s, 1H, NH(C=O)), 7.95 (d, *J* = 8.8 Hz, 2H, 3'-H, 5'-H), 7.72 (d, *J* = 8.8 Hz, 2H, 2'-H, 6'-H), 4.20 (s, 2H, 2-H), 2.53 (s, 3H, acetyl-CH<sub>3</sub>) ppm. <sup>13</sup>C NMR (126 MHz, [D<sub>6</sub>]DMSO): δ = 196.56 (acetyl-C=O), 165.73 (C-1), 150.82 (C-5'), HMBC, 142.95 (C-1'), 132.11 (C-4'), 129.60 (C-3', C-5'), 118.52 (C-2', C-6'), 31.80 (C-2), 26.48 (acetyl-CH<sub>3</sub>) ppm. MS (ESI): *m/z* = 246.0 [M+H]<sup>+</sup>. HRMS (ESI): calcd. for C<sub>11</sub>H<sub>12</sub>N<sub>2</sub>O<sub>2</sub> [M+H]<sup>+</sup> 246.0986, found 246.0980. TLC (CH<sub>2</sub>Cl<sub>2</sub>/MeOH/HCOOH 94:5:1): R<sub>f</sub> = 0.50.

**N-(4-Acetylphenyl)-2-(1H-imidazol-4-yl)acetamide (20)**: 2-(1H-imidazol-4-yl)acetic acid hydrochloride (180 mg, 1.11 mmol), HBTU (430 mg, 1.13 mmol) and DIPEA (140 μL, 0.823 mmol) were dissolved in DMF (5 mL). After 5 min stirring at RT, *p*-aminoacetophenone (101 mg, 0.747 mmol) was added, and the reaction mixture was stirred at RT for 27 h. EtOAc (200 mL) was added, and the organic layer was washed with NaHCO<sub>3</sub> solution (1.0 M, 3 × 50 mL) and brine (50 mL) and then dried over Na<sub>2</sub>SO<sub>4</sub>. The solvent was evaporated under reduced pressure, and the resultant crude product was purified by column chromatography (CH<sub>2</sub>Cl<sub>2</sub>/MeOH/NEt<sub>3</sub> 90:5:5) to give **20** as a white solid (70 mg, 39%). <sup>1</sup>H NMR (500 MHz, [D<sub>6</sub>]DMSO): δ = 11.95 (br, 1H, 1'-NH), 10.44 (s, 1H, NH(C=O)), 7.92 (d, *J* = 8.8 Hz, 2H, 3'-H, 5'-H), 7.73 (d, *J* = 8.8 Hz, 2H, 2'-H, 6'-H), 7.58 (d, *J* = 1.0 Hz, 1H, imidazole-H), 6.94 (s, 1H, imidazole-H), 3.61 (s, 2H, 2-H), 2.52 (s, 3H, acetyl-CH<sub>3</sub>) ppm. <sup>13</sup>C NMR (126 MHz, [D<sub>6</sub>]DMSO): δ = 196.46 (acetyl-C=O), 169.29 (C-1), 143.57 (C-1'), 134.95 (imidazole-C), 131.60 (C-4'), 129.47 (C-3', C-5'), 118.25 (C-2', C-6'), 35.87 (C-2), 26.40 (acetyl-CH<sub>3</sub>) ppm (due to poor relaxation, two imidazole-carbon nuclei could not be observed, but the respective hydrogen nuclei were found in the <sup>1</sup>H NMR spectrum). HRMS (ESI): calcd. for C<sub>13</sub>H<sub>14</sub>N<sub>2</sub>O<sub>2</sub> [M+H]<sup>+</sup> 244.1081, found 244.1077. TLC (CH<sub>2</sub>Cl<sub>2</sub>/MeOH/NEt<sub>3</sub> 85:10:5): R<sub>f</sub> = 0.25.

**N-(4-Acetylphenyl)-2-chloroacetamide (21)**: *p*-Aminoacetophenone (1.00 g, 7.41 mmol) and DIPEA (1.40 mL, 8.18 mmol) were dissolved in THF (5 mL). Chloroacetyl chloride (650 μL, 8.16 mmol) was added dropwise, and the reaction mixture was stirred at RT for 20 min. The reaction was quenched by addition of MeOH (15 mL). The mixture was then diluted with EtOAc (200 mL), washed with HCl (0.2 M, 3 × 30 mL) and sat. NaHCO<sub>3</sub> solution (3 × 30 mL) and then dried over Na<sub>2</sub>SO<sub>4</sub>. The solvent was evaporated under reduced pressure to give **21** as a slightly green solid (1.54 g, 98%). <sup>1</sup>H NMR (500 MHz, CDCl<sub>3</sub>): δ = 8.41 (s, 1H, NH), 7.98 (d, *J* = 8.7 Hz, 2H, 3'-H, 5'-H), 7.68 (d, *J* = 8.7 Hz, 2H, 2'-H, 6'-H), 4.22 (s, 2H, 2-H), 2.59 (s, 3H, acetyl-CH<sub>3</sub>) ppm. <sup>13</sup>C NMR (126 MHz, CDCl<sub>3</sub>): δ = 196.95 (acetyl-C=O), 164.14 (C-1), 141.00 (C-1'), 133.90 (C-4'), 129.89 (C-3', C-5'), 119.39 (C-2', C-6'), 42.99 (C-2), 26.61 (acetyl-CH<sub>3</sub>) ppm. HRMS (ESI): calcd. for C<sub>10</sub>H<sub>11</sub>ClNO<sub>2</sub> [M+H]<sup>+</sup> 212.0473, found 212.0466. TLC (CH<sub>2</sub>Cl<sub>2</sub>/MeOH 95:5): R<sub>f</sub> = 0.55.

***N*-(4-Acetylphenyl)-2-iodoacetamide (22):** Alkyl chloride **21** (364 mg, 1.72 mmol) and KI (859 mg, 5.18 mmol) were dissolved in acetone (20 mL), and the reaction mixture was stirred at RT for 15 h. EtOAc (200 mL) was added, the organic layer was washed with NaHCO<sub>3</sub> solution (0.5 M, 3 × 50 mL), HCl (0.5 M, 3 × 50 mL) and brine (50 mL) and then dried over Na<sub>2</sub>SO<sub>4</sub>. The solvent was evaporated under reduced pressure to give **22** as a slightly orange solid (472 mg, 91 %). <sup>1</sup>H NMR (500 MHz, CDCl<sub>3</sub>+CD<sub>3</sub>OD): δ = 7.91 (d, *J* = 9.0 Hz, 2H, 3'-H, 5'-H), 7.63 (d, *J* = 8.8 Hz, 2H, 2'-H, 6'-H), 3.83 (s, 2H, 2-H), 2.55 (s, 3H, acetyl-CH<sub>3</sub>) ppm. <sup>13</sup>C NMR (126 MHz, CDCl<sub>3</sub>+CD<sub>3</sub>OD): δ = 197.53 (acetyl-C=O), 166.56 (C-1), 142.42 (C-1'), 133.09 (C-4), 129.78 (C-3', C-5'), 119.04 (C-2', C-6'), 26.50 (acetyl-CH<sub>3</sub>), -0.71 (C-2) ppm. HRMS (ESI): calcd. for C<sub>10</sub>H<sub>11</sub>INO<sub>2</sub> [M+H]<sup>+</sup> 303.9829, found 303.9824. TLC (petroleum ether/EtOAc 7:3): R<sub>f</sub> = 0.15.

***N*-(4-Acetylphenyl)-2-cyanoacetamide (23):** Cyanoacetic acid (141 mg, 1.66 mmol), DIPEA (580 μL, 3.33 mmol) and EDC hydrochloride (428 mg, 2.23 mmol) were dissolved in CH<sub>2</sub>Cl<sub>2</sub> (10 mL) and the mixture was stirred at RT for 15 min. Then, *p*-aminoacetophenone (205 mg, 1.52 mmol) was added, and the reaction mixture was stirred at RT for 22 h. EtOAc (250 mL) was added, the organic layer was washed with water (2 × 50 mL), HCl (0.2 M, 1 × 50 mL) and brine (50 mL) and then dried over Na<sub>2</sub>SO<sub>4</sub>. The solvent was evaporated under reduced pressure, and the resultant crude product was purified by column chromatography (CH<sub>2</sub>Cl<sub>2</sub>/MeOH 98:2) to give **23** as a white solid (176 mg, 57 %). <sup>1</sup>H NMR (500 MHz, [D<sub>6</sub>]DMSO): δ = 10.62 (s, 1H, NH), 7.95 (d, *J* = 8.8 Hz, 2H, 3'-H, 5'-H), 7.68 (d, *J* = 8.8 Hz, 2H, 2'-H, 6'-H), 3.96 (s, 2H, 2-H), 2.53 (s, 3H, acetyl-CH<sub>3</sub>) ppm. <sup>13</sup>C NMR (126 MHz, [D<sub>6</sub>]DMSO): δ = 196.53 (acetyl-C=O), 161.71 (C-1), 142.60 (C-1'), 132.25 (C-4'), 129.58 (C-3', C-5'), 118.52 (C-2', C-6'), 115.69 (CN), 27.01 (C-2), 26.46 (acetyl-CH<sub>3</sub>) ppm. HRMS (ESI): calcd. for C<sub>11</sub>H<sub>11</sub>N<sub>2</sub>O<sub>2</sub> [M+H]<sup>+</sup> 203.0815, found 203.0813. TLC (CH<sub>2</sub>Cl<sub>2</sub>/MeOH 95:5): R<sub>f</sub> = 0.35.

**Sodium 2-((4-acetylphenyl)amino)-2-oxoethane-1-sulfonate (24):** To a suspension of alkyl chloride **21** (509 mg, 2.40 mmol) in EtOH (6 mL), a solution of Na<sub>2</sub>SO<sub>3</sub> (302 mg, 2.40 mmol) in water (6 mL) was added. The reaction mixture was stirred under reflux for 4 h. The formed precipitate was filtered off, washed with cold water and dried to give **24** as a white solid (473 mg, 70 %). <sup>1</sup>H NMR (500 MHz, [D<sub>6</sub>]DMSO): δ = 10.31 (s, 1H, NH), 7.92 (d, *J* = 8.8 Hz, 2H, 3'-H, 5'-H), 7.71 (d, *J* = 8.8 Hz, 2H, 2'-H, 6'-H), 3.57 (s, 2H, 1-H), 2.52 (s, 3H, acetyl-CH<sub>3</sub>) ppm. <sup>13</sup>C NMR (126 MHz, [D<sub>6</sub>]DMSO): δ = 196.49 (acetyl-C=O), 165.01 (C-2), 143.43 (C-1'), 131.58 (C-4'), 129.47 (C-3', C-5'), 118.18 (C-2', C-6'), 59.10 (C-1), 26.42 (acetyl-CH<sub>3</sub>) ppm. HRMS (ESI): calcd. for C<sub>10</sub>H<sub>12</sub>NO<sub>5</sub> [M(acid)+H]<sup>+</sup> 258.0431, found 258.0428. TLC (CH<sub>2</sub>Cl<sub>2</sub>/MeOH 95:5): R<sub>f</sub> = 0.00.

**Sodium 2-((4-acetylphenyl)amino)-2-oxoethyl(methyl)phosphinate (25):** General procedure **GP2** with ethyl ester **27** (50 mg, 0.18 mmol) to give **25** as a white solid (23 mg, 44 %). <sup>1</sup>H NMR (500 MHz, [D<sub>6</sub>]DMSO): δ = 10.77 (s, 1H, NH), 7.87 (d, *J* = 8.8 Hz, 2H, 3'-H, 5'-H), 7.71 (d, *J* = 8.8 Hz, 2H, 2'-H, 6'-H), 2.96 (d, *J* = 17.7 Hz, 2H, 1-H), 2.50 (br, 3H (under solvent signal), acetyl-CH<sub>3</sub>), 1.42 (d, *J* = 14.8 Hz, 3H, PCH<sub>3</sub>) ppm. <sup>13</sup>C NMR (126 MHz, [D<sub>6</sub>]DMSO): δ = 196.42 (acetyl-C=O), 166.00 (C-1), 143.69 (C-1'), 131.51 (C-4'), 129.37 (C-3', C-5'), 118.17 (C-2', C-6'), 42.13 (d, *J*<sub>CP</sub> = 78.7 Hz, C-1), 26.36 (acetyl-CH<sub>3</sub>), 16.29 (d, *J*<sub>CP</sub> = 97.7 Hz, PCH<sub>3</sub>) ppm. <sup>31</sup>P NMR (162 MHz, [D<sub>6</sub>]DMSO): δ = 37.80 ppm. HRMS (ESI): calcd. for C<sub>11</sub>H<sub>13</sub>NO<sub>3</sub>P [M(acid)+H]<sup>+</sup> 256.0733, found: 256.0730. TLC (CH<sub>2</sub>Cl<sub>2</sub>/MeOH/HCOOH 85:13:2): R<sub>f</sub> = 0.05.

**Disodium 2-((4-acetylphenyl)amino)-2-oxoethylphosphonate (26):** General procedure **GP2** with ethyl ester **28** (182 mg, 0.581 mmol) to give **26** as a slightly orange solid (89 mg, 60 %). <sup>1</sup>H NMR (500 MHz, CD<sub>3</sub>OD): δ = 8.62 (d, *J* = 8.8 Hz, 3'-H, 5'-H), 8.27 (d, *J* = 8.8 Hz, 2'-H, 6'-H), 3.64 (d, *J* = 21.0 Hz, 1-H), 3.26 (s, 3H, acetyl-

CH<sub>3</sub>) ppm. <sup>13</sup>C NMR (126 MHz, CD<sub>3</sub>OD): δ = 213.57 (acetyl-C=O), 179.12 (C-2), 153.54 (C-1'), 143.67 (C-4'), 141.13 (C-3', C-5'), 131.27 (C-2', C-6'), 49.60 (d, *J*<sub>CP</sub> = 122.2 Hz, C-1), 37.16 (acetyl-CH<sub>3</sub>). <sup>31</sup>P NMR (203 MHz, CD<sub>3</sub>OD): δ = 15.82 ppm. HRMS (ESI): calcd. for C<sub>13</sub>H<sub>21</sub>NO<sub>4</sub>P [M(acid)+H]<sup>+</sup> 258.0526, found: 258.0523.

**Ethyl 2-((4-acetylphenyl)amino)-2-oxoethyl(methyl)phosphinate (27):** Alkyl chloride **21** (113 mg, 0.536 mmol) was dissolved in a mixture of toluene (2 mL) and THF (2 mL). At 100 °C, diethyl methylphosphonate (200 μL, 1.33 mmol) was added dropwise over 10 min. The reaction mixture was stirred at 100 °C for 23 h. After cooling to RT, the solvent was evaporated under reduced pressure, and the resultant crude product was purified by column chromatography (CH<sub>2</sub>Cl<sub>2</sub>/MeOH 98:2) to give **27** as a white solid (113 mg, 75 %). <sup>1</sup>H NMR (500 MHz, CDCl<sub>3</sub>): δ = 9.97 (s, 1H, NH), 7.73 (d, *J* = 8.8 Hz, 2H, 3'-H, 5'-H), 7.51 (d, *J* = 8.8 Hz, 2H, 2'-H, 6'-H), 4.19–4.12 (m, 2H, ethyl-1-H), 3.19 (dd, *J* = 18.9, 14.3 Hz, 1H, 1-H<sub>a</sub>), 2.99 (dd, *J* = 14.3, 14.3 Hz, 1H, 1-H<sub>b</sub>), 2.50 (s, 3H, acetyl-CH<sub>3</sub>), 1.72 (d, *J* = 14.5 Hz, 3H, PCH<sub>3</sub>), 1.37 (t, *J* = 7.0 Hz, 3H, ethyl-2-H) ppm. <sup>13</sup>C NMR (126 MHz, CDCl<sub>3</sub>): δ = 197.02 (acetyl-C=O), 163.42 (d, *J*<sub>CP</sub> = 3.8 Hz, C-2), 142.54 (C-1'), 132.74 (C-4'), 129.52 (C-3', C-5'), 118.86 (C-2', C-6'), 61.57 (d, *J*<sub>CP</sub> = 6.5 Hz, ethyl-C-1), 40.35 (d, *J*<sub>CP</sub> = 81.2 Hz, C-1), 26.48 (acetyl-CH<sub>3</sub>), 16.71 (d, *J*<sub>CP</sub> = 6.2 Hz, ethyl-C-2), 14.78 (d, *J*<sub>CP</sub> = 97.3 Hz, PCH<sub>3</sub>) ppm. <sup>31</sup>P NMR (203 MHz, CDCl<sub>3</sub>): δ = 49.31 ppm. HRMS (ESI): calcd. for C<sub>13</sub>H<sub>19</sub>NO<sub>4</sub>P [M+H]<sup>+</sup> 284.1046, found 284.1043. TLC (CH<sub>2</sub>Cl<sub>2</sub>/MeOH 95:5): R<sub>f</sub> = 0.15.

**Diethyl 2-((4-acetylphenyl)amino)-2-oxoethylphosphonate (28):** Alkyl chloride **21** (146 mg, 0.692 mmol) was suspended in triethylphosphite (2.30 mL, 13.3 mmol) and the reaction mixture was stirred under reflux for 18 h. After cooling to RT, the solvent was evaporated under reduced pressure, and the resultant oily crude product was purified by column chromatography (petroleum ether/EtOAc 1:2→1:5) to give **28** as a white solid (193 mg, 89 %). <sup>1</sup>H NMR (500 MHz, CDCl<sub>3</sub>): δ = 9.53 (s, 1H, NH), 7.81 (d, *J* = 8.7 Hz, 2H, 3'-H, 5'-H), 7.56 (d, *J* = 8.8 Hz, 2H, 2'-H, 6'-H), 4.24–4.18 (m, 4H, ethyl-1-H), 3.08 (d, *J* = 21.1 Hz, 2H, 1-H), 2.53 (s, 3H, acetyl-CH<sub>3</sub>), 1.38 (t, *J* = 7.1 Hz, 6H, ethyl-2-H) ppm. <sup>13</sup>C NMR (126 MHz, CDCl<sub>3</sub>): δ = 197.03 (acetyl-C=O), 162.61 (d, *J* = 3.9 Hz, C-2), 142.32 (C-1'), 132.94 (C-4'), 129.65 (C-3', C-5'), 118.98 (C-2', C-6'), 63.33 (d, *J*<sub>CP</sub> = 6.8 Hz, ethyl-C-1), 36.50 (d, *J*<sub>CP</sub> = 129.3 Hz, C-1), 26.51 (acetyl-CH<sub>3</sub>), 16.49 (d, *J*<sub>CP</sub> = 6.1 Hz, ethyl-C-2) ppm. <sup>31</sup>P NMR (203 MHz, CDCl<sub>3</sub>): δ = 22.49 ppm. MS (ESI): *m/z* = 336.0 [M+Na]<sup>+</sup>. TLC (CH<sub>2</sub>Cl<sub>2</sub>/MeOH 9:1): R<sub>f</sub> = 0.55.

**FRET-based collagenase inhibition assay:** The peptidase domain (PD) of ColH (Uniprot: Q46085; Leu331-Gly721) and the collagenase unit of ColQ1 (ColQ1-CU; Uniprot: B9J354; Tyr94-Gly765) were expressed and purified as previously described.<sup>[24]</sup> IC<sub>50</sub> measurements were performed as previously reported.<sup>[13]</sup> ColH-PD was pretreated with the compounds at RT for 1 h. The reaction was initiated by the addition of 2 μM of the peptide substrate Mca-Ala-Gly-Pro-Gly-Pro-Dpa-Gly-Arg-NH<sub>2</sub> (FS1-1; Mca = (7-methoxycoumarin-4-yl)acetyl; Dpa = *N*-3-(2,4-dinitrophenyl)-L-2,3-diaminopropionyl). The increase in fluorescence was monitored for 2 min ( $\lambda_{\text{exc}}$  = 328 nm;  $\lambda_{\text{em}}$  = 392 nm) at 25 °C. The final concentrations were 10 nM ColH-PD and 1 nM ColQ1-CU, respectively, 2 μM FS1-1, 250 mM HEPES pH 7.5, 400 mM NaCl, 10 mM CaCl<sub>2</sub>, 10 μM ZnCl<sub>2</sub>, 2% DMSO and eight different compound concentrations. The percentage of enzyme inhibition was calculated in relation to a blank reference without compound added. All experiments were performed in triplicates and repeated at least three times. IC<sub>50</sub> values were determined using nonlinear regression with a constant Hill slope of -1. Regression analysis was performed using GraphPad Prism 5 (Graph Pad Software, San Diego, CA, USA).

**MMP inhibition assay:** The catalytic domains of MMP-1, -2, -3, -7, -8, and -14 along with the Sensolyte 520 generic MMP activity kit were purchased from AnaSpec (Fremont, CA, USA). The

assay was performed as previously described using Batimastat as a positive control<sup>[13,25]</sup> and according to the guidelines of the manufacturer.

**HDAC inhibition assay:** HDAC3 and HDAC8 inhibitor screening kits were purchased from Sigma–Aldrich. The assay was performed according to the guidelines of the manufacturer. Fluorescence signals were measured in a CLARIOstar plate reader (BMG Labtech).

**TACE inhibition assay:** A TACE (ADAM-17) inhibitor screening assay kit was purchased from Sigma–Aldrich. The assay was performed according to the guidelines of the manufacturer. Fluorescence signals were measured in a CLARIOstar plate reader (BMG Labtech).

**Cytotoxicity assay:** HepG2, HEK293, or A549 cells ( $2 \times 10^5$  cells per well) were seeded in 24-well, flat-bottomed plates. Culturing of cells, incubations, and OD measurements were performed as previously described<sup>[26]</sup> with minor modifications. 24 h after seeding the cells, the incubation was started by the addition of compounds at a final DMSO concentration of 1%. The living cell mass was determined after 48 h. At least two independent measurements were performed for each compound.

**Zebrafish embryo toxicity assay:** Toxicity testing was performed according to the procedure described in the literature<sup>[27]</sup> with minor modifications using zebrafish embryos of the AB wild-type line at 1 d post fertilisation (dpf) as previously reported.<sup>[16]</sup> All of the described experiments were performed with zebrafish embryos < 120 h post-fertilisation (hpf) and are not classified as animal experiments according to EU Directive 2010/63/EU. Protocols for husbandry and care of adult animals were in accordance with the German Animal Welfare Act (S11 Abs. 1 TierSchG).

**Ex vivo pig skin degradation assay:** The assay was performed as previously reported<sup>[6]</sup> using explants from pig ears in a 24-well plate. Compound **26** was preincubated with 300 nM of ColQ1, 4 mM CaCl<sub>2</sub>, 10 μM ZnCl<sub>2</sub> in DMEM medium at 37 °C and 5% CO<sub>2</sub> for 1 h. After preincubation, one skin explant was added into each well and incubated at 37 °C and 5% CO<sub>2</sub> for 24 h under 300 rpm shaking. Hydroxyproline release was measured using a hydroxyproline assay kit (Sigma–Aldrich) according to the guidelines of the manufacturer. Absorbance was measured using a PHERAstar plate reader (BMG Labtech). The absorbance values were converted into hydroxyproline concentrations (μg/mL) using a calibration curve of hydroxyproline (Figures S1 and S2 in the Supporting Information). The absolute concentrations were converted into percentages by setting the concentration of the 0 μM value to 100% and calculating all values from each experiment separately.

## Acknowledgements

We thank Dr. Stefan Boettcher and Stefanie Weck for the measurements of high-resolution mass spectra as well as Nathalie Andreia, Martina Jankowski, Jeannine Jung, Dennis Jener and Martina Wiesbauer for technical support. We acknowledge financial support by the Austrian Science Fund (FWF, grants P 31843 (E.S.) and W 01213 (H.B.)), the Austrian Federal Ministry of Science, Research, and Economy (H.B.), the European Research Council (ERC starting grant 757913, A.K.H.H.), and by the Helmholtz Association's Initiative and Networking Fund (A.K.H.H.). Open access funding enabled and organized by Projekt DEAL.

## Conflict of Interest

The authors declare no conflict of interest.

**Keywords:** anti-infectives · drug design · medicinal chemistry · metalloenzymes · structure–activity relationships

- [1] a) J. O'Neill, *Antimicrobial Resistance: Tackling a Crisis for the Health and Wealth of Nations*, UK Government & Wellcome Trust, London, 2014; b) *Drug-Resistant Infections: A Threat to Our Economic Future*, The World Bank, Washington DC, 2017.
- [2] *No Time to Wait: Securing the Future from Drug-Resistant Infections*, The World Health Organization, 2019.
- [3] a) A. E. Clatworthy, E. Pierson, D. T. Hung, *Nat. Chem. Biol.* **2007**, *3*, 541–548; b) D. A. Rasko, V. Sperandio, *Nat. Rev. Drug Discovery* **2010**, *9*, 117–128; c) M. B. Calvert, V. R. Jumde, A. Titz, *Beilstein J. Org. Chem.* **2018**, *14*, 2607–2617.
- [4] a) C. L. Hatheway, *Clin. Microbiol. Rev.* **1990**, *3*, 66–98; b) C. T. Supuran, in *Drug Design of Zinc-Enzyme Inhibitors* (Eds.: C. T. Supuran, J.-Y. Winum), Wiley, Hoboken, 2009, pp. 721–729.
- [5] a) H. Bruggemann, S. Baumer, W. F. Fricke, A. Wierzer, H. Liesegang, I. Decker, C. Herzberg, R. Martinez-Arias, R. Merkl, A. Henne, G. Gottschalk, *Proc. Natl. Acad. Sci. USA* **2003**, *100*, 1316–1321; b) M. P. Burke, K. Opekin, *Am. J. Forensic Med. Pathol.* **1999**, *20*, 158–162.
- [6] a) R. Stone, *Science* **2002**, *297*, 1110–1112; b) S. S. Arnon, R. Schlechter, T. V. Inglesby, D. A. Henderson, J. G. Bartlett, M. S. Ascher, E. Eitzen, A. D. Fine, J. Hauer, M. Layton, S. Lillibridge, M. T. Osterholm, T. O'Toole, G. Parker, T. M. Perl, P. K. Russell, D. L. Swerdlow, K. Tonat, *J. Am. Med. Assoc.* **2001**, *285*, 1059–1070.
- [7] D. J. Harrington, *Infect. Immun.* **1996**, *64*, 1885–1891.
- [8] a) U. Eckhard, P. F. Huesgen, H. Brandstetter, C. M. Overall, *J. Proteomics* **2014**, *100*, 102–114; b) M. R. Popoff, P. Bouvet, *Future Microbiol.* **2009**, *4*, 1021–1064.
- [9] a) N. Oshima, Y. Narukawa, T. Takeda, F. Kiuchi, *J. Nat. Med.* **2013**, *67*, 240–245; b) A. Scozzafava, C. T. Supuran, *Bioorg. Med. Chem. Lett.* **2002**, *12*, 2667–2672; c) M. Ilies, M. D. Banciu, A. Scozzafava, M. A. Ilies, M. T. Capriou, C. T. Supuran, *Bioorg. Med. Chem.* **2003**, *11*, 2227–2239; d) B. W. Clare, A. Scozzafava, C. T. Supuran, *J. Med. Chem.* **2001**, *44*, 2253–2258; e) C. T. Supuran, A. Scozzafava, *Eur. J. Pharm. Sci.* **2000**, *10*, 67–76; f) M. Amélia Santos, S. Marques, M. Gil, M. Tegoni, A. Scozzafava, C. T. Supuran, *J. Enzyme Inhib. Med. Chem.* **2003**, *18*, 233–242.
- [10] a) M. D. Shoulders, R. T. Raines, *Ann. Rev. Biochem.* **2009**, *78*, 929–958; b) M. Gauza-Włodarczyk, L. Kubisz, D. Włodarczyk, *Int. J. Biol. Macromol.* **2017**, *104*, 987–991.
- [11] U. Eckhard, E. Schönauer, D. Nüss, H. Brandstetter, *Nat. Struct. Mol. Biol.* **2011**, *18*, 1109–1114.
- [12] a) B. W. Matthews, *Acc. Chem. Res.* **1988**, *21*, 333–340; b) B. L. Vallee, D. S. Auld, *Proc. Natl. Acad. Sci. USA* **1990**, *87*, 220–224; c) L. L. Johnson, A. G. Pavlovsky, A. R. Johnson, J. A. Janowicz, C. F. Man, D. F. Ortwine, C. F. Purchase II, A. D. White, D. J. Hupe, *J. Biol. Chem.* **2000**, *275*, 11026–11033; d) D. Xu, H. Guo, *J. Am. Chem. Soc.* **2009**, *131*, 9780–9788.
- [13] E. Schönauer, A. M. Kany, J. Hauptenthal, K. Hüsecken, I. J. Hoppe, K. Voos, S. Yahiaoui, B. Elsässer, C. Ducho, H. Brandstetter, R. W. Hartmann, *J. Am. Chem. Soc.* **2017**, *139*, 12696–12703.
- [14] a) H. Nagase, R. Visse, G. Murphy, *Cardiovasc. Res.* **2006**, *69*, 562–573; b) G. B. Fields, *J. Biol. Chem.* **2013**, *288*, 8785–8793.
- [15] a) F. Graef, B. Vukosavljevic, J.-P. Michel, M. Wirth, O. Ries, C. De Rossi, M. Windbergs, V. Rosilio, C. Ducho, S. Gordon, C.-M. Lehr, *J. Controlled Release* **2016**, *243*, 214–224; b) H. Nikaïdo, *Science* **1994**, *264*, 382–388.
- [16] J. Konstantinović, S. Yahiaoui, A. Alhayek, J. Hauptenthal, E. Schönauer, A. Andreas, A. M. Kany, R. Müller, J. Köhnke, F. Berger, M. Bischoff, R. W. Hartmann, H. Brandstetter, A. K. H. Hirsch, *J. Med. Chem.* **2020**, *63*, 8359–8368.
- [17] a) R. A. Cuperus, A. O. Muijsers, R. Wever, *Arthritis Rheumatism* **1985**, *28*, 1228–1233; b) F.-M. Klingler, T. A. Wichelhaus, D. Frank, J. Cuesta-Bernal, J. El-Delik, H. F. Müller, H. Sjuts, S. Göttig, A. Koenigs, K. M. Pos, D. Pogoryelov, E. Proschak, *J. Med. Chem.* **2015**, *58*, 3626–3630; c) R. M. Rydzewski, *Real World Drug Discovery: A Chemist's Guide to Biotech and Pharmaceutical Research*, Elsevier, Oxford, 2008.
- [18] a) J. A. Jacobsen, J. L. Major Jourden, M. T. Miller, S. M. Cohen, *Biochim. Biophys. Acta Mol. Cell Res.* **2010**, *1803*, 72–94; b) C. Temperini, A.

- Innocenti, A. Guerri, A. Scozzafava, S. Rusconi, C. T. Supuran, *Bioorg. Med. Chem. Lett.* **2007**, *17*, 2210–2215; c) B. Trzaskowski, L. Adamowicz, P. A. Deymier, *J. Biol. Inorg. Chem.* **2007**, *13*, 133–137; d) L. Birch, R. Bachofen, *Experientia* **1990**, *46*, 827–834; e) J. R. Van Wazer, C. F. Callis, *Chem. Rev.* **1958**, *58*, 1011–1046.
- [19] a) R. A. Black, C. T. Rauch, C. J. Kozlosky, J. J. Peschon, J. L. Slack, M. F. Wolfson, B. J. Castner, K. L. Stocking, P. Reddy, S. Srinivasan, N. Nelson, N. Boiani, K. A. Schooley, M. Gerhart, R. Davis, J. N. Fitzner, R. S. Johnson, R. J. Paxton, C. J. March, D. P. Cerretti, *Nature* **1997**, *385*, 729–733; b) M. L. Moss, S.-L. C. Jin, M. E. Milla, W. Burkhart, H. L. Carter, W.-J. Chen, W. C. Clay, J. R. Didsbury, D. Hassler, C. R. Hoffman, T. A. Kost, M. H. Lambert, M. A. Leesnitzer, P. McCauley, G. McGeehan, J. Mitchell, M. Moyer, G. Pahel, W. Rocque, L. K. Overton, F. Schoenen, T. Seaton, J.-L. Su, J. Warner, D. Willard, J. D. Becherer, *Nature* **1997**, *385*, 733–736.
- [20] D. Schlüter, M. Deckert, *Microb. Infect.* **2000**, *2*, 1285–1292.
- [21] P. Sensi, *Clin. Infect. Dis.* **1983**, *5*, S402–S406.
- [22] a) G. Minotti, P. Menna, E. Salvatorelli, G. Cairo, L. Gianni, *Pharmacol. Rev.* **2004**, *56*, 185–229; b) C. Bertazzoli, C. Rovero, L. Ballerini, B. Lux, F. Balconi, V. Antongiovanni, U. Magrini, *Toxicol. Appl. Pharmacol.* **1985**, *79*, 412–422.
- [23] a) A. L. Rubinstein, *Expert Opin. Drug Metab. Toxicol.* **2006**, *2*, 231–240; b) Y. Li, X. Miao, T. Chen, X. Yi, R. Wang, H. Zhao, S. M.-Y. Lee, X. Wang, Y. Zheng, *Colloids Surf. B* **2017**, *156*, 227–235; c) U. J. Pyati, A. T. Look, M. Hammerschmidt, *Sem. Cancer Biol.* **2007**, *17*, 154–165; d) P. McGrath, C.-Q. Li, *Drug Discovery Today* **2008**, *13*, 394–401.
- [24] a) U. Eckhard, E. Schönauer, H. Brandstetter, *J. Biol. Chem.* **2013**, *288*, 20184–20194; b) I. J. Hoppe, H. Brandstetter, E. Schönauer, *Sci. Rep.* **2021**, *11*, 4187.
- [25] A. M. Kany, A. Sikandar, J. Haupenthal, S. Yahiaoui, C. K. Maurer, E. Proschak, J. Köhnke, R. W. Hartmann, *ACS Infect. Dis.* **2018**, *4*, 988–997.
- [26] J. Haupenthal, C. Baehr, S. Zeuzem, A. Piiper, *Int. J. Cancer* **2007**, *121*, 206–210.
- [27] J. Maes, L. Verlooy, O. E. Buenafe, P. A. M. de Witte, C. V. Esguerra, A. D. Crawford, *PLoS One* **2012**, *7*, e43850.

---

Manuscript received: December 23, 2020  
Accepted manuscript online: January 27, 2021  
Version of record online: March 16, 2021

**Chapter C: Inhibition of Collagenase Q1 of *Bacillus cereus* as a Novel Antivirulence Strategy for the Treatment of Skin-Wound Infections**

Alaa Alhayek, Essak S. Khan, Esther Schönauer, Tobias Däinghaus, Roya Shafiei, Katrin Voos, Mitchell K. L. Han, Christian Ducho, Gernot Posselt, Silja Wessler, Hans Brandstetter, Jörg Hauptenthal, Aránzazu del Campo\* and Anna K. H. Hirsch\*

\* corresponding authors

Reprinted with permission from *Adv. Ther.* **2022**, 5, 2100222

DOI: 10.1002/adtp.202100222

Copyright (2021) Wiley & Chemistry Europe

*As this chapter comprises a publication, compound numbers of this chapter are independent from other parts of this thesis.*

### III. Published Results

#### **Full contribution report:**

A. K. H. H., J. H., and A. A. conceived and coordinated the study. A. A. established and performed the *in vitro* cell-based assays, *ex vivo* pig skin model, and the *in vivo* survival study with *Galleria mellonella* model. A.A. further conducted the *in vitro* collagen-cleavage assay, the MTT assay, and the live/dead imaging of the cells. R. S. was involved in performing the *in vitro* cell-based assays and the survival study with the *in vivo* *G. mellonella* model. E. S. and H. B. performed the *in vitro* peptidolytic and gelatinolytic assays and conducted the docking study. E. S. K., T. D., and A. d. C. were involved in the imaging of the tissue. E. S. and A. A. contributed to the first analysis of the tissue images. M. K. L. H. and A. d. C. performed the final evaluation of the tissue images. K. V. synthesized compound 1. C. D. supervised the synthesis of compound 1. G. P. and S. W. prepared the supernatant of the *Bacillus cereus* bacteria. A. A. and A. K. H. H. prepared the figures and wrote the manuscript. All authors reviewed the results and approved the final version of the manuscript.

# Inhibition of Collagenase Q1 of *Bacillus cereus* as a Novel Antivirulence Strategy for the Treatment of Skin-Wound Infections

Alaa Alhayek, Essak S. Khan, Esther Schönauer, Tobias Däinghaus, Roya Shafiei, Katrin Voos, Mitchell K. L. Han, Christian Ducho, Gernot Posselt, Silja Wessler, Hans Brandstetter, Jörg Haupenthal, Aránzazu del Campo, and Anna K. H. Hirsch\*

Despite the progress in surgical techniques and antibiotic prophylaxis, opportunistic wound infections with *Bacillus cereus* remain a public health problem. Secreted toxins are one of the main factors contributing to *B. cereus* pathogenicity. A promising strategy to treat such infections is to target these toxins and not the bacteria. Although the exoenzymes produced by *B. cereus* are thoroughly investigated, little is known about the role of *B. cereus* collagenases in wound infections.

In this report, the collagenolytic activity of secreted collagenases (Col) is characterized in the *B. cereus* culture supernatant (csn) and its isolated recombinantly produced ColQ1 is characterized. The data reveals that ColQ1 causes damage on dermal collagen (COL). This results in gaps in the tissue, which might facilitate the spread of bacteria. The importance of *B. cereus* collagenases is also demonstrated in disease promotion using two inhibitors. Compound 2 shows high efficacy in peptidolytic, gelatinolytic, and COL degradation assays. It also preserves the fibrillar COLs in skin tissue challenged with ColQ1, as well as the viability of skin cells treated with *B. cereus* csn. A *Galleria mellonella* model highlights the significance of collagenase inhibition in vivo.

diarrheal food poisoning worldwide, but also associated with serious opportunistic non-gastrointestinal-tract infections.<sup>[1,2]</sup> Moreover, it is able to cause wound infections.<sup>[1,3,4]</sup> Like many pathogenic bacteria, *B. cereus* is currently evolving multi-drug resistance,<sup>[5-7]</sup> which narrows the choice of possible treatments and consequently increases economic costs, morbidity, and mortality rates.<sup>[8-10]</sup> To overcome this therapeutic crisis, the development of new antibiotics will not produce lasting success, but alternative strategies need to be employed to cope with resistance development.<sup>[11]</sup> To combat the emergence of resistance, the development of antivirulence agents targeting the pathogenicity of bacteria rather than their viability, has gained major interest.<sup>[11-13]</sup> These agents specifically block the virulence factors involved in bacterial invasion and colonization of the host.<sup>[14]</sup> This reduces the selection pressure for drug-resistant mutants

and provides a window of opportunity for the host immune system to eliminate the bacteria.<sup>[7,11,13]</sup> The pathogenicity of *B. cereus* arises from the production and dissemination of tissue-destructive exoenzymes such as hemolysins, phospholipases, and proteases.<sup>[1,15,16]</sup> It is believed that these exoenzymes assist

## 1. Introduction

*Bacillus cereus* (*B. cereus*) is a widely distributed Gram-positive bacterium. This bacterium is the major cause of emetic and

A. Alhayek, R. Shafiei, J. Haupenthal, A. K. H. Hirsch  
Helmholtz Institute for Pharmaceutical Research Saarland (HIPS)  
Helmholtz Centre for Infection Research (HZI)  
38124 Saarbrücken, Germany  
E-mail: anna.hirsch@helmholtz-hips.de


A. Alhayek, A. K. H. Hirsch  
Department of Pharmacy  
Saarland University, Saarbrücken Campus  
Campus E8.1, 66123 Saarbrücken, Germany

E. S. Khan, T. Däinghaus, M. K. L. Han, A. del Campo  
Leibniz Institute for New Materials (INM)  
Saarland University  
Campus D2 2, 66123 Saarbrücken, Germany

A. del Campo  
Chemistry Department  
Saarland University  
66123 Saarbrücken, Germany

E. Schönauer, G. Posselt, S. Wessler, H. Brandstetter  
Department of Biosciences and Medical Biology  
Hellbrunner Str. 34  
University of Salzburg  
Salzburg 5020, Austria

K. Voos, C. Ducho  
Department of Pharmacy  
Pharmaceutical and Medicinal Chemistry  
Saarland University  
Campus C2 3, 66123 Saarbrücken, Germany

 The ORCID identification number(s) for the author(s) of this article can be found under <https://doi.org/10.1002/adtp.202100222>

© 2022 The Authors. *Advanced Therapeutics* published by Wiley-VCH GmbH. This is an open access article under the terms of the Creative Commons Attribution License, which permits use, distribution and reproduction in any medium, provided the original work is properly cited.

DOI: 10.1002/adtp.202100222



in maintaining the infection, allowing the bacteria to reach multiple sites in the body and to evade the immune system. There have been only few studies to support the idea of *Bacillus* exoenzymes contributing to the pathology of wound infections and little evidence to elucidate the direct role of specific toxins during the infection.<sup>[17,18]</sup>

The skin is the largest and most exposed of all human organs and, therefore, most prone to injury.<sup>[19]</sup> The dermal layer makes up 90% of the skin structure.<sup>[20]</sup> The architecture and integrity of the dermis are maintained by COL. COL I, II, and III are predominant in the extracellular matrix (ECM) of the skin.<sup>[21,22]</sup> COL fibers are supramolecular structures, COL molecule is made up by regular packing of three supertwisted alpha helices.<sup>[21,22]</sup> The individual alpha chains consist of a repeated three amino acid motif (Glycine-X-Y), with X-Y often being proline (28%) and hydroxyproline (Hyp) (38%).<sup>[21,22]</sup> Because of its highly intertwined structure and high content of specific amino acids (i.e., Glycine-X-Y),<sup>[23]</sup> fibrillar COLs resist most proteases and can be degraded only by certain types of mammalian or bacterial collagenases with unique specificities to degrade COL.<sup>[21,24,25]</sup>

Bacterial wound infection is a public health problem occurring when bacteria adhere to an impaired skin.<sup>[26,27]</sup> After the initial local colonization, bacteria can potentially invade into deeper tissues with the help of necrotic virulence factors such as collagenases.<sup>[26,28]</sup> By degrading the structural COL scaffold of the ECM at multiple sites, bacterial collagenases assist the bacteria in invading the tissue.<sup>[29,30]</sup> Bacterial collagenases belong to the zinc metalloprotease family M9.<sup>[29]</sup> They harbor a collagenase unit, which is accompanied by accessory domains involved in substrate recognition and COL swelling.<sup>[29]</sup> To date, only a few collagenase-secreting bacterial genera (e.g., *Bacillus*, *Clostridium*, and *Vibrio*) have been identified. *Clostridium* collagenases such as ColH and ColG are the best characterized ones.<sup>[29]</sup> *Bacillus* collagenases have received less attention. Their contribution to wound infections however is assumed to be a main factor in the wound-invasion stage.

Here, we report on the establishment of a simple pre-clinical ex vivo pig-skin model to evaluate the effect of COL degradation by *B. cereus* in the skin. Our results showed that the model *B. cereus* collagenase ColQ1 degrades the dermal fibrillar COLs and confirmed it as a promising drug target. Using two small molecules, which we had recently described as inhibitors of the collagenase ColH (produced by *Clostridium histolyticum*)<sup>[31]</sup> and the elastase LasB (produced by *Pseudomonas aeruginosa*)<sup>[32]</sup> we could substantiate that these inhibitors also inhibit *B. cereus* collagenase activity. Indeed, we found that these compounds were able to protect the integrity of the dermal COL in an ex vivo pig-skin model treated with recombinant ColQ1, confirming their potency as broad-spectrum inhibitors of bacterial collagenases, as suggested earlier by Schönauer et al.<sup>[33]</sup> Moreover, these compounds reduced in vitro cytotoxic effects of the *B. cereus* csn, containing various collagenases, toward fibroblast and keratinocyte cell lines, restored their morphology, and improved their adhesion. The toxicity of *B. cereus* csn and ColQ1 was verified in vivo in *Galleria mellonella* larvae. Furthermore, we showed that treatment with collagenase inhibitors significantly improved their survival rate.

## 2. Results and Discussion

### 2.1. *B. cereus* csn and Recombinant *B. cereus* ColQ1 Act as Collagenolytic Agents

To study the effect of bacteria-derived collagenase on COL degradation in skin wounds, we used the recombinant collagenase unit of ColQ1 (Uniprot: B9J3S4)<sup>[34]</sup> and the csn of *B. cereus* ATCC 14 579<sup>[35]</sup> to challenge our skin model. ColQ1 was selected as a model *Bacillus* collagenase to study the isolated effect of this virulence factor in a skin wound setting. ColQ1 is a close homologue of ColA of *B. cereus* ATCC 14 579 (Uniprot: Q81BJ6) and similarly to ColA, it displays a remarkably high peptidolytic and collagenolytic activity compared to clostridial collagenases.<sup>[34]</sup> Both enzymes share an overall sequence identity of 72% and a similarity of 84%. Sequence conservation is higher within the collagenase unit, i.e., the catalytic core of the enzyme, increasing to 79% and 89%, respectively.<sup>[34,36]</sup> Proteolytic activity of ColQ1 and of *B. cereus* csn (which represents a more complex source of COL-degrading factors)<sup>[34,36]</sup> were validated in an in vitro peptidolytic assay using a custom-made collagenase-specific quenched fluorescence substrate.<sup>[33]</sup> The csn of *B. cereus* showed peptidolytic activity that could be completely abrogated by the addition of 20 mM EDTA and was only marginally affected by serine and cysteine protease inhibitors, consistent with its metalloprotease mechanism (Figure S1, Supporting Information). The peptidolytic activity of the csn determined in the presence of serine and cysteine protease inhibitors was comparable to the activity of  $0.9 \pm 0.1 \times 10^{-9}$  M of recombinant collagenase unit of ColQ1. These results were determined based on a standard curve that was generated using recombinant ColQ1 (Figure S2, Supporting Information).

### 2.2. *B. cereus*-Induced COL Degradation Quantified in an Ex vivo Pig-Skin Model

To analyze the collagenolytic activity of *B. cereus* csn and ColQ1 during wound infection, an ex vivo pig-skin model of *B. cereus* infection was established.<sup>[38]</sup> For this purpose, porcine ear skin biopsy punches were treated with different concentrations of *B. cereus* csn (35%, 65%, and 100% v/v) or ColQ1 ( $100 \times 10^{-9}$ ,  $300 \times 10^{-9}$ , and  $500 \times 10^{-9}$  M) to simulate COL matrix degradation after infection with *B. cereus*. The release of hydroxyproline (Hyp) was used as a biomarker for COL breakdown.<sup>[39,40]</sup> While we did not observe Hyp release in non-treated skin preparations, a significant release was detected in skin treated with various concentrations of *Bacillus* csn and ColQ1 (Figure 1a,b). In detail, incubation with 35% (v/v) of the csn led to an increase of Hyp levels to  $22 \pm 6 \mu\text{g mL}^{-1}$  release of Hyp after 24 h, and 100% (v/v) csn, Hyp levels rendered  $60 \pm 4 \mu\text{g mL}^{-1}$  (Figure 1a) Hyp in the supernatant. As we showed before,<sup>[38]</sup> treatment with  $100 \times 10^{-9}$  or  $500 \times 10^{-9}$  M of the enzyme led to  $16 \pm 6 \mu\text{g mL}^{-1}$  and  $51 \pm 10 \mu\text{g mL}^{-1}$  Hyp release after 24 h incubation, respectively (Figure 1b). Longer incubation times led to larger Hyp concentrations until a plateau value was reached. These data confirm that ColQ1 exhibited an effect on collagen degradation that was comparable to the csn. To analyze the collagenase-specific effects, we focused on ColQ1 in the following ex vivo studies.



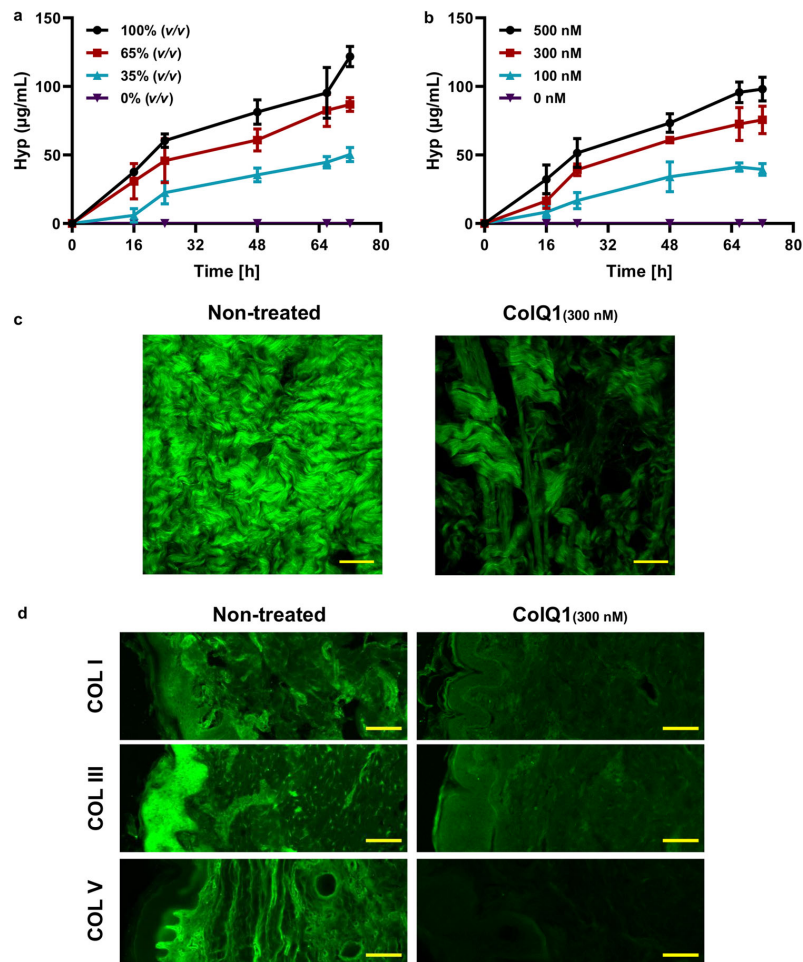


**Figure 1.** The effect of ColQ1 on dermal COL of pig-skin. **a,b)** Quantification of Hyp release over time after treatment with different concentrations of **a)** *B. cereus* csn (0–100% v/v) and **b)** ColQ1 ( $0\text{--}500 \times 10^{-9}$  M). This graph contains data adapted from our previous publication.<sup>[38]</sup> **c)** Confocal SHG Z-stack images of the COL structure in skin dermal region that was non-treated or treated with  $300 \times 10^{-9}$  M ColQ1. **d)** *B. cereus* ColQ1 ( $300 \times 10^{-9}$  M) degraded the fibrillar COLs, immunostaining of non-treated and ColQ1 treated skin with COL antibodies (COL I, III, and V). COL: collagen, Hyp: hydroxyproline, *B. cereus*: *Bacillus cereus*, csn: culture supernatant, SHG: second harmonic generation. Data point represents mean value  $\pm$  standard deviation ( $n = 3$ ). Scale bar: 100  $\mu\text{m}$  for SHG images and immunostained images. Bright-field and DAPI images of the immunostained non-treated and ColQ1-treated tissue are shown in Figure S4, Supporting Information.

We visualized the loss of matrix COL of the skin tissue challenged with ColQ1 using SHG imaging. This method allows a label-free imaging of the COL fibers.<sup>41</sup> The confocal SHG Z-stack images of non-treated skin showed COL structures with the characteristic wave-like morphology of dermal COL<sup>[42]</sup> (Figure 1c). This morphology is essential for elastic integrity and it provides the biomechanical prerequisites necessary to sustain the shape and strength of the skin tissue.<sup>[20,43,44]</sup> In contrast, skin treated with  $300 \times 10^{-9}$  M ColQ1 showed a lower SHG signal and large gaps between the COL structures (Figure 1c). Higher ColQ1 concentrations resulted in fragile

tissue samples and lower ColQ1 concentrations did not show a significant collagenolytic effect (data not shown). Therefore, a concentration of  $300 \times 10^{-9}$  M ColQ1 was chosen for further experiments.

Our evaluation of both COL structure and the released Hyp showed that *B. cereus* collagenases have a highly destructive effect on native COL in skin. Based on the disruptive effect of *B. cereus* collagenase on the collagen matrix, we hypothesize, that collagenolytic activities diminish skin tissue integrity and thus aid passage of the bacteria to deeper dermal layers in settings of wound infection.

### 2.3. ColQ1 Targets Fibrillar COLs in the Dermis

The skin dermis and hypodermis are rich in COL I, which forms heterotypic structures with other COLs such as III and/or V.<sup>[45]</sup> To test the ability of ColQ1 to target these fibrillar COLs in skin, immunostaining of skin samples after the treatment was performed with antibodies against COL I, III, and V followed by epifluorescence imaging of the stained tissue. Non-treated samples showed strong signals for COL I in the dermis, COL III in the epidermis, and around cellular components of the dermis, and COL V in the basal and dermal layers (Figure 1d). Upon treatment with ColQ1 a moderate reduction in the signal of all three fibrillar COLs (i.e., Col I, III, and V) was observed (Figure 1d). These data indicate that ColQ1 is targeting fibrillar COL subtypes enriched in the dermal region. The effect of ColQ1 on fibrillar COLs can be explained by the tertiary and primary structure of the substrate. Fibrillar COLs are mainly composed of one large triple-helical domain (e.g., COL I: 96%) with (Gly-X-Y) tripeptide repeats.<sup>[45]</sup> The active site sequence specificity of bacterial collagenases is perfectly adapted to this tripeptide motif, as it has been shown for clostridial collagenases.<sup>[46]</sup>

### 2.4. Collagenase Inhibitors Neutralize the Collagen Degradation Effect of *B. cereus* Collagenases In vitro

To study whether we could inhibit ColQ1 with small molecules, we investigated two previously described inhibitors of bacterial metalloproteases. Compound 1 is one of the first reported ColH inhibitors ( $IC_{50} = 7 \times 10^{-6}$  M) being stable and selective over several human metalloproteases.<sup>[31]</sup> Compound 2 is a moderately active LasB inhibitor ( $IC_{50} = 17.3 \times 10^{-6}$  M)<sup>[32]</sup> and was a hit in a virtual screening study performed on the active site of ColH.

Using a FRET-based peptidolytic assay with a collagenase-specific substrate as well as a COL cleavage assay with the natural triple-helical substrate of collagenases (i.e., COL I), the impact of these two inhibitors on ColQ1 activity was measured in vitro. The FRET-based assay confirmed that compounds 1 and 2 inhibit ColQ1 with  $IC_{50}$  values of  $183 \pm 7 \times 10^{-6}$  M<sup>[31]</sup> and  $95 \pm 4 \times 10^{-6}$  M, respectively (Figure S3, Supporting Information; Figure 2a). In addition, the COL cleavage assay demonstrated a full collagenase inhibition with protection of the structural integrity of COL I at  $75 \times 10^{-6}$  and  $6 \times 10^{-6}$  M with compounds 1 and 2, respectively (Figure 2b).

To further investigate the activity of compounds 1 and 2, we tested them on the *B. cereus* csn, which contains a heterogeneous mixture of ColA isoforms and other collagenase homologs. The *B. cereus* csn was treated with 1.83 mM ( $10 \times IC_{50}$ ) of compound 1. The FRET-based assay revealed that the proteolytic activity furnished by the csn could be reduced by  $84 \pm 2\%$  compared to the uninhibited control (Figure S1, Supporting Information). Due to the low solubility of compound 2 under assay conditions, compound 2 could only be tested at a concentration of  $95 \times 10^{-6}$  M ( $1 \times IC_{50}$ ). Remarkably, this concentration led to a decrease in the proteolytic activity of  $57 \pm 7\%$  (Figure S1, Supporting Information). The positive control (20 mM EDTA) completely inhibited substrate turnover, while an inhibitor cocktail specific for serine and cysteine proteases reduced the total activity by only  $14 \pm 7\%$  (Figure S1, Supporting Information).

We could qualitatively confirm the inhibitory effect of compounds 1 and 2 on the *B. cereus* csn using gelatin zymography (Figure 2c,d). For this, the csn was separated by electrophoresis and then subjected to an in-gel activity assay. Gelatinolytically active species were detected by the degradation of denatured COL I that had been co-polymerized with the polyacrylamide matrix of the SDS-PAGE gel, visible as white bands in the zymogram. Similar to previous reports,<sup>[35,48]</sup> it revealed the presence of various gelatinolytically active species in the csn of *B. cereus* most prominently at a molecular weight of approx. 115 kDa and smaller. The zymogram performed in presence of i) serine and cysteine protease inhibitors, ii) compound 1, and iii) compound 2 showed a selective reduction of the gelatinolytic activities in all cases (Figure 2c). In particular, the high molecular weight species corresponding to full-length ColA and C-terminally truncated ColA species in the range of 120–80 kDa, as identified before by Abfalter et al.,<sup>[35]</sup> were inhibited by compounds 1 and 2 (Figure 2c).

In all in vitro assays, compound 2 was more active than compound 1. Both compounds not only inhibit ColH, LasB, and ColQ1, as reported previously,<sup>[31,32]</sup> but also demonstrated an inhibitory effect on gelatinases of *B. cereus* csn. We have previously reported a similar broad-spectrum inhibition of *Bacillus* and *Clostridium* collagenases in in vitro assays for closely related compounds,<sup>[33,38]</sup> which might be beneficial in wound infections colonized by multiple bacterial genera.<sup>[28]</sup>

### 2.5. Docking Studies with Bacterial Collagenases Rationalize Differences in Inhibitory Potency

The observed difference in efficacy between compounds 1 and 2 can be rationalized based on the binding mode of both compounds to bacterial collagenases. For this purpose, molecular docking was performed using the crystal structure of the peptidase domain of ColH as target that had been determined at a resolution of 1.87 Å. The crystal structure of the homologue ColH was chosen, as there are to date no high-resolution crystal structures from a *B. cereus* collagenase available to ensure reliable docking results. The peptidase domain of ColH shares 74% and 73% sequence similarity with the peptidase domains of ColA and ColQ1 from *B. cereus*, respectively, and the sequence and topology of the active sites are highly conserved.<sup>[34,35]</sup> Since docking to metalloproteins is non-trivial in drug design, AutoDock Vina v1.2.2<sup>[48]</sup> and the Molecular Forecaster suite<sup>[49]</sup> were both evaluated for this end and their performance judged by their ability to generate poses that comply with standard atom-to-zinc distances and zinc-binding geometries.<sup>[50]</sup> Following this criterion, the Molecular Forecaster suite was used for the final docking of compounds 1 and 2 to ColH.

As expected, we found that the best docking pose for compound 1 showed a similar binding mode as was determined for the *N*-aryl mercaptoacetamide ligand in the complex crystal structure with ColH<sup>[33]</sup> (Figure 3a,b). Both compounds share the same *N*-aryl backbone, but differ in their zinc-binding group. Instead of the thiolate sulfur atom of the mercaptoacetamide compound, the phosphonate oxygen atom of compound 1 is predicted to coordinate the catalytic zinc ion (2.1 Å). The amide oxygen and nitrogen atoms form a hydrogen bond with the main-chain amide nitrogen atom of Tyr428 and the carbonyl oxygen of Glu487, re-

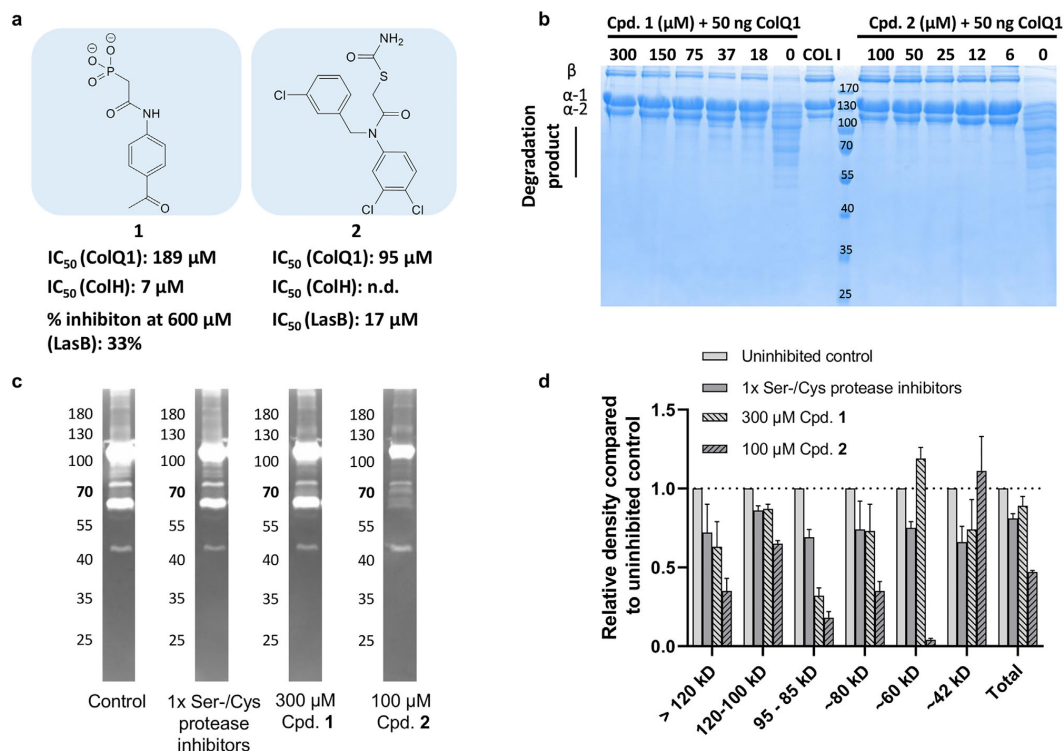


**Figure 2.** Inhibition of ColQ1 and the collagenase of *B. cereus* csn by compounds **1** and **2** in a collagenase-specific peptidic and a gelatinolytic assay. **a)** Chemical structures of compounds **1** and **2** and the calculated  $IC_{50}$  value in the FRET-based ColQ1, ColH,<sup>[31]</sup> and LasB<sup>[32]</sup> inhibition assay. **b)** Effect of ColQ1 inhibitors on the cleavage of COL I after challenge with 50 ng of ColQ1. **c,d)** Effect of compounds **1** and **2** on *B. cereus* csn monitored by **c)** gelatin zymography. The gelatin-degradation assay was performed in the presence of inhibitors or the buffer control. Due to limited solubility in the reaction buffer, compound **2** could only be tested at  $100 \times 10^{-6}$  M compared to  $300 \times 10^{-6}$  M of compound **1**. **d)** Densitometric analysis of gelatin zymography shown in **(c)**. Image analysis was performed with Image Studio Lite v5.2 software (Li-Cor Biosciences, USA). *B. cereus*: *Bacillus cereus*, csn: culture supernatant, COL: collagen, n.d.: not determined.

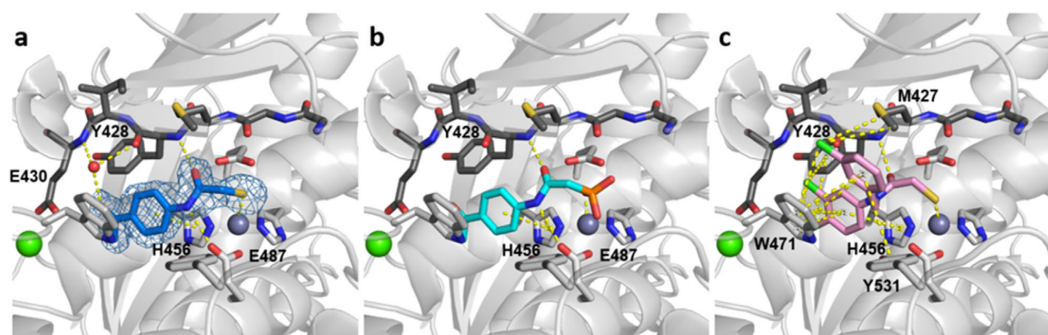


**Figure 3.** Comparison of the crystallized complex of the *N*-aryl mercaptoacetamide compound with the docking poses of compounds **1** and **2** in the active site of ColH. **a)** Close-up view of the active site in ball-and-stick representation. The co-crystallized inhibitor (blue) is shown in sticks with the maximum likelihood weighted  $2Fo - Fc$  electron density map contoured at  $1\sigma$ . Top docking poses of compounds **1** **b)** and of **2** **c)** in the active site of ColH. The catalytic zinc ion (dark gray), calcium ion (green), and water molecule (red) are shown as spheres. The edge strand formed by Gly425 to E430 is shown in dark gray sticks. The figures were prepared using the PyMOL Molecular Graphics System.

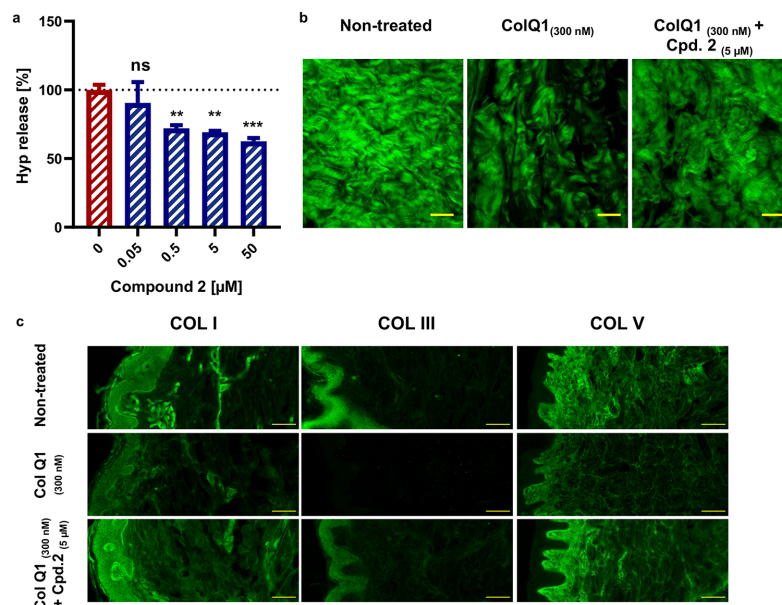


**Figure 4.** Compound 2 suppressed the collagenolytic effect of ColQ1 ex vivo in skin tissue. **a)** Dose-dependent effect of compound 2 quantified by Hyp release assay. **b)** Confocal SHG images showed an improved COL signal with  $5 \times 10^{-6}$  M of compound 2 (tissue challenged with  $300 \times 10^{-9}$  M ColQ1) compared with  $300 \times 10^{-9}$  M ColQ1 without inhibitor. **c)** Immunostaining of fibrillar COLs of the non-treated skin and treated with ColQ1 with or without compound 2. Statistical analysis was performed with one-way ANOVA and statistical significance was analyzed by Tukey test. Significance was calculated by comparing non-treated versus treated tissue with compound 2 (mean  $\pm$  SD, \*\*\*  $p \leq 0.001$ , \*\*  $p \leq 0.01$ ). Hyp: hydroxyproline, COL: collagen, SHG: second harmonic generation. Scale bar: 100  $\mu$ m for SHG images and 100  $\mu$ m for the immunostained images.

spectively, while the aryl ring of compound 1 is involved in a  $\pi$ - $\pi$ -stacking interaction with the imidazole ring of His459 (3.9 Å). In contrast to compound 1, compound 2 has a different, much larger molecular backbone, but shares the same thiol prodrug moiety with the co-crystallized *N*-aryl mercaptoacetamide,<sup>[33]</sup> i.e., a thiocarbamate group. Similarly to the *N*-aryl mercaptoacetamide, we found that the deprotonated sulfur atom of compound 2 can coordinate the active-site zinc cation (2.3 Å), while the amide oxygen forms a hydrogen bond with the main-chain nitrogen atom of Tyr428 (Figure 3c). The active site of ColH can accommodate the two aromatic moieties of compound 2 in the non-primed side via a network of  $\pi$ - $\pi$ -stacking interactions involving His456, Trp471, and Tyr531, which is supported by a parallel network of  $\pi$ -alkyl and  $\pi$ -sigma interactions via the chlorine substituents with Tyr428, Trp471, and Met427. This extensive system of  $\pi$ -interactions found by the docking experiment anchors compound 2 firmly into the active site in-between the upper and lower subdomains of the peptidase domain and it might explain the observed higher efficacy of compound 2 compared to compound 1 that lacks this dense interaction network.

## 2.6. Compounds 1 and 2 Inhibit the Collagenolytic Activity of ColQ1 in an Ex vivo Pig-Skin Model

As compounds 1 and 2 suppressed ColQ1 activity in vitro, we furthermore tested their effects on collagenase activity in the

skin model. Different concentrations of compounds 1 ( $50$ – $400 \times 10^{-6}$  M) and 2 ( $0.05$ – $50 \times 10^{-6}$  M) based on their activity in the different in vitro assays along with  $300 \times 10^{-9}$  M ColQ1 were used. Non-treated and ColQ1-treated samples were used as controls. After one day of incubation, we quantified the release of Hyp and visualized the dermal COL in the skin tissue using SHG and epifluorescence microscopic techniques. Overall, compound 1 resulted in a reduction in Hyp release in a concentration-dependent manner as we had shown previously (Figure S6, Supporting Information).<sup>[31]</sup> A concentration of  $300 \times 10^{-6}$  M of compound 1 was selected for further analysis. Addition of compound 2 at concentrations between  $5$  and  $50 \times 10^{-6}$  M caused a reduction in the release of Hyp by 35% and 48%, respectively (Figure 4a). Based on these data, a concentration of the inhibitory molecule 2 of  $5 \times 10^{-6}$  M was chosen for further analysis.

Next, we performed SHG imaging of samples treated with compounds 1 or 2. The ability of these molecules to reduce the ColQ1-mediated degradation of matrix COL fibers was confirmed compared to the ColQ1-treated control. A higher density of collagen fibers was observed in the presence of both compounds, similar to the morphology of non-treated skin (Figure 4b; Figure S6, Supporting Information). Further experiments were carried out to investigate which COL types (I, III, and V) are protected in presence of compounds 1 and 2. We performed epifluorescence imaging with the tissue treated with  $300 \times 10^{-9}$  M ColQ1 and  $300 \times 10^{-6}$  M compound 1 or  $5 \times 10^{-6}$  M compound 2. Both compounds led to a higher-intensity signal for

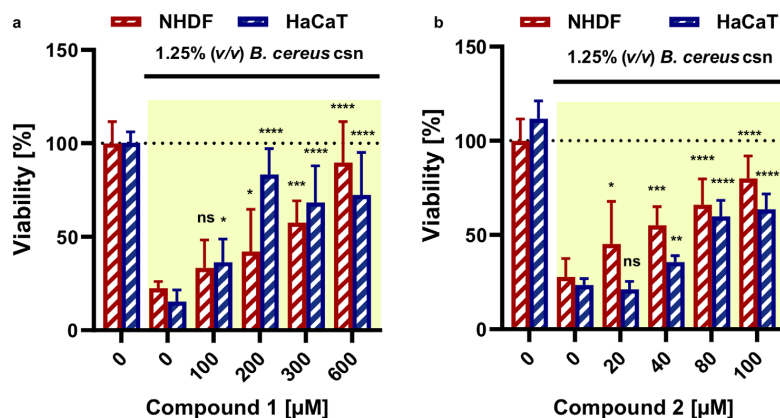


**Figure 5.** Compounds **1** and **2** maintained the viability of skin cells upon treatment with 1.25% (v/v) of *B. cereus* csn. Cell viability calculated after performance of an MTT assay for the cells challenged with *B. cereus* csn with **a**) compounds **1** and **b**) **2**. The data in yellow background indicate cells treated with the csn. Statistical analysis was performed with one-way ANOVA and statistical significance was analysed by Tukey test. Significance was calculated by comparing non-treated versus treated cells with compound **1** and **2** (mean  $\pm$  SD, \*\*\*\*  $p \leq 0.0001$ , \*\*\*  $p \leq 0.001$ , \*\*  $p \leq 0.01$ , \*  $p \leq 0.05$ , and ns: non-significant). *B. cereus*: *Bacillus cereus*, csn: culture supernatant.

COL I, V, and III when compared to the signal of the ColQ1-treated skin control (Figure 4c; Figure S6, Supporting Information). Overall, the results from the ex vivo skin model support the previous results on Hyp release and confirm that ColQ1 inhibition prevents degradation of fibrillar COL. Moreover, the findings underline the higher efficacy of compound **2** compared to compound **1** that had initially been observed in our in vitro assays.

### 2.7. Collagenase Inhibitors Reduce the Cytotoxic Effect of *B. cereus* csn on Human Skin Cell Lines

We further investigated whether the *B. cereus* csn has a cytotoxic effect on skin cells and whether this effect could be inhibited with collagenase targeting pathoblockers (i.e., compounds **1** and **2**). For this purpose, normal human dermal fibroblasts (NHDF) and human epidermal keratinocytes (HaCaT), were chosen due to their ability to produce fibrillar COLs and their roles during wound healing.<sup>[51]</sup>

These cells were exposed to different concentrations of *B. cereus* csn (0–15% v/v). The cytotoxic effect of the csn was evaluated by assessing the viability using a colorimetric MTT assay<sup>[52]</sup> and live/dead staining,<sup>[53]</sup> followed by visualization with epifluorescence microscopy.

A reduction in the viability of the cells was observed depending on the concentration of the *B. cereus* csn (Figure S7, Supporting Information). This cytotoxic effect increased slightly with incubation time of 24 h to 48 h (Figure S7, Supporting Information). The csn appeared more toxic for HaCaT cells than for NHDF cells (Figure S7, Supporting Information). The difference between the toxicity against HaCaT and NHDF cells might be due to the protective effect of fibroblasts provided by its high collagen contents, which help them to maintain the structure of the dermal layer.<sup>[54]</sup> Bright-field images showed a strong detachment of cells, rounding, and shrinkage in both cell lines (example for NHDF

cells is shown in Figure S8, Supporting Information, indicating apoptosis).

To demonstrate the inhibitory effect of compounds **1** and **2** in subsequent experiments, we used 1.25% (v/v) of the *B. cereus* csn, due to the prominent cytotoxic effects observed at this concentration in both NHDF and HaCaT cell lines. Cell viability was dose-dependent, but a significant rescue of viability ( $80 \pm 20\%$  and  $70 \pm 25\%$ ) was observed at  $600 \times 10^{-6}$  and  $100 \times 10^{-6}$  M of compounds **1** and **2**, respectively, in both NHDF and HaCaT cell lines (Figure 5). The live/dead staining results were consistent with the MTT data and showed an increase in the number of viable relative to dead cells (Figure S9, Supporting Information). Both compounds showed high viability at high concentration, which confirms their activity against the collagenase and its isoforms and maybe against other virulence factors. The property of these compounds to restore the viability of NHDF cells is important for a therapeutic context, since fibroblasts are active depositors of matrix proteins in connective tissues in the processes of wound closure.<sup>[51]</sup> Also, keratinocytes play an important role during wound healing, as they fill the gaps in the wound and produce proinflammatory mediators once pathogen invasion starts.<sup>[55,56]</sup> The protection of both cell types by collagenase inhibitors is promising, as their cross-talk is fundamental to assure wound healing and hemostasis.<sup>[57]</sup> Thus, collagenase inhibitors might serve as promising therapeutic agents in the future not only to stop bacterial dissemination but also to accelerate the immune response and subsequently accelerate the wound-healing process.<sup>[58,59]</sup>

### 2.8. Collagenase Inhibitors Diminish the Virulence Activity Induced by ColQ1 and *B. cereus* csn on *Galleria mellonella* Larvae

To examine the virulence of the *B. cereus* collagenase ColQ1 or csn and their inhibition in a simple in vivo model, *Galleria mellonella* larvae were used. This model is accepted as an



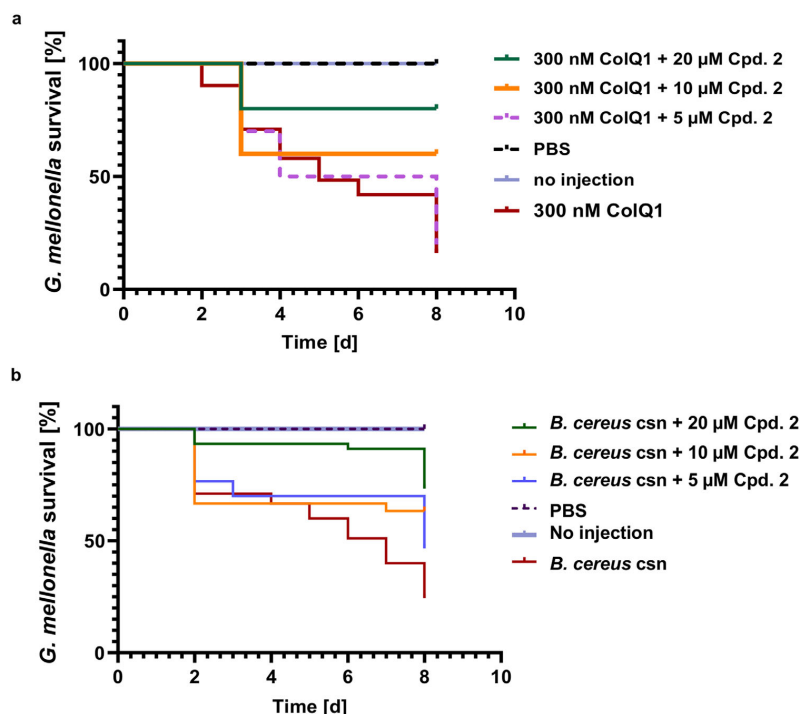


**Figure 6.** Kaplan–Meier survival analysis of larvae treated with *B. cereus* csn with and without compound 2. **a)** Survival analysis of larvae treated with  $300 \times 10^{-9}$  M ColQ1 and with various concentrations ( $5 \times 10^{-6}$ – $20 \times 10^{-6}$  M) compound 2. **b)** The improvement in the survival of larvae challenged with 100% (v/v) *B. cereus* csn and various concentrations of compound 2 ( $5 \times 10^{-6}$ – $20 \times 10^{-6}$  M). The statistical difference between groups treated with 20, 10, and  $5 \times 10^{-6}$  M of compound 2 and treated with only  $300 \times 10^{-9}$  M ColQ1 is  $p < 0.0001$ ,  $p = 0.0042$ , and  $p = 0.5800$ , sequentially (log-rank). The statistical difference between groups treated with 20, 10, and  $5 \times 10^{-6}$  M of compound 2 and treated with only 100% (v/v) *B. cereus* csn is  $p < 0.0001$ ,  $p = 0.0052$ , and  $p = 0.034$ , respectively. The survival rate for the larvae treated with compound 2 in PBS was 100%. *B. cereus*: *Bacillus cereus*, csn: culture supernatant.

alternative to murine models in microbial infection research due to its ease to obtain and use without elaborate equipment and ethical considerations.<sup>[60]</sup> Moreover, the mechanisms of the innate immune system are closely related to those of the mammals.<sup>[61,62]</sup>

To explore the effect of ColQ1 and a catalytically inactive mutant of ColQ1 (i.e., ColQ1 E502A)<sup>[34]</sup> on the larvae, we injected them with various enzyme concentrations ( $100 \times 10^{-9}$ – $500 \times 10^{-9}$  M). The survival of the larvae was monitored daily for eight days. Larvae injected with the catalytically inactive mutant enzyme survived (at all concentrations). In contrast, eight days after treatment with active ColQ1, the survival dropped to 0%, 20%, and 50% at concentrations of  $500 \times 10^{-9}$ ,  $300 \times 10^{-9}$ , and  $100 \times 10^{-9}$  M enzyme, respectively (Figure S10, Supporting Information). In a next step, we examined the effects of compounds 1 and 2 on the survival of the larvae in presence of  $300 \times 10^{-9}$  M of ColQ1. Co-injection of  $300 \times 10^{-6}$  M of compound 1 increased larvae survival by 60% while 150 and  $50 \times 10^{-6}$  M concentrations showed a lower impact (~30 and 0%, Figure S11, Supporting Information). Compound 2 maintained 60% survival at  $20 \times 10^{-6}$  M until day eight while  $10 \times 10^{-6}$  and  $5 \times 10^{-6}$  M showed a

lower effect (~40% and 0%) compared to the control (i.e., ColQ1) (Figure 6a).

Similar experiments were performed with *B. cereus* derived csn at concentrations of 35–100% (v/v). The survival of the larvae was studied for eight days after injection. After five days, only 15% of larvae injected with 100% (v/v) csn survived. With 65% and 35% (v/v) of the csn, the death of the larvae was delayed (Figure S10, Supporting Information). To investigate the effect of the collagenase inhibitors 1 and 2, we injected the larvae with 100% (v/v) of *B. cereus* csn together with compounds 1 ( $50 \times 10^{-6}$ – $300 \times 10^{-6}$  M) (Figure S11, Supporting Information) or 2 ( $5 \times 10^{-6}$ – $20 \times 10^{-6}$  M) (Figure 6b). Compound 1 at  $300 \times 10^{-6}$  M showed an increase of the survival rate from 20 to 75%, while at  $150 \times 10^{-6}$  M, the survival improved to 45% (Figure S11, Supporting Information). Compound 2 enhanced the survival from 25% to 73% at  $20 \times 10^{-6}$  M (Figure 6b). This difference between survival of larvae injected with ColQ1 and csn might be due to the high quantities of ColQ1 used in the experiment (i.e.,  $300 \times 10^{-9}$  M), which is 300-fold the collagenase concentration in csn. This indicates that the action of csn on the larvae might be connected to other virulence factors (such as sphingomyelinase and non-hemolytic

enterotoxins) as well as collagenase, which could work together to kill the larvae.<sup>[63,64]</sup> This also suggests that both compounds might target other virulence factors in the csn, therefore further experiments could be performed in the future to confirm this.

The toxic effect exerted by *B. cereus* collagenases might be related to the activation of melanization mechanisms in the larvae since the dead larvae turned black, as suggested for other metalloproteases.<sup>[65–70]</sup> In addition, it has been shown that collagenases digest hemolymph proteins of the larvae into small peptides, which trigger an immune response finally leading to their death.<sup>[65–69]</sup>

### 3. Conclusions

Virulence factors and their inhibitors are currently gaining wide attention because of their potential to limit the evolution of antibiotic resistance and to treat infections by reducing bacterial pathogenicity.<sup>[13]</sup> Therefore, full characterization of virulence factors is essential to understand their role during infection and to predict whether their inhibition is beneficial for the treatment. In the present work, we characterized the collagenolytic activity of a recently discovered recombinant *B. cereus* ColQ1 virulence factor<sup>[34]</sup> and *B. cereus* csn. In addition, we evaluated the biological effects of two small molecules that inhibit collagenases of *B. cereus* and other pathogens. In this context, an ex vivo pig-skin model of *B. cereus* infection was used to investigate *B. cereus* collagenases and the consequences of their inhibition. This model highlights the ability of *B. cereus* collagenase to decompose fibrillar COLs and disrupt their regular alignment. This mechanism might lead to an accelerated bacterial infiltration and penetration into deeper sites of the host. Moreover, as previously reported, this mechanism is one of the main obstacles to the wound-healing process.<sup>[59,73]</sup> We demonstrated that *B. cereus* csn collagenases induced cytotoxicity in fibroblasts and keratinocytes, which could be minimized using bacterial collagenase inhibitors. In an in vivo model using *G. mellonella* larvae, we showed that ColQ1 and *B. cereus* csn are toxic and induce the death of the larvae. Treatment with collagenase inhibitors significantly increased their survival rate. These findings provide new insights into the functions of *B. cereus* collagenases in wound infections and the importance of its inhibition by antivirulence, which could represent a promising therapeutic option.

### 4. Experimental Section

**Production of *B. cereus* ColQ1:** The collagenase unit of ColQ1 from *B. cereus* strain Q1 (Uniprot: B9J354; Tyr94-Gly765) was expressed and purified as previously described.<sup>[34]</sup>

***B. cereus* csn Production:** *B. cereus* ATCC 14 579 strain was prepared as described before.<sup>[35]</sup> *B. cereus* was grown in RPMI medium (+10% FCS, 1% Glutamine) (Gibco) at 30 °C ON with 160 rpm shaking. The next day, csn was harvested by centrifugation at 3000 x g for 10 min at 4 °C. The csn was sterile-filtered with 0.22 µm filter (Greiner) then, it was aliquoted and stored at –80 °C until use.

**In vitro FRET-Based Peptidolytic Assay:** IC<sub>50</sub> measurements were performed as previously reported.<sup>[33]</sup> In short, ColQ1 was incubated with compound 2 at RT for 1 h. The reaction was initiated by the addition of 2 × 10<sup>–6</sup> M of the collagenase-specific peptide substrate Mca-Ala-Gly-Pro-Gly-Pro-Dpa-Gly-Arg-NH<sub>2</sub> (FS1-1; Mca = (7-methoxycoumarin-4-yl) acetyl);

Dpa = *N*-3-(2,4-dinitrophenyl)-L-2,3-diaminopropionyl). The fluorescence was monitored for 2 min (excitation: 328 nm, emission: 392 nm) at 25 °C. The final concentrations were 1 × 10<sup>–9</sup> M ColQ1, 250 mM HEPES pH 7.5, 400 mM NaCl, 10 mM CaCl<sub>2</sub>, 10 × 10<sup>–6</sup> M ZnCl<sub>2</sub>, 2 × 10<sup>–6</sup> M FS1-1, and 0 to 120 × 10<sup>–6</sup> M compound 2. Due to poor compound solubility, the DMSO concentration was adjusted to 5%. The percentage of enzyme inhibition was calculated in relation to a blank reference without compound added. All experiments were performed in triplicate. Limited by the solubility of the compound, the IC<sub>50</sub> value could not be determined using non-linear regression, but was determined by linear regression using only data within the 40–60% inhibition range. Regression analysis was performed using GraphPad Prism 5 (Graph Pad Software, San Diego, CA, USA). To determine the peptidolytic activity versus FS1-1 of the *B. cereus* csn, a similar assay as described above was performed. Csn samples were freshly thawed and used in the assay in three different concentrations (12%, 16% and 20% v/v). Samples were preincubated with buffer control or inhibitors for 30 min at RT, before the reactions were started upon addition of 2 × 10<sup>–6</sup> M FS1-1. The final inhibitor concentrations were: 20 mM EDTA, 1x EDTA-free complete protease inhibitor cocktail (Roche, Woerden, The Netherlands) as serine and cysteine protease inhibitors, 1.83 mM compound 1 and 95 × 10<sup>–6</sup> M compound 2 at a final DMSO concentration of 5%. All results were extrapolated to 100% v/v and inhibition rates were normalized to the uninhibited control. Experiments were performed in triplicate and are presented as means ± standard deviation.

**Gelatin Zymography:** Aliquots of the *B. cereus* csn were loaded onto 10% SDS-PAGE gels containing 0.2% gelatin (Roth, Karlsruhe, Germany) and separated by electrophoresis at 4 °C. After separation, the gels were sliced into 4 pieces (marker lane plus 2 sample lanes) each and incubated in the respective renaturation buffer (50 mM HEPES pH 7.5, 200 mM NaCl, 10 × 10<sup>–3</sup> M CaCl<sub>2</sub>, 10 × 10<sup>–6</sup> M ZnCl<sub>2</sub>, 2.5% Triton X-100) supplemented with (i) nothing (control), (ii) 1x EDTA-free cComplete protease inhibitor cocktail (Roche, Woerden, The Netherlands), (iii) 300 × 10<sup>–6</sup> M compound 1 or (iv) 100 × 10<sup>–6</sup> M compound 2 at RT for 2x30 min with gentle agitation. The gel slices were then equilibrated in the respective developing buffer (50 mM HEPES pH 7.5, 200 mM NaCl, 10 mM CaCl<sub>2</sub>, 10 × 10<sup>–6</sup> M ZnCl<sub>2</sub>, 0.02% Brij-35) supplemented with the aforementioned compounds (i–iv) at RT for 2x10 min with gentle agitation, and then incubated on at 37 °C in fresh, supplemented developing buffer. Transparent bands of gelatinolytic activity were visualized by staining with 0.1% Coomassie brilliant blue G-250 dye ON. Gels were scanned using ChemiDoc XRS+ imaging system (Biorad, USA) and image analysis was performed with Image Studio Lite v5.2 software (Li-Cor Biosciences, USA). The integration area of the indicated molecular weight regions was measured, and values were expressed as a ratio of the control area from the same gel (no additional treatment; set to unity). Results were thereby standardized for each gel and expressed in dimensionless units. Results were obtained from two separate experiments for each condition.

**COL Cleavage Assay:** Acid-soluble type I COL from bovine tail (Thermo Fischer Scientific) at a final concentration of 1 mg mL<sup>–1</sup> was digested at 25 °C by 50 ng ColQ1 in 250 mM HEPES, 150 mM NaCl, 5 mM CaCl<sub>2</sub>, 5 × 10<sup>–6</sup> M ZnCl<sub>2</sub>, pH 7.5. Compounds 1 and 2 were included at different concentrations, and incubated together with COL and ColQ1 for 3 h. The reaction was stopped by the addition of 50 mM EDTA followed by visualization with 12% SDS-PAGE gels. Results were obtained from two independent experiments for each compound.

**Synthesis of Compounds 1 and 2:** The synthesis was performed according to the synthetic scheme that we published before.<sup>[32,30]</sup>

**Docking of Compounds 1 and 2:** The crystal structure of the peptidase domain of ColH (5o7e) with 1.87 Å resolution was used as target model for the docking. Ligand files were prepared as input for the docking software using OpenBabel (protonation state)<sup>71</sup> In case of compound 2, the thiolate derivative was used as input, as the mercaptoacetamide compound is known to hydrolyze in aqueous solution.<sup>[33]</sup> The final docking was performed using the Molecular Forecaster suite.<sup>[49]</sup> In short, the protein structure was prepared using the PREPARE and PROCESS modules with a ligand cutoff of 7 Å (particle water option). The ligands were prepared using the SMART module. Docking calculations were performed using FITTED. The docking software was validated via redocking the ligand 9NB, result-

ing in an RMSD of 0.43 Å. The PyMOL Molecular Graphics System, version 2.0.6.0a0, Schrödinger, LLC, was used for generating figures.<sup>[72]</sup>

**ColQ1 Activity on Ex vivo Pig-Skin Model:** The ex vivo pig-skin model was performed as reported earlier.<sup>[38]</sup> The skin explants of 15 mm diameter were made from ears of young pigs which were provided by a local slaughterhouse. Once the ears were received, several steps of sterilization were performed. The ears were punched, washed with sterile water followed with 3 x DMEM medium containing 10% FBS, 1% Pen-Strep and 250 ng mL<sup>-1</sup> amphotericin B, with a minimum of 15 min incubation time. To assess the sterilization by antibiotics, randomly selected skin punches were incubated in DMEM medium at 37 °C ON. The next day, the exposed DMEM was plated on LB-agar plate without antibiotic to check for bacterial growth. After washing the explants, they were stored at -80 °C for a maximum of one month in DMEM supplemented with 15% (v/v) glycerol. The storage conditions were selected based on the viability of the skin which we evaluated over one month with the MTT assay at 37 °C, -20 °C and -80 °C (Figure S3, Supporting Information). To investigate the activity of collagenase effect ex vivo, the skin samples were thawed and incubated at 37 °C for one hour in DMEM medium containing 10 × 10<sup>-6</sup> M ZnCl<sub>2</sub> and 4 mM CaCl<sub>2</sub>. While the epidermal side of the skin was exposed to air, the dermal side was incubated in DMEM medium with ColQ1 or csn for several time periods. The skin was incubated with different concentrations of ColQ1 ranging from 100 × 10<sup>-9</sup>–500 × 10<sup>-9</sup> M and of *B. cereus* csn (0–100% v/v) for several days in a total volume of 300 µL containing ColQ1 or csn together with DMEM and tissue explant. To estimate the release of Hyp into the DMEM medium, the medium was collected and stored at -20 °C. Hyp quantification was performed using a Hydroxyproline assay kit (Sigma Aldrich). In short, Hyp was converted into a colorimetric product after adding 100 µL chloramine T/oxidation buffer mixture, 100 µL 4-(dimethylamino)benzaldehyde diluted in perchloric acid/isopropanol to 10 µL of DMEM medium and measured at a wavelength of 560 nm. For further evaluation, the skin tissues that were treated for 24 h were fixed with 4% paraformaldehyde (PFA) and stored at 4 °C. The fixed skin was stored ON with 10% and then 25% sucrose in PBS ON in order to prevent tissue damage before downstream evaluation. The data were plotted with GraphPad Prism 8 for three independent experiments and to calculate the probability value one-way ANOVA was performed and statistical significance was analyzed by Tukey test.

**Ex vivo Pig-Skin Model for Evaluating the Effect of ColQ1 Inhibitors:** In order to select adequate inhibitor concentrations, the skin was treated with 300 × 10<sup>-9</sup> M ColQ1 (optimal concentration of ColQ1 selected from the previous assay) and gradient concentrations of collagenase inhibitors 1 and 2. A total of 12 skin punches per compound were treated in duplicate for six conditions followed by incubation at 37 °C for 24 h, 5% CO<sub>2</sub> and 300 rpm. Non-treated condition was considered as a healthy state, the other samples were incubated with 300 × 10<sup>-9</sup> M ColQ1 combined with either compound 1 (0–400 × 10<sup>-6</sup> M) or compound 2 (0–50 × 10<sup>-6</sup> M). After 24 h, all samples were fixed in 4% PFA and stored after treating them with 10% and 25% sucrose/PBS as described before and prepared for microscopic and biochemical analysis. To analyze the Hyp content in the DMEM medium for each condition, the DMEM was collected before and after treatment and stored at -20 °C. Finally, the optimal inhibitor concentration was determined by microscopy and biochemical evaluation. Results of three independent experiments were plotted, mean ± standard deviation. To estimate the probability value one-way ANOVA was performed and statistical significance was analyzed to illustrate the significant differences between non-treated versus treated samples. (\*\*\*)  $p \leq 0.001$ .

**Sample Preparation for SHG and Immunostaining of COL Subtypes:** The tissue punches were sliced into half with surgical scissors and placed into a separate holder such that the sliced edge faced inside the cavity of the holder in orthogonal direction. Next, the cryoglue (ThermoFisher) was added to the samples and skin were readjusted upright if necessary, and then frozen at -80 °C for at least 30 min. For each condition, a glass slide (Superfrost Plus, Menzel Gläser, ThermoFisher) was used and three circles were drawn using a hydrophobic liquid blocker pen (PAP pen (ab2601), Abcam). Prior to the sectioning, samples were cryo-glued onto steel molds which were then inserted into the cryostat and clamped at the correct angle (the long edge of the sample orthogonal to the blades edge). Subsequently,

the sample was trimmed to form a smooth surface and thereby reduced the risk of artefacts. Depending on the desired microscopy method, the tissue samples were sliced in 20 µm for epifluorescence microscopy or 100 µm for SHG microscopy on poly-L-lysine coated glass slides. The cryoglue was washed off with 3 × 100 µL sterile PBS carefully from the corner in order to avoid movement, overlapping or even rinsing off of the specimen. No staining was performed for SHG imaging.

For immunostaining, tissue samples were stained with primary antibodies. (COL I (Rabbit polyclonal anti-type I collagen, (600-401-103-0.1 Rockland); COL III (rabbit anti human collagen III antibody, (Abcam, ab7778)); COL V (rabbit anti human collagen V antibody, (Abcam, ab7046)) (1:200 dilutions in PBS) at RT for 1 h or at 4 °C ON. Next, the solution was removed, and all samples were gently washed with 3 × 100 µL PBS, followed by addition of 50 µL secondary antibody solution ((IgG (H+L) Highly Cross-Adsorbed; conjugated with AF647 (Abcam, A-21245)) in PBS (0.8% goat serum (Sigma-Aldrich, G9023-5ML)) and 1:5000 DAPI (Thermo Fisher)) at RT for 1 h or at 4 °C ON. Samples were washed 3 x with PBS again. For each slide, a 0.17 µm thick 24 mm x 60 mm cover glass (ThermoFisher) was placed on top of a layer of Parafilm and prepared with three evenly distributed drops of in total 60 µL FluoroMountG (ThermoFisher, 00-4958-02, refractive index: 1.4). The slides were placed at one edge of the cover glass and slowly lowered towards it in a decreasing angle, from one side to the other. Even distribution of the mounting medium required some time and a sense of applying pressure, but when performed carefully, arising air bubbles were prevented or eliminated in this step. When all slides were sealed, everything was covered with a layer of parafilm. Since the polymerization of FluoroMountG requires constant pressure, some weight (e.g., a 1 L bottle PBS on top of a book) was applied on top of it for at least 4 h but optimally ON. Prior to imaging or storage at 4 °C, all slides were cleaned using paper tissues and 70% ethanol in dH<sub>2</sub>O to remove dirt and redundant mounting medium.

**SHG and Epifluorescence Microscopy:** COL fibres in the tissue were visualized using SHG generated by a Zeiss LSM 880 confocal microscope with a two-photon femtosecond pulsed laser (Chameleon Vision I, Coherent, Santa Clara, CA (USA)) set at 900 nm wavelength for excitation. The emitted fluorescent signal was detected before the pinhole using Zeiss Big.2 non-descanned NDD detectors in combination with a 380–430 nm band pass filter. Images were obtained using 8% laser power, with a pixel dwell time of 8.24 µs with 4x averaging, and the detector gain set at 500. The resulting image had a size of 512 × 512 pixels with a pixel size of 1.38 µm. Images were taken with a Plan-Apochromat 20x/0.8 NA objective in the dermal region of the skin. Z-stack imaging was performed by selection of a representative spot in the plane with the highest SHG signal, followed by defining the first and a last plane, resulting in a Z-stack with 10 slices spanning 45 µm. Maximum intensity projections were then generated in ImageJ using the Z-project function.

Epifluorescence imaging was performed using a Nikon-Ti Eclipse inverted microscope coupled with a Lumencor SOLA white light lamp for epifluorescence. Images were captured using an Andor Clara DR-5434 camera, with filtercubes for DAPI at 365 nm staining the nuclei and the secondary antibody AF647 conjugate, which labeled COL antibodies at 640 nm. To get a good view throughout the whole skin thickness, large images with a scan area of 2 × 1 fields of view (10% overlapping) were captured using the Perfect Focus System. Parameters such as light intensity, exposure time, magnification, and tile scan area were adjusted individually for each COL type antibody. Thus, only treated and non-treated samples for one particular COL type immunostaining can be directly compared. For illustration purposes, a LUT threshold for each subtype was selected with the non-treated control of each condition and applied on all images of the related subtype. For a summary of the imaging conditions used, please see Table S1, Supporting Information. Triplicates of all samples were measured.

**In vitro Cell-Based Assay:** NHDF (Promo Cell C-12302) and HaCaT (ATCC® PCS-200-011) were purchased from commercial suppliers. 50000 cells per well of NHDF and HaCaT were seeded in 96-well plate (Greiner) with DMEM medium (Gibco) including 10% (v/v) fetal bovine serum (FBS, Gibco) and 1% (v/v) Penicillin-Streptomycin (Pen-Strep) antibiotic. The cells were incubated at 37 °C for 24 h



with 5% CO<sub>2</sub> prior to the treatment. Next, cells were incubated with varying amounts of *B. cereus* csn (0–15%) in a total volume of 200 µL containing csn, cells, DMEM. To inhibit the collagenolytic activity of *B. cereus* csn compounds **1** and **2** were added to the culture along with 1.25% (v/v) *B. cereus* csn having 1% DMSO and incubated for 24 h. On the next day, cell viability was evaluated using MTT and live/dead staining assays. The MTT assay is based on the reduction of tetrazolium dye to purple insoluble formazan by mitochondrial succinate dehydrogenase. Live/dead imaging depends on staining the live cells with fluorescein diacetate (FDA) and dead cells with propidium iodide (PI). The MTT assay and live/dead staining were performed after 24 h and 48 h incubation for csn treatment and 24 h incubation after collagenase inhibitor treatment. To conduct the MTT assay, we removed the medium and washed the cells 2 x with sterile PBS buffer. Afterwards, we added 200 µL of a mixture containing fresh DMEM and 5 mg mL<sup>-1</sup> MTT reagent in each well and incubated the plate for 2 h at 37 °C with 5% CO<sub>2</sub>. After the incubation, the medium was removed, and 200 µL of 100% DMSO was added to each well to dissolve the formazan crystals, and the plate was incubated at 37 °C for 30 min. Finally, the absorbance was measured using a PHERAstar plate reader (BMG Labtech, Ortenberg, Germany) at 0 nm for samples and at 620 nm for blanks with DMEM medium. The viability was also evaluated via epifluorescence microscope (Leica Microsystems CMS GmbH, Wetzlar, Germany) after the live/dead staining. Cells were seeded and treated with *B. cereus* csn similar to the procedures mentioned above and washed 3 x with sterile PBS. 0.03 mg mL<sup>-1</sup> FDA and 0.02 mg mL<sup>-1</sup> PI were added into each well and incubated at 37 °C for 5 min and 5% CO<sub>2</sub>. Then the viability and morphology of cells were investigated with 5x magnification to obtain an overview of the quantity of live and dead cells. The morphological changes between the non-treated cells and cells treated with the csn, treated with csn was captured at bright field channel with 20x. The viability of the cells was calculated relative to non-treated controls using ImageJ Fiji software, the results were plotted with GraphPad Prism 8 for three independent experiments for each cell type and 9 images for each condition. To calculate the probability value one-way ANOVA was performed and statistical significance was analyzed by Tukey test. For display purpose, the brightness and contrast were adjusted for each image based on the values of the control image where no treatment was applied.

**Galleria mellonella Virulence Assay:** *Galleria mellonella* larvae (TruLarv) were purchased from BioSystems Technology (Exeter, United Kingdom). Injections were performed using a LA120 syringe pump (Landgraf Laborsysteme, Langenhagen, Germany) equipped with 1 mL Injekt-F tuberculin syringes (B. Braun, Melsungen, Germany) and Sterican 0.30 × 12 mm, 30G × 1.5 needles (B. Braun). The larvae were injected in the right proleg with 10 µL of different solutions (i.e., various concentrations of *B. cereus* csn or ColQ1 or with only PBS). Based on that they were classified into different groups according to the following description: untreated group, treated with sterile PBS group, treated with different amount of *B. cereus* csn (which was diluted in sterile PBS), treated with ColQ1 diluted with sterile PBS, treated group with a mixture of 100% *B. cereus* csn or 300 × 10<sup>-9</sup> M ColQ1 and various concentrations of compounds **1** or **2** and treated group with only one of the compounds (diluted in PBS) to evaluate the toxicity level. We considered the larvae dead if they did not move and had a black color which reflected the activation of the melanization cascade due to the toxic effect induced by virulence factors. The survival of the larvae was analyzed using GraphPad Prism 8 using Kaplan-Meier analysis followed by equality test called log-rank test. The data of three independent experiments were combined and plotted in the survival curve, 45 larvae in total were included to test compounds with the csn and 30 larvae to test compounds with ColQ1 in the three experiments.

**Statistical Analysis:** Graphical data in the manuscript are communicated as the means ± SDs. Statistical comparisons were performed by Tukey one-way ANOVA test, which shows significant differences between conditions. Parametric/non-parametric statistical analysis used in the study were based on normality and homogeneity of variance. A value of  $p \leq 0.001$  was considered statistically significant while  $p > 0.05$  was considered non-significant. The normalized measurements were statistically compared between treated and non-treated groups using generalized estimating equations model to account for correlated data arising from

repeated measures. The survival of *G. mellonella* was analyzed using the Kaplan–Meier method and log-rank test was applied to calculate the significant difference between conditions.

## Supporting Information

Supporting Information is available from the Wiley Online Library or from the author.

## Acknowledgements

The authors are grateful to E. Färber GmbH & Co. KG (Zweibrücken, Germany) for providing fresh pig ears. This work was supported by Helmholtz-Zentrum für Infektionsforschung GmbH, European Research Council (ERC starting grant 757913), and Austrian Science Fund (P 31843 and I 4360).

Open Access funding enabled and organized by Projekt DEAL.

## Conflict of Interest

The authors declare no conflict of interest.

## Data Availability Statement

The data that support the findings of this study are available in the supplementary material of this article.

## Keywords

antibiotic resistance, *Bacillus cereus*, collagenase, pathoblocker, virulence factors

Received: November 9, 2021

Revised: December 15, 2021

Published online: January 15, 2022

- [1] E. J. Bottone, *Clin. Microbiol. Rev.* **2010**, *23*, 382.
- [2] P. E. Granum, T. Lund, *FEMS Microbiol. Lett.* **1997**, *157*, 223.
- [3] M. S. P. Dryden, *J. R. Soc. Med.* **1987**, *80*, 480.
- [4] X.-Y. Wu, K.-X. Ni, L. S.-B. China, *J. Orthop. Traumatol.* **2013**, *26*, 9.
- [5] F. A. Drobniowski, *Clin. Microbiol. Rev.* **1993**, *1744*, 304.
- [6] C.-W. Kim, S.-H. Cho, S.-H. Kang, Y.-B. Park, M.-H. Yoon, J.-B. Lee, W.-S. No, J.-B. Kim, *J. Food Sci.* **2015**, *80*, M123.
- [7] C. Fenselau, C. Havey, N. Teerakulkittipong, S. Swatkoski, O. Laine, N. Edwards, *Appl. Environ. Microbiol.* **2008**, *74*, 904.
- [8] Centers for Disease control and prevention <https://www.cdc.gov/drugresistance/biggest-threats.html> (accessed: December 2021)
- [9] S. B. Zaman, M. A. Hussain, R. Nye, V. Mehta, K. T. Mamun, N. Hosain, *Cureus* **2017**, *9*, 1403.
- [10] O. Jim, Antimicrobial Resistance: Tackling a crisis for the health and wealth of nations, **2014**.
- [11] S. W. Dickey, G. Y. C. Cheung, M. Otto, *Nat. Rev. Drug Discovery* **2017**, *16*, 457.
- [12] M. B. Calvert, V. R. Jumde, A. Titz, *Beilstein J. Org. Chem.* **2018**, *14*, 2607.
- [13] D. A. Rasko, V. Sperandio, *Nat. Rev. Drug Discovery* **2010**, *9*, 117.
- [14] W. Keenleyside, in *Microbiology: Canadian Edition*,
- [15] M. C. Callegan, S. T. Kane, D. C. Cochran, M. S. Gilmore, *DNA Cell Biol.* **2002**, *21*, 367.
- [16] P. C. Turnbull, K. Jørgensen, J. M. Kramer, R. J. Gilbert, J. M. Parry, *J. Clin. Pathol.* **1979**, *32*, 289.
- [17] D. J. Beecher, T. W. Olsen, E. B. Somers, A. C. L. Wong, *Infect. Immun.* **2000**, *68*, 5269.

- [18] K. K. Makinen, P. L. Makinen, *J. Biol. Chem.* **1987**, 262, 12488.
- [19] I. Negut, V. Grumezescu, A. M. Grumezescu, *Molecules* **2018**, 23, 2392.
- [20] S. H. M. D. Hussain, B. M. D. Limthongkul, T. R. M. Humphreys, *Dermatologic Surg.* **2013**, 39, 193.
- [21] K. Gelse, E. Pöschl, T. Aigner, *Adv. Drug Delivery Rev.* **2003**, 55, 1531.
- [22] V. Bansal, P. K. Sharma, N. Sharma, O. P. Pal, R. Malviya, *Biol. Res.* **2011**, 5, 28.
- [23] R. Berisio, V. Granata, L. Vitagliano, A. Zagari, *J. Am. Chem. Soc.* **2004**, 126, 11402.
- [24] D. J. Harrington, *Infect. Immun.* **1996**, 64, 1885.
- [25] Y. Z. Zhang, L. Y. Ran, C. Y. Li, X. L. Chen, *Appl. Environ. Microbiol.* **2015**, 81, 6098.
- [26] S. Patel, *Understanding Wound infection and colonisation* **2007**, 2.
- [27] P. G. Bowler, B. I. Duerden, D. G. Armstrong, *Clin. Microbiol. Rev.* **2001**, 14, 244.
- [28] H. Pîrvănescu, M. Bălăşoiu, M. E. Ciurea, A. T. Bălăşoiu, R. Mănescu, *Chirurgia* **2014**, 109, 73.
- [29] E. Schönauer, H. Brandstetter, in *Zinc Enzyme Inhibitors: Enzymes from Microorganisms* (Eds: C. T. Supuran, C. Capasso), Springer International Publishing, Cham, Switzerland **2017**, p. 69. <https://doi.org/10.1007/978-3-319-2016-9>.
- [30] A. S. Duarte, A. Correia, A. C. Esteves, *Crit. Rev. Microbiol.* **2014**, 42, 106.
- [31] K. Voos, E. Schönauer, A. Alhayek, J. Hauptenthal, A. Andreas, R. Müller, R. W. Hartmann, H. Brandstetter, A. K. H. Hirsch, C. Ducho, *ChemMedChem* **2021**, 16, 1257.
- [32] A. M. Kany, A. Sikandar, J. Hauptenthal, S. Yahiaoui, C. K. Maurer, E. Proschak, J. Köhnke, R. W. Hartmann, *ACS Infect. Dis.* **2018**, 4, 988.
- [33] A. M. Kany, J. Hauptenthal, K. Hüsecken, I. J. Hoppe, K. Voos, S. Yahiaoui, B. Elsässer, C. Ducho, H. Brandstetter, R. W. Hartmann, *J. Am. Chem. Soc.* **2017**, 139, 12696.
- [34] I. J. Hoppe, H. Brandstetter, E. Schönauer, *Sci. Rep.* **2021**, 11, 4187.
- [35] C. M. Abfalter, E. Schönauer, K. Ponnuraj, M. Huemer, G. Gadermaier, C. Regl, P. Briza, F. Ferreira, C. G. Huber, H. Brandstetter, G. Posselt, S. Wessler, *PLoS One* **2016**, 11, 0162433.
- [36] S. F. Altschul, W. Gish, W. Miller, E. W. Myers, D. J. Lipman, *J. Mol. Biol.* **1990**, 215, 403.
- [37] O. Matsushita, C. M. Jung, S. Katayama, J. Minami, Y. Takahashi, A. Okabe, *J. Bacteriol.* **1999**, 181, 923.
- [38] J. Konstantinović, S. Yahiaoui, A. Alhayek, J. Hauptenthal, E. Schönauer, A. Andreas, A. M. Kany, R. Müller, J. Köhnke, F. K. Berger, M. Bischoff, R. W. Hartmann, H. Brandstetter, A. K. H. Hirsch, *J. Med. Chem.* **2020**, 63, 8359.
- [39] G. K. Reddy, C. S. Enwemeka, *Clin. Biochem.* **1996**, 29, 225.
- [40] A. Logan, R. E. Neuman, *J. Biol. Chem.* **1950**, 184, 299.
- [41] L. Mostaço-Guidolin, N. L. Rosin, T. L. Hackett, *Int. J. Mol. Sci.* **2017**, 18, 1772.
- [42] D. Rouède, E. Schaub, J.-J. Bellanger, F. Ezan, J.-C. Scimeca, G. Baffet, F. Tiaho, *Sci. Rep.* **2017**, 7, 12197.
- [43] R. C. Haut, in *Accidental Injury: Biomechanics and Prevention*, Vol. 228 (Eds: A. M. Nahum, J. W. Melvin), Springer, New York **2002**.
- [44] P. D. Verhaegen, H. J. Schouten, W. Tigchelaar-Gutter, J. van Marle, C. J. van Noorden, E. Middelkoop, P. P. van Zuijlen, *Wound Repair Regen.* **2012**, 20, 658.
- [45] S. Ricard-Blum, *Cold Spring Harbor Perspect. Biol.* **2011**, 3, a004978.
- [46] U. Eckhard, P. F. Huesgen, H. Brandstetter, C. M. Overall, *J. Proteomics* **2014**, 100, 102.
- [47] C. Abfalter, T. Schmidt, S. Wessler, *Br. Microbiol. Res. J.* **2015**, 7, 62.
- [48] J. Eberhardt, D. Santos-martins, A. F. Tillack, S. Forli, *J. Chem. Inf. Model.* **2021**, 61, 3891.
- [49] J. Pottel, E. Therrien, J. L. Gleason, M. N. J. *Chem. Inf. Model.* **2014**, 254, 2014.
- [50] S. M. Ireland, A. C. R. Martin, *Database* **2019**, 2019, baz006.
- [51] M. A. Nilforoushzadeh, H. R. A. Ashtiani, F. Jaffary, F. Jahangiri, N. Nikkhah, M. Mahmoudbeyk, M. Fard, Z. Ansari, S. Zare, *J. Skin Stem Cell* **2017**, 4, 69080.
- [52] D. A. Scudiero, R. H. Shoemaker, K. D. Paull, A. Monks, S. Tierney, T. H. Nofziger, M. J. Currens, D. Seniff, M. R. Boyd, *Cancer Res.* **1988**, 48, 4827.
- [53] C. A. Day, A. Langfald, E. H. Hinchcliffe, *Methods in Cell Biology*, 158, Elsevier, Philadelphia **2020**, p. 43.
- [54] H. C. Stearns, V. D. Sneeden, *Am. J. Obstet. Gynecol.* **1966**, 94, 718.
- [55] M. Ito, Y. Liu, Z. Yang, J. Nguyen, F. Liang, R. J. Morris, G. Cotsarelis, *Nat. Med.* **2005**, 11, 1351.
- [56] I. Pastar, O. Stojadinovic, N. C. Yin, H. Ramirez, A. G. Nusbaum, A. Sawaya, S. B. Patel, L. Khalid, R. R. Isseroff, M. Tomic-Canic, *Adv. Wound Care* **2014**, 3, 445.
- [57] A. M. Wojtowicz, S. Oliveira, M. W. Carlson, A. Zawadzka, C. F. Rousseau, D. Baksh, *Wound Repair Regen.* **2014**, 22, 246.
- [58] S. M. McCarty, S. L. Percival, *Adv. Wound Care* **2013**, 2, 438.
- [59] L. Ovington, *Ostomy Wound Manage.* **2003**, 49, 7A.
- [60] N. Ramarao, C. Nielsen-Leroux, D. Lereclus, *J. Visualized Exp.* **2012**, 70, 4392.
- [61] P. Singkum, S. Suwanmanee, P. Purneesat, N. Luplertlop, *Acta Microbiol. Immunol. Hung.* **2019**, 66, 31.
- [62] C. J. Y. Tsai, J. M. S. Loh, T. Proft, *Virulence* **2016**, 7, 214.
- [63] V. M. Doll, M. Ehling-Schulz, R. Vogelmann, *PLoS One* **2013**, 8, 61404.
- [64] M. Ehling-Schulz, T. M. Koehler, D. Lereclus, *Microbiol. Spectr.* **2019**, 7, 139.
- [65] D. Peng, J. Lin, Q. Huang, W. Zheng, G. Liu, J. Zheng, L. Zhu, M. Sun, *Environ. Microbiol.* **2016**, 18, 846.
- [66] S. Kay, J. Edwards, J. Brown, R. Dixon, *Front. Microbiol.* **2019**, 10, 1281.
- [67] J. Griesch, M. Wedde, A. Vilcinskas, *Insect Biochem. Mol. Biol.* **2000**, 30, 461.
- [68] B. Altincicek, A. Vilcinskas, *Dev. Comp. Immunol.* **2006**, 30, 1108.
- [69] M. Andrejko, M. Mizerska-Dudka, *J. Invertebr. Pathol.* **2011**, 107, 16.
- [70] D. Peng, J. Lin, Q. Huang, W. Zheng, G. Liu, J. Zheng, L. Zhu, M. Sun, *Environ. Microbiol.* **2016**, 18, 846.
- [71] N. M. O'Boyle, M. Banck, C. A. James, C. Morley, *J. Cheminform.* **2011**, 3, 33.
- [72] The PyMOL Molecular Graphics System, <https://pymol.org/2/> (accessed: December 2021)
- [73] S. Guo, L. A. DiPietro, *J. Dent. Res.* **2010**, 89, 219.

**Chapter D: N-Aryl mercaptoacetamides as a Potential Multi-target Inhibitors of Metallo- $\beta$ -lactamases (MBLs) and the Virulence Factor LasB from *Pseudomonas aeruginosa*.**

Samir Yahiaoui, <sup>+</sup> Katrin Voos, <sup>+</sup> Jörg Hauptenthal, Thomas Wichelhaus, Denia Frank, Lilia Weizel, Marco Rotter, Steffen Brunst, Jan S. Kramer, Ewgenij Proschak, Christian Ducho\* and Anna K. H. Hirsch\*

<sup>+</sup> these authors contributed equally

\* corresponding authors

Reproduced from *RSC Med. Chem.* **2021**, *12*, 1698 – 1708

with permission from the Royal Society of Chemistry.

DOI: 10.1039/D1MD00187F

*As this chapter comprises a publication, compound numbers of this chapter are independent from other parts of this thesis.*

### III. Published Results

#### **Full contribution report:**

A. K. H. H., C. D., S. Y. and K. V. conceived and coordinated the study. S. Y. had first the idea to test further compounds against MBLs, conceived and wrote parts of the manuscript. K.V. synthesized compounds 2 – 25, contributed to SAR interpretation, conceived and wrote parts of the manuscript. S. Y and K. V. contributed equally. A. K. H. H. and C. D. edited the manuscript, supplied funding, and supervised the project. J. H. edited the manuscript and co-supervised the project. T. W. and D. F. planned and performed the growth inhibition assays with *K. Pneumoniae*. E. P., L. W., M. R., S. B. and J. S. K. Planned and performed the MBL assays. All authors reviewed the results and approved the final version of the manuscript.

## RESEARCH ARTICLE

Cite this: *RSC Med. Chem.*, 2021, 12, 1698***N*-Aryl mercaptoacetamides as potential multi-target inhibitors of metallo- $\beta$ -lactamases (MBLs) and the virulence factor LasB from *Pseudomonas aeruginosa*†**Samir Yahiaoui,<sup>†a</sup> Katrin Voos,<sup>†b</sup> Jörg Haupenthal,<sup>a</sup> Thomas A. Wichelhaus,<sup>c</sup> Denia Frank,<sup>c</sup> Lilia Weizel,<sup>d</sup> Marco Rotter,<sup>d</sup> Steffen Brunst,<sup>d</sup> Jan S. Kramer,<sup>d</sup> Evgenij Proschak,<sup>d</sup> Christian Ducho<sup>\*b</sup> and Anna K. H. Hirsch<sup>\*ae</sup>

Increasing antimicrobial resistance is evolving to be one of the major threats to public health. To reduce the selection pressure and thus to avoid a fast development of resistance, novel approaches aim to target bacterial virulence instead of growth. Another strategy is to restore the activity of antibiotics already in clinical use. This can be achieved by the inhibition of resistance factors such as metallo- $\beta$ -lactamases (MBLs). Since MBLs can cleave almost all  $\beta$ -lactam antibiotics, including the “last resort” carbapenems, their inhibition is of utmost importance. Here, we report on the synthesis and *in vitro* evaluation of *N*-aryl mercaptoacetamides as inhibitors of both clinically relevant MBLs and the virulence factor LasB from *Pseudomonas aeruginosa*. All tested *N*-aryl mercaptoacetamides showed low micromolar to submicromolar activities on the tested enzymes IMP-7, NDM-1 and VIM-1. The two most promising compounds were further examined in NDM-1 expressing *Klebsiella pneumoniae* isolates, where they restored the full activity of imipenem. Together with their LasB-inhibitory activity in the micromolar range, this class of compounds can now serve as a starting point for a multi-target inhibitor approach against both bacterial resistance and virulence, which is unprecedented in antibacterial drug discovery.

Received 4th June 2021,  
Accepted 23rd July 2021

DOI: 10.1039/d1md00187f

rsc.li/medchem

**Introduction**

Due to the emergence of drug-resistant bacteria and the lack of new antibiotics in the pipeline, novel effective and innovative treatment options are urgently needed, in particular to cure infections with Gram-negative pathogens. One of the highly problematic Gram-negative bacteria is *Pseudomonas aeruginosa*, which has been assigned critical

priority by the World Health Organization (WHO).<sup>1</sup> This opportunistic pathogen is responsible for fatal lung infections in cystic fibrosis patients and many hospital-acquired infections.<sup>2,3</sup> *P. aeruginosa* is a versatile human pathogen that easily acquires resistance against multiple classes of antibacterial agents, including aminoglycosides, quinolones, polymyxins, and  $\beta$ -lactams.<sup>4,5</sup>

The  $\beta$ -lactams are still the most commonly used group of antibiotics.<sup>6</sup> One of the main mechanisms of resistance in Gram-negative pathogens including *P. aeruginosa* is the production of  $\beta$ -lactamases.<sup>7–9</sup> These enzymes can inactivate  $\beta$ -lactam antibiotics by the hydrolysis of their four-membered  $\beta$ -lactam ring.<sup>10,11</sup> Based on their mechanism of action, two main groups of  $\beta$ -lactamases (BLs) were identified: the serine- $\beta$ -lactamases (SBLs) and the metallo- $\beta$ -lactamases (MBLs).

SBLs act *via* a nucleophilic serine residue that covalently binds to the carbonyl unit of the  $\beta$ -lactam ring to achieve its hydrolysis. They have a variable substrate spectrum ranging from small-, broad- to extended-spectrum, and even carbapenems can be degraded by some SBLs. Additionally, several effective SBL inhibitors (*e.g.*, clavulanic acid) are already in clinical use in combination with  $\beta$ -lactam antibiotics to overcome resistance.<sup>12</sup>

<sup>a</sup> Helmholtz Institute for Pharmaceutical Research Saarland (HIPS) – Helmholtz Centre for Infection Research (HZI), Campus E8 1, 66123 Saarbrücken, Germany. E-mail: Anna.Hirsch@Helmholtz-hips.de

<sup>b</sup> Department of Pharmacy, Pharmaceutical and Medicinal Chemistry, Saarland University, Campus C2 3, 66123 Saarbrücken, Germany. E-mail: Christian.Ducho@Uni-Saarland.de

<sup>c</sup> Institute of Medical Microbiology and Infection Control, University Hospital Frankfurt, Paul-Ehrlich-Straße 40, 60596 Frankfurt, Germany

<sup>d</sup> Institute of Pharmaceutical Chemistry, Goethe University Frankfurt, Max-von-Laue-Straße 9, 60438, Frankfurt, Germany

<sup>e</sup> Department of Pharmacy, Saarland University, Campus Building E8 1, 66123 Saarbrücken, Germany

† Electronic supplementary information (ESI) available. See DOI: 10.1039/d1md00187f

‡ Equal contribution.

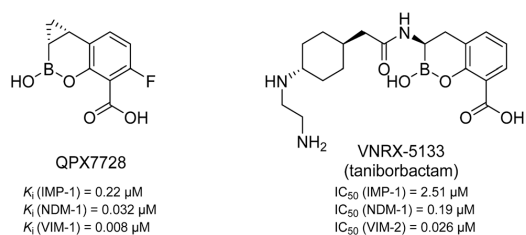


**Fig. 1** Chemical structures and reported  $K_i/IC_{50}$  values against different MBLs of QPX7728<sup>20,21</sup> and VNRX-5133 (taniborbactam),<sup>22–24</sup> two cyclic boronates that are in clinical trials.

MBLs can be divided into classes B1 to B3 which differ in their amino acid sequence homology and, as a result, their zinc coordination.<sup>13</sup> Class B2 (e.g., CphA) has only one catalytically active zinc ion and a very narrow substrate profile,<sup>14</sup> while classes B1 (e.g., NDM) and B3 (e.g., AIM) coordinate two zinc ions and show a very broad substrate spectrum.<sup>14–16</sup> In particular the B1 class is of high clinical relevance.<sup>17–19</sup> So far, two MBL inhibitors having a cyclic boronate as core structure (see Fig. 1) are in clinical trials. QPX7728 is in phase I (NCT04380207, alone and with QPX2014) and VNRX-5133 (taniborbactam) is in phase III in combination with cefepime (NCT03840148).<sup>20–24</sup> However, no clinically approved MBL inhibitors have been reported to date.<sup>25,26</sup>

It is known that bacterial pathogenesis and infectivity are mediated by microbial components called virulence factors, which play pivotal roles in adhesion, biofilm formation, invasion of host tissues, and immune evasion.<sup>27,28</sup> Targeting these factors is a newly emerging approach in the field of anti-infective drug discovery. This so-called antivirulence strategy is intended to disarm the bacteria rather than killing them. Several bacterial virulence factors have been identified including toxins, extracellular enzymes needed for cell invasion and biofilm formation, cell-surface proteins that mediate bacterial attachment, secretion systems, and quorum-sensing systems that regulate bacterial cell-to-cell communication.<sup>27,29–31</sup>

One of the major virulence factors of *P. aeruginosa* is the elastase LasB. This extracellular zinc-containing protease is responsible for the invasion of host tissues, biofilm formation, and immune evasion. It has been demonstrated that LasB can cleave important components of the connective

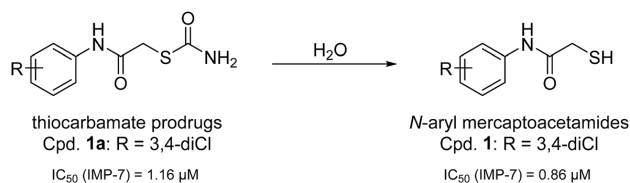
tissues such as elastin and collagen.<sup>32,33</sup> The protease was also shown to promote biofilm formation through the regulation of rhamnolipids.<sup>34</sup> Moreover, it was found to alter the human immune response by degrading host defense components such as cytokines,<sup>35</sup> antimicrobial peptides (AMP),<sup>36</sup> and surfactant proteins. These multiple roles of LasB in the infection process of *P. aeruginosa* make this protease an attractive antivirulence target.<sup>37,38</sup>

Recently, we have demonstrated the potential of thiocarbamates as prodrugs of *N*-aryl mercaptoacetamides (Scheme 1) as promising inhibitors of several bacterial proteases. Interestingly, these compounds are potent inhibitors of *P. aeruginosa* LasB and collagenases from *Clostridium* and *Bacillus* species.<sup>39,40</sup> Regarding LasB, in addition to the elucidation of the binding mode of our hit compound (1, Scheme 1), we demonstrated the *in vivo* efficacy of the same derivative in a *Galleria mellonella* larvae infection model. Moreover, compound 1 shows no cytotoxic effects on HepG2, HEK293 and A549 cells (see ESI,† Table S1) and its thiocarbamate prodrug 1a (see Scheme 1) remarkably displays high selectivity over several human matrix metalloproteases (MMPs).<sup>39</sup>

It has been demonstrated that several thiol-containing drugs such as captopril (an angiotensin converting enzyme (ACE) inhibitor which is used for the treatment of hypertension), thiorphan (the active metabolite of racecadotril used for the treatment of diarrhoea), and tiopronin (which is used in patients with cystinuria, Fig. 2), display promising *in vitro* inhibitory activities toward different MBLs.<sup>41</sup> The shown three inhibitors all consist of the same core structure, that is, a 2-substituted (2-mercaptoacetyl)- or (2-mercaptopropanoyl) glycine. Substantial synthetic work has already been done on this scaffold to obtain novel MBL inhibitors, and co-crystallization experiments have been reported.<sup>42–46</sup>

Inspired by this finding, and with respect to our slightly similar mercaptoacetamide core structure, we explored the effect of our thiol-based LasB inhibitor (compound 1) toward a class B1 MBL called impenemase 7 (IMP-7). Interestingly, our LasB inhibitor showed a strong inhibitory effect with a sub-micromolar  $IC_{50}$  value ( $IC_{50} = 0.86 \pm 0.06 \mu$ M).<sup>39</sup>

Based on the encouraging inhibitory activity of compound 1 against IMP-7, this study aimed to further investigate the inhibitory profile of the *N*-aryl mercaptoacetamide class against various MBLs. Aside from that, another goal was to explore the potential of using this class as multi-target



**Scheme 1** Hydrolysis of thiocarbamate prodrug 1a to its active thiol form 1 and their corresponding  $IC_{50}$  values reported for the inhibition of IMP-7.<sup>39</sup>

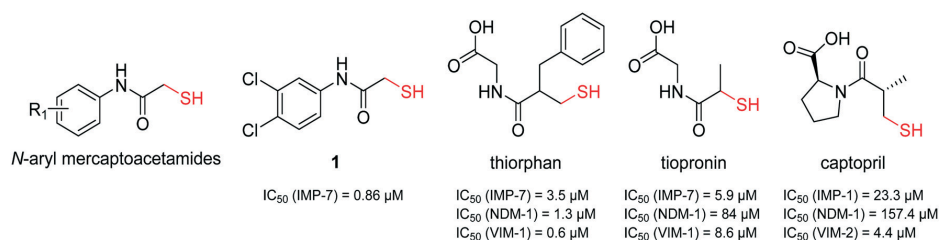


Fig. 2 Chemical structures and reported  $IC_{50}$  values of  $N$ -aryl mercaptoacetamides, compound **1**,<sup>39</sup> thiorphan,<sup>41</sup> tiopronin<sup>41</sup> and captopril<sup>47</sup> for the inhibition of different MBLs.

inhibitors tackling both virulence and bacterial resistance. In this work, we report on the design, synthesis, and *in vitro* evaluation of 13  $N$ -aryl mercaptoacetamide derivatives for inhibition of three clinically important and transferrable MBLs of the class B1: IMP-7, Verona integrin encoded metallo- $\beta$ -lactamase 1 (VIM-1) and New Delhi metallo- $\beta$ -lactamase 1 (NDM-1). Furthermore, we tested the two most active compounds in combination with the carbapenem antibiotic imipenem against a clinical NDM-1-expressing *Klebsiella pneumoniae* isolate and confirmed their activity on the bacterial level. The selectivity over nine potential human off-targets was additionally confirmed.

## Results and discussion

### Synthesis of $N$ -aryl mercaptoacetamides

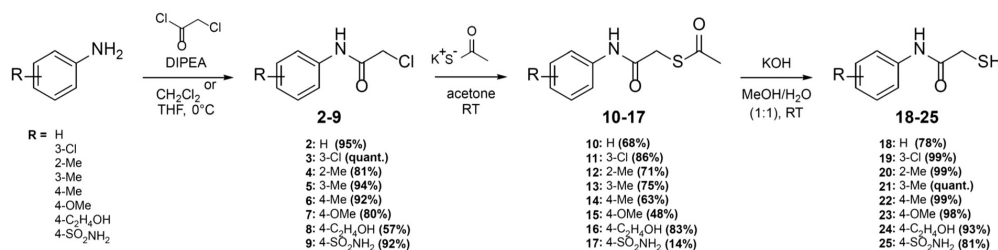
Here, we report on the biological evaluation of 13  $N$ -aryl mercaptoacetamides bearing various polar and nonpolar substituents on the aryl moiety. We have previously demonstrated that by variation of the substitution pattern on the aryl ring (and thus the electron density and H-bonding interactions), we either obtain LasB or ColH inhibitors. Additionally, the phenyl ring seems to be crucial for the selectivity of these inhibitors over human MMPs as potential off-targets.<sup>39,40</sup> Therefore, the impact of the same structural modifications on the inhibition of MBLs should also be investigated. Eight out of the 13 compounds were newly synthesised, while five had already been published as LasB or ColH inhibitors.<sup>39,40</sup> The majority of all our previously reported  $N$ -aryl mercaptoacetamides were tested against LasB and ColH

in their thiocarbamate prodrug form.<sup>39</sup> However, the co-crystal structure revealed the free thiol as the active form. This finding was confirmed by stability tests and *in vitro* assays.<sup>39,40</sup> In this work, we therefore synthesised the free-thiol forms of four compounds, which had previously been tested against LasB and ColH as thiocarbamates, as well as four novel mercaptoacetamide derivatives. The synthetic access to the mercaptoacetamide derivatives is outlined in Scheme 2.

A three-step synthetic route afforded target compounds **18–25**, starting from the corresponding aniline derivatives. In a first step, an amide formation was carried out by dropwise addition of chloroacetyl chloride to a cooled solution of the corresponding aniline and DIPEA in  $CH_2Cl_2$  or THF. Second, an  $S_N2$  reaction of the alkyl chlorides **2–9** with potassium thioacetate in acetone led to the thioacetates **10–17**. Compounds **10–17** were hydrolysed with aqueous KOH in methanol to afford the thiol target molecules **18–25**. These as well as the previously synthesised compounds **1** and **26–29** (Fig. 3) were then evaluated with respect to their biological activities.

### $N$ -Aryl mercaptoacetamides as broad-spectrum MBL inhibitors

To explore the potential of our thiol-based class to inhibit MBLs, we first tested the synthesised compounds **18–25** as well as the previously reported compounds **1** and **26–29** (Fig. 3) *in vitro* for their inhibitory potency against NDM-1, VIM-1 and IMP-7.<sup>39,40</sup> Based on their *in vitro* activity, we then selected several derivatives for further evaluation in bacteria in combination with imipenem.



Scheme 2 Synthesis of the thiols **18–25** as potential multi-target inhibitors of LasB and metallo- $\beta$ -lactamases.



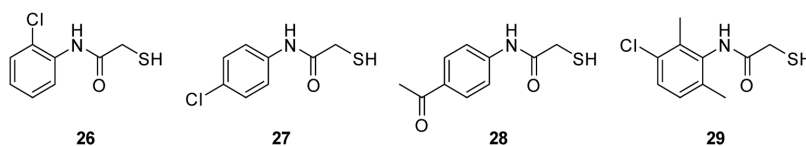


Fig. 3 Previously reported thiols 26–29 as potential multi-target inhibitors of bacterial virulence and resistance.<sup>39,40</sup>

### MBL activity assays

We used an activity assay based on kinetic fluorescence using fluorocillin as a substrate<sup>41</sup> to evaluate the inhibitory activity of the mercaptoacetamide derivatives against NDM-1, VIM-1 and IMP-7. The results can be found in Table 1.

Remarkably, all derivatives were active against all three MBL enzymes and consequently displayed broad-spectrum effects *in vitro* (Table 1). Compound **1** showed a sub-micromolar activity against both IMP-7 ( $IC_{50} = 0.86 \pm 0.06 \mu\text{M}$ )<sup>39</sup> and NDM-1 ( $IC_{50} = 0.65 \pm 0.04 \mu\text{M}$ ) and an  $IC_{50}$  of  $2.2 \pm 0.3 \mu\text{M}$  against VIM-1. All the other derivatives showed low micromolar activities against the three tested MBLs. Regarding many previously reported MBL inhibitors (a selection can be found in Fig. 2 and 4),<sup>41–43,48–50</sup> our compounds can be considered equipotent. Only the class of cyclic boronates (*e.g.* **34** (Fig. 4), QPX7728, and VNRX-5133 (Fig. 1)) was significantly more active against MBLs (with  $IC_{50}$  values in the low nanomolar range) and has already two candidates in clinical trials.<sup>20,23,50,51</sup>

In comparison to compound **1**, all structural modifications of the aryl moiety resulted in a moderate loss of activity against all MBLs. Regarding IMP-7, the  $IC_{50}$  values range from  $1.9 \mu\text{M}$  (compound **26**) to  $11 \mu\text{M}$  (compound **24**) with better tolerance for the nonpolar substituents. The most potent derivative against NDM-1 was compound **28** ( $1.5 \mu\text{M}$ ),

and as observed for IMP-7, the nonpolar groups were slightly preferred. Concerning VIM-1, all compounds showed comparable activities with  $IC_{50}$  values ranging between  $2.3 \mu\text{M}$  (**26**) and  $5.9 \mu\text{M}$  (**24**). Additionally, for mono-substituted compounds featuring a chlorine or methyl group, the position of the substituent did not have a significant effect on the biological response.

### Growth-inhibition assays

Encouraged by the promising *in vitro* activities of our *N*-aryl mercaptoacetamides, we investigated the effects of compounds **1** and **26** to restore the antibacterial effect of imipenem (ESI,† Fig. S1) in a growth inhibition assay. As we wanted to investigate MBL activity without the influence of LasB inhibition, and as our compounds were the most active on NDM-1, we selected a clinical imipenem-resistant *K. pneumoniae* isolate (strain T2301) that is able to express NDM-1 but not LasB. *K. pneumoniae* is one of the known ESKAPE pathogens and is rated critical by the WHO on their global priority list of antibiotic-resistant bacteria.<sup>52,53</sup> Nosocomial infections with *K. pneumoniae* have caused several outbreaks in multiple locations with very high mortality rates, *i.e.*, up to 72%.<sup>54–56</sup> NDM-1 (and other antibiotic resistance genes) spread between several pathogens *via* horizontal transfer,<sup>57–59</sup> and NDM-1-expressing *K.*

Table 1 Chemical structures, MBL and LasB inhibition of *N*-aryl mercaptoacetamides and their thiocarbamate prodrug forms

Cp.	R	thiol		thiocarbamate		
		Thiol $IC_{50}^a$ [ $\mu\text{M}$ ] IMP-7	Thiol $IC_{50}^a$ [ $\mu\text{M}$ ] NDM-1	Thiol $IC_{50}^a$ [ $\mu\text{M}$ ] VIM-1	Thiol $IC_{50}^a$ [ $\mu\text{M}$ ] LasB	Thiocarbamate $IC_{50}^a$ [ $\mu\text{M}$ ] LasB
<b>1</b>	3,4-DiCl	$0.86 \pm 0.06$	$0.65 \pm 0.04$	$2.2 \pm 0.3$	$6.6 \pm 0.3$ (ref. 39)	$6.2 \pm 0.3$
<b>18</b>	H	$4.7 \pm 0.7$	$3.6 \pm 0.9$	$5.1 \pm 1.3$	$39 \pm 3$	—
<b>26</b>	2-Cl	$1.9 \pm 0.5$	$1.8 \pm 0.1$	$2.3 \pm 0.2$	$11 \pm 1$	$14 \pm 1$
<b>19</b>	3-Cl	$4.1 \pm 1.6$	$2.7 \pm 0.4$	$3.6 \pm 1.2$	$14 \pm 2$	$19 \pm 1$
<b>27</b>	4-Cl	$2.4 \pm 0.3$	$2.1 \pm 0.1$	$4.7 \pm 1.8$	$21 \pm 1$ (ref. 39)	$16 \pm 1$
<b>20</b>	2-Me	$6.4 \pm 2.0$	$6.0 \pm 0.5$	$4.9 \pm 1.3$	$14 \pm 1$	—
<b>21</b>	3-Me	$4.4 \pm 1.5$	$3.4 \pm 0.2$	$4.1 \pm 0.8$	$38 \pm 3$	$48 \pm 2$
<b>22</b>	4-Me	$5.4 \pm 1.5$	$3.4 \pm 0.3$	$5.0 \pm 1.6$	$19 \pm 1$	$36 \pm 1$
<b>23</b>	4-OMe	$8.6 \pm 1.8$	$5.0 \pm 2.1$	$5.9 \pm 1.3$	$24 \pm 1$	$48 \pm 1$
<b>24</b>	4-C <sub>2</sub> H <sub>4</sub> OH	$11 \pm 4$	$6.7 \pm 3.0$	$5.9 \pm 2.0$	$52 \pm 3$	—
<b>25</b>	4-SO <sub>2</sub> NH <sub>2</sub>	$7.7 \pm 1.2$	$6.3 \pm 1.5$	$4.1 \pm 0.9$	$54 \pm 3$	—
<b>28</b>	4-Ac	$5.4 \pm 2.5$	$1.5 \pm 0.2$	$3.5 \pm 0.8$	$72 \pm 5$	$73 \pm 3$
<b>29</b>	3-Cl-2,6-diMe	$2.7 \pm 0.7$	$8.2 \pm 2.6$	$4.0 \pm 0.7$	$12 \pm 1$ (ref. 39)	—

<sup>a</sup> Means of at least two independent measurements  $\pm$  standard deviation.



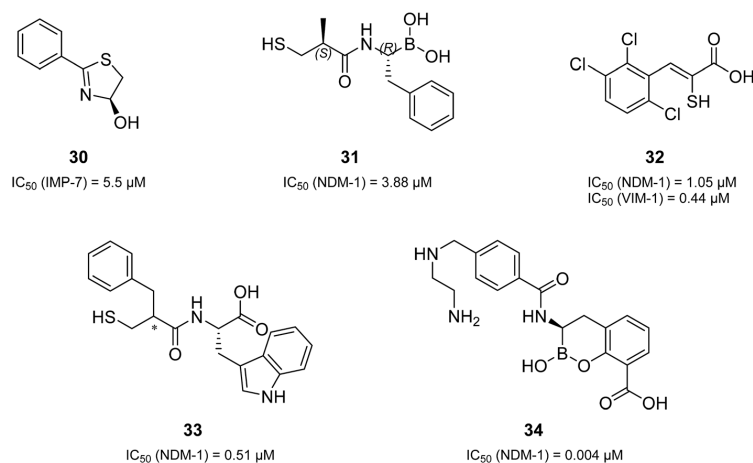


Fig. 4 A selection of the structural variations of reported MBL inhibitors and their corresponding inhibitory activities *in vitro* (30,<sup>48</sup> 31,<sup>43</sup> 32,<sup>49</sup> 33,<sup>42</sup> and 34<sup>50</sup>).

*pneumoniae* have caused several outbreaks in hospitals in the last decade.<sup>60–62</sup> Growth curves of the bacterial isolate with imipenem were determined in the presence and absence of the named compounds (two separate experiments, see Fig. 5A and B). Compounds 1 and 26 were selected based on their promising activities against MBLs.

As shown in the growth curves in Fig. 5, the presence of imipenem (at 8  $\mu$ g mL<sup>-1</sup>, *i.e.*, 0.5 $\times$  MIC) delayed the initiation of bacterial growth by a few hours, but after 24 hours, no relevant differences between the growth of imipenem-treated bacteria and the imipenem-free control were observed. Remarkably, when MBL inhibitors 1 (Fig. 5A, at 50  $\mu$ g mL<sup>-1</sup> (= 21  $\mu$ M)) or 26 (Fig. 5B, at 50  $\mu$ g mL<sup>-1</sup> (= 25  $\mu$ M)) were combined with imipenem (at 8  $\mu$ g mL<sup>-1</sup>), the inhibitory potential of imipenem was fully restored, and no growth of bacteria occurred over 24 hours. MBL inhibitors alone did not exhibit any intrinsic antibacterial activity at 50  $\mu$ g mL<sup>-1</sup>. As an additional control experiment, we employed EDTA as an MBL inhibitor, with MBL inhibition being caused by the metal-chelating properties of EDTA (ESI,<sup>†</sup> Fig. S2). The resultant growth curves were rather similar to those obtained with MBL inhibitors 1 and 26, respectively. Overall, this highlights the potency of the reported MBL inhibitors not just on the enzymatic, but also on the cellular level, making them attractive candidates for further development.

#### N-Aryl mercaptoacetamides as multi-target inhibitors of LasB and MBLs

The promising antibacterial effects of *N*-aryl mercaptoacetamides in combination with imipenem (Fig. 5) prompted us to further investigate the potential of this class as multi-target inhibitors targeting both virulence and resistance. Therefore, all synthesised compounds were evaluated for their potential inhibition of LasB as a bacterial virulence factor.

Inhibitory activity towards ColH was not determined, as the best two compounds on MBLs (1 and 26) had already been tested in their thiocarbamate form against ColH and did just show micromolar activities, which is more than three orders of magnitude less potent than the ColH-inhibiting hit compound 28.<sup>40</sup>

The evaluation of compounds 1, 19, 21, 26, and 27 in a functional LasB inhibition assay expectedly<sup>39,40</sup> showed similar activities compared to their thiocarbamate prodrug derivatives (Table 1). However, compounds 22 and 23 were two-fold more active than their thiocarbamate congeners. Regarding the novel mercaptoacetamides, the unsubstituted derivative 18 as well as the 2-methyl compound 20 showed decreased  $IC_{50}$  values relative to compound 1. Moreover, as expected based on our previous studies,<sup>39</sup> compounds 24 and 25 were the least active derivatives in the series due to the presence of polar substituents that are unfavourable for LasB inhibition.

#### Selectivity over other proteases

As most of our compounds all show activity on LasB and the three tested MBLs, and as it is known that 28 additionally is a nanomolar collagenase H (ColH) inhibitor,<sup>40</sup> it is crucial to exclude that our compounds are just non-selective zinc-chelators. Thiocarbamates 1a and 28a had already been evaluated for their selectivity over a range of six MMPs which had been chosen with respect to their structural variations in their S1' binding pockets.<sup>39,40</sup> We decided to test our hit compound 1 accordingly and, additionally, expand the selectivity panel with two histone deacetylases (HDACs) and the tumour necrosis factor  $\alpha$  converting enzyme (TACE). Those three enzymes are all zinc-dependent proteases.<sup>63–65</sup> HDACs play a crucial role in epigenetic regulation by modification of gene expression and thus in cell proliferation.<sup>66,67</sup> TACE, also known as “a disintegrin and metalloprotease 17” (ADAM17), is

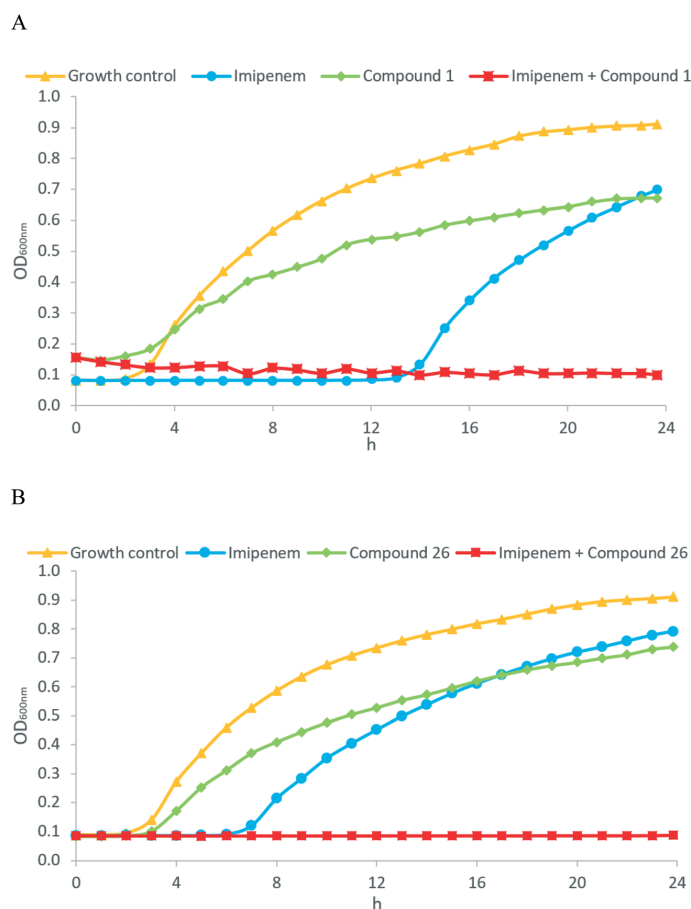


**Fig. 5** Growth-inhibition assay. Growth curves of NDM-1-expressing *K. pneumoniae* (T2301) over time (h) in the absence and presence of imipenem at  $8 \mu\text{g mL}^{-1}$  (i.e.,  $0.5 \times \text{MIC}$ )  $\pm$  MBL inhibitors at  $50 \mu\text{g mL}^{-1}$  ( $= 21 \mu\text{M}$  (**1**) or  $25 \mu\text{M}$  (**26**)); compound **1** (A) and compound **26** (B).

important for a functional immune system, for the nervous system and tissue generation.<sup>68–71</sup> Therefore, these enzymes represent important antitargets. As controls, batimastat (ESI,<sup>†</sup> Fig. S3) as unselective MMP inhibitor, trichostatin A (ESI,<sup>†</sup> Fig.

S4), a known inhibitor of HDACs, and ilomastat as TACE inhibitor (ESI,<sup>†</sup> Fig. S5) were chosen. Compound **1** was tested at a concentration of  $100 \mu\text{M}$  for its inhibitory activity on those nine enzymes. The results are reported in Table 2.

**Table 2** Inhibition values of six MMPs, TACE and two HDACs in the presence of  $100 \mu\text{M}$  **1**,  $0.5 \mu\text{M}$  trichostatin A and  $\text{IC}_{50}$  values of batimastat.<sup>40,72</sup> Ilomastat resulted in  $91 \pm 4\%$  inhibition of TACE activity at  $1 \mu\text{M}$

	1 inhibition at $100 \mu\text{M}^a$ [%]	Batimastat $\text{IC}_{50}^a$ [nM]	Trichostatin A inhibition at $0.5 \mu\text{M}^a$ [%]
MMP-1	n.i.	$2.2 \pm 0.1$	n.d.
MMP-2	n.i.	$1.8 \pm 0.1$	n.d.
MMP-3	n.i.	$5.6 \pm 0.9$	n.d.
MMP-7	n.i.	$7.0 \pm 0.2$	n.d.
MMP-8	n.i.	$0.7 \pm 0.2$	n.d.
MMP-14	n.i.	$2.8 \pm 0.2$	n.d.
TACE	$40 \pm 4$	n.d.	n.d.
HDAC-3	$9 \pm 7$	n.d.	$94 \pm 3$
HDAC-8	$11 \pm 5$	n.d.	$95 \pm 2$

<sup>a</sup> Means and SD of at least two independent measurements are displayed; n.d. = not determined; n.i. = no inhibition (if  $\leq 10\%$ ).

Compound **1** showed no inhibition of the six tested MMPs and the two HDACs. A slight inhibition of TACE ( $40 \pm 4\%$ ) at a rather high concentration of  $100 \mu\text{M}$  was found, but this still corresponds to a selectivity factor of more than five, which should be considered sufficient in particular in this early phase of development.

#### Cytotoxicity assays

It had already been demonstrated in our previous studies that compound **1** did not show any cytotoxicity against the three tested cell lines HepG2, HEK293 and A549 at a concentration of  $100 \mu\text{M}$ . The results can be found in the ESI,† Table S1.<sup>39,73</sup>

Additionally, compound **1** already had been subjected to a more complex *in vivo* toxicity model in zebrafish embryos (ESI,† Table S2).<sup>73</sup> Here the maximum tolerated concentration (MTC) was  $10 \mu\text{M}$ . At higher concentrations (e.g.  $30 \mu\text{M}$ ), the compound precipitated in this assay and the zebrafish embryos died.<sup>73</sup> Further studies to determine whether the toxicity derived from the compound's *in vivo* effect itself or from the formation of crystals will be performed in the course of future hit optimisation.

## Conclusions

In summary, based on the encouraging inhibitory activity of a previously reported LasB inhibitor (compound **1**) against IMP-7, we designed, synthesised and evaluated a series of *N*-aryl mercaptoacetamide derivatives against the three metallo- $\beta$ -lactamases IMP-7, VIM-1 and NDM-1. Interestingly, all tested compounds showed promising inhibition of all three MBLs. Compound **1** displayed the strongest inhibitory effects with submicromolar  $\text{IC}_{50}$  values toward both IMP-7 and NDM-1, and low micromolar activity against VIM-1.

To confirm the potential of our mercaptoacetamide derivatives as MBL inhibitors, compounds **1** and **26** were tested in combination with imipenem against a clinical NDM-1-expressing *K. pneumoniae* isolate. Remarkably, at  $50 \mu\text{g mL}^{-1}$  ( $\sim 20 \mu\text{M}$ ), both compounds were able to restore the activity of imipenem. Additionally, compound **1** showed high selectivity over a total of nine potential off-targets (six MMPs, TACE and two HDACs) at a concentration of  $100 \mu\text{M}$ , at which it already previously had demonstrated to also have no cytotoxic effects on human cell lines.<sup>39,73</sup> These promising effects of our *N*-aryl mercaptoacetamides against MBLs, their previously confirmed anti-LasB properties and their demonstrated high selectivity over human off-targets inspires the use of this class as multi-target inhibitors tackling both virulence and resistance of pathogens. This is a new approach that is unprecedented in antibacterial drug discovery.

Although further investigations will be needed to improve the inhibitory potencies of our inhibitors, our results demonstrate an attractive new multi-targeting approach, which can enhance the efficacy of currently used antibiotics against resistant MBL-expressing pathogens. In addition to restoring the sensitivity to antimicrobial agents, the effect of

the reported compounds on virulence factors can make bacteria less pathogenic and more vulnerable towards immune response and/or low doses of antibiotics. Even though no improvement of the *in vitro* inhibitory activities of compound **1** has been achieved so far, the reported results indicate that some structural variations in the aryl moiety appear to be feasible. This opens the way to a future optimisation of this compound class, also with respect to ADME-T properties.

## Experimental section

### Chemistry

Compounds **1**,<sup>39</sup> **26**,<sup>40</sup> **27**,<sup>39,40</sup> **28**<sup>40</sup> and **29**<sup>39</sup> were previously reported. All other compounds were synthesised according to Scheme 1 as described in detail in the ESI.†

### IMP-7, NDM-1 and VIM-1 *in vitro* inhibition assays

The assays were performed according to a previously described procedure.<sup>41</sup> They were carried out at room temperature in black polystyrol 96-well plates (Corning) using fluorocillin (prepared as described by Rukavishnikov *et al.*<sup>74</sup>), as substrate. The fluorescence emitted by the fluorescent product difluorofluorescein was kinetically monitored using a Tecan fluorescent plate reader Infinite F200.  $\text{IC}_{50}$  values were calculated using data obtained from measurements with at least six different inhibitor concentrations, applying a sigmoidal dose-response (variable slope with four parameters) equation using GraphPad Prism 5 (GraphPad software, La Jolla, CA, USA) software.

### Growth inhibition assay

A computerised incubator (Tecan Infinite M200 pro, Crailsheim, Germany) was used to obtain the growth curves over a time course. Optical density ( $\text{OD}_{600}$ ) was measured for evaluating bacterial (i.e., *K. pneumoniae* NDM-1) density in suspension. Prior to each experiment, bacteria were cultured to the exponential phase ( $\text{OD}_{600} = 0.6\text{--}0.8$ ) in cation-adjusted Mueller Hinton broth (Becton Dickinson, Heidelberg, Germany).  $5 \mu\text{L}$  of diluted bacterial suspension and  $100 \mu\text{L}$  of cation-adjusted Mueller Hinton broth either with or without imipenem (Arcos Organics, Schwerte, Germany) and/or the respective MBL inhibitor were added into wells of a 96 well plate to give a final bacterial inoculum of approx.  $5 \times 10^5 \text{ CFU mL}^{-1}$ . The temperature was adjusted to  $37 \text{ }^\circ\text{C}$ . A permanent shaking speed of 450 rpm was used and only interrupted before  $\text{OD}_{600}$  measurement. The optical densities of samples were recorded on-line every 10 minutes for 24 hours. Experiments were determined in triplicate. Representative growth curves are shown. For quality control, bacterial strain *E. coli* ATCC 25922 was used.

### LasB *in vitro* inhibition assay

The purification of LasB as well as the performance, measurement and evaluation of the FRET-based *in vitro*

inhibition assay were carried out as previously described by Kany *et al.*<sup>39</sup>

#### MMP *in vitro* inhibition assay

The assays were performed as previously described.<sup>39,40</sup>

#### TACE *in vitro* inhibition assay

ADAM-17 (TACE) inhibitor screening assay kit was purchased from Sigma-Aldrich. The assay was performed according to the guidelines of the manufacturer. Fluorescence signals were measured in a CLARIOstar plate reader (BMG Labtech).

#### HDAC *in vitro* inhibition assay

HDAC3 and HDAC8 inhibitor screening kits were purchased from Sigma-Aldrich. The assay was performed according to the guidelines of the manufacturer.

### Author contributions

Samir Yahiaoui, investigation, writing – original draft; Katrin Voos, investigation, validation, visualization, writing – original draft; Jörg Haupenthal, conceptualization, project administration, validation, writing – review & editing; Thomas A. Wichelhaus, project administration, resources, supervision, validation, visualization, writing – review & editing; Denia Frank, investigation; Lilia Weizel, investigation; Marco Rotter, investigation; Steffen Brunst, investigation; Jan S. Kramer, investigation; Ewgenij Proschak, project administration, supervision, validation, writing – review & editing; Christian Ducho, conceptualization, project administration, supervision, validation, writing – review & editing; Anna K. H. Hirsch, conceptualization, funding acquisition, project administration, supervision, validation, writing – review & editing.

### Conflicts of interest

There are no conflicts to declare.

### Acknowledgements

The authors thank Jeannine Jung and Jelena Konstantinović for excellent technical support. A. K. H. Hirsch gratefully acknowledges funding from the Helmholtz-Association's Initiative and Networking Fund. E. Proschak thanks German Research Foundation (DFG, Heisenberg-Professur PR1405/7-1) for financial support.

### Notes and references

- World Health Organization, Antibacterial Agents in Clinical Development, in *An Analysis of the Antibacterial Clinical Development Pipeline, Including Tuberculosis*, The World Health Organization, Geneva, 2017.
- R. E. W. Hancock and D. P. Speert, Antibiotic Resistance in *Pseudomonas Aeruginosa*: Mechanisms and Impact on Treatment, *Drug Resist. Updates*, 2000, 3(4), 247–255, DOI: 10.1054/drup.2000.0152.
- D. M. Ramsey and D. J. Wozniak, Understanding the Control of *Pseudomonas Aeruginosa* Alginate Synthesis and the Prospects for Management of Chronic Infections in Cystic Fibrosis: *P. Aeruginosa* Pathogenesis, *Mol. Microbiol.*, 2005, 56(2), 309–322, DOI: 10.1111/j.1365-2958.2005.04552.x.
- Z. Pang, R. Raudonis, B. R. Glick, T.-J. Lin and Z. Cheng, Antibiotic Resistance in *Pseudomonas Aeruginosa*: Mechanisms and Alternative Therapeutic Strategies, *Biotechnol. Adv.*, 2019, 37(1), 177–192, DOI: 10.1016/j.biotechadv.2018.11.013.
- M. Bassetti, A. Vena, A. Croxatto, E. Righi and B. Guery, How to Manage *Pseudomonas Aeruginosa* Infections, *Drugs Context*, 2018, 7, 1–18, DOI: 10.7573/dic.212527.
- K. Bush and P. A. Bradford,  $\beta$ -Lactams and  $\beta$ -Lactamase Inhibitors: An Overview, *Cold Spring Harb. Perspect. Med.*, 2016, 6(8), a025247, DOI: 10.1101/cshperspect.a025247.
- D. J. Wolter and P. D. Lister, Mechanisms of  $\beta$ -Lactam Resistance Among *Pseudomonas Aeruginosa*, *Curr. Pharm. Des.*, 2013, 19, 209–222, DOI: 10.2174/138161213804070311.
- D. Rawat and D. Nair, Extended-Spectrum  $\beta$ -Lactamases in Gram Negative Bacteria, *J. Global Infect. Dis.*, 2010, 2(3), 263–274, DOI: 10.4103/0974-777X.68531.
- A. A. Medeiros, Evolution and Dissemination of  $\beta$ -Lactamases Accelerated by Generations of  $\beta$ -Lactam Antibiotics, *Clin. Infect. Dis.*, 1997, 24(Supplement 1), S19–S45, DOI: 10.1093/clinids/24.supplement\_1.s19.
- A. A. Medeiros,  $\beta$ -Lactamases: Quality and Resistance, *Clin. Microbiol. Infect.*, 1997, 3, 4S2–4S9, DOI: 10.1016/S1198-743X(14)65030-8.
- M. I. Page and A. P. Laws, The Mechanism of Catalysis and the Inhibition of  $\beta$ -Lactamases, *Chem. Commun.*, 1998, 1609–1617, DOI: 10.1039/A803578D.
- K. A. Toussaint and J. C. Gallagher,  $\beta$ -Lactam/ $\beta$ -Lactamase Inhibitor Combinations: From Then to Now, *Ann. Pharmacother.*, 2015, 49(1), 86–98, DOI: 10.1177/1060028014556652.
- T. Palzkill, Metallo- $\beta$ -Lactamase Structure and Function, *Ann. N. Y. Acad. Sci.*, 2013, 1277(1), 91–104, DOI: 10.1111/j.1749-6632.2012.06796.x.
- C. Bebrone, Metallo- $\beta$ -Lactamases (Classification, Activity, Genetic Organization, Structure, Zinc Coordination) and Their Superfamily, *Biochem. Pharmacol.*, 2007, 74(12), 1686–1701, DOI: 10.1016/j.bcp.2007.05.021.
- M. I. Abboud, C. Damblon, J. Brem, N. Smargiasso, P. Mercuri, B. Gilbert, A. M. Rydzik, T. D. W. Claridge, C. J. Schofield and J.-M. Frère, Interaction of Avibactam with Class B Metallo- $\beta$ -Lactamases, *Antimicrob. Agents Chemother.*, 2016, 60(10), 5655–5662, DOI: 10.1128/AAC.00897-16.
- M.-N. Lisa, A. R. Palacios, M. Aitha, M. M. González, D. M. Moreno, M. W. Crowder, R. A. Bonomo, J. Spencer, D. L. Tierney, L. I. Llarrull and A. J. A. Vila, General Reaction Mechanism for Carbapenem Hydrolysis by Mononuclear and Binuclear Metallo- $\beta$ -Lactamases, *Nat. Commun.*, 2017, 8(1), 538, DOI: 10.1038/s41467-017-00601-9.
- P. Nordmann, L. Poirel, T. R. Walsh and D. M. Livermore, The Emerging NDM Carbapenemases, *Trends*

- Microbiol.*, 2011, **19**(12), 588–595, DOI: 10.1016/j.tim.2011.09.005.
- 18 M. F. Mojica, R. A. Bonomo and W. Fast, B1-Metallo- $\beta$ -Lactamases: Where Do We Stand?, *Curr. Drug Targets*, 2016, **17**(9), 1029–1050, DOI: 10.2174/1389450116666151001105622.
- 19 A. U. Khan, L. Maryam and R. Zarrilli, Structure, Genetics and Worldwide Spread of New Delhi Metallo- $\beta$ -Lactamase (NDM): A Threat to Public Health, *BMC Microbiol.*, 2017, **17**(1), 101, DOI: 10.1186/s12866-017-1012-8.
- 20 S. J. Hecker, K. R. Reddy, O. Lomovskaya, D. C. Griffith, D. Rubio-Aparicio, K. Nelson, R. Tsvikovski, D. Sun, M. Sabet, Z. Tarazi, J. Parkinson, M. Totrov, S. H. Boyer, T. W. Glinka, O. A. Pemberton, Y. Chen and M. N. Dudley, Discovery of Cyclic Boronic Acid QPX7728, an Ultrabroad-Spectrum Inhibitor of Serine and Metallo- $\beta$ -Lactamases, *J. Med. Chem.*, 2020, **63**(14), 7491–7507, DOI: 10.1021/acs.jmedchem.9b01976.
- 21 O. Lomovskaya, D. Rubio-Aparicio, K. Nelson, D. Sun, R. Tsvikovski, M. Castanheira, J. Lindley, J. Loutit and M. Dudley, In Vitro Activity of the Ultrabroad-Spectrum Beta-Lactamase Inhibitor QPX7728 in Combination with Multiple Beta-Lactam Antibiotics against *Pseudomonas Aeruginosa*, *Antimicrob. Agents Chemother.*, 2021, **65**(6), e00210-21, DOI: 10.1128/AAC.00210-21.
- 22 J. C. Hamrick, J.-D. Docquier, T. Uehara, C. L. Myers, D. A. Six, C. L. Chatwin, K. J. John, S. F. Vernacchio, S. M. Cusick, R. E. L. Trout, C. Pozzi, F. De Luca, M. Benvenuti, S. Mangani, B. Liu, R. W. Jackson, G. Moeck, L. Xerri, C. J. Burns, D. C. Pevear and D. M. Daigle, VNRX-5133 (Taniborbactam), a Broad-Spectrum Inhibitor of Serine- and Metallo- $\beta$ -Lactamases, Restores Activity of Cefepime in Enterobacterales and *Pseudomonas Aeruginosa*, *Antimicrob. Agents Chemother.*, 2020, **64**(3), e01963-19, DOI: 10.1128/AAC.01963-19.
- 23 B. Liu, R. E. L. Trout, G.-H. Chu, D. McGarry, R. W. Jackson, J. C. Hamrick, D. M. Daigle, S. M. Cusick, C. Pozzi, F. De Luca, M. Benvenuti, S. Mangani, J.-D. Docquier, W. J. Weiss, D. C. Pevear, L. Xerri and C. J. Burns, Discovery of Taniborbactam (VNRX-5133): A Broad-Spectrum Serine- and Metallo- $\beta$ -Lactamase Inhibitor for Carbapenem-Resistant Bacterial Infections, *J. Med. Chem.*, 2020, **63**(6), 2789–2801, DOI: 10.1021/acs.jmedchem.9b01518.
- 24 S. Mushtaq, A. Vickers, M. Doumith, M. J. Ellington, N. Woodford and D. M. Livermore, Activity of  $\beta$ -Lactam/Taniborbactam (VNRX-5133) Combinations against Carbapenem-Resistant Gram-Negative Bacteria, *J. Antimicrob. Chemother.*, 2021, **76**(1), 160–170, DOI: 10.1093/jac/dkaa391.
- 25 Faridooon and U. I. Nazar, An Update on the Status of Potent Inhibitors of Metallo- $\beta$ -Lactamases, *Sci. Pharm.*, 2013, **81**(2), 309–328, DOI: 10.3797/scipharm.1302-08.
- 26 Z. Cheng, C. A. Thomas, A. R. Joyner, R. L. Kimble, A. M. Sturgill, N.-Y. Tran, M. R. Vulcan, S. A. Klinsky, D. J. Orea, C. R. Platt, F. Cao, B. Li, Q. Yang, C. J. Yurkiewicz, W. Fast and M. W. Crowder, MBLInhibitors.Com, a Website Resource Offering Information and Expertise for the Continued Development of Metallo- $\beta$ -Lactamase Inhibitors, *Biomolecules*, 2020, **10**(3), 459, DOI: 10.3390/biom10030459.
- 27 T. J. Foster, J. A. Geoghegan, V. K. Ganesh and M. Höök, Adhesion, Invasion and Evasion: The Many Functions of the Surface Proteins of *Staphylococcus Aureus*, *Nat. Rev. Microbiol.*, 2014, **12**(1), 49–62, DOI: 10.1038/nrmicro3161.
- 28 J. W. Newman, R. V. Floyd and J. L. Fothergill, The Contribution of *Pseudomonas Aeruginosa* Virulence Factors and Host Factors in the Establishment of Urinary Tract Infections, *FEMS Microbiol. Lett.*, 2017, **364**(15), 1–11, DOI: 10.1093/femsle/fnx124.
- 29 K. Tam and V. J. Torres, *Staphylococcus aureus* Secreted Toxins and Extracellular Enzymes, in *Gram-Positive Pathogens*, ed. V. A. Fischetti, R. P. Novick, J. J. Ferretti, D. A. Portnoy, M. Braunstein and J. I. Rood, ASM Press, Washington, DC, USA, 2019, pp. 640–668, DOI: 10.1128/9781683670131.ch40.
- 30 S. T. Rutherford and B. L. Bassler, Bacterial Quorum Sensing: Its Role in Virulence and Possibilities for Its Control, *Cold Spring Harb. Perspect. Med.*, 2012, **2**(11), a012427–a012427, DOI: 10.1101/cshperspect.a012427.
- 31 M. B. Calvert, V. R. Jumde and A. Titz, Pathoblockers or Antivirulence Drugs as a New Option for the Treatment of Bacterial Infections, *Beilstein J. Org. Chem.*, 2018, **14**, 2607–2617, DOI: 10.3762/bjoc.14.239.
- 32 B. Wretling and O. R. Pavlovskis, *Pseudomonas Aeruginosa* Elastase and Its Role in *Pseudomonas* Infections, *Clin. Infect. Dis.*, 1983, **5**(Supplement\_5), S998–S1004, DOI: 10.1093/clinids/5.Supplement\_5.S998.
- 33 L. W. Heck, K. Morihara, W. B. McRae and E. J. Miller, Specific Cleavage of Human Type III and IV Collagens by *Pseudomonas Aeruginosa* Elastase, *Infect. Immun.*, 1986, **51**(1), 115–118, DOI: 10.1128/IAI.51.1.115-118.1986.
- 34 H. Yu, X. He, W. Xie, J. Xiong, H. Sheng, S. Guo, C. Huang, D. Zhang and K. Zhang, Elastase LasB of *Pseudomonas Aeruginosa* Promotes Biofilm Formation Partly through Rhamnolipid-Mediated Regulation, *Can. J. Microbiol.*, 2014, **60**(4), 227–235, DOI: 10.1139/cjm-2013-0667.
- 35 M. Parmely, A. Gale, M. Clabaugh, R. Horvat and W. W. Zhou, Proteolytic Inactivation of Cytokines by *Pseudomonas Aeruginosa*, *Infect. Immun.*, 1990, **58**(9), 3009–3014, DOI: 10.1128/IAI.58.9.3009-3014.1990.
- 36 A. Schmidtchen, I.-M. Frick, E. Andersson, H. Tapper and L. Björck, Proteinases of common pathogenic bacteria degrade and inactivate the antibacterial peptide LL-37, *Mol. Microbiol.*, 2002, **46**(1), 157–168, DOI: 10.1046/j.1365-2958.2002.03146.x.
- 37 Z. Kuang, Y. Hao, B. E. Walling, J. L. Jeffries, D. E. Ohman and G. W. Lau, *Pseudomonas Aeruginosa* Elastase Provides an Escape from Phagocytosis by Degrading the Pulmonary Surfactant Protein-A, *PLoS One*, 2011, **6**(11), e27091, DOI: 10.1371/journal.pone.0027091.
- 38 J. F. Alcorn and J. R. Wright, Degradation of Pulmonary Surfactant Protein D by *Pseudomonas Aeruginosa* Elastase Abrogates Innate Immune Function, *J. Biol. Chem.*, 2004, **279**(29), 30871–30879, DOI: 10.1074/jbc.M400796200.
- 39 A. M. Kany, A. Sikandar, J. Haupenthal, S. Yahiaoui, C. K. Maurer, E. Proschak, J. Köhnke and R. W. Hartmann, Binding Mode Characterization and Early in Vivo Evaluation of Fragment-Like Thiols as Inhibitors of the Virulence Factor



- LasB from *Pseudomonas Aeruginosa*, *ACS Infect. Dis.*, 2018, **4**(6), 988–997, DOI: 10.1021/acsinfectdis.8b00010.
- 40 E. Schönauer, A. M. Kany, J. Hauptenthal, K. Hüsecken, I. J. Hoppe, K. Voos, S. Yahiaoui, B. Elsässer, C. Ducho, H. Brandstetter and R. W. Hartmann, Discovery of a Potent Inhibitor Class with High Selectivity toward Clostridial Collagenases, *J. Am. Chem. Soc.*, 2017, **139**(36), 12696–12703, DOI: 10.1021/jacs.7b06935.
- 41 F.-M. Klingler, T. A. Wichelhaus, D. Frank, J. Cuesta-Bernal, J. El-Delik, H. F. Müller, H. Sjuts, S. Göttig, A. Koenigs, K. M. Pos, D. Pogoryelov and E. Proschak, Approved Drugs Containing Thiols as Inhibitors of Metallo- $\beta$ -Lactamases: Strategy To Combat Multidrug-Resistant Bacteria, *J. Med. Chem.*, 2015, **58**(8), 3626–3630, DOI: 10.1021/jm501844d.
- 42 J. Ma, Q. Cao, S. M. McLeod, K. Ferguson, N. Gao, A. L. Breeze and J. Hu, Target-Based Whole-Cell Screening by <sup>1</sup>H NMR Spectroscopy, *Angew. Chem., Int. Ed.*, 2015, **54**(16), 4764–4767, DOI: 10.1002/anie.201410701.
- 43 Y.-L. Wang, S. Liu, Z.-J. Yu, Y. Lei, M.-Y. Huang, Y.-H. Yan, Q. Ma, Y. Zheng, H. Deng, Y. Sun, C. Wu, Y. Yu, Q. Chen, Z. Wang, Y. Wu and G.-B. Li, Structure-Based Development of (1-(3'-Mercaptopropanamido)Methyl)Boronic Acid Derived Broad-Spectrum, Dual-Action Inhibitors of Metallo- and Serine- $\beta$ -Lactamases, *J. Med. Chem.*, 2019, **62**(15), 7160–7184, DOI: 10.1021/acs.jmedchem.9b00735.
- 44 Y. Yan, G. Li and G. Li, Principles and Current Strategies Targeting Metallo- $\beta$ -lactamase Mediated Antibacterial Resistance, *Med. Res. Rev.*, 2020, **40**(5), 1558–1592, DOI: 10.1002/med.21665.
- 45 S. Liu, L. Jing, Z.-J. Yu, C. Wu, Y. Zheng, E. Zhang, Q. Chen, Y. Yu, L. Guo, Y. Wu and G.-B. Li, ((S)-3-Mercapto-2-Methylpropanamido)Acetic Acid Derivatives as Metallo- $\beta$ -Lactamase Inhibitors: Synthesis, Kinetic and Crystallographic Studies, *Eur. J. Med. Chem.*, 2018, **145**, 649–660, DOI: 10.1016/j.ejmech.2018.01.032.
- 46 G.-B. Li, J. Brem, R. Lesniak, M. I. Abboud, C. T. Lohans, I. J. Clifton, S.-Y. Yang, J.-C. Jiménez-Castellanos, M. B. Avison, J. Spencer, M. A. McDonough and C. J. Schofield, Crystallographic Analyses of Isoquinoline Complexes Reveal a New Mode of Metallo- $\beta$ -Lactamase Inhibition, *Chem. Commun.*, 2017, **53**(43), 5806–5809, DOI: 10.1039/C7CC02394D.
- 47 J. Brem, S. S. van Berkel, D. Zollman, S. Y. Lee, O. Gileadi, P. J. McHugh, T. R. Walsh, M. A. McDonough and C. J. Schofield, Structural Basis of Metallo- $\beta$ -Lactamase Inhibition by Captopril Stereoisomers, *Antimicrob. Agents Chemother.*, 2016, **60**(1), 142–150, DOI: 10.1128/AAC.01335-15.
- 48 P. Chen, L. B. Horton, R. L. Mikulski, L. Deng, S. Sundriyal, T. Palzkill and Y. Song, 2-Substituted 4,5-Dihydrothiazole-4-Carboxylic Acids Are Novel Inhibitors of Metallo- $\beta$ -Lactamases, *Bioorg. Med. Chem. Lett.*, 2012, **22**(19), 6229–6232, DOI: 10.1016/j.bmcl.2012.08.012.
- 49 J. Brem, S. S. van Berkel, W. Aik, A. M. Rydzik, M. B. Avison, I. Pettinati, K.-D. Umland, A. Kawamura, J. Spencer, T. D. W. Claridge, M. A. McDonough and C. J. Schofield, Rhodanine Hydrolysis Leads to Potent Thioenolate Mediated Metallo- $\beta$ -Lactamase Inhibition, *Nat. Chem.*, 2014, **6**(12), 1084–1090, DOI: 10.1038/nchem.2110.
- 50 J. Brem, R. Cain, S. Cahill, M. A. McDonough, I. J. Clifton, J.-C. Jiménez-Castellanos, M. B. Avison, J. Spencer, C. W. G. Fishwick and C. J. Schofield, Structural Basis of Metallo- $\beta$ -Lactamase, Serine- $\beta$ -Lactamase and Penicillin-Binding Protein Inhibition by Cyclic Boronates, *Nat. Commun.*, 2016, **7**(1), 12406, DOI: 10.1038/ncomms12406.
- 51 S. T. Cahill, R. Cain, D. Y. Wang, C. T. Lohans, D. W. Wareham, H. P. Oswin, J. Mohammed, J. Spencer, C. W. G. Fishwick, M. A. McDonough, C. J. Schofield and J. Brem, Cyclic Boronates Inhibit All Classes of  $\beta$ -Lactamases, *Antimicrob. Agents Chemother.*, 2017, **61**(4), e02260-16, DOI: 10.1128/AAC.02260-16.
- 52 E. Tacconelli, N. Magrini, Y. Carmeli, S. Harbarth, G. Kahlmeter, J. Kluytmans, M. Mendelson, C. Pulcini, N. Singh and U. Theuretzbacher, *Global Priority List of Antibiotic-Resistant Bacteria to Guide Research, Discovery, and Development of New Antibiotics*, World Health Organization, 2017, vol. 27, pp. 318–327.
- 53 L. B. Rice, Federal Funding for the Study of Antimicrobial Resistance in Nosocomial Pathogens: No ESKAPE, *J. Infect. Dis.*, 2008, **197**(8), 1079–1081, DOI: 10.1086/533452.
- 54 A. Borer, L. Saidel-Odes, K. Riesenberger, S. Eskira, N. Peled, R. Nativ, F. Schlaeffer and M. Sherf, Attributable Mortality Rate for Carbapenem-Resistant *Klebsiella Pneumoniae* Bacteremia, *Infect. Control Hosp. Epidemiol.*, 2009, **30**(10), 972–976.
- 55 E. B. Hirsch and V. H. Tam, Detection and Treatment Options for *Klebsiella Pneumoniae* Carbapenemases (KPCs): An Emerging Cause of Multidrug-Resistant Infection, *J. Antimicrob. Chemother.*, 2010, **65**(6), 1119–1125, DOI: 10.1093/jac/dkq108.
- 56 P. Nordmann, G. Cuzon and T. Naas, The Real Threat of *Klebsiella Pneumoniae* Carbapenemase-Producing Bacteria, *Lancet Infect. Dis.*, 2009, **9**(4), 228–236, DOI: 10.1016/S1473-3099(09)70054-4.
- 57 S. Chatterjee, A. Mondal, S. Mitra and S. Basu, *Acinetobacter Baumannii* Transfers the BlaNDM-1 Gene via Outer Membrane Vesicles, *J. Antimicrob. Chemother.*, 2017, **72**(8), 2201–2207, DOI: 10.1093/jac/dkx131.
- 58 T. Krahn, D. Wibberg, I. Maus, A. Winkler, S. Bontron, A. Sczyrba, P. Nordmann, A. Pühler, L. Poirel and A. Schlüter, Intraspecies Transfer of the Chromosomal *Acinetobacter Baumannii* Bla NDM-1 Carbapenemase Gene, *Antimicrob. Agents Chemother.*, 2016, **60**(5), 3032–3040, DOI: 10.1128/AAC.00124-16.
- 59 H. Lee, J. Shin, Y.-J. Chung, M. Park, K. J. Kang, J. Y. Baek, D. Shin, D. R. Chung, K. R. Peck, J.-H. Song and K. S. Ko, Co-Introduction of Plasmids Harbouring the Carbapenemase Genes, BlaNDM-1 and BlaOXA-232, Increases Fitness and Virulence of Bacterial Host, *J. Biomed. Sci.*, 2020, **27**(1), 8, DOI: 10.1186/s12929-019-0603-0.
- 60 L. Poirel, Z. Al Maskari, F. Al Rashdi, S. Bernabeu and P. Nordmann, NDM-1-Producing *Klebsiella Pneumoniae* Isolated in the Sultanate of Oman, *J. Antimicrob. Chemother.*, 2011, **66**(2), 304–306, DOI: 10.1093/jac/dkq428.
- 61 E. Voulgari, C. Gartzonika, G. Vrioni, L. Politi, E. Priavali, S. Levidiotou-Stefanou and A. Tsakris, The Balkan Region:

- NDM-1-Producing *Klebsiella Pneumoniae* ST11 Clonal Strain Causing Outbreaks in Greece, *J. Antimicrob. Chemother.*, 2014, **69**(8), 2091–2097, DOI: 10.1093/jac/dku105.
- 62 J. A. Escobar Pérez, N. M. Olarte Escobar, B. Castro-Cardozo, I. A. Valderrama Márquez, M. I. Garzón Aguilar, L. Martínez de la Barrera, E. R. Barrero Barreto, R. A. Marquez-Ortiz, M. V. Moncada Guayazán and N. Vanegas Gómez, Outbreak of NDM-1-Producing *Klebsiella Pneumoniae* in a Neonatal Unit in Colombia, *Antimicrob. Agents Chemother.*, 2013, **57**(4), 1957–1960, DOI: 10.1128/AAC.01447-12.
- 63 A. Vannini, C. Volpari, G. Filocamo, E. C. Casavola, M. Brunetti, D. Renzoni, P. Chakravarty, C. Paolini, R. De Francesco, P. Gallinari, C. Steinkuhler and S. Di Marco, Crystal Structure of a Eukaryotic Zinc-Dependent Histone Deacetylase, Human HDAC8, Complexed with a Hydroxamic Acid Inhibitor, *Proc. Natl. Acad. Sci. U. S. A.*, 2004, **101**(42), 15064–15069, DOI: 10.1073/pnas.0404603101.
- 64 K. Maskos, C. Fernandez-Catalan, R. Huber, G. P. Bourenkov, H. Bartunik, G. A. Ellestad, P. Reddy, M. F. Wolfson, C. T. Rauch, B. J. Castner, R. Davis, H. R. G. Clarke, M. Petersen, J. N. Fitzner, D. P. Cerretti, C. J. March, R. J. Paxton, R. A. Black and W. Bode, Crystal Structure of the Catalytic Domain of Human Tumor Necrosis Factor- $\alpha$ -Converting Enzyme, *Proc. Natl. Acad. Sci. U. S. A.*, 1998, **95**(7), 3408–3412, DOI: 10.1073/pnas.95.7.3408.
- 65 P. J. Watson, L. Fairall, G. M. Santos and J. W. R. Schwabe, Structure of HDAC3 Bound to Co-Repressor and Inositol Tetraphosphate, *Nature*, 2012, **481**(7381), 335–340, DOI: 10.1038/nature10728.
- 66 K. Struhl, Histone Acetylation and Transcriptional Regulatory Mechanisms, *Genes Dev.*, 1998, **12**, 599–606.
- 67 B. G. Pogo, V. G. Allfrey and A. E. Mirsky, RNA Synthesis and Histone Acetylation during the Course of Gene Activation in Lymphocytes, *Proc. Natl. Acad. Sci. U. S. A.*, 1966, **55**(4), 805–812, DOI: 10.1073/pnas.55.4.805.
- 68 F. Zunke and S. Rose-John, The Shedding Protease ADAM17: Physiology and Pathophysiology, *Biochim. Biophys. Acta, Mol. Cell Res.*, 2017, **1864**(11), 2059–2070, DOI: 10.1016/j.bbamcr.2017.07.001.
- 69 M. Gooz, ADAM-17: The Enzyme That Does It All, *Crit. Rev. Biochem. Mol. Biol.*, 2010, **45**(2), 146–169, DOI: 10.3109/10409231003628015.
- 70 J. Scheller, A. Chalaris, C. Garbers and S. Rose-John, ADAM17: A Molecular Switch to Control Inflammation and Tissue Regeneration, *Trends Immunol.*, 2011, **32**(8), 380–387, DOI: 10.1016/j.it.2011.05.005.
- 71 R. Menghini, L. Fiorentino, V. Casagrande, R. Lauro and M. Federici, The Role of ADAM17 in Metabolic Inflammation, *Atherosclerosis*, 2013, **228**(1), 12–17, DOI: 10.1016/j.atherosclerosis.2013.01.024.
- 72 A. M. Kany, A. Sikandar, S. Yahiaoui, J. Haupenthal, I. Walter, M. Empting, J. Köhnke and R. W. Hartmann, Tackling *Pseudomonas Aeruginosa* Virulence by a Hydroxamic Acid-Based LasB Inhibitor, *ACS Chem. Biol.*, 2018, **13**(9), 2449–2455, DOI: 10.1021/acscchembio.8b00257.
- 73 J. Konstantinović, S. Yahiaoui, A. Alhayek, J. Haupenthal, E. Schönauer, A. Andreas, A. M. Kany, R. Mueller, J. Köhnke, F. Berger, M. Bischoff, R. W. Hartmann, H. Brandstetter and A. K. H. Hirsch, N-Aryl-3-Mercaptosuccinimides as Antivirulence Agents Targeting *Pseudomonas Aeruginosa* Elastase and *Clostridium* Collagenases, *J. Med. Chem.*, 2020, **63**(15), 8359–8368, DOI: 10.1021/acscimedchem.0c00584.
- 74 A. Rukavishnikov, K. R. Gee, I. Johnson and S. Corry, Fluorogenic Cephalosporin Substrates for  $\beta$ -Lactamase TEM-1, *Anal. Biochem.*, 2011, **419**(1), 9–16, DOI: 10.1016/j.ab.2011.07.020.

## IV. UNPUBLISHED RESULTS

### **Chapter E: *N*-Aryl-2-*iso*-butylmercaptoacetamides: the discovery of highly potent and selective inhibitors of *Pseudomonas aeruginosa* virulence factor LasB and *Clostridium histolyticum* virulence factor ColH**

Katrin Voos,<sup>±</sup> Samir Yahiaoui,<sup>±</sup> Jelena Konstantinović, Esther Schönauer, Alaa Alhayek, Asfandiyar Sikandar, Khadija Si Chaib, Tizian F. Ramspoth, Katharina Rox, Jörg Hauptenthal, Jesko Köhnke, Hans Brandstetter, Christian Ducho\* and Anna K. H. Hirsch\*

<sup>±</sup> these authors contributed equally

\* corresponding authors

Manuscript in preparation – Version 1  
uploaded to ChemRxiv® on April 25<sup>th</sup>, 2022  
DOI: 10.26434/chemrxiv-2022-fjrqr

*Please note that this chapter comprises a manuscript in preparation uploaded to a pre-print server and has not been peer-reviewed. Therefore, compound numbers of this chapter are independent from other parts of this thesis.*

#### **Full contribution report:**

A. K. H. H., C. D., S. Y. and K. V. conceived and coordinated the study. K.V. synthesized 81 compounds and intermediates, contributed to the SAR interpretation, conceived, and wrote parts of the manuscript. S. Y. synthesized 21 compounds and intermediates, contributed to the SAR interpretation, conceived, and wrote parts of the manuscript. S. Y and K. V. contributed equally. J. Konstantinović synthesized 8 compounds and intermediates, planned and performed the LasB functional assay, and edited the manuscript. A. K. H. H., C. D. and H.B. edited the manuscript, supplied funding, and supervised the project. J. H. edited the manuscript, planned MMP, HDAC, TACE and cytotoxicity assays. E. S. expressed and purified ColH, planned and performed the ColH functional assay, planned and performed the ColH crystallization experiments and structure determination. A. A. planned and performed the skin- (NHDF) and lung-cell (A549) degradation assays and the according microscopic evaluation, planned the *Galleria mellonella* larvae efficacy model. K. S. C. performed the *Galleria mellonella* larvae efficacy model. J. Köhnke and A. S. planned and performed the LasB crystallization experiments and structure determination. T. F. R. synthesized compounds **13**, **14** and **17**. K. R. planned and performed the *in vivo* PK study. All authors reviewed the results and approved the final version of the manuscript.



***N*-Aryl-2-*iso*-butylmercaptoacetamides: the discovery of highly potent and selective inhibitors of *Pseudomonas aeruginosa* virulence factor LasB and *Clostridium histolyticum* virulence factor ColH**

Katrin Voos,<sup>1</sup>⊥ Samir Yahiaoui,<sup>2</sup>⊥ Jelena Konstantinović,<sup>2</sup> Esther Schönauer,<sup>3</sup> Alaa Alhayek,<sup>2,4</sup> Asfandyar Sikandar,<sup>2</sup> Khadidja Si Chaib,<sup>2</sup> Tizian F. Ramspoth,<sup>2</sup> Katharina Rox,<sup>5,6</sup> Jörg Hauptenthal,<sup>2</sup> Jesko Köhnke,<sup>7</sup> Hans Brandstetter,<sup>3</sup> Christian Ducho<sup>1\*</sup> and Anna K. H. Hirsch<sup>2,4\*</sup>

⊥ these authors contributed equally

\* Corresponding authors: [Christian.Ducho@uni-saarland.de](mailto:Christian.Ducho@uni-saarland.de) & [Anna.Hirsch@helmholtz-hips.de](mailto:Anna.Hirsch@helmholtz-hips.de)

- <sup>1</sup> Department of Pharmacy, Pharmaceutical and Medicinal Chemistry, Saarland University, Campus C2 3, 66123 Saarbrücken, Germany
- <sup>2</sup> Helmholtz Institute for Pharmaceutical Research Saarland (HIPS) – Helmholtz Centre for Infection Research (HZI), Campus E8 1, 66123 Saarbrücken, Germany
- <sup>3</sup> Department of Biosciences and Christian Doppler Laboratory for Innovative Tools for Bio-similar Characterization, Division of Structural Biology, University of Salzburg, Billrothstrasse 11, 5020 Salzburg, Austria
- <sup>4</sup> Department of Pharmacy, Saarland University, Campus Building E8 1, 66123 Saarbrücken, Germany
- <sup>5</sup> Department of Chemical Biology, Helmholtz Centre for Infection Research, Inhoffenstrasse 7, 38124 Braunschweig, Germany
- <sup>6</sup> German Center for Infection Research (DZIF), Site Hannover-Braunschweig, Germany
- <sup>7</sup> School of Chemistry, University of Glasgow, Glasgow, G12 8QQ, United Kingdom

## Abstract

Antimicrobial resistance is currently one of the serious global public health threats. Unlike the conventional antimicrobial drugs, antivirulence agents disarm rather than kill bacterial pathogens and therefore represent an alternative option to skirt the problem of resistance. *Pseudomonas aeruginosa* elastase (LasB) and *Clostridium histolyticum* collagenase (ColH) are extracellular bacterial proteases which play a critical role in the establishment and progression of the respective bacterial infection. In this study, we report the modulation of the  $\alpha$ -position of the previously reported *N*-aryl mercaptoacetamide class leading to a new type of highly potent LasB and ColH inhibitors (*N*-aryl-2-*iso*-butylmercaptoacetamides). In addition to their non-toxicity and high selectivity over several human off-targets, selected derivatives may be considered unprecedented dual inhibitors of both LasB and ColH. Among the prepared derivatives, compound **37** showed the most promising properties: it had a favorable safety profile, maintained the viability and integrity of both skin- and lung-cells treated with *P. aeruginosa* supernatant, demonstrated *in vivo* efficacy in *Galleria mellonella* larvae, and revealed a good volume of distribution and moderate *in vivo* clearance in mice. Taking together, these results demonstrate that compound **37** is a promising candidate for antivirulence drug development.

## Introduction

Facing the alarming situation of antibiotic resistance worldwide, targeting bacterial virulence factors is gaining interest as a novel non-traditional antimicrobial approach.<sup>1-4</sup> Virulence factors comprise several substances produced by the bacterium that promote the establishment and the progression of the infection, but are not vital for its survival.<sup>5</sup> Unlike traditional antibiotics, the use of antivirulence agents aims at disarming pathogens rather than killing them, which may result in a weaker selection pressure on bacteria and preserves the commensal bacteria.<sup>6</sup>

Toxins, cell surface proteins and extracellular enzymes are among the most important bacterial virulence factors.<sup>7-9</sup> They contribute to the pathogenesis of the disease through several mechanisms, including the formation of biofilms (which protect bacteria from environmental changes), the adhesion to host-cell surface, the evasion of the innate immune system, and the invasion of host-cells and tissues.<sup>10,11</sup>

Produced by both Gram-positive and Gram-negative bacteria, extracellular proteases are particularly important for the growth and the proliferation of bacteria and therefore represent attractive targets for novel antivirulence drugs.<sup>12,13</sup> According to the WHO, *Pseudomonas aeruginosa* is currently one of the most problematic pathogens.<sup>14</sup> This opportunistic Gram-negative bacillus is a leading cause of nosocomial infections<sup>15</sup> and is characterized by high resistance to many classes of antibiotics.<sup>16</sup> LasB is an extracellular zinc- and calcium-containing metalloprotease<sup>17</sup> needed for the cleavage of connective tissue components such as elastin<sup>18</sup> and collagen.<sup>19</sup> Moreover, in addition to promoting biofilm formation,<sup>20</sup> LasB was also found to degrade multiple host defense barriers such as cytokines,<sup>21</sup> surfactant proteins<sup>22,23</sup> and the natural antimicrobial peptide (AMP) LL-37.<sup>24</sup>

Recently, we have identified *N*-aryl mercaptoacetamides as a novel class of inhibitors displaying low micromolar potency towards LasB (Figure 1, compd. **1**: IC<sub>50</sub> (LasB) = 6.6 ± 0.3 μM).<sup>25</sup> For those compounds, lipophilic (multi-)substitution on the aryl ring was highly favored over hydrophilic *para*-substitution (compd. **1** four times more active than compd. **2**: IC<sub>50</sub> (LasB) = 24 ± 1 μM). The same class of compounds was found to inhibit another protease from the human pathogen *Clostridium histolyticum* (since 2016 renamed to *Hathewayia histolytica*), *i.e.*, collagenase H (ColH), in the nanomolar range.<sup>26</sup> Interestingly,

mercaptoacetamides have shown an inverse activity profile on ColH compared to their LasB inhibition, with the compound bearing a 4-acetyl (4-Ac) function being the most potent congener (compd. **3**:  $IC_{50}$  (ColH) =  $0.017 \pm 0.002 \mu\text{M}$ ).<sup>26</sup> ColH is also an extracellular zinc- and calcium-containing metalloprotease that catalyzes the hydrolysis of collagen. It is therefore crucial for host invasion, colonization and toxin diffusion.<sup>27–29</sup> Recently, we were able to drastically improve the inhibitory activity of *N*-aryl mercaptoacetamides towards LasB by introducing substituted benzyl moieties in the  $\alpha$ -position (Figure 1, compds. **4** and **5**).<sup>30,31</sup> This finding revealed that the modulation of the  $\alpha$ -position might lead to inhibitors capable to occupy the lipophilic S1' binding pocket of LasB with their side chain and may therefore improve the inhibitory efficiency.

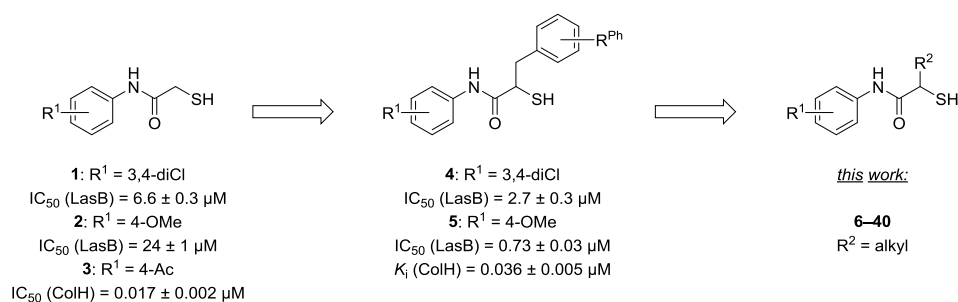


**Figure 1.** Development of *N*-aryl mercaptoacetamides as inhibitors of LasB and ColH.<sup>25,26,30,31</sup>

To further explore the effects of other substituents in the  $\alpha$ -position, we herein describe the design, synthesis, and biological evaluation of 35 novel  $\alpha$ -alkylated mercaptoacetamides **6–40**.

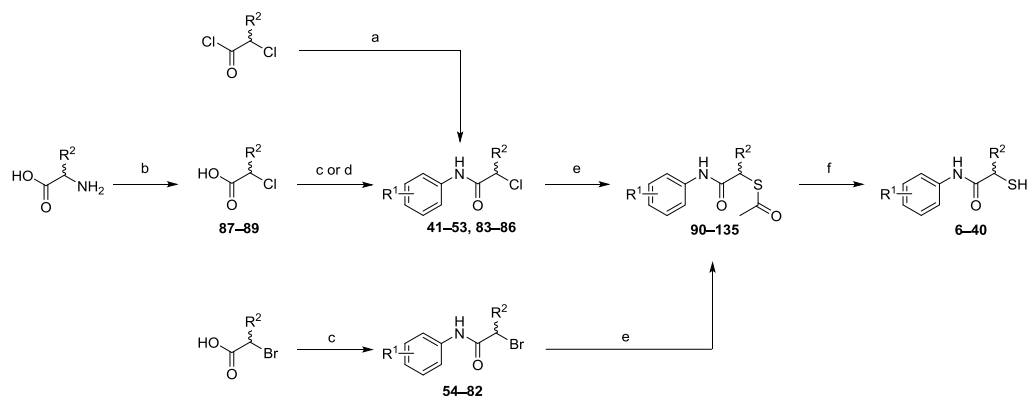
For the  $\alpha$ -unsubstituted mercaptoacetamides, we have demonstrated that nonpolar substituents on the aryl ring, in particular halogens, are more favorable for LasB inhibition than hydrophilic substituents.<sup>25</sup> However, in the case of  $\alpha$ -benzylated derivatives, both polar and nonpolar groups were found to be beneficial for the activity.<sup>30,31</sup> Based on this, we decided to modify both the  $\alpha$ -side chain with a total of nine different alkyl substituents and the aryl moiety and to investigate the resultant LasB inhibitory activity.

Following promising results on LasB inhibition, the inhibitory effects on ColH were also determined. Co-crystal structures of both LasB and ColH were solved, and our most promising hit compound was tested for cytotoxicity and its selectivity over a large panel of relevant human

off-targets. Moreover, *in vitro* assays using lung and skin cells, as well as *in vivo* studies in *Galleria mellonella* larvae were performed together with first pharmacokinetic (PK) studies in mice.

## Results and discussion

**Synthesis of *N*-aryl-2-alkylmercaptoacetamides.** The synthesis of  $\alpha$ -alkylated mercaptoacetamide derivatives **6–40** is outlined in Scheme 1. The target molecules were obtained through a multi-step synthetic route involving *N*-aryl-2-halo-2-alkylacetamides (**41–89**) and *N*-aryl-2-acetylthio-2-alkylacetamides (**90–135**) as synthetic intermediates. The *N*-aryl-2-halo-2-alkylacetamides resulted either from the condensation of a 2-haloalkanoic acid chloride and the corresponding aniline in the presence of diisopropylethylamine ((a) **41–53**) or of a 2-haloalkanoic acid and the corresponding aniline with EDC·HCl ((c) **54–82** with halo = Br, **83–85** with halo = Cl). Alternatively (in the case of compound **86**), the condensation was performed using ethyl chloroformate and trimethylamine (d). The required 2-haloalkanoic acid chlorides, as well as the 2-bromoalkanoic acids were commercially available, while the 2-chloroalkanoic acids **87–89** were prepared from their corresponding racemic amino acids *via* diazotization and subsequent chlorination using sodium nitrite and hydrochloric acid.<sup>32</sup> Using potassium thioacetate, the *N*-aryl-2-halo-2-alkylacetamides **41–89** were transformed into the *N*-aryl-2-acetylthio derivatives **90–135**. Finally, the conversion of the *N*-aryl-2-acetylthio-2-alkylacetamides into their corresponding free thiol forms **6–40** was carried out using sodium hydroxide in methanol. It should be noted that 4-Ac-substituted *N*-Aryl mercaptoacetamides gave more unwanted side products and had a lower overall yield than other hydrophilic compounds (*e.g.*, compd. **7** (*p*-OMe,  $\alpha$ -Me) overall yield 72% *vs.* 55% for compd. **10** (*p*-Ac,  $\alpha$ -Me)).

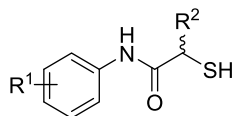


**Scheme 1.** Synthetic scheme of  $\alpha$ -alkylated derivatives (for exact structures of intermediates, see Supporting Information, Table S1). *Reagents and conditions:* (a)  $R^1$ -aniline, DIPEA, DCM, 0 °C; (b) sodium nitrite, 6 N HCl,  $-5$  °C to r.t.; (c)  $R^1$ -aniline, EDC·HCl, DCM, r.t. (d)  $R^1$ -aniline,  $\text{ClCO}_2\text{Et}$ ,  $\text{NET}_3$ , THF, r.t.; (e) potassium thioacetate, acetone, r.t.; (f) NaOH, MeOH, r.t.

**Screening of alkyl-substituted mercaptoacetamides for LasB inhibition.** First, a methyl (Me) and an *n*-propyl (*n*Pr) side chain were introduced into the  $\alpha$ -position of a total of six different *N*-aryl mercaptoacetamide derivatives to study the influence of those alkyl  $\alpha$ -side chains on the inhibitory activity. Synthesized compounds were evaluated for their inhibitory *in vitro* effects on LasB using a FRET-based inhibition assay.<sup>25</sup> The results are reported in Table 1, together with the previously obtained data for the non-alkylated derivatives **1–3**, and **136–138**.<sup>25,33</sup>

From the obtained data (Table 1), we were not able to derive a fully additive structure–activity relationship (SAR) between the introduction of a side chain in the  $\alpha$ -position and the variation of the substituents in the aryl moiety. Instead, the methyl-substituted compounds **6–11** showed similar activities as the  $\alpha$ -unsubstituted compounds, favoring nonpolar substituents in the aryl unit. For instance, the 3,4-dichlorophenyl (3,4-diCl) derivative without an  $\alpha$ -side chain **1** was up to four times more active than the corresponding 4-methoxyphenyl (4-OMe) derivative **2**. With a methyl group in the  $\alpha$ -position, the activity of compound **6** was even ten-fold higher than that of compound **7**.

**Table 1.** LasB inhibition values of compounds bearing either no side chain (**1–3**, **136–138**), a methyl group (**6–11**), or an *n*-propyl side chain (**12–17**) in the  $\alpha$ -position.



$R^2 = H$			$R^2 = Me$			$R^2 = nPr$		
Compd.	$R^1$	$IC_{50}$ ( $\mu M$ ) <sup>a</sup>	Compd.	$R^1$	$IC_{50}$ ( $\mu M$ ) <sup>a</sup>	Compd.	$R^1$	$IC_{50}$ ( $\mu M$ ) <sup>a</sup>
<b>1</b>	3,4-diCl	$6.6 \pm 0.3$ <sup>25</sup>	<b>6</b>	3,4-diCl	$4.5 \pm 0.7$	<b>12</b>	3,4-diCl	$4.0 \pm 0.6$
<b>2</b>	4-OMe	$24 \pm 1$ <sup>33</sup>	<b>7</b>	4-OMe	$45 \pm 1$	<b>13</b>	4-OMe	$2.4 \pm 0.6$
<b>136</b>	4-Me	$19 \pm 1$ <sup>33</sup>	<b>8</b>	4-Me	$40 \pm 3$	<b>14</b>	4-Me	$2.0 \pm 0.3$
<b>137</b>	4-Cl	$21 \pm 1$ <sup>25</sup>	<b>9</b>	4-Cl	$16 \pm 2$	<b>15</b>	4-Cl	$4.8 \pm 0.2$
<b>3</b>	4-Ac	$72 \pm 5$ <sup>33</sup>	<b>10</b>	4-Ac	$89 \pm 10$	<b>16</b>	4-Ac	$2.6 \pm 0.5$
<b>138</b>	H	$39 \pm 3$ <sup>33</sup>	<b>11</b>	H	$75 \pm 11$	<b>17</b>	H	$4.8 \pm 0.5$

<sup>a</sup>Means and SD of at least two independent experiments

However, when a slightly bulkier  $\alpha$ -side chain such as *n*-propyl was introduced, the activities changed significantly. With this side chain motif, the 4-OMe compound **13** ( $IC_{50} = 2.4 \pm 0.6 \mu M$ ) became two times more active than the corresponding 3,4-diCl compound **12**, and three times more active than the non-alkylated 3,4-diCl compound **1**. This was also the case, in an even more pronounced way, for the 4-acetyl (4-Ac) derivatives. Here, the *n*-propyl congener **16** was 27-fold more active than the non-alkylated derivative **3** ( $IC_{50} = 2.6 \pm 0.5 \mu M$  vs.  $IC_{50} = 72 \pm 5 \mu M$ , respectively).

Previously, we had already observed that  $\alpha$ -benzylation resulted in the 4-OMe derivative (**5**,  $IC_{50} = 0.73 \pm 0.03 \mu M$ )<sup>31</sup> becoming more potent than the corresponding 3,4-diCl compound (**4**,  $IC_{50} = 2.7 \pm 0.3 \mu M$ )<sup>30</sup> (Table 2). Having this in mind, we decided to further explore the differences of 4-OMe and 3,4-diCl derivatives by varying their  $\alpha$ -side chains, as these two aryl substitution patterns have a pronounced difference in their polarity (though the 4-Me derivative **14** and 4-Ac derivative **16** were equipotent to the 4-OMe compound **13**).

Therefore, we synthesized 3,4-diCl and 4-OMe derivatives bearing in total another seven alkyl groups from small to bulky in the  $\alpha$ -position (ethyl (Et), *iso*-propyl (*i*Pr), *iso*-butyl (*i*Bu), *sec*-butyl (*s*Bu), *n*-butyl (*n*Bu), cyclopropylmethyl and cyclohexylmethyl). The *in vitro* results are

reported in Table 2, together with the previously obtained data of the  $\alpha$ -unsubstituted (**1,2**),<sup>25,33</sup>  $\alpha$ -benzyl (**4,5**),<sup>30,31</sup>  $\alpha$ -methyl (**6,7**) and  $\alpha$ -*n*-propyl (**12,13**) derivatives.

**Table 2.** LasB inhibition values of 3,4-dichlorophenyl and 4-methoxyphenyl mercaptoacetamides bearing eleven different side chain motifs in the  $\alpha$ -position.

R <sup>1</sup> = 3,4-diCl			R <sup>1</sup> = 4-OMe		
Compd.	R <sup>2</sup>	IC <sub>50</sub> (μM) <sup>a</sup>	Compd.	R <sup>2</sup>	IC <sub>50</sub> (μM) <sup>a</sup>
<b>1</b>	H	6.6 ± 0.3 <sup>25</sup>	<b>2</b>	H	24 ± 1 <sup>33</sup>
<b>4</b>	Bn	2.7 ± 0.3 <sup>30</sup>	<b>5</b>	Bn	0.73 ± 0.03 <sup>31</sup>
<b>6</b>	Me	4.5 ± 0.7	<b>7</b>	Me	45 ± 1
<b>18</b>	Et	2.4 ± 0.4	<b>23</b>	Et	4.2 ± 0.7
<b>19</b>	<i>i</i> Pr	2.5 ± 0.3	<b>24</b>	<i>i</i> Pr	16 ± 2
<b>12</b>	<i>n</i> Pr	4.0 ± 0.6	<b>13</b>	<i>n</i> Pr	2.4 ± 0.6
<b>20</b>	<i>i</i> Bu	2.6 ± 0.3	<b>25</b>	<i>i</i> Bu	0.36 ± 0.11
<b>21</b>	<i>n</i> Bu	6.8 ± 1.1	<b>26</b>	<i>n</i> Bu	2.8 ± 0.3
<b>22</b>	<i>s</i> Bu	7.5 ± 0.3	<b>27</b>	<i>s</i> Bu	17 ± 2
<b>139</b>	cyclopropylmethyl	6.3 ± 1.2 <sup>30</sup>	<b>28</b>	cyclopropylmethyl	3.9 ± 0.7
<b>140</b>	cyclohexylmethyl	12 ± 3 <sup>30</sup>	<b>29</b>	cyclohexylmethyl	2.6 ± 1.3

<sup>a</sup>Means and SD of at least two independent experiments

As expected, the 3,4-diCl and 4-OMe derivatives of each  $\alpha$ -substituted compound displayed different inhibitory effects towards LasB. As previously observed (Table 1), the substituents on the aryl ring that are favorable for the activity depend on the structure of the  $\alpha$ -side chain. As for the  $\alpha$ -unsubstituted class, the halogen substituents turned out to be favorable for the methyl, ethyl, *iso*-propyl and *sec*-butyl side chains. However, the introduction of *n*-propyl, *iso*-butyl, *n*-butyl, cyclopropylmethyl and cyclohexylmethyl units, respectively, resulted in more potent 4-OMe derivatives, as previously found for the  $\alpha$ -benzylated compound **5**.

Among compounds bearing chlorine substituents, the most active congeners were compounds **18** (Et), **19** (*i*Pr) and **20** (*i*Bu), with IC<sub>50</sub> values similar to the benzylated derivative **4** (IC<sub>50</sub> = 2.7 ± 0.3 μM). Regarding the methoxy-substituted compounds, **25** (*i*Bu) showed the most

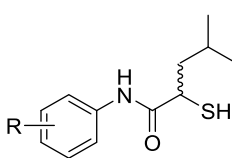


potent LasB inhibition. Interestingly, with an  $IC_{50}$  value of  $0.36 \pm 0.11 \mu\text{M}$ , **25** was two-fold more potent than compound **5**. Therefore, the *iso*-butyl motif appears to be even more advantageous for LasB inhibition than the benzyl group.

Since the inhibitory potencies strongly depended on the nature of the groups on the aryl ring and also with respect to the promising results obtained for compound **25**, we decided to further modify the aryl moiety of the  $\alpha$ -*iso*-butyl class. Consequently, nine additional *N*-aryl 2-*iso*-butylmercaptoacetamides were synthesized and evaluated for LasB inhibition.

***N*-aryl-2-*iso*-butylmercaptoacetamides as the most promising LasB inhibitors.** The novel  $\alpha$ -*iso*-butyl derivatives **30–38** were synthesized according to the aforementioned general procedure (Scheme 1). Different substituents were introduced on the aryl ring to elucidate the SAR for LasB inhibition of this novel class. The obtained  $IC_{50}$  values are reported in Table 3.

**Table 3.** LasB inhibition values of *N*-aryl-2-*iso*-butylmercaptoacetamides.



Compd.	R	$IC_{50}$ ( $\mu\text{M}$ ) <sup>a</sup>
<b>20</b>	3,4-diCl	$2.6 \pm 0.3$
<b>25</b>	4-OMe	$0.36 \pm 0.11$
<b>30</b>	3-OMe	$0.56 \pm 0.03$
<b>31</b>	2-OMe	$0.70 \pm 0.04$
<b>32</b>	2,4-di-OMe	$0.42 \pm 0.06$
<b>33</b>	3,4-di-OMe	$0.73 \pm 0.10$
<b>34</b>	4-OH	$0.96 \pm 0.13$
<b>35</b>	2-OH	$1.4 \pm 0.2$
<b>36</b>	4-Ac	$0.69 \pm 0.34$
<b>37</b>	4-Me	$0.40 \pm 0.13$
<b>38</b>	4-Cl	$0.84 \pm 0.24$

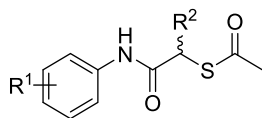
<sup>a</sup>Means and SD of at least two independent experiments.

Remarkably, nine out of eleven tested  $\alpha$ -*iso*-butyl-substituted derivatives showed sub-micromolar activities against LasB, thus highlighting the relevance of this structural variation. Comparing the 4-OMe derivatives, *para*-substitution (**25**) appeared to be slightly preferred over *ortho*- (**31**) and *meta*-substitution (**30**). The same effect was found with the phenols **34** (4-OH,  $IC_{50} = 0.96 \pm 0.13 \mu M$ ) and **35** (2-OH,  $IC_{50} = 1.4 \pm 0.2 \mu M$ ). However, differences in potencies of these derivatives were very moderate. Di-substitution on the aryl moiety was tolerated without a significant influence on the activity when polar groups were introduced, but the lipophilic 3,4-diCl substitution led to the least active inhibitor in this series (**20**,  $IC_{50} = 2.6 \pm 0.3 \mu M$ ). In contrast, the most active compounds **25** (4-OMe), **32** (2,4-diOMe) and **37** (4-Me) were five-fold more active than **20** and almost two-fold more active than the  $\alpha$ -benzylated 4-OMe derivative **5**.

**Screening of alkyl-substituted mercaptoacetamides for ColH inhibition.** Encouraged by the promising results on LasB, we investigated whether the  $\alpha$ -side chain could also positively affect the potencies of *N*-aryl mercaptoacetamides as inhibitors of the collagenase ColH.

We have previously reported that thiocarbamates can serve as precursors of *N*-aryl mercaptoacetamides, forming the latter as active ColH inhibitors by *in situ* hydrolysis of the thiocarbamate moiety in ColH assays.<sup>26</sup> Similarly, we have now employed thioacetates as hydrolytically labile thiol precursors that would be partially hydrolyzed to the corresponding thiols under the conditions of the ColH assay. The resultant inhibitory activities against ColH observed for those thioacetates were about 20- to 100-fold weaker than for the corresponding thiols, but they followed the same trend (see Supporting Information, Figures S1, S2 and Table S2). To investigate such relative trends, there is no need to use the oxidation-labile thiols directly in the assay. Instead, thioacetates (that are easier to handle and store as they cannot oxidize to the inactive disulfide form) can be used as surrogates of the free thiols. Hence, for a first exploration of ColH inhibition by novel  $\alpha$ -substituted *N*-aryl mercaptoacetamides, their thioacetate analogs with nine different aryl substitutions and either no side chain, a methyl or an *n*-propyl unit in the  $\alpha$ -position were evaluated for their inhibitory activities against ColH using the established FRET-based *in vitro* inhibition assay.<sup>26</sup> The obtained results are reported in Table 4.

**Table 4.** ColH inhibition values of thioacetate compounds bearing no side chain, a methyl or an *n*-propyl substituent in the  $\alpha$ -position.



R <sup>2</sup> = H			R <sup>2</sup> = Me			R <sup>2</sup> = <i>n</i> Pr		
Compd.	R <sup>1</sup>	Inhibition [%] at 10 $\mu$ M <sup>a</sup>	Compd.	R <sup>1</sup>	Inhibition [%] at 10 $\mu$ M <sup>a</sup>	Compd.	R <sup>1</sup>	Inhibition [%] at 10 $\mu$ M <sup>a</sup>
<b>141</b> <sup>33</sup>	4-OMe	88 $\pm$ 2	<b>93</b>	4-OMe	96 $\pm$ 1	<b>102</b>	4-OMe	98 $\pm$ 3
<b>142</b> <sup>33</sup>	2-Me	-4 $\pm$ 1	<b>94</b>	2-Me	0 $\pm$ 2	<b>103</b>	2-Me	2 $\pm$ 1
<b>143</b> <sup>33</sup>	3-Me	-1 $\pm$ 3	<b>95</b>	3-Me	11 $\pm$ 3	<b>104</b>	3-Me	26 $\pm$ 1
<b>144</b> <sup>33</sup>	4-Me	44 $\pm$ 4	<b>96</b>	4-Me	87 $\pm$ 3	<b>105</b>	4-Me	90 $\pm$ 1
<b>90</b>	2-Cl	0 $\pm$ 1	<b>97</b>	2-Cl	0 $\pm$ 2	<b>106</b>	2-Cl	6 $\pm$ 5
<b>145</b> <sup>33</sup>	3-Cl	3 $\pm$ 2	<b>98</b>	3-Cl	2 $\pm$ 3	<b>107</b>	3-Cl	23 $\pm$ 2
<b>91</b>	4-Cl	80 $\pm$ 5	<b>99</b>	4-Cl	86 $\pm$ 1	<b>108</b>	4-Cl	97 $\pm$ 1
<b>92</b>	4-Ac	73 $\pm$ 3	<b>100</b>	4-Ac	91 $\pm$ 1	<b>109</b>	4-Ac	93 $\pm$ 1
<b>146</b> <sup>33</sup>	H	0 $\pm$ 2	<b>101</b>	H	15 $\pm$ 2	<b>110</b>	H	10 $\pm$ 5

<sup>a</sup>Means and SD of at least two independent experiments

In contrast to the influence of an  $\alpha$ -side chain on LasB inhibition, one can observe an additive SAR for ColH inhibition of almost all thioacetates. Regardless of the aryl substitution, an *n*-propyl side chain in the  $\alpha$ -position proved to furnish better inhibitory activities than a methyl side chain, which provided more activity than the absence of a side chain (*e.g.*, 98% inhibition at 10  $\mu$ M (**102**) > 96% (**93**) > 88% (**141**) or 90% (**105**) > 87% (**96**) > 44% (**144**)). As already found in our previous study,<sup>26</sup> *para*-substitution of the aryl moiety was highly favored over *ortho*- and *meta*- substitution, and electron-withdrawing, polar, hydrogen-accepting substituents on the aryl ring gave higher inhibitory activities than electron-donating, lipophilic groups.

Therefore, *p*-acetyl (4-Ac) derivatives with an ethyl- (Et) and an *iso*-propyl (*i*Pr) side chain were synthesized and together with the formerly synthesized 4-Ac and 4-OMe derivatives tested for their ColH inhibition. We also included all inhibitors with an *iso*-butyl  $\alpha$ -side chain as they were the most potent congeners for LasB inhibition. For this, we used the free thiol forms of all

respective compounds.  $K_i$  values were determined with the FRET-based inhibition assay, and the obtained results are reported in Table 5 (also see Supporting Information, Table S3).<sup>26</sup>

**Table 5.** Structures, ColH and LasB inhibition values of various compounds.

Compd.	R <sup>1</sup>	R <sup>2</sup>	$K_i$ (nM) <sup>a</sup> ColH	$IC_{50}$ (μM) <sup>a</sup> LasB
2	4-OMe	H	57 ± 9	24 ± 1 <sup>33</sup>
3	4-Ac	H	20 ± 1	72 ± 5 <sup>33</sup>
7	4-OMe	Me	17 ± 3	45 ± 1
10	4-Ac	Me	3.5 ± 0.7	89 ± 10
23	4-OMe	Et	6 ± 1	4.2 ± 0.7
39	4-Ac	Et	2.3 ± 0.5	10 ± 2
24	4-OMe	<i>i</i> Pr	7 ± 1	16 ± 2
40	4-Ac	<i>i</i> Pr	2.5 ± 0.4	22 ± 1
13	4-OMe	<i>n</i> Pr	6 ± 1	2.4 ± 0.6
16	4-Ac	<i>n</i> Pr	2.0 ± 0.2	2.6 ± 0.5
25	4-OMe	<i>i</i> Bu	8 ± 1	0.36 ± 0.11
36	4-Ac	<i>i</i> Bu	11 ± 2	0.69 ± 0.34
20	3,4-diCl	<i>i</i> Bu	240 ± 40	22 ± 2
30	3-OMe	<i>i</i> Bu	>> 1000	0.56 ± 0.03
31	2-OMe	<i>i</i> Bu	>> 1000	0.70 ± 0.04
32	2,4-di-OMe	<i>i</i> Bu	>> 1000	0.42 ± 0.06
33	3,4-di-OMe	<i>i</i> Bu	> 1000	0.73 ± 0.10
34	4-OH	<i>i</i> Bu	~ 1000	0.96 ± 0.13
35	2-OH	<i>i</i> Bu	>> 1000	1.4 ± 0.2
37	4-Me	<i>i</i> Bu	22 ± 4	0.40 ± 0.13
38	4-Cl	<i>i</i> Bu	45 ± 1	0.84 ± 0.24
26	4-OMe	<i>n</i> Bu	15 ± 3	2.8 ± 0.3
27	4-OMe	<i>s</i> Bu	16 ± 3	17 ± 2
29	4-OMe	cyclohexylmethyl	111 ± 5	3.9 ± 0.7
28	4-OMe	cyclopropylmethyl	2.5 ± 0.4	2.6 ± 1.3
5	4-OMe	Bn	36 ± 5	0.73 ± 0.03 <sup>31</sup>

<sup>a</sup>Means and SD of at least two independent experiments

Remarkably, almost all introduced side chains increased the activity on ColH. We observed that the 4-Ac residue is preferred over 4-OMe for compounds bearing no or smaller  $\alpha$ -side chains, such as methyl (**10**), ethyl (**39**) and *iso*-propyl (**40**). Indeed, combining 4-Ac with an ethyl side chain gave the ColH inhibitor **39** with a  $K_i$  value of  $2.3 \pm 0.5$  nM, which is a nine-fold improvement compared to our previously published ColH inhibitor **3**.<sup>26</sup> For more bulky residues, such as *iso*-butyl, the 4-OMe derivative (**25**) was favored. A striking finding is that for 4-OMe substitution, the  $K_i$  values on ColH dropped from  $57 \pm 9$  nM for the unsubstituted compound **2** to  $2.5 \pm 0.4$  nM for the cyclopropylmethyl derivative **28**, which represents a 23-fold increase in potency.

As in our previous studies,<sup>26,34</sup> no other substitution pattern in the aryl unit than single *para*-substitution led to potent inhibition of ColH. For instance, the 4-OMe derivative **25** displayed single-digit nanomolar activity, but the activity of its 2-OMe (**31**) and 3-OMe (**30**) analogs decreased by more than a factor of 100, just affording micromolar inhibitors. We found similar results when looking into a di-substitution pattern in the aryl unit, which was not tolerated neither for polar (**32**, **33**) nor lipophilic substituents (**20**).

Overall, an *iso*-butyl group was found to be the most favorable  $\alpha$ -side chain motif for dual inhibition of LasB and ColH, as it had the best inhibitory effects on LasB and still furnished inhibitors of ColH with single digit nanomolar activities. Such dual inhibitors have the great advantage that they might be employed against several bacterial species, and hence, a broader range of bacterial infections would be covered.

**Co-crystal structures with LasB.** To rationalize the binding mode and the potency of the novel *N*-aryl-2-*iso*-butylmercaptoacetamide derivatives, crystal structures of LasB in complex with **25** and **37** were determined at 1.70 Å and 1.65 Å resolution, respectively (Figure 2). Full details of the data collection and refinement statistics can be found in Table S4. Both compounds, **25** and **37**, occupy the S1' and S2' substrate binding pockets of LasB in a fashion that is reminiscent of the binding mode previously reported for  $\alpha$ -unsubstituted *N*-aryl-mercaptoacetamide LasB inhibitors (**1**; Figure S3). The *N*-arylacetamide group mainly interacts by the formation of bidentate hydrogen bonds between the carbonyl group and Arg198 (Figure S4). The *iso*-butyl group (**R**<sup>2</sup>) is accommodated in the lipophilic S1' binding pocket and is stabilized by

hydrophobic interactions (Figure S4). However, the electron density observed for this region of the compound was blurred, which indicates some conformational flexibility of the ligands (Figure 2b and 2c). The phenyl group of the *N*-arylacetamide occupies the wide, open and solvent-accessible entrance of the S2' binding pocket (Figure 2), which rationalizes the tolerance for substitution at **R**<sup>1</sup> (Tables 1 and 3). Overall, the binding modes of **25** and **37** were found to be identical, except for a single hydrogen bond formed by the 4-OMe group of **25** with the side chain of His224 *via* a water molecule (Figure S4). This explains the identical inhibitory activities observed for **25** and **37** (Table 3,  $IC_{50} = 0.36 \pm 0.11 \mu\text{M}$  and  $IC_{50} = 0.40 \pm 0.13 \mu\text{M}$ , respectively).

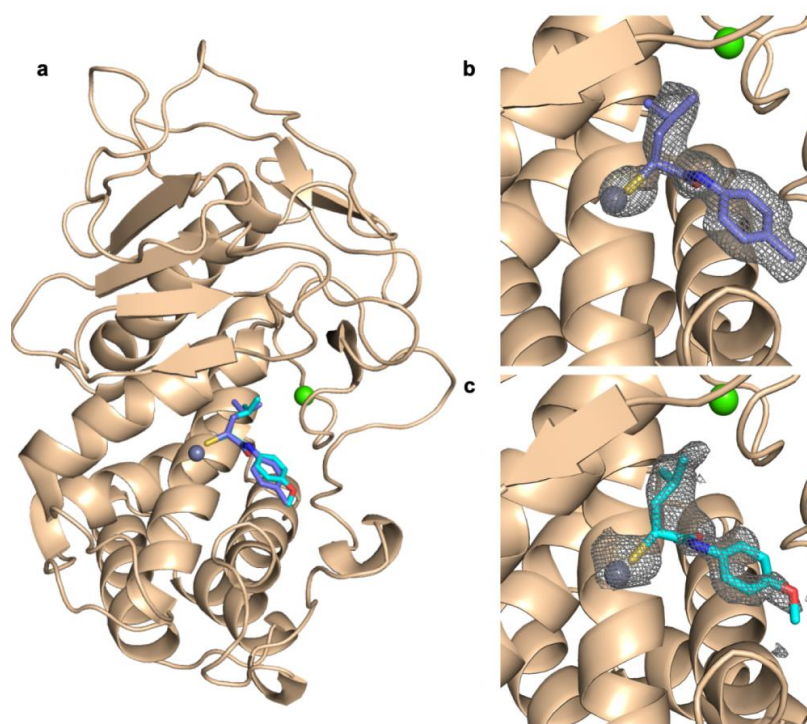


**Figure 2.** Crystal structure of LasB (cartoon, wheat) in complex with **25** (cyan) or **37** (blue). **a**) Superposition of LasB in complex with **25** (cyan) or **37** (blue). **b**) and **c**) Polder map of **25** and **37** contoured at  $3\sigma$ . The active site  $Zn^{2+}$ -ion is shown as a gray sphere and the  $Ca^{2+}$ -ion as a green sphere.

**Co-crystal structure with ColH.** We determined the crystal structure of the peptidase domain of ColH in complex with the thiol hydrolytically formed from thioacetate **100** at 1.91 Å resolution. The peptidase domain adopts the typical thermolysin-like fold, which is horizontally divided by the active-site cleft into an upper N-terminal and a lower C-terminal subdomain. The active site is composed of the catalytic zinc ion, co-ordinated by His455, His459 and Glu487, and the general acid/base Glu487. The edge strand sculpts the upper rim of the binding cleft (residues 425–430), while a wall formed by residues 443–447 frames the primed substrate-binding pocket at its end.<sup>35</sup> The well-defined electron density of the ligand in the active site revealed, as anticipated, the free thiol **10** as the binding partner of ColH (Figure 3a). Contrasting the LasB complex structures (Figure 2), the ligand occupies the non-primed substrate recognition sites in ColH. Reminiscent to our previously published co-crystal structure with the thiocarbamate compound that hydrolyzed to thiol **3**,<sup>26</sup> the co-ordination of the catalytic zinc ion by His455, His459 and Glu487 is completed by the thiolate of **10** with a sulfur-to-zinc distance of 2.30 Å. The methyl group in  $\alpha$ -position points out of the binding pocket towards the solvent and does not interact with the enzyme. The amide nitrogen atom of **10** forms a hydrogen bond with the carbonyl oxygen (OE2) of Glu487 (2.99 Å) of the C-terminal subdomain, while the aromatic ring is stabilized by a  $\pi$ - $\pi$ -stacking interaction with the imidazole ring of His459 (centroid-centroid distance of 3.81 Å) located in the N-terminal subdomain. At the end of the non-primed binding site, the acetyl oxygen atom provides water-mediated interactions (2.90 Å) with the main-chain amide of Glu430 (2.81 Å) and with the main-chain carbonyl of Tyr428 (2.96 Å) of the edge strand.

The observed conformations of the peptidase domain of ColH in the two co-crystal structures in complex with **10** and **3** agree well with each other. The average root-mean-square displacement of backbone atoms is 0.233 Å, as calculated by Pymol (The PyMOL Molecular Graphics System, Version 4.0.0 Schrödinger, LLC).

Compound **10** adopts a similar binding mode as **3**, as shown in Figure 3b, and both compounds are well-braced between the upper and lower subdomains of the peptidase domain of ColH. Yet notably, the sulfur-bearing terminus of **10** is tilted when compared to the conformation of **3**. This change in position results from the sterical accommodation of the additional  $\alpha$ -methyl group of **10** within the active-site cleft. Therefore, the position of the amide oxygen of **10** is tilted by 7.9° towards the central helix, while the sulfur atom is bent and shifted by 11.3° and 0.68 Å away

from the central helix compared to the position it occupies in the complex with **3**. As a result, and in contrast to **3**, **10** lacks the hydrogen-bond interaction of the amide oxygen atom with the main-chain amide of Tyr428 (oxygen–nitrogen distance of 3.89 Å instead of 3.11 Å, as observed with **3**). It is also notable that the edge strand adopts a slightly less contracted conformation, possibly due to the missing interaction with the amide oxygen atom of **10**.

Despite this decrease in intermolecular interactions compared to **3**, **10** was nearly six-fold more active than **3** towards ColH ( $K_i$  of  $3.5 \pm 0.7$  nM compared to  $20 \pm 1$  nM). This increase in potency might primarily result from the smaller entropic penalty paid when binding the  $\alpha$ -alkylated **10** compared to the  $\alpha$ -unsubstituted **3**, because the loss of internal degrees of freedom is less for the alkylated compound.<sup>36</sup> We suggest that this entropic advantage translated into improved inhibitory activities for all compounds with small (**7**, **10**, **13**, **16**, **23**, **24**, **39**, **40**) or not too bulky  $\alpha$ -alkyl groups (**25**, **26**, **27**, **28**, **36**) that could fit into the small S1/S1' cavity and interact with the hydrophobic protein interfaces framing the binding cleft (Figure 3c). An additionally beneficial contribution might result from an optimized hydrogen-bonding network in the non-primed binding sites, specifically involving the carbonyl oxygen and the water molecule that serves as hydrogen bridge to the protein backbone, as reflected by hydrogen-bond distances of 2.90, 2.96, and 2.81 Å compared to 3.07, 3.11, and 2.84 Å, respectively.



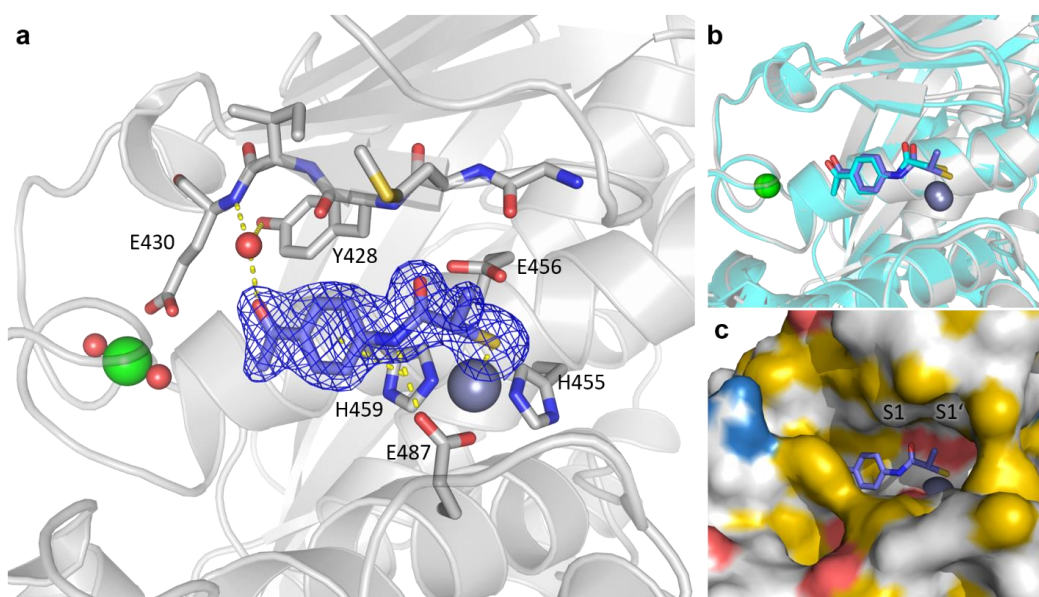


**Figure 3.** Close-up on the ligand-bound active sites of ColH. **a)** Co-crystal structure of **10** with ColH reveals thiol **10** as the binding partner. The inhibitor (blue) is shown in sticks with the maximum likelihood weighted  $2F_o - F_c$  electron density map contoured at  $1\sigma$ . The catalytic zinc ion (dark gray), calcium ion (green), and water molecule (red) are shown as spheres. The edge strand and active-site residues are shown in gray sticks. **b)** Superposition of the active sites of ColH in complex with **10** (gray; ligand in blue sticks) and with **3** (all cyan) (PDB: 5O7E). **c)** Active site of ColH bound to **10** shown in hydrophobic surface representation colored according to YRB scheme: non-polar hydrocarbons (yellow), negatively charged oxygen atoms of glutamate and aspartate (red), positively charged nitrogen atoms of lysine and arginine (red).<sup>37</sup>

**Selectivity over potential human off-targets.** As all of our inhibitors contained thiol groups, which are known for their strong zinc-binding properties,<sup>38</sup> it was crucial to screen for possible off-target inhibition. Also, the clostridial collagenases show high homology to the zinc-containing human matrix metalloproteases (MMPs), which play a significant role in various biochemical processes in humans.<sup>39,40</sup> Therefore, it is of utmost importance to retain the remarkable selectivity that we had found for the previously reported *N*-aryl mercaptoacetamides and *N*-aryl-3-mercapto succinimides.<sup>25,26,34</sup> As the MMPs can be divided into three classes based on the depth of their S1' binding pockets, two MMPs of each subclass were chosen to be tested as off-targets.

Furthermore, we decided to expand this off-target screen by other proteins for the aforementioned reasons. Therefore, we have chosen two histone deacetylases (HDAC-3 and HDAC-8), which are involved in the epigenetic regulation of gene expression,<sup>41</sup> as well as the zinc-containing TNF- $\alpha$  converting enzyme (TACE = ADAM-17), which is crucial for a functional immune response.<sup>42</sup> Our results show that all tested inhibitors of LasB and ColH had a high selectivity over most of the investigated potential off-targets. None of the tested compounds showed more than 20% inhibition at 100  $\mu$ M for all studied MMPs (Table 6) as well as both HDAC enzymes (Table 7). However, inhibition of TACE has been found for **10**, **25** and **37** (Table 7). This finding will hence be considered for further optimization studies, even though the compounds were significantly more potent against the bacterial targets LasB and ColH.

**Table 6.** Inhibition of six MMPs in presence of 100  $\mu$ M of compounds **10**, **16**, **25**, **37** and **100**<sup>a</sup>

Compd.	Inhibition [%] at 100 $\mu$ M					
	MMP-1	MMP-2	MMP-3	MMP-7	MMP-8	MMP-14
<b>10</b>	n.i.	10 $\pm$ 8	n.i.	n.i.	11 $\pm$ 6	n.i.
<b>16</b>	n.i.	n.i.	n.i.	n.i.	n.i.	n.i.
<b>25</b>	n.i.	16 $\pm$ 6	n.i.	n.i.	n.i.	n.i.
<b>37</b>	n.i.	n.i.	n.i.	n.i.	n.i.	n.i.
<b>100</b>	n.i.	14 $\pm$ 1	n.i.	n.i.	n.i.	n.i.

<sup>a</sup>Means and SD of at least two independent experiments. n.i. = <10% inhibition

**Table 7.** Activity of compounds **10**, **25**, **37** and **100** against HDAC-3, HDAC-8 and TACE

Compd.	IC <sub>50</sub> ( $\mu$ M) <sup>a</sup>		
	HDAC-3	HDAC-8	TACE
<b>10</b>	>100	>100	12.5 $\pm$ 4.8
<b>25</b>	>100	>100	4.7 $\pm$ 1.8
<b>37</b>	>100	>100	4.5 $\pm$ 1.8
<b>100</b>	>100	>100	>100

<sup>a</sup>Means and SD of at least two independent experiments.

Compound **37** showed an impressive inhibitory activity in the *in vitro* LasB and ColH assays, high selectivity over a broad range of human enzymes and no indications of cytotoxicity *in vitro* (see below). In view of further development of **37** towards a potential new investigative drug, it was subjected to a more advanced safety screening (Table 8).

Prolonged electrocardiographic QT intervals can lead to ventricular arrhythmia and with that, in the worst case, to sudden cardiac failure.<sup>43,44</sup> In the past 40 years, arrhythmogenic effects of drugs were the number one cause of withdrawals of FDA approvals in the US and number three in worldwide withdrawal.<sup>45</sup> The human ether-a-go-go related gene (hERG) potassium channel is responsible for normal ventricular repolarization.<sup>46-49</sup> Therefore, both activators and inhibitors of hERG are highly problematic for drug safety.<sup>46,49-51</sup> Consequently, the effect of **37** on hERG was analyzed. The IC<sub>50</sub> value regarding the inhibition of the hERG potassium channel was determined to be > 10 μM (see also Supporting Information, Figure S5), which suggests an at least 25-fold selectivity for LasB and a more than a 400-fold selectivity for ColH over hERG.

Furthermore, it was of particular importance to determine the effect of compound **37** on different members of the cytochrome P-450 (CYP450) family. This family of enzymes is involved in the oxidative metabolism of drugs in the human body.<sup>52,53</sup> Inhibition or induction of the CYP system can lead to major drug-drug interactions, caused by the altered metabolic pattern.<sup>54,55</sup> This can generate a loss of effect of co-administered drugs or increase toxic side effects.<sup>56,57</sup> The five human CYP450 isoforms CYP1A, CYP2C9, CYP2C19, CYP2D6 and CYP3A4 are responsible for more than 90% of all CYP-mediated metabolic transformations.<sup>58,59</sup> We tested **37** on these enzymes, and it showed weak or no inhibition on four of them. The IC<sub>50</sub> value of ~ 1.0 μM on CYP2C19 appears to be acceptable but will nevertheless be dialed out in further optimization efforts.

In addition, we also analyzed compound **37** using an AMES mutagenicity assay, where it showed no signs of mutagenic effects.

**Table 8.** Advanced safety profile of compound **37**: hERG/CYP inhibition and Ames test.

	<b>hERG</b>	<b>CYP1A</b>	<b>CYP2C9</b>	<b>CYP3A4</b>	<b>CYP2C19</b>	<b>CYP2D6</b>	<b>Ames</b>
IC <sub>50</sub> [μM]	>10	>25	>25	15	1.0	22.3	no mutagenicity @ 125 μg/mL

Compound **37** was furthermore subjected to a SafetyScreen44 panel<sup>60</sup> that is commonly used to determine the most important human off-target interactions. This screening panel comprises 44 different potential off-targets including GPCRs, transporters, ion channels, nuclear receptors, kinases and other non-kinase enzymes. Compound **37** demonstrated no inhibition of most of the investigated off-targets (see Supporting Information, Figures S5 and S6). Certain effects of the compound that were observed on cyclooxygenases, acetylcholinesterase, a calcium channel and the aforementioned CYP2C19 will be considered as a high priority in future modifications and optimizations of the structure. Since the most prominent effect was observed in case of cyclooxygenase 1 (COX1), we determined its IC<sub>50</sub> value ( $8.3 \pm 2.1 \mu\text{M}$ ) to be considerably higher than the submicromolar inhibitory activities found against LasB and ColH.

**Cytotoxicity assays.** Because of their high selectivity over a wide range of potential human off-targets, we decided to further evaluate the cytotoxicity of our compounds *in vitro*. The most promising candidates were tested in the three human cell lines HepG2 (hepatocellular carcinoma cells), HEK293 (human embryonal kidney cells) and A549 (lung carcinoma cells). Except for a slight toxicity of **10** at 100  $\mu\text{M}$ , which was not detected when the concentration was decreased to 50  $\mu\text{M}$ , none of the other selected compounds showed any noteworthy cytotoxicity at a concentration of 100  $\mu\text{M}$  (Table 9).

**Table 9.** Cytotoxicity of compounds **10**, **16**, **25**, **37**, and **100**, as well as reference compounds rifampicin and doxorubicin against HepG2, HEK293 and A549 cell lines<sup>a</sup>

Compd.	Conc. [ $\mu\text{M}$ ]	Inhibition of viability [%]		
		HepG2	HEK293	A549
<b>10</b>	100	n.i.	$48 \pm 10$	$29 \pm 5$
	50	n.d.	n.i.	n.d.
<b>16</b>	100	n.i.	$28 \pm 24$	n.i.
<b>25</b>	100	n.i.	n.i.	n.i.
<b>37</b>	100	n.i.	$14 \pm 4$	$21 \pm 12$
<b>100</b>	100	$12 \pm 15$	$23 \pm 26$	$15 \pm 1$
<b>rifampicin</b>	100	$34 \pm 12$	$27 \pm 13$	$10 \pm 11$
<b>doxorubicin</b>	1	$56 \pm 14$	$45 \pm 10$	$50 \pm 12$

<sup>a</sup>Means and SD of at least two independent experiments. n.d. = not determined; n.i. = no inhibition (if inhibition < 10%)

**Compound 37 reduced *P. aeruginosa*-related cell-toxic effects *in vitro*.** To further verify the inhibitory effect of compound **37** and to validate LasB as a target, we tested compound **37** *in vitro* in a model mimicking the disease conditions that result from the destructive effects of LasB during *P. aeruginosa* infection. Normal human dermal fibroblasts (NHDF) and A549 cells were treated with wild-type *P. aeruginosa* (wt PA14) and LasB knockout *P. aeruginosa* ( $\Delta$ LasB PA14) culture supernatants together with various concentrations of compound **37**. After one day of incubation with cells, the cytotoxic effect of the supernatants was evaluated using an MTT assay and live/dead cells visualization by epifluorescence microscopy. Our findings show that compound **37** improved cell viability and reduced the cytotoxic effect of the wt PA14 supernatant compared with the control in which no compound was applied (Figure 4a). On the other hand, compound **37** did not influence the viability of cells treated with  $\Delta$ LasB PA14 supernatant (Figure 4b). Our visualization results were consistent with the MTT data and corroborate that compound **37** enhanced cell adhesion and helped to maintain cell morphology (epithelial shape for A549<sup>61</sup> and spindle shape for NHDF<sup>62</sup>, Supporting Information, Figures S7 to S10). These results strongly suggest that compound **37** blocks pathogenic effects of *P. aeruginosa* by acting as a selective LasB inhibitor. Besides, it might reduce bacterial propagation through skin and lung epithelial tissues by maintaining their integrity. It also has a strong potential to reduce the impairment of the cells during the disease state and the infection by *P. aeruginosa* as demonstrated in this cell-based assay.<sup>10,63</sup> Moreover, **37** could accelerate wound remodeling, which is otherwise delayed due to destructive effects of LasB.<sup>63</sup>

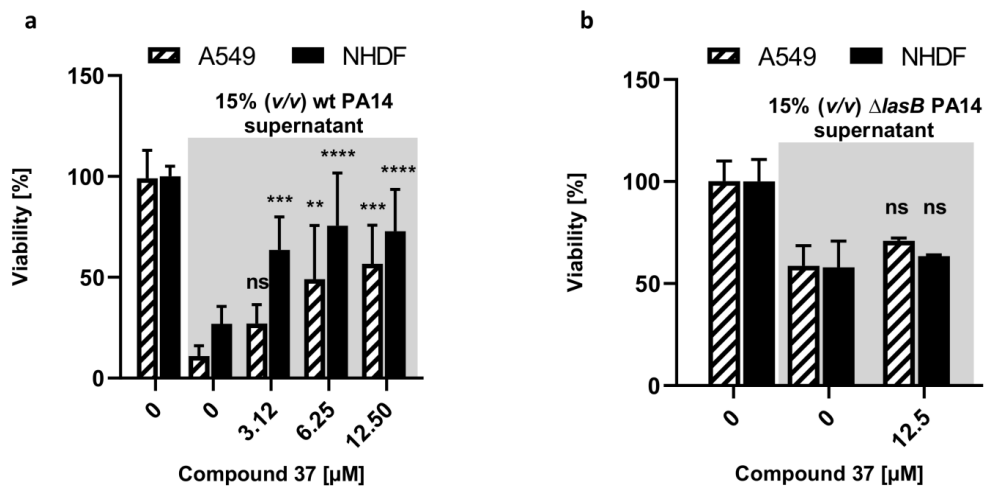


**Figure 4.** Effect of compound **37** on the viability (MTT assay) of normal human dermal fibroblasts (NHDF) and adenocarcinomic human alveolar basal epithelial (A549) cells challenged with 15% (v/v) wild-type (wt) PA14 or 15% (v/v) LasB knockout ( $\Delta lasB$ ) PA14 culture supernatants. **a**) Viability of NHDF and A549 cells treated with PA14 supernatant and various concentrations of compound **37** (data with grey background). **b**) Viability results of NHDF and A549 cells treated with  $\Delta lasB$  PA14 supernatant and 12.5  $\mu\text{M}$  of compound **37**. Each graph is a representation of the mean of three independent experiments  $\pm$  SD. One-way ANOVA was performed for each experiment following Dunnett's multiple comparisons test. The mean of each column was compared with the mean of the negative control (ns = not significant, \* =  $P \leq 0.05$ , \*\* =  $P \leq 0.01$ , \*\*\* =  $P \leq 0.001$ , \*\*\*\* =  $P \leq 0.0001$ ). PA14: *P. aeruginosa*.

**Compound 37 enhanced the survival of *G. mellonella* larvae.** To test the antivirulence effect of compound **37** *in vivo*, a *G. mellonella* larvae model was used. The larvae were treated with a mixture of compound **37** and wt PA14 supernatant, and their viability was measured once per day over six days. The obtained results show that 50% (v/v) wt PA14 supernatant decreased the survival rate of larvae and a  $70 \pm 10\%$  reduction in the viability was observed on day six. With  $\Delta lasB$  PA14 supernatant, the viability was not affected, and the survival was 100% over the time course of the experiment. An amount of 0.6 nmol of compound **37** rescued the larvae, and a 40% improvement in the viability on day six was detected relative to the control group treated only with wt PA14 supernatant. These results substantiate the potential of compound **37** as a promising antivirulence agent that reduces the pathogenicity of *P. aeruginosa* by inhibition of LasB. A crucial next step would be to study this compound in a more complex *in vivo* infection model.

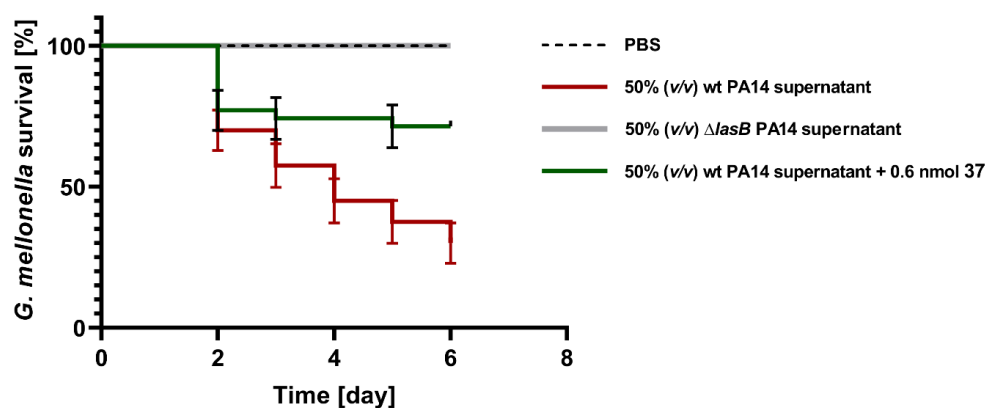


**Figure 5.** Compound **37** enhanced the survival rate of *G. mellonella* larvae treated with 50% (v/v) wild-type (wt) PA14 supernatant. The survival is improved for the group treated with compound **37** relative to the group treated with wt PA14 supernatant and 1% DMSO. Survival analysis was carried out using the Kaplan-Meier test. Each curve represents the results of three independent experiments. Statistical difference analysis between groups treated with only wt PA14 supernatant and the one treated with wt PA14 supernatant and compound **37** was performed with log-rank test  $P = 0.0010$ . The survival of the group treated with 50% (v/v)  $\Delta lasB$  PA14 supernatant did not change relative to the 50% (v/v) wt PA14 supernatant treated group ( $P = 0.0001$ ). The larvae treated with 0.6 nmol compound **37** and sterile PBS showed 100% viability. PA14: *P. aeruginosa*.

**In vivo pharmacokinetic studies.** Before conducting a more complex *in vivo* infection model, we aimed to assess the exposure and the plasma levels of compound **37** in a PK study in CD-1 male outbred mice (Supporting Information, Table S5). Compound **37** was injected intravenously (*i.v.*) at 10 mg/kg. No adverse effects were observed during the study. Unfortunately, the compound was only detected in plasma for a relatively short time frame of about 2 hours. Calculation of PK parameters showed a high *in vivo* clearance ( $Cl_{obs} = 505 \pm 119$  mL/min/kg) and a moderate half-life ( $t_{1/2} = 1.1$  h) with a low overall exposure ( $AUC_{0-t} = 241 \pm 23$  ng/mL\*h). The volume of distribution was relatively high ( $46 \pm 3$  L/kg), accounting for a good penetration into tissue. For both pathogens envisioned to be targeted, efficient tissue penetration is extremely favorable, *e.g.*, in case of tissue necrosis caused by *C. histolyticum* or in *P. aeruginosa* lung infections. In the future, we will aim for more disease-oriented ways of application, such as inhalation therapy for *P. aeruginosa* lung infections and topical application or tissue infiltration for *C. histolyticum* infections. With those ways of applications, the observed

rapid clearance and low overall exposure will be irrelevant and will not require further optimization of the compounds towards altered pharmacokinetic properties.

## Conclusions

The overall aim of this study was the investigation of novel  $\alpha$ -substituted *N*-aryl mercaptoacetamides as inhibitors of LasB and ColH, which both act as key mediators of bacterial pathogenicity. Among all structural variations, we identified the *iso*-butyl moiety as the most suitable  $\alpha$ -substituent, furnishing compounds that inhibited both LasB and ColH in the sub-micromolar range. Most remarkably, the SAR for LasB inhibitors changed significantly compared to  $\alpha$ -unsubstituted *N*-aryl mercaptoacetamides,<sup>25</sup> so that now a *para*-substitution with H-bond acceptors in the aryl unit (as seen in our previously reported ColH inhibitors<sup>26,34</sup>) has become advantageous in terms of *in vitro* inhibitory activity. Unprecedentedly, we have now identified a set of compounds (**25**, **36** and **37**) as potent inhibitors of both ColH and LasB. They have the potential to be further developed as dual inhibitors, thus covering a broader range of medical indications with just one drug candidate. All three aforementioned compounds showed a 10-fold improvement in inhibitory activity against LasB relative to the  $\alpha$ -unsubstituted 3,4-diCl derivative **1**, and still a 1.5-fold improvement relative to the  $\alpha$ -benzylated 4-OMe analog **5**. Compound **25** showed a slightly (*i.e.*, two-fold) improved activity against ColH, leading to an inhibitor with low nanomolar activity ( $K_i = 8 \pm 1$  nM). Compounds **39**, **40**, **16** and **28** were the most active ColH inhibitors, having  $K_i$  values in the range of  $2 \pm 1$  nM, which is a significant improvement of a full order of magnitude relative to our previously reported 'hit' compound **3** ( $K_i = 20 \pm 1$  nM).<sup>26</sup>

In addition, we solved the X-ray co-crystal structures of **25** and **37** in complex with LasB, as well as the structure of the hydrolyzed compound **100** in complex with ColH, thus revealing the exact binding modes of these inhibitors. These new co-crystal structures in combination with previous crystallographic insights<sup>25,26</sup> will support and facilitate future efforts of rational drug design to further improve the reported LasB and ColH inhibitors.

None of the investigated compounds showed major selectivity issues over the six tested MMPs or the two studied HDACs. Additionally, compound **37** was subjected to a safety screen 44 panel. Here, it was subjected to a variety of possible off-targets, including hERG, CYPs, COX,



GPCRs and ion channels. However, in the most cases it showed either no or rather weak inhibition. Moreover, an Ames test revealed the compound to display no mutagenicity.

We have demonstrated that compound **37** maintained the viability and integrity of both skin and lung cells treated with *P. aeruginosa* supernatant in an *in vitro* assays. Furthermore, studies with *G. mellonella* larvae demonstrate the efficacy of **37** in an *in vivo* setting, which strongly highlights the potential of such antivirulence compounds as new therapeutics for bacterial infections. A first PK *in vivo* study demonstrated the good volume of distribution of **37** which should be a favorable property for the treatment of lung infections and necrosis. Although **37** also showed a relatively rapid *in vivo* clearance and limited half-life, this will be overcome by disease-oriented ways of administration, such as inhalation or topical application. Future PK studies will aid to find the best route of administration and a good dosing regimen in order to achieve a therapeutic proof-of-concept *in vivo* for compound **37**, which we herein have shown to be a highly promising candidate for antivirulence drug development.

#### **Materials and methods**

**Chemistry.** All compounds were synthesized according to Scheme 1 using General Procedures A – D as described in more detail in the Supporting Information.

**Expression and purification of LasB and ColH-PD.** LasB and ColH-PD were expressed and purified as previously reported.<sup>25,35</sup>

***In vitro* ColH inhibition assay.** The ColH inhibition assay was performed as previously reported.<sup>26</sup> In short, enzyme and inhibitor (or buffer control) were preincubated for 1 h at rt, before the reactions were initiated by the addition of the quenched fluorescent substrate Mca-Ala-Gly-Pro-Pro-Gly-Pro-Dpa-Gly-Arg-NH<sub>2</sub> (Mca = (7-methoxycoumarin-4-yl)acetyl; Dpa = *N*-3-(2,4-dinitrophenyl)-L-2,3-diaminopropionyl) (FS1-1). The increase in fluorescence was monitored for 2 min (excitation: 328 nm, emission: 392 nm) at 25 °C. The final concentrations were 10 nM ColH-PD, 10 μM compound, 250 mM Hepes pH 7.5, 400 mM NaCl, 10 mM CaCl<sub>2</sub>, 10 μM ZnCl<sub>2</sub>, 2% DMSO, and 2 μM FS1-1. In case of poor compound solubility, the DMSO concentration was increased, but never exceeded 4.8%. The percentage of enzyme inhibition was calculated in relation to a reference without a compound added (buffer control). For the determination of the inhibition constant ( $K_i$ ), similar assay conditions were chosen. However, a

nominal final enzyme concentration of 2 nM was used, and the reactions were monitored for 144 s. For each compound, the concentrations were optimized according to Murphy's method.<sup>64</sup> Apparent inhibition constant ( $K_i^{\text{app}}$ ) values were determined by non-linear fitting to the Morrison equation<sup>65</sup> following a two-stage regression analysis strategy for tight-binding inhibitors.<sup>66</sup> Regression analysis was performed using GraphPad Prism 9.0.0 (Graph Pad Software, San Diego, CA, USA). The experiments were performed under first-order conditions ( $[S_0] \ll K_M$ ), which resulted in an approximation of the  $K_i^{\text{app}}$  to the true inhibition constant ( $K_i$ ), and therefore, the results are reported as  $K_i$  values.

**LasB Inhibition Assay.** The purification of LasB from *P. aeruginosa* P14 supernatant as well as the FRET-based *in vitro* inhibition assay were carried out as described previously.<sup>25</sup> All samples were run in duplicate for each condition, and experiments were performed independently at least twice.

***In vitro* inhibition of human off-targets.** *In vitro* inhibition assays with several human off-targets (MMPs, HDACs, TACE, COX-1) were performed as previously reported.<sup>25,26</sup> TACE and HDAC inhibitor screening kits were purchased from Sigma-Aldrich (Saint Louis, MO), MMPs 1, 2, 3, 7, 8 and 14 along with the SensoLyte 520 Generic MMP Activity Kit Fluorimetric were purchased from AnaSpec (Fremont, CA, USA), and the fluorometric cyclooxygenase 1 (COX1) inhibitor assay kit was purchased from Abcam (Cambridge, UK). The assays were performed according to the guidelines of the respective manufacturers. Fluorescence signals were measured using a CLARIOstar plate reader (BMG Labtech, Ortenberg, Germany). In-depth off-target assays with compound **37** were performed by contract research organizations (CROs). The off-target Safety Screen44<sup>TM</sup> panel comprising selected binding, inhibition and uptake assays was performed by the CRO Eurofins Cerep SA (Celle-L'Evescault, France) according to their protocols.<sup>60</sup> Experiments regarding the inhibition of cytochrome P450 enzymes as well as an Ames mutagenicity screening were performed by the CRO Cypotex (Nether Alderley, UK) according to their protocols. Inhibition of hERG was investigated by the CRO Evotec (Hamburg, Germany) according to their protocol.

**X-ray crystallography and image preparation for LasB.** LasB was concentrated to 8 mg/mL and mixed with inhibitor **25** or **37** at a final concentration of 1 mM. Complex crystals were obtained at 18 °C in 0.2 M ammonium iodine and 20% (w/v) PEG 3350 using the sitting drop

vapor diffusion method. Crystals appeared after a few days and were allowed to grow for an additional week. Crystals were cryoprotected in 35% glycerol, and data were collected at DESY (Beamline P11) in Hamburg, Germany. Data were processed by Xia<sup>2,67</sup> and the structure was solved using PHASER<sup>68</sup> molecular replacement with *P. aeruginosa* elastase (PDB entry 1EZM) as a search model. The solution was manually rebuilt with COOT<sup>69</sup> and refined using PHENIX.refine.<sup>70</sup> The images presented were created using PyMOL (The PyMOL Molecular Graphics System, Schrödinger, LLC) and Ligplot+.<sup>71</sup> The final refined structures of LasB in complex with compounds **25** and **37** were deposited in the Protein Data Bank (PDB) as entries 7NLK and 7NLM, respectively. Data collection and refinement statistics are listed in the Supporting Information, Table S4.

**X-ray crystallography for ColH.** Prior to crystallization, 9 mg/mL ColH-PD were preincubated with 5 mM compound **100** in 8 mM Hepes pH 7.5, 33 mM NaCl, 0.33 mM CaCl<sub>2</sub>, and 5% DMSO for 30 min on ice and then clarified by centrifugation for 30 min at 13,000 g at 4 °C. The co-crystal was grown using the sitting drop vapor diffusion method by mixing 1 μL protein-inhibitor solution with 1 μL crystallization buffer. The crystallization buffer contained 0.1 M Hepes/MOPS pH 7.1, 0.02 M 1,6-hexanediol, 0.02 M 1-butanol, 0.02 M 1,2-propanediol, 0.02 M 2-propanol, 0.02 M 1,4-butanediol, 0.02 M 1,3-propanediol, 12.5% v/v MPD, 12.5% PEG 1000, and 12.5% w/v PEG 3350. The drop was streak-seeded from crystals of ligand-free ColH-PD.<sup>72</sup> Crystals appeared within days. The crystals were cryoprotected with MiTeGen LV Cryo-oil (MiTeGen, Ithaca, NY) and immediately flash-frozen in liquid nitrogen. X-ray diffraction data were collected on beamline ID23-1 at the European Synchrotron Radiation Facility (ESRF) in Grenoble, France. The data set was indexed, integrated and scaled using XDS<sup>73</sup> and AIMLESS.<sup>74</sup> Molecular replacement was performed with PHASER<sup>68</sup> using as search model PDB entry 5O7E (ligand deleted). Ligand coordinates and restraints were generated using the Grade Web Server.<sup>75</sup> Final structures were obtained using PHENIX<sup>70</sup> together with model building in WinCoot.<sup>69</sup> PyMOL version 4.0.0 was used for (i) figure generation and (ii) calculation of RMSD values (The PyMOL Molecular Graphics System, Version 4.0.0 Schrödinger, LLC). The final refined structure of ColH-PD in complex with compound **100** was deposited in the Protein Data Bank (PDB) as entry 7BBK. Data collection and refinement statistics are listed in the Supporting Information, Table S4. Surface hydrophobicity was evaluated using the YRB python script.<sup>37</sup>

**Cytotoxicity assays.** Cytotoxicity assays on HepG2, HEK293 and A549 cells were performed as previously reported.<sup>76</sup>

***In vitro* cell-based experiments.** The experiments were performed as described before.<sup>31</sup>

***In vivo G. mellonella* virulence assay.** The experiments were performed as described before.<sup>31</sup>

**Pharmacokinetic (PK) studies in mice.** For PK experiments, outbred male CD-1 mice (Charles River, Netherlands), four weeks old, were used. The animal studies were conducted in accordance with the recommendations of the European Community (Directive 86/609/EEC, 24 November 1986). All animal procedures were performed in strict accordance with the German regulations of the Society for Laboratory Animal Science (GV-SOLAS) and the European Health Law of the Federation of Laboratory Animal Science Associations (FELASA). Animals were excluded from further analysis if sacrifice was necessary according to the human endpoints established by the ethical board. All experiments were approved by the ethical board of the Niedersächsisches Landesamt für Verbraucherschutz und Lebensmittelsicherheit, Oldenburg, Germany (LAVES; permit no. and 33.19-42502-04-15/1857). Compound **37** was dissolved in 20 % DMSO, 40 % PEG400, 40 % H<sub>2</sub>O (containing 1% ascorbic acid [3 mg/mL]). Mice were administered **37** at 10 mg/kg *i.v.* About 20 µL of whole blood was collected serially from the lateral tail vein at time points 0.25, 0.5, 1, 2, 4, and 8 h post administration. After 24 h, mice were sacrificed, and blood was collected from the heart. Whole blood was collected into Eppendorf tubes coated with 0.5 M EDTA and immediately spun down at 13,000 rpm at 4 °C for 10 min. The plasma was transferred into a new Eppendorf tube and then stored at –80 °C until analysis. All PK plasma samples were analyzed by HPLC-MS/MS using an Agilent 1290 Infinity II HPLC system coupled to an AB Sciex QTrap6500+ mass spectrometer. First, a calibration curve was prepared by spiking different concentrations of **37** into mouse plasma (pooled, from CD-1 mice). Caffeine was used as an internal standard. In addition, quality control samples (QCs) were prepared for **37** in mouse plasma. The following extraction procedure was used: 7.5 µL of a plasma sample (calibration samples, QCs or PK samples) was extracted with 25 µL of MeOH containing 12.5 ng/mL of caffeine as internal standard for 5 min at 2,000 rpm on an Eppendorf MixMate® vortex mixer. Then samples were spun down at 13,000 rpm for 5 min. Supernatants were transferred to standard HPLC glass vials. HPLC conditions were as follows: column: Agilent Zorbax Eclipse Plus C18, 50x2.1 mm, 1.8 µm; temperature: 30°C; injection

volume: 10  $\mu$ L; flow rate: 700  $\mu$ L/min; solvent A: water + 0.1% formic acid; solvent B: acetonitrile + 0.1% formic acid; gradient: 99% A at 0 min and until 2 min, 99% – 0% A from 2.0 min to 3.0 min, 0% A until 5.5 min, 0% – 99% A from 5.5 min to 5.7 min. Mass spectrometric conditions were as follows: Scan type: MRM, negative and positive mode; Q1 and Q3 masses for caffeine and **37** can be found in the Supporting Information, Table S6; peak areas of each sample and of the corresponding internal standard were analyzed using MultiQuant 3.0 software (AB Sciex). Peak areas of the respective sample were normalized to the internal standard peak area. For **37**  $m/z$  235.949  $\rightarrow$  178.900 was used for quantification and  $m/z$  235.949  $\rightarrow$  106.000 was used for qualification. For caffeine  $m/z$  195.024  $\rightarrow$  138.000 was used for quantification and  $m/z$  195.024  $\rightarrow$  110.000 was used for qualification. Peaks of PK samples were quantified using the calibration curve. The accuracy of the calibration curve was determined using QCs independently prepared on different days. PK parameters were determined using a non-compartmental analysis with PKSolver.<sup>77</sup>

#### **Associated content**

##### Supporting Information

Synthetic procedures for all compounds, additional information for thioacetates as surrogates of thiols in the ColH assay, crystallographic data, results from Safety Screen 44<sup>TM</sup> panel, additional figures for *in vitro* skin and lung cell assays, and additional information for *in vivo* pharmacokinetic studies (PDF).

Molecular formula strings (CSV)

PDB ID Codes: 7NLM (LasB/**37**), 7NLK (LasB/**25**) and 7BBK (ColH/**100**)

#### **Author Information**

##### Corresponding Authors

Anna K. H. Hirsch – Department of Drug Design and Optimization, Helmholtz Institute for Pharmaceutical Research, Saarland (HIPS) – Helmholtz Centre for Infection Research (HZI), 66123 Saarbrücken, Germany; Department of Pharmacy, Saarland University,

Campus E8 1, 66123 Saarbrücken, Germany; orcid.org/0000-0001-8734-4663; Email: [anna.hirsch@helmholtz-hips.de](mailto:anna.hirsch@helmholtz-hips.de)

Christian Ducho – Department of Pharmacy, Pharmaceutical and Medicinal Chemistry, Saarland University, Campus C2 3, 66123 Saarbrücken, Germany; orcid.org/0000-0002-0629-9993; Email: [christian.ducho@uni-saarland.de](mailto:christian.ducho@uni-saarland.de)

#### Author Contributions

└these authors contributed equally

#### Authors

Katrin Voos – Department of Pharmacy, Pharmaceutical and Medicinal Chemistry, Saarland University, Campus C2 3, 66123 Saarbrücken, Germany; orcid.org/0000-0001-5224-9690

Samir Yahiaoui – Department of Drug Design and Optimization, Helmholtz Institute for Pharmaceutical Research, Saarland (HIPS) – Helmholtz Centre for Infection Research (HZI), 66123 Saarbrücken, Germany; orcid.org/0000-0001-5134-5007

Jelena Konstantinović – Department of Drug Design and Optimization, Helmholtz Institute for Pharmaceutical Research, Saarland (HIPS) – Helmholtz Centre for Infection Research (HZI), 66123 Saarbrücken, Germany;

Esther Schönauer - Department of Biosciences and Christian Doppler Laboratory for Innovative Tools for Biosimilar Characterization, Division of Structural Biology, University of Salzburg, Billrothstrasse 11, 5020 Salzburg, Austria; orcid.org/0000-0002-2625-9446

Alaa Alhayek – Department of Drug Design and Optimization, Helmholtz Institute for Pharmaceutical Research, Saarland (HIPS) – Helmholtz Centre for Infection Research (HZI), 66123 Saarbrücken, Germany; Department of Pharmacy, Saarland University, Campus E8 1, 66123 Saarbrücken, Germany; orcid.org/0000-0001-8192-6574

Asfandyar Sikandar – *previous address*: Workgroup Structural Biology of Biosynthetic Enzymes, Helmholtz Institute for Pharmaceutical Research, Saarland (HIPS) – Helmholtz Centre for Infection Research (HZI), 66123 Saarbrücken, Germany; *current address*: Department of Drug Design and Optimization, Helmholtz Institute for Pharmaceutical Research, Saarland (HIPS) – Helmholtz Centre for Infection Research (HZI), 66123 Saarbrücken, Germany

Khadidja Si Chaib – Department of Drug Design and Optimization, Helmholtz Institute for Pharmaceutical Research, Saarland (HIPS) – Helmholtz Centre for Infection Research (HZI), 66123 Saarbrücken, Germany

Tizian F. Ramspoth – Department of Drug Design and Optimization, Helmholtz Institute for Pharmaceutical Research, Saarland (HIPS) – Helmholtz Centre for Infection Research (HZI), 66123 Saarbrücken, Germany

Katharina Rox – Department of Chemical Biology, Helmholtz Centre for Infection Research, Inhoffenstrasse 7, 38124 Braunschweig, Germany; German Centre for Infection Research (DZIF), Site Hannover-Braunschweig, Germany

Jörg Haupenthal – Department of Drug Design and Optimization, Helmholtz Institute for Pharmaceutical Research, Saarland (HIPS) – Helmholtz Centre for Infection Research (HZI), 66123 Saarbrücken, Germany; [orcid.org/0000-0003-3991-2800](https://orcid.org/0000-0003-3991-2800)

Jesko Köhnke – *previous address*: Workgroup Structural Biology of Biosynthetic Enzymes, Helmholtz Institute for Pharmaceutical Research, Saarland (HIPS) – Helmholtz Centre for Infection Research (HZI), 66123 Saarbrücken, Germany; *current address*: School of Chemistry, University of Glasgow, Glasgow, G12 8QQ, United Kingdom

Hans Brandstetter – Department of Biosciences and Christian Doppler Laboratory for Innovative Tools for Biosimilar Characterization, Division of Structural Biology, University of Salzburg, Billrothstrasse 11, 5020 Salzburg, Austria; [orcid.org/0000-0002-6089-3045](https://orcid.org/0000-0002-6089-3045)

## Acknowledgments

We thank Dr. Stefan Boettcher and Stefanie Weck for the measurements of high-resolution mass spectra as well as Andrea Ahlers, Nathalie Andreia, Martina Jankowski, Jeannine Jung, Dennis Jener, Janine Schreiber and Martina Wiesbauer for technical support. We acknowledge financial support by the Austrian Science Fund (FWF, grants P 31843 (E.S.) and W 01213 (H.B.)), by CARB-X (A.K.H.H.), the German Center for Infection Research (DZIF, TTU 09.710, K.R.) and by the Helmholtz Association's Initiative and Networking Fund (A.K.H.H.).

## Abbreviations

A549, lung carcinoma cell line; ColH, *Clostridium histolyticum* (*Hathewayia histolytica*) collagenase; diCl, dichloro; DIPEA, diisopropylethylamine; HepG2, hepatocellular carcinoma cell line; LasB, *Pseudomonas aeruginosa* elastase; MTT, 3-(4,5-dimethylthiazol-2-yl)-2,5-diphenyltetrazolium bromide; n.d., not determined; NHDF, normal human dermal fibroblasts; n.i., no inhibition; OMe, methoxy; PA14, *Pseudomonas aeruginosa* strain; TACE, tumor necrosis factor- $\alpha$  converting enzyme; WHO, world health organization.

## References

- (1) Maura, D.; Ballok, A. E.; Rahme, L. G. Considerations and Caveats in Anti-Virulence Drug Development. *Curr. Opin. Microbiol.* **2016**, *33*, 41–46. <https://doi.org/10.1016/j.mib.2016.06.001>.
- (2) Fleitas Martínez, O.; Cardoso, M. H.; Ribeiro, S. M.; Franco, O. L. Recent Advances in Anti-Virulence Therapeutic Strategies With a Focus on Dismantling Bacterial Membrane Microdomains, Toxin Neutralization, Quorum-Sensing Interference and Biofilm Inhibition. *Front. Cell. Infect. Microbiol.* **2019**, *9*, 74. <https://doi.org/10.3389/fcimb.2019.00074>.
- (3) Mühlen, S.; Dersch, P. Anti-Virulence Strategies to Target Bacterial Infections. In *How to Overcome the Antibiotic Crisis*; Stadler, M., Dersch, P., Eds.; Springer International Publishing: Cham, 2015; Vol. 398, pp 147–183. [https://doi.org/10.1007/82\\_2015\\_490](https://doi.org/10.1007/82_2015_490).
- (4) Calvert, M. B.; Jumde, V. R.; Titz, A. Pathoblockers or Antivirulence Drugs as a New Option for the Treatment of Bacterial Infections. *Beilstein J. Org. Chem.* **2018**, *14*, 2607–2617. <https://doi.org/10.3762/bjoc.14.239>.



- (5) Casadevall, A.; Pirofski, L. Host-Pathogen Interactions: The Attributes of Virulence. *J. Infect. Dis.* **2001**, *184* (3), 337–344. <https://doi.org/10.1086/322044>.
- (6) Anthouard, R.; DiRita, V. J. Chemical Biology Applied to the Study of Bacterial Pathogens. *Infect. Immun.* **2015**, *83* (2), 456–469. <https://doi.org/10.1128/IAI.02021-14>.
- (7) do Vale, A.; Cabanes, D.; Sousa, S. Bacterial Toxins as Pathogen Weapons Against Phagocytes. *Front. Microbiol.* **2016**, *7*. <https://doi.org/10.3389/fmicb.2016.00042>.
- (8) Vaca, D. J.; Thibau, A.; Schütz, M.; Kraiczky, P.; Happonen, L.; Malmström, J.; Kempf, V. A. J. Interaction with the Host: The Role of Fibronectin and Extracellular Matrix Proteins in the Adhesion of Gram-Negative Bacteria. *Med. Microbiol. Immunol.* **2019**. <https://doi.org/10.1007/s00430-019-00644-3>.
- (9) Chen, L. VFDB: A Reference Database for Bacterial Virulence Factors. *Nucleic Acids Res.* **2005**, *33* (Database issue), D325–D328. <https://doi.org/10.1093/nar/gki008>.
- (10) Saint-Criq, V.; Villeret, B.; Bastaert, F.; Kheir, S.; Hatton, A.; Cazes, A.; Xing, Z.; Sermet-Gaudelus, I.; Garcia-Verdugo, I.; Edelman, A.; Sallenave, J.-M. *Pseudomonas Aeruginosa* LasB Protease Impairs Innate Immunity in Mice and Humans by Targeting a Lung Epithelial Cystic Fibrosis Transmembrane Regulator–IL-6–Antimicrobial–Repair Pathway. *Thorax* **2018**, *73* (1), 49–61. <https://doi.org/10.1136/thoraxjnl-2017-210298>.
- (11) Tielen, P.; Rosenau, F.; Wilhelm, S.; Jaeger, K.-E.; Flemming, H.-C.; Wingender, J. Extracellular Enzymes Affect Biofilm Formation of Mucoid *Pseudomonas Aeruginosa*. *Microbiol.* **2010**, *156* (7), 2239–2252. <https://doi.org/10.1099/mic.0.037036-0>.
- (12) Kaman, W. E.; Hays, J. P.; Endtz, H. P.; Bikker, F. J. Bacterial Proteases: Targets for Diagnostics and Therapy. *Eur. J. Clin. Microbiol. Infect. Dis.* **2014**, *33* (7), 1081–1087. <https://doi.org/10.1007/s10096-014-2075-1>.
- (13) Suleman, L. Extracellular Bacterial Proteases in Chronic Wounds: A Potential Therapeutic Target? *Adv. Wound Care* **2016**, *5* (10), 455–463. <https://doi.org/10.1089/wound.2015.0673>.
- (14) *Antibacterial Agents in Clinical Development. In An Analysis of the Antibacterial Clinical Development Pipeline, Including Tuberculosis*; The World Health Organization: Geneva, 2017.

- (15) Van Eldere, J. Multicentre Surveillance of *Pseudomonas Aeruginosa* Susceptibility Patterns in Nosocomial Infections. *J. Antimicrob. Chemother.* **2003**, *51* (2), 347–352. <https://doi.org/10.1093/jac/dkg102>.
- (16) Pang, Z.; Raudonis, R.; Glick, B. R.; Lin, T.-J.; Cheng, Z. Antibiotic Resistance in *Pseudomonas Aeruginosa*: Mechanisms and Alternative Therapeutic Strategies. *Biotechnol. Adv.* **2019**, *37* (1), 177–192. <https://doi.org/10.1016/j.biotechadv.2018.11.013>.
- (17) Morihara, K.; Tsuzuki, H.; Oka, T.; Inoue, H.; Ebata, M. *Pseudomonas Aeruginosa* Elastase - Isolation, Crystallization and Preliminary Characterization. *J. Biol. Chem.* **1965**, *240* (8), 3295–3304.
- (18) Wretling, B.; Pavlovskis, O. R. *Pseudomonas Aeruginosa* Elastase and Its Role in *Pseudomonas* Infections. *Clini. Infect. Dis.* **1983**, *5* (Supplement\_5), S998–S1004. [https://doi.org/10.1093/clinids/5.Supplement\\_5.S998](https://doi.org/10.1093/clinids/5.Supplement_5.S998).
- (19) Heck, L. W.; Morihara, K.; McRae, W. B.; Miller, E. J. Specific Cleavage of Human Type III and IV Collagens by *Pseudomonas Aeruginosa* Elastase. *Infect. Immun.* **1986**, *51* (1), 115–118. <https://doi.org/10.1128/IAI.51.1.115-118.1986>.
- (20) Yu, H.; He, X.; Xie, W.; Xiong, J.; Sheng, H.; Guo, S.; Huang, C.; Zhang, D.; Zhang, K. Elastase LasB of *Pseudomonas Aeruginosa* Promotes Biofilm Formation Partly through Rhamnolipid-Mediated Regulation. *Can. J. Microbiol.* **2014**, *60* (4), 227–235. <https://doi.org/10.1139/cjm-2013-0667>.
- (21) Parmely, M.; Gale, A.; Clabaugh, M.; Horvat, R.; Zhou, W. W. Proteolytic Inactivation of Cytokines by *Pseudomonas Aeruginosa*. *Infect. Immun.* **1990**, *58* (9), 3009–3014. <https://doi.org/10.1128/IAI.58.9.3009-3014.1990>.
- (22) Kuang, Z.; Hao, Y.; Walling, B. E.; Jeffries, J. L.; Ohman, D. E.; Lau, G. W. *Pseudomonas aeruginosa* Elastase Provides an Escape from Phagocytosis by Degrading the Pulmonary Surfactant Protein-A. *PLoS ONE* **2011**, *6* (11), e27091. <https://doi.org/10.1371/journal.pone.0027091>.
- (23) Alcorn, J. F.; Wright, J. R. Degradation of Pulmonary Surfactant Protein D by *Pseudomonas Aeruginosa* Elastase Abrogates Innate Immune Function. *J. Biol. Chem.* **2004**, *279* (29), 30871–30879. <https://doi.org/10.1074/jbc.M400796200>.

- (24) Schmidtchen, A.; Frick, I.-M.; Andersson, E.; Tapper, H.; Björck, L. Proteinases of Common Pathogenic Bacteria Degrade and Inactivate the Antibacterial Peptide LL-37. *Mol. Microbiol.* **2002**, *46* (1), 157–168. <https://doi.org/10.1046/j.1365-2958.2002.03146.x>.
- (25) Kany, A. M.; Sikandar, A.; Hauptenthal, J.; Yahiaoui, S.; Maurer, C. K.; Proschak, E.; Köhnke, J.; Hartmann, R. W. Binding Mode Characterization and Early *in Vivo* Evaluation of Fragment-Like Thiols as Inhibitors of the Virulence Factor LasB from *Pseudomonas aeruginosa*. *ACS Infect. Dis.* **2018**, *4* (6), 988–997. <https://doi.org/10.1021/acsinfecdis.8b00010>.
- (26) Schönauer, E.; Kany, A. M.; Hauptenthal, J.; Hüsecken, K.; Hoppe, I. J.; Voos, K.; Yahiaoui, S.; Elsässer, B.; Ducho, C.; Brandstetter, H.; Hartmann, R. W. Discovery of a Potent Inhibitor Class with High Selectivity toward Clostridial Collagenases. *J. Am. Chem. Soc.* **2017**, *139* (36), 12696–12703. <https://doi.org/10.1021/jacs.7b06935>.
- (27) Matsushita, O.; Okabe, A. Clostridial Hydrolytic Enzymes Degrading Extracellular Components. *Toxicon* **2001**, *39* (11), 1769–1780. [https://doi.org/10.1016/S0041-0101\(01\)00163-5](https://doi.org/10.1016/S0041-0101(01)00163-5).
- (28) Popoff, M. R.; Bouvet, P. Clostridial Toxins. *Future Microbiol.* **2009**, *4* (8), 1021–1064. <https://doi.org/10.2217/fmb.09.72>.
- (29) Hatheway, C. L. Toxigenic Clostridia. *Clin. Microbiol. Rev.* **1990**, *3* (1), 66–98. <https://doi.org/10.1128/cmr.3.1.66>.
- (30) Kaya, C.; Walter, I.; Yahiaoui, S.; Sikandar, A.; Alhayek, A.; Konstantinović, J.; Kany, A. M.; Hauptenthal, J.; Köhnke, J.; Hartmann, R. W.; Hirsch, A. K. H. Substrate-inspired Fragment Merging and Growing Affords Efficacious LasB Inhibitors. *Angew. Chem. Int. Ed.* **2021**, anie.202112295. <https://doi.org/10.1002/anie.202112295>.
- (31) Kaya, C.; Walter, I.; Alhayek, A.; Shafiei, R.; Jézéquel, G.; Andreas, A.; Konstantinović, J.; Schönauer, E.; Sikandar, A.; Hauptenthal, J.; Müller, R.; Brandstetter, H.; Hartmann, R. W.; Hirsch, A. K. H. Structure-Based Design of  $\alpha$ -Substituted Mercaptoacetamides as Inhibitors of the Virulence Factor LasB from *Pseudomonas aeruginosa*. *ACS Infect. Dis.* **2022**, *in print*. <https://doi.org/10.1021/acsinfecdis.1c00628>.
- (32) McFadden, J. M.; Frehywot, G. L.; Townsend, C. A. A Flexible Route to (5*R*)-Thiolactomycin, a Naturally Occurring Inhibitor of Fatty Acid Synthesis. *Org. Lett.* **2002**, *4* (22), 3859–3862. <https://doi.org/10.1021/ol026685k>.

- (33) Yahiaoui, S.; Voos, K.; Haupenthal, J.; Wichelhaus, T. A.; Frank, D.; Weizel, L.; Rotter, M.; Brunst, S.; Kramer, J. S.; Proschak, E.; Ducho, C.; Hirsch, A. K. H. *N*-Aryl Mercaptoacetamides as Potential Multi-Target Inhibitors of Metallo- $\beta$ -Lactamases (MBLs) and the Virulence Factor LasB from *Pseudomonas Aeruginosa*. *RSC Med. Chem.* **2021**, *12* (10), 1698–1708. <https://doi.org/10.1039/D1MD00187F>.
- (34) Konstantinović, J.; Yahiaoui, S.; Alhayek, A.; Haupenthal, J.; Schönauer, E.; Andreas, A.; Kany, A. M.; Mueller, R.; Köhnke, J.; Berger, F.; Bischoff, M.; Hartmann, R. W.; Brandstetter, H.; Hirsch, A. K. H. *N*-Aryl-3-Mercaptosuccinimides as Antivirulence Agents Targeting *Pseudomonas Aeruginosa* Elastase and *Clostridium* Collagenases. *J. Med. Chem.* **2020**, *acs.jmedchem.0c00584*. <https://doi.org/10.1021/acs.jmedchem.0c00584>.
- (35) Eckhard, U.; Schönauer, E.; Brandstetter, H. Structural Basis for Activity Regulation and Substrate Preference of Clostridial Collagenases G, H, and T. *J. Biol. Chem.* **2013**, *288* (28), 20184–20194. <https://doi.org/10.1074/jbc.M112.448548>.
- (36) Klebe, G. Protein-Ligand Interactions as the Basis for Drug Action. In *Multifaceted Roles of Crystallography in Modern Drug Discovery*; Scapin, G., Patel, D., Arnold, E., Eds.; NATO Science for Peace and Security Series A: Chemistry and Biology; Springer Netherlands: Dordrecht, 2015; Vol. 38, pp 83–92. [https://doi.org/10.1007/978-94-017-9719-1\\_7](https://doi.org/10.1007/978-94-017-9719-1_7).
- (37) Hagemans, D.; van Belzen, I. A. E. M.; Morán Luengo, T.; Rüdiger, S. G. D. A Script to Highlight Hydrophobicity and Charge on Protein Surfaces. *Front. Mol. Biosci.* **2015**, *2*, 56. <https://doi.org/10.3389/fmolb.2015.00056>.
- (38) Maret, W. Zinc and Sulfur: A Critical Biological Partnership. *Biochemistry* **2004**, *43* (12), 3301–3309. <https://doi.org/10.1021/bi036340p>.
- (39) Sternlicht, M. D.; Werb, Z. How Matrix Metalloproteinases Regulate Cell Behavior. *Annu. Rev. Cell Dev. Biol.* **2001**, *17* (1), 463–516. <https://doi.org/10.1146/annurev.cellbio.17.1.463>.
- (40) Van Lint, P.; Libert, C. Chemokine and Cytokine Processing by Matrix Metalloproteinases and Its Effect on Leukocyte Migration and Inflammation. *J. Leukoc. Biol.* **2007**, *82* (6), 1375–1381. <https://doi.org/10.1189/jlb.0607338>.

- (41) Ropero, S.; Esteller, M. The Role of Histone Deacetylases (HDACs) in Human Cancer. *Mol. Oncol.* **2007**, *1* (1), 19–25. <https://doi.org/10.1016/j.molonc.2007.01.001>.
- (42) Gooz, M. ADAM-17: The Enzyme That Does It All. *Crit. Rev. Biochem. Mol. Biol.* **2010**, *45* (2), 146–169. <https://doi.org/10.3109/10409231003628015>.
- (43) Ahnve, S. QT Interval Prolongation in Acute Myocardial Infarction. *Eur. Heart J.* **1985**, *6* (suppl D), 85–95. [https://doi.org/10.1093/eurheartj/6.suppl\\_D.85](https://doi.org/10.1093/eurheartj/6.suppl_D.85).
- (44) Schwartz, P. J.; Wolf, S. QT Interval Prolongation as Predictor of Sudden Death in Patients with Myocardial Infarction. *Circulation* **1978**, *57* (6), 1074–1077. <https://doi.org/10.1161/01.CIR.57.6.1074>.
- (45) Piccini, J. P.; Whellan, D. J.; Berridge, B. R.; Finkle, J. K.; Pettit, S. D.; Stockbridge, N.; Valentin, J.-P.; Vargas, H. M.; Krucoff, M. W. Current Challenges in the Evaluation of Cardiac Safety during Drug Development: Translational Medicine Meets the Critical Path Initiative. *Am. Heart J.* **2009**, *158* (3), 317–326. <https://doi.org/10.1016/j.ahj.2009.06.007>.
- (46) Pearlstein, R.; Vaz, R.; Rampe, D. Understanding the Structure–Activity Relationship of the Human Ether-a-Go-Go-Related Gene Cardiac K<sup>+</sup> Channel. A Model for Bad Behavior. *J. Med. Chem.* **2003**, *46* (11), 2017–2022. <https://doi.org/10.1021/jm0205651>.
- (47) Sanguinetti, M. C.; Tristani-Firouzi, M. HERG Potassium Channels and Cardiac Arrhythmia. *Nature* **2006**, *440* (7083), 463–469. <https://doi.org/10.1038/nature04710>.
- (48) Hancox, J. C.; McPate, M. J.; El Harchi, A.; Zhang, Y. hong. The HERG Potassium Channel and HERG Screening for Drug-Induced Torsades de Pointes. *Pharmacol. Ther.* **2008**, *119* (2), 118–132. <https://doi.org/10.1016/j.pharmthera.2008.05.009>.
- (49) Raschi, E.; Vasina, V.; Poluzzi, E.; De Ponti, F. The HERG K<sup>+</sup> Channel: Target and Antitarget Strategies in Drug Development. *Pharmacol. Res.* **2008**, *57* (3), 181–195. <https://doi.org/10.1016/j.phrs.2008.01.009>.
- (50) Ponti, F. D.; Poluzzi, E.; Cavalli, A.; Recanatini, M.; Montanaro, N. Safety of Non-Antiarrhythmic Drugs That Prolong the QT Interval or Induce Torsade de Pointes: An Overview. *Drug Saf.* **2002**, *25* (4), 263–286. <https://doi.org/10.2165/00002018-200225040-00004>.
- (51) Priest, B.; Bell, I. M.; Garcia, M. Role of HERG Potassium Channel Assays in Drug Development. *Channels* **2008**, *2* (2), 87–93. <https://doi.org/10.4161/chan.2.2.6004>.

- (52) Guengerich, F. P. Cytochrome P450 and Chemical Toxicology. *Chem. Res. Toxicol.* **2008**, *21* (1), 70–83. <https://doi.org/10.1021/tx700079z>.
- (53) Denisov, I. G.; Makris, T. M.; Sligar, S. G.; Schlichting, I. Structure and Chemistry of Cytochrome P450. *Chem. Rev.* **2005**, *105* (6), 2253–2278. <https://doi.org/10.1021/cr0307143>.
- (54) Wrighton, S. A.; Stevens, J. C. The Human Hepatic Cytochromes P450 Involved in Drug Metabolism. *Crit. Rev. Toxicol.* **1992**, *22* (1), 1–21. <https://doi.org/10.3109/10408449209145319>.
- (55) Slaughter, R. L.; Edwards, D. J. Recent Advances: The Cytochrome P450 Enzymes. *Ann. Pharmacother.* **1995**, *29* (6), 619–624. <https://doi.org/10.1177/106002809502900612>.
- (56) Murray, M. Role of CYP Pharmacogenetics and Drug-Drug Interactions in the Efficacy and Safety of Atypical and Other Antipsychotic Agents. *J. Pharm. Pharmacol.* **2006**, *58* (7), 871–885. <https://doi.org/10.1211/jpp.58.7.0001>.
- (57) Tanaka, E. Clinically Important Pharmacokinetic Drug-Drug Interactions: Role of Cytochrome P450 Enzymes: Cytochrome P450 Interactions. *J. Clin. Pharm. Ther.* **1998**, *23* (6), 403–416. <https://doi.org/10.1046/j.1365-2710.1998.00086.x>.
- (58) Williams, J. A.; Hyland, R.; Jones, B. C.; Smith, D. A.; Hurst, S.; Goosen, T. C.; Peterkin, V.; Koup, J. R.; Ball, S. E. Drug-Drug Interactions for UGT Substrates: A Pharmacokinetic Explanation for Typically Observed Low Exposure (AUC<sub>i</sub>/AUC) Ratios. *Drug. Metab. Dispos.* **2004**, *32* (11), 1201–1208. <https://doi.org/10.1124/dmd.104.000794>.
- (59) Schneider, E.; Clark, D. S. Cytochrome P450 (CYP) Enzymes and the Development of CYP Biosensors. *Biosens. Bioelectron.* **2013**, *39* (1), 1–13. <https://doi.org/10.1016/j.bios.2012.05.043>.
- (60) Safety Screen Panel 44 Eurofins <https://www.eurofinsdiscoveryervices.com/catalogmanagement/viewitem/SafetyScreen44-Panel-Cerep/P270>.
- (61) Giard, D. J.; Aaronson, S. A.; Todaro, G. J.; Arnstein, P.; Kersey, J. H.; Dosik, H.; Parks, W. P. In Vitro Cultivation of Human Tumors: Establishment of Cell Lines Derived From a Series of Solid Tumors<sup>2</sup>. *JNCI: Journal of the National Cancer Institute* **1973**, *51* (5), 1417–1423. <https://doi.org/10.1093/jnci/51.5.1417>.

- (62) Kisselbach, L.; Merges, M.; Bossie, A.; Boyd, A. CD90 Expression on Human Primary Cells and Elimination of Contaminating Fibroblasts from Cell Cultures | SpringerLink. *Cytotechnology* **2009**, *59*, 31–44. <https://doi.org/10.1007/s10616-009-9190-3>.
- (63) Ruffin, M.; Brochiero, E. Repair Process Impairment by *Pseudomonas Aeruginosa* in Epithelial Tissues: Major Features and Potential Therapeutic Avenues. *Front. Cell. Infect. Microbiol.* **2019**, *9*, 182. <https://doi.org/10.3389/fcimb.2019.00182>.
- (64) Murphy, D. J. Determination of Accurate KI Values for Tight-Binding Enzyme Inhibitors: An in Silico Study of Experimental Error and Assay Design. *Analyt. Biochem.* **2004**, *327* (1), 61–67. <https://doi.org/10.1016/j.ab.2003.12.018>.
- (65) Morrison, J. F. Kinetics of the Reversible Inhibition of Enzyme-Catalysed Reactions by Tight-Binding Inhibitors. *Biochim. Biophys. Acta Enzymol.* **1969**, *185* (2), 269–286. [https://doi.org/10.1016/0005-2744\(69\)90420-3](https://doi.org/10.1016/0005-2744(69)90420-3).
- (66) Kuzmič, P.; Elrod, K. C.; Cregar, L. M.; Sideris, S.; Rai, R.; Janc, J. W. High-Throughput Screening of Enzyme Inhibitors: Simultaneous Determination of Tight-Binding Inhibition Constants and Enzyme Concentration. *Analyt. Biochem.* **2000**, *286* (1), 45–50. <https://doi.org/10.1006/abio.2000.4685>.
- (67) Winter, G.; Lobley, C. M. C.; Prince, S. M. Decision Making in Xia 2. *Acta Crystallogr., Sect. D: Biol. Crystallogr.* **2013**, *69* (7), 1260–1273. <https://doi.org/10.1107/S0907444913015308>.
- (68) McCoy, A. J. Solving Structures of Protein Complexes by Molecular Replacement with Phaser. *Acta Crystallogr., Sect. D: Biol. Crystallogr.* **2007**, *63* (1), 32–41. <https://doi.org/10.1107/S0907444906045975>.
- (69) Emsley, P.; Lohkamp, B.; Scott, W. G.; Cowtan, K. Features and Development of Coot. *Acta Crystallogr., Sect. D: Biol. Crystallogr.* **2010**, *66* (4), 486–501. <https://doi.org/10.1107/S0907444910007493>.
- (70) Adams, P. D.; Afonine, P. V.; Bunkóczi, G.; Chen, V. B.; Davis, I. W.; Echols, N.; Headd, J. J.; Hung, L.-W.; Kapral, G. J.; Grosse-Kunstleve, R. W.; McCoy, A. J.; Moriarty, N. W.; Oeffner, R.; Read, R. J.; Richardson, D. C.; Richardson, J. S.; Terwilliger, T. C.; Zwart, P. H. PHENIX: A Comprehensive Python-Based System for Macromolecular Structure Solution. *Acta Crystallogr., Sect. D: Biol. Crystallogr.* **2010**, *66* (2), 213–221. <https://doi.org/10.1107/S0907444909052925>.

- (71) Wallace, A. C.; Laskowski, R. A.; Thornton, J. M. LIGPLOT: A Program to Generate Schematic Diagrams of Protein-Ligand Interactions. *Protein Eng. Des. Sel.* **1995**, *8* (2), 127–134. <https://doi.org/10.1093/protein/8.2.127>.
- (72) Stura, E. A.; Wilson, I. A. Applications of the Streak Seeding Technique in Protein Crystallization. *J. Cryst. Growth* **1991**, *110* (1–2), 270–282. [https://doi.org/10.1016/0022-0248\(91\)90896-D](https://doi.org/10.1016/0022-0248(91)90896-D).
- (73) Kabsch, W. XDS. *Acta Crystallogr., Sect. D: Biol. Crystallogr.* **2010**, *66* (2), 125–132. <https://doi.org/10.1107/S0907444909047337>.
- (74) Evans, P. R.; Murshudov, G. N. How Good Are My Data and What Is the Resolution? *Acta Crystallogr., Sect. D: Biol. Crystallogr.* **2013**, *69* (7), 1204–1214. <https://doi.org/10.1107/S0907444913000061>.
- (75) Smart, O. S.; Womack, T. O.; Sharff, A.; Flensburg, C.; Keller, P.; Paciorek, W.; Vonrhein, C.; Bricogne, G. Grade v.1.1.1., 2011.
- (76) Hauptenthal, J.; Baehr, C.; Zeuzem, S.; Piiper, A. RNase A-like Enzymes in Serum Inhibit the Anti-Neoplastic Activity of SiRNA Targeting Polo-like Kinase 1. *Int. J. Cancer* **2007**, *121* (1), 206–210. <https://doi.org/10.1002/ijc.22665>.
- (77) Zhang, Y.; Huo, M.; Zhou, J.; Xie, S. PKSolver: An Add-in Program for Pharmacokinetic and Pharmacodynamic Data Analysis in Microsoft Excel. *Computer Methods and Programs in Biomedicine* **2010**, *99* (3), 306–314. <https://doi.org/10.1016/j.cmpb.2010.01.007>.



**Chapter F: Optimized Phosphonate Derivatives as Highly Potent Inhibitors of *P. aeruginosa* Virulence Factor Elastase B (LasB) and *Clostridium* Virulence Factor Collagenase H (ColH)**

Katrin Voos, Jelena Konstantinović, Esther Schönauer, Katharina Rox, Anna K. H. Hirsch and Christian Ducho

Please note that the following chapter is a compilation of further results on synthesized phosphonates and is thus neither published nor peer-reviewed yet.

Parts of the results from chapter **F** are included in the paper manuscript "Inhibitors of the Elastase LasB for the treatment of *Pseudomonas aeruginosa* lung infections", which was recently submitted and is currently under review. The current version can be found as preprint:

Jelena Konstantinović, Andreas M. Kany, Alaa Alhayek, Ahmed S. Abdelsamie, Asfandyar Sikandar, Katrin Voos, Yiwen Yao, Anastasia Andreas, Roya Shafiei, Brigitta Loretz, Esther Schönauer, Robert Bals, Hans Brandstetter, Rolf W. Hartmann, Christian Ducho, Claus-Michael Lehr, Christoph Beisswenger, Rolf Müller, Katharina Rox, Jörg Haupenthal, Anna K. H. Hirsch; *ChemRxiv*. Cambridge: Cambridge Open Engage; **2023**.

DOI: 10.26434/chemrxiv-2023-bszcb

#### IV. Unpublished Results

##### **Full contribution report for Chapter F:**

- Katrin Voos** synthesized compounds and intermediates **16, 21–46, and 50–55**, did the SAR interpretation and visualization, conceived, and wrote this chapter.
- Jelena Konstantinović** synthesized compounds **47–49**, expressed and purified LasB, planned and performed the LasB functional assay.
- Esther Schönauer** expressed and purified ColH, planned and performed the ColH functional assay, performed the ColH crystallization experiments and structural determination, performed visualization in Figure 9d.
- Katharina Rox** planned and performed the pharmacokinetic experiments in professional cooperation with Saretius Ltd, visualized results in Figure 11
- Anna K. H. Hirsch** supplied funding and supervised the project.
- Christian Ducho** supplied funding and supervised the project.

## Introduction

In Chapter **B** the synthesis and evaluation of compound **16** (Figure 8a) is described, which bears a phosphonate as stable alternative to the thiol zinc-binding group of our previous ColH inhibitor hit compound **17** (Chapter **A**, and Figure 8a). Unfortunately, some of the activity was lost due to this exchange, but **16** still showed remarkable efficacy in our *ex vivo* pig skin degradation assay. Additionally, the biologic effects of **16** as inhibitor of ColQ1 from *B. cereus* was evaluated in advanced cell-based *in vitro* and in *in vivo* assays (see Chapter **C**). Still, it is crucial to further optimize the phosphonate to again improve the activity on collagenases.

Furthermore, for compounds bearing the thiol ZBG, we describe in Chapter **E** the synthesis and evaluation of compounds having an alkyl side chain in their  $\alpha$ -position. This modification led to a change in the SAR of the aryl moiety in LasB inhibitors, thus furnishing compounds that can be used as dual inhibitors for ColH and LasB. Those dual inhibitors (**18** and **19**) are significantly more potent than all previously synthesized analogs (Figure 8b). An analog bearing a 4-methyl in  $R^1$  (see Chapter **E**) also showed efficacy in skin- and lung-cell assays, as well as in a *Galleria mellonella* larvae infection model.

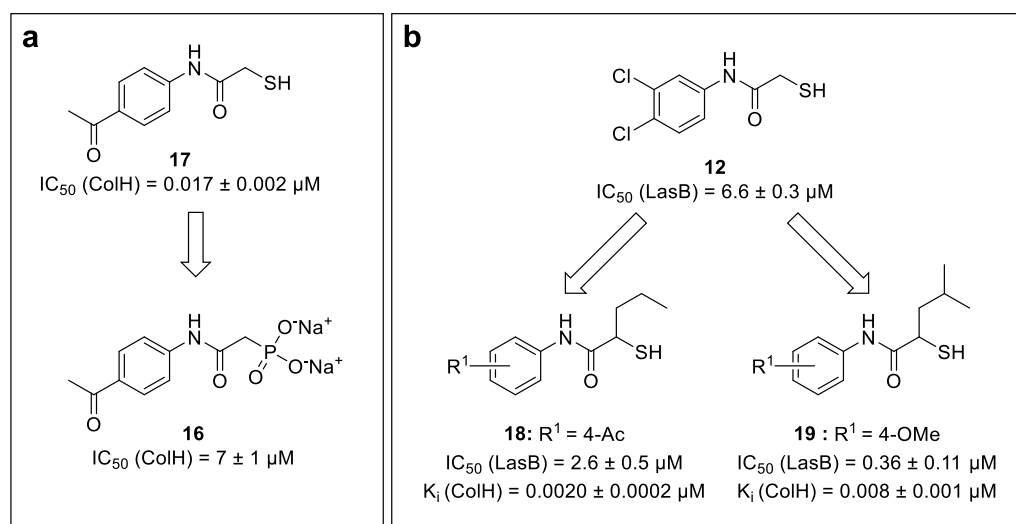


**Figure 8.** Main results and most potent compounds derived from a) ZBG variations displayed in Chapter **C** and b) introduction of alkyl side chains in the  $\alpha$ -position as described in in Chapter **D**.

Therefore, in this chapter, a co-crystal structure of **16** with ColH set the basis for the evaluation of all previously synthesized ZBG alternatives against LasB. In a second step, a first *in vivo* Absorption, Distribution, Metabolism and Excretion (ADME) assessment is performed to investigate the potential to use those phosphonates in the therapy of lung infections with *Pseudomonas aeruginosa* (LasB) or deep tissue infections, such as gas gangrene caused by *Clostridium histolyticum* (ColH). Then, a second round of synthesis was performed to check the influence of the introduction of alkyl side chains in the  $\alpha$ -position of the phosphonate analogs on LasB and ColH inhibition.

## Results and Discussion

**Co-crystal structure of 16 in complex with ColH.** We determined the X-ray crystal structure of the peptidase domain of ColH in complex with **16** at 1.76 Å resolution (Figure 9a – c). The active site is composed of the catalytic zinc ion, coordinated by His455, His459 and Glu487, and the general acid/base Glu487, as seen in the co-crystal structures of **17** (hydrolyzed from thiocarbamate **20**, PDB: 507E, Figure 9b and Figure 10d) and **21** (Chapter E,  $\alpha$ -methyl analog of **17**, PDB: 7BBK, Figure 10c) before. Our inhibitor **16** occupies the non-primed substrate recognition sites in ColH and coordinates the catalytic zinc ion with its phosphonate moiety with an oxygen-to-zinc distance of 2.0 Å. The observed conformations of the peptidase domain of ColH and the respective ligand binding in the three co-crystal structures in complex with **16**, **17** and **21** agree well with each other and reveal similar binding modes in all three complexes (Figure 9b).

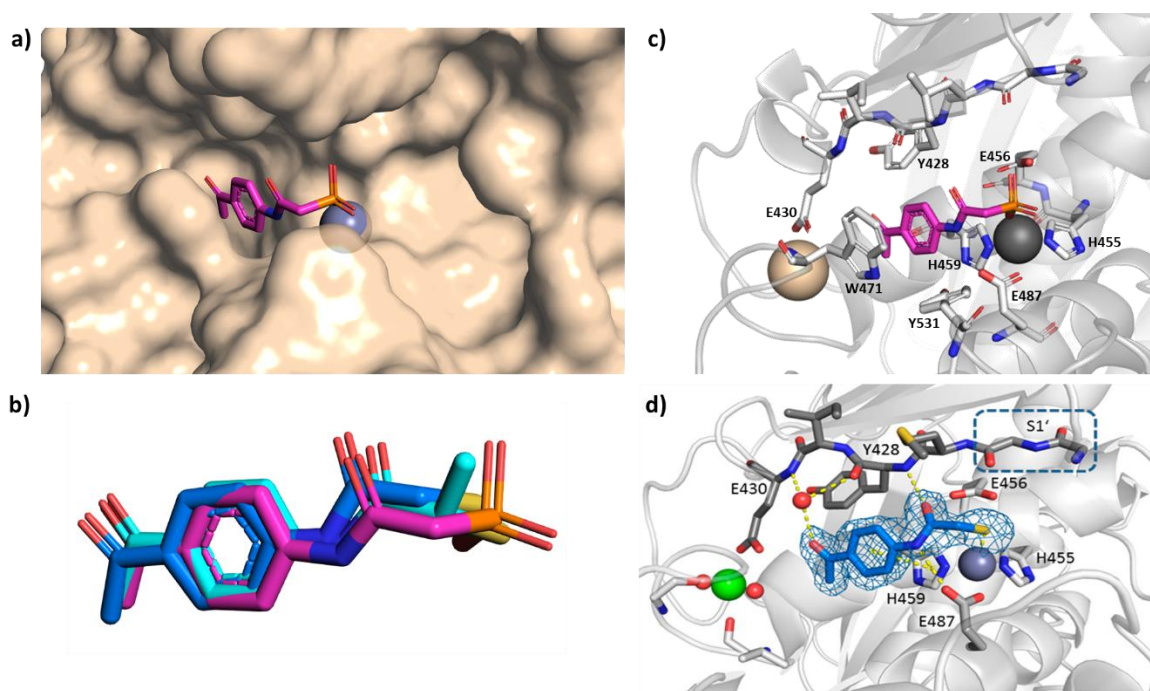


**Figure 9. Close-up on the ligand-bound active sites of ColH.** **a)** Superposition of the active sites of ColH in complex with **16** (ligand in pink sticks), surface representation colored in wheat. **b)** Close-up look on the overlay of bound **16** (ligand in purple sticks), **17** (ligand in light blue sticks, PDB: 507E) and **21** (ligand in dark blue sticks, PDB: 7BBK) reveals same binding mode to ColH for all three structures. **c)** Co-crystal structure of **16** with ColH. The inhibitor is shown in sticks (purple). The catalytic zinc ion (dark gray) and the calcium ion (wheat) are shown as spheres. The edge strand and active-site residues are shown in light gray sticks. **d)** Co-crystal structure of **21** with ColH as the binding partner (PDB: 507E).<sup>1</sup> The inhibitor is shown in sticks (blue). The catalytic zinc ion (dark gray), the calcium ion (green) and water molecules (red) are shown as spheres. The edge strand and active-site residues are shown in gray sticks.

However, looking on each co-crystal structure with surface representation (Figure 10), it can be derived, that the phosphonate as ZBG needs more space in the binding pocket itself, forcing the enzyme to open more widely (Figure 10a) compared to the complexes with **17** (Figure 10b) and **21** (Figure

#### IV. Unpublished Results

10c). This might also be the reason for the ~400-fold decrease in activity against ColH for **16** ( $IC_{50} = 7 \pm 1 \mu M$ )<sup>2</sup> compared to **17** ( $IC_{50} = 0.017 \pm 0.002 \mu M$ )<sup>1</sup>.

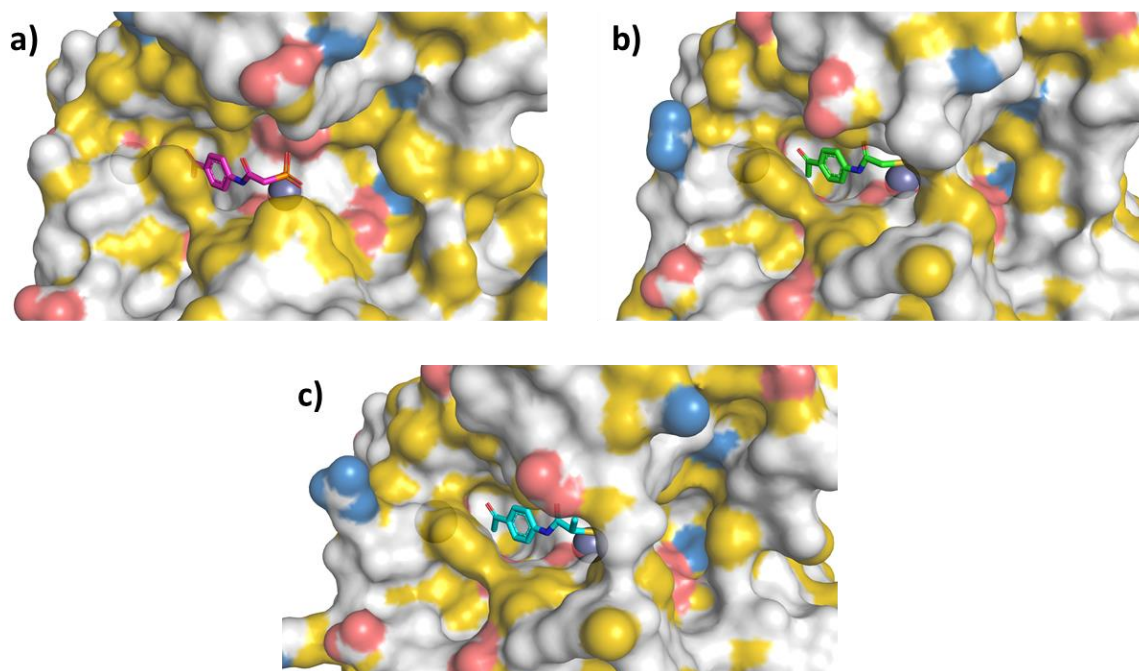


**Figure 10.** Active site of ColH bound to ligands shown in hydrophobic surface representation colored according to YRB scheme: non-polar hydrocarbons (yellow), negatively charged oxygen atoms of glutamate and aspartate (red), positively charged nitrogen atoms of lysine and arginine (blue).<sup>199</sup> All three structures are aligned and the views were taken from the same angle to give a better insight into the conformational differences of all three complexes. **a)** Co-crystal with **16** (purple sticks). The enzyme is more widely opened in the area around the catalytic zinc ion relative to the other two co-crystal structures. **b)** Co-crystal with **17** (green sticks, PDB: 507E). **c)** Co-crystal with **21** (light blue sticks, PDB: 7BBK).

#### ***In vitro* inhibition of LasB by previously synthesized components with alternative ZBG.**

Encouraged by the crystal structure of **16** in complex with ColH, which reveals very similar binding modes as previously observed for *N*-aryl mercaptoacetamides, we were encouraged to investigate whether this would also be the case for LasB, as those mercaptoacetamides comprise the main core structure for both, LasB and ColH inhibitors.<sup>1,194</sup> To not miss any possible ZBG alternative for LasB, all our previously published components with alternative ZBG for ColH<sup>2</sup> were also tested in the previously described FRET-based assay for LasB *in vitro* inhibitory activity.<sup>194</sup> Therefore, each compound was first investigated on LasB at a concentration of 600  $\mu M$ . The high concentration was chosen as the tested compounds all incorporated a *para*-acetyl phenyl group as aryl moiety, which was not favored for LasB even with the thiol as ZBG (thiocarbamate **20** as prodrug of thiol **17**). The percentages of inhibition are listed in Table 2.

#### IV. Unpublished Results

**Table 2.** *In vitro* inhibitory activities of previously synthesized target compounds **16**, **22–31**<sup>2</sup> and reference compound **20**<sup>194</sup> against LasB.

Cpd	ZBG	% Inh. @ 600 μM <sup>a</sup>	Cpd	ZBG	% Inh. @ 600 μM <sup>a</sup>	Cpd	ZBG	% Inh. @ 600 μM <sup>a</sup>
<b>20</b>		IC <sub>50</sub> = 73.1 ± 2.5 μM <sup>194</sup>	<b>25</b>		n. i.	<b>29</b>		n. i.
<b>22</b>		n. i.	<b>26</b>		n. i.	<b>30</b>		n. i.
<b>23</b>		n. i.	<b>27</b>		n. i.	<b>31</b>		n. i.
<b>24</b>		n. i.	<b>28</b>		n. i.	<b>16</b>		33 ± 4

<sup>a</sup>Means and SD of at least two independent experiments; n. i. = no inhibition (< 10% inhibition)

Interestingly, of all tested ZBG alternatives, only the phosphonate derivative **16** was able to maintain at least some inhibitory activity against LasB. However, **16** is a more than ten times weaker inhibitor than the parent thiocarbamate compound **20** (IC<sub>50</sub> > 600 μM compared to IC<sub>50</sub> = 73 μM). These observations are consistent with our previous finding for ColH inhibitors.<sup>2</sup>

***In vivo* pharmacokinetic (PK) parameters.** To investigate whether a phosphonate-based inhibitor such as **16** would be suitable for treatment of *P. aeruginosa* infections, its lung-specific *in vivo* PK parameters were investigated in mice by Katharina Rox (Helmholtz Center for Infectious Diseases HZI, Braunschweig) in professional cooperation with Saretius Ltd. (UK). After intratracheal installation at a dose of 0.25 mg/kg, the concentrations in bronchoalveolar lavage fluid (BALF), plasma, lung tissue and brain tissue were determined at designated time points (Figure 11). Additionally, we calculated the exposure in epithelial lining fluid (ELF) from the experimental BALF parameter according to previously reported formulas (Equation S3 & S4 in SI).<sup>200</sup> Unsurprisingly due to its high charge, compound **16** showed no systemic bioavailability within the time range of the PK study. It was not possible to detect it at any timepoint in the plasma or tissue samples. However, in BALF and ELF, which can be regarded as primary target sites for treatment of *P. aeruginosa* lung infections, the levels are encouraging.

The maximum concentration (C<sub>max</sub>) of **16** in BALF was 0.31 ± 0.14 μg/mL and the area under the curve within the experimental time range (AUC<sub>0-t</sub>) was 0.27 ± 0.09 μg/mL\*h (Figure 11). Therefore, the PK profile reveals **16** to be suitable for intratracheal administration with low systemic exposure.

#### IV. Unpublished Results

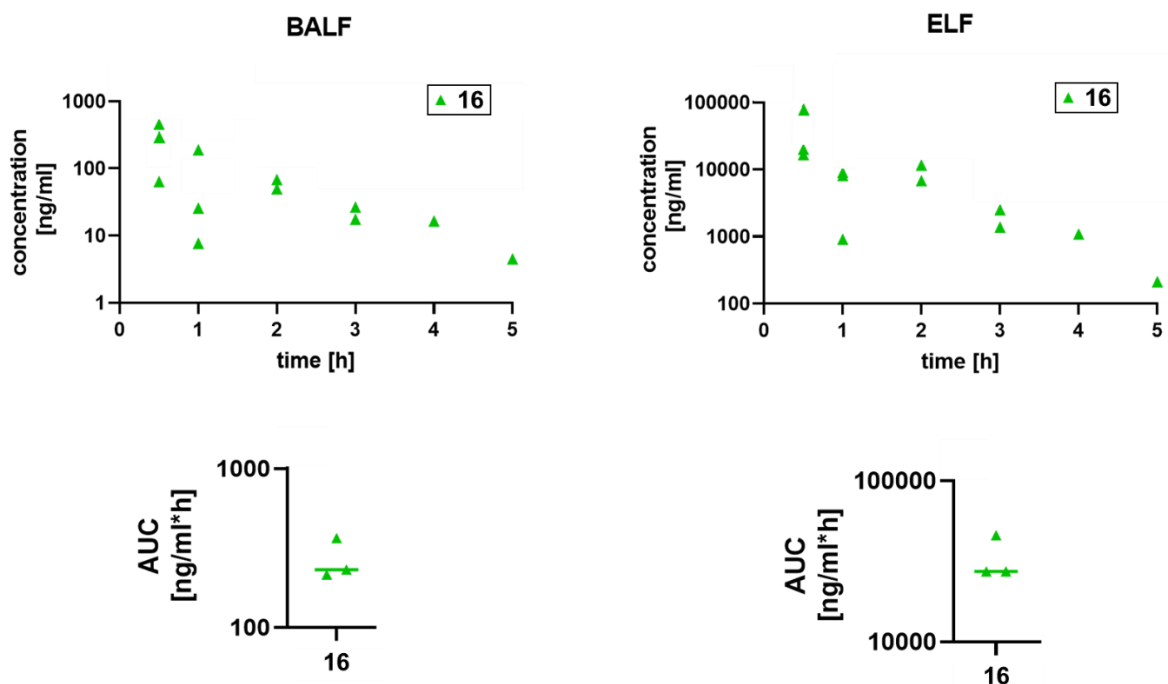


**Figure 11.** *In vivo* pharmacokinetics assessment after intratracheal instillation ( $n = 3$  mice per time point) of compound **16**.

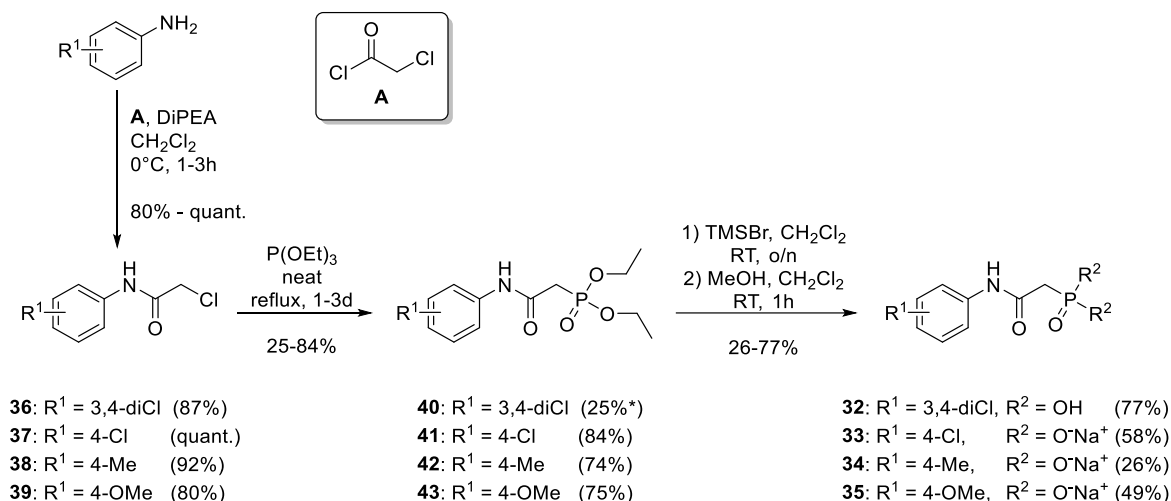
**Chemistry.** It was demonstrated that a phosphonate like **16** could be used for local *P. aeruginosa* treatment according to its PK parameters. Therefore, it was decided to test whether an improvement of the LasB inhibitory activity by modification of the currently unfavorable aryl substitution can be made. Additionally, all new phosphonates should also be evaluated against ColH, as the parent compound **16** was first published as a ColH inhibitor.

For 2-unsubstituted *N*-aryl mercaptoacetamides, lipophilic (multi-)substituents on the aryl moiety, such as chlorine, were most favored. However, additionally to the 3,4-dichlorophenyl (compd. **32**, 3,4-diCl) and 4-chlorophenyl derivatives (compd. **33**, 4-Cl), the 4-methylphenyl (compd. **34**, 4-Me) and 4-methoxyphenyl (compd. **35**, 4-OMe) derivatives were synthesized (see Scheme 1), as the respective thiols had shown higher inhibitory effects in previous studies (see Chapter E).

Starting from the corresponding aniline derivatives, the phosphonates were synthesized in three steps as previously reported.<sup>2</sup> First, anilines were acylated with chloroacetyl chloride, giving alkyl chloride intermediates **36–39** in 80% to quantitative yield. A Michaelis-Arbuzov reaction afforded the ethyl esters **40–43** (25% – 84%) which were cleaved by transesterification with trimethylsilyl bromide followed by methanol addition. It must be mentioned here that the yield of 25% for **40** is not representative, and the actual yield would have been higher, but a large mixed fraction was not purified due to time constraints. The cleaved products were converted into their sodium salts by ion exchange chromatography to afford compounds **33**, **34** and **35** in 58%, 26% and 49% yield, respectively. Unfortunately, a lot of compound **34** was lost during the purification and ion exchange process, resulting in this moderate yield. Therefore, we decided that compound **32** should be tested *in vitro* in

#### IV. Unpublished Results

its acid form and should just be converted into its salt form when tested *in vivo*. Cleavage of **40** afforded compound **32** after high-performance liquid chromatography (HPLC) purification as free acid in 77% yield.



**Scheme 1.** Synthesis of compounds **32–35**.

***In vitro* inhibition of LasB and ColH by compounds 32–35.** The four new compounds were tested using our previously reported FRET-based LasB<sup>194</sup> and FRET-based ColH<sup>1,201</sup> inhibition assays. The results are listed in Table 3.

**Table 3.** *In vitro* inhibitory activities of compounds **32–35** and reference compound **16**<sup>2</sup> against both LasB and ColH.

Compound	R <sup>1</sup>	R <sup>2</sup>	LasB Inhibition [%] at a given concentration <sup>a</sup>	ColH Inhibition [%] at a given concentration <sup>a</sup>
<b>16</b>	4-Ac	-O <sup>-</sup> Na <sup>+</sup>	33 ± 4 % @ 600 μM	IC <sub>50</sub> = 7 ± 1 μM
<b>32</b>	3,4-diCl	-OH	15 ± 3 % @ 10 μM	79 ± 5% @ 500 μM
<b>33</b>	4-Cl	-O <sup>-</sup> Na <sup>+</sup>	47 ± 0 % @ 200 μM	IC <sub>50</sub> > 500 μM
<b>34</b>	4-Me	-O <sup>-</sup> Na <sup>+</sup>	38 ± 8 % @ 200 μM	n.d.
<b>35</b>	4-OMe	-O <sup>-</sup> Na <sup>+</sup>	31 ± 3 % @ 200 μM	IC <sub>50</sub> = 268 ± 24 μM

<sup>a</sup>Means and SD of at least two independent experiments; n.d.= not determined

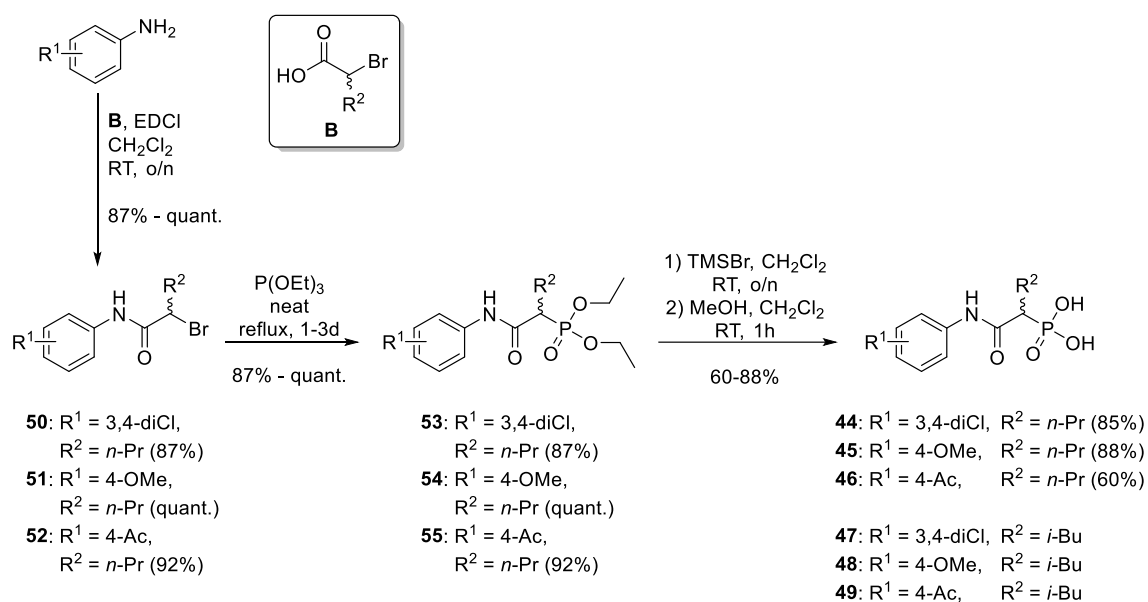
For LasB inhibition, we observed the same trend as before with the *N*-aryl-2-mercaptoacetamides, so the most active compound was the 3,4-dichloro substituted 2-phosphono acetamide **32**



#### IV. Unpublished Results

( $IC_{50}(\text{LasB}) < 200 \mu\text{M}$ ), directly followed by the 4-chloro compound **33** ( $IC_{50}(\text{LasB}) \approx 200 \mu\text{M}$ ). Hydrophilic hydrogen bond accepting moieties such as 4-acetyl **16** were the least favored for LasB ( $IC_{50}(\text{LasB}) > 600 \mu\text{M}$ ) but were the only tolerated group with respect to ColH inhibition ( $IC_{50}(\text{ColH}) = 7 \mu\text{M}$ , compared to  $> 250 \mu\text{M}$ ). In the ColH inhibition assay, **34** suffered from solubility problems, but as 4-methyl is known to be less favored than 4-methoxy against ColH, and as the LasB data were not promising, no further efforts were made to obtain the ColH inhibition value.

To investigate whether the SAR correlates fully with the SAR previously observed with 2-mercapto-2-alkyl-*N*-aryl acetamides (see Chapter E), we decided to focus on the 4-acetyl (**17** as best ColH inhibitor, Chapter A<sup>1</sup>), 3,4-diCl (**12** best non-substituted LasB inhibitor<sup>194</sup>) and 4-methoxy moieties (**19** as best  $\alpha$ -substituted dual inhibitor, Chapter E). For compounds with those moieties, an *n*-propyl side chain, which had been found to be most active for ColH inhibition, and an *iso*-butyl side chain, which had been most active against LasB and for dual inhibition (Chapter E), were introduced. The synthetic route towards compounds **44–46** followed the same scheme as before with the only difference being the first step. Here, acylation of aniline derivatives was performed using the corresponding 2-bromoalkanoic acids and *N*-(3-dimethylaminopropyl)-*N'*-ethylcarbodiimid hydrochlorid (EDCI) as coupling reagent (see Scheme 2). *iso*-butyl derivatives **47–49** were synthesized by Jelena Konstantinović at the HIPS.<sup>6</sup>



**Scheme 2.** Synthesis of compounds **44–46**.

The resulting six new phosphonates were then again tested for their inhibitory activity against both LasB and ColH and their inhibition values were compared to the values of analogs without  $\alpha$ -substitution. Results are listed in Table 4.

#### IV. Unpublished Results

**Table 4.** *In vitro* inhibitory activities of compounds **44–49** and reference compounds **16**,<sup>2</sup> **32** and **35** against both LasB and ColH.

Compound	R <sup>1</sup>	R <sup>2</sup>	IC <sub>50</sub> (LasB) [μM] <sup>a</sup>	K <sub>i</sub> (ColH) [μM] <sup>a</sup>
<b>32</b>	3,4-diCl	H	> 10	~ 500
<b>35<sup>b</sup></b>	4-OMe	H	> 200	268 ± 24
<b>16<sup>b</sup></b>	4-Ac	H	> 600	7 ± 1
<b>44</b>	3,4-diCl	<i>n</i> Pr	2.1 ± 0.3	~ 10
<b>45</b>	4-OMe	<i>n</i> Pr	1.1 ± 0.1	~ 10
<b>46</b>	4-Ac	<i>n</i> Pr	0.87 ± 0.03	0.13 ± 0.02
<b>47</b>	3,4-diCl	<i>i</i> Bu	0.026 ± 0.004 <sup>6</sup>	> 1
<b>48</b>	4-OMe	<i>i</i> Bu	0.052 ± 0.010 <sup>6</sup>	> 1
<b>49</b>	4-Ac	<i>i</i> Bu	0.040 ± 0.012 <sup>6</sup>	0.32 ± 0.07

<sup>a</sup>Means and SD of at least two independent experiments; <sup>b</sup>Substance was tested in its di-sodium salt form

For α-substituted phosphonoacetamides, the same trend as previously observed with mercaptoacetamides was found (Chapter E). Introduction of an *n*-propyl side chain boosted the activity for LasB inhibition by a factor of more than 500 for the 4-acetyl compound **46**. **46** is the most active against LasB of the three tested *n*-propyl side chain derivatives with an IC<sub>50</sub> value of 0.87 ± 0.03 μM. This is almost in the same range as our best *N*-aryl-2-alkyl-2-mercaptoacetamide (**19**, IC<sub>50</sub> = 0.36 ± 0.11 μM). When introducing an *iso*-butyl side chain to the phosphonates as in **19**, the activity again increased by a factor of more than 20 (compounds **47–49**) compared to the *n*-propyl compounds, with **47** being the most active against LasB with a remarkable IC<sub>50</sub> value of 26 ± 4 nM.

For ColH inhibition, the SAR is again slightly additive, and an *n*-propyl side chain increased activity even in the previously unfavored aryl moieties 3,4-dichloro (**44**, IC<sub>50</sub> ~10 μM) and 4-OMe methoxy (**45**, IC<sub>50</sub> ~10 μM) by a factor of more than 20. With our best aryl moiety (4-acetyl), we reached again a sub-micromolar activity (**46**, IC<sub>50</sub> = 0.13 ± 0.02 μM). The introduction of the bulkier *iso*-butyl side chain however led to less active compounds. 4-acetyl (**49**, IC<sub>50</sub> = 0.32 ± 0.07 μM) was better tolerated than 4-methoxy (**48**, IC<sub>50</sub> > 1 μM), but two to three times less active than the *n*Pr derivative **46**.

### Conclusion

In this chapter the co-crystallization of the first phosphonate-based inhibitor **16**, its *in vivo* lung-specific PK evaluation and LasB inhibitory properties are described. Moreover, seven new phosphonate derivatives were synthesized and tested (together with three more compounds synthesized at HIPS) for their LasB and ColH inhibitory activities.

For ColH, sub-micromolar inhibitors were obtained, which is a 50-fold improvement compared to the non-alkylated phosphonate **16**. The 4-methoxy compound **48** with an *iso*-butyl side chain is slightly less active than the 4-acetyl compound **46** with *n*-propyl side chain ( $IC_{50} = 0.13 \pm 0.02 \mu\text{M}$  compared to  $IC_{50} = 0.32 \pm 0.07 \mu\text{M}$ ). **46** represents the best ColH inhibitor in this series.

With respect to LasB inhibitory activity, a remarkable improvement was archived by combining the *iso*-butyl side chain, which had previously also been found to be the most suitable for thiol-based inhibitors (Chapter E), with various aryl moieties. All tested compounds had  $IC_{50}$  values well below 100 nM.

Due to their high charge, it is most likely that the *iso*-butyl compounds bear similar PK parameters as **16**. This would make them highly promising new lead compounds for the development of *P. aeruginosa* pathoblockers for local treatment.

### Experimental Section

**Chemistry.** The general methodology, together with the general procedures, synthetic descriptions and characterizations of molecules (synthesized by the author) in this chapter can be found in the Appendix 6.

**Expression and Purification of LasB and ColH-PD.** LasB and ColH-PD were expressed and purified as previously described.<sup>117,194</sup>

***In vitro* LasB and ColH Inhibition Assay.** Both LasB and ColH inhibition assays were performed as previously described.<sup>1,194</sup>

***In vivo* PK parameter determination.** The PK determination was performed by Katharina Rox at the HZI in cooperation with Saretius as previously described.<sup>202</sup> The used parameters, settings and the short description can be found in the Supporting Information (Appendix 6).

**Acknowledgments**

We thank Dr. Stefan Boettcher and Stefanie Weck for the measurements of high-resolution mass spectra, Nathalie Andreia, Martina Jankowski and Jeannine Jung for technical support and Saretius Ltd. for professional cooperation during PK evaluation.

## **Chapter G: Functionalized $\alpha$ -Side chains as Booster for the Inhibitory Activity of *N*-Aryl mercaptoacetamides on *C. histolyticum* Virulence Factor ColH**

Katrin Voos, Esther Schönauer, Jelena Konstantinović, Sebastian Dahmen, Marcel Lutz, Selina Wolter, Anna K. H. Hirsch and Christian Ducho

Please note that the following chapter is a compilation of further results on synthesized linker and side chain derivatives and is thus neither published nor peer-reviewed yet.

### **Full contribution report:**

**Katrin Voos** synthesized compounds **71–73**, **75–81**, and **83–92**, did the SAR interpretation and visualization, conceived, and wrote this chapter.

**Esther Schönauer** expressed and purified ColH, planned and performed the ColH functional assay, planned and performed the ColH crystallization experiments and structure determination, visualization in Figure 14c.

**Jelena Konstantinović** synthesized compounds **66**, **67**, **98** and **99**, planned and performed the LasB functional assay.

**Sebastian Dahmen** synthesized compounds **93–97**.

**Marcel Lutz** synthesized compounds **74** and **82**.

**Selina Wolter** expressed and purified ColH, performed the LasB functional assay.

**Anna K. H. Hirsch** supplied funding and supervised the project.

**Christian Ducho** supplied funding and supervised the project.

## Introduction

In 2020, Konstantinović *et al.* published the class of *N*-aryl-3-mercaptopuccinimides as inhibitors of both LasB and ColH.<sup>201</sup> Later investigations of this class showed that the hydrolyzed mercaptoacetamides are indeed the active moiety in this class, revealing the active form of mercapto succinimides being also  $\alpha$ -substituted mercaptoacetamides (data not published, see Figure 12).

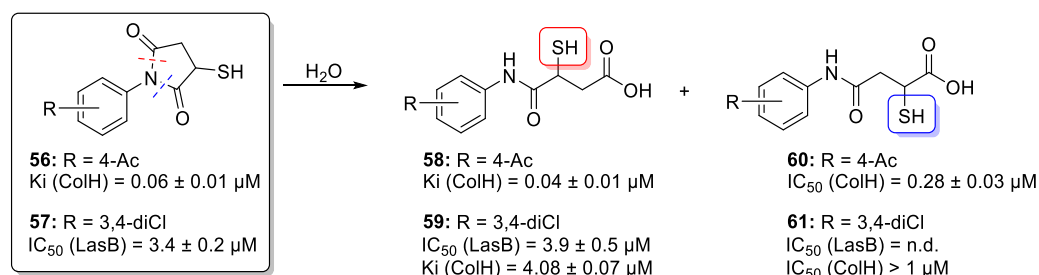


**Figure 12.** Compounds **56**<sup>201</sup> and **57**<sup>201</sup> hydrolyze in water to their actual active forms **58** and **59** and the inactive **60** and **61** (unpublished results, orally communicated by Jelena Konstantinović and Samir Yahiaoui).

An SAR study on the influence of benzyl side chains in  $\alpha$ -position of mercaptoacetamides was published by Kaya *et al.* in 2022.<sup>196,197</sup> As continuation of Kaya *et al.*'s work, Chapter E of this thesis focused on alkyl substitution. By introduction of *n*-propyl and *iso*-butyl side chains, the inhibitory activities toward LasB and ColH were highly increased. This led to sub-micromolar LasB- and single-digit nanomolar active ColH inhibitors. An overview of the different derivatizations can be found in Figure 13.

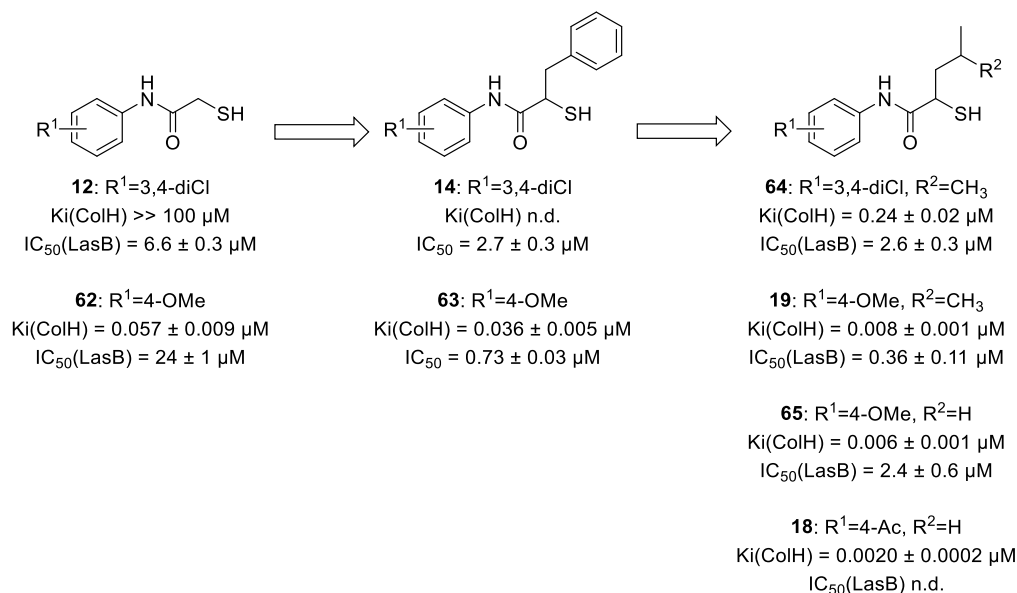


**Figure 13.** Unsubstituted *N*-aryl mercapto acetamides **12** and **62** were the first inhibitors for ColH and LasB published in 2017.<sup>1,194</sup>  $\alpha$ -benzyl substitution (compounds **14**<sup>196</sup> and **63**<sup>197</sup>) highly increased LasB activity, while ColH inhibition was only slightly improved.  $\alpha$ -alkyl substitution (compounds **18**, **19**, **64** and **65**) boosted both ColH and LasB inhibition, leading to single-digit nanomolar ColH inhibitors and sub-micromolar LasB inhibitors (see Chapter E).

## IV. Unpublished Results

*N*-Aryl-3-mercaptosuccinimides hydrolyze to mercaptoacetamides bearing acidic side chains (Figure 12, compound **58** and **59**). Despite the large SAR studies conducted by Kaya *et al.*<sup>196,197</sup> and Voos *et al.* (Chapter **E**), the influence of polar groups in the side chain of ColH inhibitors was not tested so far. From the structural information of the binding mode of various inhibitors to LasB, it is known that usually no hydrophilic residues in the S2' binding pocket are tolerated (see Introduction, 3.1.3 Inhibitors of LasB, page 12). Therefore, this chapter focused on the influence of different derivatized side chains in  $\alpha$ -position of *N*-aryl mercaptoacetamides as inhibitors of ColH.

However, the bacterial-specific binding pocket of ColH is, in contrast to LasB, quite small and as seen in the co-crystal structure PDB: 7BBK (Chapter **E**), the side chain in  $\alpha$ -position points out of the binding pocket towards the solvent and does not interact with the enzyme. Therefore, hydrophilic side chains might increase the activity of ColH inhibitors by pushing the backbone of the molecule deeper into the small binding pocket and filling the cavity between S1/S1' cavity, or by interactions with the amino acids on the surface in close surrounding to the binding pocket (*e.g.*, cation- $\pi$  or H-bond interactions with Y543, ionic or H-bond interactions with E487, ...).

Therefore, a first round of synthesis together with co-crystallization experiments was conducted to check if negatively charged compounds (*e.g.*, **58** and **59**) or neutral hydrophilic compounds are more beneficial for ColH activity. As this was proven successful, a larger round of synthesis was performed to optimize our current hit compounds especially against ColH.

### Results and Discussion

**Synthesis and biological evaluation of neutral analogs 66 and 67.** As previously described in Chapter **E**, 4-Ac moieties gave various side products during synthesis. For alkylated  $\alpha$ -side chain derivatives, 4-OMe (**65**) was proven to be almost equipotent to 4-Ac (**18**) with  $K_i$  values of  $6 \pm 1$  nM and  $2 \pm 1$  nM, respectively. Therefore, the investigation of hydrophilic side chains was mainly carried out on 4-OMe derivatives.

In a first step, the influence of the state of charge of the side chain should be investigated. Our hypothesis was that a positively charged side chain might be able to interact with Y543, forming a cation- $\pi$  interaction, but already a neutral hydrophilic side chains should be superior to negatively charged ones due to possible H-bond interactions. This hypothesis should be substantiated by an experimental setting. Thus, Jelena Konstantinović from HIPS synthesized the methyl-ester compounds **66** and **67**, which then were tested on a FRET based inhibition assay for ColH activity.<sup>1</sup> Those two compounds were compared against the acidic compounds **58** and **59** and fully 2-unsubstituted compounds **17**, **62** and **12**. The results are depicted in Table 5.

#### IV. Unpublished Results

**Table 5.** *In vitro* inhibitory activities of compounds **12**, **17**, **58**, **59**, **62**, **66** and **67** against both LasB and ColH.

Name	R <sup>1</sup>	R <sup>2</sup>	IC <sub>50</sub> (ColH) [μM] <sup>a</sup> (or K <sub>i</sub> if indicated)	IC <sub>50</sub> (LasB) [μM] <sup>a</sup>
<b>17</b>	4-Ac	-H	0.017 ± 0.002 <sup>1</sup>	73 ± 3 <sup>b</sup>
<b>58</b>	4-Ac	-CH <sub>2</sub> COOH	0.033 ± 0.004	n.d.
<b>62</b>	4-OMe	-H	K <sub>i</sub> = 0.057 ± 0.009	48 ± 1 <sup>b</sup>
<b>66</b>	4-OMe	-CH <sub>2</sub> COOMe	K <sub>i</sub> = 0.024 ± 0.005	39 ± 4
<b>12</b>	3,4-diCl	-H	10 – 100 <sup>b,c</sup>	6.6 ± 0.3
<b>59</b>	3,4-diCl	-CH <sub>2</sub> COOH	4.1 ± 0.1	3.9 ± 0.5
<b>67</b>	3,4-diCl	-CH <sub>2</sub> COOMe	0.12 ± 0.01	n.d.

<sup>a</sup> Means and SD of at least two independent experiments; <sup>b</sup> tested in its thiocarbamate prodrug form<sup>194</sup>; <sup>c</sup> 86% inhibition at 100 μM<sup>1</sup>

In direct comparison, both the acidic side chain derivative **58** and methyl ester-derivative **66** were less active than their unsubstituted counterparts against ColH. However, this only holds true, as long as we face compounds with ColH-preferred hydrophilic, H-bond accepting aryl substitution. 3,4-dichloro compound **59** with an acidic side chain gained activity by more than a factor of 2 compared to the unsubstituted compound **12** (IC<sub>50</sub> = 4.1 ± 0.1 μM compared to IC<sub>50</sub> = 10 – 100 μM, respectively). When converting the acidic side chain into a neutral hydrophilic side chain by exchanging it with the methyl ester, a tremendous activity boost was found, leading to compound **67** with an IC<sub>50</sub> value of 0.12 ± 0.01 μM. This strongly supports the hypothesis for ColH.

Looking on LasB inhibition activity, the here presented α-substitution led to only slightly more active compounds, no matter of the nature of the side chain. As already expected from the existing SARs, the improvement on LasB was far less than what had been observed with lipophilic side chains (Chapter E).

**Co-crystallization experiments.** The first round of experimental evaluation of newly synthesized compounds showed that hydrophilic α-side chains were better for ColH inhibition activity than solely lipophilic side chains. For the aryl substitution, previously only hydrophilic H-bond accepting moieties in *para*-position such as 4-acetyl or 4-methoxy were tolerated. However, compound **67** showed some promising activity despite its 3,4-dichloro substitution. As already 3 co-crystal structures were solved, it was especially interesting to investigate, why the lipophilic aryl-substitution was much more tolerated in compound **67** than in other 3,4-dichloro compounds and whether the binding mode was still the same.



#### IV. Unpublished Results

Therefore, the crystal structure of the peptidase domain of ColH in complex with **67** was determined at 2.26 Å resolution (Figure 14). As previously seen in the co-crystal structures of **17** (PDB: 507E), **21** (PDB: 7BBK) and **16** (Chapter F), the active site is composed of the catalytic zinc ion that is coordinated by His455, His459 and Glu487. Compound **67** occupied the non-primed substrate recognition sites in ColH, too, revealing the same binding mode as all previous compounds. However, one major difference was observed. The side chain of Tyr531 is tilted by 46° compared to the co-crystal of **21** (PDB:7BBK), which is shown in Figure 14c as gray sticks (current state of Tyr531) compared to the previous position of Tyr531 depicted in blue sticks. With this flip, more space is generated for the side chain of Glu487 which now generates an H-bond to the ligand's nitrogen (3.4 Å). Additionally, a second hydrogen bond is observed between the hydroxy-hydrogen atom of Tyr531 and the ester oxygen of the ligand (2.8 Å). Also, the ester side chain now comes close to the methionine Met427 side chain and might form some alkyl-alkyl interactions (3.6 Å), see Figure 14c. All these lead to a very close interaction between the enzyme and the molecule, which already can be observed by the surface representation in Figure 14d.

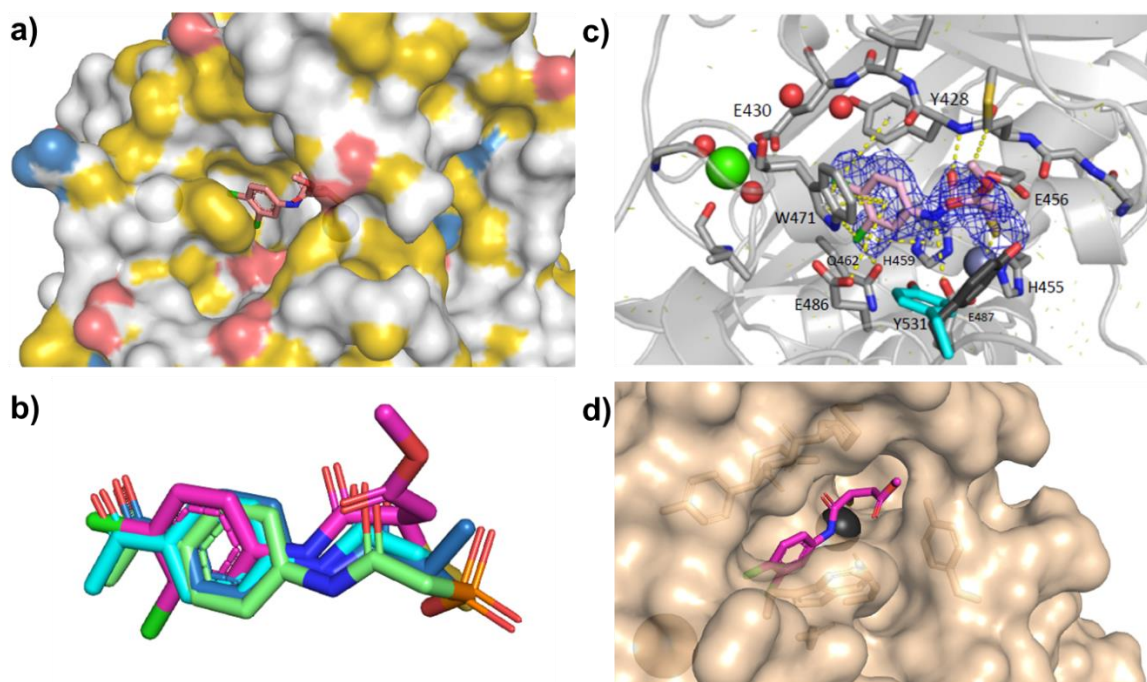


**Figure 14.** **a)** Active site of ColH bound to ligand **67** (light purple sticks) shown in hydrophobic surface representation colored according to YRB scheme: non-polar hydrocarbons (yellow), negatively charged oxygen atoms of glutamate and aspartate (red), positively charged nitrogen atoms of lysine and arginine (blue).<sup>199</sup> The view was taken from the same angle as Figure 9 in Chapter F to give a better view on the conformational differences of all complexes. The enzyme is more tightly closed in the area around the catalytic zinc ion and at the aryl compared to other co-crystal structures. **b)** Close-up look on the overlay of bound **67** (ligand in purple sticks), **16** (ligand in green sticks), **17** (ligand in light blue sticks, PDB: 507E) and **21** (ligand in dark blue sticks, PDB: 7BBK). **c)** Co-crystal structure of **67** with ColH. The inhibitor is shown in sticks (light purple). The catalytic zinc ion (dark purple) and the calcium ion (green) are shown as spheres. The edge strand and active-site residues are shown in light gray sticks. The side chain Tyr531 is depicted in dark gray, while its position in the previous co-crystal structures is shown in light blue. **d)** Superposition of the active sites of ColH in complex with **67** (ligand in pink sticks) in surface representation colored in wheat; different angle than showed in a for better view of possible interactions with the side chain.

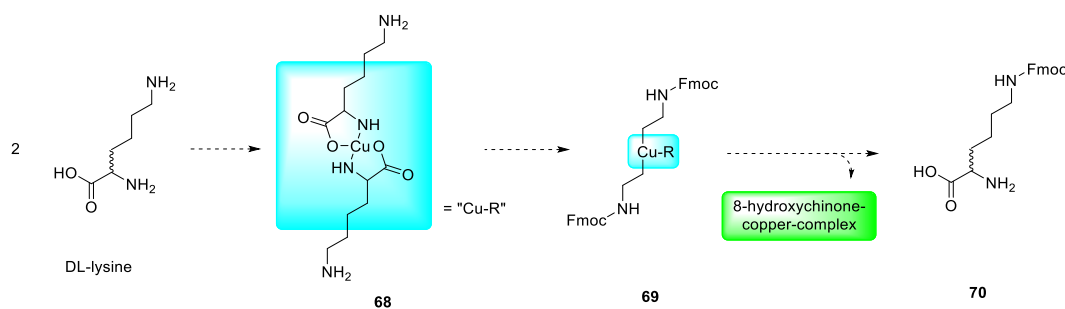
#### IV. Unpublished Results

Interestingly, comparing the co-crystal of **67** with the co-crystal of **21**, the stereochemistry of the bound ligands was different. In both cases compounds **67** and **21** were introduced into the experiment as racemic structures. However, the X-ray structure revealed the *R*-enantiomer of **67** being present in the crystal, while for **21** the *S*-enantiomer was found. This highlighted that for later optimization the influence of the stereochemistry and whether racemization takes place should be considered, but also, that so far, a preference of one isomer over the other was not confirmed yet.

A major point to consider is the flexibility of the side chain tyrosine Tyr531 which might lead to even higher potential for interactions as we thought when setting up the hypothesis of potential cation- $\pi$  interactions. Therefore, it was of utmost importance to use this possible interaction to further optimize the inhibitor regarding its side chain.

**Synthesis of derivatized side chain variations.** Different side chains can easily be introduced by using 2-amino acids as starting material and converting them to the corresponding 2-halo acids. This approach was already used to synthesize some of the alkyl side chain derivatives presented in Chapter E. Racemic amino acids served as starting material as it is not known yet, which enantiomer is the more active one and whether enantiopure compounds would be stable in buffer.

To introduce basic side chains, the respective basic amino acids were used in the first step and the side chain amine was protected. In a first approach (see Scheme 3) the protection of DL-lysine should have been performed using  $\text{CuSO}_4$  in basic aqueous solution to complex the amino acid functionality resulting in a dark blue solution (**68**). Subsequent coupling of the omega amine with 9-fluorenylmethyl chloroformate (Fmoc-Cl) in acetone gave Fmoc-protected complex **69** which precipitated as blue solid after methanol addition.<sup>203</sup> This precipitate was washed with cold methanol and dried *in vacuo*. None of these intermediates was analyzed or further purified. Decomplexation of the supposed complex **69** with 8-hydroxyquinone and extraction with water resulted in as white solid, which might have been the wanted Fmoc-lysine derivative **70**. However, it was not possible to redissolve the resulting white compound in any solvent used (DMSO, water, water and TFA, MeOH, ACN, acetone or mixtures thereof). Therefore, no analysis and no further reactions were possible, and a new protection strategy was chosen.



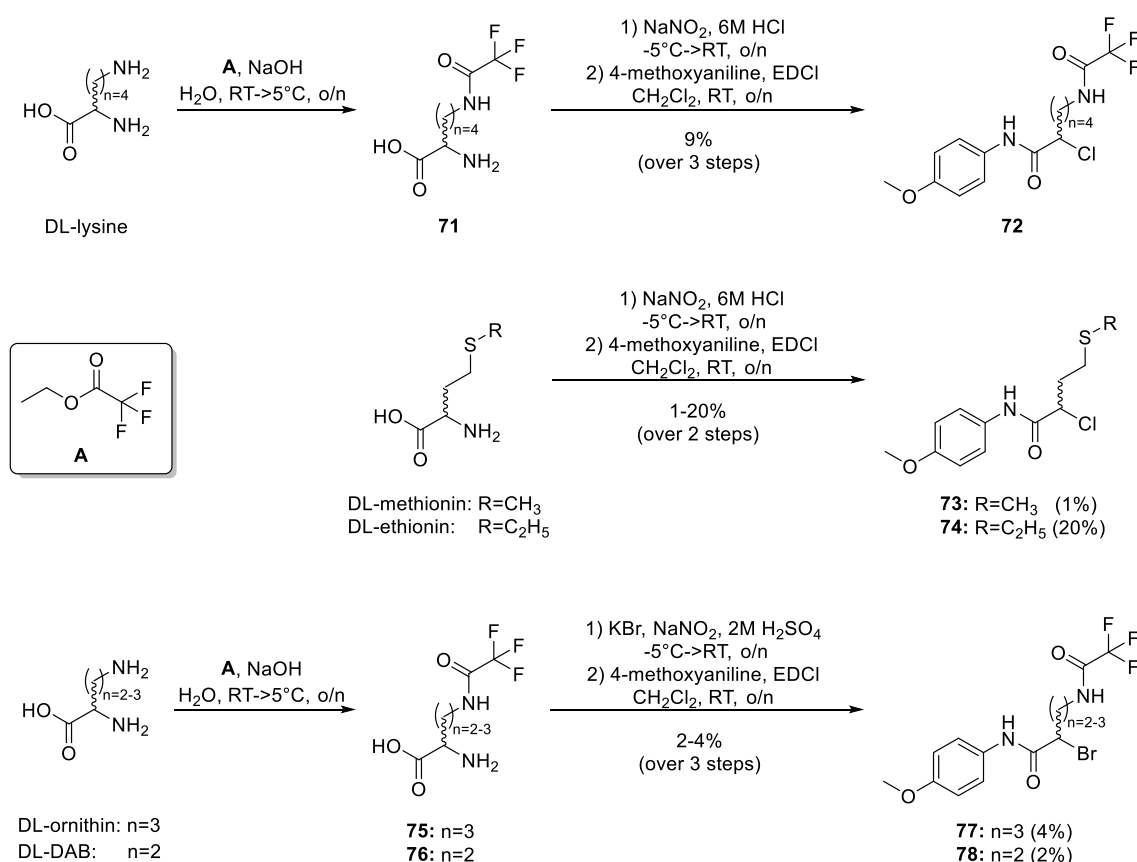
**Scheme 3.** Proposed synthetic route to access Fmoc-protected DL-lysine **70**. However, **70** could not be analyzed/isolated and further processed. The color of the complexes formed is indicated by colored boxes.

#### IV. Unpublished Results

A selective omega protection of basic amino acids DL-lysine, DL-ornithine and DL-2,4-diaminobutyric acid (DL-DAB) was successfully done using ethyl trifluoroacetate.<sup>204,205</sup> The protected amino acids precipitated as white solids in water and were filtered and washed with cold water before the next step. However, they were only soluble in acidic media, so no analysis of the precipitate took place before the next steps.

The protected DL-lysine-derivative **71**, DL-methionine and DL-ethionine were transferred to their chloro-derivatives using HCl and NaNO<sub>2</sub> in a diazotation-halogenation procedure (see also Chapter E) and after extraction and concentration directly coupled to *p*-methoxy aniline with EDCI without any further purification, giving the respective chloro acetamides **72–74** in 1–20% yield over 2 (methionine **73** and ethionine derivative **74**) or 3 (lysine derivative **72**) steps, respectively. Unfortunately, this approach did not work for the protected DL-ornithine **75** and DL-DAB **76**.

For these compounds, the protocol was changed, and the alkyl bromide was generated using KBr in H<sub>2</sub>SO<sub>4</sub> and NaNO<sub>2</sub>, as it was assumed that with having bromide as leaving group the yields might be increased. Those crude 2-bromo acids were then subsequently coupled with *p*-methoxy aniline and EDCI as done with the chloro acids. This gave compounds **77** and **78** in 4% and 2% yield over 2 steps, respectively (Scheme 4). Those yields were not satisfying, but as enough material was generated for further reactions, no further optimization was done during the frame of this work.



**Scheme 4.** Synthesis of 2-halo-*N*-(4-methoxyphenyl)acetamides **72–74**, **77** and **78**.

#### IV. Unpublished Results

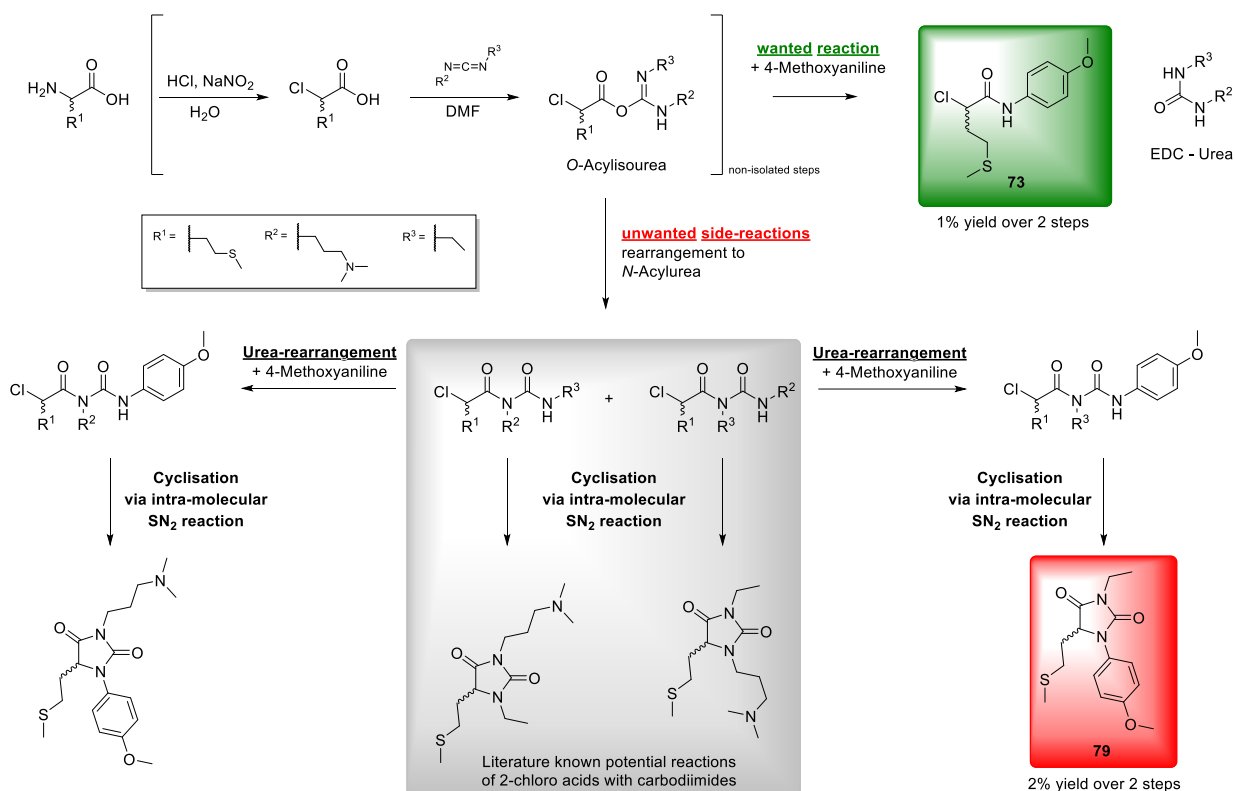
However, it has to be noted that a huge amount of side products were observed. This was especially observed during the synthesis of the methionine-derivative **73**. Here, one major side product **79** was coeluting on column chromatography with compound **73** and was only separated via HPLC purification. It was analyzed using mass spectroscopy and 2-D NMR techniques. The structure revealed that this side product was formed due to a reaction of EDCl with the 2-chloro acid with rearrangements and subsequent cyclisation (see Scheme 5). The yield for **79** was even higher than for the desired compound **73** (2% vs. 1%), which was very surprising, especially as two rearrangements have to take place to produce compound **79**.

It was already described in the literature once in 1977 by Brady and Owens, that reactions of 2-chloro acids with EDCl could form imidazolidin-2,4-diones via rearrangement of the activated *O*-acyl isourea to the *N*-acylurea and subsequent cyclisation via intramolecular S<sub>N</sub>2 reaction of the alkyl chloride with the urea nitrogen (see in grey in Scheme 5).<sup>206</sup> However, the main product observed by Brady and Owens was the 2-oxazolidinone and the imidazolidin-2,4-diones were only degradation products of the oxazolidinones. Interestingly, to give compound **79**, an additional urea rearrangement with *p*-methoxy aniline must have taken place, which so far is not literature known. It is not clear whether some more of the shown potential side reactions took place as well, as only isolated compound **79** was analyzed. It might be that the other structures were either not formed, purged during the acidic extraction work up or separated during column chromatography, as other fractions were not analyzed.

However, as the structures most probably do not bear any ColH activity due to no existing ZBG and as **79** was as instable as the analogs described by Brady and Owens (hygroscopic and turned to a brown viscos oil after 1 day at normal atmosphere), no further efforts were made to investigate the repeatability of this kind of reaction.

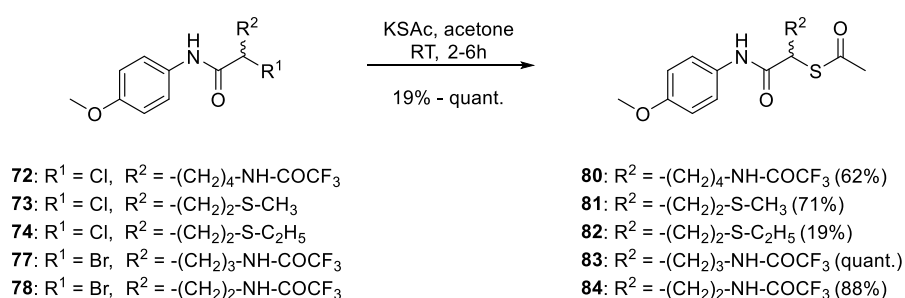
Due to the low yield in all formations of 2-halo-*N*-(4-methoxyphenyl) acetamides **72-74**, **77** and **78**, and the observed side reaction route cause, an optimization of the synthesis route using different coupling reagents and further purification steps of the intermediate 2-halo acid is highly recommended if further analogs of those structures shall be synthesized in different projects.

#### IV. Unpublished Results



**Scheme 5.** Proposed mechanism for side reactions during diazotation-halogenation reaction with following amide coupling of DL-methionine and 4-methoxyaniline leading to observed side product **79** (red) and multiple potential other side products. Ring formation as result of coupling of carbodiimides with 2-chloro acids as described by Brady and Owens in 1977 is highlighted in grey.<sup>206</sup>

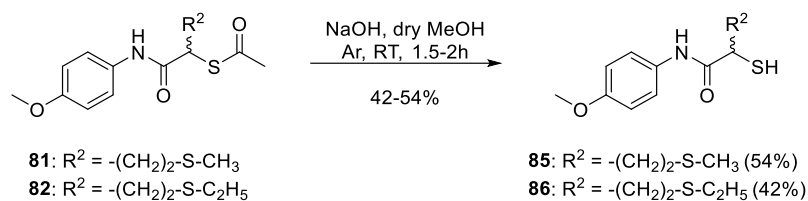
As next step towards the final thiols, the purified 2-halo-*N*-(4-methoxyphenyl) acetamides **72–74**, **77** and **78** were reacted with potassium thioacetate in an  $S_N2$  reaction in acetone to give the respective thioacetate compounds **80–84** in 19% to quantitative yield (Scheme 6).



**Scheme 6.** Synthesis of thioacetate compounds **80–84**.

Simple deprotection of the derivatives **81** and **82** with NaOH in dry methanol under argon atmosphere as previously performed (see Chapter E) gave final compounds **85** and **86** in 54% and 42% yield, respectively (Scheme 7).

#### IV. Unpublished Results

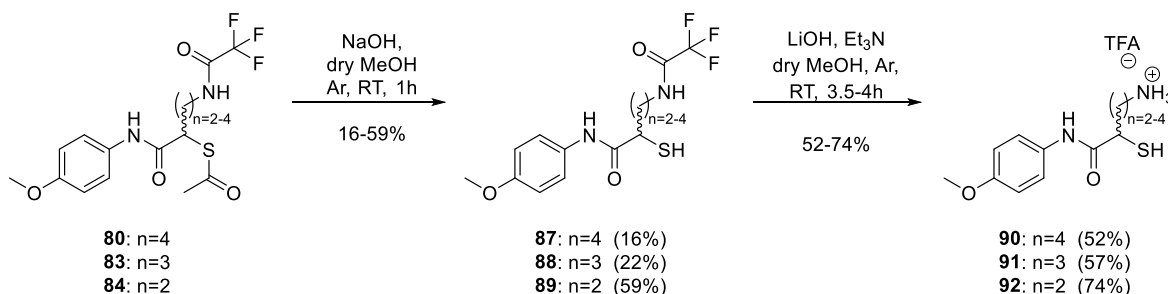


**Scheme 7.** Synthesis of thiols **85** and **86**.

However, deprotection of both acyl groups of the basic amino acid analogs **80**, **83** and **84** simultaneously failed. A fast deprotection of the thioacetate took place, but the hydrolysis of the trifluoroacetamide group was slower than the formation of the disulfide. Additionally, HPLC purification of the mixture of all three resulting compounds (mono-acyl, di-acyl and disulfide derivative) only resulted in clean mono-acyl derivatives **87–89**. Both fully deprotected derivatives **90–92** and the disulfides were not clean enough for further processing.

Therefore, it was decided to stop the deprotection reactions already after slightly more than one hour with reaction monitoring via LC-MS. The so resultant mono-deprotected thiol compounds **87–89** were purified via HPLC and also tested for their biological activities (Table 6).

The deprotection of the trifluoroacetamide group was then performed in a second step, using a mixture of LiOH and triethylamine in dry methanol under argon atmosphere monitored via LC-MS control. This condition gave compounds **90–92** after HPLC purification in 52-74% yield (Scheme 8).



**Scheme 8.** Synthesis of thiols **87–92**.

In total, eight new *N*-(4-methoxyphenyl)mercaptoacetamides **85–92** with different hydrophilic side chains in  $\alpha$ -position were synthesized to be tested for their biological activity.

As 3,4-dichlorophenyl was better tolerated by LasB in a lot of cases, Sebastian Dahmen optimized the amide coupling reactions in his Master thesis and synthesized compounds **93–97** (Figure 15).<sup>207</sup> Also, as thioether side chain variations were studied, Jelena Konstantinović from HIPS synthesized shorter ether derivatives **98** and **99** (Figure 15).

#### IV. Unpublished Results

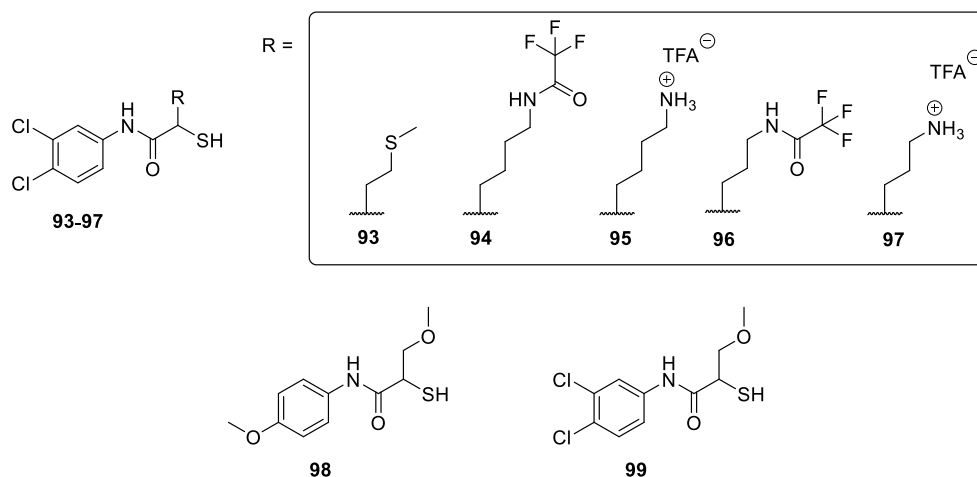


**Figure 15.** Additional compounds synthesized by S. Dahmen (93–97)<sup>207</sup> and J. Konstantinović (98, 99).

**In vitro inhibition of LasB and ColH by compounds 85–99.** The presented 15 new compounds with different hydrophilic side chains were tested using the previously reported FRET-based LasB<sup>194</sup> and FRET-based ColH<sup>1,201</sup> inhibition assays. The results are listed in Table 6.

**Table 6.** *In vitro* inhibitory activities of compounds 85–99 against both LasB and ColH.

R <sup>1</sup> = 4-OMe				R <sup>1</sup> = 3,4-diCl			
Name	R <sup>2</sup>	IC <sub>50</sub> (LasB) <sup>a</sup> [μM]	K <sub>i</sub> (ColH) <sup>a</sup> [nM]	Name	R <sup>2</sup>	IC <sub>50</sub> (LasB) <sup>a</sup> [μM]	K <sub>i</sub> (ColH) <sup>a</sup> [nM]
62	-H	24 ± 1	57 ± 9	12	-H	6.6 ± 0.3	>> 1000 <sup>b</sup>
66	-CH <sub>2</sub> -COO-CH <sub>3</sub>	39.2 ± 3.1	24 ± 5	67	-CH <sub>2</sub> -COO-CH <sub>3</sub>	n.d.	120 ± 10
85	-(CH <sub>2</sub> ) <sub>2</sub> -S-CH <sub>3</sub>	7.6 ± 0.5	0.9 ± 0.1	93	-(CH <sub>2</sub> ) <sub>2</sub> -S-CH <sub>3</sub>	> 10 <sup>207</sup>	< 1000 <sup>207, e</sup>
86	-(CH <sub>2</sub> ) <sub>2</sub> -S-C <sub>2</sub> H <sub>5</sub>	5.2 ± 0.2	68 ± 13	-	-	-	-
87	-(CH <sub>2</sub> ) <sub>4</sub> -NH-CO-CF <sub>3</sub>	10 – 100 <sup>c</sup>	2.2 ± 0.4	94	-(CH <sub>2</sub> ) <sub>4</sub> -NH-CO-CF <sub>3</sub>	5.4 ± 0.4 <sup>207</sup>	n.d.
88	-(CH <sub>2</sub> ) <sub>4</sub> -NH <sub>3</sub> <sup>+</sup>	>100 <sup>d</sup>	5.4 ± 0.5	95	-(CH <sub>2</sub> ) <sub>4</sub> -NH <sub>3</sub> <sup>+</sup>	8.3 ± 0.5 <sup>207</sup>	66 ± 6
89	-(CH <sub>2</sub> ) <sub>3</sub> -NH-CO-CF <sub>3</sub>	33.4 ± 1.0	<i>tbt</i>	96	-(CH <sub>2</sub> ) <sub>3</sub> -NH-CO-CF <sub>3</sub>	7.0 ± 0.6 <sup>207</sup>	170 ± 20
90	-(CH <sub>2</sub> ) <sub>3</sub> -NH <sub>3</sub> <sup>+</sup>	>100 <sup>d</sup>	330 ± 40	97	-(CH <sub>2</sub> ) <sub>3</sub> -NH <sub>3</sub> <sup>+</sup>	9.4 ± 0.6 <sup>207</sup>	n.d.
91	-(CH <sub>2</sub> ) <sub>2</sub> -NH-CO-CF <sub>3</sub>	10 – 100 <sup>c</sup>	110 ± 20	-	-	-	-
92	-(CH <sub>2</sub> ) <sub>2</sub> -NH <sub>3</sub> <sup>+</sup>	>100 <sup>d</sup>	<i>tbt</i>	-	-	-	-
98	-CH <sub>2</sub> -O-CH <sub>3</sub>	17.4 ± 0.2	8 ± 1	99	-CH <sub>2</sub> -O-CH <sub>3</sub>	2.4 ± 0.6	n.d.

<sup>a</sup> Means and SD of at least two independent experiments; <sup>b</sup> tested in its thiocarbamate prodrug form<sup>194</sup>; <sup>c</sup> <50% inhibition at 100 μM but >50% at 10 μM; <sup>d</sup> <50% inhibition at 100 μM; <sup>e</sup> 8 ± 5 % residual activity at 1 μM; n.d. = not determined; *tbt* = to be tested, but no results available, yet

#### IV. Unpublished Results

As already suspected by the nature of the binding pocket of LasB, none of the compounds despite **99** was able to improve the activity on LasB. **99**, which has a 3,4-dichloro aryl moiety and an ether functionality in its  $\alpha$ -position, gained only minor activity compared to the parent compound **12** ( $IC_{50}$  (LasB) =  $2.4 \pm 0.6 \mu\text{M}$  vs.  $IC_{50}$  (LasB) =  $6.6 \pm 0.3 \mu\text{M}$ ). From all 4-methoxy derivatives, positively charged and hydrophilic side chains decreased the activity, while the neutral thioether compounds **85** and **86** were active on LasB in the same range as the previous hit compound **12**. However, it must be noted that compounds with lipophilic side chains already have much increased activities towards LasB (*e.g.*,  $IC_{50}$  (LasB) =  $0.36 \pm 0.11 \mu\text{M}$  for **19**, see Figure 13 and Chapter E).

Looking on ColH inhibition, the 4-methoxy compound **62** with no side chain is more than 15 times more active on ColH than its 3,4-dichloro derivative **12** ( $K_i$  (ColH) =  $57 \pm 9 \text{ nM}$  and  $K_i$  (ColH)  $\gg 1000 \text{ nM}$ , respectively). With a neutral ester-containing side chain, this factor is decreased to only factor 5 ( $K_i$  (ColH) =  $24 \pm 5 \text{ nM}$  for **66** and  $K_i$  (ColH) =  $120 \pm 10 \text{ nM}$  for **67**, respectively). The introduction of a positively charged side chain only boosted the activity for compound **88** (lysine derivative) to  $K_i$  (ColH) =  $5.4 \pm 0.5 \text{ nM}$  (a factor of 10 compared to **62**), and also led to a medium potent inhibitor **95** in case of 3,4-dichloro substitution ( $K_i$  (ColH) =  $66 \pm 6 \text{ nM}$ ). However, all compounds with shorter side chains with positive charge suffer from a tremendous drop in activity. Compound **90** (ornithine derivative) is the least active ColH inhibitor of all tested 4-methoxy compounds ( $K_i$  (ColH) =  $330 \pm 40 \text{ nM}$ ).

Surprisingly, the neutral 4-methoxy compounds **85**, **87** and **98** all gained at least one order of magnitude activity in ColH inhibition compared to the unsubstituted compound **62**. Interestingly, compound **87** a quite long side chain with amide functionality is 25-times more active than unsubstituted compound **62**, while the shorter amide derivative **91** lost activity and is 2-times less potent than **62** ( $K_i$  (ColH, **87**) =  $2.2 \pm 0.4 \text{ nM}$  vs.  $K_i$  (ColH, **62**) =  $57 \pm 9 \text{ nM}$  vs.  $K_i$  (ColH, **91**) =  $110 \pm 20 \text{ nM}$ ). The length of the side chain seems to be needed to form the interaction of the amide within the binding pocket. Amongst the neutral compounds, compound **85** (methionine derivative) is the most active ColH inhibitor not only in this series but from all so far known compounds. Despite – or possibly even due to – the neutral and only H-bond accepting nature of the thioether side chain, it reaches levels of inhibition of almost picomolar range ( $K_i$  (ColH) =  $0.9 \pm 0.1 \text{ nM}$ ).

#### Conclusion

In this chapter the synthesis of 8 and biological evaluation of 17 compounds against LasB and ColH is described. Moreover, co-crystallization of the 3,4-dichloro containing derivative **16** with ColH is described and was used for the optimization of the further synthesized compounds.

As expected, hydrophilic side chains did not improve any activity on LasB. Interestingly, the tested 3,4-dichloro containing compounds **94–98**, as well as the 4-methoxy thioether compounds **85** and **86** are



## IV. Unpublished Results

still weak to moderate LasB inhibitors comparable to the initial LasB hit compound **12**. However, in the meanwhile, much more potent LasB inhibitors were developed, as shown in Chapter **F**.

For ColH a significant improvement of the compounds to inhibition values in the sub-nanomolar range was observed by introduction of a methylthioether side chain (compound **85**,  $K_i$  (ColH) =  $0.9 \pm 0.1$  nM). This is an improvement from the best compounds of chapter **E** (**E-16**) by a factor of 2, but even a 20-times improvement to the first hit compound **A-13** and a positive factor of 60 from the unsubstituted parent compound **62**.

All in all, compound **85** is a new and so far, the most potent compound on pure ColH, which should be further investigated for its biological (e.g. toxicity, *ex vivo* skin infection models, ...) and pharmacokinetic properties (e.g. skin permeability). If this is found successful, it might be a promising new lead for the development of pathoblockers for the treatment of Clostridial infections.

### Experimental Section

**Chemistry.** The general methodology, together with the general procedures, synthetic descriptions and characterizations of molecules (synthesized by the author) in this chapter can be found in the Appendix 7.

**Expression and Purification of LasB and ColH-PD.** LasB and ColH-PD were expressed and purified as described previously.<sup>117,194</sup>

***In vitro* LasB and ColH Inhibition Assay.** Both, LasB and ColH inhibition assays were performed as previously described.<sup>1,194</sup>

**Co-Crystallization, X-ray Data Collection and Structure Determination.** Prior to crystallization, 4 mg/mL ColH-PD were preincubated with 5 mM **67** in 8 mM Hepes pH 7.5, 33 mM NaCl, 0.33 mM CaCl<sub>2</sub>, and 5% DMSO for 1 h on ice and then clarified by centrifugation for 30 min at 13,000 g at 4°C. The co-crystal was grown by the sitting drop vapor diffusion method by mixing 1  $\mu$ L protein-inhibitor solution with 1  $\mu$ L reservoir solution. The reservoir contained 612 mM MES, 388 mM imidazole pH 6.5, 20% *v/v* polyethylene glycol methyl ether 550, 10% *w/v* polyethylene glycol 20000, 24 mM 1,6-hexanediol, 24 mM 1-butanol, 24 mM 1,2-propanediol, 24 mM 2-propanol, and 24 mM 1,4-butanediol. The drop was streak-seeded from crystals of unliganded ColH-PD. Crystals appeared within a week. The crystals were cryoprotected with MiTeGen LV Cryo-oil (MiTeGen, Ithaca, NY) and immediately flash-frozen in liquid nitrogen. X-ray diffraction data were collected on beamline ID23-1 at the European Synchrotron Radiation Facility (ESRF) in Grenoble, France. The data set was processed using XDS<sup>208</sup> and AIMLESS<sup>209</sup>. The phase problem was solved by molecular replacement with PHASER<sup>210</sup> using a ColH-PD structure as search model (PDB code 4ARF; ligand deleted). Final structures were obtained by several refinement cycles using PHENIX<sup>211</sup> interspersed with model building in WinCoot<sup>212</sup>.

### **Acknowledgments**

We thank Dr. Stefan Boettcher and Stefanie Weck for the measurements of high-resolution mass spectra, as well as Nathalie Andreia, Martina Jankowski and Jeannine Jung for technical support.

## V. FINAL DISCUSSION AND OUTLOOK

### 1. Summary

In this thesis, the synthesis, purification and biological evaluation of new pathoblockers active against *Pseudomonas aeruginosa* virulence factor LasB and *Clostridium histolyticum* virulence factor ColH is described. Additionally, in Chapter D, the potential of some inhibitors of this scaffold as multi-target inhibitors, being active not only on LasB and ColH, but also on several metallo- $\beta$ -lactamases (MBLs) was shown. This opens the potential of this class of compounds to function as multi-target inhibitors against a broad spectrum of bacterial zinc-containing proteases while being selective over human off-targets such as MMPs, TACE and HDACs. However, the main focus was the inhibition of ColH and LasB. These zinc-containing metalloproteases comprise a highly attractive target for drug development due to their essential role in the manifestation of an infection with the respective bacteria, as well as their extracellular appearance.

Please note, that due to the independent compound numbers in Chapters A – E, compounds from these chapters are mentioned in this part of the thesis with the capital letter A – E referring to the respective thesis chapter, followed by the Arabic number of the compound as depicted in the respective publications. In the case that an additional number in the later part of this thesis was assigned to the molecules, both numbers are shown.

### 1.1 2-Mercapto-*N*-(4-acetylphenyl) acetamide as starting point for further optimization towards highly active and selective ColH and LasB inhibitors

In Chapter A, a broad screening of inhibitor libraries revealed 2-mercapto-*N*-aryl acetamides as the core structure for potent and selective interaction with ColH (see Figure 16).

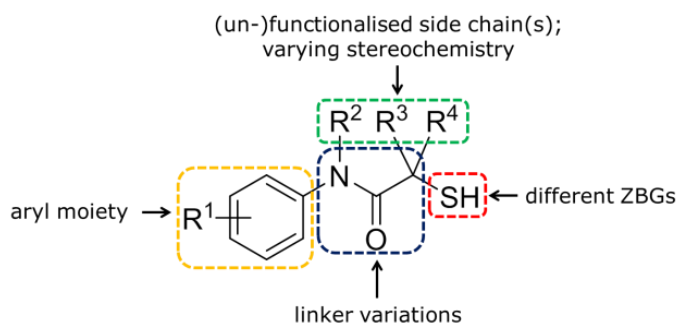


**Figure 16.** General structure of all ColH and LasB inhibitors in this thesis. The hit structure **A-13 = 17** depicted in Chapter A has the following substitution pattern: R<sup>1</sup> = *p*-Ac, R<sup>2</sup>=R<sup>3</sup>=R<sup>4</sup>=H.<sup>1</sup>

While initially thioacetamides were seen in the screening as hit structures, hydrolytic assays, and a co-crystal structure of compound **A-13 = 17** revealed that the thioacetamide (**A-3**) was a prodrug of the thiol function which then acts as the zinc-binding group when interacting with the enzyme ( $IC_{50}$  (ColH, **17**) =  $17 \pm 2$  nM).

Additionally, a substitution of the aryl function in *para*-position with a hydrophilic, hydrogen bond accepting moiety was found to be essential for ColH interaction. *Ortho*- and *meta*-substitution, as well as lipophilic residues, were unfavorable for enzyme activity. This is in contrast to what was found by Kany *et al.* in 2018 when testing the same compound class against LasB.<sup>213</sup> Here, the same basic core structure as shown in Figure 16 was found to be active. However, potent inhibitors of LasB incorporated multiple lipophilic substituents. Amongst them, compound **12** (3, 4-diCl substitution) was the most potent on LasB ( $IC_{50}$  (LasB, **12**) =  $6.6 \pm 0.3$   $\mu$ M).

### 1.2 The SAR of substituted 2-mercapto-*N*-aryl acetamides toward ColH and LasB

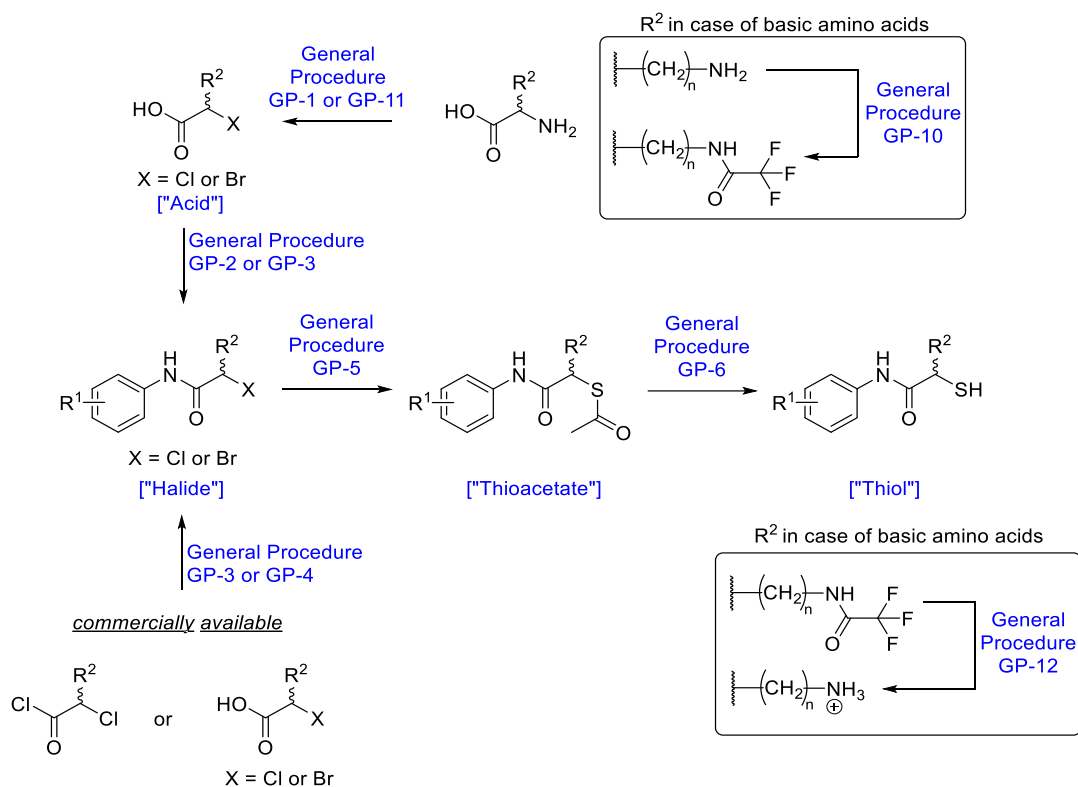
Kany *et al.* co-crystallized compound **12** with LasB, revealing 2 molecules being present in the active side of the enzyme (PDB: 6F8B).<sup>213</sup> They postulated that a fusion of both molecules by the introduction of a phenyl side chain might result in a molecule capable of fully filling in the space in the active site, as seen with two molecules of compound **12**. Therefore, the first derivatives with phenyl substitution on the nitrogen ( $R^2$ -position, Figure 16) were synthesized by Kany *et al.*, but without benefit on the activity on LasB.<sup>213</sup> The compounds were not tested towards ColH. However, in all ColH co-crystal structures shown in Chapters **A** (PDB:507E), **E** (PDB:7BBK), **F** (Figure 10a), and **G** (Figure 14c), the amide acts as a hydrogen donor, locking the molecule coordination in its specific position. Therefore, this interaction is assumed to be crucial for enzyme activity and no further attempts were made to investigate other substitutions on the amide-structure for ColH activity.

Following the same approach as Kany *et al.*, Kaya *et al.* shifted the phenyl substitution from the  $R^2$ -position into the  $\alpha$ -position of the mercaptoacetamide in 2022.<sup>196,197</sup> In contrast to the derivatives from Kany *et al.*, Kaya *et al.* were able to gain an order of magnitude in activity ( $IC_{50}$  (LasB, **63**) =  $0.73 \pm 0.03$   $\mu$ M). Surprisingly, compounds with a more hydrophilic *para*-substitution, usually only favorable for ColH, such as compound **63** (4-methoxy) and 4-hydroxy derivatives were now active against LasB as well. Compound **63** was therefore additionally tested for its ColH inhibitory activity. The activity of compound **63** was decreased by a factor of two compared to the initial hit **A-13 = 17** ( $IC_{50}$  (ColH, **63**) =  $36 \pm 5$  nM vs.  $IC_{50}$  (ColH, **63**) =  $17 \pm 2$  nM). However, this proved the  $\alpha$ -substitution as an interesting concept also for ColH.

As several co-crystal structures of LasB have been published, it is known that inhibitors occupy the lipophilic S1' and S2' binding pocket, forming main interactions with Val137, Ile186, and Leu132 in S1', and Phe129 in the S2' binding pocket (see Introduction, chapter 3.1.3 Inhibitors of LasB). Therefore, alkyl side chains were introduced as side chains and a total of 27 racemic thiols were synthesized and tested towards ColH and LasB inhibition (see Chapter **E**).

## V. Final Discussion and Outlook

To access those thiols,  $\alpha$ -halo acids were either purchased when commercially available or synthesized from their corresponding DL-amino acids via diazotation-halogenation reaction with sodium nitrite in highly acidic condition and a halogen source (see Scheme 9, GP-1 – GP-3). The general synthesis scheme used to access the compounds can be seen below in Scheme 9.



**Scheme 9.** Synthetic scheme of  $\alpha$ -substituted thiol derivatives. Adapted from the Supporting Information of Chapter E, see Appendix 5.

Focusing only on ColH inhibitory activity, compound **E-16 = 18** with a 4-acetyl moiety and an *n*-propyl side chain represented the most active analog with a remarkable  $K_i$  value of  $2 \pm 1$  nM against ColH. This is almost a full order of magnitude in gained activity against ColH, compared to the initial hit compound **17**. However, compound **18** was slightly less active against LasB than compound **63** by Kaya *et al.* ( $IC_{50}$  (LasB, **18**) =  $2.6 \pm 0.5$   $\mu$ M vs.  $IC_{50}$  (LasB, **63**) =  $0.73 \pm 0.03$   $\mu$ M). In contrast to that, compounds bearing an *iso*-butyl side chain comprise the highest LasB-only inhibitory activity, as well as best dual inhibitory activities against both LasB and ColH (compound **E-25 = 19** (4-OMe),  $IC_{50}$  (ColH, **19**) =  $8 \pm 1$  nM,  $IC_{50}$  (LasB, **19**) =  $0.36 \pm 0.11$   $\mu$ M; see Figure 17).

Unlike the LasB binding pocket, the binding pocket of ColH is relatively small and the  $\alpha$ -side chains of inhibitor molecules are more exposed to the solvent and enzyme surface area, which is also assumed to be the reason that the bulkier compound **19** is slightly less active than compound **18**. Additionally, it was shown in the co-crystal structure of compound **67** (Chapter G, Figure 14c) that the tyrosine side chain Y531 in the binding pocket of ColH is flexible and therefore, might be a good interaction partner

## V. Final Discussion and Outlook

of 8 compounds were synthesized and tested, together with 9 additional compounds (synthesized by Jelena Konstantinovic and Sebastian Dahmen), towards their ColH and LasB inhibitory activities. The synthesis of the named 8 compounds followed the same general scheme as depicted above in Scheme 9. However, an additional protection step of basic amino acids with ethyltrifluoroacetate was performed before the diazotation-halogenation reaction, as well as an additional deprotection step of the named protection group as very last step.

As hydrophilic residues are usually not tolerated in the lipophilic S1' binding pocket of LasB, no increase of inhibitory activity was assumed for those compounds and was also proven in the assay. Unfortunately, none of the positively charged derivatives improved the inhibition of ColH compared to compound **18**. However, the introduction of an ethyl thiomethyl ether in the  $\alpha$ -position of the 4-methoxy compound was revealed to be highly beneficial for ColH activity. With this introduction, for the first time, a sub-nanomolar ColH inhibitor was archived ( $K_i$  (ColH, **85**) =  $0.9 \pm 0.1 \mu\text{M}$ ). A derivative of this  $\alpha$ -side chain bearing a 4-acetyl moiety might potentially even increase the activity slightly further, but this remains to be tested.

An overview of the described compounds and their inhibitory activities is shown below in Figure 17.

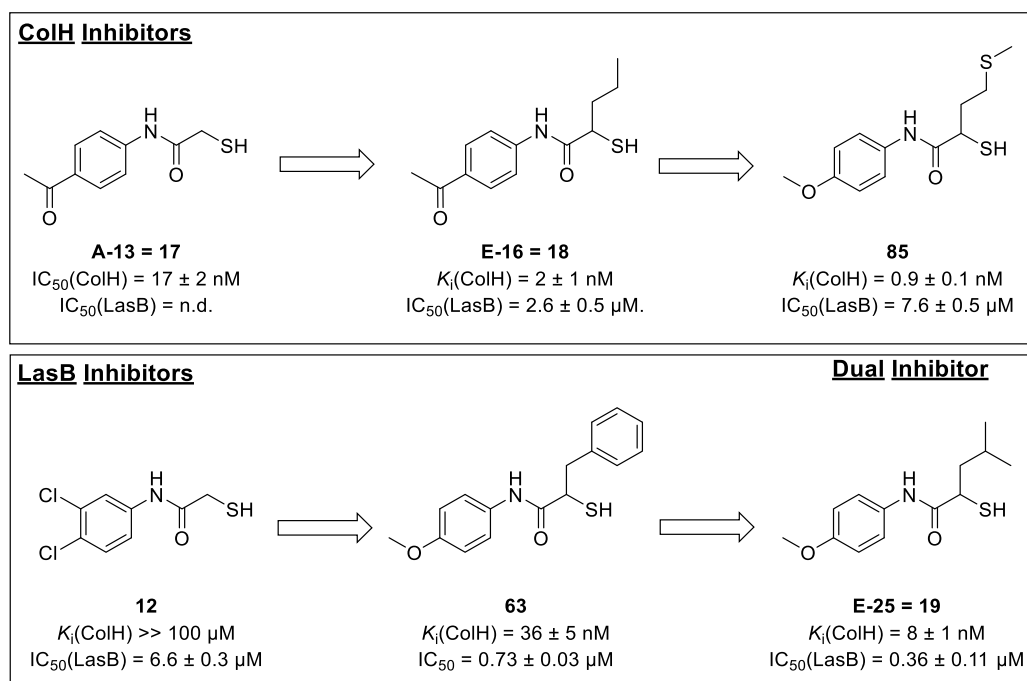


**Figure 17.** Overview of the evolution of the best ColH and LasB inhibitors throughout the presented SAR studies from Chapter A (compound **A-13 = 17**) to E (compounds **E-16 = 18** and **E-25 = 19**) and G (compound **85**). The shown LasB inhibitors **12** and **63** were described in literature by Kany *et al.* and Kaya *et al.*, respectively.<sup>197,213</sup>

### 1.3 Phosphonate as a suitable replacement of thiol function for both ColH and LasB

As thiols are known to be highly sensitive towards oxidation and the resulting disulfides are not active anymore, the potential of a replacement of the thiol ZBG with more stable ZBGs was investigated additionally. A total of 17 ZBG alternatives were synthesized and tested for their inhibitory activity against ColH (see Chapter B).

Previous publications reveal phosphinic peptide analogs as bacterial collagenase inhibitors using collagenase from *Corynebacterium*.<sup>214</sup> During our investigations, the phosphinic acid derivative **B-25** was not able to inhibit ColH. However, in the same study, it was found that a phosphonate is the only suitable replacement for the thiol zinc-binding group function from all tested derivatizations with the structural pattern shown in Figure 16 (Chapter B, compound **B-26** = **6**,  $IC_{50}$  (ColH, **6**) =  $7 \pm 1 \mu\text{M}$ ). Despite the activity loss on pure ColH compared to the first hit compound **A-13** = **17**, the good biological activity of compound **6** was shown not only on ColH and ColQ1 but also with an *ex vivo* pig skin degradation assay using ColQ1 (Chapter B), as well as *in vitro* human skin cell- and *in vivo* *Galleria mellonella* larvae models with both pure ColQ1 and *Bacillus cereus* supernatant (Chapter C, compound **B-26** = **C-1** = **6**). Additionally, compound **6** retained at least a bit of inhibitory activity against LasB ( $33 \pm 4 \%$  inhibition of LasB at a concentration of  $600 \mu\text{M}$ , Chapter F), making it a suitable ZBG to be further investigated against both ColH and LasB.

After the successful introduction of side chains into thiol-based derivatives (Chapter E), the SAR was tested and proven to be additive, when phosphonate derivatives with *n*-propyl side chains were synthesized and tested together with *i*-butyl derivatives from HIPS for their ColH and LasB activity (Chapter F). Interestingly, the ColH activity was improved to be back in the nanomolar range by the introduction of an *n*-propyl side chain (compound **46**,  $K_i$  (ColH, **46**) =  $0.13 \pm 0.02 \mu\text{M}$ ) which is a 50-fold improvement over the initial phosphonate **6** ( $IC_{50}$  (ColH, **6**) =  $7 \pm 1 \mu\text{M}$ ). However, most remarkably are the compounds with an *iso*-butyl side chain. Depending on the aryl substitution, a 7- (4-OMe, **E-25** vs. **48**) to 840-fold improvement (3,4-diCl, **E-20** vs. **47**) between the previous thiol and the new phosphonate ZBG analogs was observed, resulting in compound **47** as so far most active LasB inhibitor ( $K_i = 26 \pm 4 \text{ nM}^6$ ).

An overview of the compounds and their inhibitory activities against ColH and LasB are shown below in Figure 18.

## V. Final Discussion and Outlook

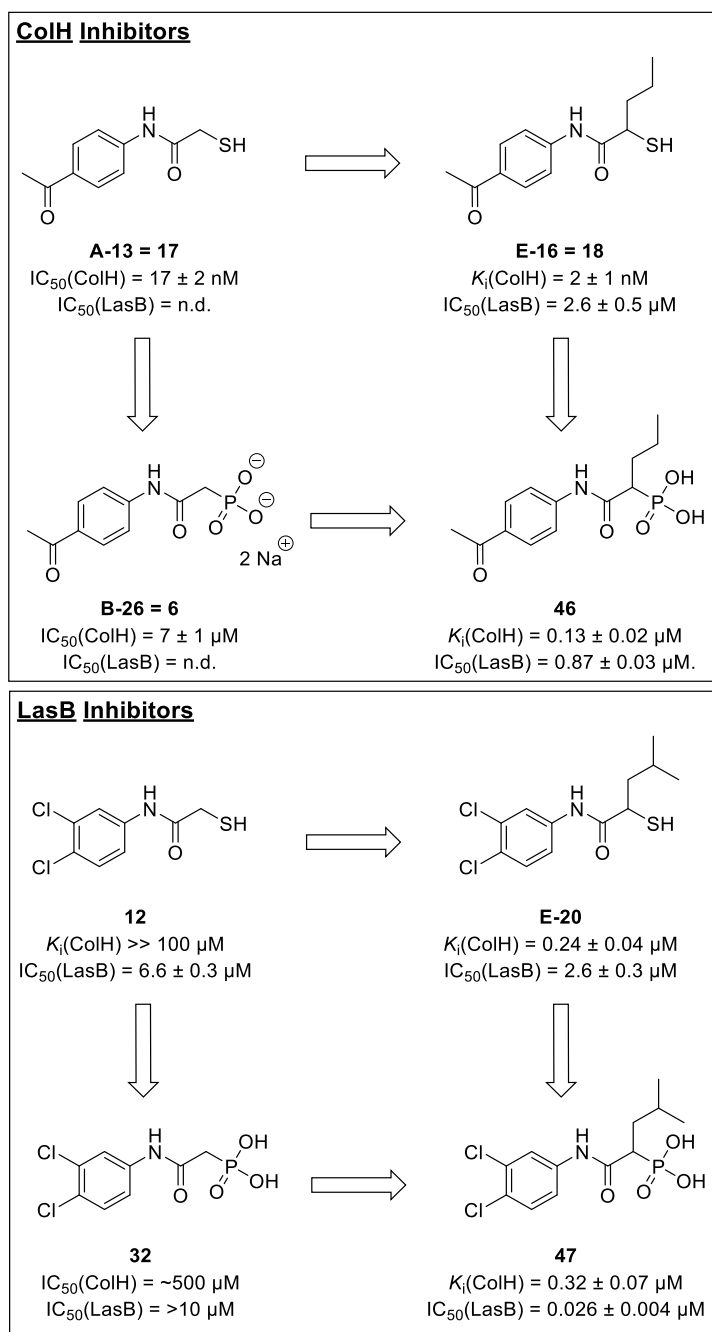


**Figure 18.** Overview of the evolution of ColH and LasB inhibitors with phosphonate as alternative ZBG. Compound 47 was synthesized by Jelena Konstantinović in the frame of our patent application.<sup>6</sup>



## 2. Outlook

### 2.1 Optimized Phosphonates for ColH by the introduction of a functionalized side chain and other aryl moieties

In Chapter G, the ethyl thiomethyl ether side chain was found to be most beneficial on the ColH activity of thiol derivatives (e.g., compound **85**,  $K_i$  (ColH) =  $0.9 \pm 0.1$  nM). However, the aryl moiety of compound **85** is substituted with a 4-methoxy group. It would be interesting to see whether this activity could be further improved by changing the aryl moiety to 4-acetyl, as this was the case for small lipophilic side chains shown in Chapter E, or even a more extended aryl substitution which can displace the water molecule present in the binding pocket, which coordinates the oxygen from the 4-acetyl moiety.

For the tested phosphonates in Chapter F, 4-acetyl was seen as the most active on ColH of all tested aryl moieties. As the SAR was found to be additive with lipophilic side chains, we propose that the introduction of functionalized side chains might also have positive effects and might produce even more potent ColH inhibitors with reduced sensitivity towards oxidization and therefore, a potentially longer half-life time and less instability during storage.

### 2.2 Phosphonate prodrugs for better bioavailability with regard to deep tissue infections

As described in Chapter F, the free phosphonate **6** shows no systemic bioavailability when administered via lung infiltration to mice (mimicking the potential inhalation application of the drug). This is highly beneficial for the local treatment of *P. aeruginosa* infections, as high concentrations are archived directly in the lung fluids where the infection is established, while systematic exposure and with that, side effects can be reduced to a minimum. However, *Clostridial* infections are usually deep tissue infections and thus, require good bioavailability and tissue penetration, which cannot be accomplished with the highly charged phosphonate group. Instead of using free phosphonate for the treatment of tissue infections, neutral prodrugs could be used as an alternative.

There are multiple potential prodrug approaches available for masking phosphate and phosphonate groups. Some examples with masked phosphates or phosphonates can be found below in Figure 19.

While ProTide (e.g., **100**) and bisPOM (e.g., **101**) prodrugs are cleaved by esterases, and HDP monoesters (e.g., **102**) are cleaved by phospholipases, the HepDirect prodrug (e.g., **103**) is cleaved by CYP3A4 mediation. All of these derivatives are significantly more lipophilic than the parent phosphonate. However, release would be needed outside of cells to reach the secreted bacterial collagenase in-between the cells in the infected tissue. If the release of the phosphonate can be archived in sufficient amounts in peripheric deep tissue infections remains unknown and must be investigated.

## V. Final Discussion and Outlook

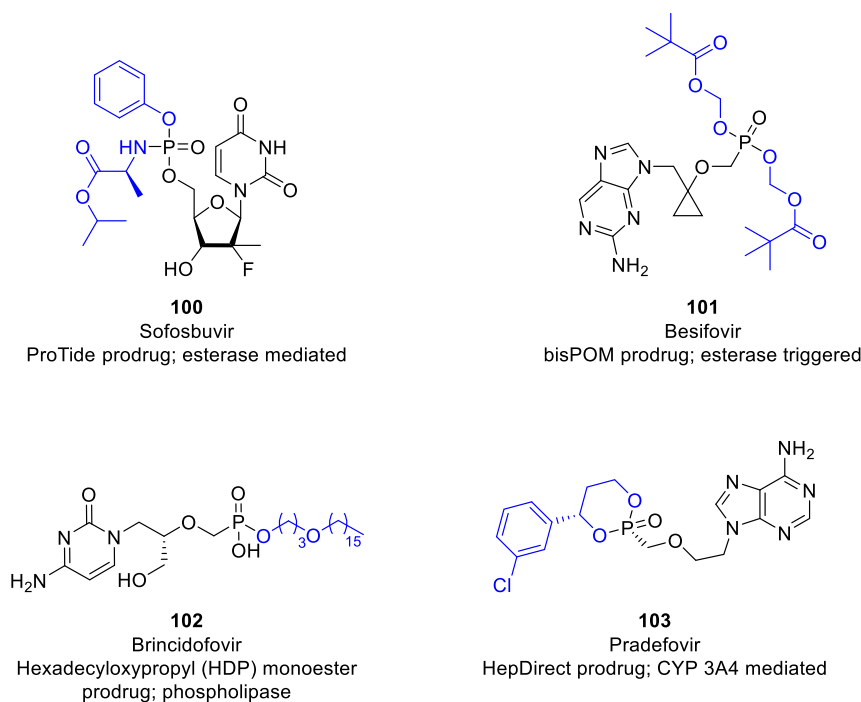


**Figure 19.** Phosphate and phosphonate prodrugs in clinical development. Masking groups of the phosphate/phosphonate group are colored in blue.

### 2.3 Combination of phosphonate with peptidic elongation

Eckhard *et al.* were able to show in 2011 and 2013 with several co-crystal structures that unselective inhibitors of collagenases such as compound **1** bind to the enzyme towards the primed binding site (see Figure 20b).<sup>117,120</sup> This is in contrast to the inhibitors presented within this thesis which bind towards the non-primed binding region. However, a ZBG is crucial in both cases.

Additionally, the inhibitors shown in Chapters **A** – **F** are relatively small. As they were shown to be highly selective, they can be used as drug candidates themselves. However, they also fulfill the “rule of three” for fragments and are therefore good candidates for further growing of the structures to enhance their activity.<sup>215</sup>

Both compounds **1** and **6** (Figure 20b and 20a, respectively) bear a phosphor-based zinc-binding group. An overlay of both co-crystal structures in the open stage of ColH (as seen for the co-crystal of **6**) shows an overlapping of both zinc-binding groups. Compound **1** bears a phosphoramidate as ZBG. This ZBG was not yet synthesized and tested for its activity in the SAR study depicted in Chapter **B**. Therefore, the potential of this ZBG in combination with *N*-arylacetamides (Figure 16) remains unknown. Additionally, merging both the unselective compound **1** and one of our selective compounds, such as compound **6** would be highly interesting to investigate the potential of compound elongation from non-primed to primed binding region with a ZBG in the middle of the molecule.

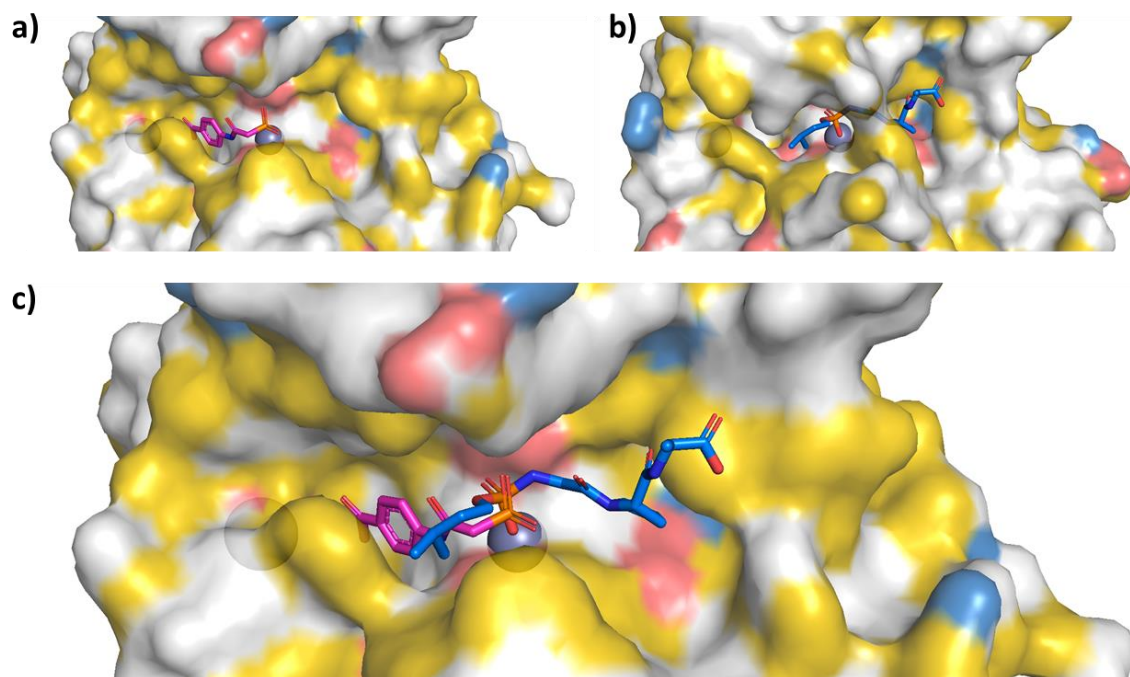


**Figure 20.** ColH cocrystal structures shown in hydrophobic surface representation colored according to the YRB scheme: non-polar hydrocarbons (yellow), negatively charged oxygen atoms of glutamate and aspartate (red), positively charged nitrogen atoms of lysine and arginine (blue).<sup>199</sup> **a)** ColH in complex with **6** (pink sticks, see Chapter F) with a widely opened catalytic region. **b)** ColH in complex with **1** (blue sticks, PDB: 4ARF).<sup>117</sup> **c)** Both co-crystal structures were aligned and an overlay of the bound unselective inhibitor **1** and the selective **6** with the enzyme in an opened stage is shown. The phosphorus atoms of both inhibitors overlap, which would account for the possibility to merge both inhibitors.

## 2.4 Additional investigations on the structure-activity relationship

Finally, it shall be noted that there is still room to further investigate the SAR of *N*-arylacetamides as depicted in Figure 16. Multiple efforts were made regarding the potential of the introduction of different side chains and their effect on LasB and ColH activity. Also, we successfully exchanged the ZBG to a phosphonate, which is less prone to oxidation and opens further optimization concepts as depicted above. Additionally, the importance of an amide in the linker was proven with several co-crystal structures all showing multiple interactions of the amide with both LasB and ColH, thus, playing a main role in inhibitor activity. The linker cannot be prolonged as the findings of Konstantinović *et al.* (introduction Chapter G) and Kaya *et al.*<sup>216</sup> reveal. Shortening the linker would lead to the loss of the potential to introduce side chains. Additionally, the formally resulting carbamothioic acid would not bear the same interaction potential as the current separate amide and thiol functions.

However, little has been done to further investigate a potential improvement of the aryl moiety. As for ColH the carbonyl function is coordinated by a water molecule, an extension of the substitution to displace the water molecule and form direct interactions with the enzyme backbone might strongly enhance inhibitor activity.

Additionally, all side-chain derivatives shown in this thesis were synthesized in their racemic forms. No conclusion on the eutomer or distomer could be drawn from the so far solved co-crystal structures,

## V. Final Discussion and Outlook

as both *R*- and *S*-enantiomers of compounds were found. Therefore, the synthesis and evaluation of enantiopure compounds is necessary and could lead to up to two times improvement in inhibitor activity. Additionally, enantiopure compounds might lead to an optimized side effect panel, as also the inhibitory activity of off-targets might be influenced. However, the stability of such enantiopure compounds should be assessed in biological media to draw a holistic picture of the compound's properties.

## VI. REFERENCES

- (1) Schönauer, E.; Kany, A. M.; Haupenthal, J.; Hüsecken, K.; Hoppe, I. J.; Voos, K.; Yahiaoui, S.; Elsässer, B.; Ducho, C.; Brandstetter, H.; Hartmann, R. W. Discovery of a Potent Inhibitor Class with High Selectivity toward Clostridial Collagenases. *J. Am. Chem. Soc.* **2017**, *139* (36), 12696–12703. <https://doi.org/10.1021/jacs.7b06935>.
- (2) Voos, K.; Schönauer, E.; Alhayek, A.; Haupenthal, J.; Andreas, A.; Müller, R.; Hartmann, R. W.; Brandstetter, H.; Hirsch, A. K. H.; Ducho, C. Phosphonate as Stable Zinc-binding Group for Inhibitors of Clostridial Collagenase H (ColH) as Pathoblocker Agents. *ChemMedChem* **2021**, *cmdc.202000994*. <https://doi.org/10.1002/cmdc.202000994>.
- (3) Alhayek, A.; Khan, E. S.; Schönauer, E.; Däinghaus, T.; Shafiei, R.; Voos, K.; Han, M. K. L.; Ducho, C.; Posselt, G.; Wessler, S.; Brandstetter, H.; Haupenthal, J.; del Campo, A.; Hirsch, A. K. H. Inhibition of Collagenase Q1 of *Bacillus Cereus* as a Novel Antivirulence Strategy for the Treatment of Skin-Wound Infections. *Adv. Ther.* **2022**, *5* (3), 2100222. <https://doi.org/10.1002/adtp.202100222>.
- (4) Yahiaoui, S.; Voos, K.; Haupenthal, J.; Wichelhaus, T. A.; Frank, D.; Weizel, L.; Rotter, M.; Brunst, S.; Kramer, J. S.; Proschak, E.; Ducho, C.; Hirsch, A. K. H. *N*-Aryl Mercaptoacetamides as Potential Multi-Target Inhibitors of Metallo- $\beta$ -Lactamases (MBLs) and the Virulence Factor LasB from *Pseudomonas Aeruginosa*. *RSC Med. Chem.* **2021**, *12* (10), 1698–1708. <https://doi.org/10.1039/D1MD00187F>.
- (5) Voos, K.; Yahiaoui, S.; Konstantinović, J.; Schönauer, E.; Alhayek, A.; Sikandar, A.; Si Chaib, K.; Ramspoth, T.; Rox, K.; Haupenthal, J.; Köhnke, J.; Brandstetter, H.; Ducho, C.; Hirsch, A. *N*-Aryl-2-Iso-Butylmercaptoacetamides: The Discovery of Highly Potent and Selective Inhibitors of *Pseudomonas Aeruginosa* Virulence Factor LasB and *Clostridium Histolyticum* Virulence Factor ColH. *ChemRxiv* **2022**. <https://doi.org/10.26434/chemrxiv-2022-fjrqr>.
- (6) Hartmann, R. W.; Konstantinović, J.; Haupenthal, J.; Kany, A. M.; Hirsch, A. K. H.; Ducho, C.; Kaya, C.; Yahiaoui, S.; Voos, K.; Walter, I.; Abdelsamie, A. S.; Schütz, C. M.; Jumde, R.; Kiefer, A. Inhibitors of *Pseudomonas Aeruginosa* Virulence Factor LasB. EP 20 192 608.6.
- (7) Konstantinovic, J.; Kany, A. M.; Alhayek, A.; Abdelsamie, A. S.; Sikandar, A.; Voos, K.; Yao, Y.; Andreas, A.; Shafiei, R.; Loretz, B.; Schönauer, E.; Bals, R.; Brandstetter, H.; Hartmann, R. W.; Ducho, C.; Lehr, C.-M.; Beisswenger, C.; Müller, R.; Rox, K.; Haupenthal, J.; Hirsch, A. K. H. Inhibitors of the Elastase LasB for the Treatment of *Pseudomonas Aeruginosa* Lung Infections. *ChemRxiv* **2023**. <https://doi.org/10.26434/chemrxiv-2023-bszcb>.
- (8) Van Leeuwenhoek, A.; de Graaf, R. A Specimen of Some Observations Made by a Microscope, Contrived by M. Leewenhoeck in Holland, Lately Communicated by Dr. Regnerus de Graaf. *Phil. Trans. R. Soc.* **1673**, *8* (94), 6037–6038. <https://doi.org/10.1098/rstl.1673.0017>.
- (9) Van Leeuwenhoek, A. Observationes D. Anthonii Lewenhoeck, de Natis'e Semine Genitali Animalculis. *Phil. Trans. R. Soc.* **1677**, *12* (142), 1040–1046. <https://doi.org/10.1098/rstl.1677.0068>.
- (10) Koch, R. Untersuchung Über Bakterien - Die Aetiologie Der Milzbrand-Krankheit, Begründet Auf Die Entwicklungsgeschichte Des Bacillus Anthracis. *Beiträge zur Biologie der Pflanzen* **1876**, *2*, 277–310.
- (11) Microbiology by Numbers. *Nat. Rev. Microbiol.* **2011**, *9* (9), 628–628. <https://doi.org/10.1038/nrmicro2644>.
- (12) WHO. *Global Burden of Disease Estimates 2000-2016*; World Health Organization (WHO): Geneva, 2018.
- (13) Mohr, K. I. *History of Antibiotics Research*; Current Topics in Microbiology and Immunology; Springer International Publishing: Cham, 2016; Vol. 398.
- (14) Fleming, A. On the Antibacterial Action of Cultures of a Penicillium, with Special Reference to Their Use in the Isolation of B. Influenzæ. *Br. J. Exp. Pathol.* **1929**, *10* (3), 226–236.

## VI. References

- (15) Chain, E.; Florey, H. W.; Gardner, A. D.; Heatley, N. G.; Jennings, M. A.; Orr-Ewing, J.; Sanders, A. G. Penicillin as a Chemotherapeutic Agent. *Lancet* **1940**, *236* (6104), 226–228.
- (16) Gaynes, R. The Discovery of Penicillin—New Insights After More Than 75 Years of Clinical Use. *Emerg. Infect. Dis.* **2017**, *23* (5), 849–853. <https://doi.org/10.3201/eid2305.161556>.
- (17) Aldridge, S.; Parascandola, J.; Sturchio, J. L.; American Chemical Society; Royal Society of Chemistry (Great Britain). *The Discovery and Development of Penicillin 1928-1945: The Alexander Fleming Laboratory Museum, London, UK, November 19, 1999: An International Historic Chemical Landmark*; American Chemical Society: Washington, D.C., 1999.
- (18) Austrian, R.; Gold, J. Pneumococcal Bacteremia with Especial Reference to Bacteremic Pneumococcal Pneumonia. *Ann. Intern. Med.* **1964**, *60* (5), 759–776. <https://doi.org/10.7326/0003-4819-60-5-759>.
- (19) Domagk, G. Chemotherapie der bakteriellen Infektionen. *Angew. Chem.* **1935**, *48* (42), 657–667. <https://doi.org/10.1002/ange.19350484202>.
- (20) Davies, J. Where Have All the Antibiotics Gone? *Canad. J. Infect. Dis. Med. Microbiol.* **2006**, *17* (5), 287–290. <https://doi.org/10.1155/2006/707296>.
- (21) Demerec, M. Origin of Bacterial Resistance to Antibiotics. *J. Bacteriol.* **1948**, *56* (1), 63–74.
- (22) Spink, W. W.; Ferris, V. Penicillin-Resistant Staphylococci: Mechanism in the Development of Resistance. *J. Clin. Invest.* **1947**, *26* (3), 379–393. <https://doi.org/10.1172/JCI101820>.
- (23) Cecchini, M.; Lee, S. Low-Value Health Care with High Stakes: Promoting the Rational Use of Antimicrobials. In *Tackling Wasteful Spending on Health*; OECD, Ed.; OECD Publishing: Paris, 2017; pp 115–158. <https://doi.org/10.1787/9789264266414-en>.
- (24) Wall, B. A.; Mateus, A.; Marshall, L.; Pfeiffer, D.; Lubroth, J.; Ormel, H. J.; Otto, P.; Patriarchi, A.; Food and Agriculture Organization of the United Nations. *Drivers, Dynamics and Epidemiology of Antimicrobial Resistance in Animal Production*; Food and Agriculture Organization of the United Nations (FAO): Rome, 2016; p 68. <http://www.fao.org/3/a-i6209e.pdf>.
- (25) Singer, A. C.; Shaw, H.; Rhodes, V.; Hart, A. Review of Antimicrobial Resistance in the Environment and Its Relevance to Environmental Regulators. *Front. Microbiol.* **2016**, *7*. <https://doi.org/10.3389/fmicb.2016.01728>.
- (26) Teillant, A.; Gandra, S.; Barter, D.; Morgan, D. J.; Laxminarayan, R. Potential Burden of Antibiotic Resistance on Surgery and Cancer Chemotherapy Antibiotic Prophylaxis in the USA: A Literature Review and Modelling Study. *Lancet Infect. Dis.* **2015**, *15* (12), 1429–1437. [https://doi.org/10.1016/S1473-3099\(15\)00270-4](https://doi.org/10.1016/S1473-3099(15)00270-4).
- (27) Cecchini, M.; Langer, J.; Slawomirski, L. *Antimicrobial Resistance in G7 Countries and Beyond: Economic Issues, Policies and Options for Action*; OECD: Paris, 2015. <https://www.oecd.org/els/health-systems/Antimicrobial-Resistance-in-G7-Countries-and-Beyond.pdf> (accessed 2020-11-03).
- (28) CDC (U.S.). *Antibiotic Resistance Threats in the United States, 2019*; U.S. Department of Health and Human Services, CDC: Atlanta, GA, 2019. <https://doi.org/10.15620/cdc:82532>.
- (29) Cassini, A.; Högberg, L. D.; Plachouras, D.; Quattrocchi, A.; Hoxha, A.; Simonsen, G. S.; Colomb-Cotinat, M.; Kretzschmar, M. E.; Devleeschauwer, B.; Cecchini, M.; Ouakrim, D. A.; Oliveira, T. C.; Struelens, M. J.; Suetens, C.; Monnet, D. L.; Strauss, R.; Mertens, K.; Struyf, T.; Catry, B.; Latour, K.; Ivanov, I. N.; Dobрева, E. G.; Tambic Andrašević, A.; Soprek, S.; Budimir, A.; Paphitou, N.; Žemlicková, H.; Schytte Olsen, S.; Wolff Sönksen, U.; Märtin, P.; Ivanova, M.; Lyytikäinen, O.; Jalava, J.; Coignard, B.; Eckmanns, T.; Abu Sin, M.; Haller, S.; Daikos, G. L.; Gikas, A.; Tsiodras, S.; Kontopidou, F.; Tóth, Á.; Hajdu, Á.; Guólaugsson, Ó.; Kristinsson, K. G.; Murchan, S.; Burns, K.; Pezzotti, P.; Gagliotti, C.; Dumpis, U.; Liuimiene, A.; Perrin, M.; Borg, M. A.; de Greeff, S. C.; Monen, J. C.; Koek, M. B.; Elstrøm, P.; Zabicka, D.; Deptula, A.; Hryniewicz, W.; Caniça, M.; Nogueira, P. J.; Fernandes, P. A.; Manageiro, V.; Popescu, G. A.; Serban, R. I.; Schréterová, E.; Litvová, S.; Štefkovicová, M.; Kolman, J.; Klavs, I.; Korošec, A.; Aracil, B.; Asensio, A.; Pérez-Vázquez, M.; Billström, H.; Larsson, S.; Reilly, J. S.; Johnson, A.; Hopkins, S. Attributable Deaths and Disability-Adjusted Life-Years Caused by Infections with Antibiotic-Resistant Bacteria in the EU and the

## VI. References

- European Economic Area in 2015: A Population-Level Modelling Analysis. *Lancet Infect. Dis.* **2019**, *19* (1), 56–66. [https://doi.org/10.1016/S1473-3099\(18\)30605-4](https://doi.org/10.1016/S1473-3099(18)30605-4).
- (30) O'Neill, J. *Antimicrobial Resistance: Tackling a Crisis for the Health and Wealth of Nations*; UK Government & Wellcome Trust: London, United Kingdom, 2014. <https://amr-review.org/>.
- (31) The World Bank. *DRUG-RESISTANT INFECTIONS: A Threat to Our Economic Future*; Final Report; The World Bank: Washington, DC, USA, 2017. <https://www.worldbank.org/en/topic/health/publication/drug-resistant-infections-a-threat-to-our-economic-future>.
- (32) Clatworthy, A. E.; Pierson, E.; Hung, D. T. Targeting Virulence: A New Paradigm for Antimicrobial Therapy. *Nat. Chem. Biol.* **2007**, *3* (9), 541–548. <https://doi.org/10.1038/nchembio.2007.24>.
- (33) Epidemiologisches Bulletin 34/2020. 2020.
- (34) UN; WHO. *No Time To Wait: Secure The Future From Drug-Resistant Infections*; Interagency Coordination Group (IACG) on Antimicrobial Resistance, 2019; p 28.
- (35) OECD; WHO; FAO; OIE. *Tackling Antimicrobial Resistance Ensuring Sustainable R&D*; Final Note; OECD, WHO, FAO & OIE, 2017. <http://www.oecd.org/health/health-systems/G20-AMR-Final-Paper-2017.pdf#page=14&zoom=160,-92,797>.
- (36) Falagas, M. E.; Fragoulis, K. N.; Karydis, I. A Comparative Study on the Cost of New Antibiotics and Drugs of Other Therapeutic Categories. *PLoS ONE* **2006**, *1* (1), e11. <https://doi.org/10.1371/journal.pone.0000011>.
- (37) Wouters, O. J.; McKee, M.; Luyten, J. Estimated Research and Development Investment Needed to Bring a New Medicine to Market, 2009-2018. *JAMA* **2020**, *323* (9), 844. <https://doi.org/10.1001/jama.2020.1166>.
- (38) Stern, S.; Chorzelski, S.; Franken, L.; Völler, S.; Rentmeister, H.; Grosch, B. *Breaking through the Wall - A Call for Concerted Action on Antibiotics Research and Development*; Follow-up Report; The Boston Consulting Group (BCG) for the German Federal Ministry of Health: Berlin, 2017. [https://www.bundesgesundheitsministerium.de/fileadmin/Dateien/5\\_Publikationen/Gesundheit/Berichte/GUARD\\_Follow\\_Up\\_Report\\_Full\\_Report\\_final.pdf](https://www.bundesgesundheitsministerium.de/fileadmin/Dateien/5_Publikationen/Gesundheit/Berichte/GUARD_Follow_Up_Report_Full_Report_final.pdf).
- (39) Stephens, P. *Stimulating Antibiotic R&D*; IMS Health: London, United Kingdom, 2015. <https://amr-review.org/sites/default/files/IMS%20HEALTH.pdf>.
- (40) Theuretzbacher, U.; Outtersson, K.; Engel, A.; Karlén, A. The Global Preclinical Antibacterial Pipeline. *Nat. Rev. Microbiol.* **2020**, *18* (5), 275–285. <https://doi.org/10.1038/s41579-019-0288-0>.
- (41) WHO. *2019 Antibacterial Agents in Clinical Development*; The World Health Organization: Geneva, 2019; p 48.
- (42) Lin, D. M.; Koskella, B.; Lin, H. C. Phage Therapy: An Alternative to Antibiotics in the Age of Multi-Drug Resistance. *WJGPT* **2017**, *8* (3), 162. <https://doi.org/10.4292/wjgpt.v8.i3.162>.
- (43) Kortright, K. E.; Chan, B. K.; Koff, J. L.; Turner, P. E. Phage Therapy: A Renewed Approach to Combat Antibiotic-Resistant Bacteria | Elsevier Enhanced Reader. *Cell Host & Microbe* **2019**, *25* (2), 219–232. <https://doi.org/10.1016/j.chom.2019.01.014>.
- (44) McConnell, M. J. Where Are We with Monoclonal Antibodies for Multidrug-Resistant Infections? *Drug Discov. Today* **2019**, *24* (5), 1132–1138. <https://doi.org/10.1016/j.drudis.2019.03.002>.
- (45) Kay, E.; Cuccui, J.; Wren, B. W. Recent Advances in the Production of Recombinant Glycoconjugate Vaccines. *npj Vaccines* **2019**, *4* (1), 16. <https://doi.org/10.1038/s41541-019-0110-z>.
- (46) Ulmer, J. B.; Deck, R. R.; Yawman, A.; Friedman, A.; Dewitt, C.; Martinez, D.; Montgomery, D. L.; Donnelly, J. J.; Liu, M. A. DNA Vaccines for Bacteria and Viruses. In *Novel Strategies in the Design and Production of Vaccines*; Cohen, S., Shafferman, A., Eds.; Advances in Experimental Medicine and Biology; Springer US: Boston, MA, 1996; Vol. 397, pp 49–53. [https://doi.org/10.1007/978-1-4899-1382-1\\_7](https://doi.org/10.1007/978-1-4899-1382-1_7).

## VI. References

- (47) Rasko, D. A.; Sperandio, V. Anti-Virulence Strategies to Combat Bacteria-Mediated Disease. *Nat. Rev. Drug Discov.* **2010**, *9* (2), 117–128. <https://doi.org/10.1038/nrd3013>.
- (48) Calvert, M. B.; Jumde, V. R.; Titz, A. Pathoblockers or Antivirulence Drugs as a New Option for the Treatment of Bacterial Infections. *Beilstein J. Org. Chem.* **2018**, *14*, 2607–2617. <https://doi.org/10.3762/bjoc.14.239>.
- (49) Mühlen, S.; Dersch, P. Anti-Virulence Strategies to Target Bacterial Infections. In *How to Overcome the Antibiotic Crisis*; Stadler, M., Dersch, P., Eds.; Springer International Publishing: Cham, 2015; Vol. 398, pp 147–183. [https://doi.org/10.1007/82\\_2015\\_490](https://doi.org/10.1007/82_2015_490).
- (50) Hutchings, M. I.; Truman, A. W.; Wilkinson, B. Antibiotics: Past, Present and Future. *Curr. Op. Microbiol.* **2019**, *51*, 72–80. <https://doi.org/10.1016/j.mib.2019.10.008>.
- (51) Walsh, C. Where Will New Antibiotics Come From? *Nat. Rev. Microbiol.* **2003**, *1* (1), 65–70. <https://doi.org/10.1038/nrmicro727>.
- (52) Tse, B. N.; Adalja, A. A.; Houchens, C.; Larsen, J.; Inglesby, T. V.; Hatchett, R. Challenges and Opportunities of Nontraditional Approaches to Treating Bacterial Infections. *Clin. Infect. Dis.* **2017**, *65* (3), 495–500. <https://doi.org/10.1093/cid/cix320>.
- (53) Czaplewski, L.; Bax, R.; Clokie, M.; Dawson, M.; Fairhead, H.; Fischetti, V. A.; Foster, S.; Gilmore, B. F.; Hancock, R. E. W.; Harper, D.; Henderson, I. R.; Hilpert, K.; Jones, B. V.; Kadioglu, A.; Knowles, D.; Ólafsdóttir, S.; Payne, D.; Projan, S.; Shaunak, S.; Silverman, J.; Thomas, C. M.; Trust, T. J.; Warn, P.; Rex, J. H. Alternatives to Antibiotics—a Pipeline Portfolio Review. *Lancet Infect. Dis.* **2016**, *16* (2), 239–251. [https://doi.org/10.1016/S1473-3099\(15\)00466-1](https://doi.org/10.1016/S1473-3099(15)00466-1).
- (54) Bartlett, J. G. Bezlotoxumab — A New Agent for *Clostridium Difficile* Infection. *N. Engl. J. Med.* **2017**, *376* (4), 381–382. <https://doi.org/10.1056/NEJMe1614726>.
- (55) Laterre, P.-F.; Colin, G.; Dequin, P.-F.; Dugernier, T.; Boulain, T.; Azeredo da Silveira, S.; Lajaunias, F.; Perez, A.; François, B. CAL02, a Novel Antitoxin Liposomal Agent, in Severe Pneumococcal Pneumonia: A First-in-Human, Double-Blind, Placebo-Controlled, Randomised Trial. *Lancet Infect. Dis.* **2019**, *19* (6), 620–630. [https://doi.org/10.1016/S1473-3099\(18\)30805-3](https://doi.org/10.1016/S1473-3099(18)30805-3).
- (56) Detke, M.; Lynch, C.; Holsinger, L.; Kapur, S.; Hennings, D.; Raha, D.; Broce, S.; Nguyen, M.; Ermini, F.; Haditsch, U.; Ryder, M.; Goodman, I.; Thein, S.; Dominy, S. COR388 for the Treatment of Alzheimer’s Disease (4098). *Neurology* **2020**, *94* (15 Supplement), 4098.
- (57) Wilson, L. M. *Eagle Pharmaceuticals Announces FDA Acceptance of Investigational New Drug Application for CAL02, a Novel First-in-Class Broad-Spectrum Anti-Virulence Agent for the Adjunct Treatment of Severe Community-Acquired Bacterial Pneumonia*. Eagle Pharmaceuticals - News. <https://investor.eagleus.com/news-releases/news-release-details/eagle-pharmaceuticals-announces-fda-acceptance-investigational> (accessed 2023-06-24).
- (58) Dehbanipour, R.; Ghalavand, Z. Anti-Virulence Therapeutic Strategies against Bacterial Infections: Recent Advances. *Germes* **2022**, *12* (2), 262–275. <https://doi.org/10.18683/germs.2022.1328>.
- (59) Raha, D.; Broce, S.; Haditsch, U.; Rodriguez, L.; Ermini, F.; Detke, M.; Kapur, S.; Hennings, D.; Roth, T.; Nguyen, M.; Holsinger, L. J.; Lynch, C. C.; Dominy, S. COR388, a Novel Gingipain Inhibitor, Decreases Fragmentation of APOE in the Central Nervous System of Alzheimer’s Disease Patients: Human/Human Trials: Other. *Alzheimers Dement.* **2020**, *16* (S9). <https://doi.org/10.1002/alz.040578>.
- (60) Ermini, F.; Haditsch, U.; Roth, T.; Rodriguez, L.; Broce, S.; Raha, D.; Nguyen, M.; Hancock, S.; Cecere, T.; Detke, M.; Kapur, S.; Holsinger, L. J.; Lynch, C. C.; Dominy, S. Comprehensive Alzheimer’s Pathology Is Induced by *P. Gingivalis* Infection: COR388 and Other Gingipain Inhibitors Protect against Synaptic Loss: Molecular and Cell Biology/Synaptic Disruption. *Alzheimers Dement.* **2020**, *16* (S3). <https://doi.org/10.1002/alz.044023>.
- (61) Yongqing, T.; Potempa, J.; Pike, R. N.; Wijeyewickrema, L. C. The Lysine-Specific Gingipain of *Porphyromonas Gingivalis*. In *Cysteine Proteases of Pathogenic Organisms*; Robinson, M. W., Dalton, J. P., Eds.; Advances in Experimental Medicine and Biology; Springer US: Boston, MA, 2011; Vol. 712, pp 15–29. [https://doi.org/10.1007/978-1-4419-8414-2\\_2](https://doi.org/10.1007/978-1-4419-8414-2_2).



## VI. References

- (62) Stathopoulou, P. G.; Benakanakere, M. R.; Galicia, J. C.; Kinane, D. F. The Host Cytokine Response to *Porphyromonas Gingivalis* Is Modified by Gingipains. *Oral Microbiol. Immunol.* **2009**, *24* (1), 11–17. <https://doi.org/10.1111/j.1399-302X.2008.00467.x>.
- (63) Baba, A.; Kadowaki, T.; Asao, T.; Yamamoto, K. Roles for Arg- and Lys-Gingipains in the Disruption of Cytokine Responses and Loss of Viability of Human Endothelial Cells by *Porphyromonas Gingivalis* Infection. *Biol. Chem.* **2002**, *383* (7–8). <https://doi.org/10.1515/BC.2002.135>.
- (64) Calkins, C. C.; Platt, K.; Potempa, J.; Travis, J. Inactivation of Tumor Necrosis Factor- $\alpha$  by Proteinases (Gingipains) from the Periodontal Pathogen, *Porphyromonas Gingivalis*: Implications of Immune Evasion. *J. Biol. Chem.* **1998**, *273* (12), 6611–6614. <https://doi.org/10.1074/jbc.273.12.6611>.
- (65) Imamura, T.; Travis, J.; Potempa, J. The Biphasic Virulence Activities of Gingipains: Activation and Inactivation of Host Proteins. *Curr. Protein Pept. Sci.* **2003**, *4* (6), 443–450. <https://doi.org/10.2174/1389203033487027>.
- (66) AlzForum Foundation Inc. *Therapeutics - Atuzaginstat*. ALZFORUM Networking for a cure. <https://www.alzforum.org/therapeutics/atuzaginstat> (accessed 2023-06-24).
- (67) Roughan, S.; Lynch, C. *Quince Therapeutics Completes the Sale of Legacy Protease Inhibitor Portfolio to Lighthouse Pharmaceuticals*. Quince Therapeutics - News Release. <https://ir.quincetx.com/news-releases/news-release-details/quince-therapeutics-completes-sale-legacy-protease-inhibitor> (accessed 2023-06-24).
- (68) Azeredo da Silveira, S.; Perez, A. CAL02 Liposomes and Other Antitoxins: A New Generation of Anti-Infectives. *Clin. Pulm. Med.* **2018**, *25* (3), 84–88. <https://doi.org/10.1097/CPM.000000000000255>.
- (69) Azeredo da Silveira, S.; Shorr, A. F. Critical Parameters for the Development of Novel Therapies for Severe and Resistant Infections—A Case Study on CAL02, a Non-Traditional Broad-Spectrum Anti-Virulence Drug. *Antibiot.* **2020**, *9* (2), 94. <https://doi.org/10.3390/antibiotics9020094>.
- (70) Bond, J. S. Proteases: History, Discovery, and Roles in Health and Disease. *J. Biol. Chem.* **2019**, *294* (5), 1643–1651. <https://doi.org/10.1074/jbc.TM118.004156>.
- (71) Barrett, A. J.; Woessner, J. F.; Rawlings, N. D. *Handbook of Proteolytic Enzymes*, 3rd ed.; Elsevier Academic Press: London, United Kingdom, 2012.
- (72) Agbowuro, A. A.; Huston, W. M.; Gamble, A. B.; Tyndall, J. D. A. Proteases and Protease Inhibitors in Infectious Diseases. *Med. Res. Rev.* **2018**, *38* (4), 1295–1331. <https://doi.org/10.1002/med.21475>.
- (73) Turk, B. Targeting Proteases: Successes, Failures and Future Prospects. *Nat. Rev. Drug Discov.* **2006**, *5* (9), 785–799. <https://doi.org/10.1038/nrd2092>.
- (74) Supuran, C. T.; Scozzafava, A.; Mastrolorenzo, A. Bacterial Proteases: Current Therapeutic Use and Future Prospects for the Development of New Antibiotics. *Expert Opin. Ther. Pat.* **2001**, *11* (2), 221–259. <https://doi.org/10.1517/13543776.11.2.221>.
- (75) Abbenante, G.; Fairlie, D. Protease Inhibitors in the Clinic. *Med. Chem.* **2005**, *1* (1), 71–104. <https://doi.org/10.2174/1573406053402569>.
- (76) Rawlings, N. D.; Barrett, A. J. Evolutionary Families of Peptidases. *Biochem. J.* **1993**, *290* (1), 205–218. <https://doi.org/10.1042/bj2900205>.
- (77) Culp, E.; Wright, G. D. Bacterial Proteases, Untapped Antimicrobial Drug Targets. *J. Antibiot.* **2017**, *70* (4), 366–377. <https://doi.org/10.1038/ja.2016.138>.
- (78) Schechter, I.; Berger, A. On the Active Site of Proteases. III. Mapping the Active Site of Papain; Specific Peptide Inhibitors of Papain. *Biochem. Biophys. Res. Commun.* **1968**, *32* (5), 898–902. [https://doi.org/10.1016/0006-291X\(68\)90326-4](https://doi.org/10.1016/0006-291X(68)90326-4).
- (79) Fischer, E. Einfluss der Configuration auf die Wirkung der Enzyme. *Ber. Dtsch. Chem. Ges.* **1894**, *27* (3), 2985–2993. <https://doi.org/10.1002/cber.18940270364>.

## VI. References

- (80) Wong, J.; Patel, R. A.; Kowey, P. R. The Clinical Use of Angiotensin-Converting Enzyme Inhibitors. *Prog. Cardiovasc. Dis.* **2004**, *47* (2), 116–130. <https://doi.org/10.1016/j.pcad.2004.04.003>.
- (81) Ho, T. C. S.; Chan, A. H. Y.; Ganesan, A. Thirty Years of HDAC Inhibitors: 2020 Insight and Hindsight. *J. Med. Chem.* **2020**, *63* (21), 12460–12484. <https://doi.org/10.1021/acs.jmedchem.0c00830>.
- (82) Eckschlager, T.; Plch, J.; Stiborova, M.; Hrabeta, J. Histone Deacetylase Inhibitors as Anticancer Drugs. *Int. J. Mol. Sci.* **2017**, *18* (7), 1414. <https://doi.org/10.3390/ijms18071414>.
- (83) Hankey, G. J.; Eikelboom, J. W. Dabigatran Etxilate: A New Oral Thrombin Inhibitor. *Circulation* **2011**, *123* (13), 1436–1450. <https://doi.org/10.1161/CIRCULATIONAHA.110.004424>.
- (84) Lv, Z.; Chu, Y.; Wang, Y. HIV Protease Inhibitors: A Review of Molecular Selectivity and Toxicity. *HIV* **2015**, *95*. <https://doi.org/10.2147/HIV.S79956>.
- (85) de Leuw, P.; Stephan, C. Protease Inhibitors for the Treatment of Hepatitis C Virus Infection. *GMS Infect. Dis.* **2017**, *5* (Doc08). <https://doi.org/10.3205/ID000034>.
- (86) Supuran, C. T.; Scozzafava, A.; Clare, B. W. Bacterial Protease Inhibitors. *Med. Res. Rev.* **2002**, *22* (4), 329–372. <https://doi.org/10.1002/med.10007>.
- (87) Hatheway, C. L. Toxigenic Clostridia. *Clin. Microbiol. Rev.* **1990**, *3* (1), 66–98. <https://doi.org/10.1128/cmr.3.1.66>.
- (88) Supuran, C. T. Clostridium Histolyticum Collagenase Inhibitors in the Drug Design. In *Drug Design of Zinc-Enzyme Inhibitors*; Supuran, C. T., Winum, J.-Y., Eds.; John Wiley & Sons, Inc.: Hoboken, NJ, USA, 2009; pp 721–729. <https://doi.org/10.1002/9780470508169.ch30>.
- (89) Bruggemann, H.; Baumer, S.; Fricke, W. F.; Wiezer, A.; Liesegang, H.; Decker, I.; Herzberg, C.; Martinez-Arias, R.; Merkl, R.; Henne, A.; Gottschalk, G. The Genome Sequence of Clostridium Tetani, the Causative Agent of Tetanus Disease. *Proc. Natl. Acad. Sci.* **2003**, *100* (3), 1316–1321. <https://doi.org/10.1073/pnas.0335853100>.
- (90) Burke, M. P.; Opeskin, K. Nontraumatic Clostridial Myonecrosis. *Am. J. Forensic Med. Pathol.* **1999**, *20* (2), 158–162. <https://doi.org/10.1097/00000433-199906000-00011>.
- (91) Stone, R. BIODEFENSE: Peering Into the Shadows: Iraq's Bioweapons Program. *Science* **2002**, *297* (5584), 1110–1112. <https://doi.org/10.1126/science.297.5584.1110>.
- (92) Arnon, S. S.; Schlechter, R.; Inglesby, T. V.; Henderson, D. A.; Bartlett, J. G.; Ascher, M. S.; Eitzen, E.; Fine, A. D.; Hauer, J.; Layton, M.; Lillibridge, S.; Osterholm, M. T.; O'Toole, T.; Parker, G.; Perl, T. M.; Russell, P. K.; Swardlow, D. L.; Tonat, K. Botulinum Toxin as a Biological Weapon: Medical and Public Health Management. *Jama* **2001**, *285* (8), 1059–1070. <https://doi.org/10.1001/jama.285.8.1059>.
- (93) Cruz-Morales, P.; Orellana, C. A.; Moutafis, G.; Moonen, G.; Rincon, G.; Nielsen, L. K.; Marcellin, E. Revisiting the Evolution and Taxonomy of Clostridia, a Phylogenomic Update. *Genome Biol. Evol.* **2019**, *11* (7), 2035–2044. <https://doi.org/10.1093/gbe/evz096>.
- (94) Yoshihara, K.; Matsushita, O.; Minami, J.; Okabe, A. Cloning and Nucleotide Sequence Analysis of the ColH Gene from Clostridium Histolyticum Encoding a Collagenase and a Gelatinase. *J. Bacteriol.* **1994**, *176* (21), 6489–6496. <https://doi.org/10.1128/jb.176.21.6489-6496.1994>.
- (95) Harrington, D. J. Bacterial Collagenases and Collagen-Degrading Enzymes and Their Potential Role in Human Disease. *Infect. Immun.* **1996**, *64* (6), 1885–1891. <https://doi.org/10.1128/IAI.64.6.1885-1891.1996>.
- (96) Bottone, E. J. *Bacillus Cereus*, a Volatile Human Pathogen. *Clin. Microbiol. Rev.* **2010**, *23* (2), 382–398. <https://doi.org/10.1128/CMR.00073-09>.
- (97) Callegan, M. C.; Kane, S. T.; Cochran, D. C.; Gilmore, M. S. Molecular Mechanisms of *Bacillus* Endophthalmitis Pathogenesis. *DNA Cell Biol.* **2002**, *21* (5), 367–373. <https://doi.org/10.1089/10445490260099647>.
- (98) Okinaka, R. T.; Cloud, K.; Hampton, O.; Hoffmaster, A. R.; Hill, K. K.; Keim, P.; Koehler, T. M.; Lamke, G.; Kumano, S.; Mahillon, J.; Manter, D.; Martinez, Y.; Ricke, D.; Svensson, R.; Jackson, P. J. Sequence and Organization of PX01, the Large *Bacillus Anthracis* Plasmid Harboring the

## VI. References

- Anthrax Toxin Genes. *J. Bacteriol.* **1999**, *181* (20), 6509–6515. <https://doi.org/10.1128/JB.181.20.6509-6515.1999>.
- (99) Bravo, A.; Likitvivatanavong, S.; Gill, S. S.; Soberón, M. *Bacillus Thuringiensis*: A Story of a Successful Bioinsecticide. *Insect Biochem. Mol. Biol.* **2011**, *41* (7), 423–431. <https://doi.org/10.1016/j.ibmb.2011.02.006>.
- (100) Granum, P. E.; Lund, T. *Bacillus Cereus* and Its Food Poisoning Toxins. *FEMS Microbiol. Lett.* **1997**, *157* (2), 223–228. <https://doi.org/10.1111/j.1574-6968.1997.tb12776.x>.
- (101) Helgason, E.; Caugant, D. A.; Olsen, I.; Kolstø, A.-B. Genetic Structure of Population of *Bacillus Cereus* and *B. Thuringiensis* Isolates Associated with Periodontitis and Other Human Infections. *J. Clin. Microbiol.* **2000**, *38* (4), 1615–1622. <https://doi.org/10.1128/JCM.38.4.1615-1622.2000>.
- (102) Mursalin, M. H.; Livingston, E. T.; Callegan, M. C. The Cereus Matter of *Bacillus Endophthalmitis*. *Exp. Eye Res.* **2020**, *193*, 107959. <https://doi.org/10.1016/j.exer.2020.107959>.
- (103) Darbar, A.; Harris, I. A.; Gosbell, I. B. Necrotizing Infection Due to *Bacillus Cereus* Mimicking Gas Gangrene Following Penetrating Trauma. *J. Orthop. Trauma* **2005**, *19* (5), 353–355. <https://doi.org/10.1001/archortho.19.5.353>.
- (104) Åkesson, A.; Hedström, S. Å.; Ripa, T. *Bacillus Cereus*: A Significant Pathogen in Postoperative and Post-Traumatic Wounds on Orthopaedic Wards. *Scand. J. Infect. Dis.* **1991**, *23* (1), 71–77. <https://doi.org/10.3109/00365549109023377>.
- (105) Peng, D.; Lin, J.; Huang, Q.; Zheng, W.; Liu, G.; Zheng, J.; Zhu, L.; Sun, M. A Novel Metalloproteinase Virulence Factor Is Involved in *B. Acillus Thuringiensis* Pathogenesis in Nematodes and Insects: *ColB* Is a Novel Virulence Factor in Bt. *Environ. Microbiol.* **2016**, *18* (3), 846–862. <https://doi.org/10.1111/1462-2920.13069>.
- (106) Beecher, D. J.; Olsen, T. W.; Somers, E. B.; Wong, A. C. L. Evidence for Contribution of Tripartite Hemolysin BL, Phosphatidylcholine-Preferring Phospholipase C, and Collagenase to Virulence of *Bacillus Cereus* Endophthalmitis. *Infect. Immun.* **2000**, *68* (9), 5269–5276. <https://doi.org/10.1128/IAI.68.9.5269-5276.2000>.
- (107) Makinen, K. K.; Makinen, P. L. Purification and Properties of an Extracellular Collagenolytic Protease Produced by the Human Oral Bacterium *Bacillus Cereus* (Strain Soc 67). *J. Biol. Chem.* **1987**, *262* (26), 12488–12495. [https://doi.org/10.1016/S0021-9258\(18\)45232-5](https://doi.org/10.1016/S0021-9258(18)45232-5).
- (108) Loesche, W. J.; Paunio, K. U.; Woolfolk, M. P.; Hockett, R. N. Collagenolytic Activity of Dental Plaque Associated with Periodontal Pathology. *Infect. Immun.* **1974**, *9* (2), 329–336. <https://doi.org/10.1128/iai.9.2.329-336.1974>.
- (109) Popoff, M. R. From Saprophytic to Toxigenic Clostridia, a Complex Evolution Based on Multiple Diverse Genetic Transfers and/or Rearrangements. *Res. Microbiol.* **2015**, *166* (4), 221–224. <https://doi.org/10.1016/j.resmic.2015.02.008>.
- (110) *Structure and Function of Collagen Types*; Mayne, R., Burgeson, R. E., Eds.; Academic Press Inc.: Orlando, Florida, 1987.
- (111) Mouw, J. K.; Ou, G.; Weaver, V. M. Extracellular Matrix Assembly: A Multiscale Deconstruction. *Nat. Rev. Mol. Cell Biol.* **2014**, *15*, 771–785.
- (112) Nagase, H.; Visse, R.; Murphy, G. Structure and Function of Matrix Metalloproteinases and TIMPs. *Cardiovasc. Res.* **2006**, *69* (3), 562–573. <https://doi.org/10.1016/j.cardiores.2005.12.002>.
- (113) Matsushita, O.; Okabe, A. Clostridial Hydrolytic Enzymes Degrading Extracellular Components. *Toxicon* **2001**, *39* (11), 1769–1780. [https://doi.org/10.1016/S0041-0101\(01\)00163-5](https://doi.org/10.1016/S0041-0101(01)00163-5).
- (114) Bond, M. D.; Van Wart, H. E. Characterization of the Individual Collagenases from *Clostridium Histolyticum*. *Biochem.* **1984**, *23* (13), 3085–3091. <https://doi.org/10.1021/bi00308a036>.
- (115) Matsushita, O.; Jung, C.-M.; Minami, J.; Katayama, S.; Nishi, N.; Okabe, A. A Study of the Collagen-Binding Domain of a 116-KDa *Clostridium Histolyticum* Collagenase. *J. Biol. Chem.* **1998**, *273* (6), 3643–3648. <https://doi.org/10.1074/jbc.273.6.3643>.

## VI. References

- (116) Jung, C.-M.; Matsushita, O.; Katayama, S.; Minami, J.; Sakurai, J.; Okabe, A. Identification of Metal Ligands in the *Clostridium Histolyticum* ColH Collagenase. *J. Bacteriol.* **1999**, *181* (9), 2816–2822. <https://doi.org/10.1128/JB.181.9.2816-2822.1999>.
- (117) Eckhard, U.; Schönauer, E.; Brandstetter, H. Structural Basis for Activity Regulation and Substrate Preference of Clostridial Collagenases G, H, and T. *J. Biol. Chem.* **2013**, *288* (28), 20184–20194. <https://doi.org/10.1074/jbc.M112.448548>.
- (118) Bond, M. D.; Van Wart, H. E. Purification and Separation of Individual Collagenases of *Clostridium Histolyticum* Using Red Dye Ligand Chromatography. *Biochemistry* **1984**, *23* (13), 3077–3085. <https://doi.org/10.1021/bi00308a035>.
- (119) Wilson, J. J. A Bacterial Collagen-Binding Domain with Novel Calcium-Binding Motif Controls Domain Orientation. *EMBO J.* **2003**, *22* (8), 1743–1752. <https://doi.org/10.1093/emboj/cdg172>.
- (120) Eckhard, U.; Schönauer, E.; Nüss, D.; Brandstetter, H. Structure of Collagenase G Reveals a Chew-and-Digest Mechanism of Bacterial Collagenolysis. *Nat. Struct. Mol. Biol.* **2011**, *18* (10), 1109–1114. <https://doi.org/10.1038/nsmb.2127>.
- (121) Abfalter, C. M.; Schönauer, E.; Ponnuraj, K.; Huemer, M.; Gadermaier, G.; Regl, C.; Briza, P.; Ferreira, F.; Huber, C. G.; Brandstetter, H.; Posselt, G.; Wessler, S. Cloning, Purification and Characterization of the Collagenase ColA Expressed by *Bacillus Cereus* ATCC 14579. *PLoS ONE* **2016**, *11* (9), e0162433. <https://doi.org/10.1371/journal.pone.0162433>.
- (122) Evans, D. G.; Wardlaw, A. C. Gelatinase and Collagenase Production by Certain Species of *Bacillus*. *J. Gen. Microbiol.* **1953**, *8* (3), 481–487. <https://doi.org/10.1099/00221287-8-3-481>.
- (123) Hoppe, I. J.; Brandstetter, H.; Schönauer, E. Biochemical Characterisation of a Collagenase from *Bacillus Cereus* Strain Q1. *Sci. Rep.* **2021**, *11* (1), 4187. <https://doi.org/10.1038/s41598-021-83744-6>.
- (124) Van Wart, H. E. Clostridium Collagenases. In *Handbook of Proteolytic Enzymes*; Rawlings, N. D., Salvesen, G., Eds.; Elsevier: London, United Kingdom, 2013; Vol. 1, pp 607–611. <https://doi.org/10.1016/B978-0-12-382219-2.00126-5>.
- (125) Eckhard, U.; Huesgen, P. F.; Brandstetter, H.; Overall, C. M. Proteomic Protease Specificity Profiling of Clostridial Collagenases Reveals Their Intrinsic Nature as Dedicated Degradors of Collagen. *J. Proteomics* **2014**, *100*, 102–114. <https://doi.org/10.1016/j.jprot.2013.10.004>.
- (126) Matsushita, O.; Jung, C.-M.; Minami, J.; Katayama, S.; Nishi, N.; Okabe, A. A Study of the Collagen-Binding Domain of a 116-KDa *Clostridium Histolyticum* Collagenase. *J. Biol. Chem.* **1998**, *273* (6), 3643–3648. <https://doi.org/10.1074/jbc.273.6.3643>.
- (127) Popoff, M. R.; Bouvet, P. Clostridial Toxins. *Future Microbiol.* **2009**, *4* (8), 1021–1064. <https://doi.org/10.2217/fmb.09.72>.
- (128) Vencill, C. F.; Rasnick, D.; Crumley, K. V.; Nishino, N.; Powers, J. C. Clostridium Histolyticum Collagenase: Development of New Thio Ester, Fluorogenic, and Depsipeptide Substrates and New Inhibitors. *Biochem.* **1985**, *24* (13), 3149–3157. <https://doi.org/10.1021/bi00334a012>.
- (129) Grobelny, D.; Galardy, R. E. Aldehyde and Ketone Substrate Analogs Inhibit the Collagenase of *Clostridium Histolyticum*. *Biochem.* **1985**, *24* (22), 6145–6152. <https://doi.org/10.1021/bi00343a017>.
- (130) Galardy, R. E.; Grobelny, D. Inhibition of the Collagenase from *Clostridium Histolyticum* by Phosphoric and Phosphonic Amides. *Biochem.* **1983**, *22* (19), 4556–4561. <https://doi.org/10.1021/bi00288a032>.
- (131) Yiotakis, A.; Hatgiannacou, A.; Dive, V.; Toma, F. New Thiol Inhibitors of Clostridium Histolyticum Collagenase. Importance of the P3' Position. *Eur. J. Biochem.* **1988**, *172* (3), 761–766. <https://doi.org/10.1111/j.1432-1033.1988.tb13954.x>.
- (132) Dive, V.; Yiotakis, A.; Nicolaou, A.; Toma, F. Inhibition of Clostridium Histolyticum Collagenases by Phosphonamide Peptide Inhibitors. *Eur. J. Biochem.* **1990**, *191* (3), 685–689. <https://doi.org/10.1111/j.1432-1033.1990.tb19175.x>.

## VI. References

- (133) Barrantes, E.; Guinea, M. Inhibition of Collagenase and Metalloproteinases by Aloins and Aloe Gel. *Life Sci.* **2003**, *72* (7), 843–850. [https://doi.org/10.1016/S0024-3205\(02\)02308-1](https://doi.org/10.1016/S0024-3205(02)02308-1).
- (134) Bols, M.; Binderup, L.; Hansen, J.; Rasmussen, P. Inhibition of Collagenase by Aranciamycin and Aranciamycin Derivatives. *J. Med. Chem.* **1992**, *35* (15), 2768–2771. <https://doi.org/10.1021/jm00093a008>.
- (135) Oshima, N.; Narukawa, Y.; Takeda, T.; Kiuchi, F. Collagenase Inhibitors from Viola Yedoensis. *J. Nat. Med.* **2013**, *67* (1), 240–245. <https://doi.org/10.1007/s11418-012-0665-8>.
- (136) Eun Lee, K.; Bharadwaj, S.; Yadava, U.; Gu Kang, S. Evaluation of Caffeine as Inhibitor against Collagenase, Elastase and Tyrosinase Using *in Silico* and *in Vitro* Approach. *J. Enzyme Inhib. Med. Chem.* **2019**, *34* (1), 927–936. <https://doi.org/10.1080/14756366.2019.1596904>.
- (137) Scozzafava, A.; Supuran, C. T. Protease Inhibitors: Synthesis of Potent Bacterial Collagenase and Matrix Metalloproteinase Inhibitors Incorporating *N*-4-Nitrobenzylsulfonylglycine Hydroxamate Moieties. *J. Med. Chem.* **2000**, *43* (9), 1858–1865. <https://doi.org/10.1021/jm990594k>.
- (138) Supuran, C. T.; Briganti, F.; Mincione, G.; Scozzafava, A. Protease Inhibitors: Synthesis of L-Alanine Hydroxamate Sulfonylated Derivatives as Inhibitors of *Clostridium Histolyticum* Collagenase. *J. Enzyme Inhib.* **2000**, *15* (2), 111–128. <https://doi.org/10.1080/14756360009030345>.
- (139) Supuran, C. T.; Scozzafava, A. Protease Inhibitors. Part 7 Inhibition of *Clostridium Histolyticum* Collagenase with Sulfonylated Derivatives of L-Valine Hydroxamate. *Eur. J. Pharm. Sci.* **2000**, *10* (1), 67–76. [https://doi.org/10.1016/S0928-0987\(99\)00090-1](https://doi.org/10.1016/S0928-0987(99)00090-1).
- (140) Clare, B. W.; Scozzafava, A.; Supuran, C. T. Protease Inhibitors: Synthesis of a Series of Bacterial Collagenase Inhibitors of the Sulfonyl Amino Acyl Hydroxamate Type. *J. Med. Chem.* **2001**, *44* (13), 2253–2258. <https://doi.org/10.1021/jm010087e>.
- (141) Ilies, M.; Banciu, M. D.; Scozzafava, A.; Ilies, M. A.; Caproiu, M. T.; Supuran, C. T. Protease Inhibitors: Synthesis of Bacterial Collagenase and Matrix Metalloproteinase Inhibitors Incorporating Arylsulfonylureido and 5-Dibenzo-Suberenyl/Suberyl Moieties. *Bioorg. Med. Chem.* **2003**, *11* (10), 2227–2239. [https://doi.org/10.1016/S0968-0896\(03\)00113-5](https://doi.org/10.1016/S0968-0896(03)00113-5).
- (142) Scozzafava, A.; Supuran, C. T. Protease Inhibitors: Synthesis of Matrix Metalloproteinase and Bacterial Collagenase Inhibitors Incorporating 5-Amino-2-Mercapto-1,3,4-Thiadiazole Zinc Binding Functions. *Bioorg. Med. Chem. Lett.* **2002**, *12* (19), 2667–2672. [https://doi.org/10.1016/S0960-894X\(02\)00564-4](https://doi.org/10.1016/S0960-894X(02)00564-4).
- (143) Amélia Santos, M.; Marques, S.; Gil, M.; Tegoni, M.; Scozzafava, A.; Supuran, C. T. Protease Inhibitors: Synthesis of Bacterial Collagenase and Matrix Metalloproteinase Inhibitors Incorporating Succinyl Hydroxamate and Iminodiacetic Acid Hydroxamate Moieties. *J. Enzyme Inhib. Med. Chem.* **2003**, *18* (3), 233–242. <https://doi.org/10.1080/1475636031000081134>.
- (144) *Antibacterial Agents in Clinical Development. In An Analysis of the Antibacterial Clinical Development Pipeline, Including Tuberculosis*; The World Health Organization: Geneva, 2017.
- (145) Tacconelli, E.; Carrara, E.; Savoldi, A.; Harbarth, S.; Mendelson, M.; Monnet, D. L.; Pulcini, C.; Kahlmeter, G.; Kluytmans, J.; Carmeli, Y.; Ouellette, M.; Outterson, K.; Patel, J.; Cavaleri, M.; Cox, E. M.; Houchens, C. R.; Grayson, M. L.; Hansen, P.; Singh, N.; Theuretzbacher, U.; Magrini, N.; Aboderin, A. O.; Al-Abri, S. S.; Awang Jalil, N.; Benzonana, N.; Bhattacharya, S.; Brink, A. J.; Burkert, F. R.; Cars, O.; Cornaglia, G.; Dyar, O. J.; Friedrich, A. W.; Gales, A. C.; Gandra, S.; Giske, C. G.; Goff, D. A.; Goossens, H.; Gottlieb, T.; Guzman Blanco, M.; Hryniewicz, W.; Kattula, D.; Jinks, T.; Kanj, S. S.; Kerr, L.; Kieny, M.-P.; Kim, Y. S.; Kozlov, R. S.; Labarca, J.; Laxminarayan, R.; Leder, K.; Leibovici, L.; Levy-Hara, G.; Littman, J.; Malhotra-Kumar, S.; Manchanda, V.; Moja, L.; Ndoye, B.; Pan, A.; Paterson, D. L.; Paul, M.; Qiu, H.; Ramon-Pardo, P.; Rodríguez-Baño, J.; Sanguinetti, M.; Sengupta, S.; Sharland, M.; Si-Mehand, M.; Silver, L. L.; Song, W.; Steinbakk, M.; Thomsen, J.; Thwaites, G. E.; van der Meer, J. W.; Van Kinh, N.; Vega, S.; Villegas, M. V.; Wechsler-Fördös, A.; Wertheim, H. F. L.; Wesangula, E.; Woodford, N.; Yilmaz, F. O.; Zorzet, A. Discovery, Research, and Development of New Antibiotics: The WHO Priority List of Antibiotic-Resistant Bacteria and Tuberculosis. *Lancet Infect. Dis.* **2018**, *18* (3), 318–327. [https://doi.org/10.1016/S1473-3099\(17\)30753-3](https://doi.org/10.1016/S1473-3099(17)30753-3).

## VI. References

- (146) CDC (U.S.). *Antibiotic Resistance Threats in the United States, 2019*; U.S. Department of Health and Human Services, CDC, 2019. <https://doi.org/10.15620/cdc:82532>.
- (147) Bodey, G. P.; Bolivar, R.; Fainstein, V.; Jadeja, L. Infections Caused by *Pseudomonas Aeruginosa*. *Clin. Infect. Dis.* **1983**, *5* (2), 279–313. <https://doi.org/10.1093/clinids/5.2.279>.
- (148) Japoni, A.; Farshad, S.; Alborzi, A. *Pseudomonas Aeruginosa*: Burn Infection, Treatment and Antibacterial Resistance. *Iran. Red Crescent Med. J.* **2009**, *11* (3), 244–253.
- (149) Van Eldere, J. Multicentre Surveillance of *Pseudomonas Aeruginosa* Susceptibility Patterns in Nosocomial Infections. *J. Antimicrob. Chemother.* **2003**, *51* (2), 347–352. <https://doi.org/10.1093/jac/dkg102>.
- (150) Obritsch, M. D.; Fish, D. N.; MacLaren, R.; Jung, R. Nosocomial Infections Due to Multidrug-Resistant *Pseudomonas Aeruginosa* : Epidemiology and Treatment Options. *Pharmacotherapy* **2005**, *25* (10), 1353–1364. <https://doi.org/10.1592/phco.2005.25.10.1353>.
- (151) Estahbanati, H. K.; Kashani, P. P.; Ghanaatpisheh, F. Frequency of *Pseudomonas Aeruginosa* Serotypes in Burn Wound Infections and Their Resistance to Antibiotics. *Burns* **2002**, *28* (4), 340–348. [https://doi.org/10.1016/S0305-4179\(02\)00024-4](https://doi.org/10.1016/S0305-4179(02)00024-4).
- (152) Burns, R. P.; Rhodes, D. H. *Pseudomonas* Eye Infection as a Cause of Death in Premature Infants. *Arch. Ophthalmol.* **1961**, *65* (4), 517–525. <https://doi.org/10.1001/archopht.1961.01840020519010>.
- (153) Preston, M. J.; Seed, P. C.; Toder, D. S.; Iglewski, B. H.; Ohman, D. E.; Gustin, J. K.; Goldberg, J. B.; Pier, G. B. Contribution of Proteases and LasR to the Virulence of *Pseudomonas Aeruginosa* during Corneal Infections. *Infect. Immun.* **1997**, *65* (8), 3086–3090. <https://doi.org/10.1128/IAI.65.8.3086-3090.1997>.
- (154) Fleiszig, S. M.; Evans, D. J. The Pathogenesis of Bacterial Keratitis: Studies with *Pseudomonas Aeruginosa*. *Clin. Exp. Optom.* **2002**, *85* (5), 271–278. <https://doi.org/10.1111/j.1444-0938.2002.tb03082.x>.
- (155) Sorde, R.; Albert Pahissa; Jordi Rello. Management of Refractory *Pseudomonas Aeruginosa* Infection in Cystic Fibrosis. *IDR* **2011**, *31*. <https://doi.org/10.2147/IDR.S16263>.
- (156) Oliver, A. High Frequency of Hypermutable *Pseudomonas Aeruginosa* in Cystic Fibrosis Lung Infection. *Science* **2000**, *288* (5469), 1251–1253. <https://doi.org/10.1126/science.288.5469.1251>.
- (157) Zolin, A.; Orenti, A.; Naehrlich, L.; van Rens, J. *ECFSPR Annual Report 2018*; Annual Data Report; ECFS, 2020; p 175. <https://www.ecfs.eu/projects/ecfs-patient-registry/annual-reports> (accessed 2021-07-10).
- (158) Hauser, A. R.; Jain, M.; Bar-Meir, M.; McColley, S. A. Clinical Significance of Microbial Infection and Adaptation in Cystic Fibrosis. *Clin. Microbiol. Rev.* **2011**, *24* (1), 29–70. <https://doi.org/10.1128/CMR.00036-10>.
- (159) Mulcahy, L. R.; Isabella, V. M.; Lewis, K. *Pseudomonas Aeruginosa* Biofilms in Disease. *Microb. Ecol.* **2014**, *68* (1), 1–12. <https://doi.org/10.1007/s00248-013-0297-x>.
- (160) Høiby, N.; Ciofu, O.; Bjarnsholt, T. *Pseudomonas Aeruginosa* Biofilms in Cystic Fibrosis. *Future Microbiol.* **2010**, *5* (11), 1663–1674. <https://doi.org/10.2217/fmb.10.125>.
- (161) Gaspar, M. C.; Couet, W.; Olivier, J.-C.; Pais, A. A. C. C.; Sousa, J. J. S. *Pseudomonas Aeruginosa* Infection in Cystic Fibrosis Lung Disease and New Perspectives of Treatment: A Review. *Eur. J. Clin. Microbiol. Infect. Dis.* **2013**, *32* (10), 1231–1252. <https://doi.org/10.1007/s10096-013-1876-y>.
- (162) Pang, Z.; Raudonis, R.; Glick, B. R.; Lin, T.-J.; Cheng, Z. Antibiotic Resistance in *Pseudomonas Aeruginosa*: Mechanisms and Alternative Therapeutic Strategies. *Biotechnol. Adv.* **2019**, *37* (1), 177–192. <https://doi.org/10.1016/j.biotechadv.2018.11.013>.
- (163) Buret, A.; Cripps, A. W. The Immuno-evasive Activities of *Pseudomonas Aeruginosa* : Relevance for Cystic Fibrosis. *Am. Rev. Respir. Dis.* **1993**, *148* (3), 793–805. <https://doi.org/10.1164/ajrccm/148.3.793>.

## VI. References

- (164) Venturi, V. Regulation of Quorum Sensing in *Pseudomonas*. *FEMS Microbiol. Rev.* **2006**, *30* (2), 274–291. <https://doi.org/10.1111/j.1574-6976.2005.00012.x>.
- (165) Rocha, A. J.; Barsottini, M. R. de O.; Rocha, R. R.; Laurindo, M. V.; Moraes, F. L. L. de; Rocha, S. L. da. *Pseudomonas Aeruginosa*: Virulence Factors and Antibiotic Resistance Genes. *Braz. Arch. Biol. Technol.* **2019**, *62*, e19180503. <https://doi.org/10.1590/1678-4324-2019180503>.
- (166) Balasubramanian, D.; Schneper, L.; Kumari, H.; Mathee, K. A Dynamic and Intricate Regulatory Network Determines *Pseudomonas Aeruginosa* Virulence. *Nucleic Acids Res.* **2013**, *41* (1), 1–20. <https://doi.org/10.1093/nar/gks1039>.
- (167) Galdino, A. C. M.; Branquinha, M. H.; Santos, A. L. S.; Viganor, L. *Pseudomonas Aeruginosa* and Its Arsenal of Proteases: Weapons to Battle the Host. In *Pathophysiological Aspects of Proteases*; Chakraborti, S., Dhalla, N. S., Eds.; Springer Singapore: Singapore, 2017; pp 381–397. [https://doi.org/10.1007/978-981-10-6141-7\\_16](https://doi.org/10.1007/978-981-10-6141-7_16).
- (168) Everett, M. J.; Davies, D. T. *Pseudomonas Aeruginosa* Elastase (LasB) as a Therapeutic Target. *Drug Discov. Today* **2021**, *26* (9), 2108–2123. <https://doi.org/10.1016/j.drudis.2021.02.026>.
- (169) Woods, D. E.; Cryz, S. J.; Friedman, R. L.; Iglewski, B. H. Contribution of Toxin A and Elastase to Virulence of *Pseudomonas Aeruginosa* in Chronic Lung Infections of Rats. *Infect. Immun.* **1982**, *36* (3), 1223–1228. <https://doi.org/10.1128/IAI.36.3.1223-1228.1982>.
- (170) Wretling, B.; Pavlovskis, O. R. *Pseudomonas Aeruginosa* Elastase and Its Role in *Pseudomonas* Infections. *Clin. Infect. Dis.* **1983**, *5* (Supplement\_5), S998–S1004. [https://doi.org/10.1093/clinids/5.Supplement\\_5.S998](https://doi.org/10.1093/clinids/5.Supplement_5.S998).
- (171) Morihara, K.; Tsuzuki, H.; Oka, T.; Inoue, H.; Ebata, M. *Pseudomonas Aeruginosa* Elastase - Isolation, Crystallization and Preliminary Characterization. *J. Biol. Chem.* **1965**, *240* (8), 3295–3304.
- (172) Galdino, A. C. M.; Viganor, L.; de Castro, A. A.; da Cunha, E. F. F.; Mello, T. P.; Mattos, L. M.; Pereira, M. D.; Hunt, M. C.; O’Shaughnessy, M.; Howe, O.; Devereux, M.; McCann, M.; Ramalho, T. C.; Branquinha, M. H.; Santos, A. L. S. Disarming *Pseudomonas Aeruginosa* Virulence by the Inhibitory Action of 1,10-Phenanthroline-5,6-Dione-Based Compounds: Elastase B (LasB) as a Chemotherapeutic Target. *Front. Microbiol.* **2019**, *10*, 1701. <https://doi.org/10.3389/fmicb.2019.01701>.
- (173) Casilag, F.; Lorenz, A.; Krueger, J.; Klawonn, F.; Weiss, S.; Häussler, S. The LasB Elastase of *Pseudomonas Aeruginosa* Acts in Concert with Alkaline Protease AprA To Prevent Flagellin-Mediated Immune Recognition. *Infect. Immun.* **2016**, *84* (1), 162–171. <https://doi.org/10.1128/IAI.00939-15>.
- (174) Kessler, E.; Safrin, M.; Gustin, J. K.; Ohman, D. E. Elastase and the LasA Protease of *Pseudomonas Aeruginosa* Are Secreted with Their Propeptides. *J. Biol. Chem.* **1998**, *273* (46), 30225–30231. <https://doi.org/10.1074/jbc.273.46.30225>.
- (175) Yu, H.; He, X.; Xie, W.; Xiong, J.; Sheng, H.; Guo, S.; Huang, C.; Zhang, D.; Zhang, K. Elastase LasB of *Pseudomonas Aeruginosa* Promotes Biofilm Formation Partly through Rhamnolipid-Mediated Regulation. *Can. J. Microbiol.* **2014**, *60* (4), 227–235. <https://doi.org/10.1139/cjm-2013-0667>.
- (176) Parmely, M.; Gale, A.; Clabaugh, M.; Horvat, R.; Zhou, W. W. Proteolytic Inactivation of Cytokines by *Pseudomonas Aeruginosa*. *Infect. Immun.* **1990**, *58* (9), 3009–3014. <https://doi.org/10.1128/IAI.58.9.3009-3014.1990>.
- (177) Schmidtchen, A.; Frick, I.-M.; Andersson, E.; Tapper, H.; Björck, L. Proteinases of Common Pathogenic Bacteria Degrade and Inactivate the Antibacterial Peptide LL-37. *Mol. Microbiol.* **2002**, *46* (1), 157–168. <https://doi.org/10.1046/j.1365-2958.2002.03146.x>.
- (178) Schultz, D. R.; Miller, K. D. Elastase of *Pseudomonas Aeruginosa*: Inactivation of Complement Components and Complement-Derived Chemotactic and Phagocytic Factors. *Infect. Immun.* **1974**, *10* (1), 128.
- (179) Mariencheck, W. I.; Alcorn, J. F.; Palmer, S. M.; Wright, J. R. *Pseudomonas Aeruginosa* Elastase Degrades Surfactant Proteins A and D. *Am. J. Respir. Cell Mol. Biol.* **2003**, *28* (4), 528–537. <https://doi.org/10.1165/rcmb.2002-01410C>.

## VI. References

- (180) Alcorn, J. F.; Wright, J. R. Degradation of Pulmonary Surfactant Protein D by *Pseudomonas Aeruginosa* Elastase Abrogates Innate Immune Function. *J. Biol. Chem.* **2004**, *279* (29), 30871–30879. <https://doi.org/10.1074/jbc.M400796200>.
- (181) Kuang, Z.; Hao, Y.; Walling, B. E.; Jeffries, J. L.; Ohman, D. E.; Lau, G. W. *Pseudomonas Aeruginosa* Elastase Provides an Escape from Phagocytosis by Degrading the Pulmonary Surfactant Protein-A. *PLoS ONE* **2011**, *6* (11), e27091. <https://doi.org/10.1371/journal.pone.0027091>.
- (182) Senyürek, I.; Kempf, W. E.; Klein, G.; Maurer, A.; Kalbacher, H.; Schäfer, L.; Wanke, I.; Christ, C.; Stevanovic, S.; Schaller, M.; Rousselle, P.; Garbe, C.; Biedermann, T.; Schittek, B. Processing of Laminin  $\alpha$  Chains Generates Peptides Involved in Wound Healing and Host Defense. *J. Innate Immun.* **2014**, *6* (4), 467–484. <https://doi.org/10.1159/000357032>.
- (183) Wretlind, B.; Pavlovskis, O. R. *Pseudomonas Aeruginosa* Elastase and Its Role in *Pseudomonas* Infections. *Clin. Infect. Dis.* **1983**, *5* (Supplement\_5), S998–S1004. [https://doi.org/10.1093/clinids/5.Supplement\\_5.S998](https://doi.org/10.1093/clinids/5.Supplement_5.S998).
- (184) Heck, L. W.; Morihara, K.; McRae, W. B.; Miller, E. J. Specific Cleavage of Human Type III and IV Collagens by *Pseudomonas Aeruginosa* Elastase. *Infect. Immun.* **1986**, *51* (1), 115–118. <https://doi.org/10.1128/IAI.51.1.115-118.1986>.
- (185) Cowell, B. A.; Twining, S. S.; Hobden, J. A.; Kwong, M. S. F.; Fleiszig, S. M. J. Mutation of LasA and LasB Reduces *Pseudomonas Aeruginosa* Invasion of Epithelial Cells. *Microbiol.* **2003**, *149* (8), 2291–2299. <https://doi.org/10.1099/mic.0.26280-0>.
- (186) Tan, M.-W.; Rahme, L. G.; Sternberg, J. A.; Tompkins, R. G.; Ausubel, F. M. *Pseudomonas Aeruginosa* Killing of *Caenorhabditis Elegans* Used to Identify *P. Aeruginosa* Virulence Factors. *Proc. Natl. Acad. Sci.* **1999**, *96* (5), 2408–2413. <https://doi.org/10.1073/pnas.96.5.2408>.
- (187) Tang, H. B.; DiMango, E.; Bryan, R.; Gambello, M.; Iglewski, B. H.; Goldberg, J. B.; Prince, A. Contribution of Specific *Pseudomonas Aeruginosa* Virulence Factors to Pathogenesis of Pneumonia in a Neonatal Mouse Model of Infection. *Infect. Immun.* **1996**, *64* (1), 37–43. <https://doi.org/10.1128/iai.64.1.37-43.1996>.
- (188) Morihara, K.; Tsuzuki, H. Phosphoramidon as an Inhibitor of Elastase from *Pseudomonas Aeruginosa*. *Jpn. J. Exp. Med.* **1978**, *48* (1), 81–84.
- (189) Leiris, S.; Davies, D. T.; Sprynski, N.; Castandet, J.; Beyria, L.; Bodnarchuk, M. S.; Sutton, J. M.; Mullins, T. M. G.; Jones, M. W.; Forrest, A. K.; Pallin, T. D.; Karunakar, P.; Martha, S. K.; Parusharamulu, B.; Ramula, R.; Kotha, V.; Pottabathini, N.; Pothukanuri, S.; Lemonnier, M.; Everett, M. Virtual Screening Approach to Identifying a Novel and Tractable Series of *Pseudomonas Aeruginosa* Elastase Inhibitors. *ACS Med. Chem. Lett.* **2021**, *12* (2), 217–227. <https://doi.org/10.1021/acsmchemlett.0c00554>.
- (190) Velázquez-Libera, J. L.; Murillo-López, J. A.; F. de la Torre, A.; Caballero, J. Structural Requirements of N-Alpha-Mercaptoacetyl Dipeptide (NAMdP) Inhibitors of *Pseudomonas Aeruginosa* Virulence Factor LasB: 3D-QSAR, Molecular Docking, and Interaction Fingerprint Studies. *Int. J. Mol. Sci.* **2019**, *20* (24), 6133. <https://doi.org/10.3390/ijms20246133>.
- (191) Yokota, S.; Ohtsuka, H.; Noguchi, H. Monoclonal Antibodies against *Pseudomonas Aeruginosa* Elastase: A Neutralizing Antibody Which Recognizes a Conformational Epitope Related to an Active Site of Elastase. *Eur. J. Biochem.* **1992**, *206* (2), 587–593. <https://doi.org/10.1111/j.1432-1033.1992.tb16963.x>.
- (192) Cathcart, G. R. A.; Quinn, D.; Greer, B.; Harriott, P.; Lynas, J. F.; Gilmore, B. F.; Walker, B. Novel Inhibitors of the *Pseudomonas Aeruginosa* Virulence Factor LasB: A Potential Therapeutic Approach for the Attenuation of Virulence Mechanisms in Pseudomonas Infection. *Antimicrob. Agents Chemother.* **2011**, *55* (6), 2670–2678. <https://doi.org/10.1128/AAC.00776-10>.
- (193) Zhu, J.; Cai, X.; Harris, T. L.; Gooyit, M.; Wood, M.; Lardy, M.; Janda, K. D. Disarming *Pseudomonas Aeruginosa* Virulence Factor LasB by Leveraging a *Caenorhabditis Elegans* Infection Model. *Chem. Biol.* **2015**, *22* (4), 483–491. <https://doi.org/10.1016/j.chembiol.2015.03.012>.
- (194) Kany, A. M.; Sikandar, A.; Haupenthal, J.; Yahiaoui, S.; Maurer, C. K.; Proschak, E.; Köhnke, J.; Hartmann, R. W. Binding Mode Characterization and Early in Vivo Evaluation of Fragment-Like



## VI. References

- Thiols as Inhibitors of the Virulence Factor LasB from *Pseudomonas Aeruginosa*. *ACS Infect. Dis.* **2018**, *4* (6), 988–997. <https://doi.org/10.1021/acsinfecdis.8b00010>.
- (195) Kany, A. M.; Sikandar, A.; Yahiaoui, S.; Hauptenthal, J.; Walter, I.; Empting, M.; Köhnke, J.; Hartmann, R. W. Tackling *Pseudomonas Aeruginosa* Virulence by a Hydroxamic Acid-Based LasB Inhibitor. *ACS Chem. Biol.* **2018**, *13* (9), 2449–2455. <https://doi.org/10.1021/acschembio.8b00257>.
- (196) Kaya, C.; Walter, I.; Yahiaoui, S.; Sikandar, A.; Alhayek, A.; Konstantinović, J.; Kany, A. M.; Hauptenthal, J.; Köhnke, J.; Hartmann, R. W.; Hirsch, A. K. H. Substrate-inspired Fragment Merging and Growing Affords Efficacious LasB Inhibitors. *Angew. Chem. Int. Ed.* **2022**, *61*, e202112295. <https://doi.org/10.1002/anie.202112295>.
- (197) Kaya, C.; Walter, I.; Alhayek, A.; Shafiei, R.; Jézéquel, G.; Andreas, A.; Konstantinović, J.; Schönauer, E.; Sikandar, A.; Hauptenthal, J.; Müller, R.; Brandstetter, H.; Hartmann, R. W.; Hirsch, A. K. H. Structure-Based Design of  $\alpha$ -Substituted Mercaptoacetamides as Inhibitors of the Virulence Factor LasB from *Pseudomonas Aeruginosa*. *ACS Infect. Dis.* **2022**, *8* (5), 1010–1021. <https://doi.org/10.1021/acsinfecdis.1c00628>.
- (198) Kany, A. Development of Pathoblockers by Targeting Secreted Bacterial Proteases, Universität des Saarlandes, Saarbrücken, 2018.
- (199) Hagemans, D.; van Belzen, I. A. E. M.; Morán Luengo, T.; Rüdiger, S. G. D. A Script to Highlight Hydrophobicity and Charge on Protein Surfaces. *Front. Mol. Biosci.* **2015**, *2*, 56. <https://doi.org/10.3389/fmolb.2015.00056>.
- (200) Kiem, S.; Schentag, J. J. Interpretation of Antibiotic Concentration Ratios Measured in Epithelial Lining Fluid. *Antimicrob. Agents Chemother.* **2008**, *52* (1), 24–36. <https://doi.org/10.1128/AAC.00133-06>.
- (201) Konstantinović, J.; Yahiaoui, S.; Alhayek, A.; Hauptenthal, J.; Schönauer, E.; Andreas, A.; Kany, A. M.; Mueller, R.; Köhnke, J.; Berger, F.; Bischoff, M.; Hartmann, R. W.; Brandstetter, H.; Hirsch, A. K. H. N-Aryl-3-Mercaptosuccinimides as Antivirulence Agents Targeting *Pseudomonas Aeruginosa* Elastase and *Clostridium* Collagenases. *J. Med. Chem.* **2020**, acs.jmedchem.0c00584. <https://doi.org/10.1021/acs.jmedchem.0c00584>.
- (202) Schütz, C.; Ho, D.; Hamed, M. M.; Abdelsamie, A. S.; Röhrig, T.; Herr, C.; Kany, A. M.; Rox, K.; Schmelz, S.; Siebenbürger, L.; Wirth, M.; Börger, C.; Yahiaoui, S.; Bals, R.; Scrima, A.; Blankenfeldt, W.; Horstmann, J. C.; Christmann, R.; Murgia, X.; Koch, M.; Berwanger, A.; Loretz, B.; Hirsch, A. K. H.; Hartmann, R. W.; Lehr, C.; Empting, M. A New PqsR Inverse Agonist Potentiates Tobramycin Efficacy to Eradicate *Pseudomonas Aeruginosa* Biofilms. *Adv. Sci.* **2021**, *8* (12), 2004369. <https://doi.org/10.1002/advs.202004369>.
- (203) Henczi, M.; Weaver, D. F. An Improved Synthesis of N $\epsilon$ -Fmoc-L-Lysine and N $\delta$ -Fmoc-L-Ornithine. *Org. Prep. Proced. Int.* **1994**, *26* (5), 578–580. <https://doi.org/10.1080/00304949409458061>.
- (204) Raghava Reddy, A. V. Synthesis and Characterization of Compounds Related to Lisinopril. *Sci. Pharm.* **2016**, *84* (2), 269–278. <https://doi.org/10.3797/scipharm.1507-08>.
- (205) Aviron-Violet, P.; Gervais, C. Process for the n-omega-trifluoroacetylation of alpha, omega-saturated aliphatic diamino-monocarboxylic acids. EP0279716, April 17, 1991. <https://register.epo.org/application?number=EP88400088&tab=main>.
- (206) Brady, W. T.; Owens, R. A. Reactions of  $\alpha$ -Halo Acid Chlorides with Diisopropylcarbodiimide. 5-Oxazolidinones. *J. Org. Chem.* **1977**, *42* (20), 3220–3222.
- (207) Dahmen, S. Synthese Neuer Potentieller Pathoblocker Gegen Clostridien-Infektionen. Masterarbeit, Universität des Saarlandes, Saarbrücken, 2021.
- (208) Kabsch, W. XDS. *Acta Crystallogr., Sect. D: Biol. Crystallogr.* **2010**, *66* (2), 125–132. <https://doi.org/10.1107/S0907444909047337>.
- (209) Evans, P. R.; Murshudov, G. N. How Good Are My Data and What Is the Resolution? *Acta Crystallogr., Sect. D: Biol. Crystallogr.* **2013**, *69* (7), 1204–1214. <https://doi.org/10.1107/S0907444913000061>.

## VI. References

- (210) McCoy, A. J. Solving Structures of Protein Complexes by Molecular Replacement with *Phaser*. *Acta Cryst.* **2007**, *D63* (1), 32–41. <https://doi.org/10.1107/S0907444906045975>.
- (211) Adams, P. D.; Afonine, P. V.; Bunkóczi, G.; Chen, V. B.; Davis, I. W.; Echols, N.; Headd, J. J.; Hung, L.-W.; Kapral, G. J.; Grosse-Kunstleve, R. W.; McCoy, A. J.; Moriarty, N. W.; Oeffner, R.; Read, R. J.; Richardson, D. C.; Richardson, J. S.; Terwilliger, T. C.; Zwart, P. H. *PHENIX*: A Comprehensive Python-Based System for Macromolecular Structure Solution. *Acta Cryst.* **2010**, *D66* (2), 213–221. <https://doi.org/10.1107/S0907444909052925>.
- (212) Emsley, P.; Lohkamp, B.; Scott, W. G.; Cowtan, K. Features and Development of *Coot*. *Acta Cryst.* **2010**, *D66* (4), 486–501. <https://doi.org/10.1107/S0907444910007493>.
- (213) Kany, A. M.; Sikandar, A.; Hauptenthal, J.; Yahiaoui, S.; Maurer, C. K.; Proschak, E.; Köhnke, J.; Hartmann, R. W. Binding Mode Characterization and Early *in Vivo* Evaluation of Fragment-Like Thiols as Inhibitors of the Virulence Factor LasB from *Pseudomonas Aeruginosa*. *ACS Infect. Dis.* **2018**, *4* (6), 988–997. <https://doi.org/10.1021/acsinfecdis.8b00010>.
- (214) Yiotakis, A.; Lecoq, A.; Nicolaou, A.; Labadie, J.; Dive, V. Phosphinic Peptide Analogues as Potent Inhibitors of *Corynebacterium Rathayii* Bacterial Collagenase. *Biochem. J.* **1994**, *303* (1), 323–327. <https://doi.org/10.1042/bj3030323>.
- (215) Congreve, M.; Carr, R.; Murray, C.; Jhoti, H. A ‘Rule of Three’ for Fragment-Based Lead Discovery? *Drug Discov. Today* **2003**, *8* (19), 876–877. [https://doi.org/10.1016/S1359-6446\(03\)02831-9](https://doi.org/10.1016/S1359-6446(03)02831-9).
- (216) Kaya, C.; Konstantinović, J.; Kany, A. M.; Andreas, A.; Kramer, J. S.; Brunst, S.; Weizel, L.; Rotter, M. J.; Frank, D.; Yahiaoui, S.; Müller, R.; Hartmann, R. W.; Hauptenthal, J.; Proschak, E.; Wichelhaus, T. A.; Hirsch, A. K. H. *N*-Aryl Mercaptopropionamides as Broad-Spectrum Inhibitors of Metallo- $\beta$ -Lactamases. *J. Med. Chem.* **2022**, *65* (5), 3913–3922. <https://doi.org/10.1021/acs.jmedchem.1c01755>.

**APPENDIX**

***Synthesis of  
Bacterial Protease Inhibitors as new  
Antibiotics***

**TABLE OF CONTENTS**

<b>Table of Contents</b> .....	<b>2</b>
<b>A1. Supporting Information to Chapter A</b> .....	<b>3</b>
<b>A2. Supporting Information to Chapter B</b> .....	<b>23</b>
<b>A3. Supporting Information to Chapter C</b> .....	<b>52</b>
<b>A4. Supporting Information to Chapter D</b> .....	<b>67</b>
<b>A5. Supporting Information to Chapter E</b> .....	<b>109</b>
<b>A6. Supporting Information to Chapter F</b> .....	<b>164</b>
1. General Procedures.....	165
2. Compounds 16, 20, 22–31 (already published).....	166
3. Synthesis of compounds 32–55.....	166
4. HPLC procedures.....	174
5. PK Sample Preparation and Analysis.....	175
<b>A7. Supporting Information to Chapter G</b> .....	<b>177</b>
1. General Procedures.....	178
2. Compounds 66, 67 and 93–99.....	179
3. Synthesis of compounds 72–74, 77–92.....	180
4. HPLC procedures.....	188
<b>Danksagung</b> .....	<b>190</b>

## A1. SUPPORTING INFORMATION TO CHAPTER A

### **Discovery of a Potent Inhibitor Class with High Selectivity toward Clostridial Collagenases.**

Esther Schönauer,<sup>±</sup> Andreas M. Kany,<sup>±</sup> Jörg Haupenthal, Kristina Hüsecken, Isabel J. Hoppe, Katrin Voos, Samir Yahiaoui, Brigitta Elsässer, Christian Ducho, Hans Brandstetter\* and Rolf W. Hartmann\*

<sup>±</sup> these authors contributed equally

\* corresponding authors

Reprinted with permission from *J. Am. Chem. Soc.* **2017**, *139*, 12696–12703.

DOI:10.1021/jacs.7b06935

Copyright (2017) American Chemical Society

## **Discovery of a potent inhibitor class with high selectivity towards clostridial collagenases**

Esther Schönauer†‡, Andreas M. Kany†‡, Jörg Hauptenthal‡, Kristina Hüsecken‡, Isabel J.

Hoppe†, Katrin Voos§, Samir Yahiaoui‡, Brigitta Elsässer†, Christian Ducho§, Hans

Brandstetter†\*, Rolf W. Hartmann‡§\*

† Division of Structural Biology, Department of Molecular Biology, University of Salzburg, Billrothstr. 11, 5020 Salzburg, Austria

‡ Helmholtz Institute for Pharmaceutical Research Saarland (HIPS), Department of Drug Design and Optimization, Campus E8.1, 66123, Saarbrücken, Germany

§ Department of Pharmacy, Pharmaceutical and Medicinal Chemistry, Saarland University, Campus C2.3, 66123 Saarbrücken, Germany

## Table of Contents

1. Supporting Figures and Tables	S2
2. Experimental Section	S10
3. References	S19

### 1. Supporting Figures and Tables

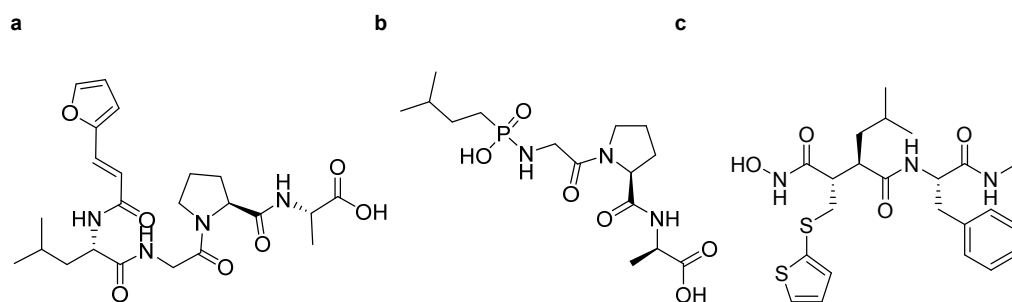


**Figure S1.** Molecular structures of the positive-control compounds (a) FALGPA, (b) isoamylphosphonyl-Gly-Pro-Ala and (c) batimastat.

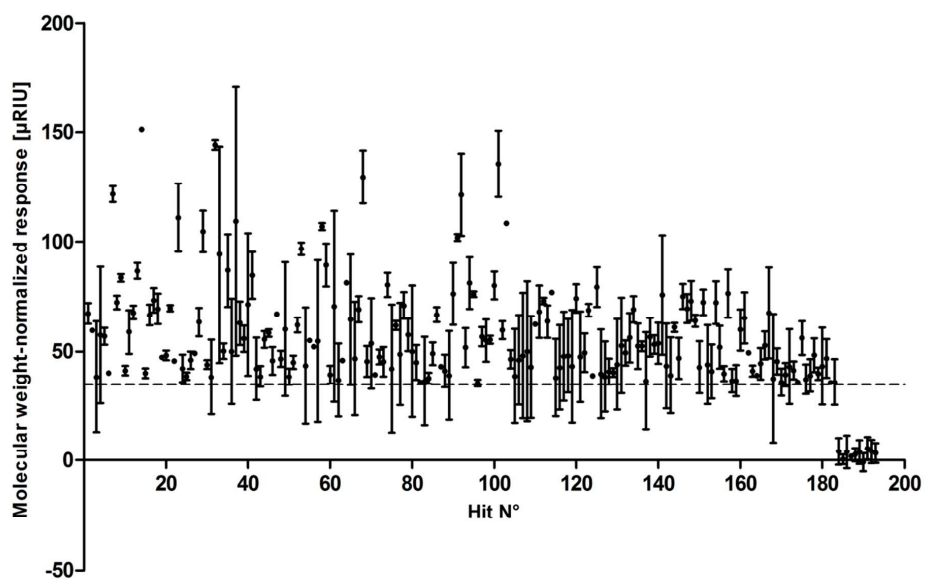


**Figure S2.** SPR screening for ColH inhibitor discovery. Screening data for 183 hits and 10 selected non-hits of the TimTec Acti-Targ-P library are shown. Compounds at 100  $\mu\text{M}$  that showed a higher response than 500  $\mu\text{M}$  FALGPA (35  $\mu\text{RIU}$ ; line) were designated as hits.

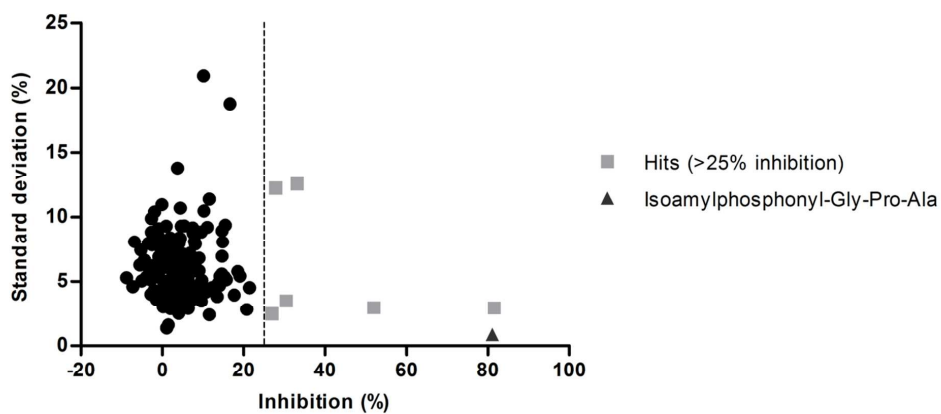


**Figure S3.** Functional screening hits of the peptidolytic activity of ColH-PD. Compounds were screened at 40  $\mu\text{M}$ .



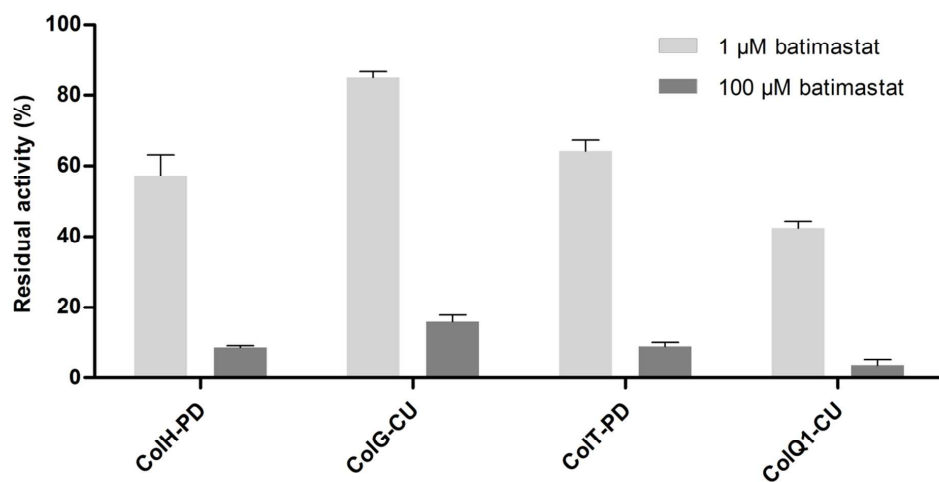


Figure S4. Inhibition of bacterial collagenases by batimastat.

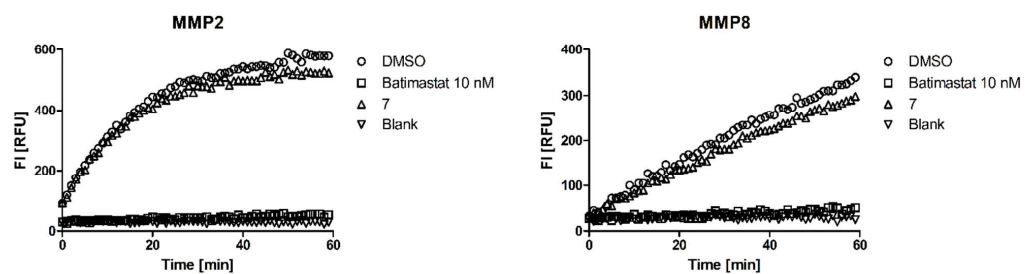


Figure S5. MMP inhibition assay. Exemplary representation of fluorescence intensity curves indicating protease activity of MMP-2 and -8. The influence of selected compounds on MMP activity is shown. The fluorescence intensity at 520 nm was determined every 60 s for a period of one hour.

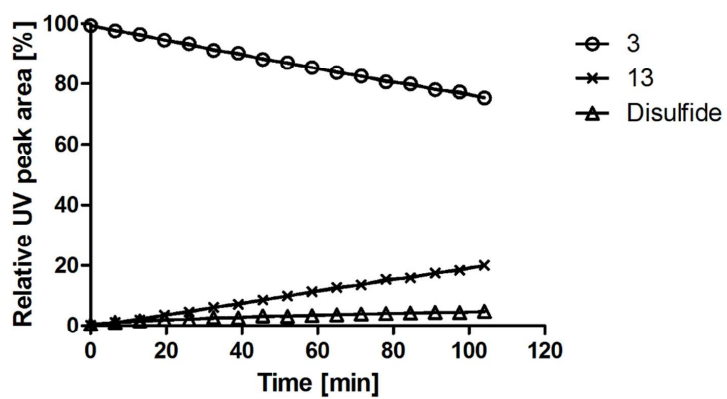


Figure S6. LC-MS stability assay of cp. **3** in 10 mM MES pH 7.4 (10% methanol) at 22.5°C.

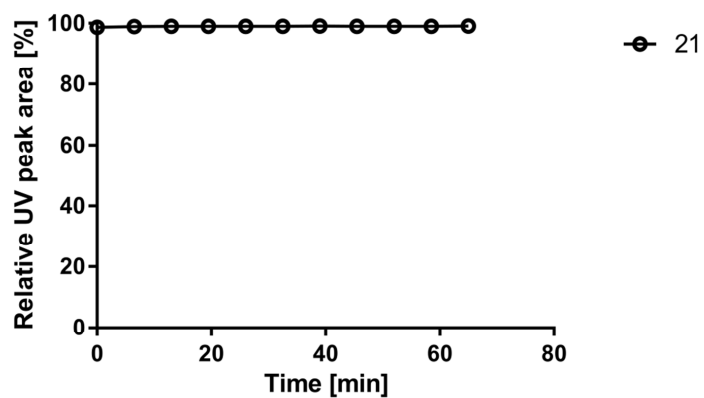
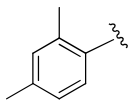
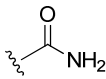
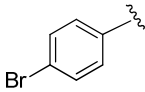
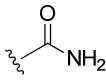
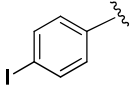
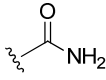
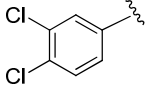
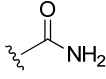
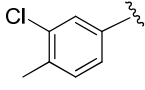
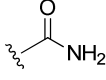
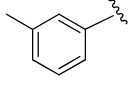
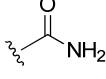
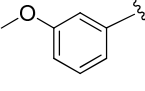
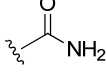
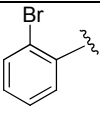
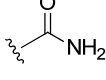
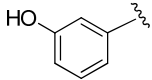
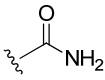
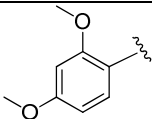
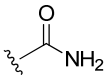
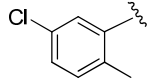
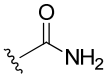
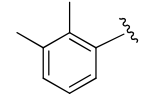
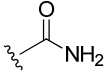
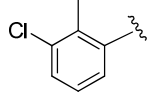
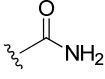
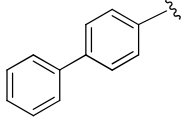
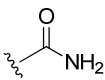
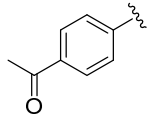
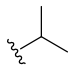
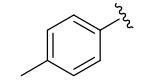
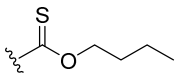


Figure S7. LC-MS stability assay of dithiocarbamate **21** in 10 mM HEPES pH 7.4 (10% methanol) at 22.5°C, illustrating that the dithiocarbamates are stable within the experimental time frame as no hydrolysis to the corresponding free thiol **13** occurs.

**Table S1.** Structure and activity of thiocarbamates and related compounds.

$\text{R}_1\text{-NH-CO-CH}_2\text{-S-R}_2$			
Compound	R <sub>1</sub>	R <sub>2</sub>	Inhibition at 100 μM (%)
22			90 ± 3
23			89 ± 5
24			89 ± 2
25			86 ± 2
26			85 ± 2
27			75 ± 1
28			72 ± 1
29			71 ± 4

30			$69 \pm 2$
31			$68 \pm 6$
32			$49 \pm 6$
33			$44 \pm 6$
34			$39 \pm 9$
35			$28 \pm 10$
36			$13 \pm 3$
37			no inhibition

**Table S2.** IC<sub>50</sub> values of batimastat towards MMP-1, -2, -3, -7, -8 and -14

	IC <sub>50</sub> (nM)
MMP-1	2.2 ± 0.1
MMP-2	1.8 ± 0.1
MMP-3	5.6 ± 0.9
MMP-7	7.0 ± 0.2
MMP-8	0.7 ± 0.2
MMP-14	2.8 ± 0.2

**Table S3.** Data collection and refinement statistics for ColH-PD in complex with compound **3**.

Data collection	
Space Group	P 1 2 <sub>1</sub> 1
Cell dimensions	
a (Å)	51.3
b (Å)	79.7
c (Å)	57.0
α (°)	90.0
β (°)	91.2
γ (°)	90.0
Wavelength (Å)	0.97623
Resolution range (Å)	46.33 - 1.87 (1.937 - 1.87) <sup>a</sup>
R <sub>merge</sub>	0.083 (0.636)
Mean I/sigma(I)	8.7 (1.9)
Completeness (%)	99.6 (99.8)
Multiplicity	3.5 (3.6)
CC <sub>1/2</sub>	0.998 (0.771)
CC*	0.999 (0.933)
Wilson B-factor	21.73

Refinement	
<b>Resolution range (Å)</b>	<b>46.33 - 1.87 (1.937 - 1.87)</b>
<b>No. of unique reflections</b>	<b>37834 (3810)</b>
<b>R<sub>work</sub>/R<sub>free</sub></b>	<b>0.1903/0.2264</b>
<b>No. of non-hydrogen atoms</b>	<b>3258</b>
<b>Protein</b>	<b>3129</b>
<b>Ligand</b>	<b>16</b>
<b>Solvent</b>	<b>113</b>
<b>B factors</b>	
<b>Protein</b>	<b>25.70</b>
<b>Ligand</b>	<b>29.00</b>
<b>Solvent</b>	<b>23.80</b>
<b>RMSD</b>	
<b>Bond lengths (Å)</b>	<b>0.005</b>
<b>Bond angles (°)</b>	<b>0.82</b>
<b>Ramachandran favoured (%)</b>	<b>99.5</b>
<b>Ramachandran allowed (%)</b>	<b>0.5</b>
<b>Ramachandran outliers (%)</b>	<b>0.0</b>

<sup>a</sup> Statistics for the highest-resolution shell are shown in parentheses.

## 2. Experimental Section

**Protein Expression and Purification of ColH-PD.** The peptidase domain of ColH (Uniprot: Q46085; Leu331-Gly721) was expressed and purified as published previously<sup>1</sup>. The homogeneous protein, as judged by SDS-PAGE and size-exclusion chromatography, was flash-frozen in thin-walled PCR tubes at 12.3 mg/mL concentration in 10  $\mu$ L aliquots in 10 mM Hepes pH 7.5, 100 mM NaCl, 1 mM CaCl<sub>2</sub>, 3% (v/v) glycerol, and 3 mM NaN<sub>3</sub>. For functional assays, the protein samples were prepared immediately before usage. After thawing, the protein solution was clarified by centrifugation at 13,000 g at 4°C for 30 min and protein concentrations were determined by UV<sub>280</sub> measurements using the molar extinction coefficient calculated by ProtParam ( $\epsilon = 77130 \text{ M}^{-1} \text{ cm}^{-1}$ )<sup>2</sup>.

**Screening Library.** The screening library comprising 1,520 low-molecular weight compounds was purchased from TimTec (Newark, DE, USA). The compounds had an average molecular weight (MW) of 390 Da and were provided as 10 mM stock solutions in DMSO.

**SPR-based Primary Screening.** The surface plasmon resonance experiments were performed using a Reichert SR 7500DC equipped with CMD500m sensor chip (Xantec Bioanalytics, Düsseldorf, Germany). For immobilization, standard amine coupling chemistry was applied. Both channels were activated for 7 min with a mixture of 0.1 M NHS (*N*-hydroxysuccinimide) and 0.1 M EDC (3-(Ethyl-iminomethyleneamino)-*N,N*-dimethylpropan-1-amine) at a flow rate of 10  $\mu$ L/min. The peptidase domain of ColH (1 mg/mL; 45.8 kDa; crystallization grade) was diluted 1:20 in 10 mM sodium acetate buffer pH 4.0 and coupled to the sensor surface via standard amine coupling chemistry on one of the channels to 15-20,000  $\mu$ RIU. Flow cell 2 was left blank to serve as a reference surface. Both channels were blocked with a 3 min injection of 1 M ethanolamine, pH 8.0. The 1,520 analytes were diluted in running buffer (10 mM Hepes pH 7.4, 150 mM NaCl, 0.005 % (v/v) Tween 20, 5 % (v/v) DMSO) to a final concentration of 100  $\mu$ M. The screening was run at 18 °C and a flow rate of 50  $\mu$ L/min. An initial series of buffer injections was carried out on both flow cells to equilibrate the system. Each cycle consisted of a 60 s injection of 100  $\mu$ M analyte, followed by a 120 s dissociation phase. Every 12 injections included 500  $\mu$ M FALGPA (*N*-[3-(2-furyl)acryloyl]-Leu-Gly-Pro-Ala) as positive and 100  $\mu$ M ampicillin as negative control. All screening experiments comprised two seven-point DMSO injections, to produce a DMSO calibration curve in order to correct differences in solvent effects on empty and target surface. They consisted of 60 s injections ranging from 4.25 to 5.75 % (v/v) DMSO. Data were zeroed, referenced, and calibrated using Scrubber 2.0 software. SPR responses, expressed in refractive index units [ $\mu$ RIU] that were used for analysis correspond to the corrected response recorded 45 s after start of the injection.

**Determination of Kinetic Parameters.** Steady state measurements were used to determine  $K_M$  for the custom-made FRET substrate Mca-Ala-Gly-Pro-Pro-Gly-Pro-Dpa-Gly-Arg-NH<sub>2</sub> (FS1-1) (Mca = (7-Methoxycoumarin-4-yl)acetyl; Dpa = *N*-3-(2,4-dinitrophenyl)-*L*-2,3-diaminopropionyl). The substrate was dissolved in DMSO. The enzymatic reaction was started by adding

S10

ColH-PD to a final concentration of 2, 4, and 6 nM. The final reaction buffer contained 250 mM Hepes pH 7.5, 400 mM NaCl, 10 mM CaCl<sub>2</sub>, 10 μM ZnCl<sub>2</sub>, 2% DMSO, and 2.5 – 120 μM substrate. Cleavage of the substrate was followed by measuring the fluorescence signal every 5 s for 2 min (Excitation: 328 nm, Emission: 392 nm) in an Infinite M200 plate reader (Tecan, Grödig, Austria) at 25°C. The initial velocity was determined from the progress curves (<10% substrate conversion) using regression analysis<sup>3</sup> and inner filter effect-correction<sup>4</sup>. The  $\epsilon_{\text{ex}328}$  and  $\epsilon_{\text{em}392}$  were estimated in the buffer used for the kinetic assays to be 21794 M<sup>-1</sup> cm<sup>-1</sup> and 9561 M<sup>-1</sup> cm<sup>-1</sup>.  $K_M$  and  $k_{\text{cat}}$  were calculated by non-linear regression from the resulting Michaelis – Menten plot using GraphPad Prism 5 (Graph Pad Software, San Diego, CA, USA).

**FRET-Based Inhibition Assay.** In the secondary screening, ColH-PD was pretreated with the compounds for 1 h at room temperature. The reaction was initiated by the addition of 5 μM FS1-1. The increase in fluorescence was monitored for 2 min (Excitation: 328 nm, Emission: 392 nm) at 25°C. The final concentrations were 50 nM ColH-PD, 40 μM compound or isoamylphosphonyl-Gly-Pro-Ala, 250 mM Hepes pH 7.5, 400 mM NaCl, 10 mM CaCl<sub>2</sub>, 10 μM ZnCl<sub>2</sub>, and 2% DMSO. In case of poor compound solubility, the DMSO concentration was increased, but never exceeded 4.8%. The percentage of enzyme inhibition was calculated in relation to a reference without a compound added, only plus buffer control. For IC<sub>50</sub> measurements, the experiments were performed as described above, but using 10 nM ColH-PD, 2 μM FS1-1, 2% DMSO and employing 8 different compound concentrations. The compound concentrations were chosen to be evenly distributed above and below the estimated IC<sub>50</sub>. All experiments were performed in triplicates and repeated at least three times. IC<sub>50</sub> values were determined using non-linear regression with a constant Hill slope of -1. In case of tight binding conditions ( $E_T \approx K_{i(\text{app})}$ ), the initial velocities were fit to the Morrison equation<sup>5</sup>. Enzyme concentration was held at a constant value  $E_T = 10$  nM (when  $K_{i(\text{app})} > E_T$ ), whereas  $v_0$  and  $K_{i(\text{app})}$  were treated as adjustable parameters<sup>6</sup>. IC<sub>50</sub> values are given as mean values of three independent experiments ± standard deviation. Reported apparent inhibition constants ( $K_{i(\text{app})}$ ) were measured under first-order conditions ( $S_0 \ll K_M$ ) and with  $K_{i(\text{app})}/E_T > 10^7$  and in the presence of 3.5% DMSO. Measurements under reducing conditions were performed in the presence of 5 mM TCEP. Regression analysis was performed using GraphPad Prism 5 (Graph Pad Software, San Diego, CA, USA) and DYNAFIT (BioKin, Ltd., Madison, WI, USA).

**Bacterial Collagenase Inhibition Assay.** These assays were performed as described above for the IC<sub>50</sub> measurements using 100 μM of the indicated compounds. The final enzyme concentrations used were 10 nM ColH-PD, 30 nM ColT-PD, 40 nM ColG-CU, and 2 nM ColQ1-CU, respectively.

**Human matrix metalloproteinases (MMP) inhibition assay.** The catalytic domains of MMP-1, -2, -3, -7, -8 and -14 along with the SensoLyte 520 Generic MMP Activity Kit were purchased from AnaSpec (Fremont, CA, USA). The assay was performed according to the guidelines of the manufacturer. Fluorescence signals were measured in a CLARIOstar plate reader (BMG LABTECH, Ortenberg, Germany) every 60 s for a period of 1 h. Compounds synthesized by us were tested at 100 μM. IC<sub>50</sub> values



were determined for the hydroxamate-based peptidomimetic batimastat which was used as a positive control. The calculation of the  $IC_{50}$  value was performed by plotting the percent inhibition vs. the different inhibitor concentrations on a semi-log plot. At least three independent measurements were performed for each compound.

**Isothermal Titration Calorimetry (ITC).** ITC experiments were carried out using an ITC200 instrument (Microcal Inc., GE Healthcare). Final ligand concentrations were obtained by dilution 1:20 (v/v) in the experimental buffer resulting in a final DMSO concentration of 5% (v/v). Protein concentration was determined by measuring the absorbance at 280 nm using the molar extinction coefficient calculated by ProtParam ( $\epsilon = 77130 \text{ M}^{-1} \text{ cm}^{-1}$ )<sup>2</sup>. DMSO concentration in the protein solution was adjusted to 5% (v/v). ITC measurements were routinely performed at 25 °C in 10 mM Hepes pH 7.5, 100 mM NaCl, 1 mM CaCl<sub>2</sub>, 3% (v/v) glycerol, and 3 mM NaN<sub>3</sub>. Titrations were performed on 40–50  $\mu\text{M}$  ColH peptidase domain in the 200  $\mu\text{L}$  sample cell using 2  $\mu\text{L}$  injections of 250–500  $\mu\text{M}$  ligand solution every 180 s. Raw data was collected and the area under each peak was integrated. To correct for heats of dilution and mixing, the final baseline consisting of small peaks of the same size at the end of the experiment was subtracted.

Experimental data was fitted to a theoretical titration curve (one site binding model) using MicroCal Origin 7 software, with  $\Delta H$  (enthalpy change in kcal mol<sup>-1</sup>),  $K_A$  (association constant in M<sup>-1</sup>), and N (number of binding sites) as adjustable parameters. Thermodynamic parameters were calculated from equation  $\Delta G = \Delta H - T\Delta S = RT \ln K_A = -RT \ln K_D$  where  $\Delta G$ ,  $\Delta H$ , and  $\Delta S$  are the changes in Gibbs free energy, enthalpy, and entropy of binding, respectively. T is the absolute temperature, and R = 1.98 cal mol<sup>-1</sup> K<sup>-1</sup>. For every sample, at least two independent measurements were performed.

**LC-MS method.** The stability assay was performed measuring the UV<sub>254</sub> chromatogram of 20  $\mu\text{M}$  thiocarbamate compound in 10 mM HEPES pH 7.5 or in 10 mM MES pH 6.4 in presence of 20  $\mu\text{M}$  caffeine as internal standard. Injections were performed every 6.5 minutes during 104 minutes in total. Samples of the respective free thiols to determine the retention time were analyzed before thiocarbamate injection using the same method. Compounds and ISTD were dissolved in MeOH and diluted 1:20 in assay buffer, respectively, giving a final volume of 200  $\mu\text{L}$  with a methanol concentration of 10% (v/v). The solution of internal standard in assay buffer was incubated at 22.5°C for at least 10 min before adding thiocarbamates. Measurements were started directly after compound addition.

The analyses were performed using a TF UltiMate 3000 binary RSLC UHPLC (Thermo Fisher, Dreieich, Germany) equipped with a degasser, a binary pump, an autosampler and a thermostated column compartment and a MWD, coupled to a TF TSQ Quantum Access Max mass spectrometer with heated electrospray ionization source (HESI-II). For gradient elution, a NUCLEODUR C18 Pyramid column (150 × 2 mm, 3  $\mu\text{m}$ , Macherey-Nagel, Düren, Germany) was used with a mobile phase consisting of acetonitrile containing 1% formic acid (FA; v/v; eluent A) and water containing 1% FA (v/v; eluent B) and a flow rate of 600  $\mu\text{L}/\text{min}$  under the following conditions: 0 – 0.5 min 10% A, 0.5 – 4 min 10 – 95% A, 4 – 5 min hold, 5 – 5.5 min 10% A for column equilibra-

S12

tion giving a total run time of 5.5 min. The injection volume was 5  $\mu$ L. The divert valve was set to 1.5 min. Before injecting samples the column was equilibrated with 10% methanol (v/v) in assay buffer using this method.

For UV detection we monitored the following wavelengths: 254 nm, 272 nm and 290 nm. The following MS conditions were used: electrospray ionization (ESI), positive mode, sheath gas, nitrogen at a flow rate of 60 arbitrary units; auxiliary gas, nitrogen at flow rate of 20 arbitrary units; vaporizer temperature, 300 °C; ion transfer capillary temperature, 350 °C; capillary offset, 15 V; spray voltage, 3500 V. The mass spectrometer was operated in the SIM mode with the following masses: caffeine  $m/z$  194.0 (tube lens offset 100 V), cp. **3**  $m/z$  252.1, cp. **7/12**  $m/z$  245.0 (tube lens offset 88 V), cp. **13**  $m/z$  252.1, cp. **14/15**  $m/z$  202.1 (tube lens offset 129 V) with a scan width of  $m/z$  2.0 and a scan time of 0.1 s, respectively. Three independent measurements were performed.

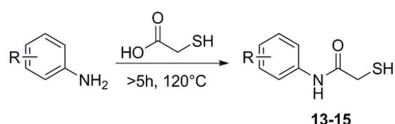
Observed retention times were as follows: caffeine 2.29 min, cp. **3** 2.68, cp. **12** 3.08 min, cp. **7** 3.22 min, cp. **13** 3.00 min, cp. **14** 3.57 min, cp. **15** 3.52 min. Additional peaks were found at 3.51 min, 4.32 min and 4.19 min for cp. **13**, **14** and **15**, respectively, hinting at disulfide formation. Peak areas were determined using TF Xcalibur Software. Peak areas were normalized by ISTD peak area and divided by total peak area. Half-life was determined using a one-phase decay model (GraphPad Prism 5 software).

**Cytotoxicity assay.** Hep G2 cells ( $2 \times 10^5$  cells per well) were seeded in 24-well, flat-bottomed plates. Culturing of cells, incubations and OD measurements were performed as described previously<sup>8</sup> with small modifications. 24 h after seeding the cells the incubation was started by the addition of compounds in a final DMSO concentration of 1%. The living cell mass was determined after 48 h. At least two independent measurements were performed for each compound.

**Co-Crystallization, X-ray Data Collection and Analysis.** Prior to crystallization, 4 mg/mL ColH-PD were preincubated with 260  $\mu$ M compound **3** in 8 mM Hepes pH 7.5, 33 mM NaCl, 0.33 mM CaCl<sub>2</sub>, and 2% DMSO for 1 h on ice and then clarified by centrifugation for 30 min at 13,000 g at 4°C. The co-crystal was grown by the sitting drop vapour diffusion method by mixing 1  $\mu$ L protein-inhibitor solution with 1  $\mu$ L reservoir solution. The reservoir contained 0.1 M MES pH 6.4, 25% w/v polyethylene glycol methyl ether 2000, and 50 mM NaCl. The drop was streak-seeded from crystals of unliganded ColH-PD<sup>9</sup>. Crystals appeared within several days. The crystals were cryoprotected with MiTeGen LV Cryo-oil (MiTeGen, Ithaca, NY) and immediately flash-frozen in liquid nitrogen. X-ray diffraction data were collected on beamline ID29 at the European Synchrotron Radiation Facility (ESRF) in Grenoble, France. The data set was processed using XDS<sup>10</sup> and AIMLESS<sup>11</sup>. The phase problem was solved by molecular replacement with PHASER<sup>12</sup> using a ColH-PD structure as search model (PDB code 4arf; ligand deleted). Final structures were obtained by several refinement cycles using PHENIX<sup>13</sup> interspersed with model building in WinCoot<sup>14</sup>. The PyMOL Molecular Graphics System, version 1.7.6.0, Schrodinger, LLC, was used for (i) figure generation, (ii) calculation of RMSD values (apo ColH-PD: 4ar1, MMP1: 3shi) and (iii) for comparison of ligand-bound edge strand conformations (MMP-1: 1hfc, MMP-2: 3ayu, MMP-3: 1b8y, MMP8: 1i76, MMP-12: 1jjz, MMP-13: 4jpd, ColT: 4ar8, ColG: 2y6i)<sup>15</sup>. The final refined structure of ColH-PD in complex with compound **3** was deposited in the Protein Data Bank (PDB) as entry 5O7E.

S13

**Chemistry. General Procedures.** Compounds **2-12** and **21-37** were commercially available (ChemBridge, San Diego, CA, USA). Synthesis of free thiols **13-15** was achieved by treating the respective anilines with thioglycolic acid in a neat reaction (see Scheme Si).<sup>16</sup> Selected thiocarbamates were synthesized according to the procedures described below.

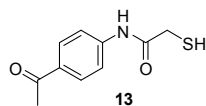


**Scheme Si.** Synthesis of free thiol compounds **13-15**.

All reagents were used from commercial suppliers without further purification. Procedures were not optimized regarding yield. NMR spectra were recorded on a Bruker Fourier 300 (300 MHz) spectrometer. Chemical shifts are given in parts per million (ppm) and referenced against the residual proton, <sup>1</sup>H, or carbon, <sup>13</sup>C, resonances of the >99% deuterated solvents as internal reference. Coupling constants (J) are given in Hertz. Data are reported as follows: chemical shift, multiplicity (s = singlet, d = doublet, t = triplet, m = multiplet, br = broad and combinations of these) coupling constants and integration. Mass spectrometry was performed on a SpectraSystems-MSQ LCMS system (Thermo Fisher, Dreieich, Germany). Flash chromatography was performed on silica gel 60 M, 0.04 - 0.063 mm (Machery-Nagel, Düren, Germany) or using the automated flash chromatography system CombiFlash Rf+ (Teledyne Isco, Lincoln, NE, USA) equipped with RediSepRf silica columns (Axel Semrau, Sprockhövel Germany) or Chromabond Flash C<sub>18</sub> columns (Machery-Nagel, Düren, Germany). Purity of compounds synthesized by us was determined by LCMS using the area percentage method on the UV trace recorded at a wavelength of 254 nm and found to be >95%.

### Thiol synthesis

*N*-(4-acetylphenyl)-2-mercaptoacetamide (**13**)

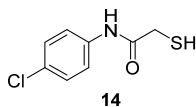


4'-Aminoacetophenone (300 mg, 2.21 mmol) was placed in a crimp vial. The vial was evacuated and flushed with nitrogen three times, followed by addition of thioglycolic acid (160  $\mu$ L, 2.3 mmol). The vial was flushed with argon and heated to 120°C for 18 hours. The crude was purified by automated flash chromatography (petroleum ether:ethyl acetate 70:30 to 0:100) to yield the

S14

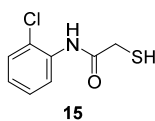
title compound as a white powder (50 mg, 11%). <sup>1</sup>H NMR (300 MHz, Methanol-d<sub>4</sub>) δ ppm 2.58 (s, 3 H), 3.34 (s, 2 H), 7.69 - 7.77 (m, 2 H), 7.95 - 8.03 (m, 2 H); <sup>13</sup>C NMR (75 MHz, Methanol-d<sub>4</sub>) δ ppm 26.61, 29.55, 120.32, 130.89, 134.09, 144.75, 172.04, 199.56; MS (ESI<sup>+</sup>) *m/z* 210 (M+H)<sup>+</sup>

*N*-(4-chlorophenyl)-2-mercaptoacetamide (**14**)



4-chloroaniline (200 mg, 1.57 mmol) was placed in a crimp vial. The vial was evacuated and flushed with nitrogen three times, followed by addition of thioglycolic acid (120 μL, 1.72 mmol). The vial was flushed with argon and heated to 120°C for 5 hours. The crude was purified by flash chromatography (petroleum ether:ethyl acetate 90:10 to 70:30) to yield the title compound as a white powder (187 mg, 59%). <sup>1</sup>H NMR (300 MHz, DMSO-d<sub>6</sub>) δ ppm 2.97 (br s, 1 H) 3.29 (s, 2 H) 7.30 - 7.42 (m, 2 H) 7.53 - 7.68 (m, 2 H) 10.21 (s, 1 H); <sup>13</sup>C NMR (75 MHz, DMSO-d<sub>6</sub>) δ ppm 28.24, 120.61, 126.92, 128.67, 137.92, 168.72; MS (ESI<sup>+</sup>) *m/z* 202 (M+H)<sup>+</sup>

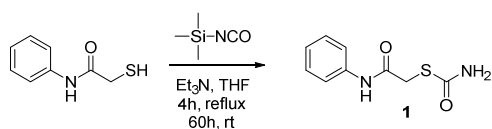
*N*-(2-chlorophenyl)-2-mercaptoacetamide (**15**)



2-chloroaniline (164 μL, 1.57 mmol) was placed in a crimp vial. The vial was evacuated and flushed with nitrogen three times, followed by addition of thioglycolic acid (120 μL, 1.72 mmol). The vial was flushed with argon and heated to 120°C for 5 hours. The crude was purified by automated flash chromatography (petroleum ether:ethyl acetate 70:30 to 50:50) to yield the title compound as a white powder (160 mg, 51%). <sup>1</sup>H NMR (300 MHz, DMSO-d<sub>6</sub>) δ ppm 3.02 (s, 1 H), 7.19 (dt, *J* = 7.6, 1.7 Hz, 1 H), 7.33 (dt, *J* = 7.6, 1.4 Hz, 1 H), 7.50 (dd, *J* = 8.0, 1.5 Hz, 1 H), 7.80 (dd, *J* = 8.1, 1.4 Hz, 1 H), 9.66 (br. s., 1 H), <sup>13</sup>C NMR (75 MHz, DMSO-d<sub>6</sub>) δ ppm 27.79, 125.23, 125.81, 126.20, 127.48, 129.45, 134.62, 168.93; MS (ESI<sup>+</sup>) *m/z* 202 (M+H)<sup>+</sup>

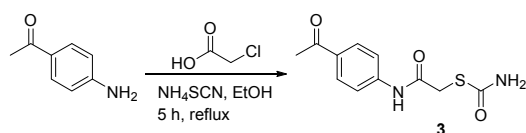
#### Thiocarbamate synthesis

*S*-(2-oxo-2-(phenylamino)ethyl) carbamothioate (**1**)



Under nitrogen atmosphere, *N*-phenyl-2-mercaptoacetamide (209 mg, 1.25 mmol) was dissolved in 20 mL dry THF and triethylamine (200  $\mu$ L, 1.44 mmol) and trimethylsilyl isocyanate (200  $\mu$ L, 1.48 mmol) were added. The reaction mixture was refluxed for 4 hours and then stirred at room temperature for 60 hours. After that, the reaction was quenched for 30 min with methanol. The crude was purified using flash chromatography (petroleum ether:ethyl acetate 7:3) to yield the title compound as a white powder (50 mg, 19%).  $^1\text{H}$  NMR (500 MHz,  $\text{DMSO-d}_6$ )  $\delta$  ppm 3.69 (s, 2H), 7.04 (t,  $J = 7.4$  Hz, 1H), 7.30 (t,  $J = 7.1$  Hz, 2H), 7.57 (dd,  $J = 8.4$ , 0.8 Hz, 2H), 7.40-7.90 (b, 2H), 10.09 (s, 1H);  $^{13}\text{C}$  NMR (126 MHz,  $\text{DMSO-d}_6$ )  $\delta$  ppm 34.10, 119.03, 123.31, 128.75, 139.02, 166.24, 166.89; MS (ESI $^+$ )  $m/z$  211 (M+H) $^+$

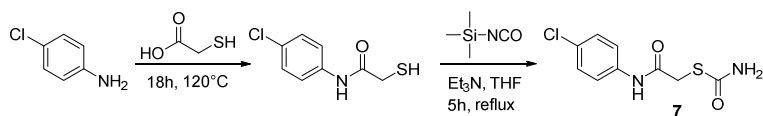
*S*-(2-((4-acetylphenyl)amino)-2-oxoethyl) carbamothioate (3)



Following the procedure described by Koulberg<sup>17</sup> 4'-Aminoacetophenone (200 mg, 1.5 mmol) was added to a solution of chloroacetic acid (140 mg, 1.5 mmol) and ammonium thiocyanate (90 mg, 1.5 mmol) in 5 mL absolute ethanol. The reaction was refluxed for 5 hours and then stirred at room temperature for 14 hours. Addition of water, followed by extraction with ethyl acetate gave the crude which was purified using automated flash chromatography (acetonitrile + 0.1% formic acid:water + 0.1% formic acid 5:95 to 70:30) to yield the title compound as a white powder (39 mg, 10%).

$^1\text{H}$  NMR (300 MHz,  $\text{DMSO-d}_6$ )  $\delta$  ppm 2.52 (s, 3 H), 3.74 (s, 2 H), 7.50 - 7.87 (br s, 2H), 7.67 - 7.74 (m, 2 H), 7.89 - 7.97 (m, 2 H), 10.46 (s, 1 H);  $^{13}\text{C}$  NMR (75 MHz,  $\text{DMSO-d}_6$ )  $\delta$  ppm 26.39, 34.19, 118.27, 129.48, 131.74, 143.28, 166.08, 167.52, 196.46; MS (ESI $^+$ )  $m/z$  253 (M+H) $^+$

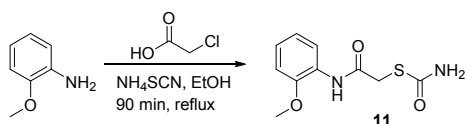
*S*-(2-((4-chlorophenyl)amino)-2-oxoethyl) carbamothioate (7)



S16

*N*-(4-chlorophenyl)-2-mercaptoacetamide (**14**) was prepared according to the described procedure and the crude was taken in 6 mL THF without further workup or purification. Triethylamine (260  $\mu$ L, 1.9 mmol) was added, followed by trimethylsilyl isocyanate (250  $\mu$ L, 1.9 mmol). The reaction mixture was kept under argon atmosphere and refluxed for 5 hours. After cooling to room temperature the reaction was quenched for 10 min with methanol. The crude was purified by flash chromatography (petroleum ether:ethyl acetate 75:25 to 50:50) to yield the title compound as a white powder (70 mg, 18% over two steps).  $^1\text{H}$  NMR (300 MHz, DMSO- $d_6$ )  $\delta$  ppm 3.69 (s, 2 H), 7.30 – 8.00 (br s, 2 H), 7.32 – 7.40 (m, 2 H), 7.57 – 7.65 (m, 2 H), 10.25 (s, 1 H);  $^{13}\text{C}$  NMR (75 MHz, DMSO- $d_6$ )  $\delta$  ppm 34.05, 120.57, 126.82, 128.63, 137.94, 166.10, 167.06; MS (ESI $^+$ )  $m/z$  245 (M+H) $^+$

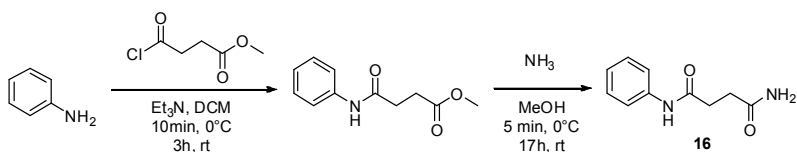
*S*-(2-((2-methoxyphenyl)amino)-2-oxoethyl) carbamothioate (**11**)



*O*-anisidine (380  $\mu$ L, 3.4 mmol) was added to a solution of chloroacetic acid (318 mg, 3.4 mmol) and ammonium thiocyanate (205 mg, 2.7 mmol) in 6 mL absolute ethanol. The reaction was refluxed for 1.5 hours until formation of a precipitate. Addition of water, followed by filtration gave the crude which was purified using automated flash chromatography (petroleum ether:ethyl acetate 80:20 to 0:100) to yield the title compound as a white powder (140 mg, 22%).

$^1\text{H}$  NMR (300 MHz, DMSO- $d_6$ )  $\delta$  ppm 3.69 (s, 2 H), 3.83 (s, 3 H), 6.84 – 6.95 (m, 1 H), 6.98 – 7.11 (m, 2 H), 7.59 – 8.00 (br s, 2 H), 8.04 (d,  $J$  = 7.5 Hz, 1 H), 9.25 (s, 1 H);  $^{13}\text{C}$  NMR (75 MHz, DMSO- $d_6$ )  $\delta$  ppm 33.79, 55.80, 111.08, 120.34, 124.10, 127.28, 148.76, 166.29, 167.16; MS (ESI $^+$ )  $m/z$  240 (M+H) $^+$

*N*-phenylsuccinamide (**16**)



Methyl succinyl chloride (170  $\mu$ L, 1.4 mmol) was added dropwise over 5 min to a solution of aniline (100  $\mu$ L, 1.1 mmol) and triethylamine (300  $\mu$ L, 2.2 mmol) in dry dichloromethane at 0°C. After another 5 min, the reaction was allowed to warm up to room temperature and was stirred for 3 hours. Washing with sodium bicarbonate solution and evaporation of the solvent gave the crude which was purified using radial thin-layer chromatography (dichloromethane) to yield methyl-4-oxo-4-(phenylamino)butanoate as a white powder (222 mg, 98%).

S17

<sup>1</sup>H NMR (500 MHz, CDCl<sub>3</sub>) δ ppm 2.66 (t, *J* = 6.5 Hz, 2H), 2.75 (t, *J* = 6.5 Hz, 2H), 3.70 (s, 3H), 7.09 (t, *J* = 7.4 Hz, 1H), 7.30 (t, *J* = 7.9 Hz, 2H), 7.50 (d, *J* = 7.9 Hz, 2H), 7.71 (s, 1H); <sup>13</sup>C NMR (126 MHz, CDCl<sub>3</sub>) δ ppm 29.37, 32.21, 52.13, 119.91, 124.36, 129.08, 137.98, 169.86, 173.80; MS (ESI<sup>+</sup>) *m/z* 208 (M+H)<sup>+</sup>

Methyl-4-oxo-4-(phenylamino)butanoate (26 mg, 0.13 mmol) was added to a 10% ammonia solution in methanol (9 mL) at 0°C. After addition, the reaction was allowed to warm up to room temperature and was stirred for 17 h. The reaction mixture was concentrated in air stream and the crude was purified using flash chromatography (dichloromethane:methanol:triethylamine 97:2:1) to give the title compound (29 mg, quant.).

<sup>1</sup>H NMR (500 MHz, DMSO-*d*<sub>6</sub>) δ ppm 2.38 (t, *J* = 7.2 Hz, 2H), 2.38 (t, *J* = 7.2 Hz, 2H), 6.76 (s, 1H), 7.00 (t, *J* = 7.4 Hz, 1H), 7.27 (t, *J* = 7.9 Hz, 2H), 7.33 (s, 1H), 7.58 (d, *J* = 7.7 Hz, 2H), 9.92 (s, 1H); <sup>13</sup>C NMR (126 MHz, DMSO-*d*<sub>6</sub>) δ ppm 29.96, 31.51, 118.87, 122.83, 128.63, 139.38, 170.55, 173.33; MS (ESI<sup>+</sup>) *m/z* 215 (M+Na)<sup>+</sup>

#### Peptide synthesis

Solid-phase synthesis of the peptide Mca-Ala-Gly-Pro-Pro-Gly-Pro-Dpa-Gly-Arg-amide (with Mca = 7-methoxycoumarin-4-acetyl and Dpa = Dap(Dnp) = N-beta-2,4-dinitrophenyl-L-2,3-diaminopropionyl) was carried out on a scale of 100 μmol with a Syro Multiple Peptide Synthesizer (MultiSynTech, Witten, Germany) on Rapp S RAM resin (Rapp Polymere, Tübingen, Germany) for the generation of the C-terminal amide. Fmoc chemistry with TBTU / diisopropylethyl amine activation with tenfold excess was employed for the coupling of the amino acids. Coupling time was 1 hour. Side chain protection of arginine was Pbf. After assembly of the peptide chain Mca was coupled in a threefold excess with activation by TBTU / diisopropylethyl amine in DMF over 3 hours at room temperature. The crude peptide was cleaved from the resin and deprotected by a 3 hour treatment with TFA containing 3% triisopropylsilane and 2% water (10 mL/g resin). After precipitation with *t*-butylmethyl ether, the resulting crude peptide was purified by preparative HPLC on C<sub>18</sub> material with water/acetonitrile gradients containing 0.1% TFA and characterized by analytical HPLC and MALDI-MS. The final product was lyophilized from water. For the calculation of the concentration of stock solutions of the peptide one counter ion of trifluoroacetic acid (mol. weight 114.02) was taken into account. Yield: 56 mg (44.6 μmol).

### 3. References

- (1) Eckhard, U.; Schönauer, E.; Brandstetter, H. *J. Biol. Chem.* **2013**, *288*, 20184–20194.
- (2) Gasteiger, E.; Hoogland, C. In *The Proteomics Protocols Handbook*; Humana Press Inc: Totowa, NJ, 2005; pp 571–607.
- (3) Briers, Y.; Lavigne, R.; Volckaert, G.; Hertveldt, K. *J. Biochem. Biophys. Methods* **2007**, *70*, 531–533.
- (4) Liu, Y.; Kati, W.; Chen, C.-M.; Tripathi, R.; Molla, A.; Kohlbrenner, W. *Anal. Biochem.* **1999**, *267*, 331–335.
- (5) Williams, J.; Morrison, J. *Methods Enzymol.* **1979**, *63*, 437–467.
- (6) Kuzmic, P.; Elrod, K. C.; Cregar, L. M.; Sideris, S.; Rai, R.; Janc, J. W. *Anal. Biochem.* **2000**, *286*, 45–50.
- (7) Copeland, R. A. *Methods Biochem. Anal.* **2005**, *46*, 1–265.
- (8) Hauptenthal, J.; Baehr, C.; Zeuzem, S.; Piiper, A. *Int. J. Cancer* **2007**, *121*, 206–210.
- (9) Stura, E. A.; Wilson, I. A. *J. Cryst. Growth* **1991**, *110*, 270–282.
- (10) Kabsch, W. *Acta Crystallogr. D. Biol. Crystallogr.* **2010**, *66*, 125–132.
- (11) Evans, P. R.; Murshudov, G. N. *Acta Crystallogr. Sect. D Biol. Crystallogr.* **2013**, *69*, 1204–1214.
- (12) McCoy, A. J. *Acta Crystallogr. D. Biol. Crystallogr.* **2007**, *63*, 32–41.
- (13) Adams, P. D.; Afonine, P. V.; Bunkóczi, G.; Chen, V. B.; Davis, I. W.; Echols, N.; Headd, J. J.; Hung, L.-W.; Kapral, G. J.; Grosse-Kunstleve, R. W.; McCoy, A. J.; Moriarty, N. W.; Oeffner, R.; Read, R. J.; Richardson, D. C.; Richardson, J. S.; Terwilliger, T. C.; Zwart, P. H. *Acta Crystallogr. Sect. D, Biol. Crystallogr.* **2010**, *66*, 213–221.
- (14) Emsley, P.; Lohkamp, B.; Scott, W. G.; Cowtan, K. *Acta Crystallogr. Sect. D, Biological Crystallogr.* **2010**, *66*, 486–501.
- (15) DeLano, W. L. The PyMOL Molecular Graphics System, Version-1.3r1, 2010.
- (16) Shaitanov, P. V.; Lukashov, S. S.; Turov, O. V.; Yarmoluk, S. M. *Ukr. Bioorganica Acta* **2007**, *5*, 56–61.



## A2. SUPPORTING INFORMATION TO CHAPTER B

**Phosphonate as a Stable Zinc-Binding Group for “Pathoblocker” Inhibitors of Clostridial Collagenase H (ColH).**

Katrin Voos, Esther Schönauer, Alaa Alhayek, Jörg Hauptenthal, Anastasia Andreas, Rolf Müller, Rolf W. Hartmann, Hans Brandstetter, Anna K. H. Hirsch\* and Christian Ducho\*

\* corresponding authors

Reprinted with permission from *ChemMedChem* **2021**, *16*, 1257 – 1267.

DOI: 10.1002/cmdc.202000994

Copyright (2021) Wiley & Chemistry Europe

# ChemMedChem

Supporting Information

## **Phosphonate as a Stable Zinc-Binding Group for “Pathoblocker” Inhibitors of Clostridial Collagenase H (ColH)**

Katrin Voos, Esther Schönauer, Alaa Alhayek, Jörg Haupenthal, Anastasia Andreas,  
Rolf Müller, Rolf W. Hartmann, Hans Brandstetter, Anna K. H. Hirsch,\* and Christian Ducho\*

**Table of Contents**

Additional data for the <i>ex vivo</i> pig skin degradation model.....	S2
<sup>1</sup> H, <sup>13</sup> C and <sup>31</sup> P NMR spectra of synthesised compounds.....	S3

**Additional data for the *ex vivo* pig skin degradation model**

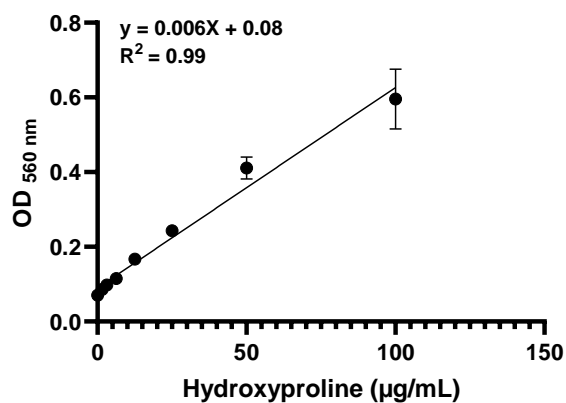


**Figure S1.** Calibration curve for hydroxyproline. Mean  $\pm$  SD of three independent measurements are depicted.

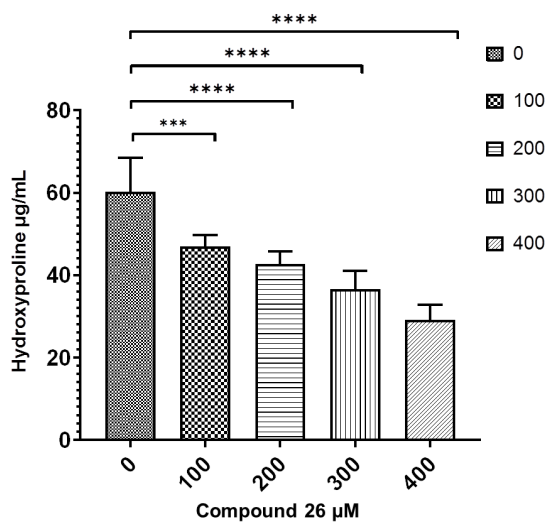
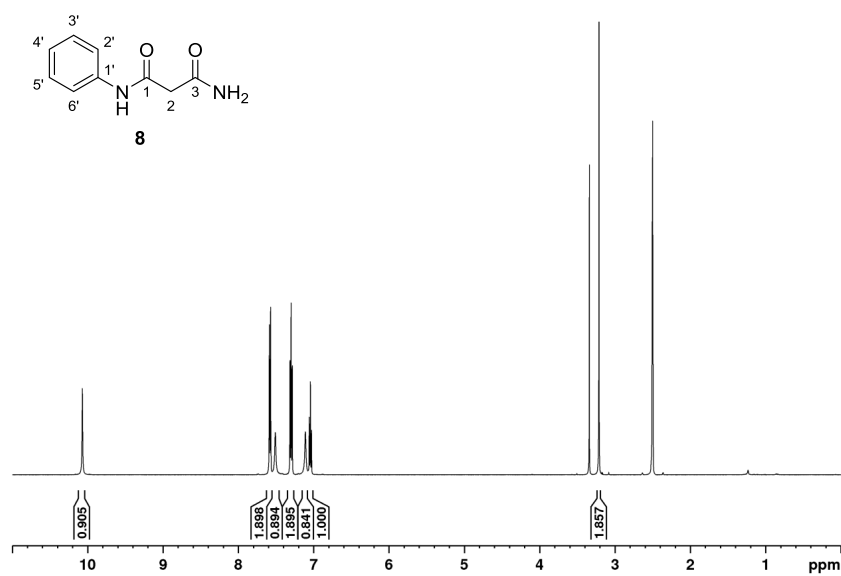
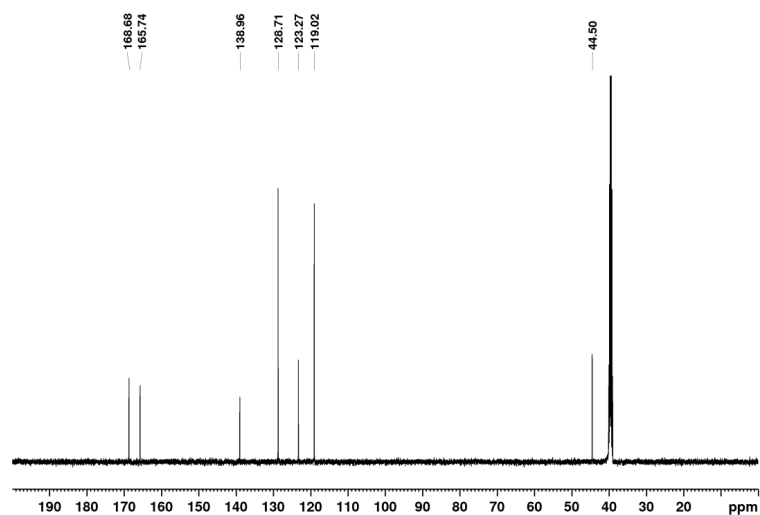


**Figure S2.** Amount of hydroxyproline release at different concentrations of **26**. Data shown represent the means  $\pm$  SD from three independent measurements. One-way ANOVA followed by Tukey's HSD test (\*\*\*:  $p = 0.0003$ ; \*\*\*\*:  $p < 0.0001$ ).

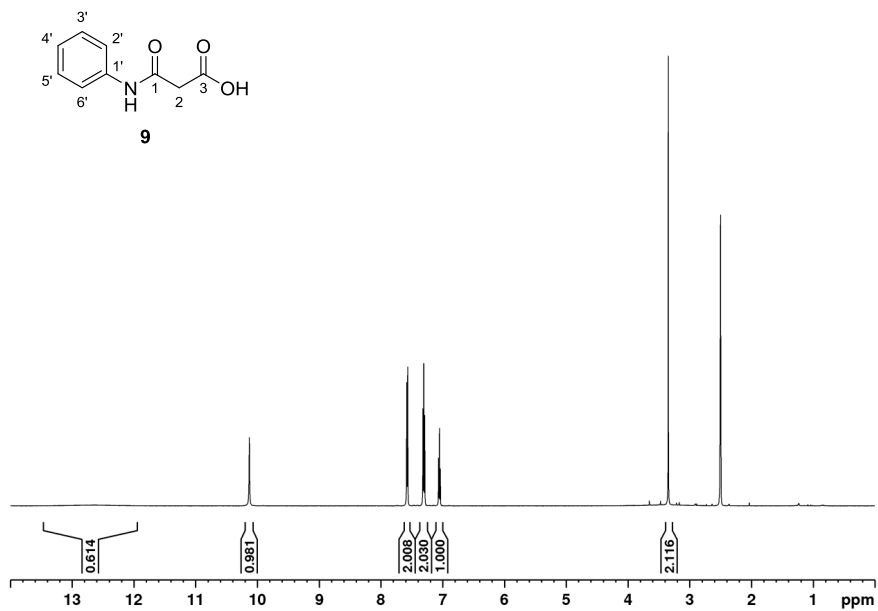
$^1\text{H}$ ,  $^{13}\text{C}$  and  $^{31}\text{P}$  NMR spectra of synthesised compounds



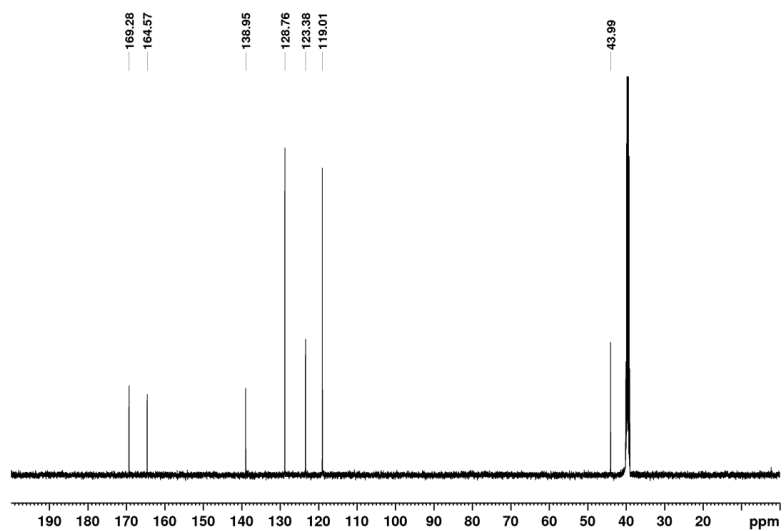
$^1\text{H}$  NMR spectrum of **8** (500 MHz, DMSO- $d_6$ ).



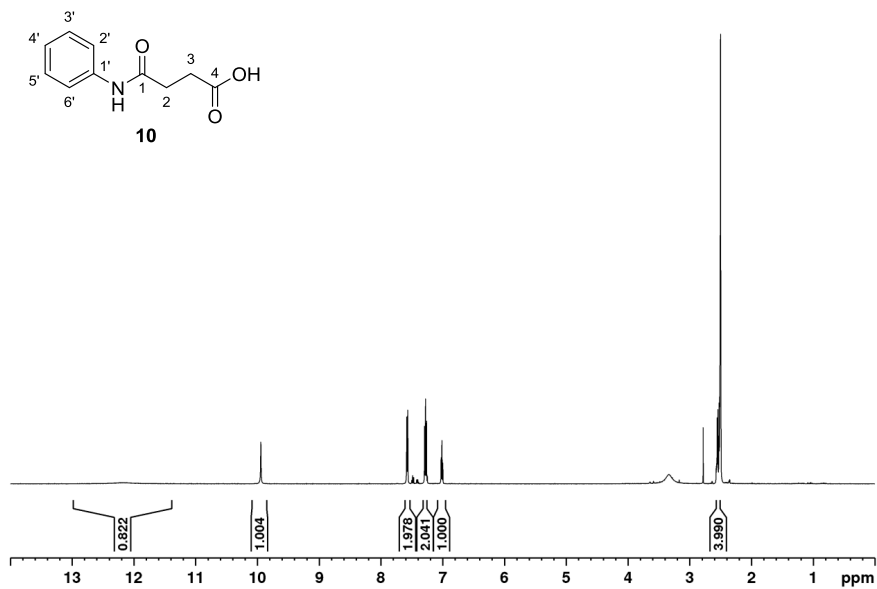
$^{13}\text{C}$  NMR spectrum of **8** (126 MHz, DMSO- $d_6$ ).



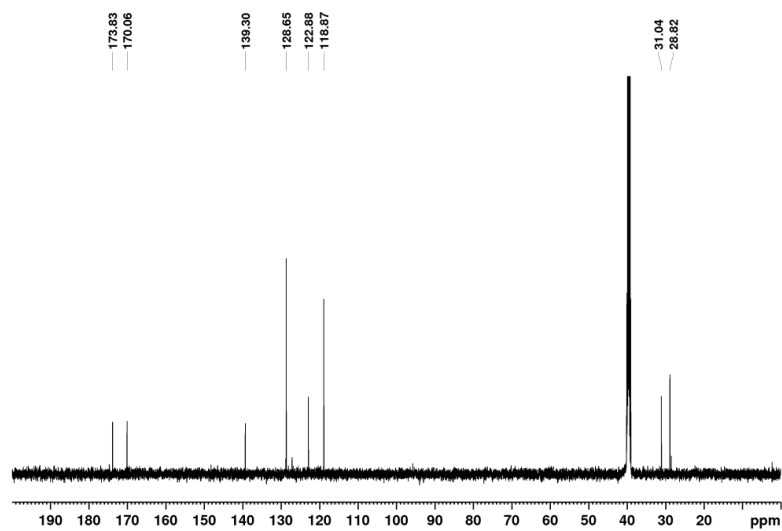
$^1\text{H}$  NMR spectrum of **9** (500 MHz, DMSO- $d_6$ ).



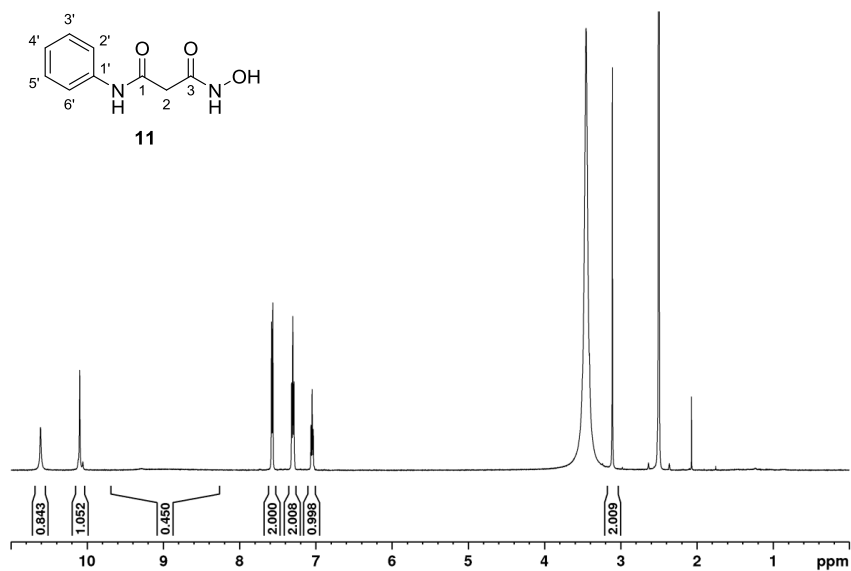
$^{13}\text{C}$  NMR spectrum of **9** (126 MHz, DMSO- $d_6$ ).



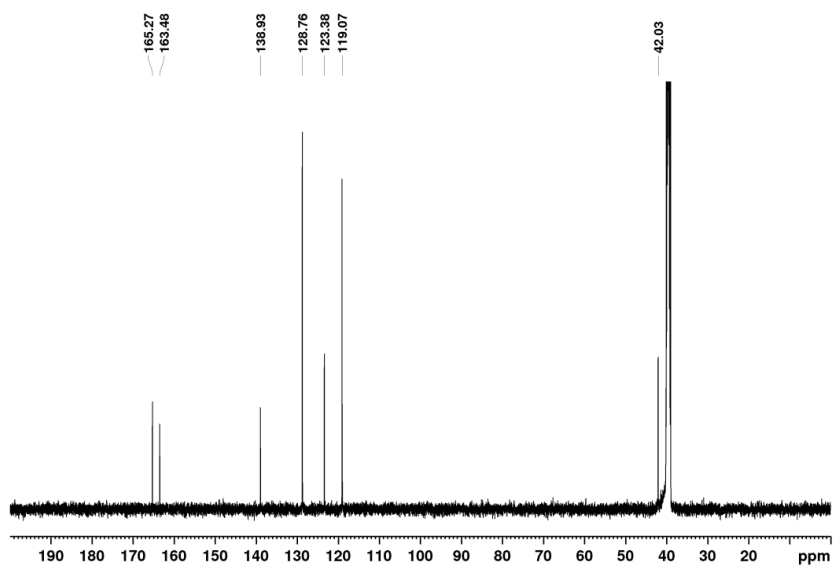
$^1\text{H}$  NMR spectrum of **10** (500 MHz, DMSO- $d_6$ ).



$^{13}\text{C}$  NMR spectrum of **10** (126 MHz, DMSO- $d_6$ ).

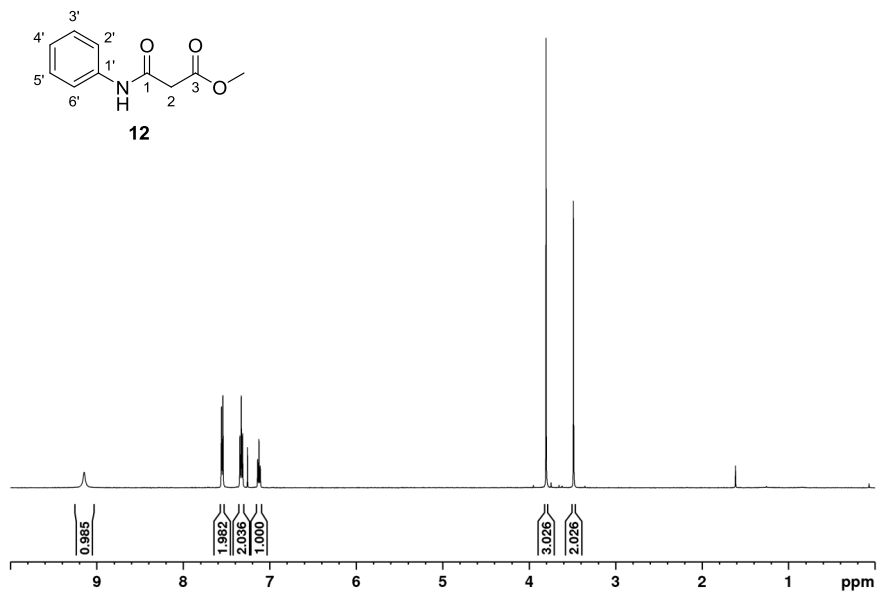


<sup>1</sup>H NMR spectrum of **11** (500 MHz, DMSO-d<sub>6</sub>).

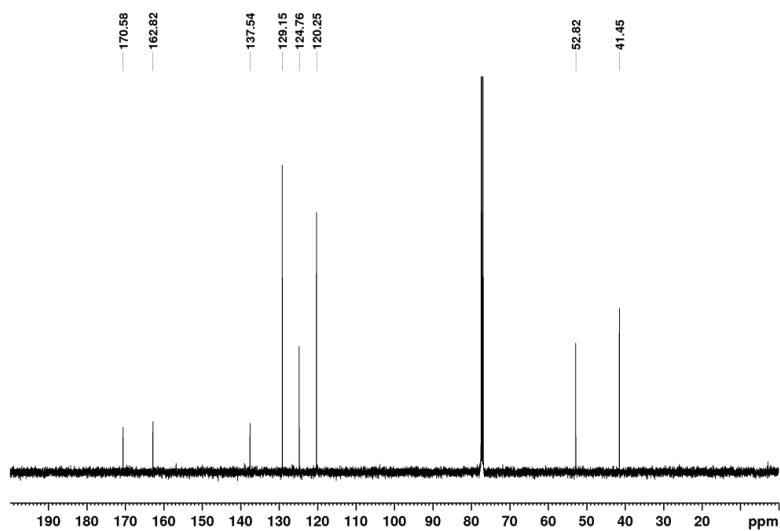


<sup>13</sup>C NMR spectrum of **11** (126 MHz, DMSO-d<sub>6</sub>).

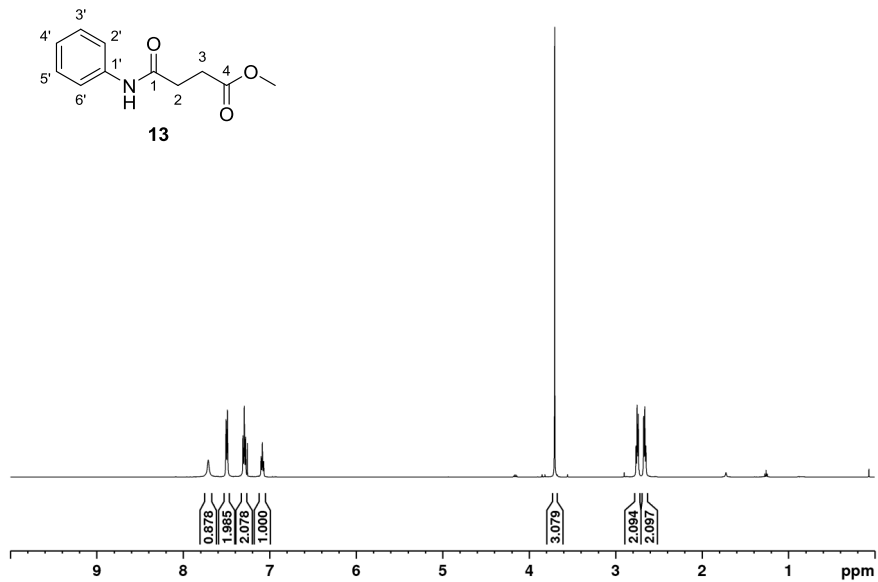




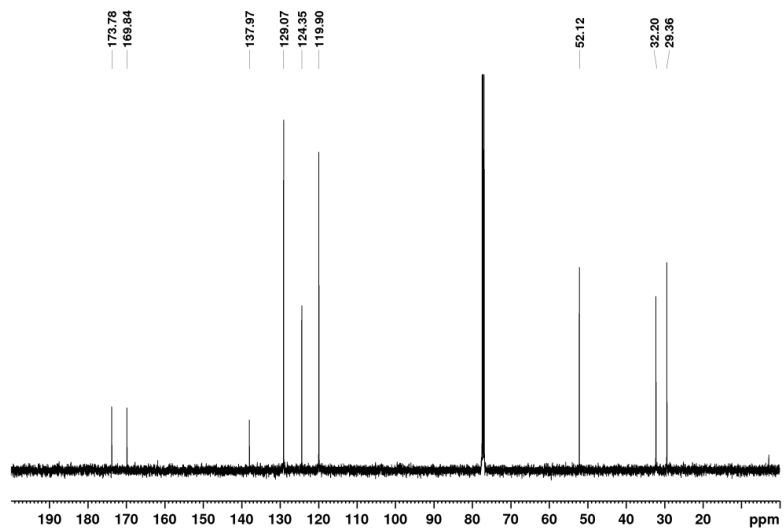
<sup>1</sup>H NMR spectrum of **12** (500 MHz, CDCl<sub>3</sub>).



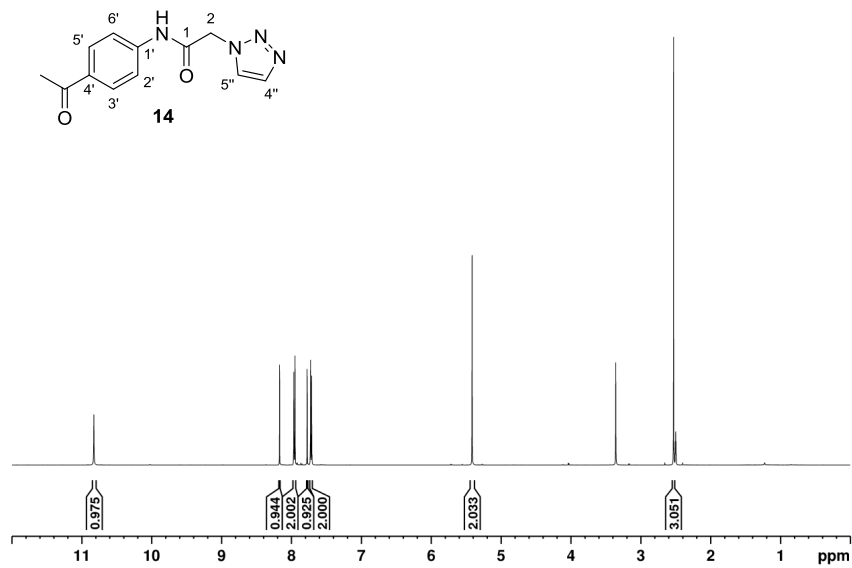
<sup>13</sup>C NMR spectrum of **12** (126 MHz, CDCl<sub>3</sub>).



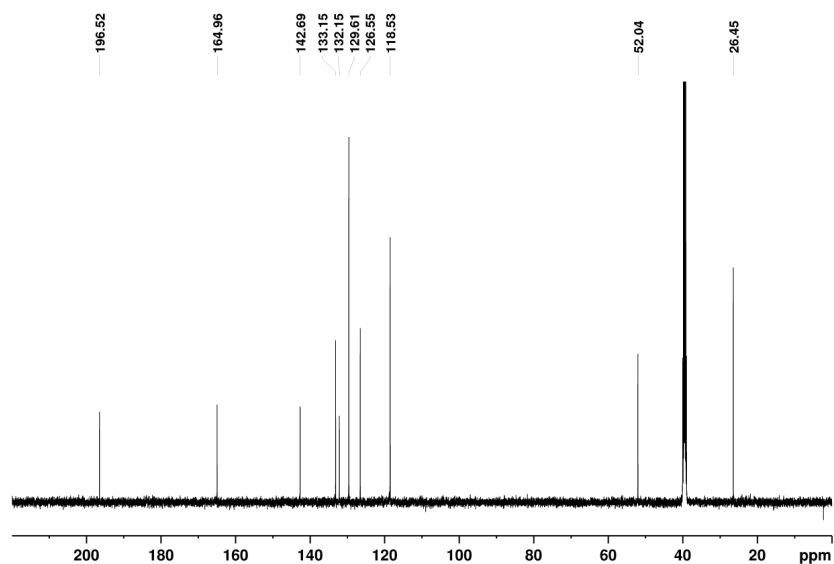
<sup>1</sup>H NMR spectrum of **13** (500 MHz, CDCl<sub>3</sub>).



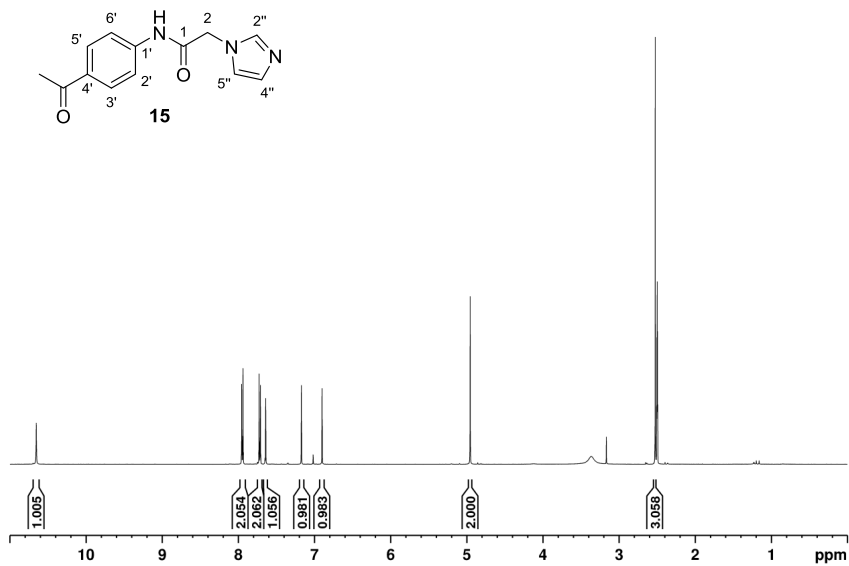
<sup>13</sup>C NMR spectrum of **13** (126 MHz, CDCl<sub>3</sub>).



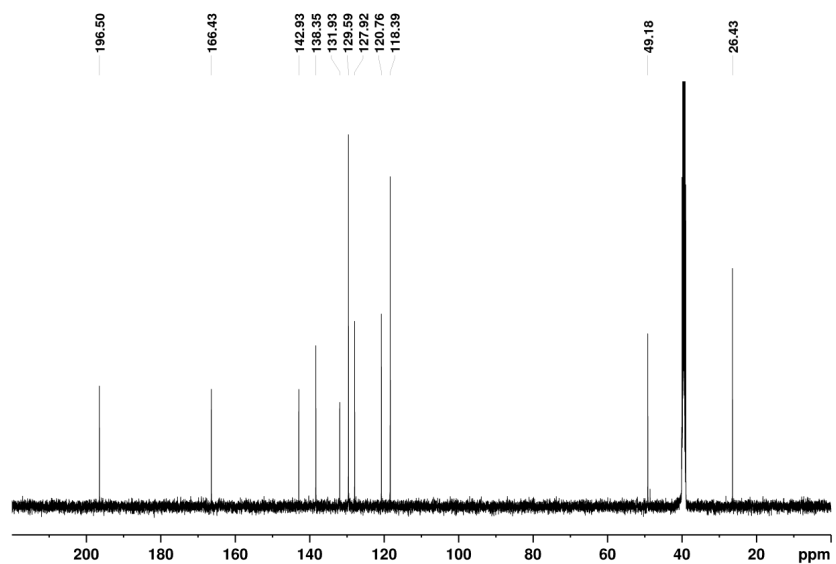
<sup>1</sup>H NMR spectrum of **14** (500 MHz, DMSO-d<sub>6</sub>).



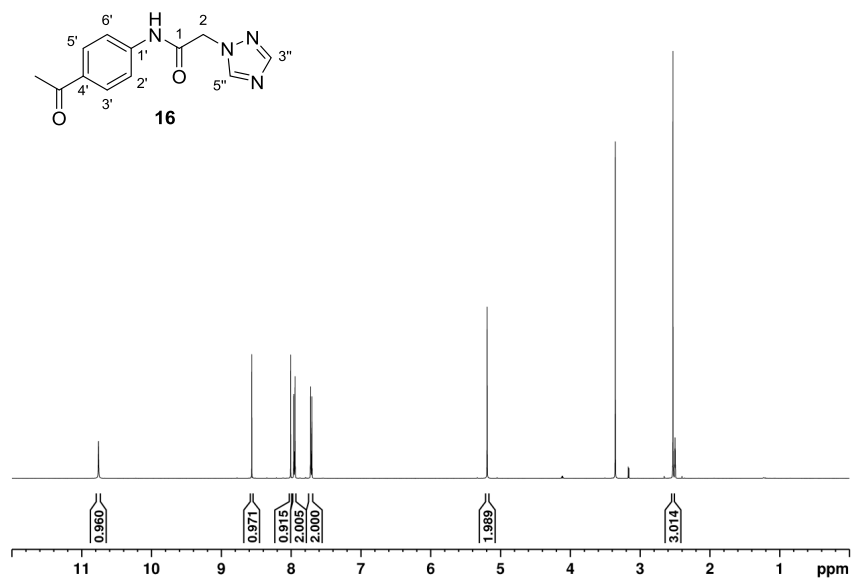
<sup>13</sup>C NMR spectrum of **14** (126 MHz, DMSO-d<sub>6</sub>).



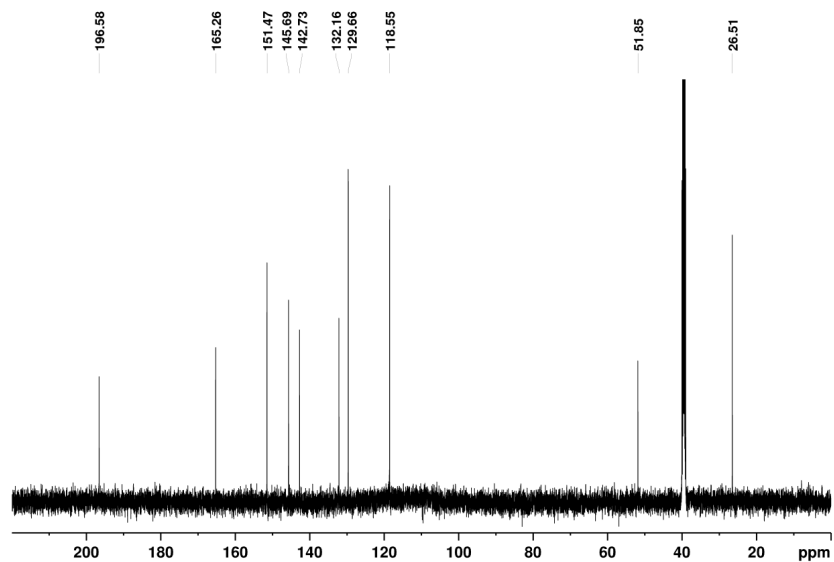
$^1\text{H}$  NMR spectrum of **15** (500 MHz,  $\text{DMSO-d}_6$ ).



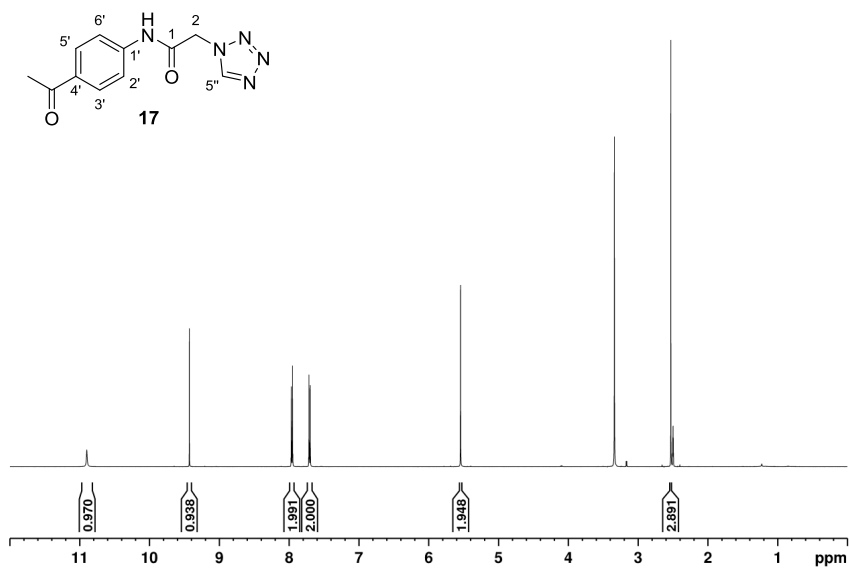
$^{13}\text{C}$  NMR spectrum of **15** (126 MHz,  $\text{DMSO-d}_6$ ).



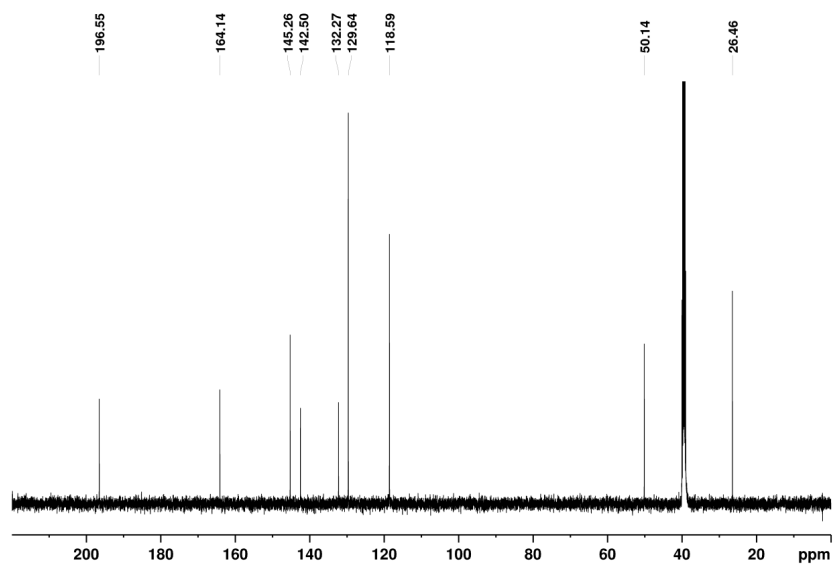
$^1\text{H}$  NMR spectrum of **16** (500 MHz, DMSO- $d_6$ ).



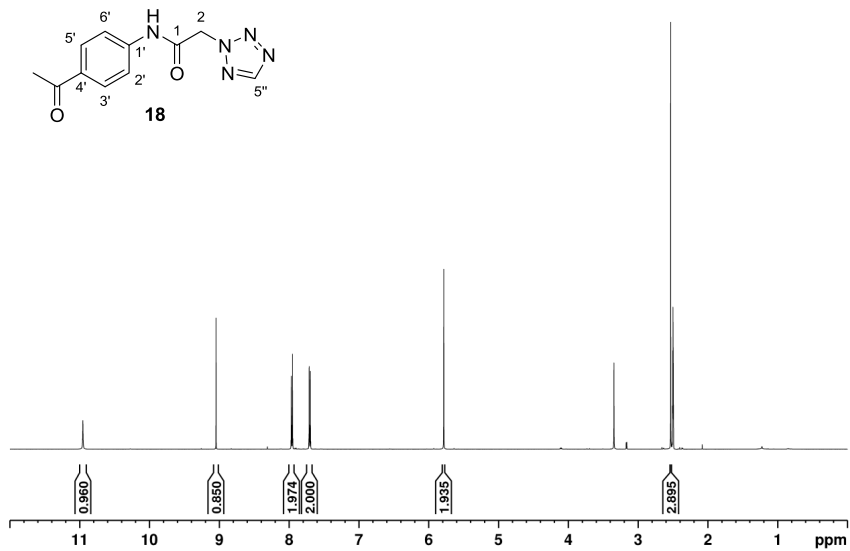
$^{13}\text{C}$  NMR spectrum of **16** (126 MHz, DMSO- $d_6$ ).



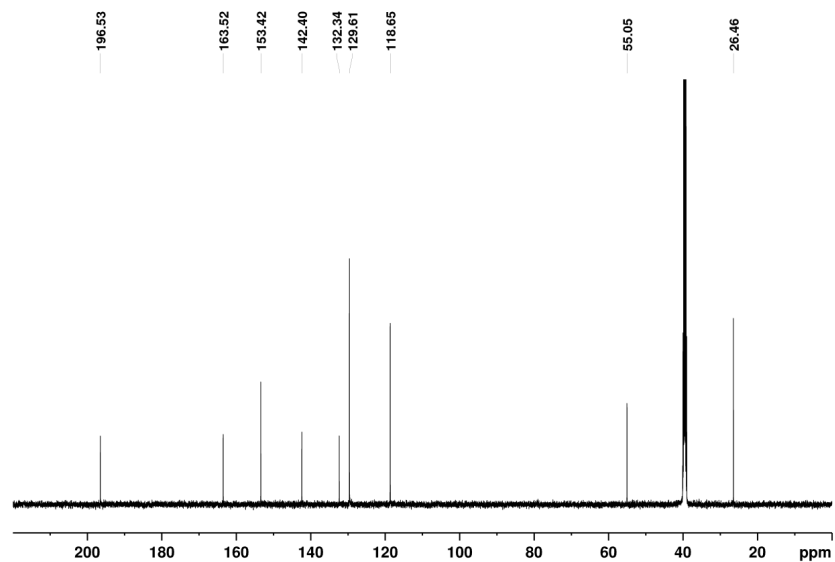
<sup>1</sup>H NMR spectrum of **17** (500 MHz, DMSO-d<sub>6</sub>).



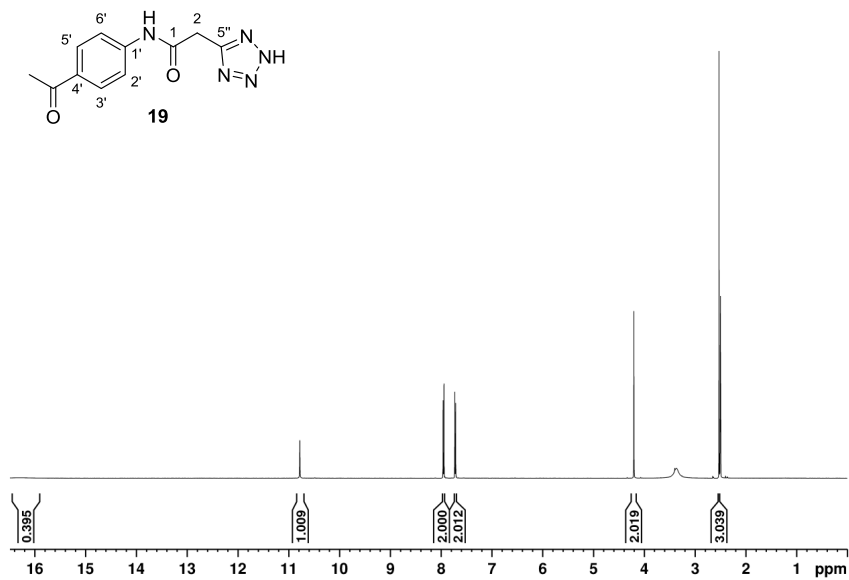
<sup>13</sup>C NMR spectrum of **17** (126 MHz, DMSO-d<sub>6</sub>).



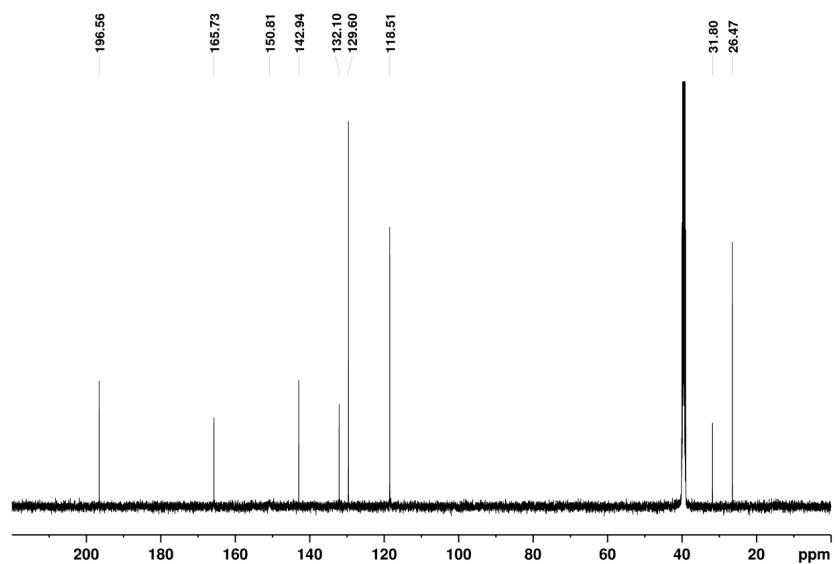
<sup>1</sup>H NMR spectrum of **18** (500 MHz, DMSO-d<sub>6</sub>).



<sup>13</sup>C NMR spectrum of **18** (126 MHz, DMSO-d<sub>6</sub>).

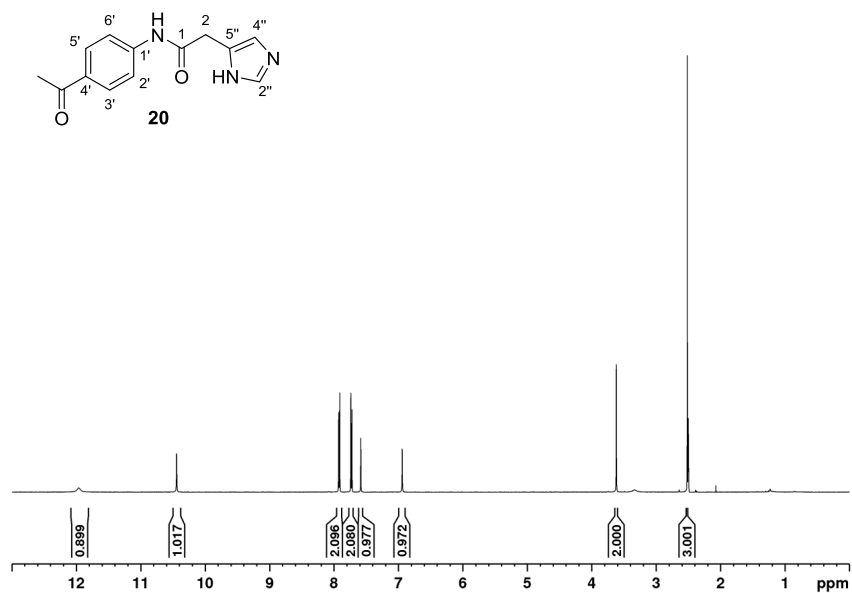


$^1\text{H}$  NMR spectrum of **19** (500 MHz, DMSO- $d_6$ ).

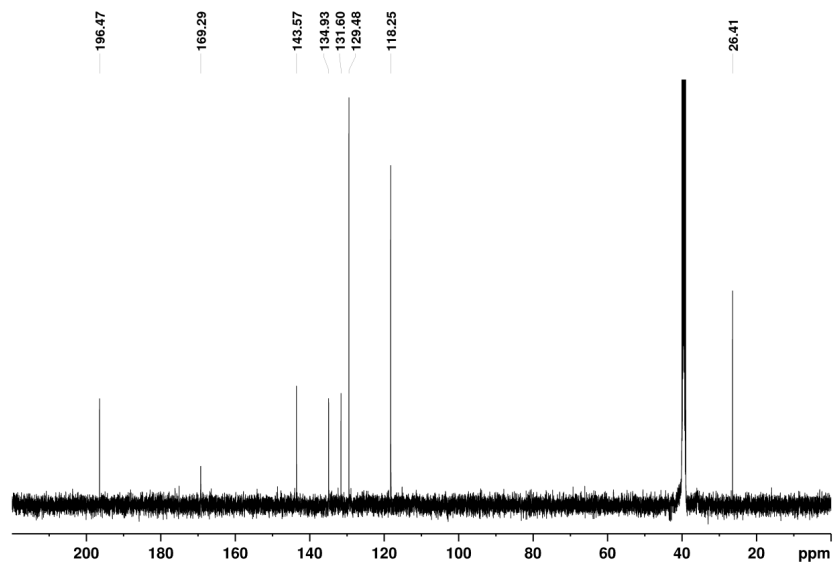


$^{13}\text{C}$  NMR spectrum of **19** (126 MHz, DMSO- $d_6$ ).



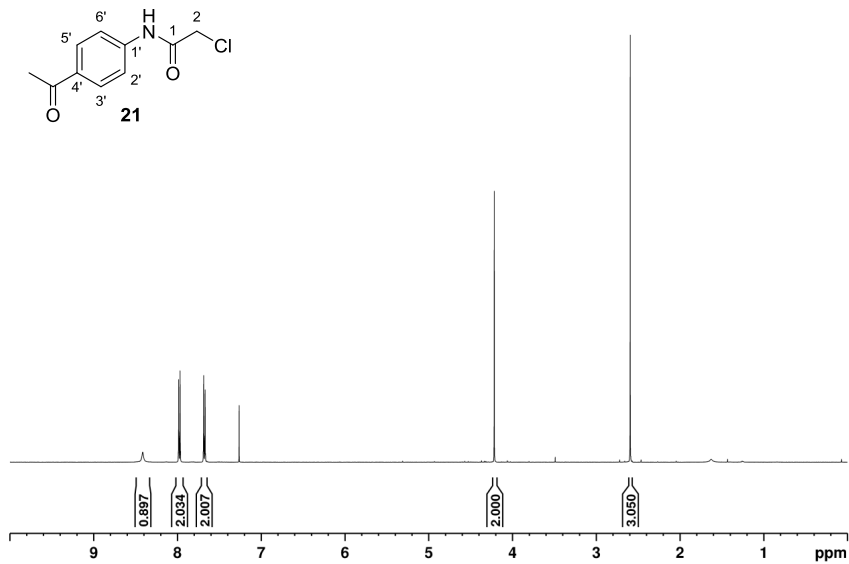


$^1\text{H}$  NMR spectrum of **20** (500 MHz,  $\text{DMSO-d}_6$ ).

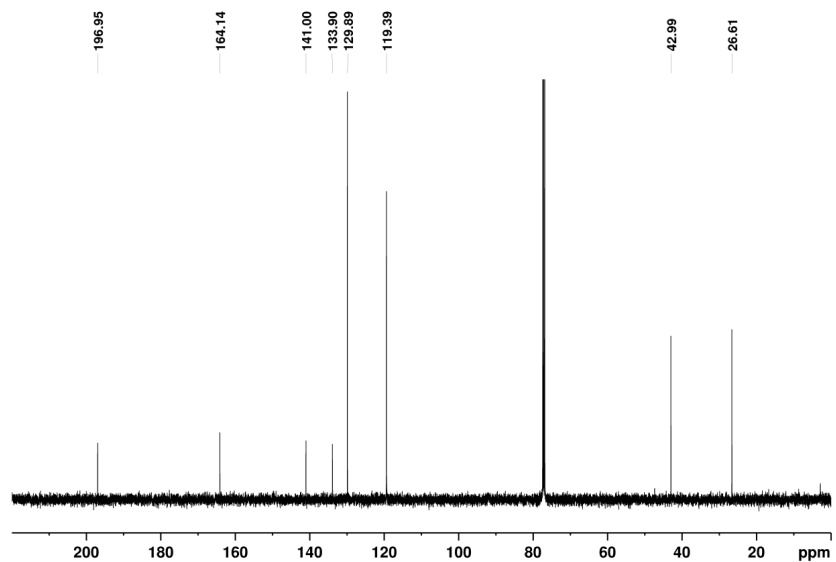


$^{13}\text{C}$  NMR spectrum of **20** (126 MHz,  $\text{DMSO-d}_6$ ).

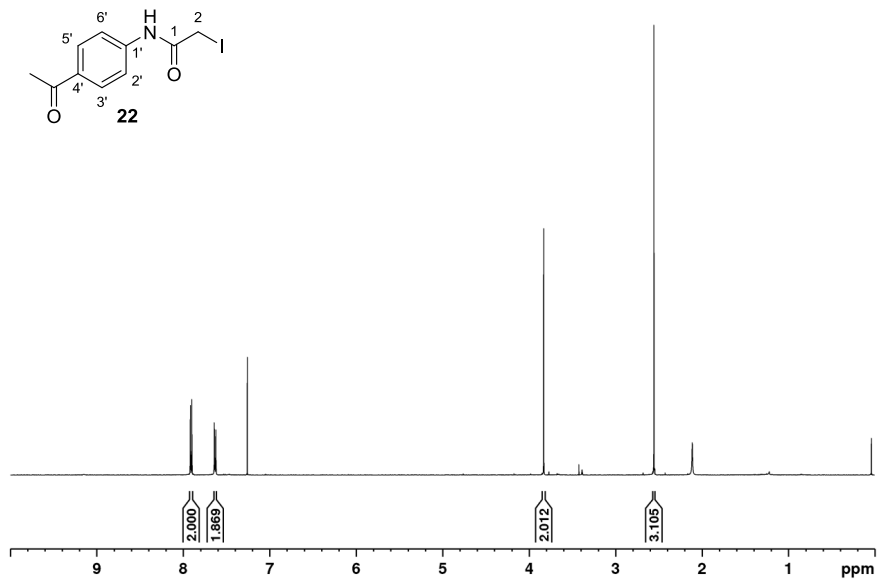
S15



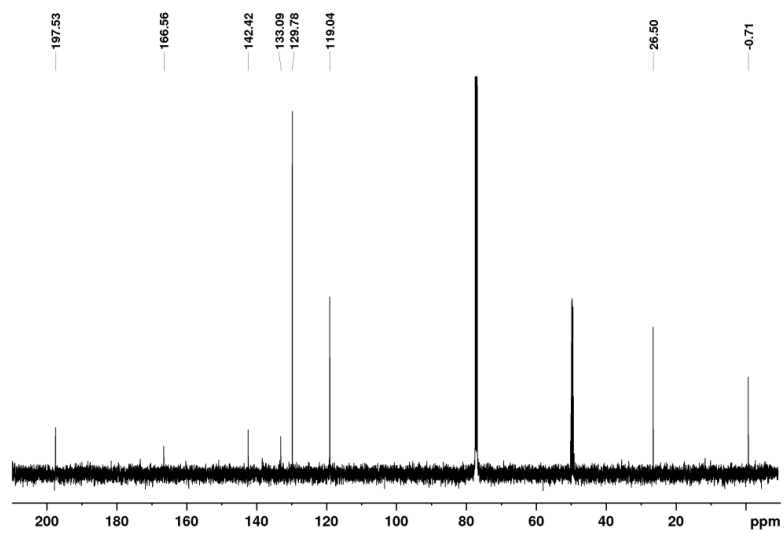
<sup>1</sup>H NMR spectrum of **21** (500 MHz, CDCl<sub>3</sub>).



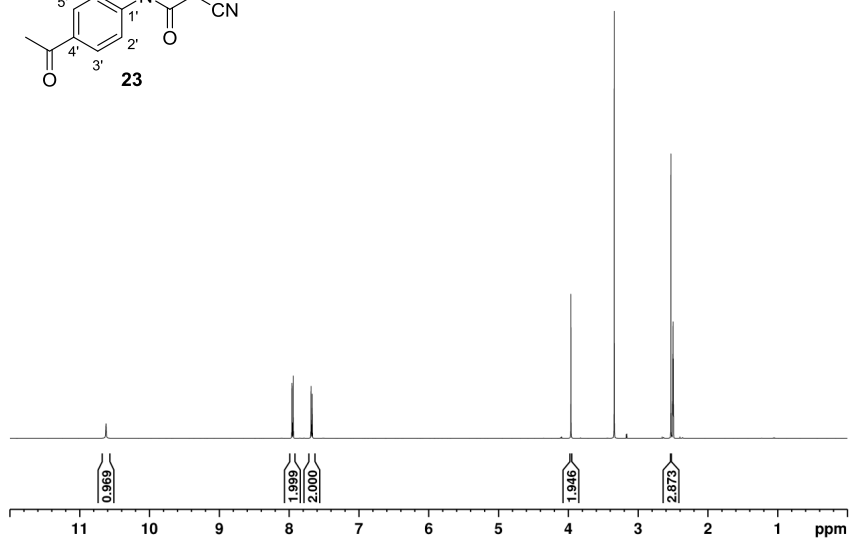
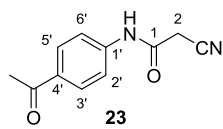
<sup>13</sup>C NMR spectrum of **21** (126 MHz, CDCl<sub>3</sub>).



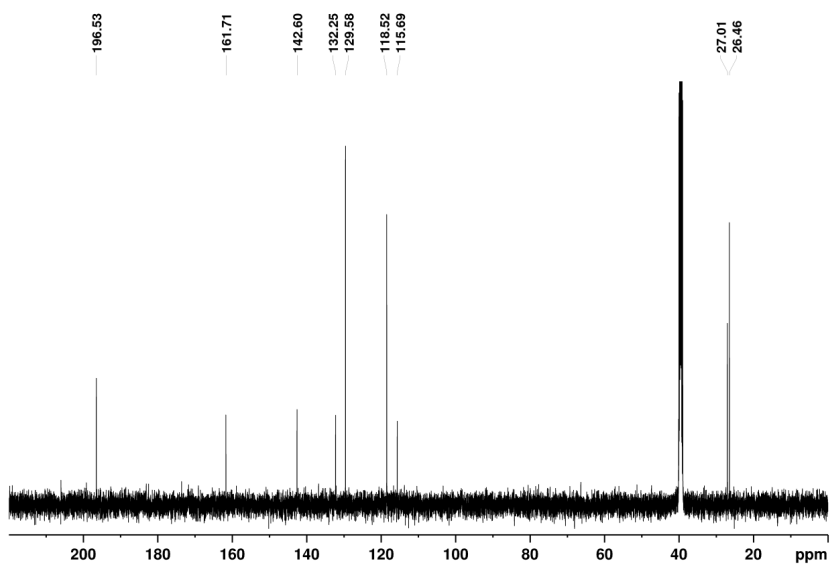
<sup>1</sup>H NMR spectrum of **22** (500 MHz, CDCl<sub>3</sub> + CD<sub>3</sub>OD).



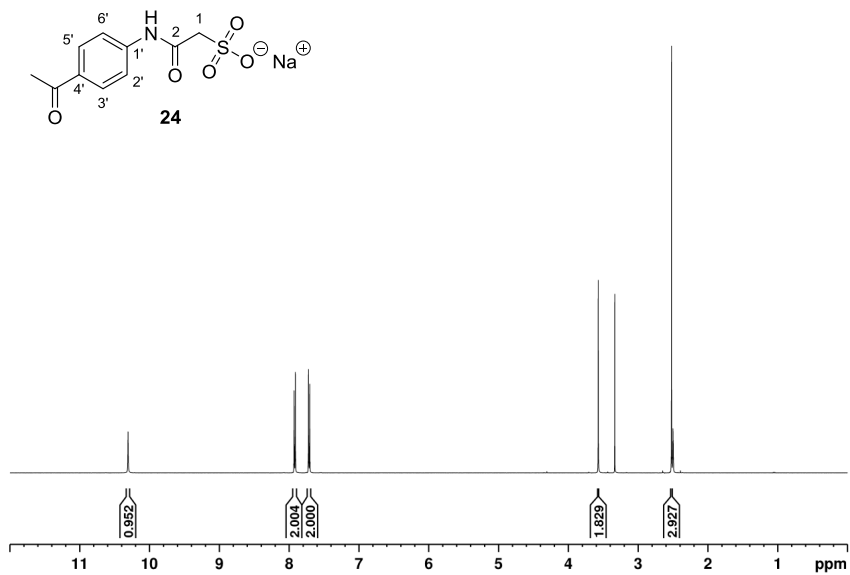
<sup>13</sup>C NMR spectrum of **22** (126 MHz, CDCl<sub>3</sub> + CD<sub>3</sub>OD).



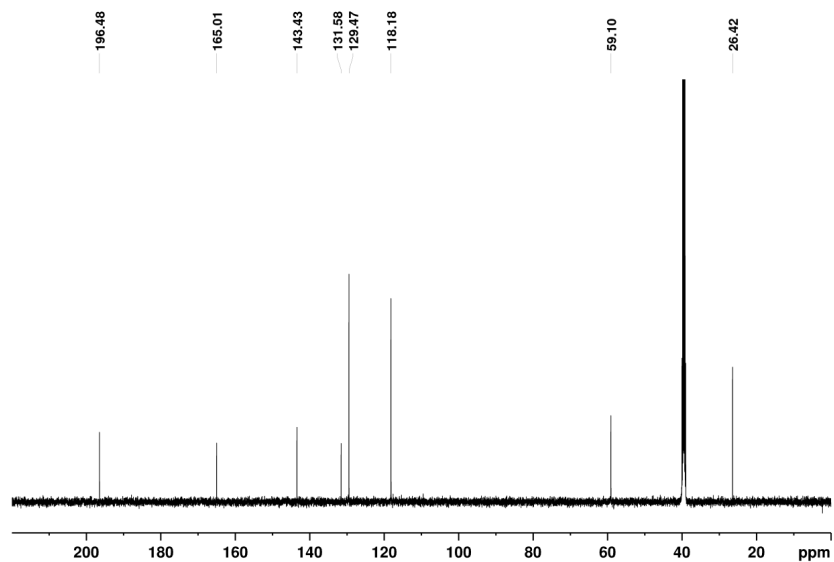
$^1\text{H}$  NMR spectrum of **23** (500 MHz, DMSO- $d_6$ ).



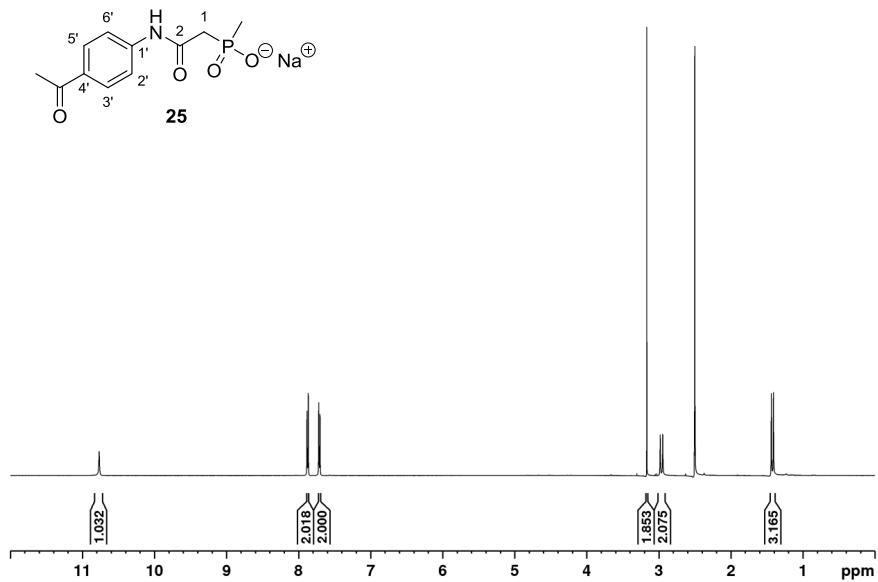
$^{13}\text{C}$  NMR spectrum of **23** (126 MHz, DMSO- $d_6$ ).



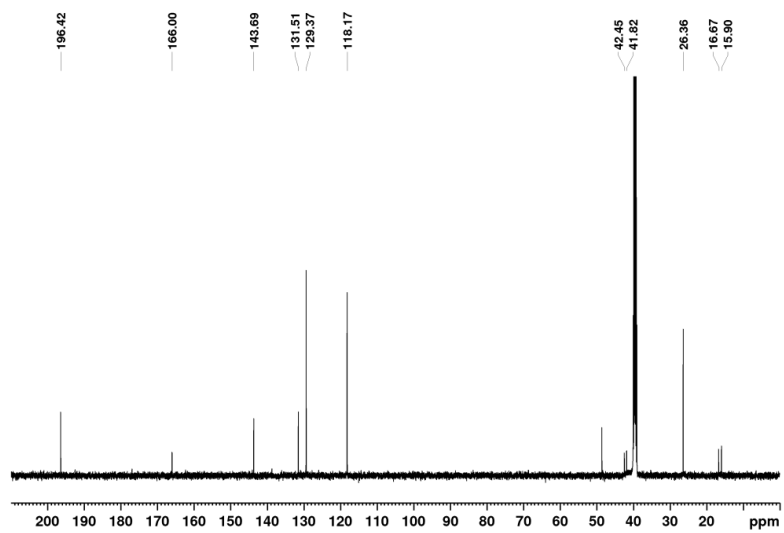
$^1\text{H}$  NMR spectrum of **24** (500 MHz,  $\text{DMSO-d}_6$ ).



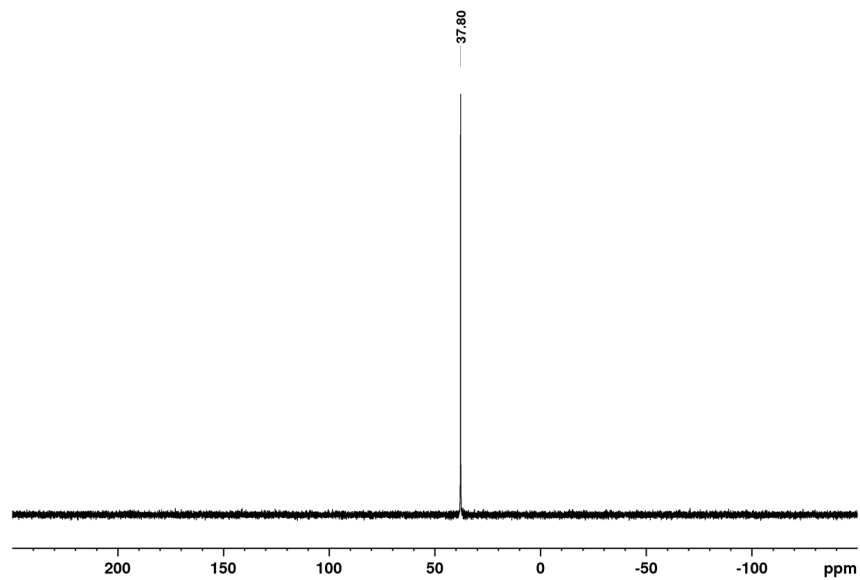
$^{13}\text{C}$  NMR spectrum of **24** (126 MHz,  $\text{DMSO-d}_6$ ).



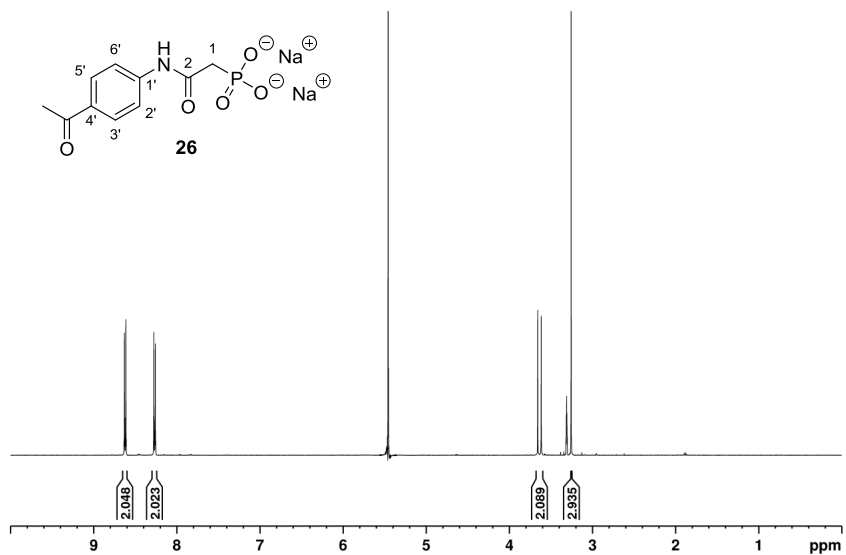
$^1\text{H}$  NMR spectrum of **25** (500 MHz, DMSO- $d_6$ ).



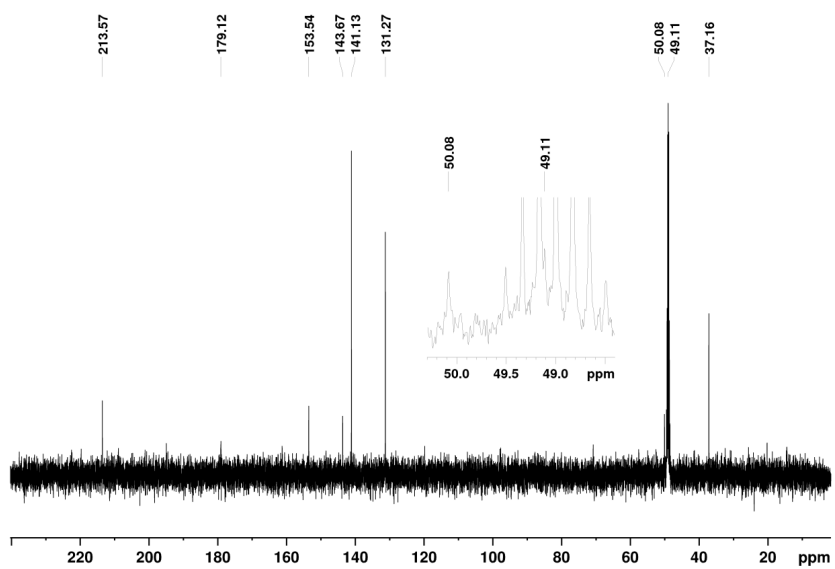
$^{13}\text{C}$  NMR spectrum of **25** (126 MHz, DMSO- $d_6$ ).



$^{31}\text{P}$  NMR spectrum of **25** (162 MHz, DMSO- $d_6$ ).

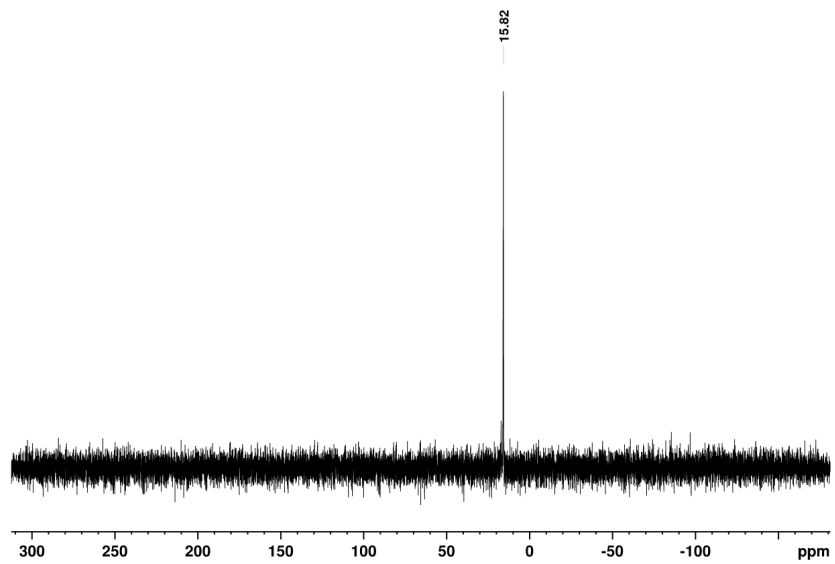


<sup>1</sup>H NMR spectrum of **26** (500 MHz, CD<sub>3</sub>OD).

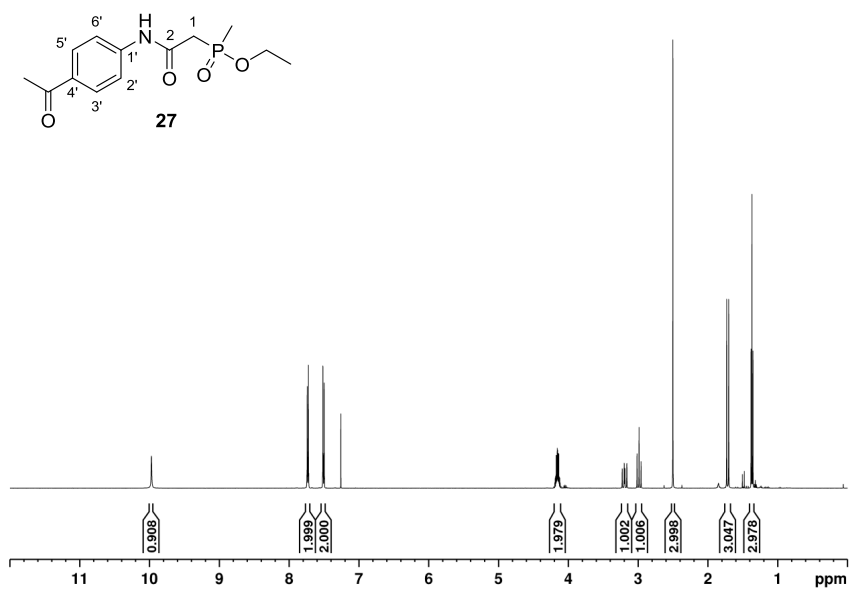


<sup>13</sup>C NMR spectrum of **26** (126 MHz, CD<sub>3</sub>OD).

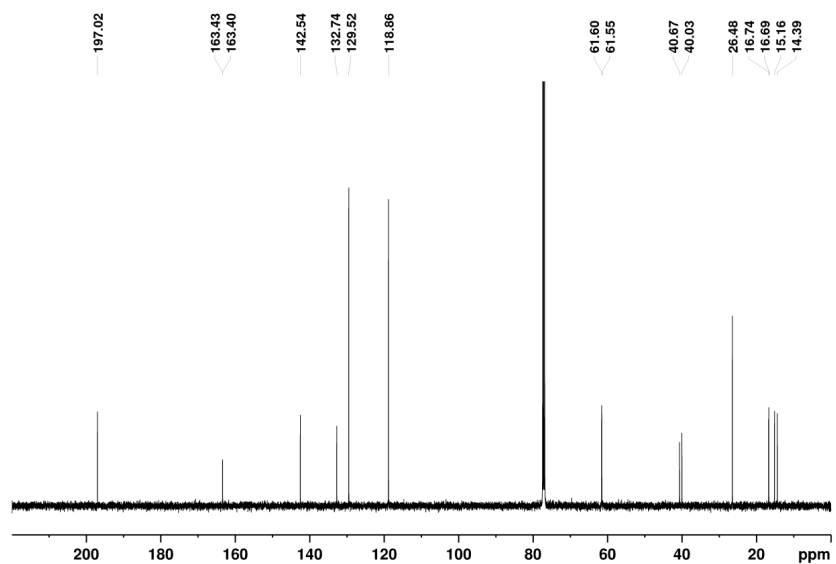




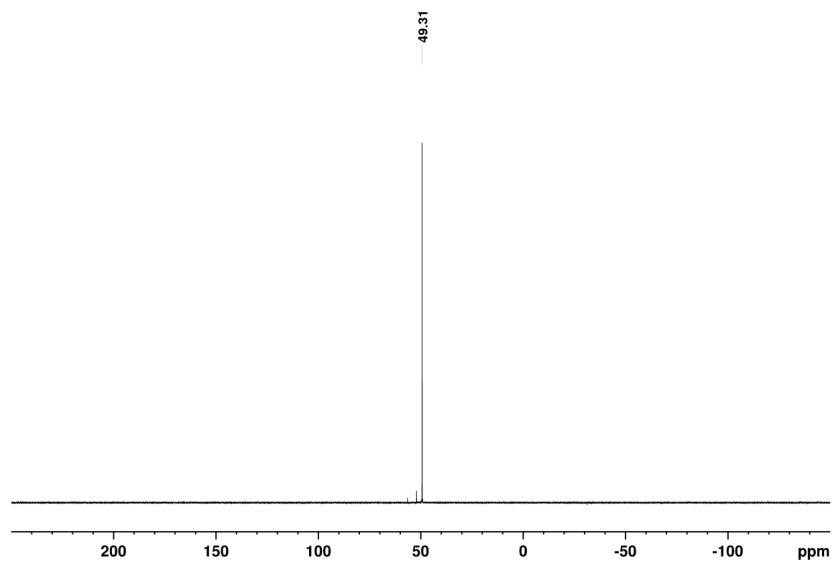
$^{31}\text{P}$  NMR spectrum of **26** (203 MHz,  $\text{CD}_3\text{OD}$ ).



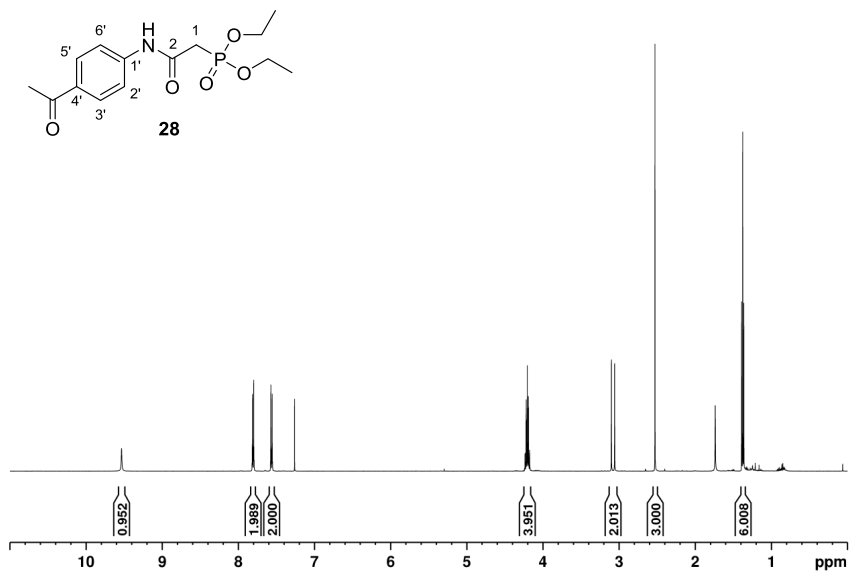
$^1\text{H}$  NMR spectrum of **27** (500 MHz,  $\text{CDCl}_3$ ).



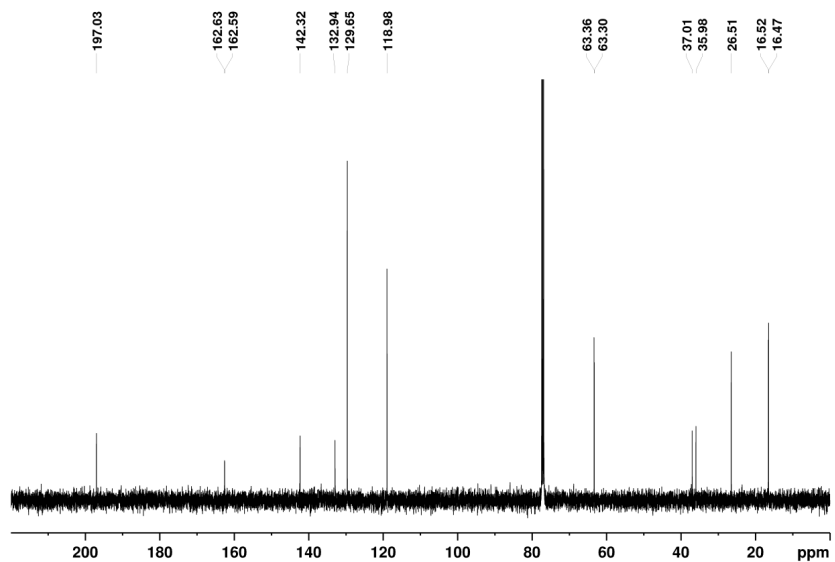
$^{13}\text{C}$  NMR spectrum of **27** (126 MHz,  $\text{CDCl}_3$ ).



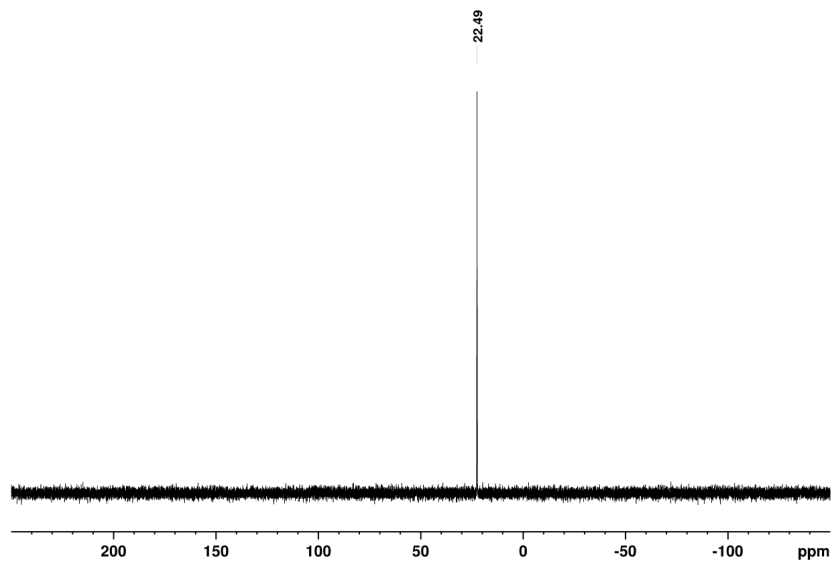
$^{31}\text{P}$  NMR spectrum of **27** (203 MHz,  $\text{CDCl}_3$ ).



$^1\text{H}$  NMR spectrum of **28** (500 MHz,  $\text{CDCl}_3$ ).



$^{13}\text{C}$  NMR spectrum of **28** (126 MHz,  $\text{CDCl}_3$ ).



$^{31}\text{P}$  NMR spectrum of **28** (203 MHz,  $\text{CDCl}_3$ ).

## A3. SUPPORTING INFORMATION TO CHAPTER C

### **Inhibition of Collagenase Q1 of *Bacillus cereus* as a Novel Antivirulence Strategy for the Treatment of Skin-Wound Infections**

Alaa Alhayek, Essak S. Khan, Esther Schönauer, Tobias Däinghaus, Roya Shafiei, Katrin Voos, Mitchell K. L. Han, Christian Ducho, Gernot Posselt, Silja Wessler, Hans Brandstetter, Jörg Haupenthal, Aránzazu del Campo\* and Anna K. H. Hirsch\*

\* corresponding authors

Reprinted with permission from *Adv. Ther.* **2022**, *5*, 2100222

DOI: 10.1002/adtp.202100222

Copyright (2021) Wiley & Chemistry Europe

# Supporting Information

## Inhibition of collagenase Q1 of *Bacillus cereus* as a novel antivirulence strategy for the treatment of skin wound infections

*Alaa Alhayek*<sup>1,2</sup>, *Essak S. Khan*<sup>3,4</sup>, *Esther Schönauer*<sup>5</sup>, *Tobias Däinghaus*<sup>3</sup>, *Roya Shafiei*<sup>1</sup>,  
*Katrin Voos*<sup>6</sup>, *Mitchell K. L. Han*<sup>3,4</sup>, *Christian Ducho*<sup>6</sup>, *Gernot Posselt*<sup>5</sup>, *Silja Wessler*<sup>5</sup>, *Hans Brandstetter*<sup>5</sup>, *Jörg Haupenthal*<sup>1</sup>, *Aránzazu del Campo*<sup>3,4</sup>, and *Anna K. Hirsch*<sup>1,2,\*</sup>

- 
- (1) A. Alhayek, R. Shafiei, Dr. J. Haupenthal, Prof. Dr. A. K. Hirsch  
Department of Drug Design and Optimization  
Helmholtz Institute for Pharmaceutical Research Saarland (HIPS)  
Helmholtz Centre for Infection Research (HZI)
  - (2) A. Alhayek, Prof. Dr. A. K. Hirsch  
Department of Pharmacy, Saarland University, Campus, Saarbrücken, GERMANY  
Email: [anna.hirsch@helmholtz-hips.de](mailto:anna.hirsch@helmholtz-hips.de)
  - (3) T. Däinghaus, Dr. E. S. Khan, Prof. Dr. A. d. Campo  
Leibniz Institute for New Materials (INM)  
Chemistry Department, Saarland University, Campus, Saarbrücken, GERMANY
  - (4) Dr. E. Schönauer, Dr. G. Posselt, Prof. Dr. S. Wessler, Prof. Dr. H. Brandstetter  
Department of Biosciences  
University of Salzburg, Hellbrunner Str., Salzburg, AUSTRIA
  - (5) K. Voos, Prof. Dr. C. Ducho  
Department of Pharmacy, Pharmaceutical and Medicinal Chemistry  
Saarland University, Campus, Saarbrücken, GERMANY

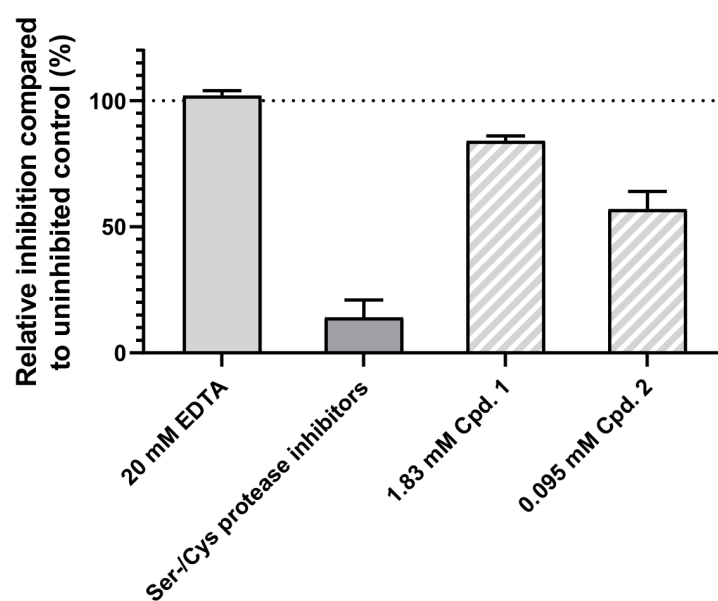
## Table of Contents

<i>Supplementary figures</i> .....	<i>S3–S12</i>
<i>Supplementary tables</i> .....	<i>S14</i>
<i>References</i> .....	<i>S14</i>



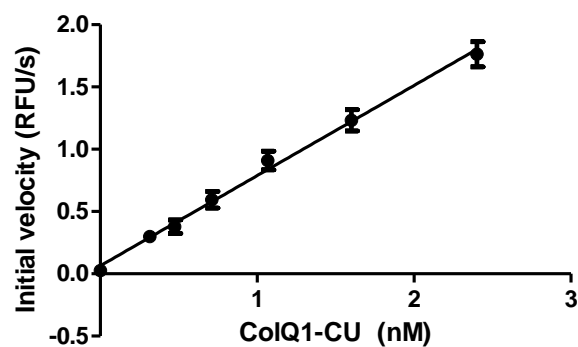
## Supplementary figures

### Peptidolytic activity of the *B. cereus* csn (Figure S1)



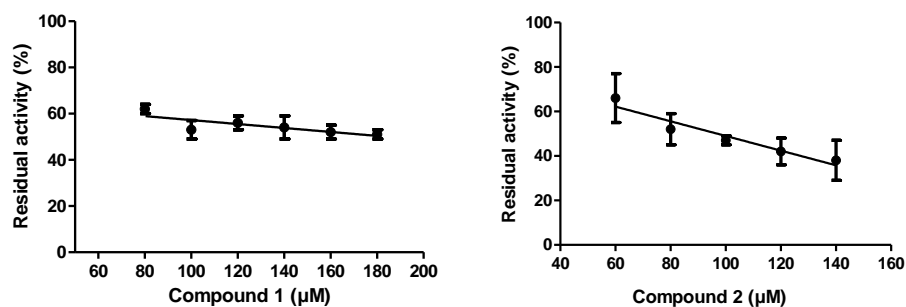
**Figure S1. *B. cereus* csn activity in a collagenase-specific peptidic assay.** Peptidolytic activity towards a collagenase-specific substrate by csn from *B. cereus* ATCC 14579 and inhibited with compounds **1** and **2** ( $n = 3$ , results are shown as mean  $\pm$  standard deviation). Compound **1** was used at a concentration of 10x its  $IC_{50}$  vs ColQ1. Due to limited solubility in the reaction buffer, compound **2** could only be tested at a concentration of 1x  $IC_{50}$ . *B. cereus*: *Bacillus cereus*, csn: culture supernatant.

### Standard curve of ColQ1 (Figure S2)



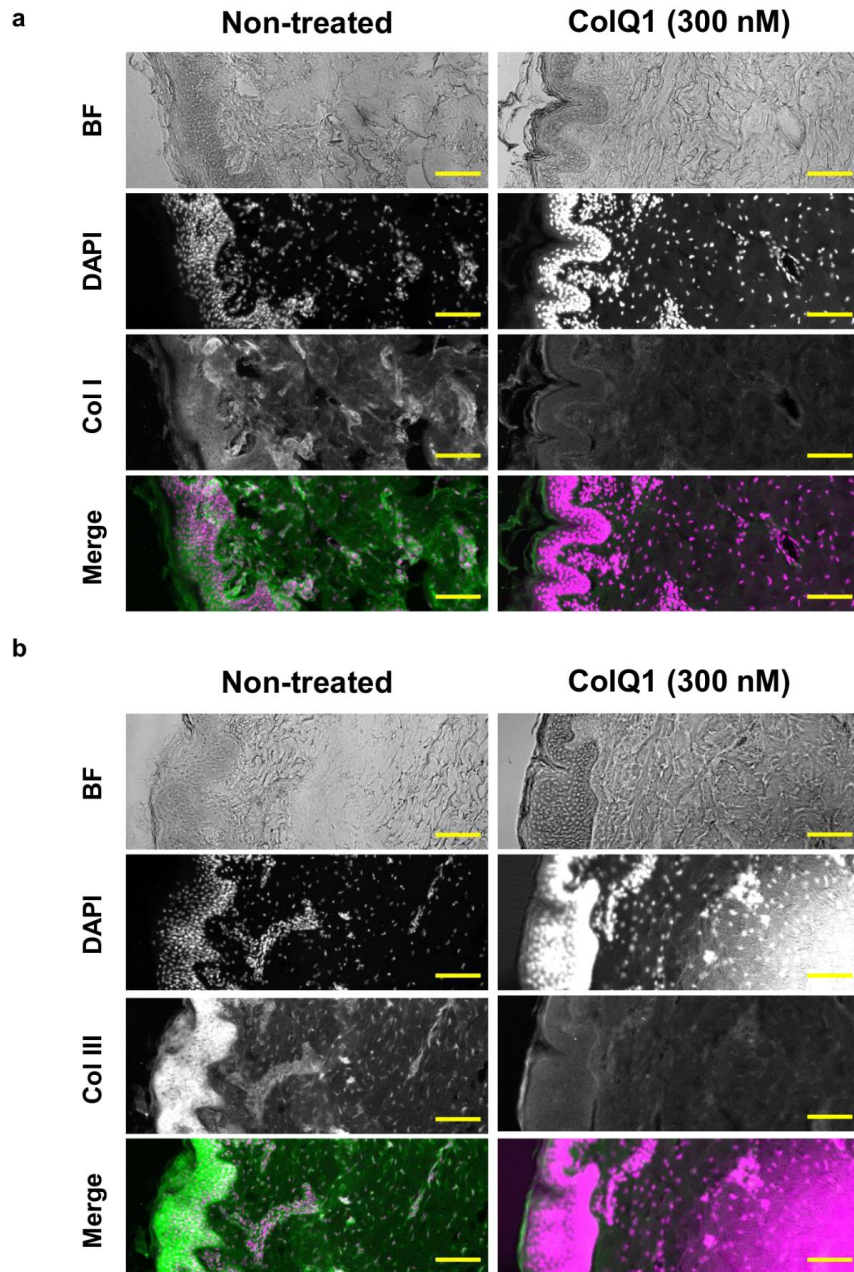
**Figure S2. Representative standard curve of peptidolytic activity of ColQ1 in presence of serine and cysteine inhibitors.** A 2.4 nM/ml stock solution of ColQ1 was serially diluted in the reaction buffer of the *in vitro* FRET-based peptidolytic assay. The reactions were initiated by the addition of 2  $\mu$ M FS1-1 and the reactions monitored for 2 min (excitation: 328 nm, emission: 392 nm) at 25  $^{\circ}$ C. Initial velocities were calculated via linear regression. All experiments were performed in triplicates and results are shown as mean  $\pm$  standard deviation.

### Dose-response curves for compound 1 and compound 2 vs ColQ1 (Figure S3)



**Figure S3. Representative dose-response curve for the  $IC_{50}$  value determination of compound 1 and 2 on ColQ1.** Due to limited compound solubility, the  $IC_{50}$  determination had to be performed via linear regression and was limited to the linear portion of the sigmoidal response curve.<sup>[1]</sup> The compounds were preincubated for 1 h at RT before initiating the reaction by addition of 2  $\mu$ M FS1-1. The reactions were monitored for 2 min (excitation: 328 nm, emission: 392 nm) at 25  $^{\circ}$ C. Initial velocities were calculated via linear regression and normalized to a non-inhibited control reaction. All experiments were performed in triplicates and results are shown as mean  $\pm$  standard deviation.

**Bright-field and DAPI signals of the tissue used for the immunostaining of fibrillar collagens (Figure S4)**



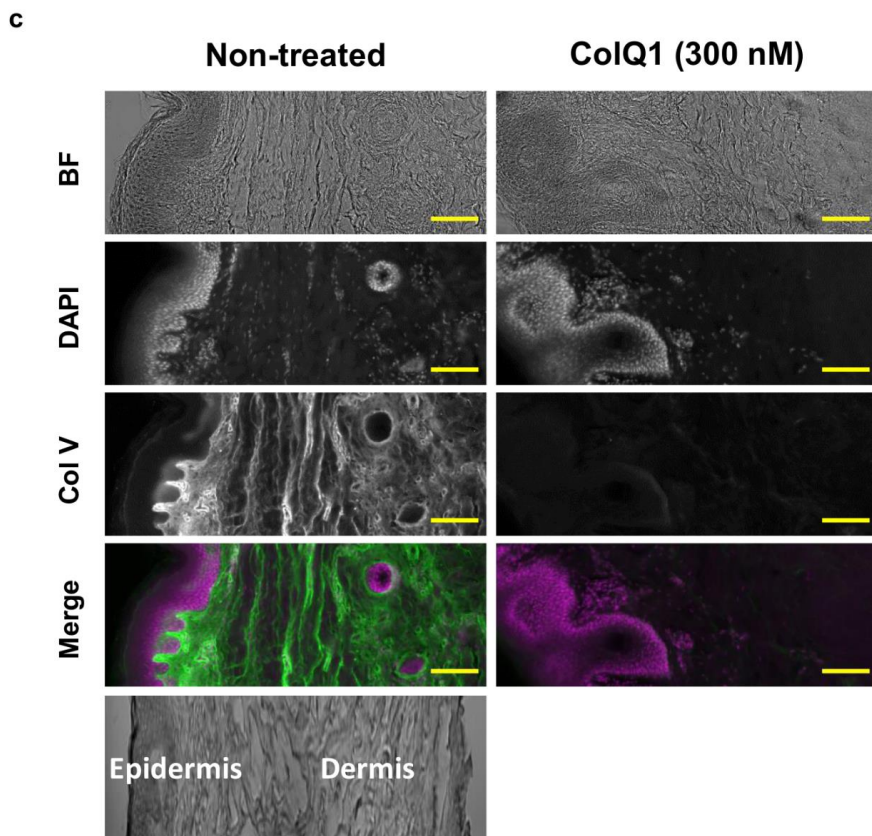


**Figure S4.** Bright-field and DAPI images of the non-treated tissue and ColQ1-treated tissue (a) COL I (Collagen I), (b) COL III (collagen III), (c) COL V (collagen V). Dermal and epidermal regions are labeled. Scale bar: 100  $\mu$ m.

**Effect of storage conditions on skin tissue (Figure S5)**

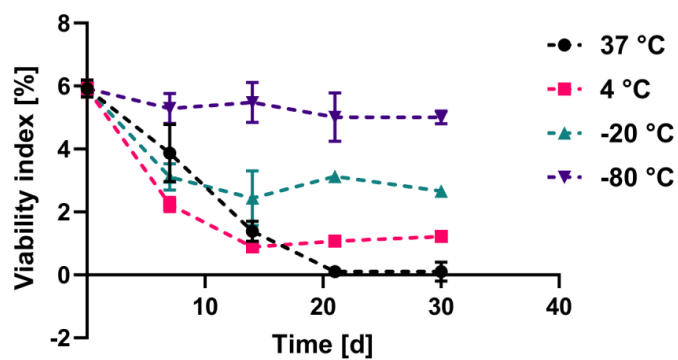


**Figure S5.** The influence of storage temperature on skin viability.

**SHG and fibrillar collagen imaging for the tissue challenged with ColQ1 with or without compound 1 (Figure S6)**

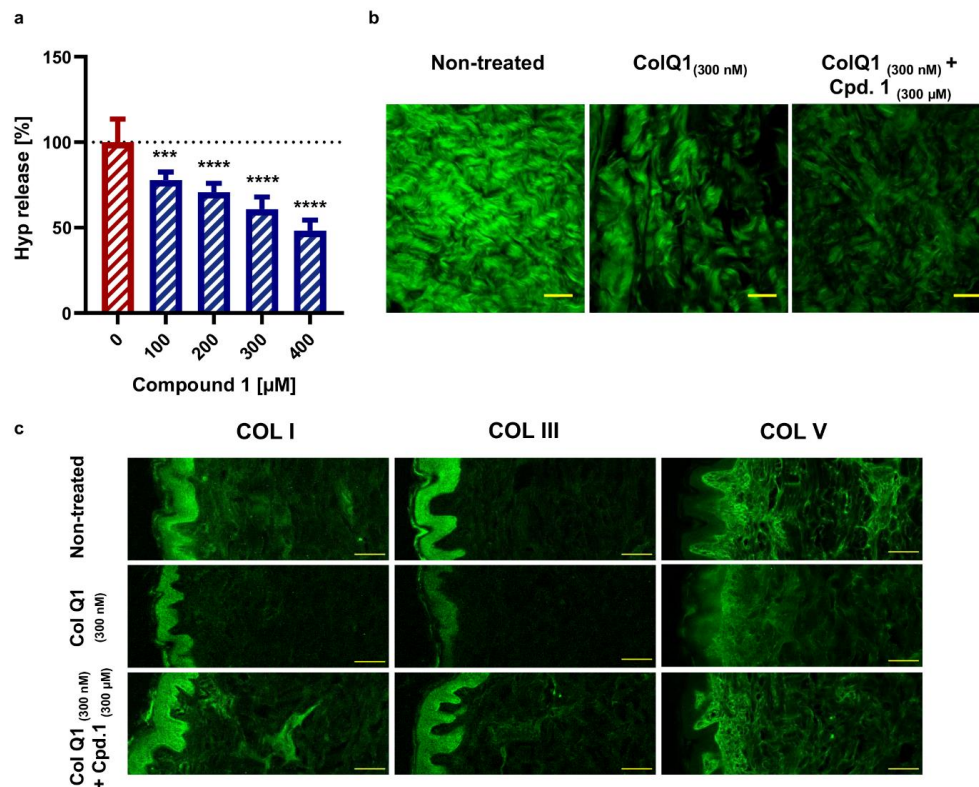


**Figure S6. Compound 1 inhibited the collagenolytic effect of ColQ1 *ex vivo* in skin tissue. (a)** Dose-dependent effect of compound 1 in Hyp release assay. **(b)** Confocal SHG images revealed an improved collagen signal with 300  $\mu$ M of compound 1 (tissue challenged with 300 nM ColQ1) compared with 300 nM ColQ1 without inhibitor. **(c)** Immunostaining of fibrillar COLs of the non-treated skin and treated with ColQ1 with or without compound 1. Statistical analysis was performed with one-way ANOVA and statistical significance was analyzed by Tukey test. Significance was calculated by comparing non-treated vs treated tissue with compound 1 (mean  $\pm$  SD, \*\*\*\*  $p \leq 0.0001$ , \*\*\*  $p \leq 0.001$ ). Hyp: hydroxyproline, COLs: collagens, SHG: second-harmonic generation. Scale bar: 100  $\mu$ m for SHG images and for the immunostained images.

**Viability and imaging data of fibroblast and keratinocyte cells challenged with *B. cereus* csn (Figure S7–S9)**

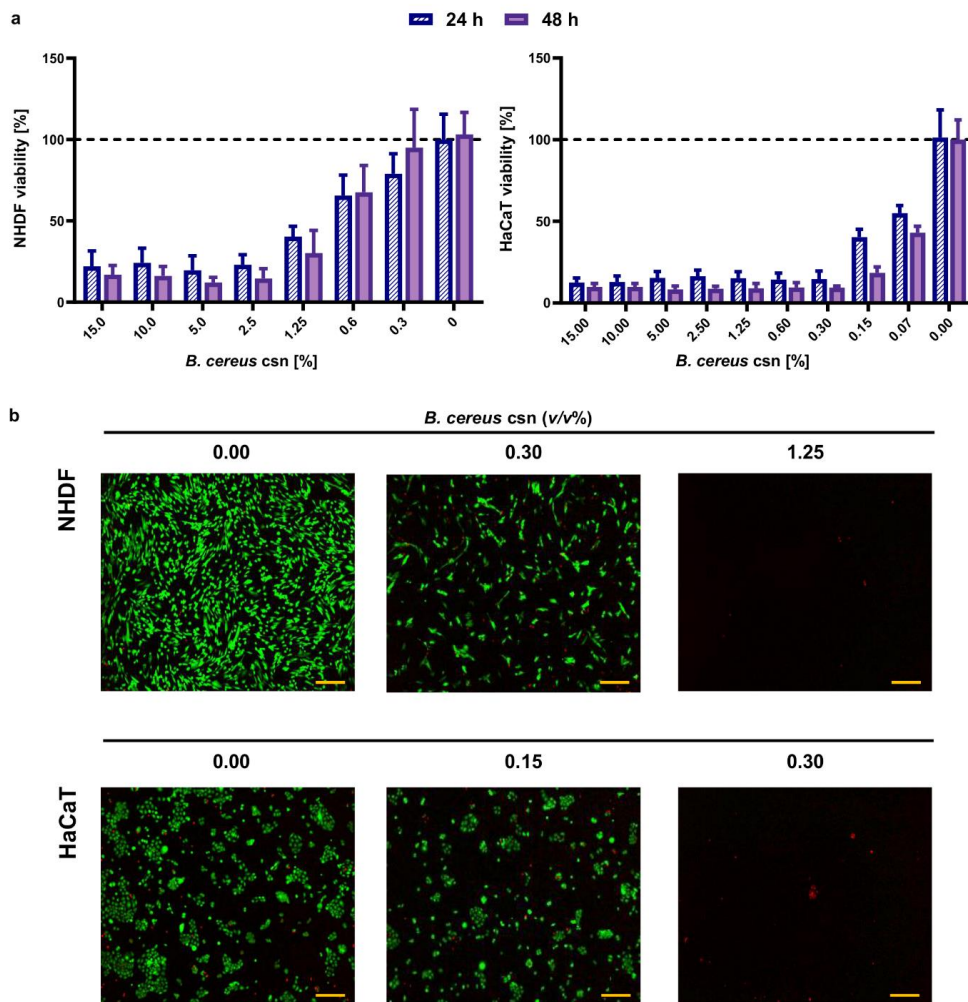


**Figure S7. Viability data of fibroblast (NHDF) and keratinocyte (HaCaT) cells upon the treatment with *B. cereus* csn. (a)** Representations of MTT data of skin cells after 1 and 2 days of incubation with various concentrations of *B. cereus* csn. **(b)** Composite signal of live and dead skin cells challenged with various concentrations of *B. cereus*. Green signals: living cells and red signals: dead cells, red signal in some cases was lost because the detached cells were washed away after the rinsing step with PBS. ( $n = 3$ , results are shown as mean  $\pm$  standard deviation), *B. cereus*: *Bacillus cereus*, csn: culture supernatant. Scale bar: 200  $\mu$ m.



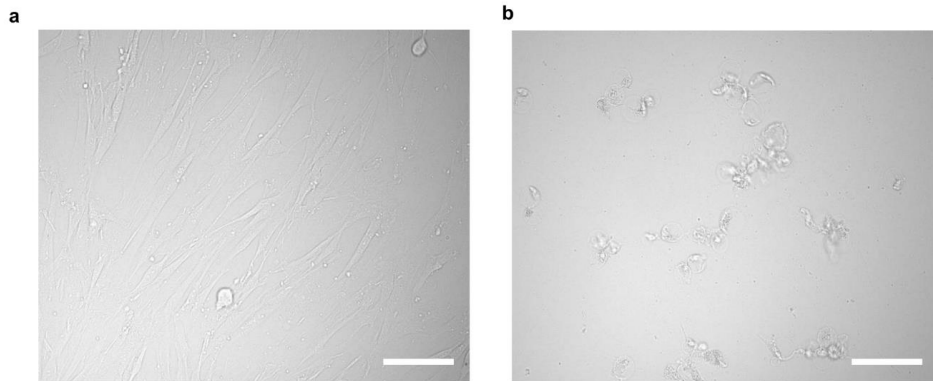


**Figure S8. Bright-field signals of skin cells challenged with *B. cereus* csn visualized with 20X objective. (a)** Non-treated NHDF cells compared with **(b)** NHDF cells treated with 1.25% (v/v) *B. cereus* csn. *B. cereus*: *Bacillus cereus*, csn: culture supernatant Scale bar: 100  $\mu$ m

**Live/dead imaging of the effect of compounds 1 and 2 on skin cells challenged with *B. cereus* csn (Figure S9)**

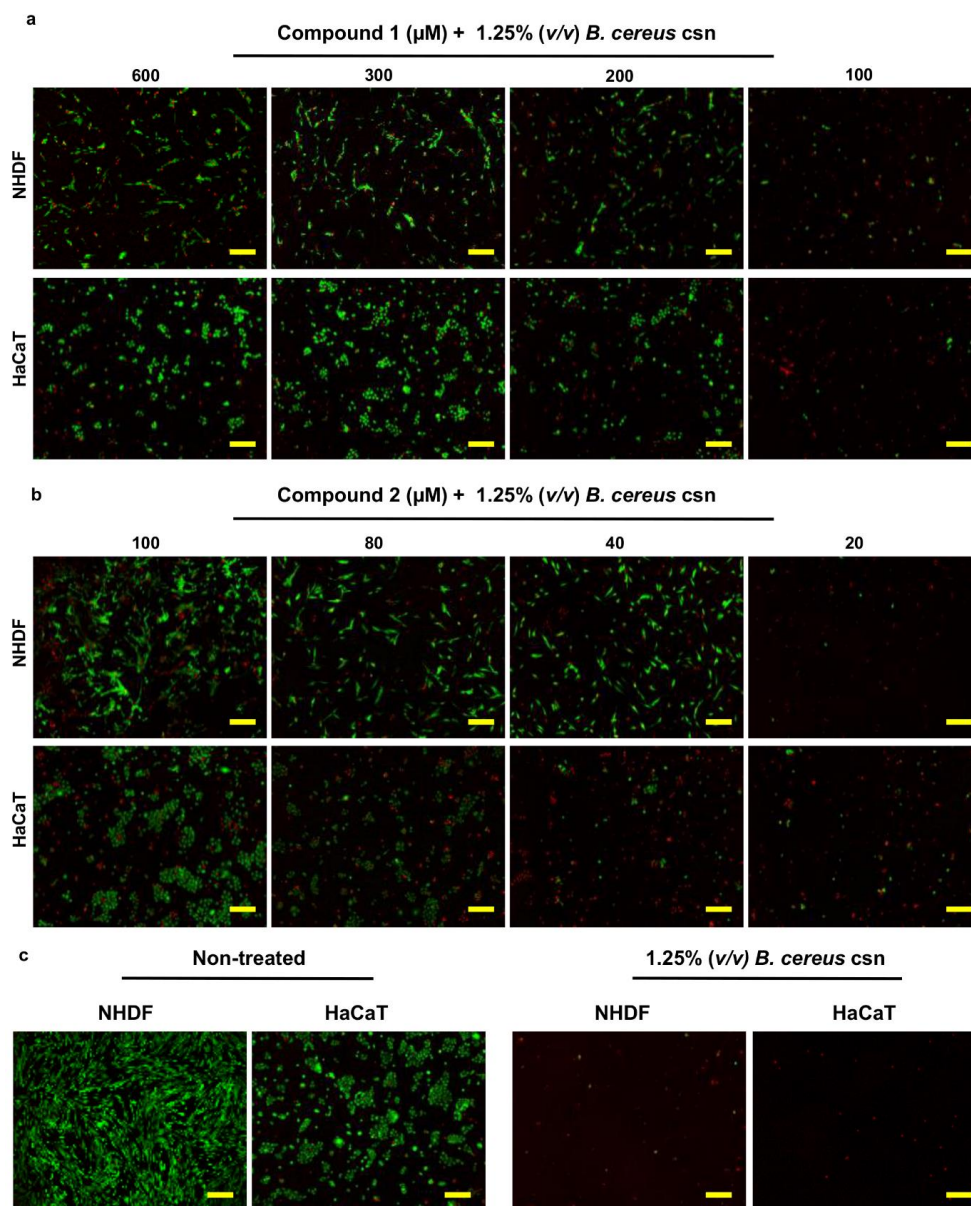


**Figure S9. Compounds 1 and 2 maintained the viability of skin cells upon the treatment with 1.25% (v/v) of *B. cereus* csn.** Live/dead imaging with fibroblasts (NHDF) and keratinocytes (HaCaT) challenged with 1.25% (v/v) of *B. cereus* csn with and without compounds (a) 1 and (b) 2 and (c) non-treated cells. Green signals: living cells and red signals: dead cells, red signals in some cases were lost because the detached cells were washed away after the rinsing step with PBS. *B. cereus*: *Bacillus cereus*, csn: culture supernatant. Scale bar: 200 μm for images.





*G. mellonella* survival analysis of the larvae challenged with *B. cereus* csn or with ColQ1 (with or without compound 1) and its inactive mutant version (Figure S10–S11)

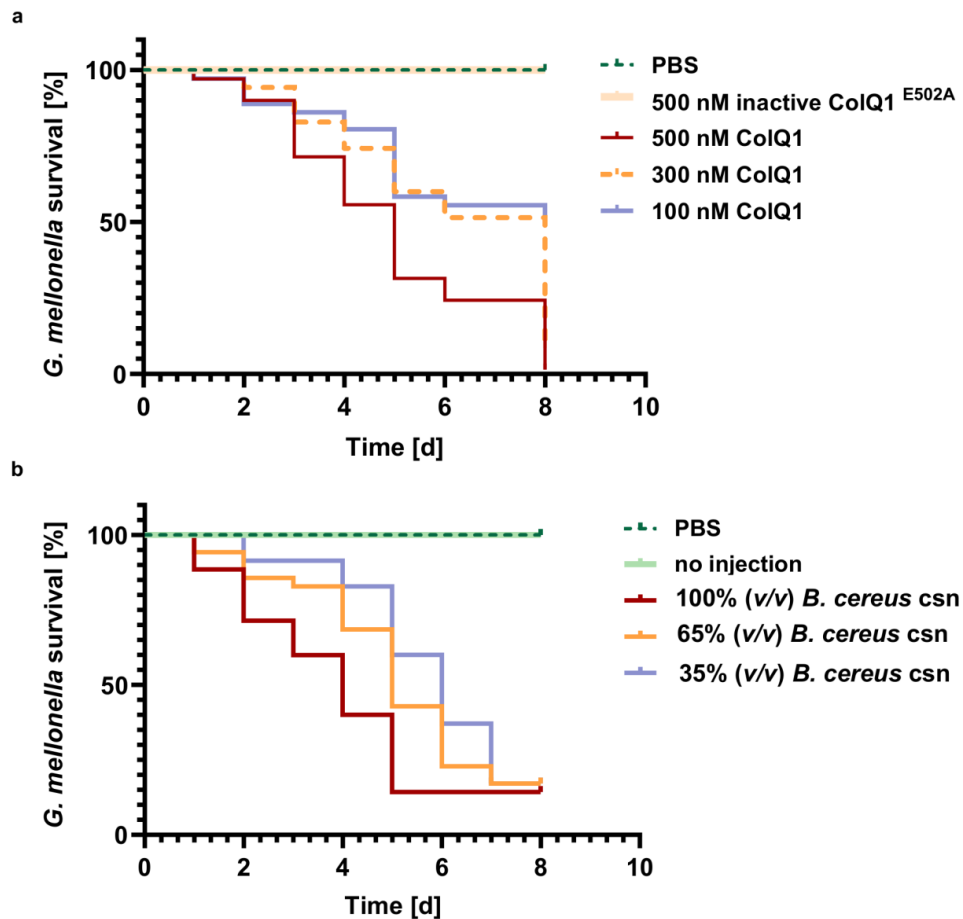


**Figure S11. Probability of survival of the *Galleria mellonella* larvae treated *B. cereus* csn or ColQ1.** (a) The survival of larvae challenged with different concentrations of ColQ1 (active and inactive mutant), the survival rate of larvae treated with 300 and 100  $\mu$ M of the inactive mutant ColQ1 E502A was 100%. (b) The survival of larvae challenged with different concentrations of *B. cereus* csn. *B. cereus*: *Bacillus cereus*, csn: culture supernatant. Each curve represents results of three independent experiments.

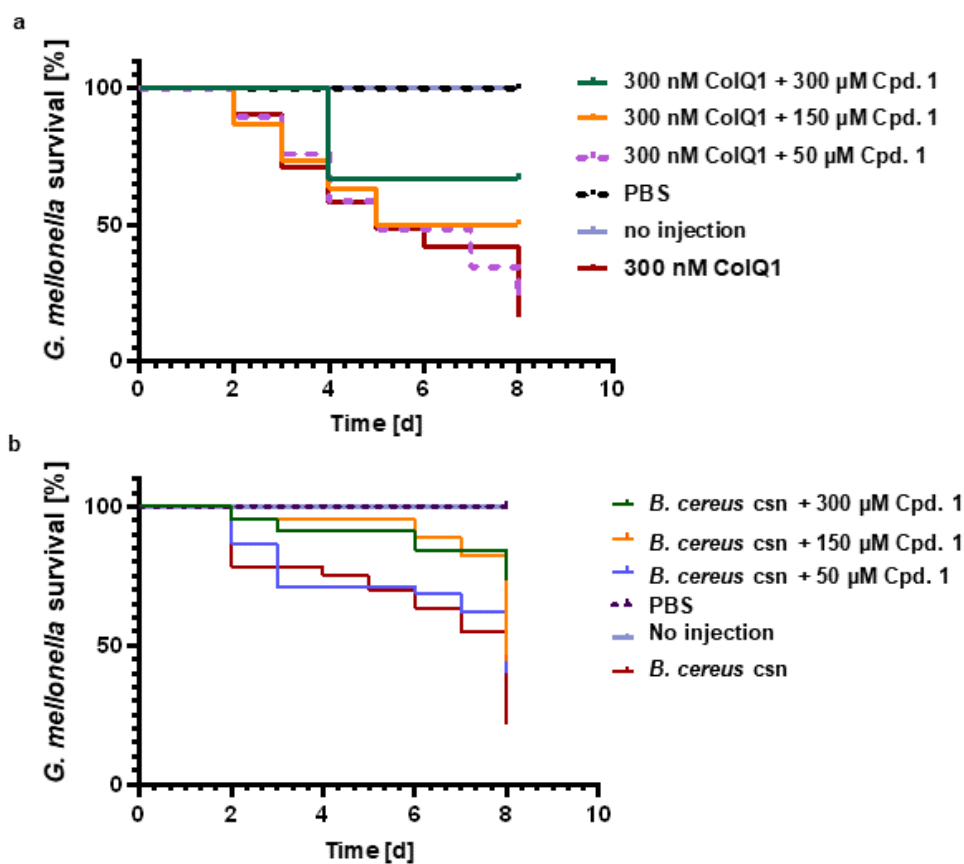


**Figure S11. Kaplan–Meier survival analysis of larvae treated with *B. cereus* csn with and without compound 1. (a) Survival analysis of larvae treated with 300 nM ColQ1 and with various concentrations (50–300 μM) compound 1. (b) The improvement in the survival of larvae challenged with 100% (*v/v*) *B. cereus* csn and various concentrations of compound 1 (50–300 μM). The statistical difference between groups treated with 300, 150, and 50 μM of compound 1 and treated with only 300 nM ColQ1 is  $p = 0.0002$ ,  $p = 0.0510$ , and  $p = 0.7593$ , sequentially (log-rank). The statistical difference between groups treated with 300, 150, and 50 μM of compound 1 and treated with only 100% (*v/v*) *B. cereus* csn is  $p < 0.0001$ ,  $p = 0.0096$ , and  $p = 0.0107$ , respectively. The survival rate for the larvae treated with compound 1 in PBS was 100%. *B. cereus*: *Bacillus cereus*, csn: culture supernatant.**

## Supplementary tables

**Table S1. Summary of epifluorescence imaging conditions**

Imaging conditions Collagen	Objective	Exposure time	LUT settings (Min–Max)
<b>Fig 1 – ColQ1 effect</b>			
<b>COL I</b>	Plan Apo $\lambda$ 10x	700 ms	500–1200
<b>COL III</b>	Plan Apo $\lambda$ 10x	700 ms	500–1200
<b>COL V</b>	SPlanFluor 20x LWD Dry	200 ms	500–5600
<b>Fig 3 – (compound 2)</b>			
<b>COL I</b>	SPlanFluor 20x LWD Dry	200 ms	500–8000
<b>COL III</b>	SPlanFluor 20x LWD Dry	200 ms	500–1400
<b>COL V</b>	SPlanFluor 20x LWD Dry	1 s	500–1600
<b>S4 Fig – (compound 1)</b>			
<b>COL I</b>	SPlanFluor 20x ELWD DIC N1	200 ms	500–560
<b>COL III</b>	SPlanFluor 20x ELWD DIC N1	200 ms	500–560
<b>COL V</b>	SPlanFluor 20x ELWD DIC N1	1 s	500–800

## References

1. Sebaugh, J. L. & McCray, P. D. Defining the linear portion of a sigmoid-shaped curve: bend points. *Pharm. Stat.* **2**, 167–174 (2003).

## A4. SUPPORTING INFORMATION TO CHAPTER D

***N*-Aryl mercaptoacetamides as a Potential Multi-target Inhibitors of Metallo- $\beta$ -lactamases (MBLs) and the Virulence Factor LasB from *Pseudomonas aeruginosa*.**

Samir Yahiaoui,<sup>±</sup> Katrin Voos,<sup>±</sup> Jörg Haupenthal, Thomas Wichelhaus, Denia Frank, Lilia Weizel, Marco Rotter, Steffen Brunst, Jan S. Kramer, Ewgenij Proschak, Christian Ducho\* and Anna K. H. Hirsch\*

<sup>±</sup> these authors contributed equally

\* corresponding authors

Reproduced from *RSC Med. Chem.* **2021**, *12*, 1698 – 1708

with permission from the Royal Society of Chemistry.

DOI: 10.1039/D1MD00187F

Copyright (2021) Royal Society of Chemistry

## -Supporting Information-

*N*-Aryl mercaptoacetamides as potential multi-target inhibitors of metallo- $\beta$ -  
lactamases (MBLs) and the virulence factor LasB from *Pseudomonas*  
*aeruginosa*

Samir Yahiaoui<sup>1,#</sup>, Katrin Voos<sup>2,#</sup>, Jörg Haupenthal<sup>1</sup>, Thomas A. Wichelhaus<sup>4</sup>, Denia Frank<sup>4</sup>,  
Lilia Weizel,<sup>5</sup> Marco Rotter,<sup>5</sup> Steffen Brunst,<sup>5</sup> Jan S. Kramer,<sup>5</sup> Ewgenij Proschak<sup>5</sup>, Christian  
Ducho<sup>2,\*</sup>, Anna K.H. Hirsch<sup>1,3\*</sup>

<sup>1</sup> Helmholtz Institute for Pharmaceutical Research Saarland (HIPS) – Helmholtz Centre for  
Infection Research (HZI), Campus E8 1, 66123 Saarbrücken, Germany

<sup>2</sup> Department of Pharmacy, Pharmaceutical and Medicinal Chemistry, Saarland University,  
Campus C2 3, 66123 Saarbrücken, Germany

<sup>3</sup> Department of Pharmacy, Saarland University, Campus Building E8 1, 66123 Saarbrücken,  
Germany

<sup>4</sup> Institute of Medical Microbiology and Infection Control, University Hospital Frankfurt, Paul-  
Ehrlich-Straße 40, 60596 Frankfurt, Germany

<sup>5</sup> Institute of Pharmaceutical Chemistry, Goethe University Frankfurt, Max-von-Laue-Straße  
9, 60438, Frankfurt, Germany

\* Corresponding authors. E-mail: [Anna.Hirsch@Helmholtz-hips.de](mailto:Anna.Hirsch@Helmholtz-hips.de); [Christian.Ducho@Uni-Saarland.de](mailto:Christian.Ducho@Uni-Saarland.de)

# Equal contribution

## **Table of contents**

Assays.....	3
Cytotoxicity assay <sup>1,2</sup> .....	3
<i>In vivo</i> zebrafish-embryo toxicity assay <sup>1</sup> .....	3
Growth inhibition assay .....	3
Selectivity assay over several human off-targets .....	4
Chemistry .....	6
General procedures for the synthesis of compounds <b>2 – 25</b> .....	7
Synthesis of alkyl chlorides <b>2 – 9</b> .....	8
Synthesis of thioacetates <b>10 – 17</b> .....	11
Synthesis of thiols <b>18 – 25</b> .....	14
<sup>1</sup> H and <sup>13</sup> C NMR spectra of compounds <b>2 – 25</b> .....	17
References .....	41

## Assays

### Cytotoxicity assay<sup>1,2</sup>

**Table S1.** Previously published cytotoxicity data of compound **1** against HepG2, HEK293, and A549 cell lines.

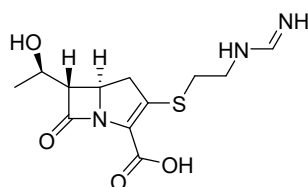
Cpd.	IC <sub>50</sub> ( $\mu$ M) <sup>a</sup>		
	HepG2	HEK293	A549
<b>1</b>	>100	>100	>100
<sup>a</sup> Means and SD of at least two independent experiments			

### In vivo zebrafish-embryo toxicity assay<sup>1</sup>

**Table S2.** Previously published results of zebrafish-embryo toxicity for compound **1**.

Cpd.	Conc. ( $\mu$ M)	Observation after 1 day of incubation	Observation after 2 days of incubation	Observation after 3 days of incubation	Observation after 4 days of incubation	Final survival rate (%)
<b>1</b>	100	all embryos dead, cpd precipitation	all embryos dead, cpd precipitation	all embryos dead, cpd precipitation	all embryos dead, cpd precipitation	0
	30	all embryos dead, cpd precipitation	all embryos dead, cpd precipitation	all embryos dead, cpd precipitation	all embryos dead, cpd precipitation	0
	10	no pigmentation	impaired pigmentation	impaired pigmentation	impaired pigmentation	90
	2	-	-	-	-	80

### Growth-inhibition assay



**Imipenem  
(Imi)**

**Figure S1.** Structure of the carbapenem antibiotic imipenem used in the growth-curve assay.



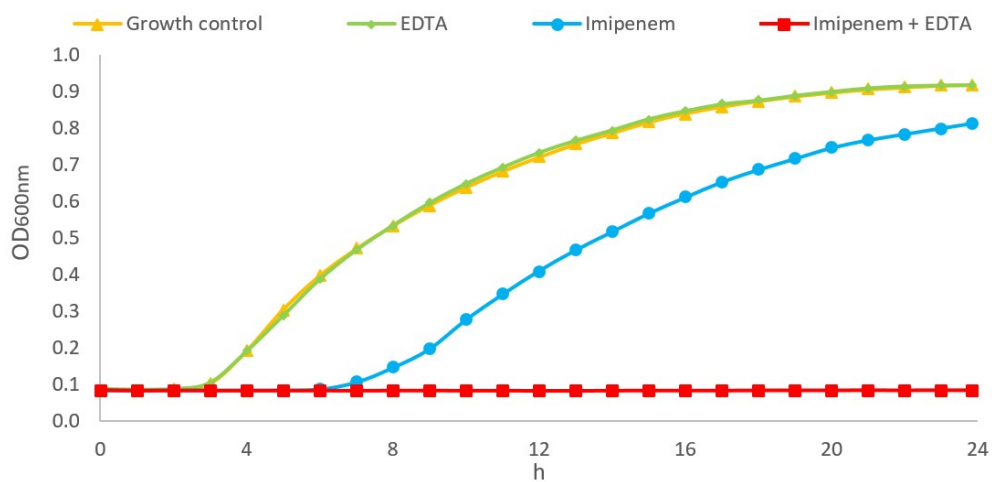
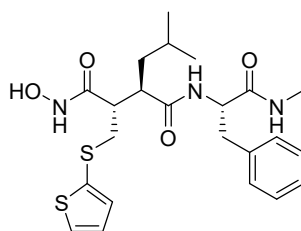


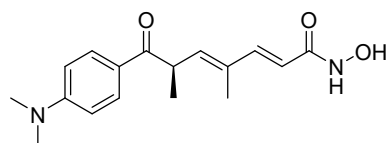
**Figure S2.** Growth curve of NDM-1-expressing *K. pneumoniae* (T2301) in the absence and presence of imipenem at 8  $\mu\text{g}/\text{mL}$  (*i.e.*, 0.5x MIC)  $\pm$  EDTA as MBL inhibitor at 50  $\mu\text{g}/\text{mL}$ .

#### Selectivity assay over several human off-targets



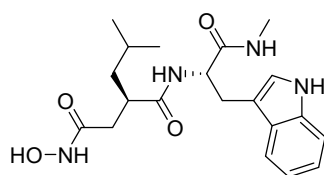
**Batimastat**

**Figure S3.** Structure of batimastat, an unselective MMP inhibitor used as reference in the MMP selectivity study.



**Trichostatin A**

**Figure S4.** Structure of trichostatin A, an HDAC inhibitor used as reference in the HDAC selectivity study.



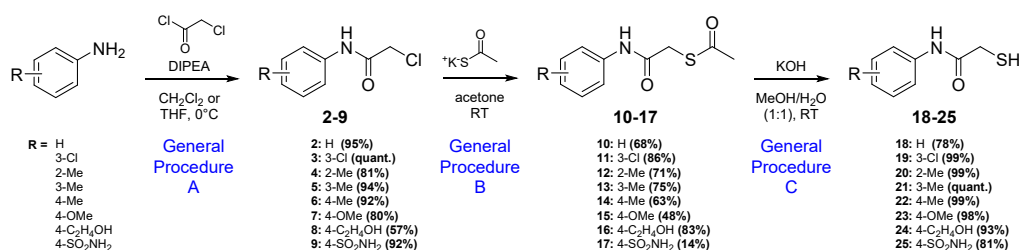
**Ilomastat**

**Figure S5.** Structure of ilomastat, an MMP and TACE inhibitor used as reference in the TACE selectivity study.

## Chemistry

**General.** All chemicals were purchased from standard suppliers. Acetone and MeOH were purchased in HPLC quality, all other solvents were of technical quality and distilled before use. Deionized water was used throughout. The reactions were monitored by thin-layer chromatography (TLC) using aluminum plates precoated with silica gel 60 F<sub>254</sub> (VWR) and visualized using UV light (254 nm) and staining under heating (CAM stain: 12 g ammonium molybdate, 0.5 g ceric ammonium molybdate, 235 mL H<sub>2</sub>O, 15 mL conc. H<sub>2</sub>SO<sub>4</sub>). All organic extracts were dried over Na<sub>2</sub>SO<sub>4</sub>, and solvents were removed by a rotary evaporator equipped with a water bath at 40 °C. 300 MHz- and 500 MHz-<sup>1</sup>H NMR spectra and 75 MHz- and 125 MHz-<sup>13</sup>C NMR spectra were recorded on Bruker Fourier 300 or Bruker UltraShield™ 500 (Bruker Corporation, Billerica, MA, USA) spectrometers. All spectra were recorded at room temperature and were referenced internally to solvent reference frequencies. Chemical shifts ( $\delta$ ) are provided in parts per million (ppm) and coupling constants ( $J$ ) are given in Hz. Low-resolution mass spectra were measured on a Thermo Finnigan Surveyor MSQ Plus mass spectrometer. High-resolution mass spectrometry (HRMS) was performed on a Thermo Scientific Q Exactive Orbitrap mass spectrometer equipped with an electrospray (ESI) source.

## General procedures for the synthesis of compounds 2–25



**General Procedure A.** Aniline (1 equiv.) and DIPEA (1.2 equiv.) were dissolved in dry CH<sub>2</sub>Cl<sub>2</sub> and cooled on ice to 0 °C. To this solution, acid chloride (1.2 equiv.) was added dropwise, and the resulting mixture was stirred at 0 °C for 1-2 h. The reaction mixture was quenched with 0.5 M NaHCO<sub>3</sub>. After dilution with CH<sub>2</sub>Cl<sub>2</sub>, the mixture was extracted thrice with 0.5 M NaHCO<sub>3</sub> and 0.5 M HCl, as well as once with brine. The CH<sub>2</sub>Cl<sub>2</sub> layer was dried with Na<sub>2</sub>SO<sub>4</sub> and concentrated under reduced pressure to give the titled compounds in clean form without any further purification.

**General Procedure B.** Alpha-chloride (1 equiv.) was dissolved in acetone, and then potassium thioacetate (1.2 equiv.) was added. The resulting suspension was stirred at rt until the TLC indicated complete transformation. The reaction mixture was concentrated under reduced pressure. The resulting residue was diluted with EtOAc and extracted thrice with 0.5 M NaHCO<sub>3</sub> and 0.5 M HCl, as well as once with brine. The EtOAc layer was dried with Na<sub>2</sub>SO<sub>4</sub> and concentrated under reduced pressure to give a solid or oily residue, which was further purified using flash chromatography on high performance silica gel, to yield the named thioacetates.

**General Procedure C.** The thioacetate compound was dissolved in methanol and heated to 35 °C. Then 2 M aqueous KOH was added to give a 1:1 mixture. The solution was stirred at this temperature until the TLC indicated complete transformation (0.5-2 h). The reaction mixture was diluted with EtOAc and extracted twice with 0.5 M NaHCO<sub>3</sub> and once with 0.5 M HCl and brine. The EtOAc layer was dried with Na<sub>2</sub>SO<sub>4</sub> and concentrated under reduced pressure to give the final compounds without further purification.

### Synthesis of alkyl chlorides 2 – 9

**2-Chloro-*N*-phenylacetamide 2.** Compound **2** was synthesized according to the general procedure **A**, using aniline (1.00 mL, 11.0 mmol), DIPEA (4.00 mL, 23.0 mmol) and chloroacetyl chloride (1.00 mL, 12.6 mmol) in 15 mL of dry CH<sub>2</sub>Cl<sub>2</sub>. The reaction was stirred for 2 h at 0 °C. After extraction, **2** was obtained as brown solid without further purification (1.76 g, 95%). <sup>1</sup>H NMR (500 MHz, CDCl<sub>3</sub>) δ 8.27 (br, 1 H, NH), 7.55 (dd, *J* = 1.1, 8.6 Hz, 2 H, 2'-H, 6'-H), 7.36 (dd, *J* = 7.6, 8.4 Hz, 2 H, 3'-H, 5'-H), 7.17 (t, *J* = 7.5 Hz, 1 H, 4'-H), 4.19 (s, 2 H, 2-H). <sup>13</sup>C NMR (126 MHz, CDCl<sub>3</sub>) δ 163.99 (1-C), 136.78 (1'-C), 129.25 (3'-C, 5'-C), 125.38 (4'-C), 120.27 (2'-C, 6'-C), 43.00 (2-C). HRMS (ESI) *m/z* calculated for C<sub>8</sub>H<sub>9</sub>ClNO 170.0367 [M+H]<sup>+</sup>, found 170.0363. TLC (petroleum ether-EtOAc, 7:3): R<sub>f</sub> = 0.30.

**2-Chloro-*N*-(3'-chlorophenyl)acetamide 3.** Compound **3** was synthesized according to the general procedure **A**, using 3-chloroaniline (150 μL, 1.42 mmol), DIPEA (500 μL, 2.87 mmol) and 2-chloroacetyl chloride (130 μL, 1.63 mmol) in 10 mL of dry CH<sub>2</sub>Cl<sub>2</sub>. The reaction was stirred for 4 h 20 min at 0 °C. After extraction, **3** was obtained as brown solid without further purification (323 mg, quant.). <sup>1</sup>H NMR (500 MHz, CDCl<sub>3</sub>) δ 8.20 (br, 1 H, NH), 7.66 (t, *J* = 2.0 Hz, 1 H, 2'-H), 7.40 (ddd, *J* = 0.7, 1.9, 8.2 Hz, 1 H, 4'-H or 6'-H), 7.28 (t, *J* = 8.2 Hz, 1 H, 5'-H), 6.99 (ddd, *J* = 0.9, 1.9, 8.0 Hz, 1 H, 4'-H or 6'-H), 4.19 (s, 2 H). <sup>13</sup>C NMR (126 MHz, CDCl<sub>3</sub>) δ 164.03 (1-C), 137.88 (1'-C or 3'-C), 134.95 (1'-C or 3'-C), 130.25 (5'-C), 125.45 (4'-C or 6'-C), 120.32 (2'-C), 118.17 (4'-C or 6'-C), 42.93 (2-C). HRMS (ESI) *m/z* calcd. for C<sub>8</sub>H<sub>8</sub>Cl<sub>2</sub>NO [M+H]<sup>+</sup> 203.9977, found: 203.9974. TLC (petroleum ether-EtOAc, 7:3): R<sub>f</sub> = 0.30.

**2-Chloro-*N*-(*o*-tolyl)acetamide 4.** Compound **4** was synthesized according to the general procedure **A**, using *o*-toluidine (500 μL, 4.70 mmol), DIPEA (1.70 mL, 9.76 mmol) and 2-chloroacetyl chloride (410 μL, 5.15 mmol) in 10 mL of dry CH<sub>2</sub>Cl<sub>2</sub>. The reaction was stirred for 6 h at 0 °C that slowly warmed up to room temperature. After extraction, **4** was obtained as brown solid without further purification (700 mg, 81%). <sup>1</sup>H NMR (500 MHz, CDCl<sub>3</sub>) δ 8.23 (br, 1 H, NH), 7.87 (d, *J* = 8.2 Hz, 1 H, 6'-H), 7.26 – 7.20 (m, 2 H, 3'-H, 4'-H), 7.12 (td, *J* = 1.1, 7.5 Hz, 1 H, 5'-H), 4.24 (s, 2 H, 2-H), 2.31 (s, 3 H, 2'-CH<sub>3</sub>). <sup>13</sup>C NMR (126 MHz, CDCl<sub>3</sub>) δ 163.92 (1-C), 134.76 (1'-C or 2'-C), 130.72 (3'-C), 129.14 (1'-C or 2'-C), 127.05 (4'-C), 125.92 (5'-C), 122.55 (6'-C), 43.28 (2-C), 17.62 (2'-CH<sub>3</sub>). MS (ESI<sup>+</sup>) *m/z* 184 (M+H)<sup>+</sup>. TLC (petroleum ether-EtOAc, 7:3): R<sub>f</sub> = 0.30.

**2-Chloro-*N*-(*m*-tolyl)acetamide 5.** Compound **5** was synthesized according to the general procedure **A**, using *m*-toluidine (400  $\mu$ L, 3.73 mmol), DIPEA (1.30 mL, 7.46 mmol) and chloroacetyl chloride (330  $\mu$ L, 4.14 mmol) in 7 mL of dry  $\text{CH}_2\text{Cl}_2$ . The reaction was stirred for 3 h 30 min at 0  $^\circ\text{C}$ . After extraction, **5** was obtained as brown solid without further purification (642 mg, 94%).  $^1\text{H}$  NMR (500 MHz,  $\text{CDCl}_3$ )  $\delta$  8.20 (br, 1 H, NH), 7.37 (s, 1 H, 2'-H), 7.33 (d,  $J$  = 8.3 Hz, 1 H, 6'-H), 7.23 (t,  $J$  = 7.7 Hz, 1 H, 5'-H), 6.99 (d,  $J$  = 7.5 Hz, 1 H, 4'-H), 4.17 (s, 2 H, 2-H), 2.35 (s, 3 H, 3'- $\text{CH}_3$ ).  $^{13}\text{C}$  NMR (126 MHz,  $\text{CDCl}_3$ )  $\delta$  163.91 (1-C), 139.26 (3'-C), 136.66 (1'-C), 129.07 (5'-C), 126.20 (4'-C), 120.88 (2'-C), 117.35 (6'-C), 43.02 (2-C), 21.57 (3'- $\text{CH}_3$ ). HRMS (ESI)  $m/z$  calcd. for  $\text{C}_9\text{H}_{11}\text{ClNO}$   $[\text{M}+\text{H}]^+$  184.0524, found: 184.0519. TLC (petroleum ether-EtOAc, 7:3):  $R_f$  = 0.40.

**2-Chloro-*N*-(*p*-tolyl)acetamide 6.** Compound **6** was synthesized according to the general procedure **A**, using *p*-toluidine (499 mg, 4.66 mmol), DIPEA (1.70 mL, 9.76 mmol) and chloroacetyl chloride (450  $\mu$ L, 5.65 mmol) in 10 mL of dry  $\text{CH}_2\text{Cl}_2$ . The reaction was stirred for 2 h 30 min at 0  $^\circ\text{C}$ . After extraction **6** was obtained as brown solid without further purification (784 mg, 92%).  $^1\text{H}$  NMR (500 Hz,  $\text{CDCl}_3$ )  $\delta$  8.18 (br, 1 H, NH), 7.42 (d,  $J$  = 8.4 Hz, 2 H, aryl- $\text{H}_a$ ), 7.16 (d,  $J$  = 8.3 Hz, 2 H, aryl- $\text{H}_b$ ), 4.18 (s, 2 H, 2-H), 2.33 (s, 3 H, 4'- $\text{CH}_3$ ).  $^{13}\text{C}$  NMR (126 Hz,  $\text{CDCl}_3$ )  $\delta$  163.84 (1-C), 135.15 (1'-C or 4'-C), 134.22 (1'-C or 4'-C), 129.77 (aryl- $\text{C}_b$ ), 120.36 (aryl- $\text{C}_a$ ), 43.01 (2-H), 21.05 (4'- $\text{CH}_3$ ). HRMS (ESI)  $m/z$  calcd. for  $\text{C}_9\text{H}_{11}\text{ClNO}$   $[\text{M}+\text{H}]^+$  184.0524, found: 184.0520. TLC (petroleum ether-EtOAc, 7:3):  $R_f$  = 0.40.

**2-Chloro-*N*-(4'-methoxyphenyl)acetamide 7.** Compound **7** was synthesized according to the general procedure **A**, using 4-methoxyaniline (1.41 g, 11.5 mmol), DIPEA (4.00 mL, 23.0 mmol) and chloroacetyl chloride (1.00 mL, 12.56 mmol) in 15 mL of dry  $\text{CH}_2\text{Cl}_2$ . The reaction was stirred for 2 h 20 min at 0  $^\circ\text{C}$ . After extraction **7** was obtained as brown solid without further purification (1.83 g, 80%).  $^1\text{H}$  NMR (500 Hz,  $\text{CDCl}_3$ )  $\delta$  8.18 (br, 1 H, NH), 7.43 (d,  $J$  = 9.0 Hz, 2 H, 3'-H, 5'-H), 6.88 (d,  $J$  = 9.0 Hz, 2 H, 2'-C, 6'-C), 4.18 (s, 2 H, 2-H), 3.80 (s, 3 H, 4'- $\text{OCH}_3$ ).  $^{13}\text{C}$  NMR (126 Hz,  $\text{CDCl}_3$ )  $\delta$  163.90 (1-C), 157.22 (4'-C), 129.78 (1'-C), 122.22 (3'-C, 5'-C), 114.38 (2'-C, 6'-C), 55.60 (4'- $\text{OCH}_3$ ), 42.96 (2-C). HRMS (ESI)  $m/z$  calculated for  $\text{C}_9\text{H}_{11}\text{ClNO}_2$  200.0473  $[\text{M}+\text{H}]^+$ , found 200.0466. TLC (petroleum ether-EtOAc, 2:8):  $R_f$  = 0.50.

**2-Chloro-*N*-(4'-(2'-hydroxyethyl)phenyl)acetamide 8.** Compound **8** was synthesized according to the general procedure **A**, using 4-(2'-hydroxyethyl)aniline (1.00 g, 7.30 mmol), DIPEA (1.40 mL, 8.04 mmol) and chloroacetyl chloride (640  $\mu$ L, 8.04 mmol) in 20 mL of dry

9

THF. The reaction was stirred for 2 h 20 min at 0 °C. After extraction, **8** was obtained as white solid without further purification (885 mg, 57%).  $R_f = 0.06$  (PE/EtOAc 65:35).  $^1\text{H NMR}$  (500 MHz,  $\text{DMSO-}d_6$ )  $\delta$  10.21 (s, 1 H, NH), 7.47 (d,  $J = 8.5$  Hz, 2 H, 3'-H, 5'-H), 7.16 (d,  $J = 8.5$  Hz, 2 H, 2'-H, 6'-H), 4.62 (t,  $J = 5.1$  Hz, 1 H, 2''-OH), 4.23 (s, 2 H, 2-H), 3.56 (td,  $J = 4.8, 7.0$  Hz, 2 H, 2''-H), 2.67 (t,  $J = 7.1$  Hz, 2 H, 1''-H).  $^{13}\text{C NMR}$  (126 MHz,  $\text{DMSO-}d_6$ )  $\delta$  164.39 (1-C), 136.37 (1'-C), 135.07 (4'-C), 129.19 (2'-C, 6'-C), 119.31 (3'-C, 5'-C), 62.19 (2''-C), 43.56 (2-C), 38.46 (1''-C). MS (ESI<sup>+</sup>)  $m/z$  214 (M+H)<sup>+</sup>. TLC (petroleum ether-EtOAc, 65:35):  $R_f = 0.05$ .

**2-Chloro-*N*-(4'-sulfamoylphenyl)acetamide 9.** Compound **9** was synthesized according to the general procedure **A**, using sulfanilamid (2.03 g, 11.8 mmol), DIPEA (2.30 mL, 13.2 mmol) and chloroacetyl chloride (1.10 mL, 13.8 mmol) in 45 mL of dry THF. The reaction was stirred for 1 h 30 min at 0 °C. After extraction **9** was obtained as orange solid without further purification (2.70 g, 92%).  $^1\text{H NMR}$  (500 MHz,  $\text{DMSO-}d_6$ )  $\delta$  10.63 (s, 1 H, NH), 7.79 (d,  $J = 9.0$  Hz, 2 H, aryl-H<sub>a</sub>), 7.75 (d,  $J = 9.0$  Hz, 2 H, aryl-H<sub>b</sub>), 7.29 (s, 2 H, SO<sub>2</sub>NH<sub>2</sub>), 4.30 (s, 2 H, 2-C).  $^{13}\text{C NMR}$  (126 MHz,  $\text{DMSO-}d_6$ )  $\delta$  165.18 (1-C), 141.34 (1'-C or 4'-C), 138.95 (1'-C or 4'-C), 126.81 (aryl-C<sub>a</sub>), 118.97 (aryl-C<sub>b</sub>), 43.55 (2-C). MS (ESI<sup>+</sup>)  $m/z$  249 (M+H)<sup>+</sup>. TLC ( $\text{CH}_2\text{Cl}_2$ - MeOH, 95:5):  $R_f = 0.10$ .

### Synthesis of thioacetates 10–17

**2-S-(Acetylthio)-N-phenylacetamide 10.** Compound **10** was synthesized according to the general procedure **B**, using intermediate **2** (242 mg, 1.43 mmol) and potassium thioacetate (200 mg, 1.75 mmol) in 10 mL acetone. The reaction was stirred for 3 h at room temperature. After extraction and column chromatography (PE/EtOAc 8:2) **10** was obtained as yellow solid (204 mg, 68%). <sup>1</sup>H NMR (500 MHz, CDCl<sub>3</sub>) δ 8.11 (br, 1 H, NH), 7.49 (d, *J* = 7.6 Hz, 2 H, 2'-H, 6'-H), 7.29 (t, *J* = 7.7 Hz, 2 H, 3'-H, 5'-H), 7.11 (t, *J* = 7.5 Hz, 1 H, 4'-H), 3.64 (s, 2 H, 2-H), 2.43 (s, 3 H, S(CO)CH<sub>3</sub>). <sup>13</sup>C NMR (126 MHz, CDCl<sub>3</sub>) δ 197.26 (S(CO)CH<sub>3</sub>), 166.46 (1-C), 137.73 (1'-C), 129.13 (3'-C, 5'-C), 124.68 (4'-C), 119.94 (2'-C, 6'-C), 34.38 (2-C), 30.40 (S(CO)CH<sub>3</sub>). HRMS (ESI) *m/z* calculated for C<sub>10</sub>H<sub>12</sub>NO<sub>2</sub>S 210.0583 [M+H]<sup>+</sup>, found: 210.0576. TLC (petroleum ether-EtOAc, 7:3): R<sub>f</sub> = 0.20.

**2-S-(Acetylthio)-N-(3'-chlorophenyl)acetamide 11.** Compound **11** was synthesized according to the general procedure **B**, using intermediate **3** (125 mg, 0.61 mmol) and potassium thioacetate (90 mg, 0.79 mmol) in 5 mL acetone. The reaction was stirred for 3 h at room temperature. After extraction and column chromatography (PE/EtOAc 8:2) **11** was obtained as yellow solid (128 mg, 86%). <sup>1</sup>H NMR (500 MHz, CDCl<sub>3</sub>) δ 8.18 (br, 1 H, NH), 7.60 (t, *J* = 2.0 Hz, 1 H, 2'-H), 7.34 (ddd, *J* = 0.9, 2.0, 8.2 Hz, 1 H, 4'-H or 6'-H), 7.23 (t, *J* = 8.1 Hz, 1 H, 5'-H), 7.06 (ddd, *J* = 0.9, 1.9, 8.0 Hz, 1 H, 4'-H or 6'-H), 3.64 (s, 2 H, 2-H), 2.46 (s, 3 H, S(CO)CH<sub>3</sub>). <sup>13</sup>C NMR (126 MHz, CDCl<sub>3</sub>) δ 197.62 (S(CO)CH<sub>3</sub>), 166.60 (1-C), 138.87 (1'-C or 3'-C), 134.81 (1'-C or 3'-C), 130.12 (5'-C), 124.70 (4'-C or 6'-C), 119.99 (2'-C), 117.87 (4'-C or 6'-C), 34.36 (2-C), 30.41 (S(CO)CH<sub>3</sub>). HRMS (ESI) *m/z* calculated for C<sub>10</sub>H<sub>11</sub>ClNO<sub>2</sub>S 244.0194 [M+H]<sup>+</sup>, found: 244.0183. TLC (petroleum ether-EtOAc, 7:3): R<sub>f</sub> = 0.20.

**2-S-(Acetylthio)-N-(*o*-tolyl)acetamide 12.** Compound **12** was synthesized according to the general procedure **B**, using intermediate **4** (458 mg, 2.29 mmol) and potassium thioacetate (321 mg, 2.81 mmol) in 10 mL acetone. The reaction was stirred for 3 h 30 min at room temperature. After extraction and column chromatography (PE/EtOAc 7:3) **12** was obtained as yellow solid (193 mg, 71%). <sup>1</sup>H NMR (300 MHz, CDCl<sub>3</sub>) δ 7.93 (br, 1 H, NH), 7.88 (d, *J* = 8.1 Hz, 1 H, 6'-H), 7.21-7.13 (m, 2 H, 3'-H, 4'-H), 7.04 (td, *J* = 1.1, 7.4 Hz, 1 H, 5'-H), 3.67 (s, 2 H, 2-H), 2.44 (s, 3 H, S(CO)CH<sub>3</sub>), 2.23 (s, 3 H, 2'-CH<sub>3</sub>). <sup>13</sup>C NMR (126 MHz, CDCl<sub>3</sub>) δ 197.21 (S(CO)CH<sub>3</sub>), 166.63 (1-C), 135.76 (1'-C or 2'-C), 130.59 (3'-C), 128.57 (1'-C or 2'-C), 126.91 (4'-C), 125.21 (5'-C), 122.38 (6'-C), 34.21 (2-C), 30.37 (S(CO)CH<sub>3</sub>), 17.80 (2'-CH<sub>3</sub>). MS (ESI<sup>+</sup>) *m/z* 224 (M+H)<sup>+</sup>. TLC (petroleum ether-EtOAc, 7:3): R<sub>f</sub> = 0.25.



**2-S-(Acetylthio)-N-(*m*-tolyl)acetamide 13.** Compound **13** was synthesized according to the general procedure **B**, using intermediate **5** (145 mg, 0.79 mmol) and potassium thioacetate (118 mg, 1.03 mmol) in 15 mL acetone. The reaction was stirred for 4 h at room temperature. After extraction and column chromatography (PE/EtOAc 9:1→8:2), **13** was obtained as yellow solid (132 mg, 75%). <sup>1</sup>H NMR (500 MHz, CDCl<sub>3</sub>) δ 8.07 (br, 1 H, NH), 7.32 (s, 1 H, 2'-H), 7.29 (d, *J* = 8.0 Hz, 1 H, 6'-H), 7.19 (t, *J* = 7.8 Hz, 1 H, 5'-H), 6.92 (d, *J* = 7.5 Hz, 1 H, 4'-H), 3.65 (s, 2 H, 2-H), 2.45 (s, 3 H, S(CO)CH<sub>3</sub>), 2.33 (s, 3 H, 3'-CH<sub>3</sub>). <sup>13</sup>C NMR (126 MHz, CDCl<sub>3</sub>) δ 197.20 (S(CO)CH<sub>3</sub>), 166.40 (1-C), 139.06 (3'-C), 137.64 (1'-C), 128.97 (5'-C), 125.47 (4'-C), 120.54 (2'-C), 117.03 (6'-C), 34.39 (2-C), 30.38 (S(CO)CH<sub>3</sub>), 21.56 (3'-CH<sub>3</sub>). MS (ESI<sup>+</sup>) *m/z* 224 (M+H)<sup>+</sup>. TLC (petroleum ether-EtOAc, 7:3): R<sub>f</sub> = 0.25.

**2-S-(Acetylthio)-N-(*p*-tolyl)acetamide 14.** Compound **14** was synthesized according to the general procedure **B**, using intermediate **6** (122 mg, 0.66 mmol) and potassium thioacetate (92 mg, 0.81 mmol) in 5 mL acetone. The reaction was stirred for 2 h 30 min at room temperature. After extraction and column chromatography (PE/EtOAc 8:2) **14** was obtained as yellow solid (94 mg, 63%). <sup>1</sup>H NMR (300 MHz, CDCl<sub>3</sub>) δ 8.03 (br, 1 H, NH), 7.37 (d, *J* = 8.4 Hz, 2 H, aryl-H<sub>a</sub>), 7.11 (d, *J* = 8.2 Hz, 2 H, aryl-H<sub>b</sub>), 3.64 (s, 2 H, 2-H), 2.44 (s, 3 H, S(CO)CH<sub>3</sub>), 2.30 (s, 3 H, 4'-CH<sub>3</sub>). <sup>13</sup>C NMR (75 MHz, CDCl<sub>3</sub>) δ 197.21 (S(CO)CH<sub>3</sub>), 166.32 (1-C), 135.17 (1'-C or 4'-C), 134.36 (1'-C or 4'-C), 129.62 (aryl-C<sub>b</sub>), 120.00 (aryl-C<sub>a</sub>), 34.33 (2-C), 30.42 (S(CO)CH<sub>3</sub>), 21.02 (4'-CH<sub>3</sub>). MS (ESI<sup>+</sup>) *m/z* 224 (M+H)<sup>+</sup>. TLC (petroleum ether-EtOAc, 7:3): R<sub>f</sub> = 0.20.

**2-S-(Acetylthio)-N-(4'-methoxyphenyl)acetamide 15.** Compound **15** was synthesized according to the general procedure **B**, using intermediate **7** (458 mg, 2.29 mmol) and potassium thioacetate (321 mg, 2.81 mmol) in 10 mL acetone. The reaction was stirred for 3 h 30 min at room temperature. After extraction and column chromatography (PE/EtOAc 7:3) **15** was obtained as yellow solid (262 mg, 48%). <sup>1</sup>H NMR (500 MHz, CDCl<sub>3</sub>) δ 7.98 (s, 1 H, NH), 7.39 (d, *J* = 9.0 Hz, 2 H, 3'-H, 5'-H), 6.85 (d, *J* = 9.0 Hz, 2 H, 2'-C, 6'-C), 3.78 (s, 3 H, 4'-OCH<sub>3</sub>), 3.64 (s, 2 H, 2-H), 2.44 (s, 3 H, S(CO)CH<sub>3</sub>). <sup>13</sup>C NMR (126 MHz, CDCl<sub>3</sub>) δ 197.12 (S(CO)CH<sub>3</sub>), 166.25 (1-C), 156.73 (4'-C), 130.85 (1'-C), 121.77 (3'-C, 5'-C), 114.28 (2'-C, 6'-C), 55.63 (4'-OCH<sub>3</sub>), 34.21 (2-C), 30.42 (S(CO)CH<sub>3</sub>). HRMS (ESI) *m/z* calculated for C<sub>11</sub>H<sub>14</sub>NO<sub>3</sub>S 240.0689 [M+H]<sup>+</sup>, found 240.0679. TLC (petroleum ether-EtOAc, 6:4): R<sub>f</sub> = 0.20.

**2-S-(Acetylthio)-N-(4'-(2''-hydroxyethyl)phenyl)acetamide 16.** Compound **16** was synthesized according to the general procedure **B**, using intermediate **8** (201 mg, 0.94 mmol) and potassium thioacetate (136 mg, 1.19 mmol) in 7 mL acetone. The reaction was stirred for

12

5 h at room temperature. After extraction, **16** was obtained as white solid (197 mg, 83%). <sup>1</sup>H NMR (500 MHz, DMSO-d<sub>6</sub>) δ 10.14 (s, 1 H, NH), 7.44 (d, *J* = 8.5 Hz, 2 H, 3'-H, 5'-H), 7.14 (d, *J* = 8.5 Hz, 2 H, 2'-H, 6'-H), 4.60 (t, *J* = 5.2 Hz, 1 H, 2''-OH), 3.80 (s, 2 H, 2-H), 3.56 (td, *J* = 5.2, 7.1 Hz, 2 H, 2''-H), 2.66 (t, *J* = 7.1 Hz, 2 H, 1''-H), 2.38 (s, 3 H, S(CO)CH<sub>3</sub>). <sup>13</sup>C NMR (126 MHz, DMSO-d<sub>6</sub>) δ 194.57 (S(CO)CH<sub>3</sub>), 165.43 (1-C), 136.75 (1'-C), 134.63 (4'-C), 129.08 (2'-C, 6'-C), 119.04 (3'-C, 5'-C), 62.20 (2''-C), 38.44 (1''-C), 33.78 (2-C), 30.11 (S(CO)CH<sub>3</sub>). MS (ESI<sup>+</sup>) *m/z* 254 (M+H)<sup>+</sup>. TLC (CH<sub>2</sub>Cl<sub>2</sub>-MeOH, 95:5): R<sub>f</sub> = 0.15.

**2-S-(Acetylthio)-N-(4'-sulfamoylphenyl)acetamide 17.** Compound **17** was synthesized according to the general procedure **B**, using intermediate **9** (300 mg, 1.21 mmol) and potassium thioacetate (166 mg, 1.45 mmol) in 7 mL acetone. The reaction was stirred for 5 h at room temperature. After extraction, **17** was obtained as white solid (48 mg, 14%). <sup>1</sup>H NMR (500 MHz, DMSO-d<sub>6</sub>) δ 10.59 (s, 1 H, NH), 7.76 (d, *J* = 8.8 Hz, 2 H, aryl-H<sub>a</sub>), 7.72 (d, *J* = 8.8 Hz, 2 H, aryl-H<sub>b</sub>), 7.27 (s, 2 H, SO<sub>2</sub>NH<sub>2</sub>), 3.86 (s, 2 H, 2-C), 2.39 (s, 3 H, S(CO)CH<sub>3</sub>). <sup>13</sup>C NMR (126 MHz, DMSO-d<sub>6</sub>) δ 194.58 (S(CO)CH<sub>3</sub>), 166.33 (1-C), 141.68 (1'-C or 4'-C), 138.57 (1'-C or 4'-C), 126.75 (aryl-C<sub>a</sub>), 118.66 (aryl-C<sub>b</sub>), 33.90 (2-C), 30.10 (S(CO)CH<sub>3</sub>). MS (ESI<sup>+</sup>) *m/z* 289 (M+H)<sup>+</sup>. TLC (petroleum ether-EtOAc, 4:6): R<sub>f</sub> = 0.15.

### Synthesis of thiols 18–25

**2-mercapto-*N*-phenylacetamide 18.** Compound **18** was synthesized according to the general procedure **C**, using thioacetate **10** (29 mg, 0.14 mmol) and 5 mL KOH (1 M, H<sub>2</sub>O/MeOH 1:1). The mix was stirred at room temperature for 40 min. Extraction gave the final compound **18** without any further purification as white solid (17 mg, 78%). <sup>1</sup>H NMR (500 MHz, CDCl<sub>3</sub>) δ 8.52 (s, 1 H, NH), 7.55 (dd, *J* = 0.9, 8.5 Hz, 2 H, 2'-H, 6'-H), 7.35 (t, *J* = 8.0 Hz, 2 H, 3'-H, 5'-H), 7.15 (t, *J* = 7.4 Hz, 1 H, 4'-H), 3.41 (d, *J* = 9.2 Hz, 2 H, 2-H), 2.03 (t, *J* = 9.2 Hz, 1 H, SH). <sup>13</sup>C NMR (126 MHz, CDCl<sub>3</sub>) δ 167.23 (1-C), 137.37 (1'-C), 129.22 (3'-C, 5'-C), 124.97 (4'-C), 119.96 (2'-C, 6'-C), 29.29 (2-C). HRMS (ESI) *m/z* calculated for C<sub>8</sub>H<sub>10</sub>NOS 168.0478 [M+H]<sup>+</sup>, found 168.0474.

**2-mercapto-*N*-(3'-chlorophenyl)acetamide 19.** Compound **19** was synthesized according to the general procedure **C**, using thioacetate **11** (28 mg, 0.12 mmol) and 5 mL KOH (1 M, H<sub>2</sub>O/MeOH 1:1). The mix was stirred at room temperature for 1 h 20 min. Extraction gave the final compound **19** without any further purification as white solid (23 mg, 99%). <sup>1</sup>H NMR (300 MHz, DMSO-*d*<sub>6</sub>) δ 10.26 (s, 1 H, NH), 7.80 (t, *J* = 2.0 Hz, 1 H, 2'-H), 7.40 (ddd, *J* = 1.1, 1.9, 8.2 Hz, 1 H, 4'-H or 6'-H), 7.34 (t, *J* = 8.0 Hz, 1 H, 5'-H), 7.12 (ddd, *J* = 1.1, 2.1, 7.8 Hz, 1 H, 4'-H or 6'-H), 3.30\* (br, 2 H, 2-H), 2.97\*\* (br, 1 H, SH). <sup>13</sup>C NMR (126 MHz, DMSO-*d*<sub>6</sub>) δ 169.06 (1-C), 140.46 (1'-C or 3'-C), 133.13 (1'-C or 3'-C), 130.57 (5'-C), 123.14 (4'-C or 6'-C), 118.52 (2'-C), 117.49 (4'-C or 6'-C), 28.32 (2-C). HRMS (ESI) *m/z* calculated for C<sub>8</sub>H<sub>9</sub>ClNOS 202.0088 [M+H]<sup>+</sup>, found 202.0085.

\* 3.30 (d, *J* = 7.7 Hz, 2H, 2-H), when measured at 500 MHz, DMSO-*d*<sub>6</sub>

\*\* 2.99 (t, *J* = 7.9 Hz, 1H, SH), when measured at 500 MHz, DMSO-*d*<sub>6</sub>

**2-mercapto-*N*-(*o*-tolyl)acetamide 20.** Compound **20** was synthesized according to the general procedure **C**, using thioacetate **12** (32 mg, 0.14 mmol) and 5 mL KOH (1 M, H<sub>2</sub>O/MeOH 1:1). The mix was stirred at room temperature for 45 min. Extraction gave the final compound **20** without any further purification as slightly yellow solid (26 mg, 99%). <sup>1</sup>H NMR (300 MHz, CDCl<sub>3</sub>) δ 8.57 (br, 1 H, NH), 7.91 (d, *J* = 8.0 Hz, 1 H, 6'-H), 7.25–7.18 (m, 2 H, 3'-H, 4'-H), 7.09 (td, *J* = 0.9, 7.5 Hz, 1 H, 5'-H), 3.45 (d, *J* = 9.2 Hz, 2 H, 2-H), 2.31 (s, 3 H, 2'-CH<sub>3</sub>), 2.04 (t, *J* = 9.3 Hz, 1 H, SH). <sup>13</sup>C NMR (126 MHz, CDCl<sub>3</sub>) δ 167.18 (1-C), 135.39 (1'-C or 2'-C), 130.66 (3'-C), 128.80 (1'-C or 2'-C), 127.04 (4'-C), 125.48 (5'-C), 122.25 (6'-C), 29.40 (2-C), 17.85 (2'-CH<sub>3</sub>). HRMS (ESI) *m/z* calculated for C<sub>9</sub>H<sub>12</sub>NOS 182.0634 [M+H]<sup>+</sup>, found 182.0631.

**2-mercapto-*N*-(*m*-tolyl)acetamide 21.** Compound **21** was synthesized according to the general procedure **C**, using thioacetate **13** (30 mg, 0.13 mmol) and 5 mL KOH (1 M, H<sub>2</sub>O/MeOH 1:1). The mix was stirred at room temperature for 45 min. Extraction gave the final compound **7** without any further purification as slightly yellow solid (27 mg, quant.). <sup>1</sup>H NMR (300 MHz, CDCl<sub>3</sub>) δ 8.50 (br, 1 H, NH), 7.39 (s, 1 H, 2'-H), 7.34 (d, *J* = 8.1 Hz, 1 H, 6'-H), 7.22 (t, *J* = 7.8 Hz, 1 H, 5'-H), 6.96 (d, *J* = 7.4 Hz, 1 H, 4'-H), 3.39 (d, *J* = 8.8 Hz, 2 H, 2-H), 2.34 (s, 3 H, 3'-CH<sub>3</sub>), 2.03 (t, *J* = 9.1 Hz, 1 H, SH). <sup>13</sup>C NMR (75 MHz, CDCl<sub>3</sub>) δ 167.32 (1-C), 139.16 (3'-C), 137.26 (1'-C), 129.01 (5'-C), 125.77 (4'-C), 120.62 (2'-C), 117.07 (6'-C), 29.29 (2-C), 21.58 (3'-CH<sub>3</sub>). HRMS (ESI) *m/z* calculated for C<sub>9</sub>H<sub>12</sub>NOS 182.0634 [M+H]<sup>+</sup>, found 182.0631.

**2-mercapto-*N*-(*p*-tolyl)acetamide 22.** Compound **22** was synthesized according to the general procedure **C**, using thioacetate **14** (31 mg, 0.14 mmol) and 5 mL KOH (1 M, H<sub>2</sub>O/MeOH 1:1). The mix was stirred at room temperature for 45 min. Extraction gave the final compound **22** without any further purification as white solid (25 mg, 99%). <sup>1</sup>H NMR (300 MHz, DMSO-*d*<sub>6</sub>) δ 9.97 (br, 1 H, NH), 7.46 (d, *J* = 8.4 Hz, 2 H, aryl-H<sub>a</sub>), 7.11 (d, *J* = 8.3 Hz, 2 H, aryl-H<sub>b</sub>), 3.27 (d, *J* = 8.0 Hz, 2 H, 2-C), 2.90 (t, *J* = 8.0 Hz, 1 H, SH), 2.24 (s, 3 H, 4'-CH<sub>3</sub>). <sup>13</sup>C NMR (126 MHz, DMSO-*d*<sub>6</sub>) δ 168.35 (1-C), 136.52 (1'-C or 4'-C), 132.32 (1'-C or 4'-C), 129.18 (aryl-C<sub>b</sub>), 119.08 (aryl-C<sub>a</sub>), 28.25 (2-C), 20.47 (4'-CH<sub>3</sub>). HRMS (ESI) *m/z* calculated for C<sub>9</sub>H<sub>12</sub>NOS 182.0634 [M+H]<sup>+</sup>, found 182.0630.

**2-mercapto-*N*-(4'-methoxyphenyl)acetamide 23.** Compound **23** was synthesized according to the general procedure **C**, using thioacetate **16** (37 mg, 0.15 mmol) and 5 mL KOH (1 M, H<sub>2</sub>O/MeOH 1:1). The mix was stirred at room temperature for 45 min. Extraction gave the final compound **23** without any further purification as white solid (30 mg, 98%). <sup>1</sup>H NMR (500 MHz, CDCl<sub>3</sub>) δ 8.42 (br, 1 H, NH), 7.44 (d, *J* = 9.0 Hz, 2 H, 3'-H, 5'-H), 6.88 (d, *J* = 9.0 Hz, 2 H, 2'-C, 6'-C), 3.80 (s, 3 H, 4'-OCH<sub>3</sub>), 3.39 (d, *J* = 9.3 Hz, 2 H, 2-H), 2.01 (t, *J* = 9.3 Hz, 1 H, SH). <sup>13</sup>C NMR (126 MHz, CDCl<sub>3</sub>) δ 167.09 (1-C), 156.92 (4'-C), 130.48 (1'-C), 121.87 (3'-C, 5'-C), 114.36 (2'-C, 6'-C), 55.62 (4'-OCH<sub>3</sub>), 29.13 (2-C). HRMS (ESI) *m/z* calculated for C<sub>9</sub>H<sub>11</sub>NO<sub>2</sub>S 198.0583 [M+H]<sup>+</sup>, found 198.0580.

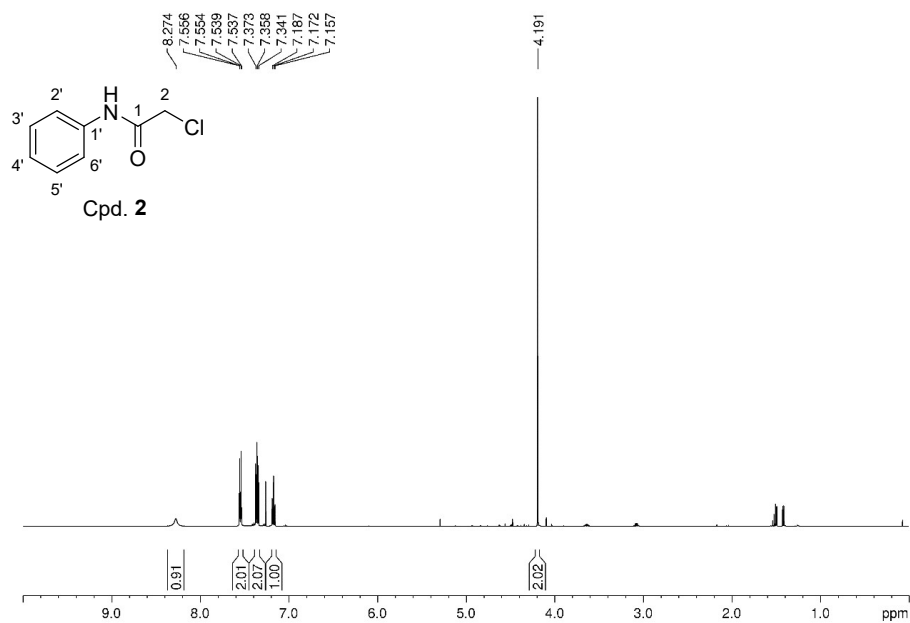
**2-mercapto-*N*-(4'-(2''-hydroxyethyl)phenyl)acetamide 24.** Compound **24** was synthesized according to the general procedure **C**, using thioacetate **16** (36 mg, 0.14 mmol) and 5 mL KOH (1 M, H<sub>2</sub>O/MeOH 1:1). The mix was stirred at room temperature for 1 h. Extraction gave **24** as white solid (28 mg, 93%). <sup>1</sup>H NMR (500 MHz, DMSO-*d*<sub>6</sub>) δ 9.99 (s, 1 H, NH), 7.46 (d, *J* = 8.5 Hz, 2 H, 3'-H, 5'-H), 7.14 (d, *J* = 8.5 Hz, 2 H, 2'-H, 6'-H), 4.63-4.58 (m, 1 H, 2''-OH),

15

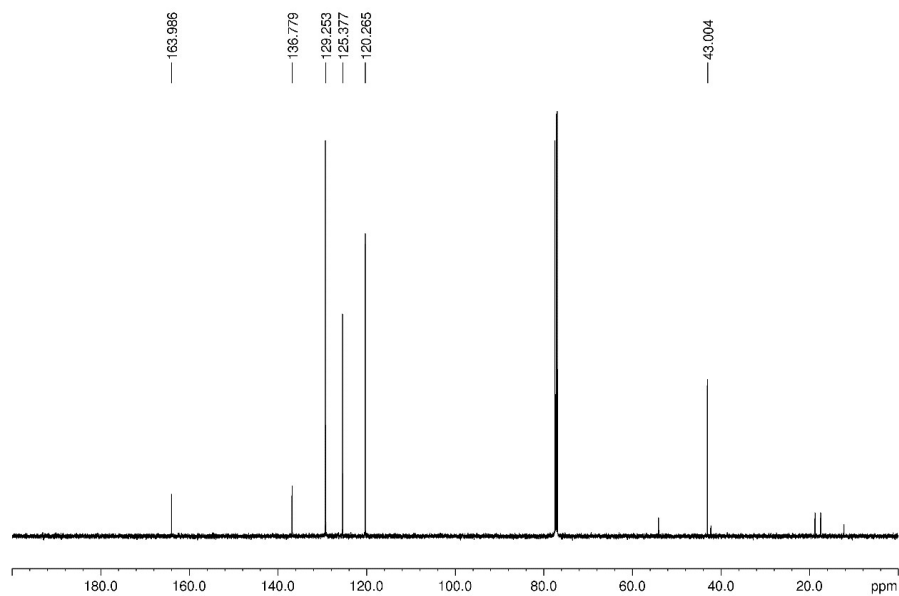
3.58-3.54 (m, 2 H, 2''-H), 3.27 (d,  $J = 8.0$  Hz, 2 H, 2-H), 2.91 (t,  $J = 8.0$  Hz, 1 H, SH), 2.66 (t,  $J = 7.1$  Hz, 2 H, 1''-H).  $^{13}\text{C}$  NMR (126 MHz, DMSO- $d_6$ )  $\delta$  168.32 (1-C), 136.90 (1'-C), 134.56 (4'-C), 129.10 (2'-C, 6'-C), 119.04 (3'-C, 5'-C), 62.23 (2''-C), 38.46 (1''-C), 28.24 (2-C). HRMS (ESI)  $m/z$  calcd. for  $\text{C}_{10}\text{H}_{14}\text{NO}_2\text{S}$   $[\text{M}+\text{H}]^+$  212.0740, found 212.0733.

**2-mercapto-*N*-(4'-sulfamoylphenyl)acetamide 25.** Compound **25** was synthesized according to the general procedure **C**, using thioacetate **17** (23 mg, 0.08 mmol) and 5 mL KOH (1 M,  $\text{H}_2\text{O}/\text{MeOH}$  1:1). The mix was stirred at room temperature for 1 h 15 min. After extraction, **25** was obtained as white solid (16 mg, 81%).  $^1\text{H}$  NMR (500 MHz, DMSO- $d_6$ )  $\delta$  10.41 (s, 1 H, NH), 7.77 (d,  $J = 9.0$  Hz, 2 H, aryl- $\text{H}_a$ ), 7.73 (d,  $J = 9.0$  Hz, 2 H, aryl- $\text{H}_b$ ), 7.25 (s, 2 H,  $\text{SO}_2\text{NH}_2$ ), 3.33 (m, 2H, 2-C (HMBC)), 2.99 (t,  $J = 8.0$  Hz, 1 H, SH)  $^{13}\text{C}$  NMR (126 MHz, DMSO- $d_6$ )  $\delta$  169.19 (1-C), 141.87 (1'-C or 4'-C), 138.52 (1'-C or 4'-C), 126.76 (aryl- $\text{C}_a$ ), 118.66 (aryl- $\text{C}_b$ ), 28.34 (2-C). HRMS (ESI)  $m/z$  calcd. for  $\text{C}_8\text{H}_{11}\text{N}_2\text{O}_3\text{S}_2$   $[\text{M}+\text{H}]^+$  247.0206, found 247.0201.

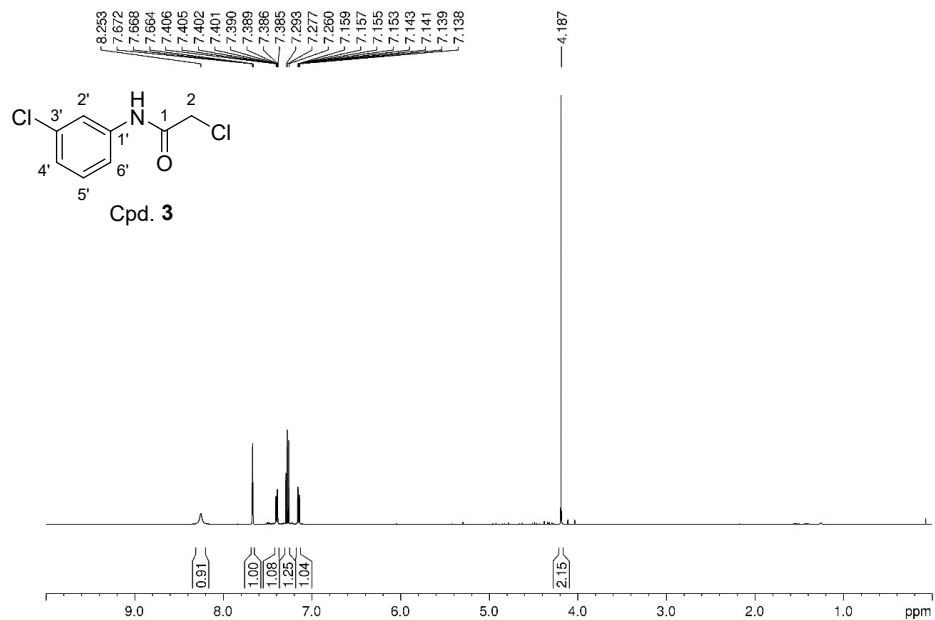
*<sup>1</sup>H and <sup>13</sup>C NMR spectra of compounds 2–25*



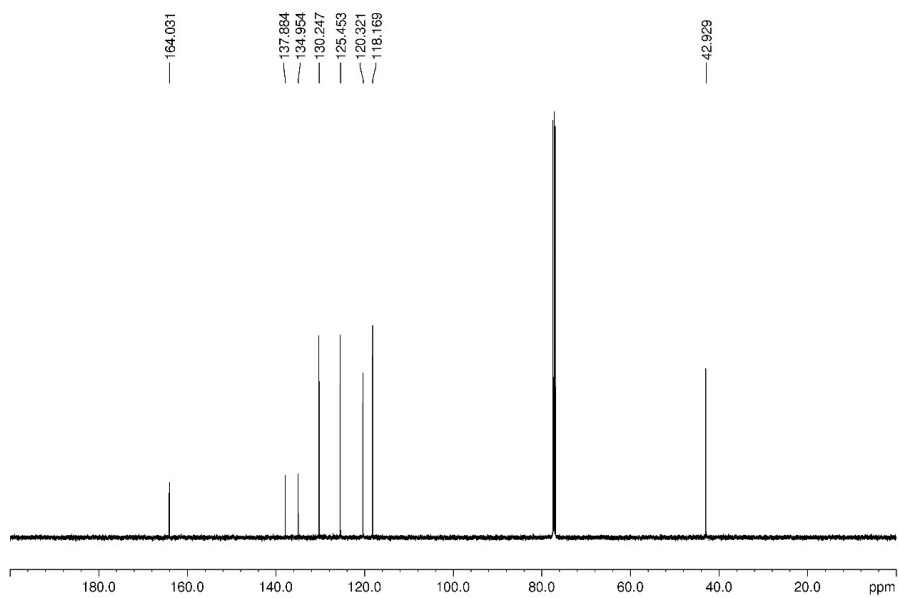
<sup>1</sup>H NMR of Cpd. 2 (500 MHz, CDCl<sub>3</sub>)



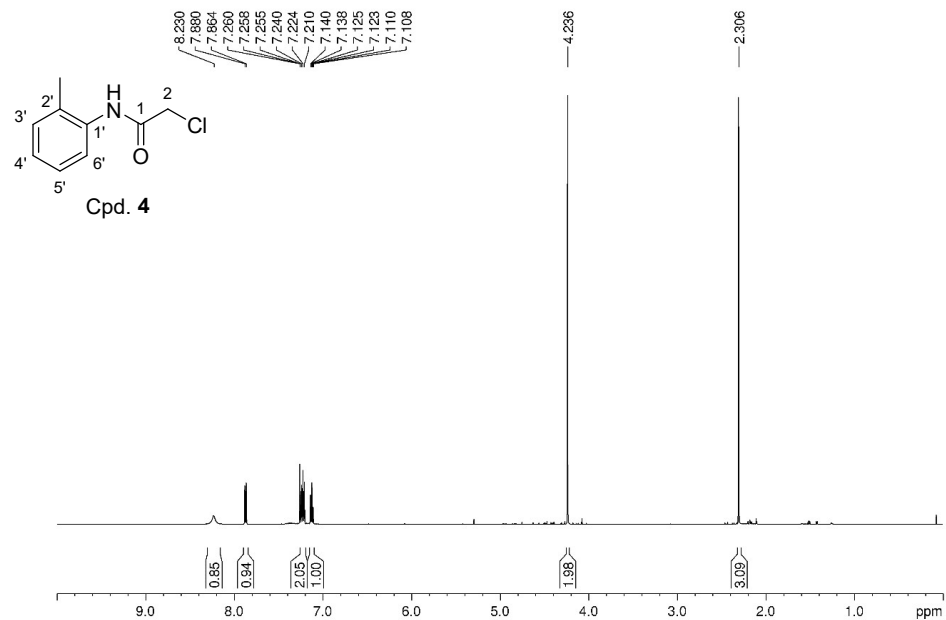
<sup>13</sup>C NMR of Cpd. 2 (126 MHz, CDCl<sub>3</sub>)



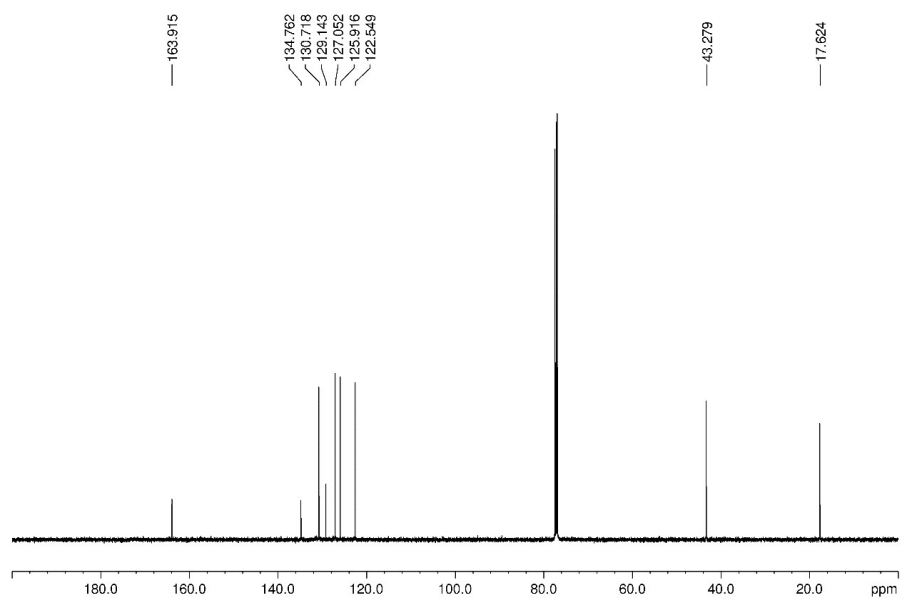
<sup>1</sup>H NMR of Cpd. 3 (500 MHz, CDCl<sub>3</sub>)



<sup>13</sup>C NMR of Cpd. 3 (126 MHz, CDCl<sub>3</sub>)

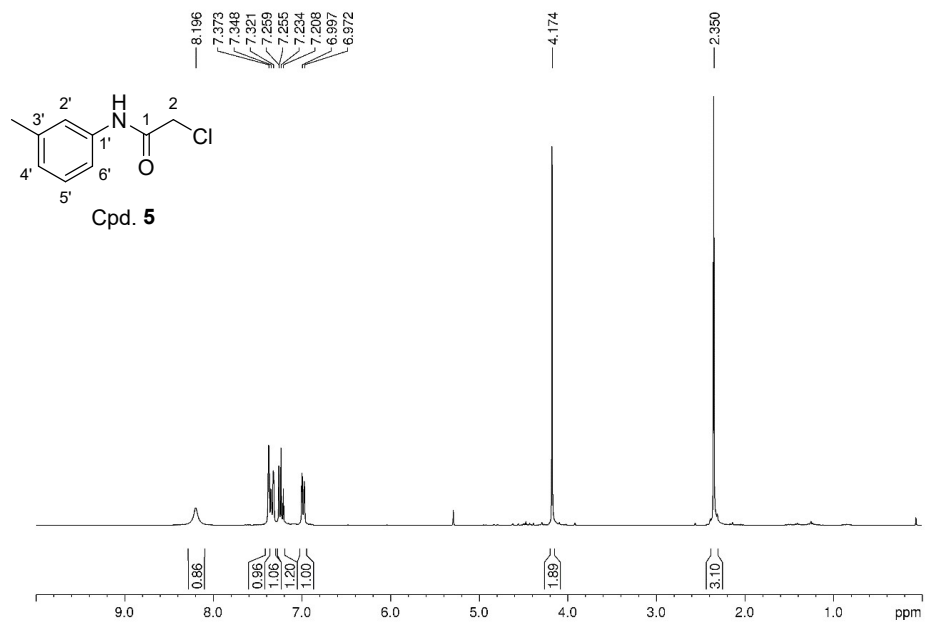


<sup>1</sup>H NMR of Cpd. 4 (500 MHz, CDCl<sub>3</sub>)

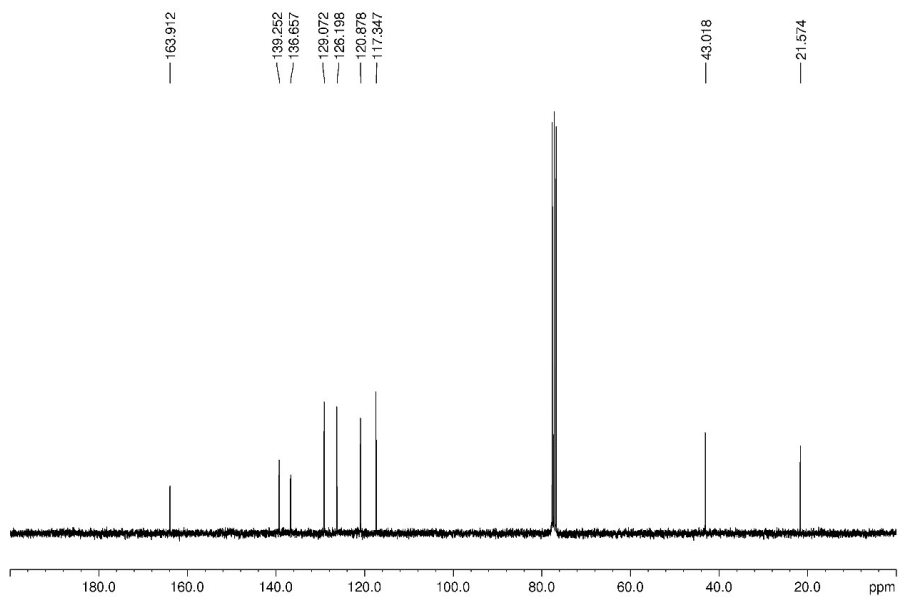


<sup>13</sup>C NMR of Cpd. 4 (126 MHz, CDCl<sub>3</sub>)

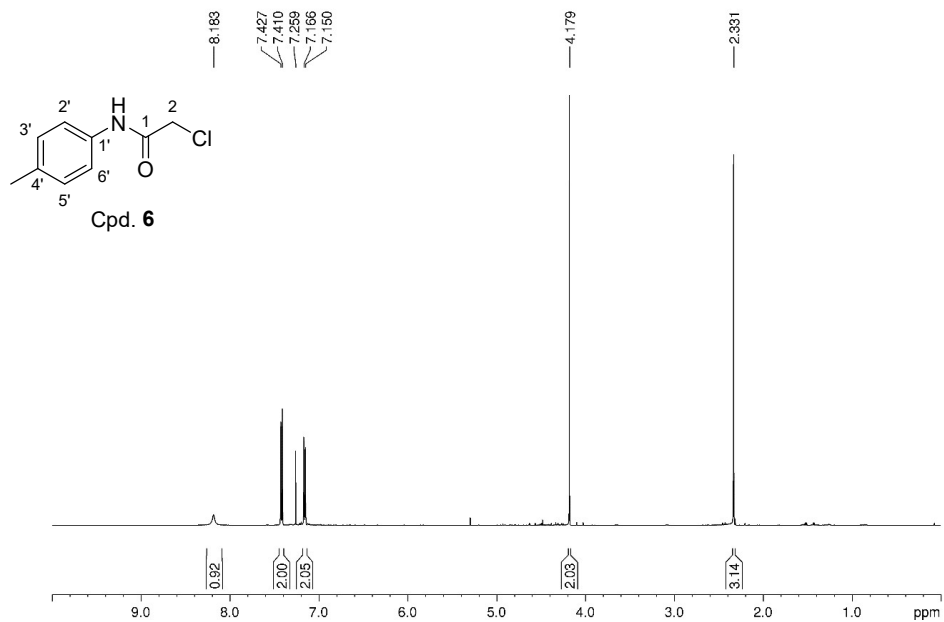




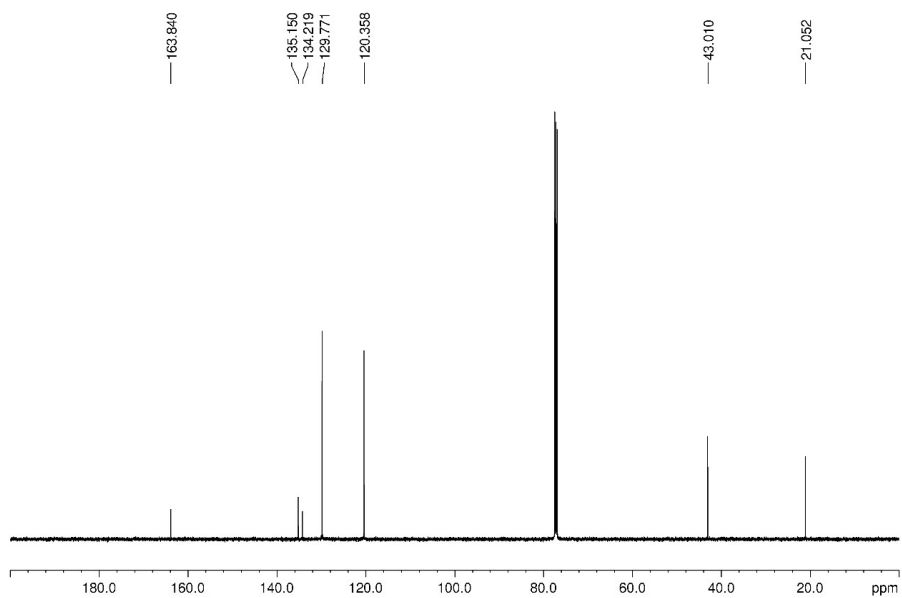
<sup>1</sup>H NMR of Cpd. 5 (500 MHz, CDCl<sub>3</sub>)



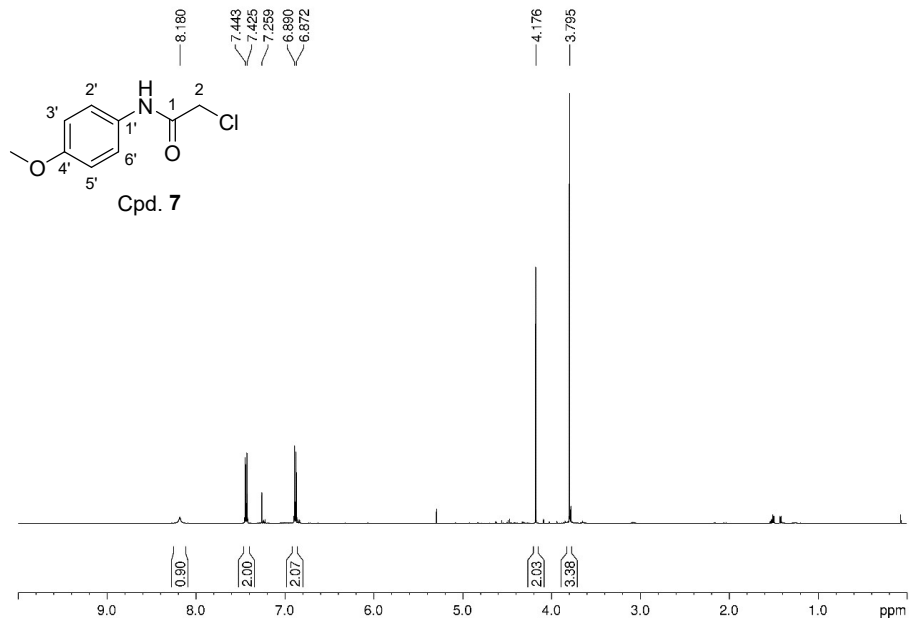
<sup>13</sup>C NMR of Cpd. 5 (126 MHz, CDCl<sub>3</sub>)



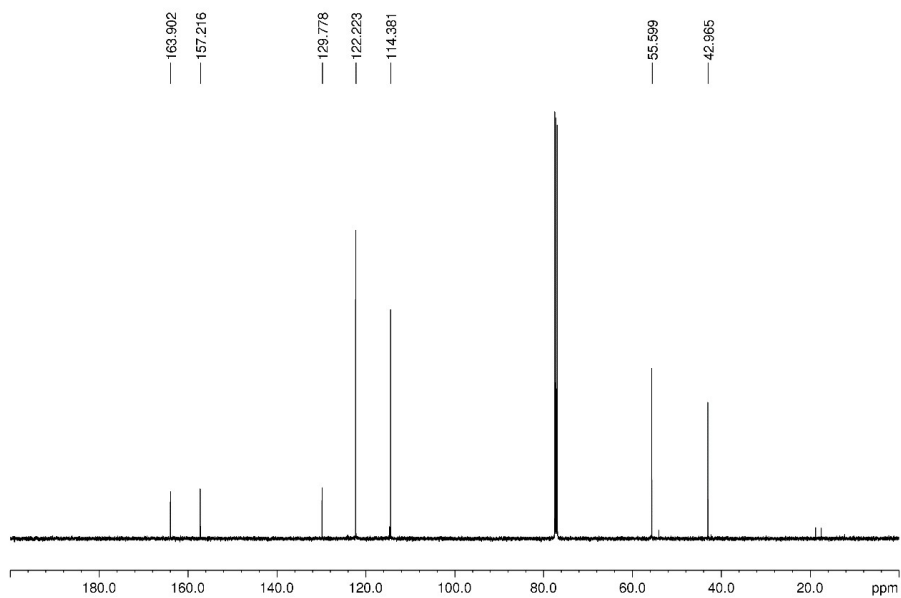
<sup>1</sup>H NMR of Cpd. 6 (500 MHz, CDCl<sub>3</sub>)



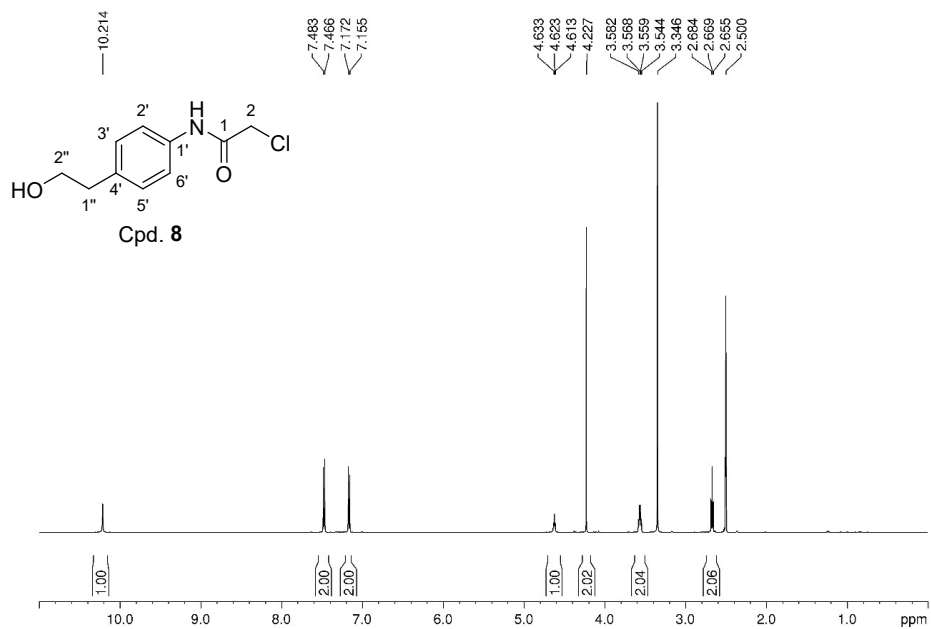
<sup>13</sup>C NMR of Cpd. 6 (126 MHz, CDCl<sub>3</sub>)



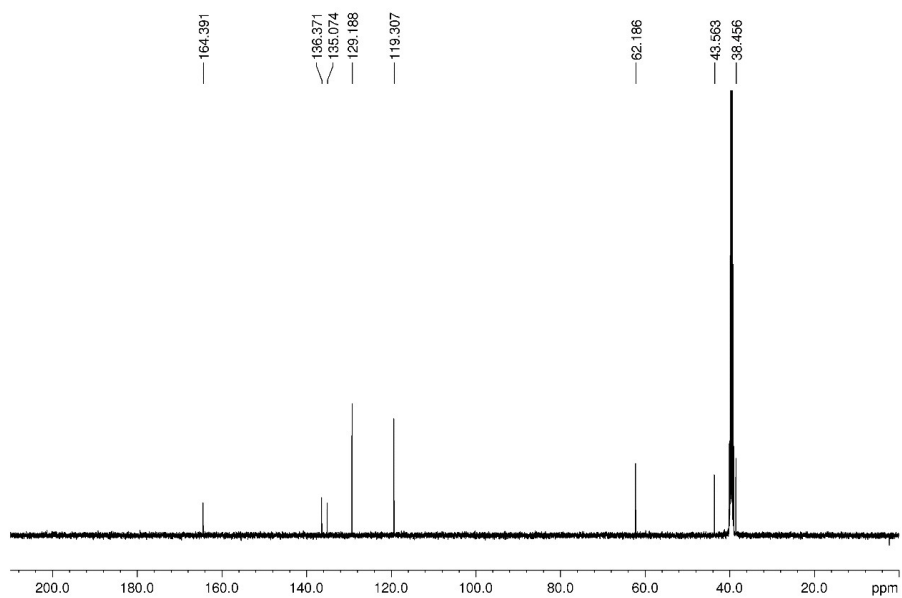
<sup>1</sup>H NMR of Cpd. 7 (500 MHz, CDCl<sub>3</sub>)



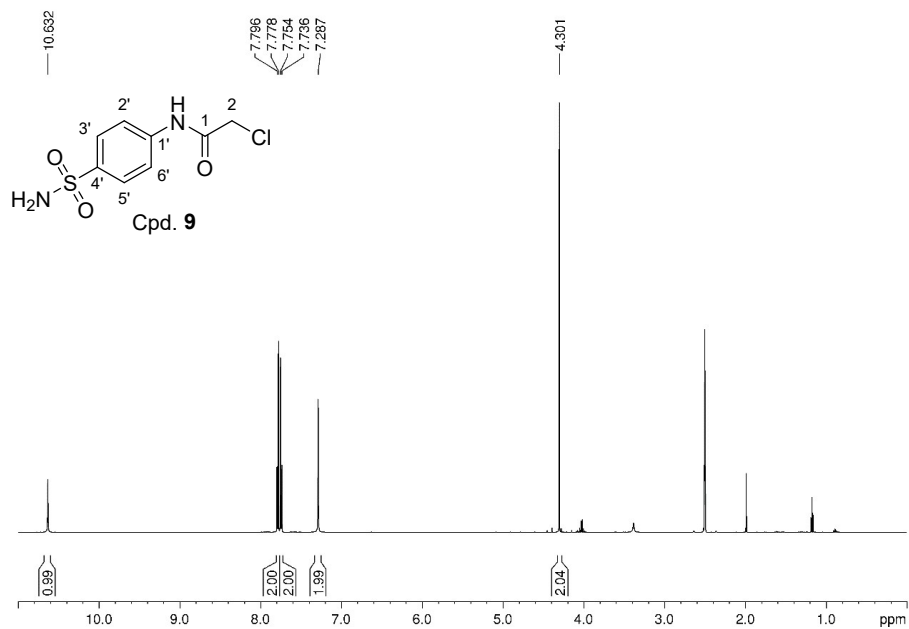
<sup>13</sup>C NMR of Cpd. 7 (126 MHz, CDCl<sub>3</sub>)



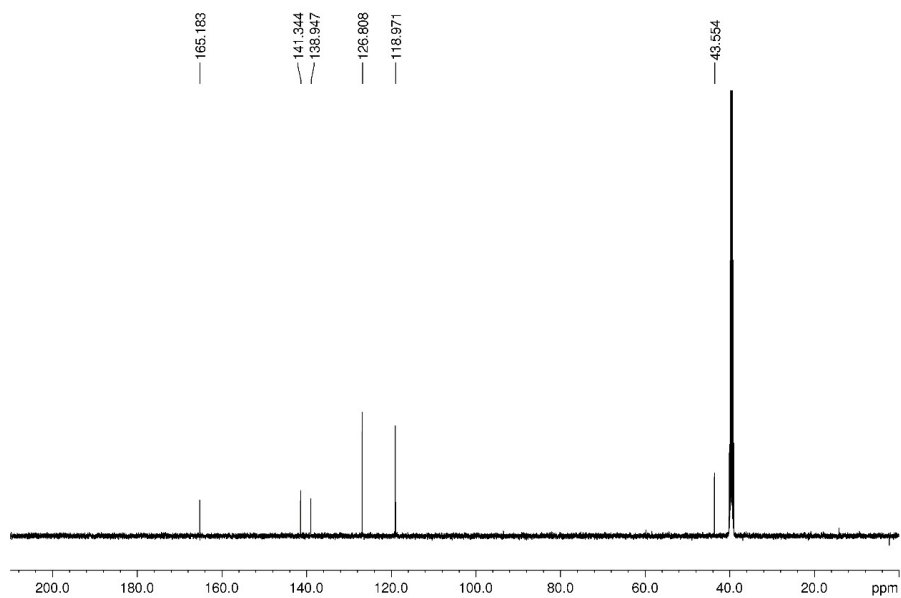
<sup>1</sup>H NMR of Cpd. 8 (500 MHz, DMSO-*d*<sub>6</sub>)



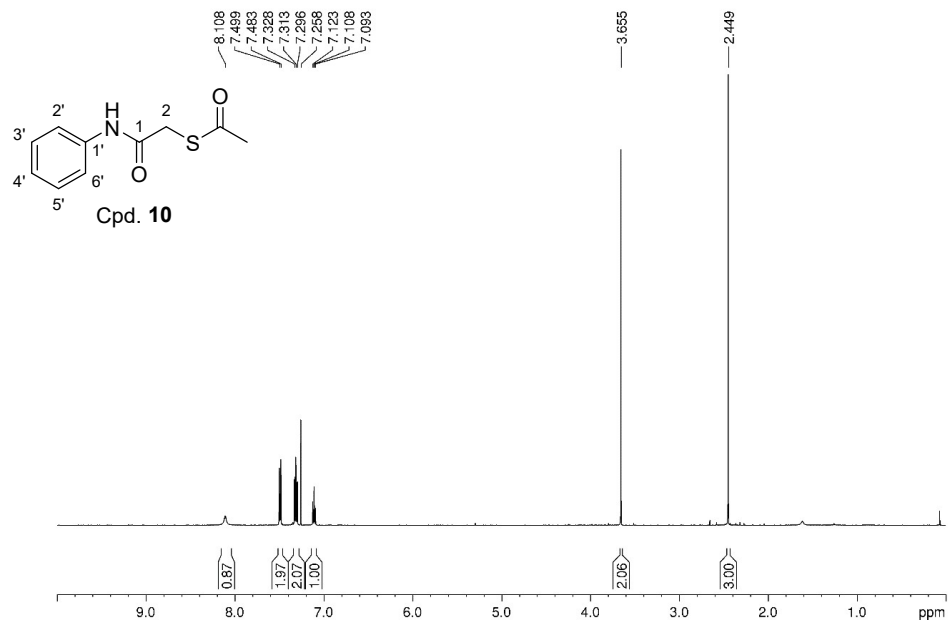
<sup>13</sup>C NMR of Cpd. 8 (126 MHz, DMSO-*d*<sub>6</sub>)



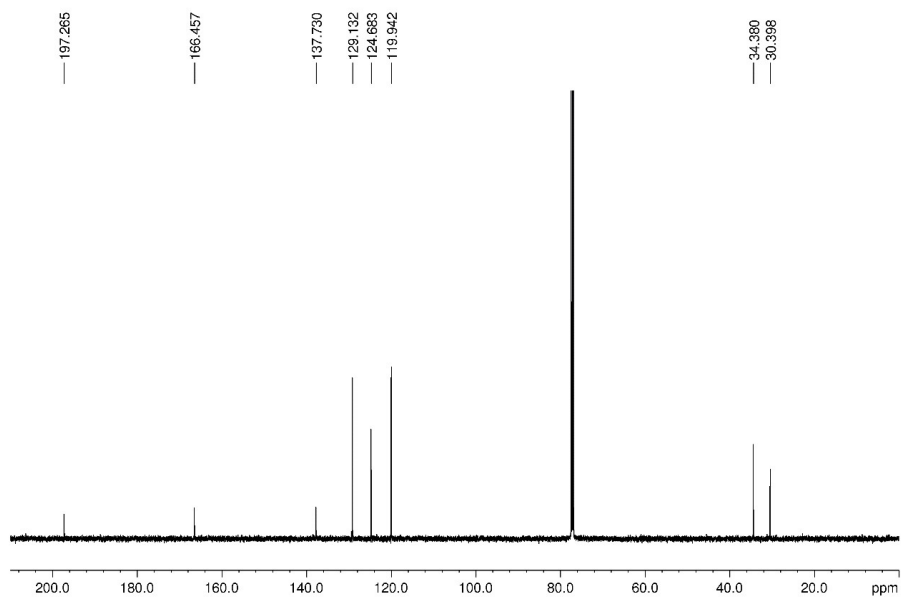
<sup>1</sup>H NMR of Cpd. 9 (500 MHz, DMSO-*d*<sub>6</sub>)



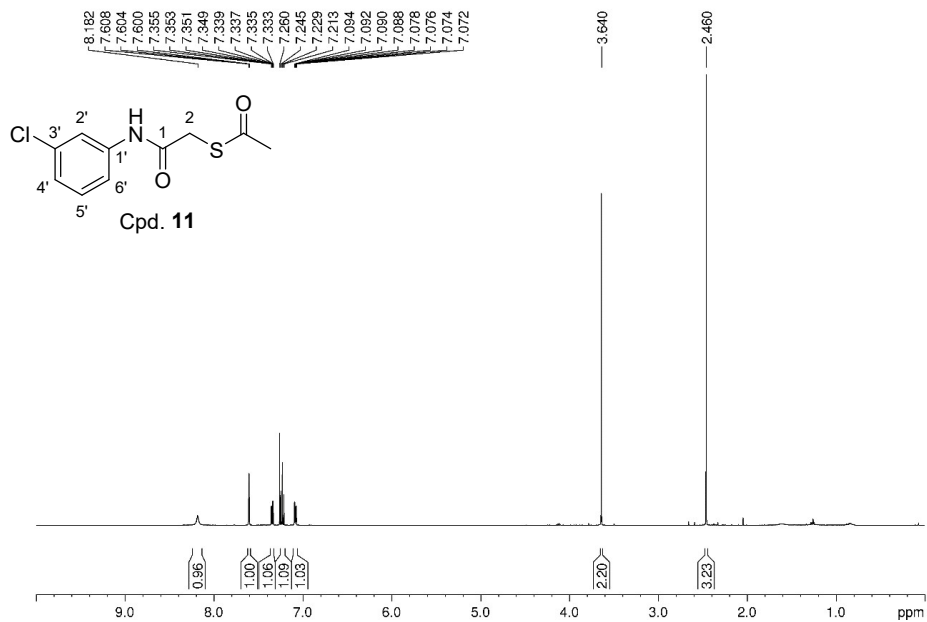
<sup>13</sup>C NMR of Cpd. 9 (126 MHz, DMSO-*d*<sub>6</sub>)



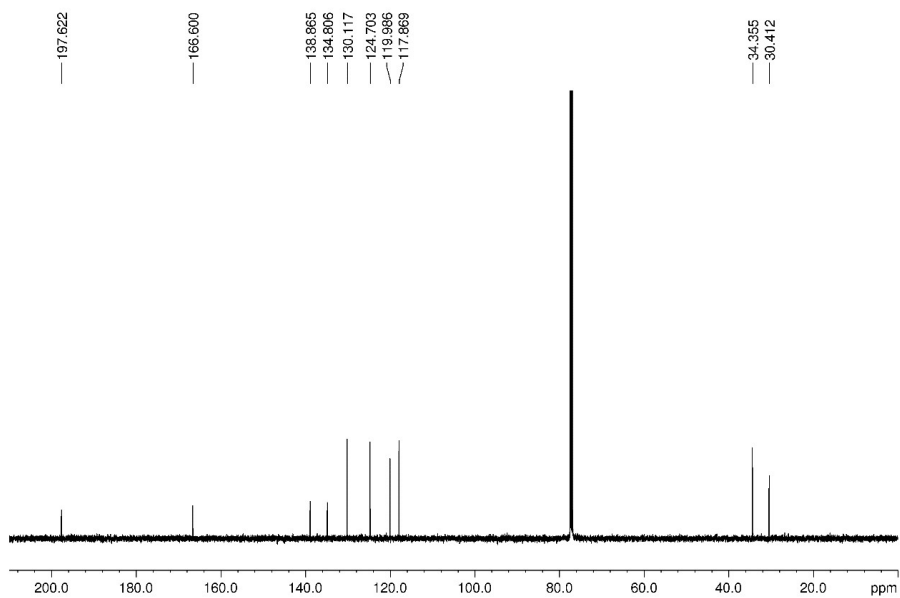
<sup>1</sup>H NMR of Cpd. 10 (500 MHz, CDCl<sub>3</sub>)



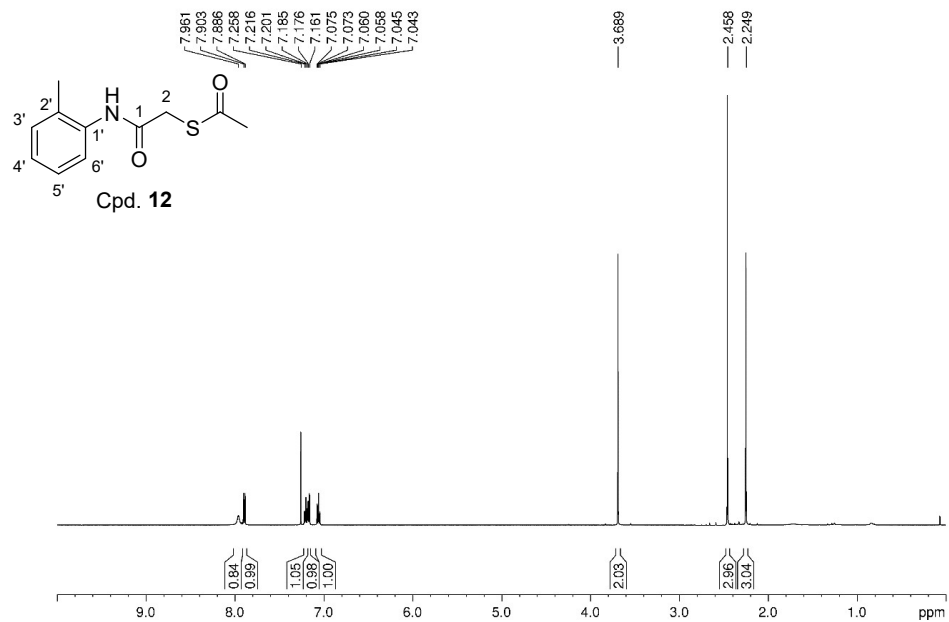
<sup>13</sup>C NMR of Cpd. 10 (126 MHz, CDCl<sub>3</sub>)



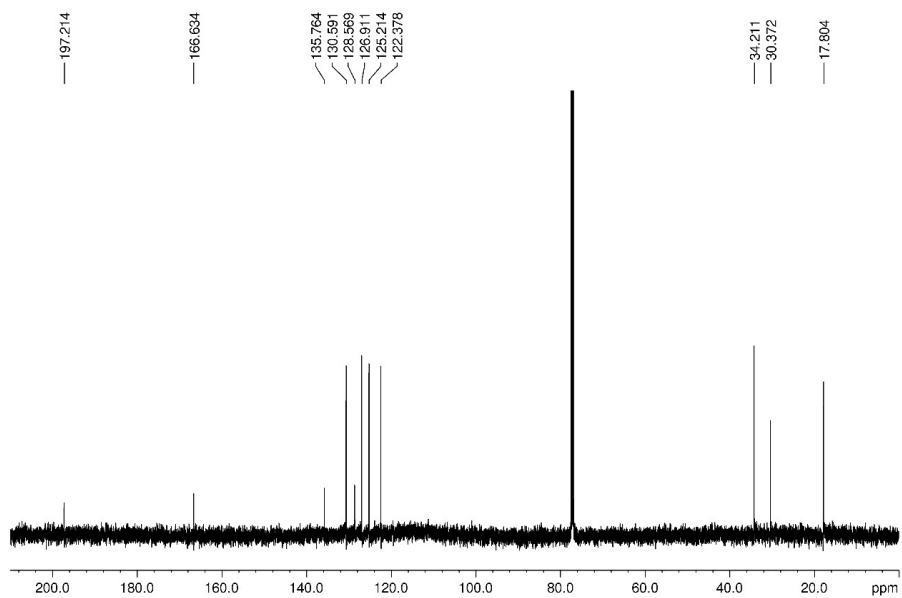
<sup>1</sup>H NMR of Cpd. 11 (500 MHz, CDCl<sub>3</sub>)



<sup>13</sup>C NMR of Cpd. 11 (126 MHz, CDCl<sub>3</sub>)

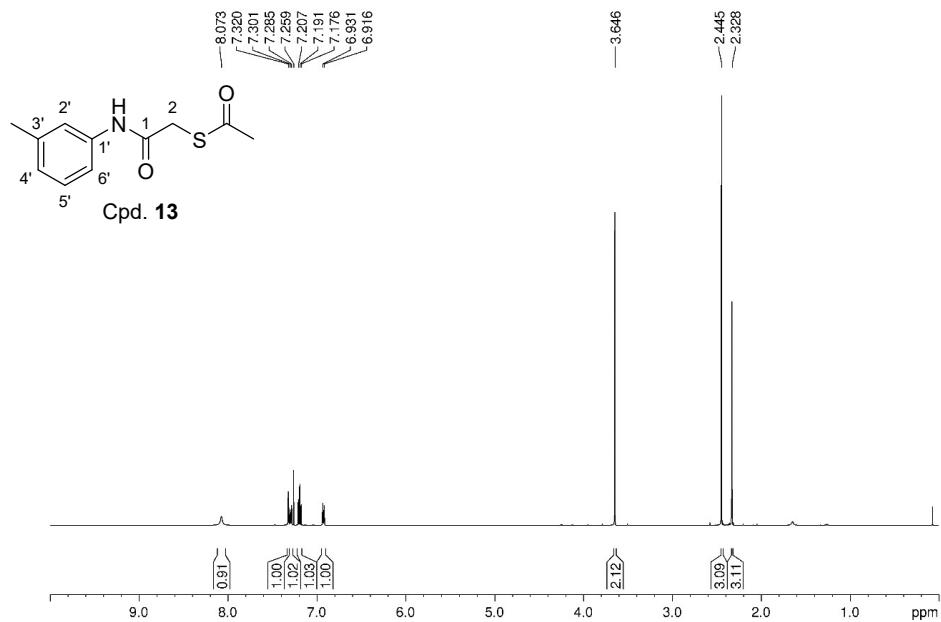


<sup>1</sup>H NMR of Cpd. 12 (500 MHz, CDCl<sub>3</sub>)

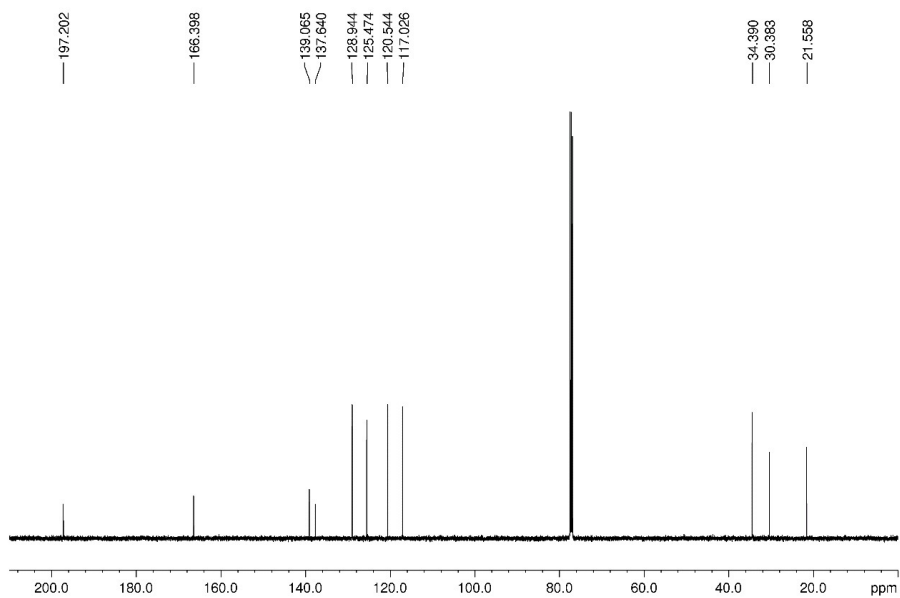


<sup>13</sup>C NMR of Cpd. 12 (126 MHz, CDCl<sub>3</sub>)

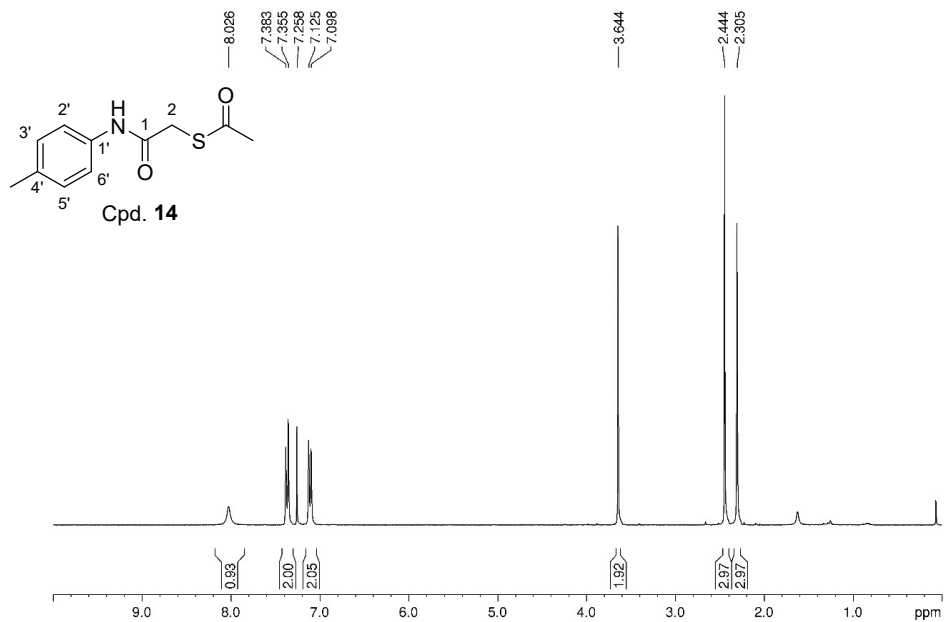




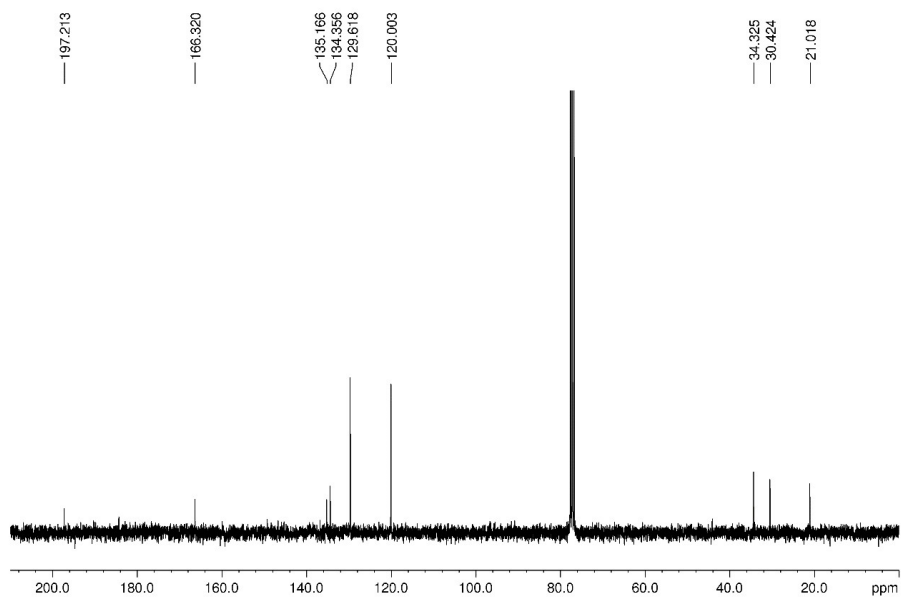
<sup>1</sup>H NMR of Cpd. 13 (500 MHz, CDCl<sub>3</sub>)



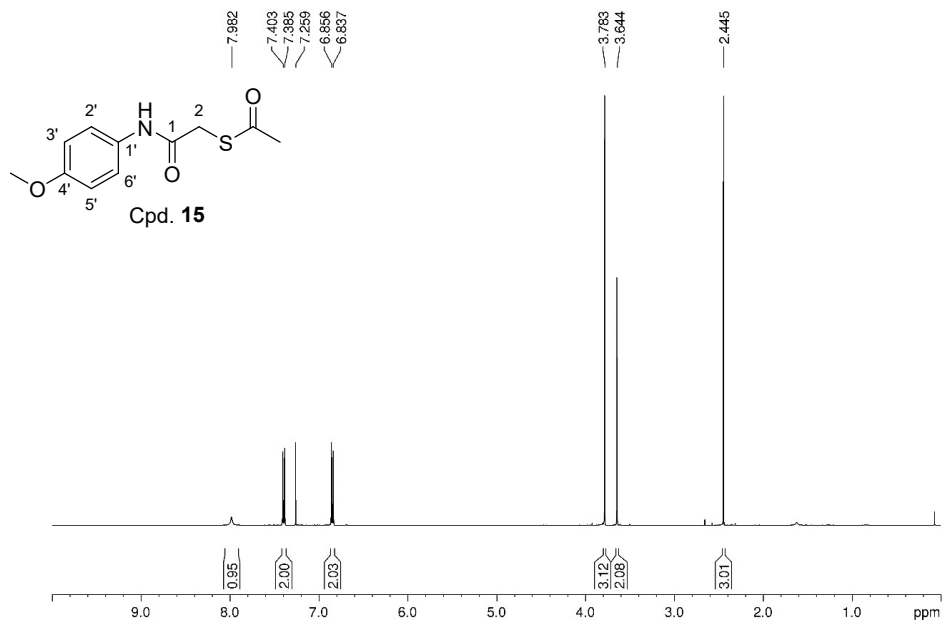
<sup>13</sup>C NMR of Cpd. 13 (126 MHz, CDCl<sub>3</sub>)



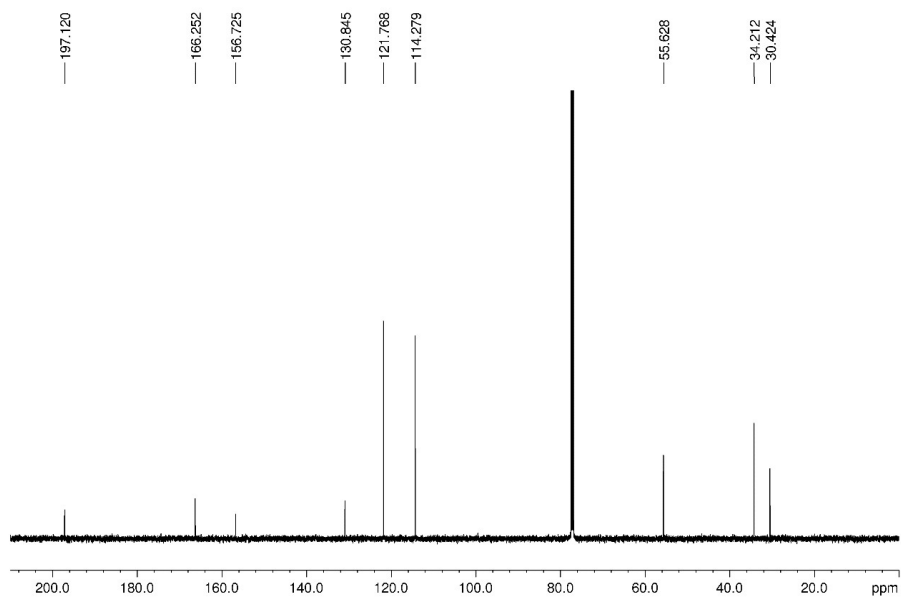
<sup>1</sup>H NMR of Cpd. 14 (300 MHz, CDCl<sub>3</sub>)



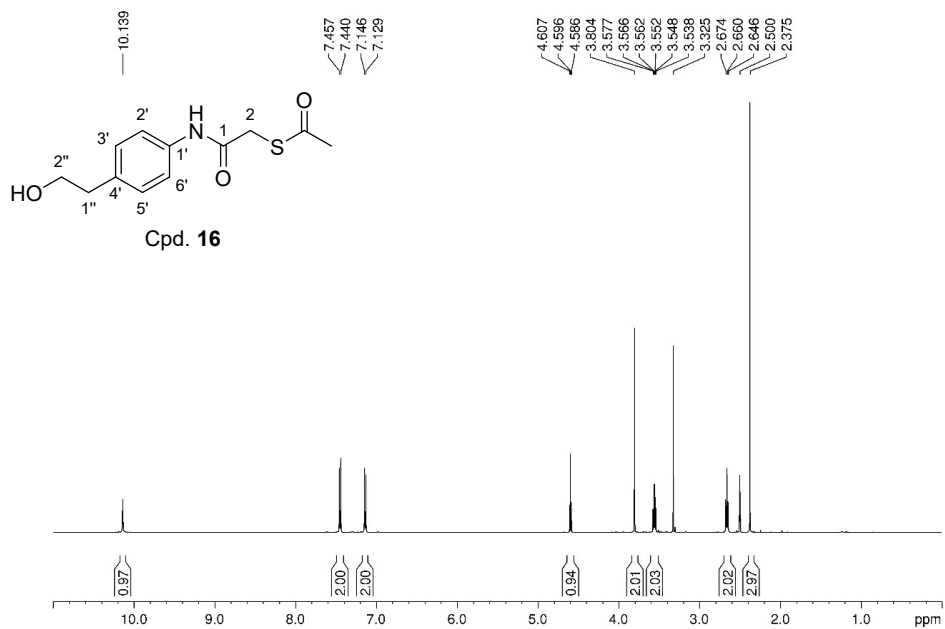
<sup>13</sup>C NMR of Cpd. 14 (75 MHz, CDCl<sub>3</sub>)



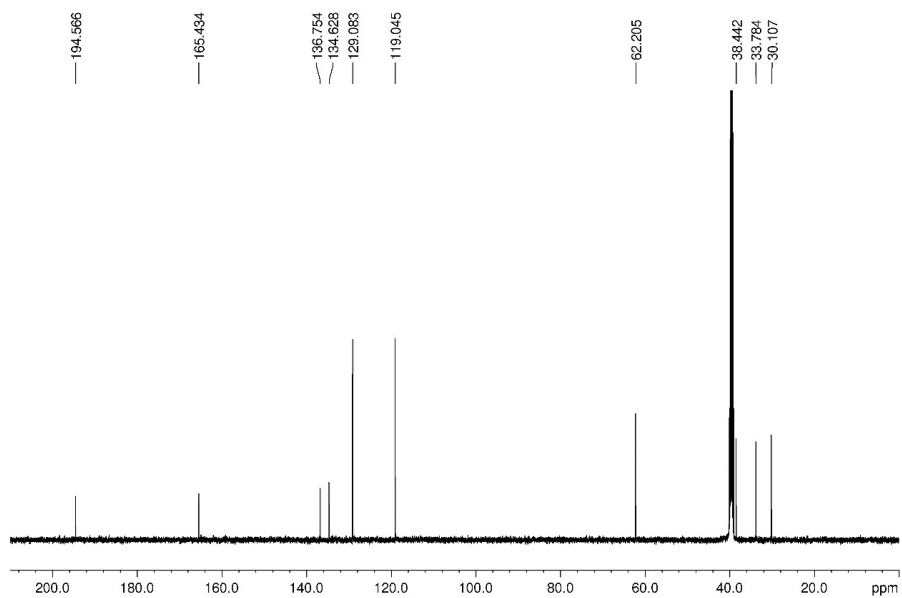
<sup>1</sup>H NMR of Cpd. 15 (500 MHz, CDCl<sub>3</sub>)



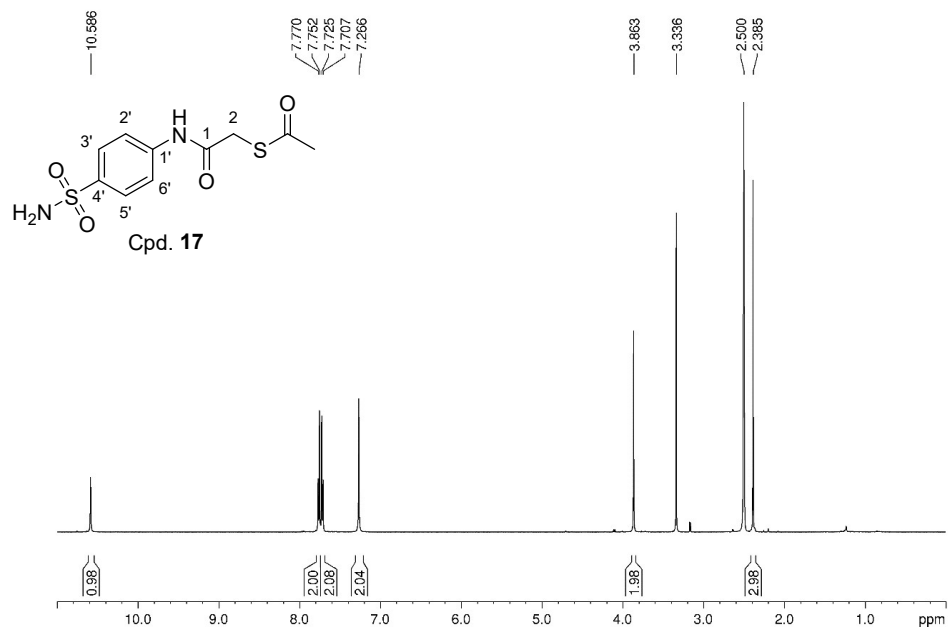
<sup>13</sup>C NMR of Cpd. 15 (126 MHz, CDCl<sub>3</sub>)



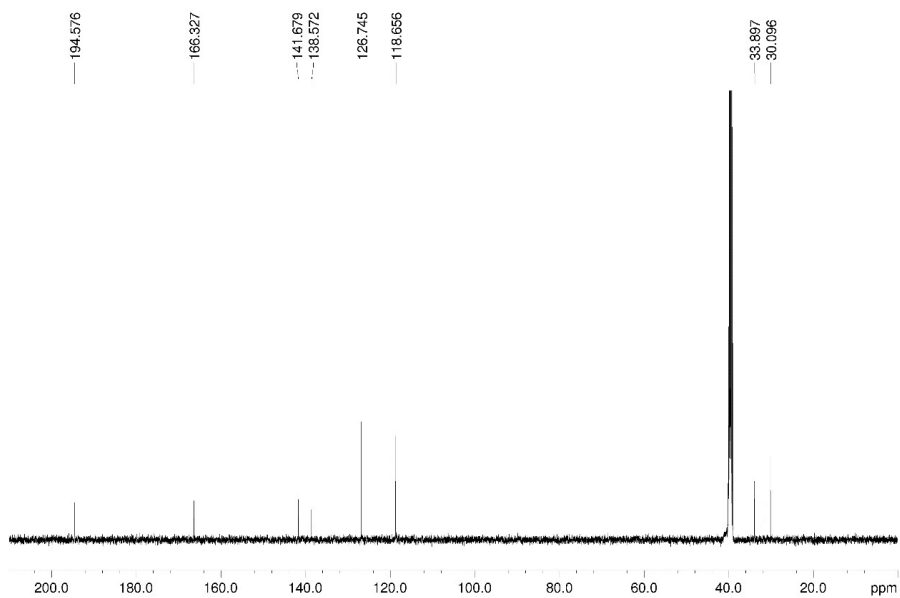
<sup>1</sup>H NMR of Cpd. 16 (500 MHz, DMSO-*d*<sub>6</sub>)



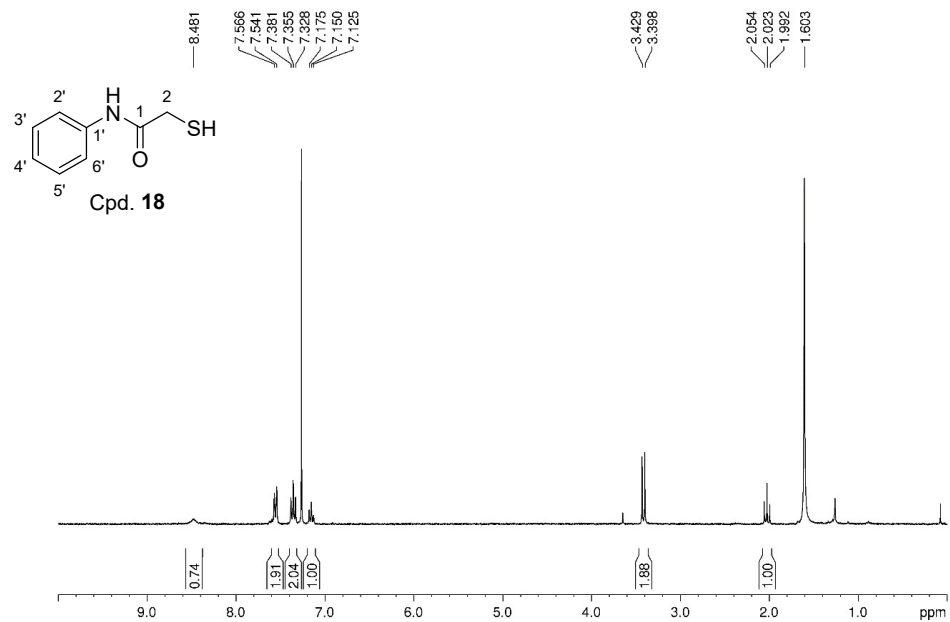
<sup>13</sup>C NMR of Cpd. 16 (126 MHz, DMSO-*d*<sub>6</sub>)



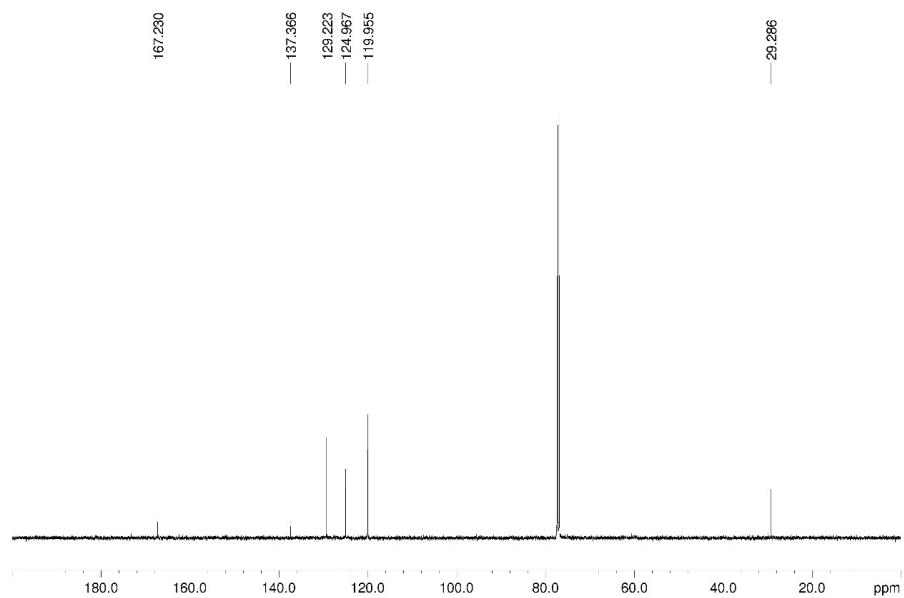
<sup>1</sup>H NMR of Cpd. 17 (500 MHz, DMSO-*d*<sub>6</sub>)



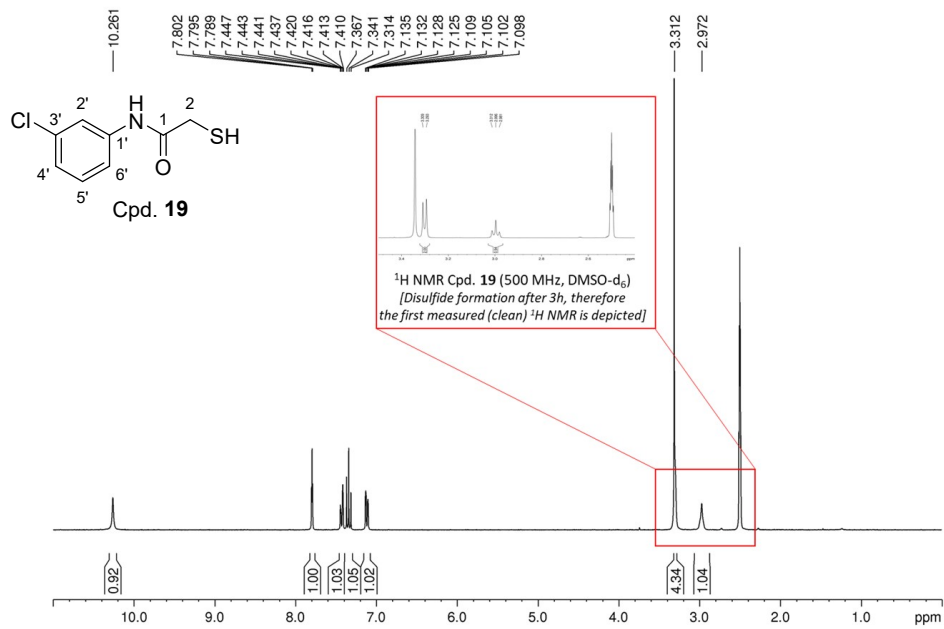
<sup>13</sup>C NMR of Cpd. 17 (126 MHz, DMSO-*d*<sub>6</sub>)



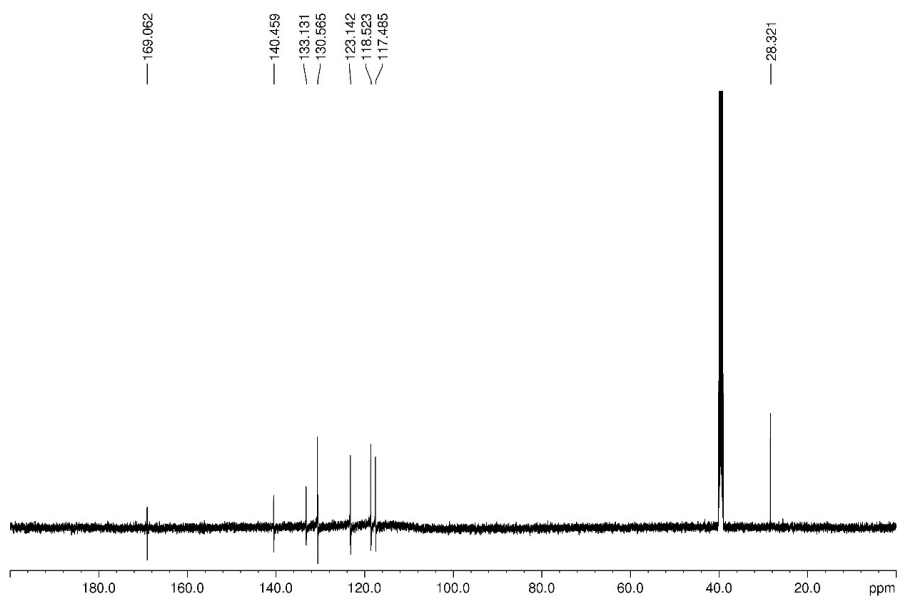
$^1\text{H}$  NMR of Cpd. **18** (300 MHz,  $\text{CDCl}_3$ )

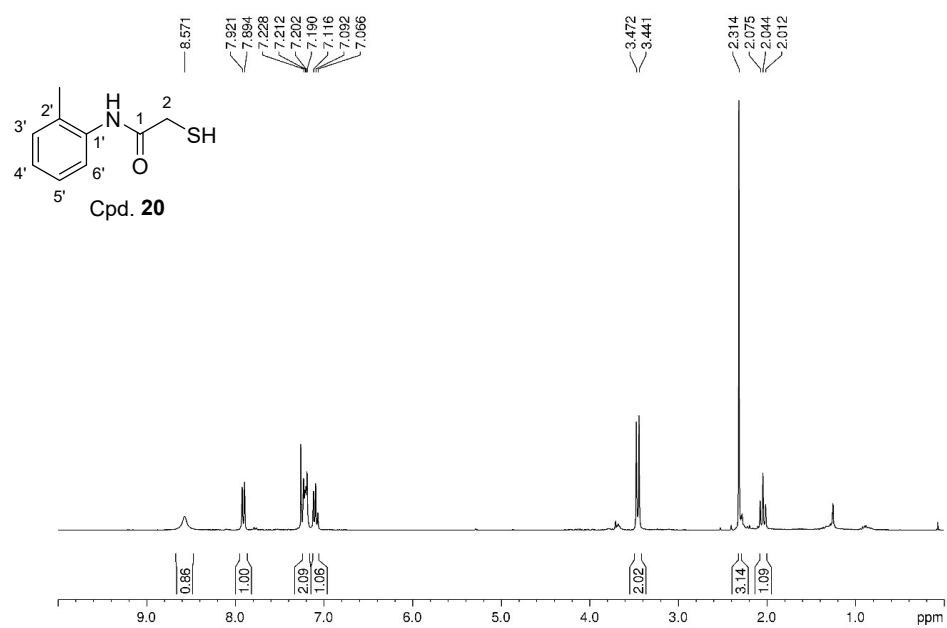


$^{13}\text{C}$  NMR of Cpd. **18** (126 MHz,  $\text{CDCl}_3$ )

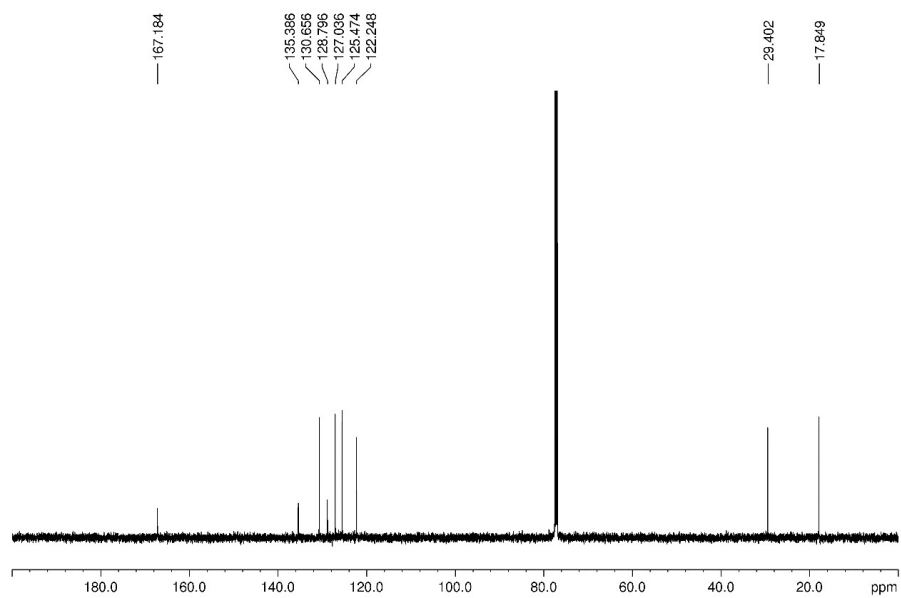


$^1\text{H NMR of Cpd. 19 (300 MHz, DMSO-}d_6)$



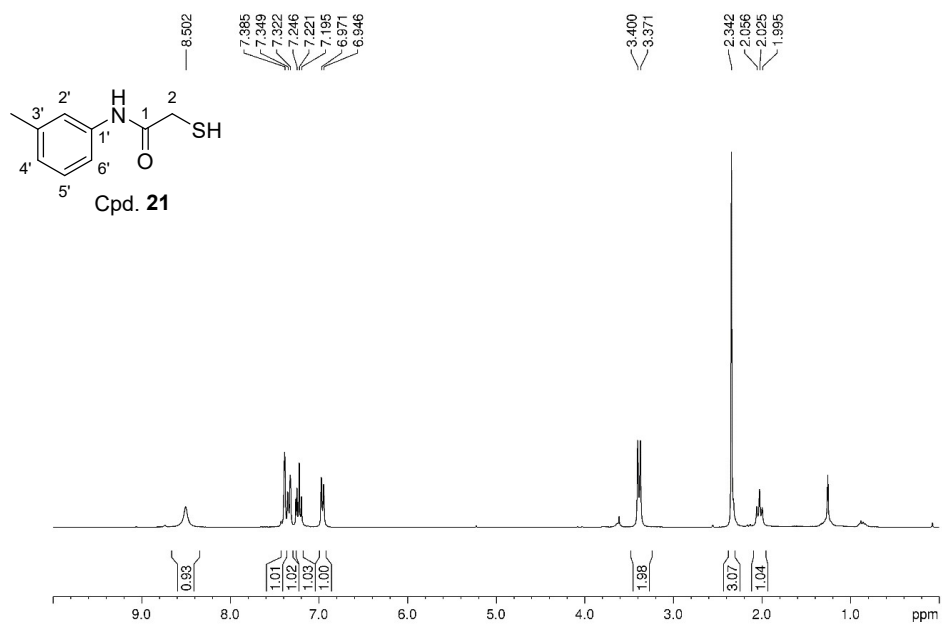


<sup>1</sup>H NMR of Cpd. 20 (300 MHz, CDCl<sub>3</sub>)

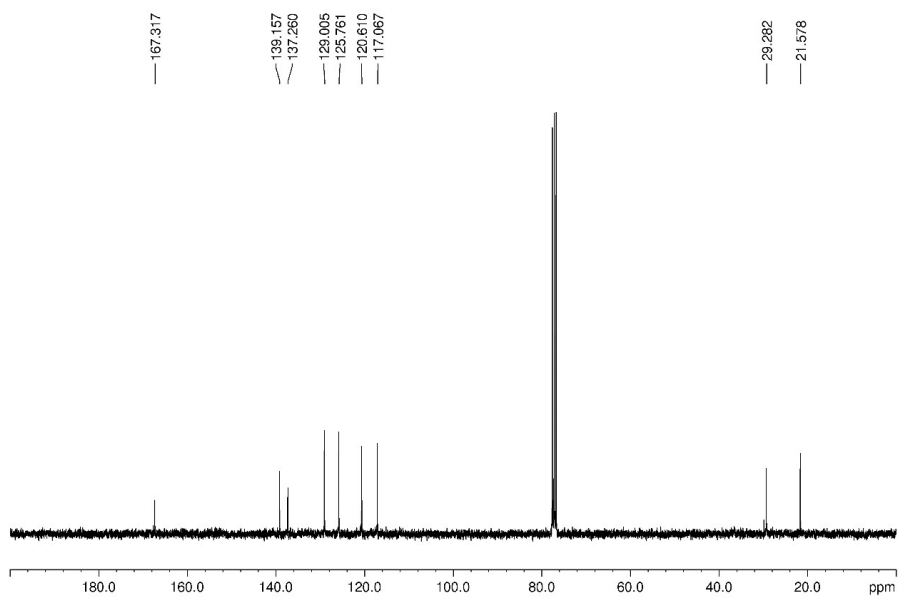


<sup>13</sup>C NMR of Cpd. 20 (126 MHz, CDCl<sub>3</sub>)

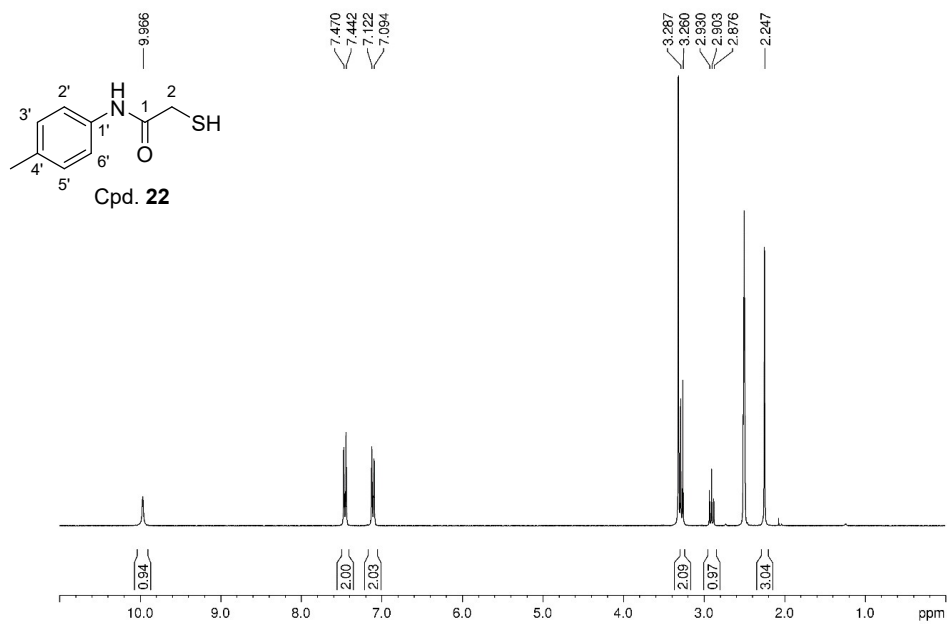




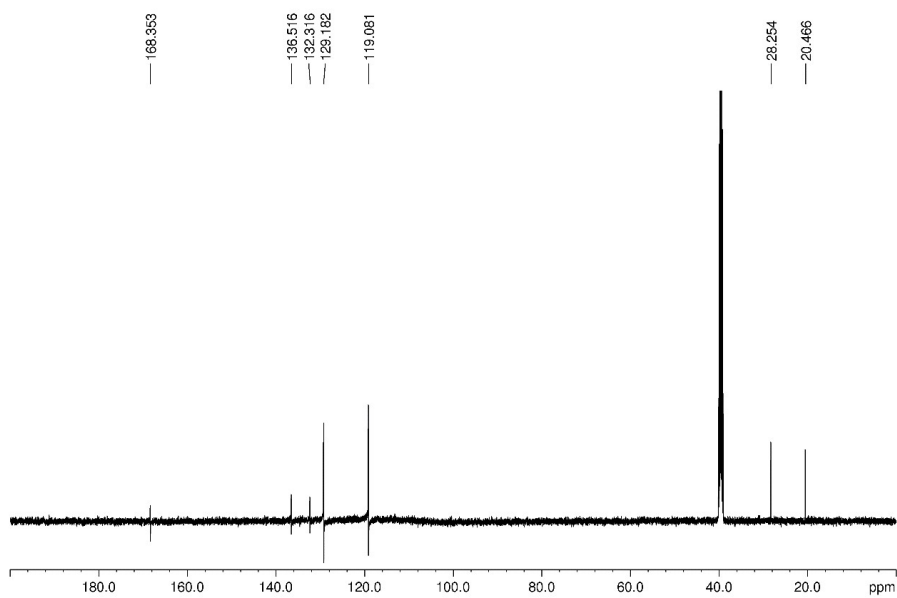
<sup>1</sup>H NMR of Cpd. 21 (300 MHz, CDCl<sub>3</sub>)



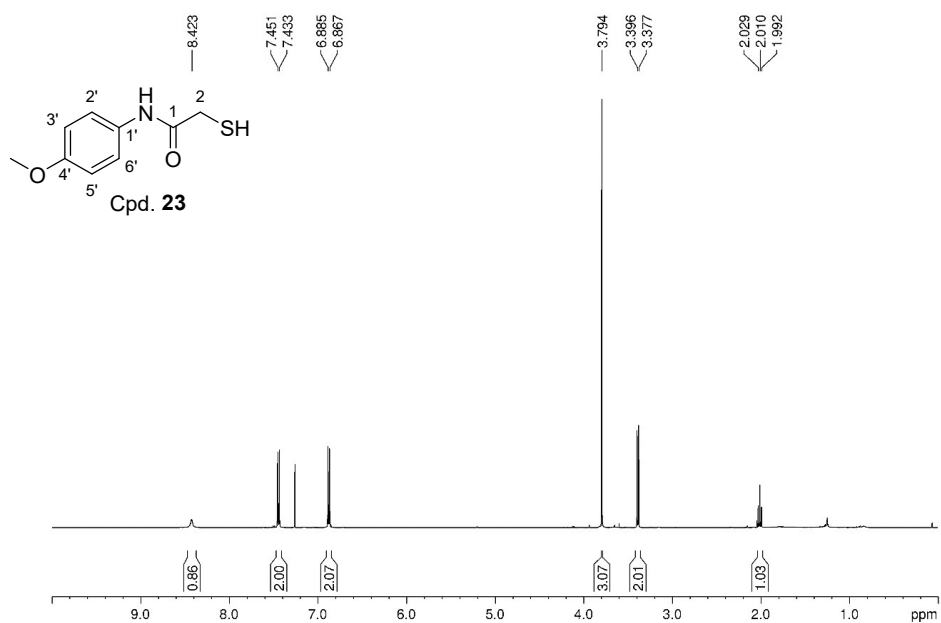
<sup>13</sup>C NMR of Cpd. 21 (75 MHz, CDCl<sub>3</sub>)



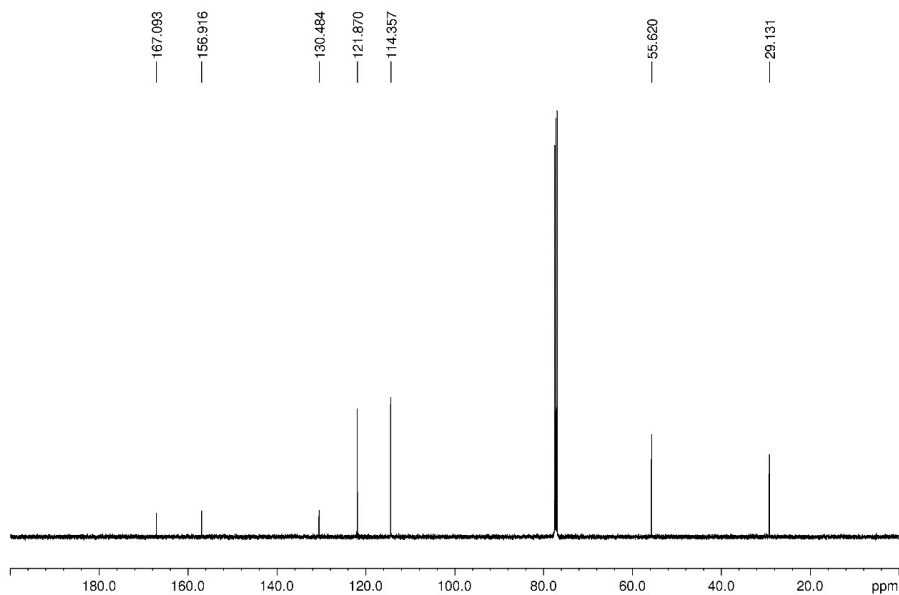
<sup>1</sup>H NMR of Cpd. 22 (300 MHz, DMSO-*d*<sub>6</sub>)



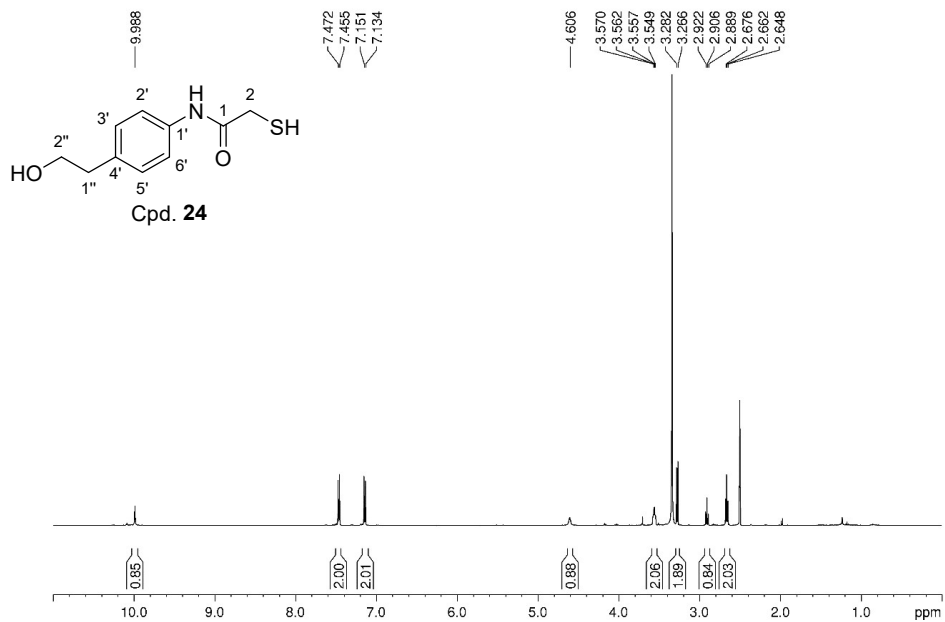
<sup>13</sup>C NMR of Cpd. 22 (126 MHz, DMSO-*d*<sub>6</sub>)



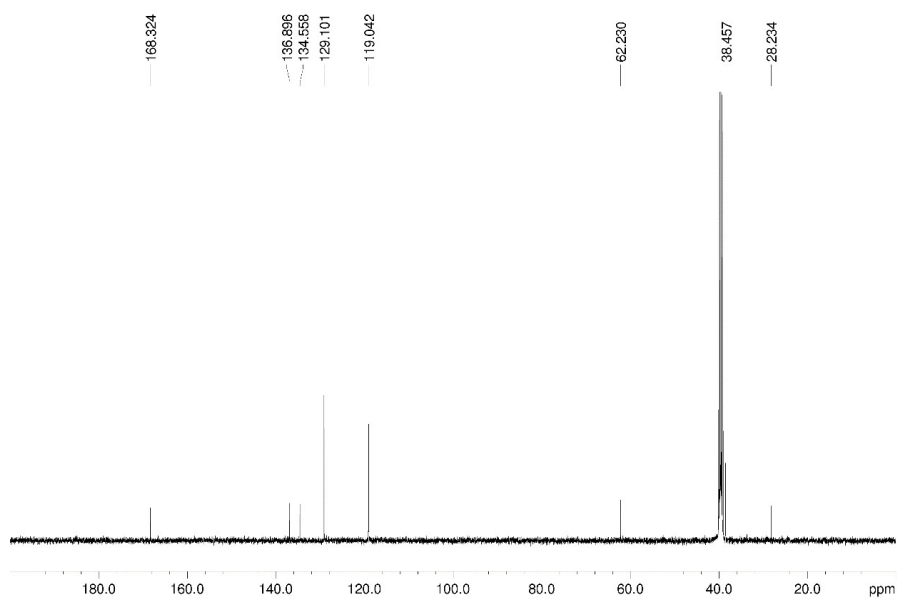
<sup>1</sup>H NMR of Cpd. 23 (500 MHz, CDCl<sub>3</sub>)



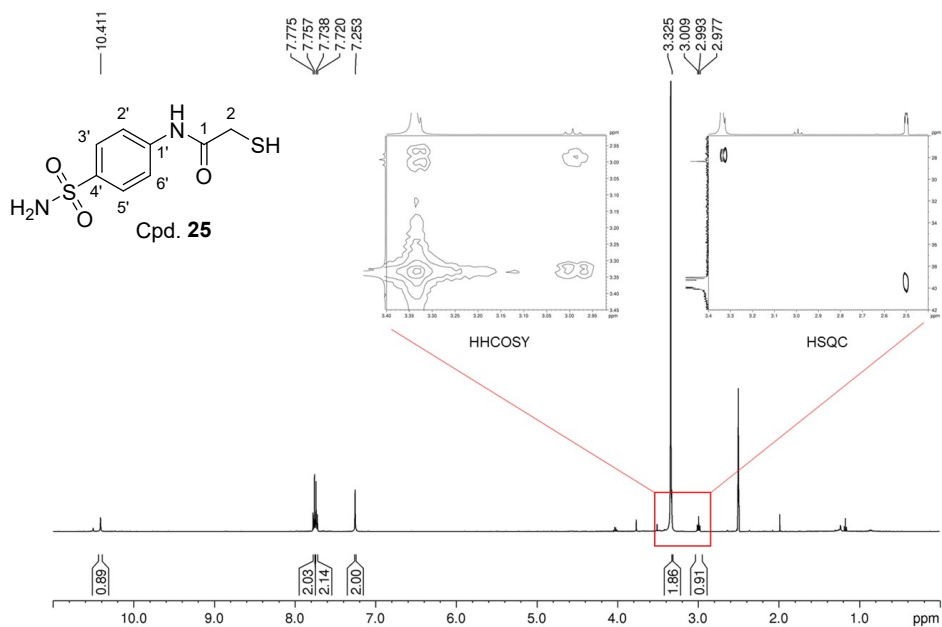
<sup>13</sup>C NMR of Cpd. 23 (126 MHz, CDCl<sub>3</sub>)



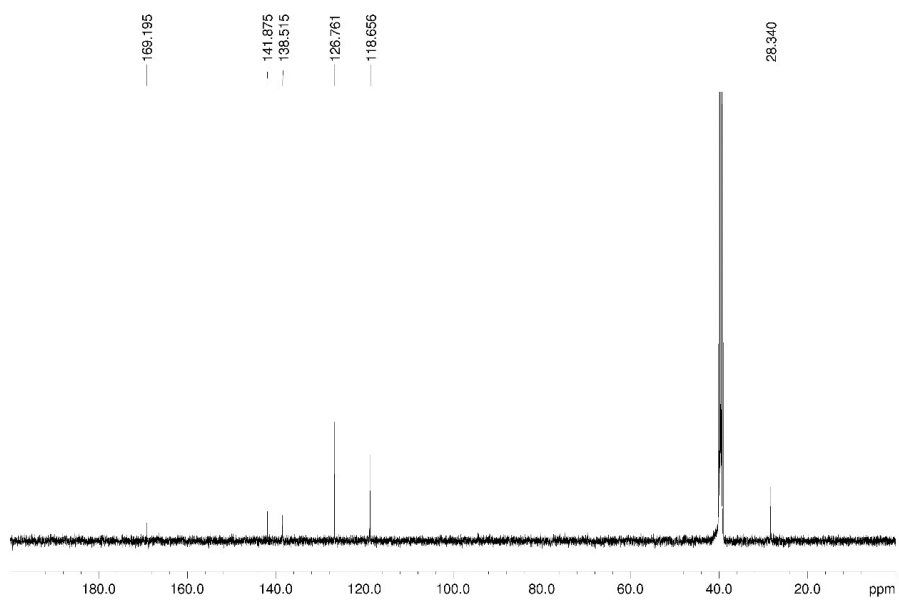
<sup>1</sup>H NMR of Cpd. 24 (500 MHz, DMSO-*d*<sub>6</sub>)



<sup>13</sup>C NMR of Cpd. 24 (126 MHz, DMSO-*d*<sub>6</sub>)



<sup>1</sup>H NMR of Cpd. 25 (500 MHz, DMSO-*d*<sub>6</sub>)



<sup>13</sup>C NMR of Cpd. 25 (126 MHz, DMSO-*d*<sub>6</sub>)

## References

- (1) Konstantinović, J.; Yahiaoui, S.; Alhayek, A.; Haupenthal, J.; Schönauer, E.; Andreas, A.; Kany, A. M.; Mueller, R.; Köhnke, J.; Berger, F.; Bischoff, M.; Hartmann, R. W.; Brandstetter, H.; Hirsch, A. K. H. N-Aryl-3-Mercaptosuccinimides as Antivirulence Agents Targeting *Pseudomonas Aeruginosa* Elastase and *Clostridium* Collagenases. *J. Med. Chem.* **2020**, *63* (15), 8359–8368. <https://doi.org/10.1021/acs.jmedchem.0c00584>.
- (2) Kany, A. M.; Sikandar, A.; Haupenthal, J.; Yahiaoui, S.; Maurer, C. K.; Proschak, E.; Köhnke, J.; Hartmann, R. W. Binding Mode Characterization and Early *in Vivo* Evaluation of Fragment-Like Thiols as Inhibitors of the Virulence Factor LasB from *Pseudomonas Aeruginosa*. *ACS Infect. Dis.* **2018**, *4* (6), 988–997. <https://doi.org/10.1021/acsinfecdis.8b00010>.

## A5. SUPPORTING INFORMATION TO CHAPTER E

***N*-Aryl-2-*iso*-butylmercaptoacetamides: the discovery of highly potent and selective inhibitors of *P. aeruginosa* virulence factor LasB and *C. histolyticum* virulence factor ColH.**

Katrin Voos,<sup>±</sup> Samir Yahiaoui,<sup>±</sup> Jelena Konstantinović, Esther Schönauer, Alaa Alhayek, Jörg Hauptenthal, Asfandyar Sikandar, Khadija Si Chaib, Tizian F. Ramspoth, Katharina Rox, Hans Brandstetter, Christian Ducho\* and Anna K. H. Hirsch\*

<sup>±</sup> these authors contributed equally

\* corresponding authors

Please note that the following chapter is the supporting information of a manuscript in preparation and thus, neither published nor peer-reviewed yet!

# Supporting Information

## *N*-Aryl-2-*iso*-butylmercaptoacetamides: the discovery of highly potent and selective inhibitors of *Pseudomonas aeruginosa* virulence factor LasB and *Clostridium histolyticum* virulence factor ColH

Katrin Voos,<sup>1</sup>⊥ Samir Yahiaoui,<sup>2</sup>⊥ Jelena Konstantinović,<sup>2</sup> Esther Schönauer,<sup>3</sup> Alaa Alhayek,<sup>2,4</sup> Asfandyar Sikandar,<sup>2</sup> Khadidja Si Chaib,<sup>2</sup> Tizian F. Ramspoth,<sup>2</sup> Katharina Rox,<sup>5,6</sup> Jörg Hauptenthal,<sup>2</sup> Jesko Köhnke,<sup>7</sup> Hans Brandstetter,<sup>3</sup> Christian Ducho<sup>1\*</sup> and Anna K. H. Hirsch<sup>2,4\*</sup>

⊥ these authors contributed equally

\* corresponding authors: [Christian.Ducho@uni-saarland.de](mailto:Christian.Ducho@uni-saarland.de) & [Anna.Hirsch@helmholtz-hips.de](mailto:Anna.Hirsch@helmholtz-hips.de)

- <sup>1.</sup> Department of Pharmacy, Pharmaceutical and Medicinal Chemistry, Saarland University, Campus C2 3, 66123 Saarbrücken, Germany
- <sup>2.</sup> Department of Drug Design and Optimization, Helmholtz Institute for Pharmaceutical Research Saarland (HIPS) – Helmholtz Centre for Infection Research (HZI), Campus E8 1, 66123 Saarbrücken, Germany
- <sup>3.</sup> Department of Biosciences and Christian Doppler Laboratory for Innovative Tools for Biosimilar Characterization, Division of Structural Biology, University of Salzburg, Billrothstrasse 11, 5020 Salzburg, Austria
- <sup>4.</sup> Department of Pharmacy, Saarland University, Campus Building E8 1, 66123 Saarbrücken, Germany
- <sup>5.</sup> Department of Chemical Biology, Helmholtz Centre for Infection Research, Inhoffenstrasse 7, 38124 Braunschweig, Germany
- <sup>6.</sup> German Center for Infection Research (DZIF), Site Hannover-Braunschweig, Germany
- <sup>7.</sup> School of Chemistry, University of Glasgow, Glasgow, G12 8QQ, United Kingdom

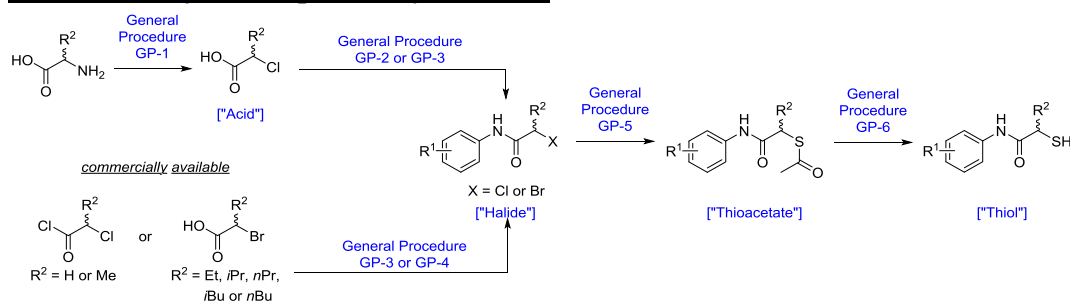


## Content

Content .....	2
Chemistry .....	3
<i>An overview of all compounds synthesized</i> .....	3
<i>General</i> .....	4
<i>General Procedures GP-1 – GP-6</i> .....	5
<i>Synthesis of compounds 6–135</i> .....	7
Thioacetates as surrogates for ColH inhibition of thiols .....	42
Inhibition [%] of ColH at 1 $\mu$ M concentration .....	43
Crystallographic data .....	44
<i>Co-crystal structures of LasB with 25 and 37 and ColH with 100</i> .....	44
SafetyScreen44™ Panel .....	47
<i>In Vitro Pharmacology: Binding Assays (Figure S5)</i> .....	47
<i>In Vitro Pharmacology: Enzyme and Uptake Assays (Figure S6)</i> .....	48
Additional information on the <i>in vitro</i> lung and skin-cell assays .....	49
<i>In vivo</i> pharmacokinetic studies .....	53
References .....	54

# Chemistry

## An overview of all compounds synthesized



**Scheme S1.** Synthetic scheme of  $\alpha$ -alkylated derivatives. General Procedures can be found in section “Chemistry”, the corresponding structures to the compound numbers can be found in Table S1.

**Table S1.** Overview of compound structures according to Scheme S1 with their corresponding compound numbers. Previously published compounds are colored in green, and their references are given in the table. Non-isolated compounds are colored in blue. Their syntheses can be found as part of the corresponding next step with an isolated product.

R <sup>1</sup>	R <sup>2</sup>	Halide	Thioacetate	Thiol	R <sup>1</sup>	R <sup>2</sup>	Acid	Halide	Thioacetate	Thiol
3,4-diCl	benzyl	-	-	4 <sup>1</sup>	3,4-diCl	<i>n</i> -propyl	-	60	118	12
4-OMe	benzyl	-	-	5 <sup>2</sup>	4-OMe	<i>n</i> -propyl	-	61	102	13
3,4-diCl	H	-	-	1 <sup>3</sup>	2-Me	<i>n</i> -propyl	-	62	103	-
4-OMe	H	-	141 <sup>4</sup>	2 <sup>4</sup>	3-Me	<i>n</i> -propyl	-	63	104	-
2-Me	H	-	142 <sup>4</sup>	-	4-Me	<i>n</i> -propyl	-	64	105	14
3-Me	H	-	143 <sup>4</sup>	-	2-Cl	<i>n</i> -propyl	-	65	106	-
4-Me	H	-	144 <sup>4</sup>	136 <sup>4</sup>	3-Cl	<i>n</i> -propyl	-	66	107	-
2-Cl	H	41	90	-	4-Cl	<i>n</i> -propyl	-	67	108	15
3-Cl	H	-	145 <sup>4</sup>	-	4-Ac	<i>n</i> -propyl	-	68	109	16
4-Cl	H	42	91	137 <sup>3</sup>	H	<i>n</i> -propyl	-	69	110	17
4-Ac	H	43	92	3 <sup>5</sup>	3,4-diCl	<i>i</i> -butyl	-	70	119	20
H	H	-	146 <sup>4</sup>	138 <sup>4</sup>	4-OMe	<i>i</i> -butyl	-	71	120	25
3,4-diCl	methyl	44	111	6	3-OMe	<i>i</i> -butyl	-	72	121	30
4-OMe	methyl	45	93	7	2-OMe	<i>i</i> -butyl	-	73	122	31
2-Me	methyl	46	94	-	2,4-di-OMe	<i>i</i> -butyl	-	74	123	32
3-Me	methyl	47	95	-	3,4-di-OMe	<i>i</i> -butyl	-	75	124	33
4-Me	methyl	48	96	8	4-OH	<i>i</i> -butyl	-	76	125	34
2-Cl	methyl	49	97	-	2-OH	<i>i</i> -butyl	-	77	126	35
3-Cl	methyl	50	98	-	4-Ac	<i>i</i> -butyl	-	78	127	36
4-Cl	methyl	51	99	9	4-Me	<i>i</i> -butyl	-	79	128	37
4-Ac	methyl	52	100	10	4-Cl	<i>i</i> -butyl	-	80	129	38
H	methyl	53	101	11	3,4-diCl	<i>n</i> -butyl	-	81	130	21
3,4-diCl	ethyl	54	112	18	4-MeO	<i>n</i> -butyl	-	82	131	26
4-OMe	ethyl	55	113	23	3,4-diCl	<i>sec</i> -butyl	87	83	132	22
4-Ac	ethyl	56	114	39	4-OMe	<i>sec</i> -butyl	87	84	133	27
3,4-diCl	<i>i</i> -propyl	57	115	19	3,4-diCl	cy-hex	-	-	-	140 <sup>1</sup>
4-OMe	<i>i</i> -propyl	58	116	24	4-OMe	cy-hex	88	85	134	29
4-Ac	<i>i</i> -propyl	59	117	40	3,4-diCl	cy-pr	-	-	-	139 <sup>1</sup>
					4-OMe	cy-pr	89	86	135	28

## **General**

All chemicals were purchased using standard suppliers. Acetone and methanol were purchased in HPLC quality, all other solvents were of technical quality and distilled prior to use. Deionized water was used throughout. None of the procedures was optimized regarding yield. The reactions were monitored by thin-layer chromatography (TLC) using aluminum plates precoated with silica gel 60 F<sub>254</sub> (VWR, Bruchsal, Germany) and visualized using UV light (254 nm) and staining under heating (VSS stain: 4 g vanillin, 25 mL conc. H<sub>2</sub>SO<sub>4</sub>, 80 mL AcOH, and 680 mL MeOH; CAM stain: 12 g ammonium molybdate, 0.5 g ceric ammonium molybdate, 235 mL H<sub>2</sub>O, 15 mL conc. H<sub>2</sub>SO<sub>4</sub>). All organic extracts were dried over Na<sub>2</sub>SO<sub>4</sub>, filtered, and solvents were removed under reduced pressure. Radial chromatography was performed on a Chromatotron (Harrison Research, Model 7924T-01, T-Squared Technology) using glass plates coated with a layer of silica gel containing a fluorescent indicator (VWR 60 PF254). 300 MHz- and 500 MHz-<sup>1</sup>H NMR spectra and 75 MHz- and 125 MHz-<sup>13</sup>C NMR spectra were recorded on Bruker Fourier 300 or Bruker UltraShield™ 500 (Bruker Corporation, Billerica, MA, USA) spectrometers. All spectra were recorded at room temperature and were referenced internally to solvent reference frequencies. Chemical shifts ( $\delta$ ) are expressed in parts per million (ppm) and coupling constants ( $J$ ) are expressed in Hertz (Hz). The following abbreviations were used to identify the multiplicities: s = singlet, d = doublet, t = triplet, q = quartet, m = multiplet, br = broad. The assignment of the signals was done using <sup>1</sup>H,<sup>1</sup>H-COSY, HSQC and HMBC spectra obtained on the aforementioned spectrometers. Low-resolution mass spectra (LCMS) were measured on a Thermo Finnigan Surveyor MSQ Plus mass spectrometer. The purity of synthesized target compounds was determined by LCMS using the area percentage method on the UV trace recorded at a wavelength of 254 nm and found to be >95%. High-resolution mass spectrometry (HRMS) was performed on a Thermo Scientific Q Exactive Orbitrap mass spectrometer equipped with an electrospray ionization (ESI) source. Melting points (m.p.) were measured on a melting point apparatus SMP3 (Stuart Scientific, Staffordshire, United Kingdom) and are not corrected.

## **General Procedures GP-1 – GP-6**

### **General procedure GP-1: Synthesis of 2-chloroalkanoic acids**

Amino acid (1.0 eq) was dissolved in 6 M HCl (2 mL/mmol or until mostly dissolved) under nitrogen atmosphere and cooled to  $-5\text{ }^{\circ}\text{C}$ . Sodium nitrite (2.5 eq) was dissolved in water (0.3 mL/mmol amino acid) and added slowly dropwise. The reaction was stirred overnight while warming to room temperature. The reaction was extracted with EtOAc/THF (3x, 3:1). The combined organic extracts were washed with saturated aqueous NaCl solution and dried over anhydrous  $\text{Na}_2\text{SO}_4$  and filtered. The solvent was removed under reduced pressure to afford the crude product. The crude product obtained was used in the next step without further purification.

### **General procedure GP-2: Synthesis of *N*-aryl-2-halo-2-alkylacetamide derivatives**

2-Haloalkanoic acid (1.2 eq) (purified or as crude) was dissolved in THF.  $\text{NEt}_3$  (1.2 eq) was added to this solution at room temperature, followed by dropwise addition of ethylchloroformate (1.3 eq). A solution of the corresponding aniline (1.0 eq) was dissolved in THF and added dropwise to this mixture. The reaction was stirred at room temperature overnight. THF was evaporated, the crude product was dissolved in  $\text{CH}_2\text{Cl}_2$  and washed with aqueous  $\text{KHCO}_3$  (10% wt) and water. The solvent was removed under reduced pressure, the compound was dried over anhydrous  $\text{Na}_2\text{SO}_4$  and filtered. Purification was carried out by flash chromatography.

### **General procedure GP-3: Synthesis of *N*-aryl-2-halo-2-alkylacetamide derivatives**

2-Haloalkanoic acid (1.2 eq) (2-chloroalkanoic acid as crude or commercially available 2-bromoalkanoic acid) and EDC·HCl (1.2 eq) were added to a solution of the corresponding aniline (1.0 eq) in  $\text{CH}_2\text{Cl}_2$ . The resultant mixture was stirred at room temperature. The reaction was stopped and  $\text{CH}_2\text{Cl}_2$  was added. The solution obtained was washed with 1 M HCl and with saturated aqueous NaCl solution. The organic layer was dried over anhydrous  $\text{Na}_2\text{SO}_4$ , filtered and concentrated under reduced pressure to afford the crude product. The crude product was used for the next step without further purification or purified using column chromatography.

### **General procedure GP-4: Synthesis of *N*-aryl-2-halo-2-alkylacetamide derivatives**

Aniline (1.0 eq) and DIPEA (1.2 eq) were dissolved in dry  $\text{CH}_2\text{Cl}_2$  or THF and cooled on ice to  $0\text{ }^{\circ}\text{C}$ . To this solution, 2-haloalkanoic acid chloride (1.2 eq) was added dropwise, and the resultant mixture was stirred at  $0\text{ }^{\circ}\text{C}$ . The reaction was quenched with 0.5 M  $\text{NaHCO}_3$ . After dilution with  $\text{CH}_2\text{Cl}_2$ , the reaction was extracted with 0.5 M  $\text{NaHCO}_3$  (3x), 0.5 M HCl (3x), and saturated aqueous NaCl solution (1x). The  $\text{CH}_2\text{Cl}_2$  layer was dried over anhydrous  $\text{Na}_2\text{SO}_4$ , filtered, and concentrated under reduced pressure to give the title compounds in pure form without any further purification.

**General procedure GP-5: Synthesis of *N*-aryl-2-thioacetyl-2-alkylacetamide derivatives**

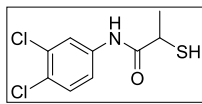
*N*-aryl-2-halo-2-alkylacetamide derivative (1.0 eq) (purified or as crude) was dissolved in acetone, and potassium thioacetate (1–2 eq) was added to the solution. The resultant mixture was stirred at room temperature. After concentration under vacuum, the resultant residue was diluted with H<sub>2</sub>O and extracted with EtOAc. The organic layer was washed with saturated aqueous NaCl solution, dried over anhydrous Na<sub>2</sub>SO<sub>4</sub>, filtered and evaporated under reduced pressure. The crude residue was purified using column chromatography.

**General procedure GP-6: Synthesis of 2-mercapto-*N*-aryl-2-alkylacetamide derivatives**

NaOH (3–4 eq) was added to a solution of *N*-aryl-2-thioacetyl-2-alkylacetamide (1.0 eq) in MeOH under argon atmosphere. The reaction was stirred at room temperature. The reaction was acidified with 2 M HCl and extracted with EtOAc and 0.5 M HCl. The organic layer was washed with 0.5 M HCl and with saturated aqueous NaCl solution, dried over anhydrous Na<sub>2</sub>SO<sub>4</sub>, filtered and evaporated under reduced pressure. The product was obtained in pure form or purified using column chromatography or preparative HPLC.

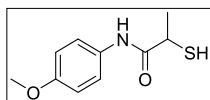
## Synthesis of compounds 6–135

**2-Mercapto-*N*-(3',4'-dichlorophenyl)propanamide 6.** Compound **6** was synthesized according to



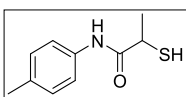
the general procedure **GP-6**, using thioacetate **111** (41 mg, 0.14 mmol) and NaOH (200 mg, 5.00 mmol) in MeOH (5 mL). The reaction was stirred at room temperature for 1 h. Extraction gave the final compound **6** without any further purification as white solid (35 mg, 98%). m.p. = 123 °C. <sup>1</sup>H NMR (500 MHz, CDCl<sub>3</sub>) δ 8.41 (br, 1H), 7.81 (d, *J* = 2.0 Hz, 1H), 7.39 (d, *J* = 8.7 Hz, 1H), 7.37 (dd, *J* = 2.1, 8.7 Hz, 1H), 4.16 (dq, *J* = 7.2, 8.5 Hz, 1H), 2.16 (d, *J* = 8.5 Hz, 1H), 1.65 (d, *J* = 7.2 Hz, 3H). <sup>13</sup>C NMR (126 MHz, CDCl<sub>3</sub>) δ 171.0, 137.1, 133.1, 130.7, 128.0, 119.1, 39.1, 22.1. HRMS (ESI) *m/z* calculated for C<sub>9</sub>H<sub>10</sub>Cl<sub>2</sub>NOS 249.9855 [M+H]<sup>+</sup>, found 249.9850.

**2-Mercapto-*N*-(4'-methoxyphenyl)propanamide 7.** Compound **7** was synthesized according to the



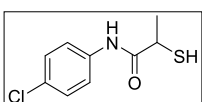
general procedure **GP-6**, using thioacetate **93** (28 mg, 0.11 mmol) and NaOH (200 mg, 5.00 mmol) in MeOH (5 mL). The reaction was stirred at room temperature for 1.5 h. Extraction gave the final compound **7** without any further purification as white solid (23 mg, 98%). m.p. = 93 °C. <sup>1</sup>H NMR (500 MHz, CDCl<sub>3</sub>) δ 8.25 (br, 1H), 7.44 (d, *J* = 9.0 Hz, 2H), 6.87 (d, *J* = 9.0 Hz, 2H), 3.79 (s, 3H), 3.61–3.55 (m, 1H), 2.15 (d, *J* = 8.3 Hz, 1H), 1.65 (d, *J* = 7.2 Hz, 3H). <sup>13</sup>C NMR (126 MHz, CDCl<sub>3</sub>) δ 170.8, 156.8, 130.7, 121.8, 114.3, 55.6, 39.1, 22.3. HRMS (ESI) *m/z* calculated for C<sub>10</sub>H<sub>12</sub>NO<sub>2</sub>S 210.0594 [M-H]<sup>-</sup>, found 210.0577.

**2-Mercapto-*N*-(4'-methylphenyl)propanamide 8.** Compound **8** was synthesized according to the



general procedure **GP-6**, using thioacetate **96** (20 mg, 0.084 mmol) and NaOH (50 mg, 1.3 mmol) in MeOH (3 mL). The reaction was stirred at room temperature for 1 h. Extraction followed by column chromatography (PE/EtOAc 9:1) gave the final compound **8** as white solid (14 mg, 85%). m.p. = 137 °C. *R<sub>f</sub>* = 0.53 (PE/EtOAc 1:1). <sup>1</sup>H NMR (500 MHz, CDCl<sub>3</sub>) δ 8.30 (br, 1H), 7.42 (d, *J* = 8.4 Hz, 2H), 7.13 (d, *J* = 8.3 Hz, 2H), 3.58 (ddd, *J* = 7.6, 7.9, 14.6 Hz, 1H), 2.32 (s, 3H), 2.15 (d, *J* = 8.4 Hz, 1H), 1.64 (d, *J* = 7.2 Hz, 3H). <sup>13</sup>C NMR (126 MHz, CDCl<sub>3</sub>) δ 170.9, 135.1, 134.4, 129.7, 120.0, 39.1, 22.3, 21.0. HRMS (ESI) *m/z* calculated for C<sub>10</sub>H<sub>14</sub>NOS 196.0791 [M+H]<sup>+</sup>, found 196.0788.

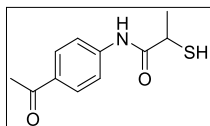
**2-Mercapto-*N*-(4'-chlorophenyl)propanamide 9.** Compound **9** was synthesized according to the



general procedure **GP-6**, using thioacetate **93** (28 mg, 0.11 mmol) and NaOH (200 mg, 5.00 mmol) in MeOH (5 mL). The reaction was stirred at room temperature for 1.5 h. Extraction gave the final compound **9** without any further purification as white solid (23 mg, 98%). m.p. = 113 °C. *R<sub>f</sub>* = 0.29 (PE/EtOAc 7:3). <sup>1</sup>H NMR (300 MHz, DMSO-*d*<sub>6</sub>) δ 10.15 (s, 1H), 7.62 (d, *J* = 8.9 Hz, 2H), 7.37 (d, *J* = 8.9 Hz, 2H), 3.62 (dq, *J* = 6.9, 8.6 Hz, 1H), 3.12 (d, *J* = 8.7 Hz, 1H), 1.43 (d, *J* = 6.9 Hz, 3H). <sup>13</sup>C NMR (75 MHz, DMSO-*d*<sub>6</sub>)

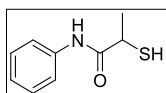
$\delta$  171.6, 138.0, 128.6, 126.9, 120.7, 36.7, 21.4. HRMS (ESI)  $m/z$  calculated for  $C_9H_{11}ClNOS$  216.0244  $[M+H]^+$ , found 216.0243.

**2-Mercapto-*N*-(4'-acetylphenyl)propanamide 10.** Compound **10** was synthesized according to the



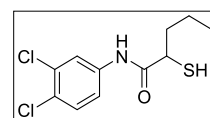
general procedure **GP-6**, using thioacetate **100** (199 mg, 0.750 mmol) and NaOH (100 mg, 2.50 mmol) in MeOH (7 mL). The reaction was stirred at room temperature for 3 h. Extraction followed by column chromatography (PE/EtOAc 7:3) gave the final compound **10** as clear oil (128 mg, 73%).  $R_f = 0.14$  (PE/EtOAc 7:3).  $^1H$  NMR (500 MHz,  $CDCl_3$ )  $\delta$  8.67 (br, 1H), 7.95 (d,  $J = 8.8$  Hz, 2H), 7.67 (d,  $J = 8.8$  Hz, 2H), 3.61 (qd,  $J = 7.2, 8.5$  Hz, 1H), 2.58 (s, 3H), 2.20 (d,  $J = 8.7$  Hz, 1H), 1.65 (d,  $J = 7.2$  Hz, 3H).  $^{13}C$  NMR (126 MHz,  $CDCl_3$ )  $\delta$  197.2, 171.4, 142.0, 133.3, 129.9, 119.1, 39.1, 26.6, 22.1. HRMS (ESI)  $m/z$  calculated for  $C_{11}H_{12}NO_2S$  222.0594  $[M-H]^-$ , found 222.0577.

**2-Mercapto-*N*-phenylpropanamide 11.** Compound **11** was synthesized according to the general



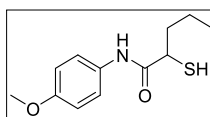
procedure **GP-6**, using thioacetate **101** (35 mg, 0.16 mmol) and NaOH (50 mg, 1.3 mmol) in MeOH (3 mL). The reaction was stirred at room temperature for 1 h. Extraction gave the final compound **11** without any further purification as white solid (23 mg, 79%). m.p. = 93 °C.  $^1H$  NMR (500 MHz,  $CDCl_3$ )  $\delta$  8.35 (br, 1H), 7.54 (d,  $J = 7.8$  Hz, 2H), 7.34 (t,  $J = 7.9$  Hz, 2H), 7.13 (t,  $J = 7.4$  Hz, 1H), 3.60 (dq,  $J = 7.5, 7.5$  Hz, 1H), 2.16 (d,  $J = 8.5$  Hz, 1H), 1.65 (d,  $J = 7.3$  Hz, 3H).  $^{13}C$  NMR (126 MHz,  $CDCl_3$ )  $\delta$  171.0, 137.6, 129.2, 124.8, 119.9, 39.2, 22.2. HRMS (ESI)  $m/z$  calculated for  $C_9H_{10}NOS$  180.0483  $[M-H]^-$ , found 180.0474.

**2-Mercapto-*N*-(3',4'-dichlorophenyl)pentanamide 12.** Compound **12** was synthesized according to



the general procedure **GP-6**, using compound **118** (91 mg, 0.28 mmol), NaOH (34 mg, 0.85 mmol) and MeOH (10 mL). The reaction was stirred at room temperature for 2.5 h. After extraction, compound **12** was obtained as pure white solid without any further purification (77 mg, 97%). m.p. = 74 °C.  $^1H$  NMR (500 MHz,  $DMSO-d_6$ )  $\delta$  10.36 (s, 1H), 8.00 (d,  $J = 2.5$  Hz, 1H), 7.57 (d,  $J = 9.0$  Hz, 1H), 7.48 (dd,  $J = 2.5, 9.0$  Hz, 1H), 3.44 (t,  $J = 7.3$  Hz, 1H), 3.06 (s, 1H), 1.92–1.77 (m, 1H), 1.68–1.54 (m, 1H), 1.45–1.20 (m, 2H), 0.88 (t,  $J = 7.5$  Hz, 3H).  $^{13}C$  NMR (126 MHz,  $DMSO-d_6$ )  $\delta$  171.6, 139.0, 131.1, 130.8, 124.9, 120.4, 119.3, 41.6, 37.2, 20.1, 13.5. HRMS (ESI)  $m/z$  calculated for  $C_{11}H_{14}Cl_2NOS$   $[M+H]^+$  278.0173, found 278.0167.

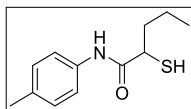
**2-Mercapto-*N*-(4'-methoxyphenyl)pentanamide 13.** Compound **13** was synthesized according to the



general procedure **GP-6**, using thioacetate **102** (80 mg, 0.28 mmol) and NaOH (38 mg, 0.94 mmol) in MeOH (5 mL). The mixture was stirred at room temperature for 4 h. After extraction, the final compound **13** was obtained as colorless crystals (64 mg, 96%).  $^1H$  NMR (500 MHz,  $DMSO-d_6$ )  $\delta$  9.91 (s, 1H), 7.49 (d,  $J = 8.2$  Hz, 2H), 6.88 (d,  $J = 8.2$  Hz, 2H), 3.72 (s, 3H), 3.43 (m, 1H), 2.90 (d,  $J = 9.2$  Hz, 1H), 1.91–1.80 (m, 1H),

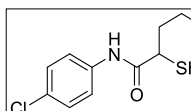
1.65–1.56 (m, 1H), 1.43–1.26 (m, 2H), 0.89 (t,  $J = 7.4$  Hz, 3H).  $^{13}\text{C}$  NMR (126 MHz,  $\text{DMSO-}d_6$ )  $\delta$  170.5, 155.3, 132.1, 120.7, 113.9, 55.5, 41.8, 37.7, 20.3, 13.5. HRMS (ESI)  $m/z$  calculated for  $\text{C}_{12}\text{H}_{18}\text{NO}_2\text{S}$  240.1053  $[\text{M}+\text{H}]^+$ , found 240.1043.

**2-Mercapto-*N*-(4'-methylphenyl)pentanamide 14.** Compound **14** was synthesized according to the



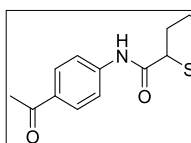
general procedure **GP-6**, using thioacetate **105** (80 mg, 0.30 mmol) and NaOH (41 mg, 1.00 mmol) in MeOH (5 mL). The mixture was stirred at room temperature for 4 h. After extraction the final compound **14** was obtained as colorless crystals (63 mg, 93%). m.p. = 86 °C.  $^1\text{H}$  NMR (500 MHz,  $\text{DMSO-}d_6$ )  $\delta$  9.96 (s, 1H), 7.47 (d,  $J = 8.2$  Hz, 2H), 7.11 (d,  $J = 8.2$  Hz, 2H), 3.45 (m, 1H), 2.91 (d,  $J = 9.3$  Hz, 1H), 2.25 (s, 3H), 1.90–1.80 (m, 1H), 1.66–1.58 (m, 1H), 1.44–1.25 (m, 2H), 0.88 (t,  $J = 7.4$  Hz, 3H).  $^{13}\text{C}$  NMR (126 MHz,  $\text{DMSO-}d_6$ )  $\delta$  170.8, 136.5, 132.3, 129.2, 119.3, 41.7, 37.7, 20.5, 20.2, 13.5. HRMS (ESI)  $m/z$  calculated for  $\text{C}_{12}\text{H}_{18}\text{NOS}$  224.1104  $[\text{M}+\text{H}]^+$ , found 224.1094.

**2-Mercapto-*N*-(4'-chlorophenyl)pentanamide 15.** Compound **15** was synthesized according to the



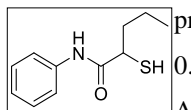
general procedure **GP-6**, using thioacetate **116** (23 mg, 0.080 mmol) and NaOH (15 mg, 0.38 mmol) in MeOH (2 mL). The reaction was stirred at room temperature for 4 h. Extraction followed by preparative HPLC ( $\text{CH}_3\text{CN}$  (HCOOH 0.05%)/ $\text{H}_2\text{O}$  (HCOOH 0.05%) 5:95  $\rightarrow$  95:5) gave the final compound **15** as white solid (13 mg, 67%). m.p. = 89 °C.  $^1\text{H}$  NMR (300 MHz,  $\text{CDCl}_3$ )  $\delta$  8.29 (br, 1H), 7.50 (d,  $J = 8.8$  Hz, 2H), 7.29 (d,  $J = 8.8$  Hz, 2H), 3.46 (td,  $J = 6.1, 8.0$  Hz, 1H), 2.11–2.00 (m, 2H), 1.83–1.71 (m, 1H), 1.61–1.40 (m, 2H), 0.96 (t,  $J = 7.3$  Hz, 3H).  $^{13}\text{C}$  NMR (75 MHz,  $\text{CDCl}_3$ )  $\delta$  170.8, 136.2, 129.8, 129.2, 121.2, 44.4, 37.7, 20.6, 13.7. HRMS (ESI)  $m/z$  calculated for  $\text{C}_{11}\text{H}_{15}\text{ClNOS}$  244.0557  $[\text{M}+\text{H}]^+$ , found 244.0554.

**2-Mercapto-*N*-(4'-acetylphenyl)pentanamide 16.** Compound **16** was synthesized according to the



general procedure **GP-6**, using thioacetate **109** (30 mg, 0.10 mmol) and NaOH (200 mg, 5.00 mmol) in MeOH (5 mL). The reaction was stirred at room temperature for 3.5 h. Extraction gave the final compound **16** without any further purification as colorless oil (25 mg, 97%).  $R_f = 0.53$  ( $\text{CH}_2\text{Cl}_2/\text{MeOH}$  95:5).  $^1\text{H}$  NMR (500 MHz,  $\text{CDCl}_3$ )  $\delta$  8.70 (br, 1H), 7.93 (d,  $J = 8.8$  Hz, 2H), 7.67 (d,  $J = 8.8$  Hz, 2H), 3.48 (dt,  $J = 6.6, 8.1$  Hz, 1H), 2.57 (s, 3H), 2.10 (d,  $J = 8.6$  Hz, 1H), 2.08–2.01 (m, 1H), 1.80–1.72 (m, 1H), 1.58–1.40 (m, 2H), 0.93 (t,  $J = 7.3$  Hz, 3H).  $^{13}\text{C}$  NMR (126 MHz,  $\text{CDCl}_3$ )  $\delta$  197.3, 171.3, 142.1, 133.1, 119.1, 44.2, 37.6, 26.6, 20.6, 13.6. HRMS (ESI)  $m/z$  calculated for  $\text{C}_{13}\text{H}_{18}\text{NO}_2\text{S}$  252.1053  $[\text{M}+\text{H}]^+$ , found 252.1047.

**2-Mercapto-*N*-phenylpentanamide 17.** Compound **17** was synthesized according to the general

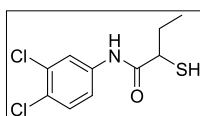


procedure **GP-6**, using thioacetate **110** (60 mg, 0.24 mmol) and NaOH (32 mg, 0.80 mmol) in MeOH (4 mL). The mixture was stirred at room temperature for 4 h. After extraction, the final compound **17** was obtained as colorless crystals (45 mg,



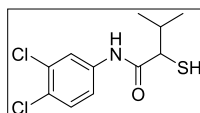
87%). m.p. = 76 °C. <sup>1</sup>H NMR (500 MHz, DMSO-*d*<sub>6</sub>) δ 10.05 (s, 1H), 7.59 (d, *J* = 8.6 Hz, 2H), 7.31 (d, *J* = 7.4 Hz, 2H), 7.06 (t, *J* = 7.4 Hz, 1H), 3.57 (m, 1H), 2.95 (d, *J* = 9.2 Hz, 1H), 1.91–1.82 (m, 1H), 1.66–1.58 (m, 1H), 1.44–1.25 (m, 2H), 0.89 (t, *J* = 7.4 Hz, 3H). <sup>13</sup>C NMR (126 MHz, DMSO-*d*<sub>6</sub>) δ 171.0, 139.0, 128.9, 123.6, 119.3, 41.8, 37.7, 20.5, 13.7. HRMS (ESI) *m/z* calculated for C<sub>11</sub>H<sub>16</sub>NOS 210.0947 [M+H]<sup>+</sup>, found 210.0939.

**2-Mercapto-*N*-(3',4'-dichlorophenyl)butanamide 18.** Compound **18** was synthesized according to



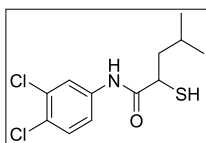
the general procedure **GP-6**, using thioacetate **112** (51 mg, 0.17 mmol) and NaOH (200 mg, 5.00 mmol) in MeOH (5 mL). The reaction was stirred at room temperature for 75 min. Extraction gave the final compound **18** without any further purification as white solid (38 mg, 86%). m.p. = 99 °C. <sup>1</sup>H NMR (500 MHz, CDCl<sub>3</sub>) δ 8.33 (br, 1H), 7.80 (d, *J* = 1.8 Hz, 1H), 7.40–7.35 (m, 2H), 3.41 (dt, *J* = 6.2, 8.0 Hz, 1H), 2.15–2.07 (m, 1H), 2.04 (d, *J* = 8.5 Hz, 1H), 1.90–1.81 (m, 1H), 1.07 (t, *J* = 7.4 Hz, 3H). <sup>13</sup>C NMR (126 MHz, CDCl<sub>3</sub>) δ 170.6, 137.1, 133.1, 130.7, 128.0, 121.6, 119.1, 46.1, 28.9, 11.8. HRMS (ESI) *m/z* calculated for C<sub>10</sub>H<sub>12</sub>Cl<sub>2</sub>NOS 264.0011 [M+H]<sup>+</sup>, found 264.0008.

**2-Mercapto-*N*-(3',4'-dichlorophenyl)-3-methylbutanamide 19.** Compound **19** was synthesized



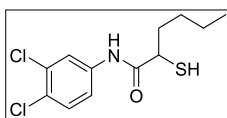
according to the general procedure **GP-6**, using thioacetate **115** (37 mg, 0.12 mmol) and NaOH (200 mg, 5.00 mmol) in MeOH (5 mL). The reaction was stirred at room temperature for 30 min. Extraction gave the final compound **19** without any further purification as white solid (30 mg, 93%). m.p. = 107 °C. R<sub>f</sub> = 0.51 (PE/EtOAc 7:3). <sup>1</sup>H NMR (300 MHz, CDCl<sub>3</sub>) δ 8.43 (br, 1H), 7.82–7.79 (m, 1H), 7.41–7.34 (m, 2H), 3.37 (dd, *J* = 5.7, 8.6 Hz, 1H), 2.49–2.38 (m, 1H), 1.90 (d, *J* = 8.6 Hz, 1H), 1.10 (d, *J* = 6.7 Hz, 3H), 1.00 (d, *J* = 6.7 Hz, 3H). <sup>13</sup>C NMR (75 MHz, CDCl<sub>3</sub>) δ 170.4, 137.0, 133.0, 130.7, 128.1, 121.6, 119.1, 52.0, 32.0, 21.1, 18.4. HRMS (ESI) *m/z* calculated for C<sub>11</sub>H<sub>14</sub>Cl<sub>2</sub>NOS 278.0168 [M+H]<sup>+</sup>, found 278.0162.

**2-Mercapto-*N*-(3',4'-dichlorophenyl)-4-methylpentanamide 20.** Compound **20** was synthesized



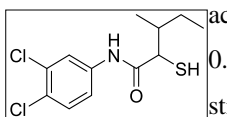
according to the general procedure **GP-6**, using compound **119** (98 mg, 0.29 mmol), NaOH (35 mg, 0.88 mmol) and MeOH (10 mL). The reaction was stirred at room temperature for 2 h. After extraction, compound **20** was obtained as pure white solid without any further purification (80 mg, 93%). m.p. = 122 °C. <sup>1</sup>H NMR (500 MHz, DMSO-*d*<sub>6</sub>) δ 10.39 (s, 1H), 8.00 (d, *J* = 2.5 Hz, 1H), 7.57 (d, *J* = 9.0 Hz, 1H), 7.47 (dd, *J* = 2.5, 9.0 Hz, 1H), 3.50 (dd, *J* = 7.0, 8.0 Hz, 1H), 3.09 (s, 1H), 1.85–1.73 (m, 1H), 1.68–1.57 (m, 1H), 1.56–1.45 (m, 1H), 0.90 (d, *J* = 6.5 Hz, 3H), 0.85 (d, *J* = 6.5 Hz, 3H). <sup>13</sup>C NMR (126 MHz, DMSO-*d*<sub>6</sub>) δ 171.7, 139.1, 131.1, 130.8, 124.9, 120.4, 119.3, 44.0, 39.8, 25.8, 22.2, 22.1. HRMS (ESI) *m/z* calculated for C<sub>12</sub>H<sub>16</sub>Cl<sub>2</sub>NOS [M+H]<sup>+</sup> 292.0330, found 292.0321.

**2-Mercapto-*N*-(3',4'-dichlorophenyl)hexanamide 21.** Compound **21** was synthesized according to



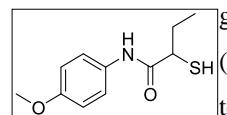
the general procedure **GP-6**, using compound **130** (93 mg, 0.28 mmol), NaOH (33 mg, 0.83 mmol) and MeOH (10 mL). The reaction was stirred at room temperature for 2.5 h. After extraction, **21** was obtained as pure white solid without any further purification (61 mg, 75%). m.p. = 78 °C. <sup>1</sup>H NMR (500 MHz, DMSO-*d*<sub>6</sub>) δ 10.36 (s, 1H), 8.00 (d, *J* = 2.5 Hz, 1H), 7.58 (d, *J* = 9.0 Hz, 1H), 7.48 (dd, *J* = 2.5, 9.0 Hz, 1H), 3.42 (t, *J* = 7.5 Hz, 1H), 3.07 (s, 1H), 1.94–1.80 (m, 1H), 1.71–1.55 (m, 1H), 1.41–1.23 (m, 4H), 0.86 (t, *J* = 7.3 Hz, 3H). <sup>13</sup>C NMR (126 MHz, DMSO-*d*<sub>6</sub>) δ 171.6, 139.0, 131.1, 130.8, 124.9, 120.4, 119.3, 41.9, 34.9, 29.1, 21.7, 13.8. HRMS (ESI) *m/z* calculated for C<sub>12</sub>H<sub>16</sub>Cl<sub>2</sub>NOS [M+H]<sup>+</sup> 292.0330, found 292.0323.

**2-Mercapto-*N*-(3',4'-dichlorophenyl)-3-methylpentanamide 22.** Compound **22** was synthesized



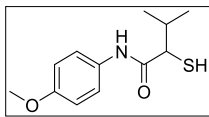
according to the general procedure **GP-6**, using compound **132** (50 mg, 0.15 mmol), NaOH (18 mg, 0.44 mmol) and MeOH (5 mL). The reaction was stirred at room temperature for 3 h. The crude product was purified using preparative HPLC (CH<sub>3</sub>CN (HCOOH 0.05%)/H<sub>2</sub>O (HCOOH 0.05%) 5:95 → 90:10). The product **22** was obtained as beige solid (16 mg, 37%). m.p. = 84 °C. <sup>1</sup>H NMR (500 MHz, DMSO-*d*<sub>6</sub>) δ 10.38 (s, 1H+1H\*), 8.00 (t, *J* = 2.8 Hz, 1H+1H\*), 7.58 (d, *J* = 9.0 Hz, 1H+1H\*), 7.48 (dd, *J* = 2.5, 9.0 Hz, 1H+1H\*), 3.44–3.27 (m, 1H), 3.24 (d, *J* = 9.0 Hz, 1H\*), 2.88 (br, 1H+1H\*), 1.90–1.67 (m, 2H+1H\*), 1.48–1.34 (m, 1H\*), 1.31–1.09 (m, 1H+1H\*), 0.99 (d, *J* = 6.5 Hz, 3H), 0.90 (d, *J* = 6.5 Hz, 3H\*), 0.89–0.83 (m, 3H+3H\*). <sup>13</sup>C NMR (126 MHz, DMSO-*d*<sub>6</sub>) δ 171.4, 171.3\*, 138.98, 138.96\*, 131.1, 130.8, 125.0, 120.45, 120.43\*, 119.3, 48.5, 48.0\*, 38.19, 38.17\*, 27.0, 25.3\*, 16.5, 15.6\*, 11.2, 10.4\*. **22** was obtained as a diastereomeric mixture (53:47). The values labeled with \* belong to the second diastereomer. HRMS (ESI) *m/z* calculated for C<sub>12</sub>H<sub>16</sub>Cl<sub>2</sub>NOS [M+H]<sup>+</sup> 292.0330, found 292.0321.

**2-Mercapto-*N*-(4'-methoxyphenyl)butanamide 23.** Compound **23** was synthesized according to the



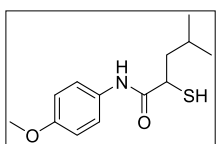
general procedure **GP-6**, using thioacetate **113** (35 mg, 0.13 mmol) and NaOH (200 mg, 5.00 mmol) in MeOH (5 mL). The reaction was stirred at room temperature for 30 min. Extraction gave the final compound **23** without any further purification as white solid (31 mg, quant.). m.p. = 103 °C. <sup>1</sup>H NMR (300 MHz, CDCl<sub>3</sub>) δ 8.18 (br, 1H), 7.44 (d, *J* = 8.9 Hz, 2H), 6.87 (d, *J* = 8.9 Hz, 2H), 3.79 (s, 3H), 3.41 (dd, *J* = 7.6, 14.0 Hz, 1H), 2.19–2.02 (m, 2H), 1.90–1.78 (m, 1H), 1.07 (t, *J* = 7.4 Hz, 3H). <sup>13</sup>C NMR (126 MHz, CDCl<sub>3</sub>) δ 170.4, 156.8, 130.7, 121.8, 114.3, 55.6, 46.1, 29.1, 11.8. HRMS (ESI) *m/z* calculated for C<sub>11</sub>H<sub>16</sub>NO<sub>2</sub>S 226.0896 [M+H]<sup>+</sup>, found 226.0891.

**2-Mercapto-N-(4'-methoxyphenyl)-3-methylbutanamide 24.** Compound **24** was synthesized



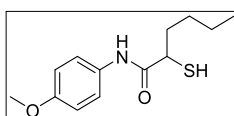
according to the general procedure **GP-6**, using thioacetate **116** (46 mg, 0.16 mmol) and NaOH (200 mg, 5.00 mmol) in MeOH (5 mL). The reaction was stirred at room temperature for 2.5 h 10 min. Extraction gave the final compound **24** without any further purification as white solid (40 mg, quant.). m.p. = 125 °C.  $R_f$  = 0.27 (PE/EtOAc 7:3).  $^1\text{H}$  NMR (300 MHz,  $\text{CDCl}_3$ )  $\delta$  8.26 (br, 1H), 7.45 (d,  $J$  = 8.8 Hz, 2H), 6.87 (d,  $J$  = 8.8 Hz, 2H), 3.79 (s, 3H), 3.36 (dd,  $J$  = 5.9, 8.2 Hz, 1H), 2.49–2.38 (m, 1H), 1.90 (d,  $J$  = 8.5 Hz, 1H), 1.10 (d,  $J$  = 6.7 Hz, 3H), 1.01 (d,  $J$  = 6.7 Hz, 3H).  $^{13}\text{C}$  NMR (75 MHz,  $\text{CDCl}_3$ )  $\delta$  170.1, 156.8, 130.7, 121.9, 114.3, 55.6, 52.0, 32.2, 21.1, 18.5. HRMS (ESI)  $m/z$  calculated for  $\text{C}_{12}\text{H}_{16}\text{NO}_2\text{S}$  238.0907 [M-H] $^-$ , found 238.0890.

**2-Mercapto-N-(4'-methoxyphenyl)-4-methylpentanamide 25.** Compound **25** was synthesized



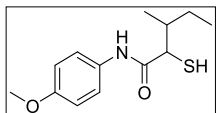
according to the general procedure **GP-6**, using compound **120** (90 mg, 0.31 mmol), NaOH (37 mg, 0.92 mmol) and MeOH (5 mL). The reaction was stirred at room temperature for 2 h. The crude product was purified using preparative HPLC ( $\text{CH}_3\text{CN}$  (HCOOH 0.05%)/ $\text{H}_2\text{O}$  (HCOOH 0.05%): 10:90  $\rightarrow$  100:0) to give **25** as white solid (47 mg, 61%). m.p. = 89 °C.  $^1\text{H}$  NMR (500 MHz,  $\text{DMSO}-d_6$ )  $\delta$  9.94 (s, 1H), 7.49 (d,  $J$  = 9.0 Hz, 2H), 6.88 (d,  $J$  = 9.0 Hz, 2H), 3.72 (s, 3H), 3.50 (dd,  $J$  = 7.0, 8.5 Hz, 1H), 2.92 (s, 1H), 1.83–1.72 (m, 1H), 1.68–1.55 (m, 1H), 1.54–1.43 (m, 1H), 0.91 (d,  $J$  = 7.0 Hz, 3H), 0.86 (d,  $J$  = 6.5 Hz, 3H).  $^{13}\text{C}$  NMR (126 MHz,  $\text{DMSO}-d_6$ )  $\delta$  170.6, 155.3, 132.1, 120.7, 113.9, 55.2, 44.5, 39.8, 25.8, 22.2, 22.1. HRMS (ESI)  $m/z$  calculated for  $\text{C}_{13}\text{H}_{20}\text{NO}_2\text{S}$  [M+H] $^+$  254.1215, found 254.1203.

**2-Mercapto-N-(4'-methoxyphenyl)hexanamide 26.** Compound **26** was synthesized according to the



general procedure **GP-6**, using thioacetate **131** (74 mg, 0.25 mmol) and NaOH (40 mg, 1.0 mmol) in MeOH (5 mL). The reaction was stirred at room temperature for 2.5. Extraction gave the final compound **26** without any further purification as white solid (63 mg, 99%). m.p. = 77 °C.  $^1\text{H}$  NMR (500 MHz,  $\text{DMSO}-d_6$ )  $\delta$  9.91 (s, 1H), 7.50 (d,  $J$  = 9.1 Hz, 2H), 6.88 (d,  $J$  = 9.1 Hz, 2H), 3.72 (s, 3H), 3.41 (td,  $J$  = 7.1, 8.7 Hz, 1H), 2.91 (d,  $J$  = 9.2 Hz, 1H), 1.90–1.83 (m, 1H), 1.66–1.59 (m, 1H), 1.37–1.20 (m, 4H), 0.86 (t,  $J$  = 7.1 Hz, 3H).  $^{13}\text{C}$  NMR (126 MHz,  $\text{DMSO}-d_6$ )  $\delta$  170.5, 155.3, 132.1, 120.7, 113.9, 55.2, 41.9, 35.4, 29.2, 21.7, 13.8. HRMS (ESI)  $m/z$  calculated for  $\text{C}_{13}\text{H}_{20}\text{NO}_2\text{S}$  252.1064 [M+H] $^+$ , found 252.1048.

**2-Mercapto-N-(4'-methoxyphenyl)-3-methylpentanamide 27.** Compound **27** was synthesized

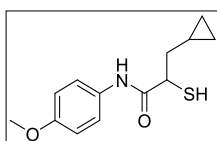


according to the general procedure **GP-6**, using compound **133** (37 mg, 0.13 mmol), NaOH (15 mg, 0.38 mmol) and MeOH (5 mL). The reaction was stirred at room temperature for 1.5 h. The crude product was purified using preparative HPLC ( $\text{CH}_3\text{CN}$  (HCOOH 0.05%)/ $\text{H}_2\text{O}$  (HCOOH 0.05%) 10:90  $\rightarrow$  90:10) to give **27** as beige solid (17 mg, 54%). m.p. = 101 °C.  $^1\text{H}$  NMR (500 MHz,  $\text{DMSO}-d_6$ )  $\delta$  9.93 (s, 1H+1H\*), 7.494

S12

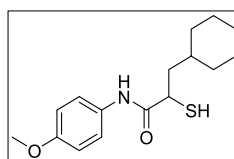
(d,  $J = 9.5$  Hz, 2H), 7.489 (d,  $J = 9.0$  Hz, 2H\*), 6.88 (d,  $J = 9.0$  Hz, 2H+2H\*), 3.72 (s, 3H+3H\*), 3.31 (d,  $J = 8.0$  Hz, 1H), 3.23 (d,  $J = 8.5$  Hz, 1H\*), 2.71 (br, 1H+1H\*), 1.85–1.66 (m, 2H+1H\*), 1.50–1.36 (m, 1H\*), 1.32–1.08 (m, 1H+1H\*), 0.99 (d,  $J = 7.0$  Hz, 3H), 0.90 (d,  $J = 6.5$  Hz, 3H\*), 0.89–0.83 (m, 3H+3H\*).  $^{13}\text{C}$  NMR (126 MHz, DMSO- $d_6$ )  $\delta$  170.3, 170.2\*, 155.4, 132.0, 120.83, 120.81\*, 113.9, 55.2, 48.6, 48.0\*, 38.54, 38.50\*, 27.0, 25.3\*, 16.5, 15.7\*, 11.3, 10.4\*. **27** was obtained as a diastereomeric mixture (54:46). The values labeled with \* belong to the second diastereomer. HRMS (ESI)  $m/z$  calculated for  $\text{C}_{13}\text{H}_{20}\text{NO}_2\text{S}$   $[\text{M}+\text{H}]^+$  254.1215, found 254.1188.

**2-Mercapto-*N*-(4'-methoxyphenyl)-3-cyclopropylpropanamide 28.** Compound **28** was synthesized



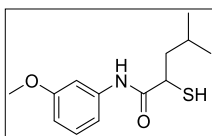
according to the general procedure **GP-6**, using compound **135** (39 mg, 0.13 mmol), NaOH (16 mg, 0.40 mmol) and MeOH (2.5 mL). The reaction was stirred at room temperature for 2 h. After extraction, the product was purified using preparative HPLC ( $\text{CH}_3\text{CN}$  (HCOOH 0.05%)/ $\text{H}_2\text{O}$  (HCOOH 0.05%) 5:95  $\rightarrow$  95:5) to give **28** as white solid (6 mg, 19%). m.p. = 121 °C.  $^1\text{H}$  NMR (500 MHz,  $\text{CDCl}_3$ )  $\delta$  8.16 (br, 1H), 7.44 (d,  $J = 8.5$  Hz, 2H), 6.86 (d,  $J = 8.7$  Hz, 2H), 3.78 (s, 3H), 3.54 (q,  $J = 7.1$  Hz, 1H), 2.09 (d,  $J = 8.4$  Hz, 1H), 1.93–1.80 (m, 2H), 0.92–0.83 (m, 1H), 0.54–0.45 (m, 2H), 0.19–0.13 (m, 2H).  $^{13}\text{C}$  NMR (126 MHz,  $\text{CDCl}_3$ )  $\delta$  170.2, 156.6, 130.6, 121.6, 114.2, 55.5, 44.8, 40.6, 8.8, 4.5, 4.5. HRMS (ESI)  $m/z$  calculated for  $\text{C}_{13}\text{H}_{16}\text{NO}_2\text{S}$   $[\text{M}-\text{H}]^-$  250.0907, found 250.0893.

**2-Mercapto-*N*-(4'-methoxyphenyl)-3-cyclohexylpropanamide 29.** Compound **29** was synthesized



according to the general procedure **GP-6**, using compound **134** (48 mg, 0.14 mmol), NaOH (17 mg, 0.43 mmol) and MeOH (5 mL). The reaction was stirred at room temperature for 1.5 h. The crude product was purified using preparative HPLC ( $\text{CH}_3\text{CN}$  (HCOOH 0.05%)/ $\text{H}_2\text{O}$  (HCOOH 0.05%) 10:90  $\rightarrow$  90:10) to give **29** as beige solid (28 mg, 67%). m.p. = 88 °C.  $^1\text{H}$  NMR (500 MHz, DMSO- $d_6$ )  $\delta$  9.92 (s, 1H), 7.49 (d,  $J = 9.0$  Hz, 2H), 6.88 (d,  $J = 9.0$  Hz, 2H), 3.72 (s, 3H), 3.52 (dd,  $J = 6.5, 8.5$  Hz, 1H), 2.91 (s, 1H), 1.85–1.44 (m, 7H), 1.37–1.25 (m, 1H), 1.22–1.03 (m, 3H), 0.96–0.80 (m, 2H).  $^{13}\text{C}$  NMR (126 MHz, DMSO- $d_6$ )  $\delta$  170.7, 155.3, 132.2, 120.7, 113.9, 55.2, 43.1, 39.2, 35.2, 32.5, 32.4, 26.0, 25.7, 25.6. HRMS (ESI)  $m/z$  calculated for  $\text{C}_{16}\text{H}_{24}\text{NO}_2\text{S}$   $[\text{M}+\text{H}]^+$  294.1528, found 294.1499.

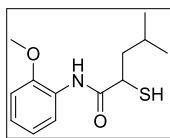
**2-Mercapto-*N*-(3'-methoxyphenyl)-4-methylpentanamide 30.** Compound **30** was synthesized



according to the general procedure **GP-6**, using compound **121** (132 mg, 0.450 mmol), NaOH (54 mg, 1.3 mmol) and MeOH (8 mL). The reaction was stirred at room temperature for 2 h. After extraction, the product was purified using preparative HPLC ( $\text{CH}_3\text{CN}$  (HCOOH 0.05%)/ $\text{H}_2\text{O}$  (HCOOH 0.05%) 5:95  $\rightarrow$  95:5) to give **30** as colorless oil (53 mg, 47%).  $^1\text{H}$  NMR (500 MHz, DMSO- $d_6$ )  $\delta$  10.05 (s, 1H), 7.31–7.27 (m, 1H), 7.20 (t,  $J = 8.2$  Hz, 1H), 7.13–7.08 (m, 1H), 6.65–6.61 (m, 1H), 3.72 (s, 3H), 3.55–3.48 (m, 1H), 2.95 (d,  $J = 9.2$  Hz, 1H), 1.82–1.74 (m, 1H), 1.67–1.57 (m, 1H), 1.53–1.45 (m, 1H), 0.90

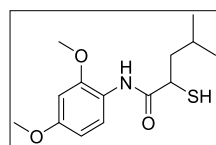
(d,  $J = 6.7$  Hz, 3H), 0.85 (d,  $J = 6.6$  Hz, 3H).  $^{13}\text{C}$  NMR (126 MHz,  $\text{DMSO-}d_6$ )  $\delta$  171.2, 159.5, 140.2, 129.6, 111.4, 109.0, 104.8, 55.0, 44.3, 39.8, 25.8, 22.2, 22.1. HRMS (ESI)  $m/z$  calculated for  $\text{C}_{13}\text{H}_{20}\text{NO}_2\text{S}$   $[\text{M}+\text{H}]^+$  254.1209, found 254.1205.

**2-Mercapto-*N*-(2'-methoxyphenyl)-4-methylpentanamide 31.** Compound **31** was synthesized



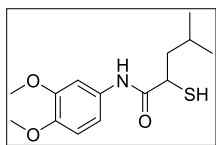
according to the general procedure **GP-6**, using compound **122** (138 mg, 0.470 mmol), NaOH (56 mg, 1.4 mmol) and MeOH (8 mL). The reaction was stirred at room temperature for 2 h. After extraction, the product was purified using preparative HPLC ( $\text{CH}_3\text{CN}$  ( $\text{HCOOH}$  0.05%)/ $\text{H}_2\text{O}$  ( $\text{HCOOH}$  0.05%) 5:95  $\rightarrow$  95:5) to give **31** as colourless oil (50 mg, 42%).  $^1\text{H}$  NMR (500 MHz,  $\text{DMSO-}d_6$ )  $\delta$  9.35 (s, 1H), 7.96 (dd,  $J = 1.5, 7.9$  Hz, 1H), 7.10–7.01 (m, 2H), 6.92–6.86 (m, 1H), 3.83 (br, 3H+1H), 2.85 (br, 1H), 1.80–1.72 (m, 1H), 1.70–1.60 (m, 1H), 1.52–1.44 (m, 1H), 0.91 (d,  $J = 6.6$  Hz, 3H), 0.85 (d,  $J = 6.6$  Hz, 3H).  $^{13}\text{C}$  NMR (126 MHz,  $\text{DMSO-}d_6$ )  $\delta$  171.5, 149.6, 127.1, 124.5, 121.6, 120.2, 111.2, 55.7, 44.5, 39.7, 25.8, 22.2, 22.1. HRMS (ESI)  $m/z$  calculated for  $\text{C}_{13}\text{H}_{20}\text{NO}_2\text{S}$   $[\text{M}+\text{H}]^+$  254.1209, found 254.1205.

**2-Mercapto-*N*-(2',4'-dimethoxyphenyl)-4-methylpentanamide 32.** Compound **32** was synthesized



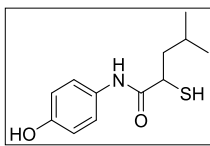
according to the general procedure **GP-6**, using thioacetate **123** (54 mg, 0.17 mmol), NaOH (19 mg, 0.48 mmol) and MeOH (3 mL). The reaction was stirred at room temperature for 2.5 h. After extraction and preparative HPLC ( $\text{CH}_3\text{CN}$  ( $\text{HCOOH}$  0.1%)/ $\text{H}_2\text{O}$  ( $\text{HCOOH}$  0.1%) 5:95  $\rightarrow$  95:5), compound **32** was obtained as colorless oil (36 mg, 76%).  $^1\text{H}$  NMR (300 MHz,  $\text{DMSO-}d_6$ )  $\delta$  9.20 (s, 1H), 7.72 (d,  $J = 8.8$  Hz, 1H), 6.61 (d,  $J = 2.7$  Hz, 1H), 6.48 (dd,  $J = 2.7, 8.8$  Hz, 1H), 3.81 (s, 3H), 3.79–3.71 (m, 1H+3H), 2.79 (d,  $J = 9.4$  Hz, 1H), 1.81–1.59 (m, 1H), 1.52–1.43 (m, 1H), 0.92 (d,  $J = 6.5$  Hz, 3H), 0.86 (d,  $J = 6.5$  Hz, 3H).  $^{13}\text{C}$  NMR (75 MHz,  $\text{DMSO-}d_6$ )  $\delta$  171.1, 156.8, 151.4, 123.3, 120.2, 104.1, 98.8, 55.8, 55.3, 44.7, 39.5 (HSQC), 25.8, 22.2. HRMS (ESI)  $m/z$  calculated for  $\text{C}_{14}\text{H}_{22}\text{NO}_3\text{S}$  282.1169  $[\text{M}-\text{H}]^-$ , found 282.1150.

**2-mercapto-*N*-(3',4'-dimethoxyphenyl)-4-methylpentanamide 33.** Compound **33** was synthesized



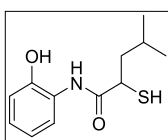
according to the general procedure **GP-6**, using thioacetate **124** (36 mg, 0.111 mmol), NaOH (28 mg, 0.70 mmol) and MeOH (3 mL). The reaction was stirred at room temperature for 1 h. After extraction and column chromatography (PE/EtOAc 8:2), compound **33** was obtained as colorless oil (21 mg, 67%).  $R_f = 0.15$  (PE/EtOAc 7:3).  $^1\text{H}$  NMR (500 MHz,  $\text{DMSO-}d_6$ )  $\delta$  8.24 (s, 1H), 7.36 (d,  $J = 2.4$  Hz, 1H), 6.90 (dd,  $J = 2.4, 8.6$  Hz, 1H), 6.79 (d,  $J = 8.6$  Hz, 1H), 3.86 (s, 3H), 3.84 (s, 3H), 3.46 (td,  $J = 6.5, 8.4$  Hz, 1H), 2.04 (d,  $J = 8.3$  Hz, 1H), 1.97–1.91 (m, 1H), 1.89–1.80 (m, 1H), 1.64–1.58 (m, 1H), 0.96 (d,  $J = 6.6$  Hz, 1H), 0.92 (d,  $J = 6.5$  Hz, 1H).  $^{13}\text{C}$  NMR (126 MHz,  $\text{DMSO-}d_6$ )  $\delta$  171.0, 149.2, 146.1, 131.4, 111.9, 111.4, 104.8, 56.2, 26.0, 44.7, 42.8, 26.1, 22.8, 21.7. HRMS (ESI)  $m/z$  calculated for  $\text{C}_{14}\text{H}_{22}\text{NO}_3\text{S}$  284.1315  $[\text{M}+\text{H}]^+$ , found 284.1312.

**2-Mercapto-*N*-(4'-hydroxyphenyl)-4-methylpentanamide 34.** Compound **34** was synthesized



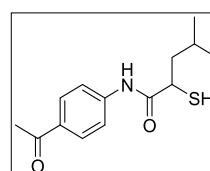
according to the general procedure **GP-6**, using thioacetate **125** (50 mg, 0.18 mmol), NaOH (28 mg, 0.70 mmol) and MeOH (3 mL). The reaction was stirred at room temperature for 1 h. After extraction, the product was purified using preparative HPLC (CH<sub>3</sub>CN (HCOOH 0.1%) /H<sub>2</sub>O (HCOOH 0.1%) 5:95 → 95:5) to give **34** as colorless oil (22 mg, 52%). <sup>1</sup>H NMR (300 MHz, DMSO-*d*<sub>6</sub>) δ 9.82 (s, 1H), 9.20 (s, 1H), 7.37 (d, *J* = 8.9 Hz, 2H), 6.70 (d, *J* = 8.9 Hz, 2H), 3.50 (dt, *J* = 6.8, 8.8 Hz, 1H), 2.87 (d, *J* = 9.3 Hz, 1H), 1.83–1.74 (m, 1H), 1.67–1.58 (m, 1H), 1.53–1.44 (m, 1H), 0.89 (dd, *J* = 6.5, 15.3 Hz, 6H). <sup>13</sup>C NMR (75 MHz, DMSO-*d*<sub>6</sub>) δ 170.4, 153.4, 130.6, 120.9, 115.1, 44.6, 25.8, 22.2, 22.1. HRMS (ESI) *m/z* calculated for C<sub>12</sub>H<sub>18</sub>NO<sub>2</sub>S 238.0907 [M-H]<sup>-</sup>, found 238.0893.

**2-Mercapto-*N*-(2'-hydroxyphenyl)-4-methylpentanamide 35.** Compound **35** was synthesized



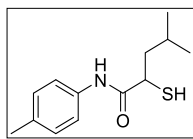
according to the general procedure **GP-6**, using compound **126** (36 mg, 0.13 mmol), NaOH (21 mg, 0.51 mmol) and MeOH (2.5 mL). The reaction was stirred at room temperature for 2 h. After extraction, the product was purified using preparative HPLC (CH<sub>3</sub>CN (HCOOH 0.05%) /H<sub>2</sub>O (HCOOH 0.05%) 5:95 → 95:5) to give **35** as white solid (7 mg, 21%). m.p. = 94 °C. <sup>1</sup>H NMR (500 MHz, DMSO-*d*<sub>6</sub>) δ 9.84 (br, 1H), 9.40 (br, 1H), 7.83 (dd, *J* = 1.5, 8.1 Hz, 1H), 6.95–6.89 (m, 1H), 6.87–6.84 (m, 1H), 6.77–6.72 (m, 1H), 3.82 (t, *J* = 7.6 Hz, 1H), 2.52–2.50 (m, 1H), 1.80–1.73 (m, 1H), 1.69–1.60 (m, 1H), 1.52–1.44 (m, 1H), 0.91 (d, *J* = 6.6 Hz, 3H), 0.85 (d, *J* = 6.6 Hz, 3H). <sup>13</sup>C NMR (126 MHz, DMSO-*d*<sub>6</sub>) δ 171.6, 147.6, 126.2, 124.5, 121.8, 118.9, 115.3, 44.5, 39.8, 25.8, 22.2, 22.1. HRMS (ESI) *m/z* calculated for C<sub>12</sub>H<sub>16</sub>NO<sub>2</sub>S [M-H]<sup>-</sup> 238.0907, found 238.0905.

**2-Mercapto-*N*-(4'-acetylphenyl)-4-methylpentanamide 36.** Compound **36** was synthesized



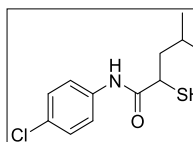
according to the general procedure **GP-6**, using thioacetate **127** (25 mg, 0.082 mmol) and NaOH (5 mL, 1 M, H<sub>2</sub>O/MeOH 1:1). The reaction was stirred at room temperature for 1 h. After extraction, the product **36** was obtained as white solid (19 mg, 0.072 mmol, 87%). m.p. = 95 °C. R<sub>f</sub> = 0.22 (PE/EtOAc 7:3). <sup>1</sup>H NMR (500 MHz, CDCl<sub>3</sub>) δ 8.40 (s, 1H), 7.96 (d, *J* = 8.8 Hz, 2H), 7.66 (d, *J* = 8.8 Hz, 2H), 4.11 (td, *J* = 6.2, 8.5 Hz, 1H), 2.58 (s, 3H), 2.06 (d, *J* = 8.1 Hz, 1H), 1.96 (ddd, *J* = 6.1, 8.0, 13.7 Hz, 1H), 1.91–1.85 (m, 1H), 1.64 (ddd, *J* = 5.8, 8.8, 13.7 Hz, 1H), 1.62–1.56 (m, 1H), 0.98 (d, *J* = 6.5 Hz, 3H), 0.95 (d, *J* = 6.5 Hz, 3H). <sup>13</sup>C NMR (126 MHz, CDCl<sub>3</sub>) δ 197.1, 171.3, 142.0, 133.3, 129.9, 119.1, 44.4, 43.0, 26.6, 26.1, 22.8, 21.7, 20.6. HRMS (ESI) *m/z* calculated for C<sub>14</sub>H<sub>20</sub>NO<sub>2</sub>S [M+H]<sup>+</sup> 266.1209, found 266.1198.

**2-Mercapto-N-(p-tolyl)-4-methylpentanamide 37.** Compound **37** was synthesized according to the



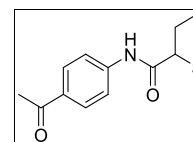
general procedure **GP-6**, using compound **128** (90 mg, 0.32 mmol), NaOH (39 mg, 0.97 mmol) and MeOH (5 mL). The reaction was stirred at room temperature for 2 h. The crude product was purified using preparative HPLC (CH<sub>3</sub>CN (HCOOH 0.05%)/H<sub>2</sub>O (HCOOH 0.05%) 10:90 → 100:0) to give **37** as beige solid (38 mg, 50%). m.p. = 90 °C. <sup>1</sup>H NMR (500 MHz, DMSO-*d*<sub>6</sub>) δ 9.99 (s, 1H), 7.47 (d, *J* = 8.0 Hz, 2H), 7.11 (d, *J* = 8.0 Hz, 2H), 3.51 (t, *J* = 7.8 Hz, 1H), 2.93 (s, 1H), 2.25 (s, 3H), 1.84–1.73 (m, 1H), 1.67–1.56 (m, 1H), 1.54–1.43 (m, 1H), 0.91 (d, *J* = 7.0 Hz, 3H), 0.86 (d, *J* = 6.5 Hz, 3H). <sup>13</sup>C NMR (126 MHz, DMSO-*d*<sub>6</sub>) δ 170.9, 136.5, 132.4, 129.2, 119.2, 44.4, 39.9, 25.8, 22.2, 22.1, 20.5. HRMS (ESI) *m/z* calculated for C<sub>13</sub>H<sub>20</sub>NOS [M+H]<sup>+</sup> 238.1266, found 238.1254.

**2-Mercapto-N-(4'-chlorophenyl)-4-methylpentanamide 38.** Compound **38** was synthesized



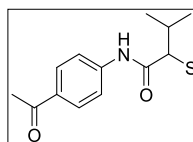
according to the general procedure **GP-6**, using compound **129** (90 mg, 0.30 mmol), NaOH (36 mg, 0.90 mmol) and MeOH (5 mL). The reaction was stirred at room temperature for 2 h. The crude product was purified using preparative HPLC (CH<sub>3</sub>CN (HCOOH 0.05%)/H<sub>2</sub>O (HCOOH 0.05%) 10:90 → 100:0) to give **38** as white solid (37 mg, 48%). m.p. = 120 °C. <sup>1</sup>H NMR (500 MHz, DMSO-*d*<sub>6</sub>) δ 10.22 (s, 1H), 7.62 (d, *J* = 8.5 Hz, 2H), 7.37 (d, *J* = 9.0 Hz, 2H), 3.51 (dd, *J* = 7.0, 8.0 Hz, 1H), 3.02 (s, 1H), 1.85–1.73 (m, 1H), 1.68–1.57 (m, 1H), 1.55–1.45 (m, 1H), 0.91 (d, *J* = 6.5 Hz, 3H), 0.86 (d, *J* = 7.0 Hz, 3H). <sup>13</sup>C NMR (126 MHz, DMSO-*d*<sub>6</sub>) δ 171.3, 138.0, 128.7, 127.0, 120.7, 44.2, 39.8, 25.8, 22.2, 22.1. HRMS (ESI) *m/z* calculated for C<sub>12</sub>H<sub>17</sub>ClNOS [M+H]<sup>+</sup> 258.0719, found 258.0705.

**2-Mercapto-N-(4'-acetylphenyl)butanamide 39.** Compound **39** was synthesized according to the



general procedure **GP-6**, using thioacetate **114** (46 mg, 0.16 mmol) and NaOH (100 mg, 2.50 mmol) in MeOH (5 mL). The reaction was stirred at room temperature for 2 h. Extraction gave the final compound **39** without any further purification as colorless oil (38 mg, 98%). <sup>1</sup>H NMR (500 MHz, CDCl<sub>3</sub>) δ 8.78 (br, 1H), 7.93 (d, *J* = 8.8 Hz, 2H), 7.67 (d, *J* = 8.8 Hz, 2H), 3.41 (ddd, *J* = 6.6, 7.3, 8.8 Hz, 1H), 2.57 (s, 3H), 2.12–2.05 (m, 2H), 1.88–1.79 (m, 1H), 1.05 (t, *J* = 7.4 Hz, 3H). <sup>13</sup>C NMR (126 MHz, CDCl<sub>3</sub>) δ 197.4, 171.2, 142.2, 133.1, 129.8, 119.2, 45.9, 29.0, 26.6, 11.9. HRMS (ESI) *m/z* calculated for C<sub>12</sub>H<sub>16</sub>NO<sub>2</sub>S 238.0896 [M+H]<sup>+</sup>, found 238.0890.

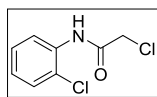
**2-Mercapto-N-(4'-acetylphenyl)-3-methylbutanamide 40.** Compound **40** was synthesized according



to the general procedure **GP-6**, using thioacetate **117** (46 mg, 0.16 mmol) and NaOH (100 mg, 2.50 mmol) in MeOH (5 mL). The reaction was stirred at room temperature for 4.5 h. Extraction gave the final compound **40** without any further purification as white solid (29 mg, 98%). m.p. = 121 °C. *R*<sub>f</sub> = 0.53 (CH<sub>2</sub>Cl<sub>2</sub>/MeOH 95:5). <sup>1</sup>H NMR (500 MHz, CDCl<sub>3</sub>) δ 8.80 (br, 1H), 7.93 (d, *J* = 8.8 Hz, 2H), 7.67 (d, *J* = 8.8 Hz, 2H),

3.34 (dd,  $J = 6.5, 8.9$  Hz, 1H), 2.57 (s, 3H), 2.36 (dq,  $J = 6.7, 6.7, 6.7$  Hz, 1H), 1.96 (d,  $J = 8.9$  Hz, 1H), 1.07 (d,  $J = 6.7$  Hz, 3H), 1.02 (d,  $J = 6.7$  Hz, 3H).  $^{13}\text{C}$  NMR (126 MHz,  $\text{CDCl}_3$ )  $\delta$  197.3, 170.9, 142.1, 133.2, 129.8, 119.2, 51.9, 32.3, 26.6, 21.0, 18.7. HRMS (ESI)  $m/z$  calculated for  $\text{C}_{13}\text{H}_{16}\text{NO}_2\text{S}$  250.0907  $[\text{M}-\text{H}]^-$ , found 250.0889.

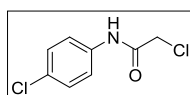
**2-Chloro-*N*-(2'-chlorophenyl)acetamide 41.** Compound **41** was synthesized according to the general



procedure **GP-4**, using 2-chloroaniline (1.20 mL, 11.3 mmol), DIPEA (4.00 mL, 23.0 mmol) and chloroacetyl chloride (1.00 mL, 12.6 mmol) in dry  $\text{CH}_2\text{Cl}_2$  (15 mL).

The reaction was stirred at 0 °C for 2 h. After extraction, **41** was obtained as brown solid without further purification (1.98 g, 86%).  $R_f = 0.49$  (PE/EtOAc 7:3).  $^1\text{H}$  NMR (500 MHz,  $\text{CDCl}_3$ )  $\delta$  8.93 (br, 1H), 8.36 (dd,  $J = 1.5, 8.3$  Hz, 1H), 7.40 (dd,  $J = 1.5, 8.0$  Hz, 1H), 7.32–7.28 (m, 1H), 7.10 (td,  $J = 1.6, 7.7$  Hz, 1H), 4.24 (s, 2H).  $^{13}\text{C}$  NMR (126 MHz,  $\text{CDCl}_3$ )  $\delta$  164.1, 133.8, 129.3, 127.9, 125.6, 123.6, 121.4, 43.3. HRMS (ESI)  $m/z$  calculated for  $\text{C}_8\text{H}_8\text{Cl}_2\text{NO}$   $[\text{M}+\text{H}]^+$  203.9977, found 203.9973.

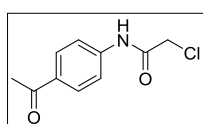
**2-Chloro-*N*-(4'-chlorophenyl)acetamide 42.** Compound **42** was synthesized according to the general



procedure **GP-4**, using 4-chloroaniline (143 mg, 1.13 mmol), DIPEA (220  $\mu\text{L}$ , 1.29 mmol) and chloroacetyl chloride (110  $\mu\text{L}$ , 1.38 mmol) in dry THF (8 mL). The

reaction was stirred at 0 °C for 1 h. After extraction, **42** was obtained as yellow solid without further purification (258 mg, quant.).  $R_f = 0.34$  ( $\text{CH}_2\text{Cl}_2/\text{MeOH}$  9:1).  $^1\text{H}$  NMR (300 MHz,  $\text{CDCl}_3$ )  $\delta$  8.22 (br, 1H), 7.51 (d,  $J = 8.3$  Hz, 2H), 7.33 (d,  $J = 8.9$  Hz, 2H), 4.19 (s, 2H).  $^{13}\text{C}$  NMR (75 MHz,  $\text{CDCl}_3$ )  $\delta$  163.9, 135.4, 130.5, 129.3, 121.5, 43.0. HRMS (ESI)  $m/z$  calculated for  $\text{C}_8\text{H}_8\text{Cl}_2\text{NO}$   $[\text{M}+\text{H}]^+$  203.9977, found 203.9972.

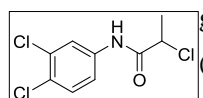
**2-Chloro-*N*-(4'-acetylphenyl)acetamide 43.** Compound **43** was synthesized according to the general



procedure **GP-4**, using 4-aminoacetophenone (803 mg, 5.94 mmol), DIPEA

(1.20 mL, 6.89 mmol) and chloroacetyl chloride (620  $\mu\text{L}$ , 7.78 mmol) in dry THF (10 mL). The reaction was stirred at 0 °C for 1 h. After extraction, **43** was obtained as yellow solid without further purification (1.11 g, 89%).  $R_f = 0.31$  (PE/EtOAc, 1:1).  $^1\text{H}$  NMR (500 MHz,  $\text{CDCl}_3$ )  $\delta$  8.43 (br, 1H), 7.97 (d,  $J = 8.5$  Hz, 2H), 7.67 (d,  $J = 8.5$  Hz, 2H), 4.21 (s, 2H), 2.58 (s, 3H).  $^{13}\text{C}$  NMR (126 MHz,  $\text{CDCl}_3$ )  $\delta$  197.0, 164.2, 141.0, 133.9, 129.9, 119.4, 43.0, 26.6. HRMS (ESI)  $m/z$  calculated for  $\text{C}_{10}\text{H}_{11}\text{ClNO}_2$   $[\text{M}+\text{H}]^+$  212.0473, found 212.0466.

**2-Chloro-*N*-(3',4'-dichlorophenyl)propanamide 44.** Compound **44** was synthesized according to the



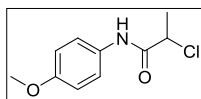
general procedure **GP-4**, using 3,4-dichloroaniline (121 mg, 0.747 mmol), DIPEA

(260  $\mu\text{L}$ , 1.49 mmol) and 2-chloropropionyl chloride (80  $\mu\text{L}$ , 0.82 mmol) in dry  $\text{CH}_2\text{Cl}_2$  (5 mL). The reaction was stirred at 0 °C for 2.5. After extraction, **44** was obtained as yellow solid without further purification (187 mg, 99%).  $R_f = 0.42$  (PE/EtOAc 7:3).  $^1\text{H}$  NMR (500 MHz,  $\text{CDCl}_3$ )  $\delta$  8.29 (br, 1H), 7.80 (d,  $J = 2.3$  Hz, 1H), 7.41 (d,  $J = 8.7$  Hz, 1H), 7.38



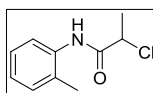
(dd,  $J = 2.3, 8.7$  Hz, 1H), 4.55 (q,  $J = 7.1$  Hz, 1H), 1.82 (d,  $J = 7.1$  Hz, 3H).  $^{13}\text{C}$  NMR (126 MHz,  $\text{CDCl}_3$ )  $\delta$  167.7, 136.5, 133.1, 130.8, 128.5, 121.9, 119.3, 56.2, 22.7. HRMS (ESI)  $m/z$  calculated for  $\text{C}_9\text{H}_9\text{Cl}_3\text{NO}$  251.9744  $[\text{M}+\text{H}]^+$ , found 251.9738.

**2-Chloro-*N*-(4'-methoxyphenyl)propanamide 45.** Compound **45** was synthesized according to the



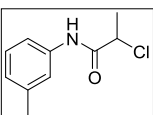
general procedure **GP-4**, using 4-methoxyaniline (910 mg, 7.39 mmol), DIPEA (1.80 mL, 10.3 mmol) and 2-chloropropionyl chloride (790  $\mu\text{L}$ , 8.14 mmol) in dry  $\text{CH}_2\text{Cl}_2$  (10 mL). The reaction was stirred at 0  $^\circ\text{C}$  for 5.5 h and was slowly allowed to warm up to room temperature. After extraction, **45** was obtained as white solid without further purification (1.53 g, 97%).  $R_f = 0.29$  (PE/EtOAc 7:3).  $^1\text{H}$  NMR (500 MHz,  $\text{CDCl}_3$ )  $\delta$  8.19 (br, 1H), 7.44 (d,  $J = 9.0$  Hz, 2H), 6.88 (d,  $J = 9.0$  Hz, 2H), 4.54 (q,  $J = 7.0$  Hz, 1H), 3.80 (s, 3H), 1.82 (d,  $J = 7.0$  Hz, 3H).  $^{13}\text{C}$  NMR (126 MHz,  $\text{CDCl}_3$ )  $\delta$  167.5, 157.1, 130.1, 122.1, 114.4, 56.4, 55.6, 22.9. HRMS (ESI)  $m/z$  calculated for  $\text{C}_{10}\text{H}_{13}\text{ClNO}_2$  214.0629  $[\text{M}+\text{H}]^+$ , found: 214.0624.

**2-Chloro-*N*-(*o*-tolyl)propanamide 46.** Compound **46** was synthesized according to the general



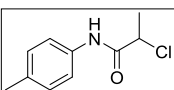
procedure **GP-4**, using *o*-toluidine (500  $\mu\text{L}$ , 4.70 mmol), DIPEA (1.70 mL, 9.76 mmol) and 2-chloropropionyl chloride (500  $\mu\text{L}$ , 5.15 mmol) in dry  $\text{CH}_2\text{Cl}_2$  (10 mL). The reaction was stirred at 0  $^\circ\text{C}$  for 6 h and was slowly allowed to warm up to room temperature. After extraction, **46** was obtained as yellow solid without further purification (965 mg, quant.).  $R_f = 0.39$  (PE/EtOAc 7:3).  $^1\text{H}$  NMR (500 MHz,  $\text{CDCl}_3$ )  $\delta$  8.26 (br, 1H), 7.87 (d,  $J = 8.1$  Hz, 1H), 7.26–7.20 (m, 2H), 7.12 (td,  $J = 1.1, 11.2$  Hz, 1H), 4.60 (q,  $J = 7.1$  Hz, 1H), 2.30 (s, 3H), 1.86 (d,  $J = 7.1$  Hz, 3H).  $^{13}\text{C}$  NMR (126 MHz,  $\text{CDCl}_3$ )  $\delta$  167.6, 135.0, 130.7, 129.2, 127.0, 125.8, 122.5, 56.9, 23.1, 17.7. HRMS (ESI)  $m/z$  calculated for  $\text{C}_{10}\text{H}_{13}\text{ClNO}$  198.0680  $[\text{M}+\text{H}]^+$ , found 198.0675.

**2-Chloro-*N*-(*m*-tolyl)propanamide 47.** Compound **47** was synthesized according to the general



procedure **GP-4**, using *m*-toluidine (400  $\mu\text{L}$ , 3.73 mmol), DIPEA (1.30 mL, 7.46 mmol) and 2-chloropropionyl chloride (400  $\mu\text{L}$ , 4.12 mmol) in dry  $\text{CH}_2\text{Cl}_2$  (7 mL). The reaction was stirred at 0  $^\circ\text{C}$  for 3.5 h and was slowly allowed to warm up to room temperature. After extraction, **47** was obtained as brown oil without further purification (727 mg, 99%).  $R_f = 0.46$  (PE/EtOAc 7:3).  $^1\text{H}$  NMR (300 MHz,  $\text{CDCl}_3$ )  $\delta$  8.24 (br, 1H), 7.40 (s, 1H), 7.34 (d,  $J = 8.3$  Hz, 1H), 7.23 (t,  $J = 7.7$  Hz, 1H), 6.98 (d,  $J = 7.5$  Hz, 1H), 4.54 (q,  $J = 7.1$  Hz, 1H), 2.35 (s, 3H), 1.82 (d,  $J = 7.1$  Hz, 3H).  $^{13}\text{C}$  NMR (75 MHz,  $\text{CDCl}_3$ )  $\delta$  167.5, 139.2, 137.0, 129.0, 126.0, 120.8, 117.2, 56.4, 22.9, 21.6. HRMS (ESI)  $m/z$  calculated for  $\text{C}_{10}\text{H}_{13}\text{ClNO}$  198.0680  $[\text{M}+\text{H}]^+$ , found 198.0671.

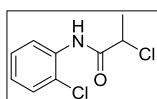
**2-Chloro-*N*-(*p*-tolyl)propanamide 48.** Compound **48** was synthesized according to the general



procedure **GP-4**, using *p*-toluidine (434 mg, 4.05 mmol), DIPEA (1.50 mL, 8.61 mmol) and 2-chloropropionyl chloride (430  $\mu\text{L}$ , 4.43 mmol) in dry  $\text{CH}_2\text{Cl}_2$  (10 mL). The reaction was stirred at 0  $^\circ\text{C}$  for 2.5 h and was slowly allowed to warm

up to room temperature. After extraction, **48** was obtained as orange solid without further purification (815 mg, quant.).  $R_f = 0.50$  (PE/EtOAc 7:3).  $^1\text{H NMR}$  (500 MHz,  $\text{CDCl}_3$ )  $\delta$  8.22 (br, 1H), 7.42 (d,  $J = 8.4$  Hz, 2H), 7.15 (d,  $J = 8.3$  Hz, 2H), 4.54 (q,  $J = 7.1$  Hz, 1H), 2.33 (s, 3H), 1.82 (d,  $J = 7.0$  Hz, 3H).  $^{13}\text{C NMR}$  (126 MHz,  $\text{CDCl}_3$ )  $\delta$  167.4, 134.9, 134.5, 129.7, 120.2, 56.4, 22.9, 21.0. HRMS (ESI)  $m/z$  calculated for  $\text{C}_{10}\text{H}_{13}\text{ClNO}$  198.0680  $[\text{M}+\text{H}]^+$ , found 198.0675.

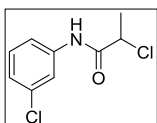
**2-Chloro-*N*-(2'-chlorophenyl)propanamide 49.** Compound **49** was synthesized according to the



general procedure **GP-4**, using 2-chloroaniline (500  $\mu\text{L}$ , 4.75 mmol), DIPEA (1.70 mL, 9.76 mmol) and 2-chloropropionyl chloride (500  $\mu\text{L}$ , 5.15 mmol) in dry  $\text{CH}_2\text{Cl}_2$  (10 mL). The reaction was stirred at 0  $^\circ\text{C}$  for 5 h and was slowly allowed to warm up to

room temperature. After extraction, **49** was obtained as orange oil without further purification (990 mg, 96%).  $R_f = 0.53$  (PE/EtOAc 7:3).  $^1\text{H NMR}$  (500 MHz,  $\text{CDCl}_3$ )  $\delta$  8.94 (br, 1H), 8.36 (dd,  $J = 1.5, 8.3$  Hz, 1H), 7.40 (dd,  $J = 1.5, 8.1$  Hz, 1H), 7.29 (td,  $J = 1.5, 8.7$  Hz, 1H), 7.09 (td,  $J = 1.6, 7.7$  Hz, 1H), 4.59 (q,  $J = 7.1$  Hz, 1H), 1.85 (d,  $J = 7.1$  Hz, 3H).  $^{13}\text{C NMR}$  (126 MHz,  $\text{CDCl}_3$ )  $\delta$  167.7, 134.0, 129.3, 127.9, 125.5, 123.7, 121.3, 56.5, 22.9. HRMS (ESI)  $m/z$  calculated for  $\text{C}_9\text{H}_{10}\text{Cl}_2\text{NO}$  218.0134  $[\text{M}+\text{H}]^+$ , found 218.0129.

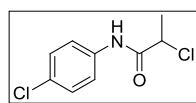
**2-Chloro-*N*-(3'-chlorophenyl)propanamide 50.** Compound **50** was synthesized according to the



general procedure **GP-4**, using 3-chloroaniline (150  $\mu\text{L}$ , 1.42 mmol), DIPEA (500  $\mu\text{L}$ , 2.87 mmol) and 2-chloropropionyl chloride (150  $\mu\text{L}$ , 1.55 mmol) in dry  $\text{CH}_2\text{Cl}_2$  (10 mL). The reaction was stirred at 0  $^\circ\text{C}$  for 4.5 h and was slowly allowed to warm up to

room temperature. After extraction, **50** was obtained as orange oil without further purification (312 mg, quant.).  $R_f = 0.42$  (PE/EtOAc 7:3).  $^1\text{H NMR}$  (500 MHz,  $\text{CDCl}_3$ )  $\delta$  8.27 (br, 1H), 7.68 (t,  $J = 2.0$  Hz, 1H), 7.39 (ddd,  $J = 1.0, 2.0, 8.2$  Hz, 1H), 7.27 (t,  $J = 7.9$  Hz, 1H), 7.14 (ddd,  $J = 1.0, 2.0, 8.0$  Hz, 1H), 4.54 (q,  $J = 7.1$  Hz, 1H), 1.83 (d,  $J = 7.0$  Hz, 3H).  $^{13}\text{C NMR}$  (126 MHz,  $\text{CDCl}_3$ )  $\delta$  167.6, 138.2, 135.0, 130.2, 125.3, 120.3, 118.1, 56.3, 22.8. HRMS (ESI)  $m/z$  calculated for  $\text{C}_9\text{H}_{10}\text{Cl}_2\text{NO}$  218.0134  $[\text{M}+\text{H}]^+$ , found 218.0129.

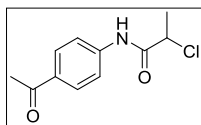
**2-Chloro-*N*-(4'-chlorophenyl)propanamide 51.** Compound **51** was synthesized according to the



general procedure **GP-4**, using 4-chloroaniline (396 mg, 3.10 mmol), DIPEA (1.10 mL, 6.32 mmol) and 2-chloropropionyl chloride (330  $\mu\text{L}$ , 3.40 mmol) in dry  $\text{CH}_2\text{Cl}_2$  (7 mL). The reaction was stirred at 0  $^\circ\text{C}$  for 3.5 h and was slowly allowed to

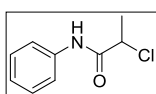
warm up to room temperature. After extraction, **51** was obtained as orange solid without further purification (669 mg, 99%).  $R_f = 0.44$  (PE/EtOAc 7:3).  $^1\text{H NMR}$  (300 MHz,  $\text{CDCl}_3$ )  $\delta$  8.28 (br, 1H), 7.51 (d,  $J = 8.9$  Hz, 2H), 7.31 (d,  $J = 8.9$  Hz, 2H), 4.54 (q,  $J = 7.1$  Hz, 1H), 1.82 (d,  $J = 7.1$  Hz, 3H).  $^{13}\text{C NMR}$  (75 MHz,  $\text{CDCl}_3$ )  $\delta$  167.6, 135.6, 130.3, 129.3, 121.4, 56.3, 22.8. HRMS (ESI)  $m/z$  calculated for  $\text{C}_9\text{H}_{10}\text{Cl}_2\text{NO}$  218.0134  $[\text{M}+\text{H}]^+$ , found 218.0129.

**2-Chloro-*N*-(4'-acetylphenyl)propanamide 52.** Compound **52** was synthesized according to the



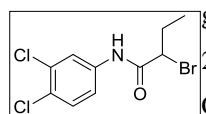
general procedure **GP-4**, using 4-aminoacetophenone (502 mg, 3.71 mmol), DIPEA (700  $\mu$ L, 4.09 mmol) and 2-chloropropionyl chloride (400  $\mu$ L, 4.12 mmol) in dry THF (5 mL). The reaction was stirred at 0  $^{\circ}$ C for 2 h. After extraction, **52** was obtained as orange solid without further purification (827 mg, 99%).  $R_f$  = 0.19 (PE/EtOAc 7:3).  $^1\text{H}$  NMR (500 MHz,  $\text{CDCl}_3$ )  $\delta$  8.46 (br, 1H), 7.96 (d,  $J$  = 8.5 Hz, 2H), 7.67 (d,  $J$  = 8.4 Hz, 2H), 4.56 (q,  $J$  = 7.0 Hz, 1H), 2.58 (s, 3H), 1.83 (d,  $J$  = 7.1 Hz, 3H).  $^{13}\text{C}$  NMR (126 MHz,  $\text{CDCl}_3$ )  $\delta$  197.0, 167.8, 141.3, 133.7, 129.9, 119.3, 56.2, 26.6, 22.7. HRMS (ESI)  $m/z$  calculated for  $\text{C}_{11}\text{H}_{13}\text{ClNO}_2$  226.0629  $[\text{M}+\text{H}]^+$ , found 226.0623.

**2-Chloro-*N*-phenylpropanamide 53.** Compound **53** was synthesized according to the general



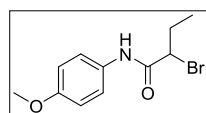
procedure **GP-4**, using aniline (200  $\mu$ L, 2.19 mmol), DIPEA (800  $\mu$ L, 4.59 mmol) and 2-chloropropionyl chloride (240  $\mu$ L, 2.47 mmol) in dry  $\text{CH}_2\text{Cl}_2$  (5 mL). The reaction was stirred at 0  $^{\circ}$ C for 70 min. After extraction, **53** was obtained as yellow solid without further purification (407 mg, quant.).  $R_f$  = 0.38 (PE/EtOAc 7:3).  $^1\text{H}$  NMR (300 MHz,  $\text{CDCl}_3$ )  $\delta$  8.28 (br, 1H), 7.55 (d,  $J$  = 7.6 Hz, 2H), 7.36 (t,  $J$  = 7.9 Hz, 2H), 7.16 (t,  $J$  = 7.4 Hz, 1H), 4.55 (q,  $J$  = 7.1 Hz, 1H), 1.83 (d,  $J$  = 7.1 Hz, 3H).  $^{13}\text{C}$  NMR (75 MHz,  $\text{CDCl}_3$ )  $\delta$  167.5, 137.1, 129.2, 125.2, 120.1, 56.4, 22.8. HRMS (ESI)  $m/z$  calculated for  $\text{C}_9\text{H}_{11}\text{ClNO}$  184.0524  $[\text{M}+\text{H}]^+$ , found 184.0520.

**2-Bromo-*N*-(3',4'-dichlorophenyl)butanamide 54.** Compound **54** was synthesized according to the



general procedure **GP-3**, using 3,4-dichloroaniline (149 mg, 0.920 mmol), 2-bromobutyric acid (120  $\mu$ L, 1.13 mmol) and EDC $\cdot$ HCl (218 mg, 1.14 mmol) in  $\text{CH}_2\text{Cl}_2$  (5 mL). The reaction was stirred at room temperature overnight. After extraction, **54** was obtained as white solid without further purification (275 mg, 96%).  $R_f$  = 0.33 (PE/EtOAc 7:3).  $^1\text{H}$  NMR (500 MHz,  $\text{CDCl}_3$ )  $\delta$  8.08 (br, 1H), 7.79 (d,  $J$  = 2.4 Hz, 1H), 7.40 (d,  $J$  = 8.7 Hz, 1H), 7.36 (dd,  $J$  = 2.4, 8.7 Hz, 1H), 4.41 (dd,  $J$  = 5.1, 7.8 Hz, 1H), 2.29–2.20 (m, 1H), 2.17–2.09 (m, 1H), 1.10 (t,  $J$  = 7.3 Hz, 3H).  $^{13}\text{C}$  NMR (126 MHz,  $\text{CDCl}_3$ )  $\delta$  166.8, 136.7, 133.1, 130.8, 128.5, 121.8, 119.3, 53.8, 29.4, 11.9. HRMS (ESI)  $m/z$  calculated for  $\text{C}_{10}\text{H}_{11}\text{BrCl}_2\text{NO}$  309.9396  $[\text{M}+\text{H}]^+$ , found 309.9388.

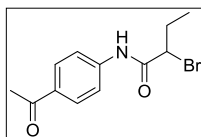
**2-Bromo-*N*-(4'-methoxyphenyl)butanamide 55.** Compound **55** was synthesized according to the



general procedure **GP-3**, using 4-methoxyaniline (120 mg, 0.974 mmol), 2-bromobutyric acid (130  $\mu$ L, 1.22 mmol) and EDC $\cdot$ HCl (236 mg, 1.23 mmol) in  $\text{CH}_2\text{Cl}_2$  (5 mL). The reaction was stirred at room temperature overnight. After extraction, **55** was obtained as white solid without further purification (226 mg, 85%).  $R_f$  = 0.37 (PE/EtOAc 7:3).  $^1\text{H}$  NMR (500 MHz,  $\text{CDCl}_3$ )  $\delta$  8.00 (br, 1H), 7.43 (d,  $J$  = 9.0 Hz, 2H), 6.88 (d,  $J$  = 9.0 Hz, 2H), 4.42 (dd,  $J$  = 5.0, 7.7 Hz, 1H), 3.80 (s, 3H), 2.55 (hd,  $J$  = 5.0, 7.3 Hz, 1H), 2.19–2.10 (m, 1H), 1.11 (t,  $J$  = 7.3 Hz, 1H).  $^{13}\text{C}$  NMR (126 MHz,  $\text{CDCl}_3$ )  $\delta$  166.5, 157.1, 130.3, 122.1, 114.4,

55.7, 54.3, 29.6, 11.9. HRMS (ESI)  $m/z$  calculated for  $C_{11}H_{15}BrNO_2$  272.0281  $[M+H]^+$ , found 272.0273.

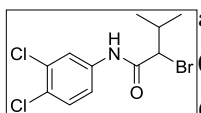
**2-Bromo-*N*-(4'-acetylphenyl)butanamide 56.** Compound **56** was synthesized according to the



general procedure **GP-3**, using 4-aminoacetophenone (303 mg, 2.24 mmol), 2-bromobutyric acid (200  $\mu$ L, 1.87 mmol) and EDC·HCl (540 mg, 2.84 mmol) in  $CH_2Cl_2$  (15 mL). The reaction was stirred at room temperature overnight.

Extraction followed by column chromatography (PE/EtOAc 8:2) yielded **56** as colorless oil (240 mg, 38%).  $R_f$  = 0.17 (PE/EtOAc 7:3).  $^1H$  NMR (500 MHz,  $CDCl_3$ )  $\delta$  8.29 (br, 1H), 7.96 (d,  $J$  = 8.8 Hz, 2H), 7.66 (d,  $J$  = 8.8 Hz, 2H), 4.43 (dd,  $J$  = 5.2, 7.8 Hz, 1H), 2.59 (s, 3H), 2.30–2.21 (m, 1H), 2.19–2.07 (m, 1H), 1.11 (t,  $J$  = 7.3 Hz, 1H).  $^{13}C$  NMR (126 MHz,  $CDCl_3$ )  $\delta$  197.0, 167.0, 141.5, 133.7, 129.9, 119.3, 53.7, 29.4, 26.6, 12.0. HRMS (ESI)  $m/z$  calculated for  $C_{12}H_{15}BrNO_2$  284.0281  $[M+H]^+$ , found 284.0272.

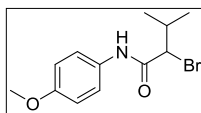
**2-Bromo-*N*-(3',4'-dichlorophenyl)-3-methylbutanamide 57.** Compound **57** was synthesized



according to the general procedure **GP-3**, using 3,4-dichloroaniline (153 mg, 0.940 mmol), 2-bromo-3-methylbutyric acid (210 mg, 1.16 mmol) and EDC·HCl (222 mg, 1.16 mmol) in  $CH_2Cl_2$  (5 mL). The reaction was stirred at room

temperature overnight. After extraction, **57** was obtained as slightly green solid without further purification (290 mg, 94%).  $R_f$  = 0.51 (PE/EtOAc 7:3).  $^1H$  NMR (500 MHz,  $CDCl_3$ )  $\delta$  8.20 (br, 1H), 7.79 (d,  $J$  = 2.4 Hz, 1H), 7.40 (d,  $J$  = 8.7 Hz, 1H), 7.36 (dd,  $J$  = 2.4, 8.7 Hz, 1H), 4.42 (d,  $J$  = 4.7 Hz, 1H), 2.45 (dq,  $J$  = 4.7, 6.6, 6.6 Hz, 1H), 1.11 (d,  $J$  = 6.7 Hz, 3H), 1.04 (d,  $J$  = 6.6 Hz, 3H).  $^{13}C$  NMR (126 MHz,  $CDCl_3$ )  $\delta$  166.5, 136.6, 133.1, 130.7, 128.5, 121.8, 119.3, 61.6, 32.8, 21.1, 18.6. HRMS (ESI)  $m/z$  calculated for  $C_{11}H_{13}BrCl_2NO$  323.9552  $[M+H]^+$ , found 323.9536.

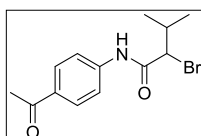
**2-Bromo-*N*-(4'-methoxyphenyl)-3-methylbutanamide 58.** Compound **58** was synthesized according



to the general procedure **GP-3**, using 4-methoxyaniline (217 mg, 1.76 mmol), 2-bromo-3-methylbutyric acid (375 mg, 2.07 mmol) and EDC·HCl (406 mg, 2.12 mmol) in  $CH_2Cl_2$  (5 mL). The reaction was stirred at room temperature

overnight. After extraction, **58** was obtained as white solid without further purification (484 mg, 96%).  $^1H$  NMR (500 MHz,  $CDCl_3$ )  $\delta$  8.12 (br, 1H), 7.43 (d,  $J$  = 9.0 Hz, 2H), 6.88 (d,  $J$  = 9.0 Hz, 2H), 4.44 (d,  $J$  = 4.6 Hz, 1H), 3.80 (s, 3H), 2.49 (dq,  $J$  = 4.5, 6.6, 6.6 Hz, 1H), 1.11 (d,  $J$  = 6.7 Hz, 3H), 1.04 (d,  $J$  = 6.6 Hz, 3H).  $^{13}C$  NMR (126 MHz,  $CDCl_3$ )  $\delta$  166.2, 157.1, 130.2, 122.1, 114.4, 62.2, 55.6, 32.8, 21.2, 18.6. HRMS (ESI)  $m/z$  calculated for  $C_{12}H_{17}BrNO_2$  286.0437  $[M+H]^+$ , found 286.0428.

**2-Bromo-*N*-(4'-acetylphenyl)-3-methylbutanamide 59.** Compound **59** was synthesized according to

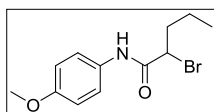


the general procedure **GP-3**, using 4-aminoacetophenone (276 mg, 2.04 mmol), 2-bromo-3-methylbutyric acid (310 mg, 1.71 mmol) and EDC·HCl (496 mg, 2.59 mmol) in  $CH_2Cl_2$  (15 mL). The reaction was stirred at room temperature

overnight. Extraction followed by column chromatography (PE/EtOAc 8:2) yielded **59** as white solid (123 mg, 26%). <sup>1</sup>H NMR (500 MHz, CDCl<sub>3</sub>) δ 8.42 (br, 1H), 7.96 (d, *J* = 8.7 Hz, 2H), 7.66 (d, *J* = 8.7 Hz, 2H), 4.42 (d, *J* = 5.0 Hz, 1H), 2.58 (s, 3H), 2.49 (dq, *J* = 5.0, 6.8, 6.8 Hz, 1H), 1.11 (d, *J* = 6.7 Hz, 3H), 1.05 (d, *J* = 6.6 Hz, 3H). <sup>13</sup>C NMR (126 MHz, CDCl<sub>3</sub>) δ 197.0, 166.7, 141.4, 133.7, 129.9, 119.3, 61.4, 32.8, 26.6, 21.1, 18.8. HRMS (ESI) *m/z* calculated for C<sub>13</sub>H<sub>17</sub>BrNO<sub>2</sub> 298.0437 [M+H]<sup>+</sup>, found 298.0428.

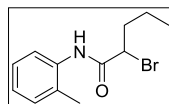
**2-Bromo-N-(3',4'-dichlorophenyl)pentanamide 60.** Non-isolated compound. Please see the synthesis of compound **118**.

**2-Bromo-N-(4'-methoxyphenyl)pentanamide 61.** Compound **61** was synthesized according to the



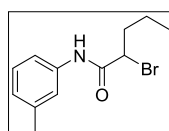
general procedure **GP-3**, using 4-methoxyaniline (301 mg, 2.44 mmol), 2-bromopentanoic acid (390 μL, 2.98 mmol) and EDC·HCl (562 mg, 2.91 mmol) in CH<sub>2</sub>Cl<sub>2</sub> (7.5 mL). The reaction was stirred at room temperature overnight. After extraction, **61** was obtained as white solid without further purification (496 mg, 70%). *R<sub>f</sub>* = 0.37 (PE/EtOAc 7:3). <sup>1</sup>H NMR (500 MHz, CDCl<sub>3</sub>) δ 8.01 (br, 1H), 7.43 (d, *J* = 9.0 Hz, 2H), 6.88 (d, *J* = 9.0 Hz, 2H), 4.45 (dd, *J* = 5.1, 8.3 Hz, 1H), 3.80 (s, 3H), 2.23–2.14 (m, 1H), 2.11–2.03 (m, 1H), 1.64–1.46 (m, 1H), 0.98 (t, *J* = 7.4 Hz, 3H). <sup>13</sup>C NMR (126 MHz, CDCl<sub>3</sub>) δ 166.8, 157.0, 130.3, 122.0, 114.3, 55.6, 52.4, 38.1, 20.7, 13.4. HRMS (ESI) *m/z* calculated for C<sub>12</sub>H<sub>17</sub>BrNO<sub>2</sub> 286.0437 [M+H]<sup>+</sup>, found 286.0427.

**2-Bromo-N-(o-tolyl)pentanamide 62.** Compound **62** was synthesized according to the general



procedure **GP-3**, using *o*-toluidine (140 μL, 1.32 mmol), 2-bromopentanoic acid (200 μL, 1.53 mmol) and EDC·HCl (291 mg, 1.52 mmol) in CH<sub>2</sub>Cl<sub>2</sub> (5 mL). The reaction was stirred at room temperature overnight. After extraction, **62** was obtained as yellow solid without further purification (243 mg, 68%). *R<sub>f</sub>* = 0.50 (PE/EtOAc 7:3). <sup>1</sup>H NMR (300 MHz, CDCl<sub>3</sub>) δ 8.08 (br, 1H), 7.83 (d, *J* = 8.0 Hz, 1H), 7.23–7.19 (m, 2H), 7.11 (d, *J* = 7.4 Hz, 1H), 4.53 (dd, *J* = 5.0, 8.2 Hz, 1H), 2.30 (s, 3H), 2.26–2.04 (m, 2H), 1.67–1.51 (m, 2H), 0.99 (t, *J* = 7.4 Hz, 3H). <sup>13</sup>C NMR (75 MHz, CDCl<sub>3</sub>) δ 166.9, 135.2, 130.7, 129.3, 127.0, 125.8, 122.6, 53.1, 38.3, 20.7, 17.8, 13.4. HRMS (ESI) *m/z* calculated for C<sub>12</sub>H<sub>17</sub>BrNO 270.0488 [M+H]<sup>+</sup>, found 270.0480.

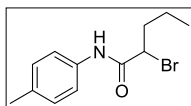
**2-Bromo-N-(m-tolyl)pentanamide 63.** Compound **63** was synthesized according to the general



procedure **GP-3**, using *m*-toluidine (200 μL, 1.87 mmol), 2-bromopentanoic acid (300 μL, 2.29 mmol) and EDC·HCl (411 mg, 2.14 mmol) in CH<sub>2</sub>Cl<sub>2</sub> (10 mL). The reaction was stirred at room temperature overnight. After extraction, **63** was obtained as brown oil without further purification (375 mg, 74%). *R<sub>f</sub>* = 0.38 (PE/EtOAc 7:3). <sup>1</sup>H NMR (300 MHz, CDCl<sub>3</sub>) δ 8.04 (br, 1H), 7.39 (s, 1H), 7.32 (d, *J* = 8.3 Hz, 1H), 7.23 (t, *J* = 7.8 Hz, 1H), 6.97 (d, *J* = 7.5 Hz, 1H), 4.45 (dd, *J* = 5.3, 8.1 Hz, 1H), 2.35 (s, 3H), 2.20–2.05 (m, 2H), 1.63–1.45 (m,

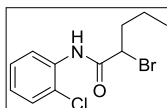
2H), 0.97 (t,  $J = 7.4$  Hz, 3H).  $^{13}\text{C}$  NMR (75 MHz,  $\text{CDCl}_3$ )  $\delta$  166.9, 139.2, 137.2, 129.0, 125.9, 120.7, 117.2, 52.3, 38.1, 21.6, 20.7, 13.4. HRMS (ESI)  $m/z$  calculated for  $\text{C}_{12}\text{H}_{17}\text{BrNO}$  270.0488  $[\text{M}+\text{H}]^+$ , found 270.0480.

**2-Bromo-*N*-(*p*-tolyl)pentanamide 64.** Compound **64** was synthesized according to the general



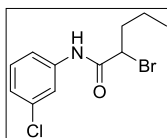
procedure **GP-3**, using *p*-toluidine (137 mg, 1.28 mmol), 2-bromopentanoic acid (200  $\mu\text{L}$ , 1.53 mmol) and EDC·HCl (291 mg, 1.52 mmol) in  $\text{CH}_2\text{Cl}_2$  (5 mL). The reaction was stirred at room temperature overnight. After extraction, **64** was obtained as yellow solid without further purification (275 mg, 80%).  $R_f = 0.49$  (PE/EtOAc 7:3).  $^1\text{H}$  NMR (300 MHz,  $\text{CDCl}_3$ )  $\delta$  8.04 (br, 1H), 7.41 (d,  $J = 8.4$  Hz, 2H), 7.15 (d,  $J = 8.3$  Hz, 2H), 4.45 (dd,  $J = 5.2, 8.2$  Hz, 1H), 2.33 (s, 3H), 2.23–2.01 (m, 2H), 1.63–1.45 (m, 2H), 0.97 (t,  $J = 7.4$  Hz, 3H).  $^{13}\text{C}$  NMR (75 MHz,  $\text{CDCl}_3$ )  $\delta$  166.8, 134.9, 134.7, 129.7, 120.2, 52.4, 38.1, 21.0, 20.7, 13.4. HRMS (ESI)  $m/z$  calculated for  $\text{C}_{12}\text{H}_{17}\text{BrNO}$  270.0488  $[\text{M}+\text{H}]^+$ , found 270.0480.

**2-Bromo-*N*-(2'-chlorophenyl)pentanamide 65.** Compound **65** was synthesized according to the



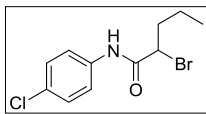
general procedure **GP-3**, using 2-chloroaniline (140  $\mu\text{L}$ , 1.33 mmol), 2-bromopentanoic acid (200  $\mu\text{L}$ , 1.53 mmol) and EDC·HCl (291 mg, 1.52 mmol) in  $\text{CH}_2\text{Cl}_2$  (5 mL). The reaction was stirred at room temperature overnight. After extraction, **65** was obtained as white solid without further purification (240 mg, 62%).  $R_f = 0.54$  (PE/EtOAc 7:3).  $^1\text{H}$  NMR (500 MHz,  $\text{CDCl}_3$ )  $\delta$  8.69 (br, 1H), 8.34 (dd,  $J = 1.4, 8.3$  Hz, 1H), 7.40 (dd,  $J = 1.3, 8.0$  Hz, 1H), 7.30 (t,  $J = 8.6$  Hz, 1H), 7.08 (td,  $J = 1.6, 7.7$  Hz, 1H), 4.49 (dd,  $J = 5.2, 8.4$  Hz, 1H), 2.24–2.16 (m, 1H), 2.15–2.05 (m, 1H), 1.65–1.51 (m, 1H), 0.99 (t,  $J = 7.4$  Hz, 3H).  $^{13}\text{C}$  NMR (126 MHz,  $\text{CDCl}_3$ )  $\delta$  167.0, 134.2, 129.3, 127.9, 125.4, 123.6, 121.5, 52.3, 38.1, 20.7, 13.4. HRMS (ESI)  $m/z$  calculated for  $\text{C}_{11}\text{H}_{14}\text{BrClNO}$  289.9942  $[\text{M}+\text{H}]^+$ , found 289.9932.

**2-Bromo-*N*-(3'-chlorophenyl)pentanamide 66.** Compound **66** was synthesized according to the



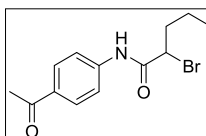
general procedure **GP-3**, using 3-chloroaniline (140  $\mu\text{L}$ , 1.33 mmol), 2-bromopentanoic acid (200  $\mu\text{L}$ , 1.53 mmol) and EDC·HCl (291 mg, 1.52 mmol) in  $\text{CH}_2\text{Cl}_2$  (5 mL). The reaction was stirred at room temperature overnight. After extraction, **66** was obtained as yellow oil without further purification (317 mg, 82%).  $^1\text{H}$  NMR (500 MHz,  $\text{CDCl}_3$ )  $\delta$  8.13 (br, 1H), 7.67 (t,  $J = 2.0$  Hz, 1H), 7.38 (ddd,  $J = 0.8, 2.0, 8.2$  Hz, 1H), 7.26 (t,  $J = 8.0$  Hz, 1H), 7.12 (ddd,  $J = 0.8, 2.0, 8.0$  Hz, 1H), 4.45 (dd,  $J = 5.3, 8.3$  Hz, 1H), 2.24–2.14 (m, 1H), 2.10–2.03 (m, 1H), 1.61–1.47 (m, 2H), 0.97 (t,  $J = 7.4$  Hz, 3H).  $^{13}\text{C}$  NMR (126 MHz,  $\text{CDCl}_3$ )  $\delta$  167.1, 138.4, 134.9, 130.2, 125.2, 120.2, 118.0, 51.9, 37.9, 20.7, 13.4. HRMS (ESI)  $m/z$  calculated for  $\text{C}_{11}\text{H}_{14}\text{BrClNO}$  289.9942  $[\text{M}+\text{H}]^+$ , found 289.9932.

**2-Bromo-N-(4'-chlorophenyl)pentanamide 67.** Compound **67** was synthesized according to the



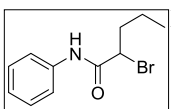
general procedure **GP-3**, using 4-chloroaniline (167 mg, 1.31 mmol), 2-bromopentanoic acid (200  $\mu$ L, 1.53 mmol) and EDC·HCl (309 mg, 1.61 mmol) in  $\text{CH}_2\text{Cl}_2$  (10 mL). The reaction was stirred at room temperature overnight. After extraction, **67** was obtained as white solid without further purification (353 mg, 93%).  $^1\text{H}$  NMR (300 MHz,  $\text{CDCl}_3$ )  $\delta$  8.06 (br, 1H), 7.49 (d,  $J = 8.6$  Hz, 2H), 7.31 (d,  $J = 8.6$  Hz, 2H), 4.44 (dd,  $J = 5.1, 8.2$  Hz, 1H), 2.25–2.01 (m, 2H), 1.63–1.47 (m, 2H), 0.98 (t,  $J = 7.3$  Hz, 3H).  $^{13}\text{C}$  NMR (75 MHz,  $\text{CDCl}_3$ )  $\delta$  166.9, 135.8, 130.5, 129.3, 121.3, 52.1, 38.0, 20.7, 13.4.

**2-Bromo-N-(4'-acetylphenyl)pentanamide 68.** Compound **68** was synthesized according to the



general procedure **GP-3**, using 4-aminoacetophenone (300 mg, 2.22 mmol), 2-bromopentanoic acid (350  $\mu$ L, 2.55 mmol) and EDC·HCl (515 mg, 2.69 mmol) in  $\text{CH}_2\text{Cl}_2$  (10 mL). The reaction was stirred at room temperature overnight. After extraction, **68** was obtained as yellow oil without further purification (676 mg, quant.).  $R_f = 0.32$  (PE/EtOAc 7:3).  $^1\text{H}$  NMR (300 MHz,  $\text{CDCl}_3$ )  $\delta$  8.24 (br, 1H), 7.97 (d,  $J = 8.7$  Hz, 2H), 7.66 (d,  $J = 8.7$  Hz, 2H), 4.46 (dd,  $J = 5.4, 8.1$  Hz, 1H), 2.59 (s, 3H), 2.26–2.02 (m, 2H), 1.66–1.45 (m, 1H), 0.98 (t,  $J = 7.4$  Hz, 3H).  $^{13}\text{C}$  NMR (75 MHz,  $\text{CDCl}_3$ )  $\delta$  197.0, 167.2, 141.5, 133.6, 129.9, 119.3, 51.8, 37.9, 26.6, 20.7, 13.4. HRMS (ESI)  $m/z$  calculated for  $\text{C}_{13}\text{H}_{17}\text{BrNO}_2$  298.0437  $[\text{M}+\text{H}]^+$ , found 298.0422.

**2-Bromo-N-phenylpentanamide 69.** Compound **69** was synthesized according to the general

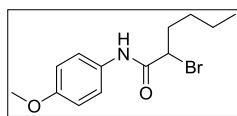


procedure **GP-3**, using aniline (120  $\mu$ L, 1.32 mmol), 2-bromopentanoic acid (200  $\mu$ L, 1.53 mmol) and EDC·HCl (291 mg, 1.52 mmol) in  $\text{CH}_2\text{Cl}_2$  (5 mL). The reaction was stirred at room temperature overnight. After extraction, **69** was obtained as yellow solid without further purification (235 mg, 70%).  $R_f = 0.53$  (PE/EtOAc 7:3).  $^1\text{H}$  NMR (300 MHz,  $\text{CDCl}_3$ )  $\delta$  8.08 (br, 1H), 7.53 (d,  $J = 8.5$  Hz, 2H), 7.35 (t,  $J = 8.0$  Hz, 2H), 7.15 (t,  $J = 7.4$  Hz, 1H), 4.45 (dd,  $J = 5.2, 8.2$  Hz, 1H), 2.26–2.01 (m, 2H), 1.64–1.47 (m, 2H), 0.98 (t,  $J = 7.4$  Hz, 3H).  $^{13}\text{C}$  NMR (75 MHz,  $\text{CDCl}_3$ )  $\delta$  166.9, 137.3, 129.2, 125.1, 120.1, 52.3, 38.0, 20.7, 13.4. HRMS (ESI)  $m/z$  calculated for  $\text{C}_{12}\text{H}_{17}\text{BrNO}_2$  256.0332  $[\text{M}+\text{H}]^+$ , found 256.0324.

**2-Bromo-N-aryl-4-methylpentanamides 70-80.** Non-isolated compound. Please see the synthesis of compounds **119–129**.

**2-Bromo-N-(3',4'-dichlorophenyl)hexanamide 81.** Non-isolated compound. Please see the synthesis of compound **130**.

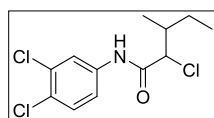
**2-Bromo-*N*-(4'-methoxyphenyl)hexanamide 82.** Compound **82** was synthesized according to the



general procedure **GP-3**, using 4-methoxyaniline (495 mg, 4.02 mmol), 2-bromohexanoic acid (700  $\mu$ L, 4.92 mmol) and EDC·HCl (926 mg, 4.83 mmol) in  $\text{CH}_2\text{Cl}_2$  (5 mL). The reaction was stirred at room temperature overnight. After

extraction, **82** was obtained as white solid without further purification (1.08 g, 89%).  $R_f = 0.43$  (PE/EtOAc 7:3).  $^1\text{H}$  NMR (500 MHz,  $\text{CDCl}_3$ )  $\delta$  7.99 (s, 1H), 7.43 (d,  $J = 9.0$  Hz, 2H), 6.88 (d,  $J = 9.0$  Hz, 2H), 4.43 (dd,  $J = 5.2, 8.2$  Hz, 1H), 3.80 (s, 3H), 2.25–2.18 (m, 1H), 2.12–2.04 (m, 1H), 1.57–1.32 (m, 4H), 0.93 (t,  $J = 7.3$  Hz, 3H).  $^{13}\text{C}$  NMR (126 MHz,  $\text{CDCl}_3$ )  $\delta$  166.8, 157.1, 130.3, 122.0, 114.4, 55.6, 52.6, 35.9, 29.5, 22.1, 14.0. HRMS (ESI)  $m/z$  calculated for  $\text{C}_{13}\text{H}_{19}\text{BrNO}_2$  300.0594  $[\text{M}+\text{H}]^+$ , found 300.0577.

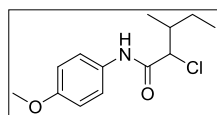
**2-Chloro-*N*-(3',4'-dichlorophenyl)-3-methylpentanamide 83.** Compound **83** was synthesized in two



steps. The first step was performed according to the general procedure **GP-1**, using DL-isoleucine (200 mg, 1.53 mmol) and sodium nitrite (263 mg, 3.81 mmol).

The resultant crude product of **87** was used without further purification. The second step was achieved according to the general procedure **GP-3**, using the crude product of **87** obtained from the first step, 3,4-dichloroaniline (206 mg, 1.27 mmol), EDC·HCl (292 mg, 1.53 mmol) and  $\text{CH}_2\text{Cl}_2$  (10 mL). The reaction was stirred at room temperature overnight. The crude product was purified using column chromatography (100%  $\text{CH}_2\text{Cl}_2$ ) to give **83** as yellow solid (192 mg, 51% over two steps). m.p. = 89  $^\circ\text{C}$ .  $^1\text{H}$  NMR (500 MHz,  $\text{DMSO}-d_6$ )  $\delta$  10.59 (s, 1H), 10.54 (s, 1H\*), 7.99 (t,  $J = 2.5$  Hz, 1H+1H\*), 7.60 (dd,  $J = 1.5, 8.5$  Hz, 1H+1H\*), 7.51 (td,  $J = 2.5, 8.5$  Hz, 1H+1H\*), 4.42 (d,  $J = 7.0$  Hz, 1H), 4.31 (d,  $J = 8.5$  Hz, 1H\*), 2.11–1.97 (m, 1H+1H\*), 1.75–1.62 (m, 1H), 1.47–1.36 (m, 1H\*), 1.33–1.16 (m, 1H+1H\*), 0.99 (d,  $J = 6.5$  Hz, 3H), 0.93 (d,  $J = 7.0$  Hz, 3H\*), 0.91–0.84 (m, 3H+3H\*).  $^{13}\text{C}$  NMR (126 MHz,  $\text{DMSO}-d_6$ )  $\delta$  167.21, 167.17\*, 138.4, 138.3\*, 131.2, 131.1\*, 130.89, 130.86\*, 125.62, 125.57\*, 120.9, 120.8\*, 119.71, 119.66\*, 64.7, 64.1\*, 38.0, 37.7\*, 26.1, 24.5\*, 15.4, 14.8\*, 11.2, 10.2\*. **83** was obtained as a diastereomeric mixture (51:49). The values labeled with \* belong to the second diastereomer. HRMS (ESI)  $m/z$  calculated for  $\text{C}_{12}\text{H}_{15}\text{Cl}_3\text{NO}$   $[\text{M}+\text{H}]^+$  294.0219, found 294.0190.

**2-Chloro-*N*-(4'-methoxyphenyl)-3-methylpentanamide 84.** Compound **84** was synthesized in two



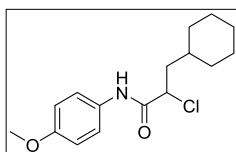
steps. The first step was performed according to the general procedure **GP-1**, using DL-isoleucine (200 mg, 1.53 mmol) and sodium nitrite (263 mg, 3.81 mmol). The resultant crude product of **87** was used without further

purification. The second step was achieved according to the general procedure **GP-3**, using the crude product of **87** obtained from the first step, *p*-anisidine (157 mg, 1.27 mmol), EDC·HCl (292 mg, 1.53 mmol) and  $\text{CH}_2\text{Cl}_2$  (10 mL). The reaction was stirred at room temperature overnight. The crude product was purified using column chromatography (100%  $\text{CH}_2\text{Cl}_2$ ). Compound **84** was obtained as white solid (210 mg, 65% over two steps). m.p. = 89  $^\circ\text{C}$ .  $^1\text{H}$  NMR (500 MHz,  $\text{DMSO}-d_6$ )  $\delta$  10.15 (s,



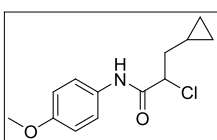
1H), 10.10 (s, 1H\*), 7.502 (d,  $J = 9.0$  Hz, 2H), 7.497 (d,  $J = 9.0$  Hz, 2H\*), 6.904 (d,  $J = 9.0$  Hz, 2H), 6.901 (d,  $J = 9.0$  Hz, 2H\*), 4.38 (d,  $J = 7.5$  Hz, 1H), 4.28 (d,  $J = 9.0$  Hz, 1H\*), 3.72 (s, 3H+3H\*), 2.09–1.95 (m, 1H+1H\*), 1.76–1.63 (m, 1H), 1.48–1.36 (m, 1H\*), 1.33–1.14 (m, 1H+1H\*), 1.01 (d,  $J = 6.5$  Hz, 3H), 0.92 (d,  $J = 7.0$  Hz, 3H\*), 0.91–0.86 (m, 3H+3H\*).  $^{13}\text{C}$  NMR (126 MHz, DMSO- $d_6$ )  $\delta$  166.24, 166.18\*, 155.7, 131.42, 131.40\*, 121.2, 121.1\*, 114.01, 113.98\*, 65.0, 64.3\*, 55.2, 38.1, 37.8\*, 26.1, 24.7\*, 15.4, 15.0\*, 11.1, 10.1\*. **84** was obtained as a diastereomeric mixture (51:49). The values labeled with \* belong to the second diastereomer. HRMS (ESI)  $m/z$  calculated for  $\text{C}_{13}\text{H}_{19}\text{ClNO}_2$   $[\text{M}+\text{H}]^+$  256.1104, found 256.1077.

**2-Chloro-*N*-(4'-methoxyphenyl)-3-cyclohexylpropanamide 85.** Compound **85** was synthesized in



two steps. The first step was performed according to the general procedure **GP-1**, using DL-3-cyclohexylalanine (260 mg, 1.52 mmol) and sodium nitrite (262 mg, 3.80 mmol). The resultant crude product of **88** was used without further purification. The second step was achieved according to the general procedure **GP-3**, using the crude product of **88** obtained from the first step, *p*-anisidine (156 mg, 1.27 mmol), EDC·HCl (291 mg, 1.52 mmol) and  $\text{CH}_2\text{Cl}_2$  (10 mL). The reaction was stirred at room temperature overnight. The crude product was purified using column chromatography (100%  $\text{CH}_2\text{Cl}_2$ ) to give **85** as beige solid (99 mg, 26 % over two steps). m.p. = 70 °C.  $^1\text{H}$  NMR (500 MHz, DMSO- $d_6$ )  $\delta$  10.19 (s, 1H), 7.51 (d,  $J = 9.5$  Hz, 2H), 6.91 (d,  $J = 9.0$  Hz, 2H), 4.58 (dd,  $J = 7.5, 8.0$  Hz, 1H), 3.72 (s, 3H), 1.93–1.54 (m, 7H), 1.44–1.30 (m, 1H), 1.26–1.05 (m, 3H), 1.02–0.85 (m, 2H).  $^{13}\text{C}$  NMR (126 MHz, DMSO- $d_6$ )  $\delta$  166.5, 155.7, 131.5, 121.0, 114.0, 57.3, 55.2, 41.5, 34.3, 32.6, 31.9, 25.9, 25.6, 25.5. HRMS (ESI)  $m/z$  calculated for  $\text{C}_{16}\text{H}_{23}\text{ClNO}_2$   $[\text{M}+\text{H}]^+$  296.1417, found 296.1388.

**2-Chloro-*N*-(4'-methoxyphenyl) 3-cyclopropylpropanamide 86.** Compound **86** was synthesized in



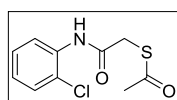
two steps. The first step was performed according to the general procedure **GP-1**, using DL-3-cyclopropylalanine (250 mg, 1.93 mmol) and sodium nitrite (334 mg, 4.84 mmol). The resultant crude product of **89** was used in the next step without further purification. The second step was performed according to the general procedure **GP-2**, using the crude product of **89** obtained from the first step (246 mg), *p*-anisidine (170 mg, 1.38 mmol),  $\text{ClCO}_2\text{Et}$  (175  $\mu\text{L}$ , 1.84 mmol),  $\text{NEt}_3$  (230  $\mu\text{L}$ , 1.65 mmol) and THF (20 mL). The reaction was stirred at room temperature overnight. The crude product was purified using column chromatography (cyclohexane/EtOAc 8:2) to give **86** as beige solid (109 mg, 22% over two steps).  $^1\text{H}$  NMR (500 MHz,  $\text{CDCl}_3$ )  $\delta$  8.20 (br, 1H), 7.43 (d,  $J = 8.2$  Hz, 2H), 6.88 (d,  $J = 8.2$  Hz, 2H), 4.52 (t,  $J = 6.0$  Hz, 1H), 3.79 (s, 3H), 2.02 (t,  $J = 8.2$  Hz, 2H), 1.02–0.94 (m, 1H), 0.56–0.47 (m, 2H), 0.26–0.14 (m, 2H). MS (ESI $^+$ )  $m/z$  253.96  $[\text{M}+\text{H}]^+$ .

**2-Chloro-3-methylpentanoic acid 87.** Non-isolated compound. Please see the synthesis of compounds **83** and **84**.

**2-Chloro-3-cyclohexylpropanoic acid 88.** Non-isolated compound. Please see the synthesis of compound **85**.

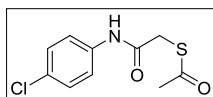
**2-Chloro-3-cyclopropylpropanoic acid 89.** Non-isolated compound. Please see the synthesis of compound **86**.

**2-(Acetylthio)-N-(2'-chlorophenyl)acetamide 90.** Compound **90** was synthesized according to the



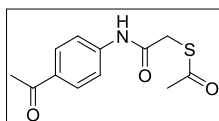
general procedure **GP-5**, using intermediate **41** (397 mg, 1.95 mmol) and potassium thioacetate (276 mg, 2.42 mmol) in acetone (10 mL). The reaction was stirred at room temperature for 2.5 h. After extraction and column chromatography (PE/EtOAc 8:2), **90** was obtained as yellow solid (297 mg, 63%).  $R_f = 0.22$  (PE/EtOAc 8:2).  $^1\text{H NMR}$  (500 MHz,  $\text{CDCl}_3$ )  $\delta$  8.49 (br, 1H), 8.33 (dd,  $J = 1.2, 8.3$  Hz, 1H), 7.36 (dd,  $J = 1.5, 8.1$  Hz, 1H), 7.26 (td,  $J = 1.4, 7.9$  Hz, 1H), 3.74 (s, 2H), 2.46 (s, 3H).  $^{13}\text{C NMR}$  (126 MHz,  $\text{CDCl}_3$ )  $\delta$  195.8, 166.5, 134.6, 129.2, 127.8, 125.1, 123.2, 121.8, 34.3, 30.3. HRMS (ESI)  $m/z$  calculated for  $\text{C}_{10}\text{H}_{11}\text{ClNO}_2\text{S}$  244.0194  $[\text{M}+\text{H}]^+$ , found 244.0186.

**2-(Acetylthio)-N-(4'-chlorophenyl)acetamide 91.** Intermediate **42** (110 mg, 0.539 mmol), thioacetic



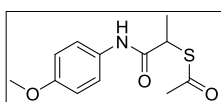
acid (50  $\mu\text{L}$ , 0.71 mmol) and  $\text{Cs}_2\text{CO}_3$  (200 mg, 0.614 mmol) were dissolved in DMF (5 mL) and stirred for 3 h at room temperature. The reaction was diluted with EtOAc (200 mL) and washed with  $\text{H}_2\text{O}$  (3x 100 mL) and saturated NaCl solution (1x 30 mL). The organic layer was dried over  $\text{Na}_2\text{SO}_4$ , filtered and concentrated *in vacuo* until dryness. The crude product was purified using column chromatography (PE/EtOAc 9:1) to give **91** as white solid (112 mg, 85%).  $R_f = 0.37$  (PE/EtOAc 7:3).  $^1\text{H NMR}$  (300 MHz,  $\text{CDCl}_3$ )  $\delta$  8.21 (br, 1 H), 7.45 (d,  $J = 8.8$  Hz, 2H), 7.27 (d,  $J = 8.8$  Hz, 2H), 3.64 (s, 2H), 2.45 (s, 3 H).  $^{13}\text{C NMR}$  (75 MHz,  $\text{CDCl}_3$ )  $\delta$  197.5, 166.5, 136.3, 129.6, 129.1, 121.1, 34.3, 30.4. HRMS (ESI)  $m/z$  calculated for  $\text{C}_{10}\text{H}_{11}\text{ClNO}_2\text{S}$  244.0194  $[\text{M}+\text{H}]^+$ , found 244.0188.

**2-(Acetylthio)-N-(4'-acetylphenyl)acetamide 92.** Intermediate **43** (340 mg, 1.61 mmol), thioacetic



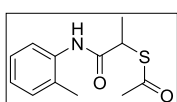
acid (140  $\mu\text{L}$ , 1.99 mmol) and  $\text{Cs}_2\text{CO}_3$  (580 mg, 1.78 mmol) were dissolved in DMF (15 mL) and stirred at room temperature for 3 h. The reaction was diluted with EtOAc (200 mL) and washed with  $\text{H}_2\text{O}$  (3x 100 mL) and saturated NaCl solution (1x 30 mL). The organic layer was dried over  $\text{Na}_2\text{SO}_4$ , filtered and concentrated *in vacuo* until dryness. The crude product was purified using column chromatography ( $\text{CH}_2\text{Cl}_2/\text{MeOH}$  97:3) to give **92** as off-white solid (320 mg, 79%).  $R_f = 0.41$  ( $\text{CH}_2\text{Cl}_2/\text{MeOH}$  9:1).  $^1\text{H NMR}$  (300 MHz,  $\text{DMSO}-d_6$ )  $\delta$  10.58 (s, 1H), 7.93 (d,  $J = 8.8$  Hz, 2H), 7.70 (d,  $J = 8.8$  Hz, 2H), 3.86 (s, 2H), 2.52 (s, 3 H), 2.38 (s, 3H).  $^{13}\text{C NMR}$  (75 MHz,  $\text{DMSO}-d_6$ )  $\delta$  196.5, 194.6, 166.4, 143.1, 131.9, 129.5, 118.4, 34.0, 30.1, 26.4. HRMS (ESI)  $m/z$  calculated for  $\text{C}_{12}\text{H}_{14}\text{ClNO}_3\text{S}$  252.0689  $[\text{M}+\text{H}]^+$ , found 252.0667.

**2-(Acetylthio)-N-(4'-methoxyphenyl)propanamide 93.** Compound **93** was synthesized according to



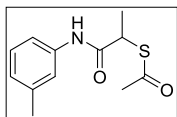
the general procedure **GP-5**, using intermediate **45** (188 mg, 0.880 mmol) and potassium thioacetate (124 mg, 1.09 mmol) in acetone (5 mL). The reaction was stirred at room temperature for 3.5 h. After extraction and column chromatography (PE/EtOAc 8:2), **93** was obtained as white solid (170 mg, 76%). m.p. = 97 °C.  $R_f$  = 0.25 (PE/EtOAc 7:3).  $^1\text{H}$  NMR (500 MHz,  $\text{CDCl}_3$ )  $\delta$  8.09 (br, 1H), 7.42 (d,  $J$  = 9.0 Hz, 2H), 6.84 (d,  $J$  = 9.0 Hz, 2H), 4.17 (q,  $J$  = 7.3 Hz, 1H), 3.78 (s, 3H), 2.39 (s, 3H), 1.52 (d,  $J$  = 7.3 Hz, 3H).  $^{13}\text{C}$  NMR (126 MHz,  $\text{CDCl}_3$ )  $\delta$  198.1, 169.2, 156.5, 131.2, 121.5, 114.3, 55.6, 41.5, 30.4, 15.5. HRMS (ESI)  $m/z$  calculated for  $\text{C}_{12}\text{H}_{16}\text{NO}_3\text{S}$  254.0845  $[\text{M}+\text{H}]^+$ , found 254.0837.

**2-(Acetylthio)-N-(o-tolyl)propanamide 94.** Compound **94** was synthesized according to the general



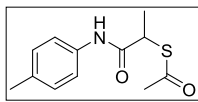
procedure **GP-5**, using intermediate **46** (187 mg, 0.946 mmol) and potassium thioacetate (131 mg, 1.15 mmol) in acetone (5 mL). The reaction was stirred at room temperature for 3 h. After extraction and column chromatography (PE/EtOAc 8:2), **94** was obtained as yellow solid (198 mg, 88%). m.p. = 85 °C.  $R_f$  = 0.34 (PE/EtOAc 7:3).  $^1\text{H}$  NMR (500 MHz,  $\text{CDCl}_3$ )  $\delta$  8.00 (br, 1H), 7.96 (d,  $J$  = 8.2 Hz, 1H), 7.19 (t,  $J$  = 8.4 Hz, 1H), 7.16 (d,  $J$  = 7.5 Hz, 1H), 7.04 (td,  $J$  = 1.1, 7.5 Hz, 1H), 4.25 (q,  $J$  = 7.3 Hz, 1H), 2.40 (s, 3H), 2.25 (s, 3H), 1.54 (d,  $J$  = 7.3 Hz, 3H).  $^{13}\text{C}$  NMR (126 MHz,  $\text{CDCl}_3$ )  $\delta$  197.9, 169.5, 136.0, 130.5, 128.3, 126.8, 124.9, 122.1, 41.3, 30.3, 17.8, 15.4. HRMS (ESI)  $m/z$  calculated for  $\text{C}_{12}\text{H}_{16}\text{NO}_2\text{S}$  238.0896  $[\text{M}+\text{H}]^+$ , found 238.0888.

**2-(Acetylthio)-N-(m-tolyl)propanamide 95.** Compound **95** was synthesized according to the general



procedure **GP-5**, using intermediate **47** (264 mg, 1.34 mmol) and potassium thioacetate (190 mg, 1.66 mmol) in acetone (15 mL). The reaction was stirred at room temperature for 2.5 h. After extraction and column chromatography (PE/EtOAc 9:1), **95** was obtained as yellow oil (288 mg, 91%).  $R_f$  = 0.44 (PE/EtOAc 7:3).  $^1\text{H}$  NMR (500 MHz,  $\text{CDCl}_3$ )  $\delta$  8.16 (br, 1H), 7.36 (s, 1H), 7.30 (d,  $J$  = 8.1 Hz, 1H), 7.19 (d,  $J$  = 7.8 Hz, 1H), 6.91 (d,  $J$  = 7.6 Hz, 1H), 4.18 (q,  $J$  = 7.3 Hz, 1H), 2.40 (s, 3H), 2.32 (s, 3H), 1.52 (d,  $J$  = 7.3 Hz, 3H).  $^{13}\text{C}$  NMR (126 MHz,  $\text{CDCl}_3$ )  $\delta$  198.2, 169.4, 130.1, 137.9, 128.9, 125.2, 120.4, 116.9, 41.5, 30.4, 21.6, 15.4. HRMS (ESI)  $m/z$  calculated for  $\text{C}_{12}\text{H}_{16}\text{NO}_2\text{S}$  238.0896  $[\text{M}+\text{H}]^+$ , found 238.0892.

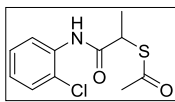
**2-(Acetylthio)-N-(p-tolyl)propanamide 96.** Compound **96** was synthesized according to the general



procedure **GP-5**, using intermediate **48** (135 mg, 0.683 mmol) and potassium thioacetate (97 mg, 0.85 mmol) in acetone (5 mL). The reaction was stirred at room temperature for 3 h. After extraction and column chromatography (PE/EtOAc 85:15), **96** was obtained as yellow solid (134 mg, 86%). m.p. = 87 °C.  $R_f$  = 0.32 (PE/EtOAc 7:3).  $^1\text{H}$  NMR (300 MHz,  $\text{CDCl}_3$ )  $\delta$  8.13 (br, 1H), 7.39 (d,  $J$  = 8.4 Hz, 2H), 7.11 (d,  $J$  = 8.1 Hz, 2H), 4.18 (q,  $J$  = 7.3 Hz, 1H), 2.40 (s, 3H), 2.30 (s, 3H), 1.52 (d,  $J$  = 7.3 Hz, 3H).  $^{13}\text{C}$  NMR (75 MHz,  $\text{CDCl}_3$ )  $\delta$

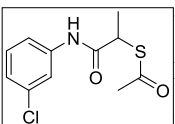
198.2, 169.3, 135.5, 134.1, 129.6, 119.8, 41.5, 30.4, 21.0, 15.4. HRMS (ESI)  $m/z$  calculated for  $C_{12}H_{16}NO_2S$  238.0896  $[M+H]^+$ , found 238.0889.

**2-(Acetylthio)-*N*-(2'-chlorophenyl)propanamide 97.** Compound **97** was synthesized according to



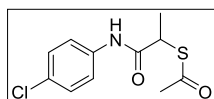
the general procedure **GP-5**, using intermediate **49** (187 mg, 0.857 mmol) and potassium thioacetate (120 mg, 1.05 mmol) in acetone (5 mL). The reaction was stirred at room temperature for 2.5 h. After extraction and column chromatography (PE/EtOAc 9:1), **97** was obtained as yellow oil (173 mg, 78%).  $R_f = 0.41$  (PE/EtOAc 7:3).  $^1H$  NMR (300 MHz,  $CDCl_3$ )  $\delta$  8.52 (br, 1H), 8.35 (dd,  $J = 1.4, 8.3$  Hz, 1H), 7.36 (dd,  $J = 1.5, 8.0$  Hz, 1H), 7.26 (td,  $J = 1.4, 7.9$  Hz, 1H), 7.03 (td,  $J = 1.5, 7.9$  Hz, 1H), 4.30 (q,  $J = 7.3$  Hz, 1H), 2.42 (s, 3H), 1.56 (d,  $J = 7.3$  Hz, 3H).  $^{13}C$  NMR (126 MHz,  $CDCl_3$ )  $\delta$  196.7, 169.8, 134.8, 129.3, 127.7, 124.9, 123.2, 121.8, 41.6, 30.3, 15.7. HRMS (ESI)  $m/z$  calculated for  $C_{12}H_{13}ClNO_2S$  258.0350  $[M+H]^+$ , found 258.0338.

**2-(Acetylthio)-*N*-(3'-chlorophenyl)propanamide 98.** Compound **98** was synthesized according to



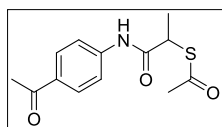
the general procedure **GP-5**, using intermediate **50** (116 mg, 0.532 mmol) and potassium thioacetate (77 mg, 0.67 mmol) in acetone (5 mL). The reaction was stirred at room temperature for 3.5 h. After extraction and column chromatography (PE/EtOAc 85:15), **98** was obtained as yellow oil (119 mg, 87%).  $R_f = 0.33$  (PE/EtOAc 7:3).  $^1H$  NMR (300 MHz,  $CDCl_3$ )  $\delta$  8.31 (br, 1H), 7.63 (t,  $J = 2.0$  Hz, 1H), 7.35 (ddd,  $J = 1.0, 2.0, 8.2$  Hz, 1H), 7.22 (t,  $J = 8.0$  Hz, 1H), 7.07 (ddd,  $J = 1.0, 2.0, 7.9$  Hz, 1H), 4.17 (q,  $J = 7.3$  Hz, 1H), 2.42 (s, 3H), 1.52 (d,  $J = 7.3$  Hz, 3H).  $^{13}C$  NMR (75 MHz,  $CDCl_3$ )  $\delta$  198.6, 169.6, 139.1, 134.8, 130.1, 124.4, 119.9, 117.7, 41.4, 30.4, 15.1. HRMS (ESI)  $m/z$  calculated for  $C_{12}H_{13}ClNO_2S$  258.0350  $[M+H]^+$ , found 258.0344.

**2-(Acetylthio)-*N*-(4'-chlorophenyl)propanamide 99.** Compound **99** was synthesized according to



the general procedure **GP-5**, using intermediate **51** (200 mg, 0.917 mmol) and potassium thioacetate (128 mg, 1.12 mmol) in acetone (5 mL). The reaction was stirred at room temperature for 3.5 h. After extraction and column chromatography (PE/EtOAc 8:2), **99** was obtained as off-white solid (198 mg, 84%).  $R_f = 0.33$  (PE/EtOAc 7:3).  $^1H$  NMR (500 MHz,  $CDCl_3$ )  $\delta$  8.28 (s, 1H), 7.46 (d,  $J = 8.9$  Hz, 2H), 7.26 (d,  $J = 8.9$  Hz, 2H), 4.17 (q,  $J = 7.3$  Hz, 1H), 2.41 (s, 3H), 1.52 (d,  $J = 7.3$  Hz, 3H).  $^{13}C$  NMR (126 MHz,  $CDCl_3$ )  $\delta$  198.5, 169.5, 136.6, 129.4, 129.1, 121.0, 41.4, 30.4, 15.2. HRMS (ESI)  $m/z$  calculated for  $C_{12}H_{13}ClNO_2S$  258.0350  $[M+H]^+$ , found 258.0351.

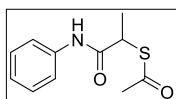
**2-(Acetylthio)-*N*-(4'-acetylphenyl)propanamide 100.** Intermediate **52** (305 mg, 1.35 mmol),



thioacetic acid (100  $\mu$ L, 1.42 mmol) and  $Cs_2CO_3$  (481 mg, 1.48 mmol) were dissolved in DMF (5 mL) and stirred at room temperature for 70 min. The reaction was diluted with EtOAc (200 mL) and washed with  $H_2O$  (3x 100 mL) and saturated NaCl solution (1x 30 mL). The organic layer was dried over  $Na_2SO_4$ , filtered and concentrated *in vacuo* until dryness. The crude product was purified using column chromatography

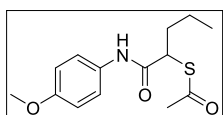
(PE/EtOAc 8:2) to give **100** as white solid (310 mg, 86%). m.p. = 89 °C.  $R_f$  = 0.19 (PE/EtOAc 7:3).  $^1\text{H NMR}$  (500 MHz,  $\text{CDCl}_3$ )  $\delta$  8.52 (br, 1H), 7.93 (d,  $J$  = 8.8 Hz, 2H), 7.61 (d,  $J$  = 8.8 Hz, 2H), 4.20 (q,  $J$  = 7.3 Hz, 1H), 2.57 (s, 3H), 2.42 (s, 3H), 1.53 (d,  $J$  = 7.3 Hz, 3H).  $^{13}\text{C NMR}$  (126 MHz,  $\text{CDCl}_3$ )  $\delta$  198.7, 197.0, 169.8, 142.3, 133.1, 129.9, 119.1, 41.5, 30.4, 26.6, 15.1. HRMS (ESI)  $m/z$  calculated for  $\text{C}_{13}\text{H}_{16}\text{NO}_3\text{S}$  266.0845  $[\text{M}+\text{H}]^+$ , found 266.0840.

**2-(Acetylthio)-*N*-phenylpropanamide 101.** Compound **101** was synthesized according to the general



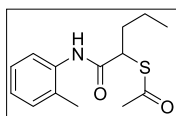
procedure **GP-5**, using intermediate **53** (206 mg, 1.12 mmol) and potassium thioacetate (168 mg, 1.47 mmol) in acetone (5 mL). The reaction was stirred at room temperature for 2.5 h. After extraction and column chromatography (PE/EtOAc 9:1), **101** was obtained as white solid (220 mg, 88%).  $R_f$  = 0.39 (PE/EtOAc 7:3).  $^1\text{H NMR}$  (500 MHz,  $\text{CD}_3\text{OD}$ )  $\delta$  7.53 (d,  $J$  = 7.6 Hz, 2H), 7.30 (t,  $J$  = 7.9 Hz, 2H), 7.09 (t,  $J$  = 7.4 Hz, 1H), 4.32 (q,  $J$  = 7.2 Hz, 1H), 2.35 (s, 3H), 1.52 (d,  $J$  = 7.2 Hz, 3H).  $^{13}\text{C NMR}$  (126 MHz,  $\text{CD}_3\text{OD}$ )  $\delta$  196.4, 172.2, 139.4, 129.7, 125.5, 121.3, 44.4, 30.2, 18.1. HRMS (ESI)  $m/z$  calculated for  $\text{C}_{11}\text{H}_{14}\text{NO}_2\text{S}$  224.0740  $[\text{M}+\text{H}]^+$ , found 224.0729.

**2-(Acetylthio)-*N*-(4'-methoxyphenyl)pentanamide 102.** Compound **102** was synthesized according



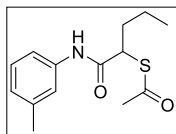
to the general procedure **GP-5**, using intermediate **61** (185 mg, 0.640 mmol) and potassium thioacetate (95 mg, 0.83 mmol) in acetone (5 mL). The reaction was stirred at room temperature for 6 h. After extraction and column chromatography (PE/EtOAc 9:1), **102** was obtained as yellow solid (157 mg, 87%). m.p. = 100 °C.  $R_f$  = 0.33 (PE/EtOAc 7:3).  $^1\text{H NMR}$  (300 MHz,  $\text{CDCl}_3$ )  $\delta$  7.97 (br, 1H), 7.43 (d,  $J$  = 9.0 Hz, 2H), 6.84 (d,  $J$  = 9.0 Hz, 2H), 4.02 (t,  $J$  = 7.6 Hz, 1H), 3.78 (s, 3H), 2.40 (s, 3H), 2.13–2.01 (m, 1H), 1.75–1.63 (m, 1H), 1.52–1.39 (m, 2H), 0.95 (t,  $J$  = 7.3 Hz, 3H).  $^{13}\text{C NMR}$  (75 MHz,  $\text{CDCl}_3$ )  $\delta$  197.9, 168.9, 156.5, 131.1, 121.5, 114.2, 55.6, 46.8, 31.7, 30.5, 20.7, 13.8. HRMS (ESI)  $m/z$  calculated for  $\text{C}_{14}\text{H}_{20}\text{NO}_3\text{S}$  282.1158  $[\text{M}+\text{H}]^+$ , found 282.1151.

**2-(Acetylthio)-*N*-(*o*-tolyl)pentanamide 103.** Compound **103** was synthesized according to the



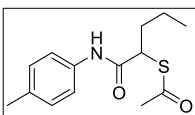
general procedure **GP-5**, using intermediate **62** (144 mg, 0.533 mmol) and potassium thioacetate (85 mg, 0.74 mmol) in acetone (5 mL). The reaction was stirred at room temperature for 2.5 h. After extraction and column chromatography (PE/EtOAc 9:1), **103** was obtained as white solid (129 mg, 91%). m.p. = 87 °C.  $R_f$  = 0.39 (PE/EtOAc 7:3).  $^1\text{H NMR}$  (300 MHz,  $\text{CDCl}_3$ )  $\delta$  7.96 (d,  $J$  = 8.1 Hz, 1H), 7.91 (br, 1H), 7.23–7.15 (m, 2H), 7.04 (td,  $J$  = 1.0, 7.4 Hz, 1H), 4.10 (dd,  $J$  = 7.6 Hz, 1H), 2.41 (s, 3H), 2.26 (s, 3H), 2.16–2.04 (m, 1H), 1.78–1.66 (m, 1H), 1.53–1.44 (m, 2H), 0.97 (t,  $J$  = 7.3 Hz, 3H).  $^{13}\text{C NMR}$  (75 MHz,  $\text{CDCl}_3$ )  $\delta$  197.8, 169.2, 136.0, 130.6, 128.3, 126.9, 124.9, 122.2, 46.7, 31.6, 30.5, 20.8, 17.9, 13.9. HRMS (ESI)  $m/z$  calculated for  $\text{C}_{14}\text{H}_{20}\text{NO}_2\text{S}$  266.1209  $[\text{M}+\text{H}]^+$ , found 266.1201.

**2-(Acetylthio)-N-(*m*-tolyl)pentanamide 104.** Compound **104** was synthesized according to the



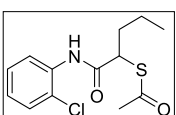
general procedure **GP-5**, using intermediate **63** (152 mg, 0.563 mmol) and potassium thioacetate (83 mg, 0.73 mmol) in acetone (5 mL). The reaction was stirred at room temperature for 2.5 h. After extraction and column chromatography (PE/EtOAc 85:15), **104** was obtained as yellow oil (117 mg, 75%).  $R_f = 0.42$  (PE/EtOAc 7:3).  $^1\text{H NMR}$  (300 MHz,  $\text{CDCl}_3$ )  $\delta$  8.06 (br, 1H), 7.38 (s, 1H), 7.30 (d,  $J = 8.3$  Hz, 1H), 7.19 (t,  $J = 7.8$  Hz, 1H), 6.91 (d,  $J = 7.5$  Hz, 1H), 4.03 (t,  $J = 7.6$  Hz, 1H), 2.40 (s, 3H), 2.33 (s, 3H), 2.14–2.01 (m, 1H), 1.75–1.63 (m, 1H), 1.53–1.40 (m, 2H), 0.95 (t,  $J = 7.3$  Hz, 3H).  $^{13}\text{C NMR}$  (75 MHz,  $\text{CDCl}_3$ )  $\delta$  198.0, 169.0, 139.0, 137.9, 128.9, 125.2, 120.4, 116.8, 46.8, 31.6, 30.5, 21.6, 20.7, 13.8. HRMS (ESI)  $m/z$  calculated for  $\text{C}_{14}\text{H}_{20}\text{NO}_2\text{S}$  266.1209  $[\text{M}+\text{H}]^+$ , found 266.1202.

**2-(Acetylthio)-N-(*p*-tolyl)pentanamide 105.** Compound **105** was synthesized according to the



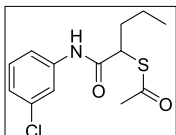
general procedure **GP-5**, using intermediate **64** (143 mg, 0.529 mmol) and potassium thioacetate (75 mg, 0.66 mmol) in acetone (5 mL). The reaction was stirred at room temperature for 5 h. After extraction and radial chromatography (PE/EtOAc 10:0  $\rightarrow$  9:1), **105** was obtained as yellow solid (123 mg, 88%). m.p. = 106 °C.  $R_f = 0.46$  (PE/EtOAc 7:3).  $^1\text{H NMR}$  (300 MHz,  $\text{CDCl}_3$ )  $\delta$  8.03 (br, 1H), 7.40 (d,  $J = 8.5$  Hz, 2H), 7.11 (d,  $J = 8.2$  Hz, 2H), 4.03 (dd,  $J = 7.1, 8.1$  Hz, 1H), 2.40 (s, 3H), 2.30 (s, 3H), 2.13–2.01 (m, 1H), 1.75–1.63 (m, 1H), 1.53–1.39 (m, 2H), 0.95 (t,  $J = 7.3$  Hz, 3H).  $^{13}\text{C NMR}$  (75 MHz,  $\text{CDCl}_3$ )  $\delta$  198.0, 169.0, 135.4, 134.1, 129.6, 119.8, 46.8, 31.7, 30.5, 21.0, 20.7, 13.8. HRMS (ESI)  $m/z$  calculated for  $\text{C}_{14}\text{H}_{20}\text{NO}_2\text{S}$  266.1209  $[\text{M}+\text{H}]^+$ , found 266.1201.

**2-(Acetylthio)-N-(2'-chlorophenyl)pentanamide 106.** Compound **106** was synthesized according to



the general procedure **GP-5**, using intermediate **65** (116 mg, 0.400 mmol) and potassium thioacetate (60 mg, 0.53 mmol) in acetone (5 mL). The reaction was stirred at room temperature for 3.5 h. After extraction and radial chromatography (PE/EtOAc 9:1), **106** was obtained as yellow oil (104 mg, 91%).  $R_f = 0.46$  (PE/EtOAc 7:3).  $^1\text{H NMR}$  (300 MHz,  $\text{CDCl}_3$ )  $\delta$  8.45 (br, 1H), 8.36 (dd,  $J = 1.4, 8.3$  Hz, 1H), 7.36 (dd,  $J = 1.4, 8.0$  Hz, 1H), 7.25 (td,  $J = 1.3, 7.9$  Hz, 1H), 7.04 (td,  $J = 1.5, 7.7$  Hz, 1H), 4.15 (t,  $J = 7.5$  Hz, 1H), 3.78 (s, 3H), 2.41 (s, 3H), 2.14–2.02 (m, 1H), 1.80–1.68 (m, 1H), 1.57–1.42 (m, 2H), 0.96 (t,  $J = 7.3$  Hz, 3H).  $^{13}\text{C NMR}$  (75 MHz,  $\text{CDCl}_3$ )  $\delta$  196.6, 169.5, 134.8, 129.2, 127.7, 124.9, 123.2, 121.8, 47.0, 31.9, 30.5, 20.7, 13.8. HRMS (ESI)  $m/z$  calculated for  $\text{C}_{13}\text{H}_{17}\text{ClNO}_2\text{S}$  286.0663  $[\text{M}+\text{H}]^+$ , found 286.0652.

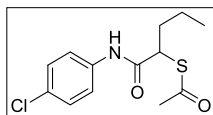
**2-(Acetylthio)-N-(3'-chlorophenyl)pentanamide 107.** Compound **107** was synthesized according to



the general procedure **GP-5**, using intermediate **66** (131 mg, 0.451 mmol) and potassium thioacetate (66 mg, 0.58 mmol) in acetone (7 mL). The reaction was stirred at room temperature for 5 h. After extraction and column chromatography (PE/EtOAc 9:1), **107** was obtained as yellow oil (100 mg, 78%).  $R_f = 0.56$  (PE/EtOAc 7:3).  $^1\text{H NMR}$  (300 MHz,  $\text{CDCl}_3$ )  $\delta$  8.18 (br, 1H), 7.65 (t,  $J = 2.0$  Hz, 1H), 7.35 (ddd,

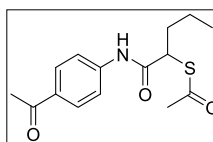
$J = 1.0, 1.9, 8.2$  Hz, 1H), 7.22 (t,  $J = 8.1$  Hz, 1H), 7.07 (ddd,  $J = 0.9, 1.9, 7.9$  Hz, 1H), 4.02 (dd,  $J = 7.3, 8.0$  Hz, 1H), 2.42 (s, 3H), 2.13–2.01 (m, 1H), 1.75–1.65 (m, 1H), 1.52–1.40 (m, 2H), 0.96 (t,  $J = 7.3$  Hz, 3H).  $^{13}\text{C}$  NMR (75 MHz,  $\text{CDCl}_3$ )  $\delta$  169.3, 139.1, 130.1, 124.5, 119.9, 117.8, 46.7, 31.4, 30.5, 20.7, 13.8. HRMS (ESI)  $m/z$  calculated for  $\text{C}_{13}\text{H}_{17}\text{ClNO}_2\text{S}$  286.0663  $[\text{M}+\text{H}]^+$ , found 286.0647.

**2-(Acetylthio)-*N*-(4'-chlorophenyl)pentanamide 108.** Compound **108** was synthesized according to



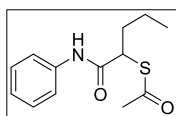
the general procedure **GP-5**, using intermediate **67** (134 mg, 0.461 mmol) and potassium thioacetate (69 mg, 0.60 mmol) in acetone (5 mL). The reaction was stirred at room temperature for 2 h. After extraction, **108** was obtained without further purification as white solid (127 mg, 96%).  $^1\text{H}$  NMR (300 MHz,  $\text{CDCl}_3$ )  $\delta$  8.17 (br, 1H), 7.47 (d,  $J = 8.9$  Hz, 2H), 7.26 (d,  $J = 8.9$  Hz, 2H), 4.02 (dd,  $J = 7.2, 8.0$  Hz, 1H), 2.41 (s, 3H), 2.13–2.00 (m, 1H), 1.75–1.63 (m, 1H), 1.52–1.39 (m, 2H), 0.95 (t,  $J = 7.3$  Hz, 3H).  $^{13}\text{C}$  NMR (75 MHz,  $\text{CDCl}_3$ )  $\delta$  198.3, 169.2, 136.5, 129.4, 129.1, 121.0, 46.7, 31.4, 30.5, 20.7, 13.8.

**2-(Acetylthio)-*N*-(4'-acetylphenyl)pentanamide 109.** Intermediate **68** (119 mg, 0.400 mmol),



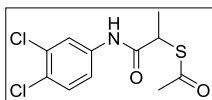
thioacetic acid (35  $\mu\text{L}$ , 0.50 mmol) and  $\text{Cs}_2\text{CO}_3$  (151 mg, 0.463 mmol) were dissolved in DMF (6 mL) and stirred at room temperature for 3.5 h. The reaction was diluted with EtOAc (150 mL) and washed with  $\text{H}_2\text{O}$  (3x 100 mL) and saturated NaCl solution (1x 30 mL). The organic layer was dried over  $\text{Na}_2\text{SO}_4$ , filtered, and concentrated *in vacuo* until dryness. The crude product was purified using column chromatography (PE/EtOAc 8:2) to give **109** as white solid (95 mg, 81%). m.p. = 121  $^\circ\text{C}$ .  $R_f = 0.13$  (PE/EtOAc 8:2).  $^1\text{H}$  NMR (500 MHz,  $\text{DMSO}-d_6$ )  $\delta$  10.65 (s, 1H), 7.93 (d,  $J = 8.8$  Hz, 2H), 7.53 (d,  $J = 8.8$  Hz, 2H), 4.27 (dd,  $J = 6.9, 8.0$  Hz, 1H), 2.52 (s, 3H), 2.36 (s, 3H), 1.92–1.84 (m, 1H), 1.68–1.61 (m, 1H), 1.42–1.26 (m, 2H), 0.89 (t,  $J = 7.4$  Hz, 3H).  $^{13}\text{C}$  NMR (126 MHz,  $\text{DMSO}-d_6$ )  $\delta$  196.5, 194.5, 169.4, 143.0, 132.1, 129.5, 118.7, 47.9, 34.6, 30.3, 26.5, 20.0, 13.5. HRMS (ESI)  $m/z$  calculated for  $\text{C}_{15}\text{H}_{20}\text{NO}_3\text{S}$  294.1158  $[\text{M}+\text{H}]^+$ , found 294.1149.

**2-(Acetylthio)-*N*-phenylpentanamide 110.** Compound **110** was synthesized according to the general



procedure **GP-5**, using intermediate **69** (138 mg, 0.539 mmol) and potassium thioacetate (76 mg, 0.67 mmol) in acetone (5 mL). The reaction was stirred at room temperature for 4 h. After extraction and column chromatography (PE/EtOAc 9:1), **110** was obtained as white solid (116 mg, 86%). m.p. = 98  $^\circ\text{C}$ .  $R_f = 0.41$  (PE/EtOAc 7:3).  $^1\text{H}$  NMR (300 MHz,  $\text{CDCl}_3$ )  $\delta$  8.11 (br, 1H), 7.52 (d,  $J = 8.7$  Hz, 2H), 7.31 (t,  $J = 8.0$  Hz, 2H), 7.10 (t,  $J = 7.4$  Hz, 1H), 4.04 (dd,  $J = 7.2, 8.0$  Hz, 1H), 2.40 (s, 3H), 2.14–2.02 (m, 1H), 1.76–1.64 (m, 1H), 1.53–1.40 (m, 2H), 0.96 (t,  $J = 7.3$  Hz, 3H).  $^{13}\text{C}$  NMR (75 MHz,  $\text{CDCl}_3$ )  $\delta$  198.1, 169.1, 138.0, 129.1, 124.4, 119.8, 46.8, 31.6, 30.5, 20.7, 13.8. HRMS (ESI)  $m/z$  calculated for  $\text{C}_{13}\text{H}_{18}\text{NO}_2\text{S}$  252.1053  $[\text{M}+\text{H}]^+$ , found 252.1046.

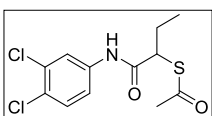
**2-(Acetylthio)-N-(3',4'-dichlorophenyl)propanamide 111.** Compound **111** was synthesized



according to the general procedure **GP-5**, using intermediate **44** (132 mg, 0.520 mmol) and potassium thioacetate (79 mg, 0.69 mmol) in acetone (5 mL).

The reaction was stirred at room temperature for 2.5 h. After extraction and column chromatography (PE/EtOAc 9:1), **111** was obtained as yellow oil (128 mg, 84%).  $R_f = 0.36$  (PE/EtOAc 7:3).  $^1\text{H NMR}$  (500 MHz,  $\text{CDCl}_3$ )  $\delta$  8.36 (br, 1H), 7.75 (d,  $J = 2.2$  Hz, 1H), 7.35 (d,  $J = 8.5$  Hz, 1H), 7.33 (dd,  $J = 2.2, 8.7$  Hz, 1H), 4.16 (q,  $J = 7.3$  Hz, 1H), 2.42 (s, 3H), 1.51 (d,  $J = 7.3$  Hz, 3H).  $^{13}\text{C NMR}$  (126 MHz,  $\text{CDCl}_3$ )  $\delta$  198.8, 169.6, 137.5, 132.9, 130.6, 127.6, 121.5, 119.0, 41.4, 30.4, 15.0. HRMS (ESI)  $m/z$  calculated for  $\text{C}_{11}\text{H}_{12}\text{Cl}_2\text{NO}_2\text{S}$  291.9960  $[\text{M}+\text{H}]^+$ , found 291.9943.

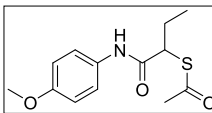
**2-(Acetylthio)-N-(3',4'-dichlorophenyl)butanamide 112.** Compound **112** was synthesized according



to the general procedure **GP-5**, using intermediate **54** (160 mg, 0.515 mmol) and potassium thioacetate (77 mg, 0.67 mmol) in acetone (5 mL). The reaction was

stirred at room temperature for 3.5 h. After extraction and column chromatography (PE/EtOAc 9:1), **112** was obtained as clear oil (142 mg, 90%).  $R_f = 0.30$  (PE/EtOAc 7:3).  $^1\text{H NMR}$  (500 MHz,  $\text{CDCl}_3$ )  $\delta$  8.23 (br, 1H), 7.77 (d,  $J = 2.0$  Hz, 1H), 7.38-7.30 (m, 2H), 3.92 (dd,  $J = 7.2, 7.9$  Hz, 1H), 2.42 (s, 3H), 2.19-2.04 (m, 1H), 1.82-1.68 (m, 1H), 1.05 (t,  $J = 7.4$  Hz, 3H).  $^{13}\text{C NMR}$  (126 MHz,  $\text{CDCl}_3$ )  $\delta$  198.6, 169.2, 137.4, 132.9, 130.6, 127.6, 121.5, 119.0, 48.5, 30.6, 22.8, 12.1. HRMS (ESI)  $m/z$  calculated for  $\text{C}_{12}\text{H}_{14}\text{Cl}_2\text{NO}_2\text{S}$  306.0117  $[\text{M}+\text{H}]^+$ , found 306.0101.

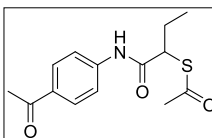
**2-(Acetylthio)-N-(4'-methoxyphenyl)butanamide 113.** Compound **113** was synthesized according to



the general procedure **GP-5**, using intermediate **55** (94 mg, 0.35 mmol) and potassium thioacetate (53 mg, 0.46 mmol) in acetone (5 mL). The reaction was

stirred at room temperature for 3.5 h. After extraction and column chromatography (PE/EtOAc 9:1), **113** was obtained as white solid (81 mg, 88%).  $R_f = 0.14$  (PE/EtOAc 9:1).  $R_f = 0.31$  (PE/EtOAc 7:3).  $^1\text{H NMR}$  (500 MHz,  $\text{CDCl}_3$ )  $\delta$  7.98 (br, 1H), 7.43 (d,  $J = 9.0$  Hz, 2H), 6.84 (d,  $J = 9.0$  Hz, 2H), 3.95 (dd,  $J = 7.3, 7.8$  Hz, 1H), 3.78 (s, 3H), 2.40 (s, 3H), 2.16-2.07 (m, 1H), 1.80-1.71 (m, 1H), 1.05 (t,  $J = 7.3$  Hz, 1H).  $^{13}\text{C NMR}$  (126 MHz,  $\text{CDCl}_3$ )  $\delta$  197.8, 168.8, 156.5, 131.1, 121.5, 114.2, 55.6, 48.7, 30.6, 2336, 12.1. HRMS (ESI)  $m/z$  calculated for  $\text{C}_{13}\text{H}_{18}\text{NO}_3\text{S}$  268.1002  $[\text{M}+\text{H}]^+$ , found 268.0987.

**2-(Acetylthio)-N-(4'-acetylphenyl)butanamide 114.** Intermediate **56** (135 mg, 0.475 mmol),



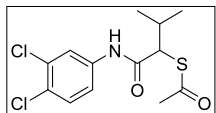
thioacetic acid (35  $\mu\text{L}$ , 0.50 mmol) and  $\text{Cs}_2\text{CO}_3$  (172 mg, 0.528 mmol) were dissolved in DMF (10 mL) and stirred at room temperature for 2.5 h. The reaction

was diluted with EtOAc (200 mL) and washed with  $\text{H}_2\text{O}$  (3x 100 mL) and saturated NaCl solution (1x 30 mL). The organic layer was dried over  $\text{Na}_2\text{SO}_4$ , filtered, and concentrated *in vacuo* until dryness. The crude product was purified using column chromatography (PE/EtOAc 8:2) to give **114** as white solid (137 mg, quant.).  $R_f = 0.29$  (PE/EtOAc 6:4).  $^1\text{H NMR}$  (500 MHz,  $\text{CDCl}_3$ )  $\delta$  8.42 (br, 1H), 7.92 (d,  $J = 8.8$  Hz, 2H), 7.62 (d,  $J = 8.8$  Hz, 2H),



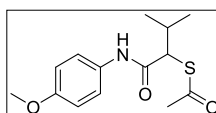
3.97 (dd,  $J = 7.2, 7.9$  Hz, 1H), 2.57 (s, 3H), 2.42 (s, 3H), 2.17–2.08 (m, 1H), 1.81–1.72 (m, 1H), 1.06 (t,  $J = 7.3$  Hz, 1H).  $^{13}\text{C}$  NMR (126 MHz,  $\text{CDCl}_3$ )  $\delta$  198.4, 197.0, 169.4, 142.2, 133.1, 129.8, 119.1, 48.7, 30.6, 26.6, 22.9, 12.1. HRMS (ESI)  $m/z$  calculated for  $\text{C}_{14}\text{H}_{18}\text{NO}_3\text{S}$  280.1002  $[\text{M}+\text{H}]^+$ , found 280.0995.

**2-(Acetylthio)-*N*-(3',4'-dichlorophenyl)-3-methylbutanamide 115.** Compound **115** was synthesized



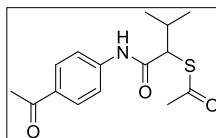
according to the general procedure **GP-5**, using intermediate **57** (184 mg, 0.566 mmol) and potassium thioacetate (84 mg, 0.74 mmol) in acetone (5 mL). The reaction was stirred at room temperature for 2.5 h. After extraction and column chromatography (PE/EtOAc 9:1), **115** was obtained as white solid (125 mg, 69%).  $R_f = 0.48$  (PE/EtOAc 7:3).  $^1\text{H}$  NMR (500 MHz,  $\text{CDCl}_3$ )  $\delta$  8.06 (br, 1H), 7.77 (d,  $J = 2.3$  Hz, 1H), 7.35 (d,  $J = 8.7$  Hz, 1H), 7.32 (dd,  $J = 2.3, 8.7$  Hz, 1H), 3.79 (d,  $J = 8.5$  Hz, 1H), 2.43 (s, 3H), 2.45 (dq,  $J = 6.7, 6.7, 8.5$  Hz, 1H), 1.09 (d,  $J = 6.7$  Hz, 3H), 1.07 (d,  $J = 6.8$  Hz, 3H).  $^{13}\text{C}$  NMR (126 MHz,  $\text{CDCl}_3$ )  $\delta$  197.7, 169.3, 137.3, 132.9, 130.6, 127.7, 121.6, 119.1, 54.7, 30.8, 28.5, 21.2, 20.1. HRMS (ESI)  $m/z$  calculated for  $\text{C}_{13}\text{H}_{16}\text{Cl}_2\text{NO}_2\text{S}$  320.0273  $[\text{M}+\text{H}]^+$ , found 320.0258.

**2-(Acetylthio)-*N*-(4'-methoxyphenyl)-3-methylbutanamide 116.** Compound **116** was synthesized



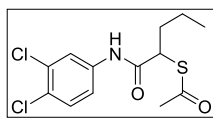
according to the general procedure **GP-5**, using intermediate **58** (195 mg, 0.681 mmol) and potassium thioacetate (101 mg, 0.884 mmol) in acetone (5 mL). The reaction was stirred at room temperature for 3 h. After extraction and column chromatography (PE/EtOAc 9:1), **116** was obtained as white solid (177 mg, 92%).  $R_f = 0.28$  (PE/EtOAc 7:3).  $^1\text{H}$  NMR (500 MHz,  $\text{CDCl}_3$ )  $\delta$  7.83 (br, 1H), 7.42 (d,  $J = 9.0$  Hz, 2H), 6.84 (d,  $J = 9.0$  Hz, 2H), 3.81 (d,  $J = 8.5$  Hz, 1H), 3.78 (s, 3H), 2.41 (s, 3H), 2.40–2.34 (m, 1H), 1.09 (d,  $J = 6.6$  Hz, 3H), 1.06 (d,  $J = 6.7$  Hz, 3H).  $^{13}\text{C}$  NMR (126 MHz,  $\text{CDCl}_3$ )  $\delta$  197.1, 168.8, 156.6, 131.0, 121.7, 114.3, 55.7, 55.0, 30.8, 28.9, 21.2, 20.1. HRMS (ESI)  $m/z$  calculated for  $\text{C}_{14}\text{H}_{20}\text{NO}_3\text{S}$  282.1158  $[\text{M}+\text{H}]^+$ , found 282.1144.

**2-(Acetylthio)-*N*-(4'-acetylphenyl)-3-methylbutanamide 117.** Intermediate **59** (111 mg,



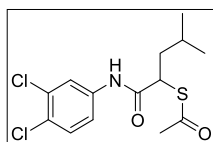
0.372 mmol), thioacetic acid (35  $\mu\text{L}$ , 0.50 mmol) and  $\text{Cs}_2\text{CO}_3$  (135 mg, 0.413 mmol) were dissolved in DMF (6 mL) and stirred at room temperature for 3 h. The reaction was diluted with EtOAc (150 mL) and washed with  $\text{H}_2\text{O}$  (3x 100 mL) and saturated NaCl solution (1x 30 mL). The organic layer was dried over  $\text{Na}_2\text{SO}_4$ , filtered, and concentrated *in vacuo* until dryness. The crude product was purified using column chromatography (PE/EtOAc 10:0  $\rightarrow$  8:2) to give **117** as yellow oil (95 mg, 87%).  $R_f = 0.18$  (PE/EtOAc 7:3).  $^1\text{H}$  NMR (500 MHz,  $\text{CDCl}_3$ )  $\delta$  8.44 (br, 1H), 7.90 (d,  $J = 8.7$  Hz, 2H), 7.62 (d,  $J = 8.8$  Hz, 2H), 3.86 (d,  $J = 8.5$  Hz, 1H), 2.55 (s, 3H), 2.39 (s, 3H), 2.39–2.31 (m, 1H), 1.07 (d,  $J = 6.6$  Hz, 3H), 1.05 (d,  $J = 6.7$  Hz, 3H).  $^{13}\text{C}$  NMR (126 MHz,  $\text{CDCl}_3$ )  $\delta$  197.2, 197.1, 169.5, 142.2, 133.0, 129.8, 119.1, 55.0, 30.7, 28.9, 26.5, 21.1, 20.0. HRMS (ESI)  $m/z$  calculated for  $\text{C}_{15}\text{H}_{20}\text{NO}_3\text{S}$  294.1158  $[\text{M}+\text{H}]^+$ , found 294.1146.

**2-(Acetylthio)-N-(3',4'-dichlorophenyl)pentanamide 118.** Compound **118** was synthesized in two



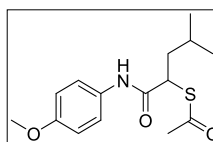
steps. The first step was performed according to the general procedure **GP-3**, using 3,4-dichloroaniline (200 mg, 1.23 mmol), 2-bromovaleric acid (268 mg, 1.48 mmol), EDC·HCl (284 mg, 1.48 mmol) and CH<sub>2</sub>Cl<sub>2</sub> (10 mL). The reaction was stirred at room temperature overnight. The resultant crude product of **60** was used without further purification. The second step was achieved according to the general procedure **GP-5**, using the crude product of **60** obtained from the first step, potassium thioacetate (282 mg, 2.47 mmol) and acetone (10 mL). The reaction was stirred at room temperature for 4 h. The crude product was purified using column chromatography (hexane/EtOAc 95:5 → 80:20) to give **118** as colorless oil (180 mg, 46% (over two steps)). <sup>1</sup>H NMR (500 MHz, DMSO-*d*<sub>6</sub>) δ 10.61 (s, 1H), 7.98 (br, 1H), 7.57 (d, *J* = 9.0 Hz, 1H), 7.49 (d, *J* = 8.5 Hz, 1H), 4.20 (t, *J* = 7.3 Hz, 1H), 2.36 (s, 3H), 1.92–1.78 (m, 1H), 1.70–1.56 (m, 1H), 1.42–1.18 (m, 2H), 0.89 (t, *J* = 7.3 Hz, 3H). <sup>13</sup>C NMR (126 MHz, DMSO-*d*<sub>6</sub>) δ 194.5, 169.4, 138.7, 131.1, 130.8, 125.2, 120.6, 119.4, 47.8, 34.5, 30.3, 20.0, 13.5. HRMS (ESI) *m/z* calculated for C<sub>13</sub>H<sub>16</sub>Cl<sub>2</sub>NO<sub>2</sub>S [M+H]<sup>+</sup> 320.0279, found 320.0272.

**2-(Acetylthio)-N-(3',4'-dichlorophenyl)-3-methylpentanamide 119.** Compound **119** was



synthesized in two steps. The first step was performed according to the general procedure **GP-3**, using 3,4-dichloroaniline (200 mg, 1.23 mmol), 2-bromo-4-methylpentanoic acid (289 mg, 1.48 mmol), EDC·HCl (284 mg, 1.48 mmol) and CH<sub>2</sub>Cl<sub>2</sub> (10 mL). The reaction was stirred at room temperature overnight. The resultant crude product of **70** was used without further purification. The second step was achieved according to the general procedure **GP-5**, using the crude product of **70** obtained from the first step, potassium thioacetate (282 mg, 2.47 mmol) and acetone (10 mL). The reaction was stirred at room temperature for 4 h. The crude product was purified using column chromatography (hexane/EtOAc 95:5 → 80:20) to give **119** as colorless oil (230 mg, 56% (over two steps)). <sup>1</sup>H NMR (500 MHz, DMSO-*d*<sub>6</sub>) δ 10.63 (s, 1H), 7.98 (d, *J* = 2.0 Hz, 1H), 7.57 (d, *J* = 9.0 Hz, 1H), 7.50 (dd, *J* = 2.5, 9.0 Hz, 1H), 4.25 (dd, *J* = 7.0, 8.5 Hz, 1H), 2.36 (s, 3H), 1.88–1.75 (m, 1H), 1.60–1.42 (m, 2H), 0.94 (d, *J* = 6.5 Hz, 3H), 0.87 (d, *J* = 6.0 Hz, 3H). <sup>13</sup>C NMR (126 MHz, DMSO-*d*<sub>6</sub>) δ 194.4, 169.5, 138.8, 131.1, 130.8, 125.2, 120.6, 119.5, 46.3, 41.3, 30.3, 25.9, 22.4, 22.1. HRMS (ESI) *m/z* calculated for C<sub>14</sub>H<sub>18</sub>Cl<sub>2</sub>NO<sub>2</sub>S [M+H]<sup>+</sup> 334.0435, found 334.0426.

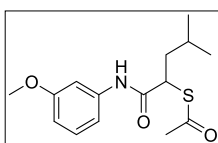
**2-(Acetylthio)-N-(4'-methoxyphenyl)-3-methylpentanamide 120.** Compound **120** was synthesized



in two steps. The first step was performed according to the general procedure **GP-3**, using *p*-anisidine (92 mg, 0.75 mmol), 2-bromo-4-methylpentanoic acid (175 mg, 0.896 mmol), EDC·HCl (172 mg, 0.896 mmol) and CH<sub>2</sub>Cl<sub>2</sub> (5 mL). The reaction was stirred at room temperature for 5.5 h. The resultant crude product of **71** was used without further purification. The second step was achieved according to the general procedure **GP-5**, using the crude product of **71** obtained from the first step, potassium thioacetate

(171 mg, 1.49 mmol) and acetone (7 mL). The reaction was stirred at room temperature for 2.5 h. The crude product was purified using column chromatography (CH<sub>2</sub>Cl<sub>2</sub>) to give **120** as beige solid (149 mg, 68% (over two steps)). m.p. = 69 °C. <sup>1</sup>H NMR (500 MHz, DMSO-*d*<sub>6</sub>) δ 10.18 (s, 1H), 7.49 (d, *J* = 8.5 Hz, 2H), 6.87 (d, *J* = 8.5 Hz, 2H), 4.25 (t, *J* = 7.8 Hz, 1H), 3.71 (s, 3H), 2.35 (s, 3H), 1.88–1.76 (m, 1H), 1.62–1.39 (m, 2H), 0.95 (d, *J* = 6.0 Hz, 3H), 0.88 (d, *J* = 6.5 Hz, 3H). <sup>13</sup>C NMR (126 MHz, DMSO-*d*<sub>6</sub>) δ 194.5, 168.3, 155.5, 131.9, 121.0, 113.9, 55.2, 46.4, 41.8, 30.3, 25.9, 22.6, 22.1. HRMS (ESI) *m/z* calculated for C<sub>15</sub>H<sub>22</sub>NO<sub>3</sub>S [M+H]<sup>+</sup> 296.1320, found 296.1305.

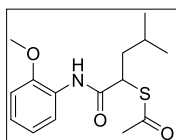
**2-(Acetylthio)-*N*-(3'-methoxyphenyl)-3-methylpentanamide 121.** Compound **121** was synthesized



in two steps. The first step was performed according to the general procedure **GP-3**, using *m*-anisidine (92 mg, 0.75 mmol), 2-bromo-4-methylpentanoic acid (175 mg, 0.896 mmol), EDC·HCl (172 mg, 0.896 mmol) and CH<sub>2</sub>Cl<sub>2</sub> (5 mL).

The reaction was stirred at room temperature for 4.5 h. The resultant crude product of **72** was used in the next step without further purification. The second step was achieved according to the general procedure **GP-5**, using the crude product of **72** obtained from the first step (230 mg), potassium thioacetate (175 mg, 1.53 mmol) and acetone (9 mL). The reaction was stirred at room temperature for 3 h. The crude product was purified using column chromatography (hexane/EtOAc 9:1) to give **121** as pale-yellow oil (136 mg, 61% (over two steps)). <sup>1</sup>H NMR (500 MHz, DMSO-*d*<sub>6</sub>) δ 10.29 (s, 1H), 7.29–7.26 (m, 1H), 7.19 (t, *J* = 8.1 Hz, 1H), 7.15–7.12 (m, 1H), 6.66–6.61 (m, 1H), 4.27 (dd, *J* = 6.6, 8.7 Hz, 1H), 3.71 (s, 3H), 2.34 (s, 3H), 1.86–1.79 (m, 1H), 1.59–1.50 (m, 1H), 1.50–1.43 (m, 1H), 0.94 (d, *J* = 6.6 Hz, 3H), 0.87 (d, *J* = 6.4 Hz, 3H). <sup>13</sup>C NMR (126 MHz, DMSO-*d*<sub>6</sub>) δ 194.4, 168.9, 159.5, 139.9, 129.5, 111.6, 109.2, 105.0, 55.0, 46.4, 41.6, 30.3, 25.9, 22.5, 22.0. MS (ESI<sup>+</sup>) *m/z* 296.03 [M+H]<sup>+</sup>.

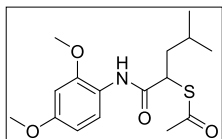
**2-(Acetylthio)-*N*-(2'-methoxyphenyl)-3-methylpentanamide 122.** Compound **122** was synthesized



in two steps. The first step was performed according to the general procedure **GP-3**, using *o*-anisidine (92 mg, 0.75 mmol), 2-bromo-4-methylpentanoic acid (175 mg, 0.896 mmol), EDC·HCl (172 mg, 0.896 mmol) and CH<sub>2</sub>Cl<sub>2</sub> (5 mL). The reaction was stirred at room temperature for 4 h. The resultant crude product of **73** was used in the next step without further purification. The second step was achieved according to the general procedure **GP-5**, using the crude product of **73** obtained from the first step (220 mg), potassium thioacetate (167 mg, 1.46 mmol) and acetone (8 mL). The reaction was stirred at room temperature for 3 h. The crude product was purified using column chromatography (hexane/EtOAc 9:1) to give **122** as pale-yellow oil (142 mg, 64% (over two steps)). <sup>1</sup>H NMR (500 MHz, DMSO-*d*<sub>6</sub>) δ 9.40 (s, 1H), 7.83 (dd, *J* = 1.4, 8.0 Hz, 1H), 7.11–7.06 (m, 1H), 7.05–7.01 (m, 1H), 6.91–6.86 (m, 1H), 4.42 (dd, *J* = 6.9, 8.4 Hz, 1H), 3.81 (s, 3H), 2.36 (s, 3H), 1.86–1.78 (m, 1H), 1.66–1.56 (m, 1H), 1.53–1.45 (m, 1H), 0.94 (d, *J* = 6.6 Hz, 3H), 0.87 (d, *J* = 6.6 Hz, 3H). <sup>13</sup>C NMR (126 MHz, DMSO-*d*<sub>6</sub>) δ 194.7, 168.9,

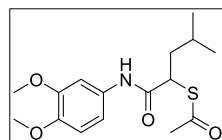
149.9, 126.8, 124.9, 122.1, 120.2, 111.3, 55.8, 45.8, 41.0, 30.3, 25.8, 22.4, 22.2. MS (ESI<sup>+</sup>) *m/z* 296.07 [M+H]<sup>+</sup>.

**2-(Acetylthio)-*N*-(2',4'-dimethoxyphenyl)-4-methylpentanamide 123.** Compound **123** was



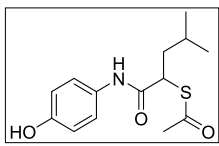
synthesized in two steps. The first step was performed according to the general procedure **GP-3**, using 2,4-dimethoxyaniline (115 mg, 0.748 mmol), 2-bromo-4-methylpentanoic acid (175 mg, 0.897 mmol), EDC·HCl (172 mg, 0.897 mmol) and CH<sub>2</sub>Cl<sub>2</sub> (5 mL). The reaction was stirred at room temperature for 4 h. The resultant crude product of **74** was obtained as dark violet solid (248 mg) and was used in the next step without further purification. The second step was achieved according to the general procedure **GP-5**, using the crude product of **74** (239 mg) obtained from the first step, potassium thioacetate (118 mg, 1.03 mmol) and acetone (5 mL). The reaction was stirred at room temperature for 2 h. The crude product was purified using column chromatography (PE/EtOAc 9:1) to give **123** as pale-yellow oil (143 mg, 59% (over two steps)). *R<sub>f</sub>* = 0.31 (PE/EtOAc 7:3). <sup>1</sup>H NMR (300 MHz, CDCl<sub>3</sub>) δ 8.25 (br, 1H), 8.19 (d, *J* = 8.2 Hz, 1H), 6.45–6.39 (m, 2H), 4.14 (t, *J* = 7.8 Hz, 1H), 3.85 (s, 3H), 3.76 (s, 3H), 2.35 (s, 3H), 2.01–1.91 (m, 1H), 1.76 (sept., *J* = 6.6 Hz, 1H), 1.62–1.53 (m, 1H), 0.95 (d, *J* = 6.5 Hz, 3H), 0.90 (d, *J* = 6.5 Hz, 3H). <sup>13</sup>C NMR (75 MHz, CDCl<sub>3</sub>) δ 196.4, 168.8, 156.7, 149.6, 121.4, 120.8, 103.8, 98.8, 56.0, 55.7, 45.7, 38.8, 30.4, 26.1, 22.5, 22.5. HRMS (ESI) *m/z* calculated for C<sub>16</sub>H<sub>24</sub>NO<sub>4</sub>S 326.1421 [M+H]<sup>+</sup>, found 326.1403.

**2-(Acetylthio)-*N*-(3',4'-dimethoxyphenyl)-4-methylpentanamide 124.** Compound **124** was



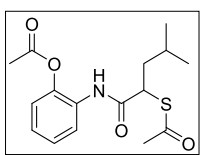
synthesized in two steps. The first step was performed according to the general procedure **GP-3**, using 3,4-dimethoxyaniline (115 mg, 0.748 mmol), 2-bromo-4-methylpentanoic acid (175 mg, 0.897 mmol), EDC·HCl (172 mg, 0.897 mmol) and CH<sub>2</sub>Cl<sub>2</sub> (5 mL). The reaction was stirred at room temperature for 4 h. The resultant crude product of **75** was obtained as dark violet solid (301 mg) and was used in the next step without further purification. The second step was achieved according to the general procedure **GP-5**, using the crude product of **75** (292 mg) obtained from the first step, potassium thioacetate (120 mg, 1.05 mmol) and acetone (5 mL). The reaction was stirred at room temperature for 2.5 h. The crude product was purified using column chromatography (PE/EtOAc 9:1) to give **124** as white solid (230 mg, 95% (over two steps)). *R<sub>f</sub>* = 0.25 (PE/EtOAc 7:3). <sup>1</sup>H NMR (300 MHz, CDCl<sub>3</sub>) δ 8.02 (br, 1H), 7.40 (d, *J* = 2.2 Hz, 1H), 6.87 (dd, *J* = 2.3, 8.6 Hz, 1H), 6.78 (d, *J* = 8.6 Hz, 1H), 4.09 (t, *J* = 7.8 Hz, 1H), 3.88 (s, 3H), 3.85 (s, 3H), 2.40 (s, 3H), 2.01–1.94 (m, 1H), 1.82–1.69 (m, 1H), 1.63–1.53 (m, 1H), 0.97 (d, *J* = 6.5 Hz, 3H), 0.93 (d, *J* = 6.5 Hz, 3H). <sup>13</sup>C NMR (75 MHz, CDCl<sub>3</sub>) δ 198.1, 169.0, 149.2, 146.0, 131.8, 111.5, 111.5, 104.6, 56.3, 56.1, 45.3, 38.2, 30.5, 26.0, 22.5. HRMS (ESI) *m/z* calculated for C<sub>16</sub>H<sub>24</sub>NO<sub>4</sub>S 326.1421 [M+H]<sup>+</sup>, found 326.1413.

**2-(Acetylthio)-N-(4'-hydroxyphenyl)-4-methylpentanamide 125.** Compound **125** was synthesized



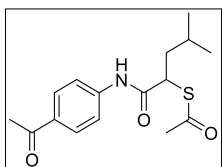
in two steps. The first step was performed according to the general procedure **GP-3**, using 4-aminophenol (82 mg, 0.75 mmol), 2-bromo-4-methylpentanoic acid (175 mg, 0.896 mmol), EDC·HCl (172 mg, 0.896 mmol) and CH<sub>2</sub>Cl<sub>2</sub> (5 mL). The reaction was stirred at room temperature for 4 h. The resultant crude product of **76** was used in the next step without further purification. The second step was achieved according to the general procedure **GP-5**, using the crude product of **76** obtained from the first step (201 mg), potassium thioacetate (112 mg, 0.981 mmol) and acetone (5 mL). The reaction was stirred at room temperature for 4 h. The crude product was purified using column chromatography (PE/EtOAc 9:1 → 7:3) to give **125** as clear colorless oil (140 mg, 66% (over two steps)). <sup>1</sup>H NMR (500 MHz, DMSO-*d*<sub>6</sub>) δ 10.04 (s, 1H), 9.21 (s, 1H), 7.35 (d, *J* = 8.9 Hz, 2H), 6.68 (d, *J* = 8.9 Hz, 2H), 4.34 (dd, *J* = 6.4, 8.9 Hz, 1H), 2.34 (s, 3H), 1.82 (ddd, *J* = 6.0, 8.9, 13.2 Hz, 1H), 1.58–1.50 (m, 1H), 1.48–1.42 (m, 1H), 0.95 (d, *J* = 6.5 Hz, 3H), 0.88 (d, *J* = 6.5 Hz, 3H). <sup>13</sup>C NMR (126 MHz, DMSO-*d*<sub>6</sub>) δ 194.4, 168.0, 153.6, 130.3, 121.1, 115.0, 46.3, 41.8, 30.3, 25.9, 22.6, 22.0. HRMS (ESI) *m/z* calculated for C<sub>14</sub>H<sub>20</sub>NO<sub>3</sub>S 282.1158 [M+H]<sup>+</sup>, found 282.1151.

**2-(Acetylthio)-N-(2'-(acetyloxy)phenyl)-4-methylpentanamide 126.** Compound **126** was



synthesized in two steps. The first step was performed according to the general procedure **GP-3**, using 2-aminophenol (82 mg, 0.75 mmol), 2-bromo-4-methylpentanoic acid (176 mg, 0.901 mmol), EDC·HCl (173 mg, 0.901 mmol) and CH<sub>2</sub>Cl<sub>2</sub> (5 mL). The reaction was stirred at room temperature for 4.5 h. The resultant crude product of **77** was used in the next step without further purification. The second step was achieved according to the general procedure **GP-5**, using the crude product of **77** obtained from the first step (190 mg), potassium thioacetate (152 mg, 1.33 mmol) and acetone (7 mL). The reaction was stirred at room temperature overnight. The crude product was purified using column chromatography (hexane/EtOAc 9:1 → 85:15) to give **126** as yellow oil (36 mg, 15% (over two steps)). <sup>1</sup>H NMR (500 MHz, DMSO-*d*<sub>6</sub>) δ 9.78 (s, 1H), 7.62 (dd, *J* = 1.9, 7.7 Hz, 1H), 7.24–7.12 (m, 3H), 4.36 (dd, *J* = 6.4, 9.2 Hz, 1H), 2.35 (s, 3H), 2.26 (s, 3H), 1.84–1.76 (m, 1H), 1.62–1.53 (m, 1H), 1.49–1.42 (m, 1H), 0.96 (d, *J* = 6.6 Hz, 3H), 0.87 (d, *J* = 6.6 Hz, 3H). <sup>13</sup>C NMR (126 MHz, DMSO-*d*<sub>6</sub>) δ 194.6, 169.0, 168.6, 142.6, 129.7, 125.8, 125.4, 124.8, 123.2, 45.6, 41.2, 30.2, 25.8, 22.6, 22.0, 21.0. MS (ESI<sup>+</sup>) *m/z* 282.01 [M-Ac+H]<sup>+</sup>, 240.00 [M-2Ac+H]<sup>+</sup>.

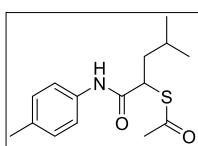
**2-(Acetylthio)-N-(4'-acetylphenyl)-4-methylpentanamide 127.** Compound **127** was synthesized in



two steps. The first step was performed according to the general procedure **GP-3**, using 4-aminoacetophenone (138 mg, 1.02 mmol), 2-bromo-4-methylpentanoic acid (213 mg, 1.09 mmol), EDC·HCl (212 mg, 1.11 mmol) and CH<sub>2</sub>Cl<sub>2</sub> (5 mL). The reaction was stirred at room temperature for 2 d. The resultant crude product of **78** was used in the next step without further purification. The second step was achieved according

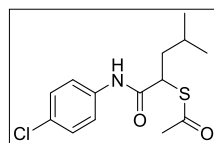
to the general procedure **GP-5**, using the crude product of **78** obtained from the first step, potassium thioacetate (151 mg, 1.32 mmol) and acetone (5 mL). The reaction was stirred at room temperature for 3 h. The crude product was purified using column chromatography (PE/EtOAc 9:1) to give **127** as white solid (162 mg, 52% (over two steps)).  $R_f = 0.28$  (PE/EtOAc 7:3).  $^1\text{H NMR}$  (500 MHz,  $\text{CDCl}_3$ )  $\delta$  8.41 (s, 1H), 7.93 (d,  $J = 8.8$  Hz, 2H), 7.62 (d,  $J = 8.8$  Hz, 2H), 4.11 (t,  $J = 7.8$  Hz, 1H), 2.57 (s, 3H), 2.42 (s, 3H), 2.00 (ddd,  $J = 7.2, 8.1, 13.9$  Hz, 1H), 1.76 (sept.,  $J = 6.7$  Hz, 1H), 1.62–1.56 (m, 1H), 0.97 (d,  $J = 6.6$  Hz, 3H), 0.93 (d,  $J = 6.6$  Hz, 3H).  $^{13}\text{C NMR}$  (126 MHz,  $\text{CDCl}_3$ )  $\delta$  198.5, 197.0, 169.5, 142.3, 133.1, 129.8, 119.1, 45.3, 37.8, 30.5, 26.6, 26.0, 22.5, 22.4. HRMS (ESI)  $m/z$  calculated for  $\text{C}_{16}\text{H}_{22}\text{NO}_3\text{S}$  308.1315  $[\text{M}+\text{H}]^+$ , found 308.1298.

**2-(Acetylthio)-N-(*p*-tolyl)-4-methylpentanamide 128.** Compound **128** was synthesized in two steps.



The first step was performed according to the general procedure **GP-3**, using *p*-toluidine (80 mg, 0.75 mmol), 2-bromo-4-methylpentanoic acid (175 mg, 0.896 mmol), EDC·HCl (172 mg, 0.896 mmol) and  $\text{CH}_2\text{Cl}_2$  (5 mL). The reaction was stirred at room temperature for 5 h. The resultant crude product of **79** was used without further purification. The second step was achieved according to the general procedure **GP-5**, using the crude product of **79** obtained from the first step, potassium thioacetate (171 mg, 1.49 mmol) and acetone (7 mL). The reaction was stirred at room temperature for 2.5 h. The crude product was purified using column chromatography ( $\text{CH}_2\text{Cl}_2$ ) to give **128** as peach solid (131 mg, 63% (over two steps)). m.p. = 66 °C.  $^1\text{H NMR}$  (500 MHz,  $\text{DMSO}-d_6$ )  $\delta$  10.23 (s, 1H), 7.46 (d,  $J = 8.0$  Hz, 2H), 7.10 (d,  $J = 8.0$  Hz, 2H), 4.27 (t,  $J = 7.5$  Hz, 1H), 2.35 (s, 3H), 2.24 (s, 3H), 1.88–1.75 (m, 1H), 1.62–1.40 (m, 2H), 0.95 (d,  $J = 6.5$  Hz, 3H), 0.88 (d,  $J = 6.5$  Hz, 3H).  $^{13}\text{C NMR}$  (126 MHz,  $\text{DMSO}-d_6$ )  $\delta$  194.5, 168.6, 136.2, 132.6, 129.1, 119.4, 46.4, 41.7, 30.3, 25.9, 22.5, 22.1, 20.5. HRMS (ESI) calculated for  $\text{C}_{15}\text{H}_{22}\text{NO}_2\text{S}$   $[\text{M}+\text{H}]^+$  280.1371, found 280.1358.

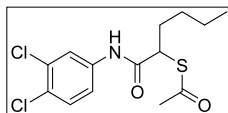
**2-(Acetylthio)-N-(4'-chlorophenyl)-4-methylpentanamide 129.** Compound **129** was synthesized in



two steps. The first step was performed according to the general procedure **GP-3**, using 4-chloroaniline (95 mg, 0.75 mmol), 2-bromo-4-methylpentanoic acid (174 mg, 0.894 mmol), EDC·HCl (171 mg, 0.894 mmol) and  $\text{CH}_2\text{Cl}_2$  (5 mL). The reaction was stirred at room temperature for 5.5 h. The resultant crude product of **80** was used without further purification. The second step was achieved according to the general procedure **GP-5**, using the crude product of **80** obtained from the first step, potassium thioacetate (170 mg, 1.49 mmol) and acetone (7 mL). The reaction was stirred at room temperature for 2.5 h. The crude product was purified using column chromatography ( $\text{CH}_2\text{Cl}_2$ ) to give **129** as yellow solid (139 mg, 62% (over two steps)). m.p. = 82 °C.  $^1\text{H NMR}$  (500 MHz,  $\text{DMSO}-d_6$ )  $\delta$  10.46 (s, 1H), 7.62 (d,  $J = 8.5$  Hz, 2H), 7.36 (d,  $J = 8.5$  Hz, 2H), 4.27 (t,  $J = 7.5$  Hz, 1H), 2.36 (s, 3H), 1.90–1.74 (m, 1H), 1.61–1.42 (m, 2H), 0.95 (d,  $J = 6.5$  Hz, 3H), 0.88 (d,  $J = 6.5$  Hz, 3H).  $^{13}\text{C NMR}$  (126 MHz,  $\text{DMSO}-d_6$ )

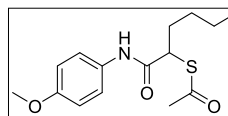
$\delta$  194.4, 169.1, 137.7, 128.7, 127.3, 121.0, 46.4, 41.5, 30.3, 25.9, 22.5, 22.1. HRMS (ESI)  $m/z$  calculated for  $C_{14}H_{19}ClNO_2S$   $[M+H]^+$  300.0825, found 300.0813.

**2-(Acetylthio)-*N*-(3',4'-dichlorophenyl)hexanamide 130.** Compound **130** was synthesized in two



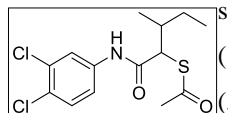
steps. The first step was performed according to the general procedure **GP-3**, using 3,4-dichloroaniline (200 mg, 1.23 mmol), 2-bromohexanoic acid (289 mg, 1.48 mmol), EDC·HCl (284 mg, 1.48 mmol) and  $CH_2Cl_2$  (10 mL). The reaction was stirred at room temperature overnight. The resultant crude product of **81** was used without further purification. The second step was achieved according to the general procedure **GP-5**, using the crude product of **81** obtained from the first step, potassium thioacetate (282 mg, 2.47 mmol) and acetone (10 mL). The reaction was stirred at room temperature for 4 h. The crude product was purified using column chromatography (hexane/EtOAc 95:5  $\rightarrow$  80:20) to give **130** as colorless oil (180 mg, 44% (over two steps)).  $^1H$  NMR (500 MHz,  $DMSO-d_6$ )  $\delta$  10.60 (s, 1H), 7.98 (br, 1H), 7.57 (d,  $J = 9.0$  Hz, 1H), 7.49 (d,  $J = 9.0$  Hz, 1H), 4.18 (t,  $J = 7.5$  Hz, 1H), 2.36 (s, 3H), 1.95–1.80 (m, 1H), 1.72–1.57 (m, 1H), 1.39–1.14 (m, 4H), 0.84 (t,  $J = 6.5$  Hz, 3H).  $^{13}C$  NMR (126 MHz,  $DMSO-d_6$ )  $\delta$  194.5, 169.4, 138.7, 131.1, 130.8, 125.2, 120.5, 119.4, 48.0, 32.2, 30.3, 28.8, 21.7, 13.8. HRMS (ESI)  $m/z$  calculated for  $C_{14}H_{18}Cl_2NO_2S$   $[M+H]^+$  334.0435, found 334.0429.

**2-(Acetylthio)-*N*-(4'-methoxyphenyl)hexanamide 131.** Compound **131** was synthesized according to



the general procedure **GP-5**, using intermediate **82** (305 mg, 1.01 mmol) and potassium thioacetate (150 mg, 1.31 mmol) in acetone (6 mL). The reaction was stirred at room temperature for 2 h. After extraction and column chromatography (PE/EtOAc 9:1), **131** was obtained as white solid (265 mg, 88%).  $R_f = 0.38$  (PE/EtOAc 7:3).  $^1H$  NMR (500 MHz,  $CDCl_3$ )  $\delta$  7.98 (s, 1H), 7.43 (d,  $J = 9.0$  Hz, 2H), 6.84 (d,  $J = 9.0$  Hz, 2H), 4.00 (dd,  $J = 7.2, 8.1$  Hz, 1H), 3.78 (s, 3H), 2.40 (s, 3H), 2.12–2.04 (m, 1H), 1.74–1.67 (m, 1H), 1.44–1.32 (m, 4H), 0.91 (t,  $J = 7.1$  Hz, 1H).  $^{13}C$  NMR (126 MHz,  $CDCl_3$ )  $\delta$  197.9, 168.9, 156.6, 131.2, 121.5, 114.3, 55.6, 47.1, 30.5, 29.6, 29.5, 22.5, 14.0. HRMS (ESI)  $m/z$  calculated for  $C_{15}H_{22}NO_3S$  296.1315  $[M+H]^+$ , found 296.1298.

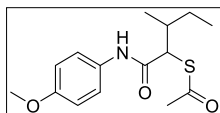
**2-(Acetylthio)-*N*-(3',4'-dichlorophenyl)-3-methylpentanamide 132.** Compound **132** was



synthesized according to the general procedure **GP-5**, using compound **83** (100 mg, 0.339 mmol), potassium thioacetate (77 mg, 0.68 mmol) and acetone (5 mL). The reaction was stirred at room temperature overnight. The crude product was purified using column chromatography ( $CH_2Cl_2$ ) to give **132** as red oil (64 mg, 56%).  $^1H$  NMR (500 MHz,  $DMSO-d_6$ )  $\delta$  10.58 (s, 1H+1H\*), 7.98 (br, 1H+1H\*), 7.57 (d,  $J = 9.0$  Hz, 1H+1H\*), 7.49 (d,  $J = 8.5$  Hz, 1H+1H\*), 4.18 (d,  $J = 7.0$  Hz, 1H), 4.11 (d,  $J = 8.0$  Hz, 1H\*), 2.37 (s, 3H+3H\*), 2.00–1.78 (m, 1H+1H\*), 1.68–1.52 (m, 1H), 1.48–1.34 (m, 1H\*), 1.29–1.04 (m, 1H+1H\*), 1.02–0.79 (m, 6H+6H\*).  $^{13}C$  NMR (126 MHz,  $DMSO-d_6$ )  $\delta$  194.5, 169.32, 169.29\*, 138.8, 138.7\*, 131.0, 130.8, 125.14, 125.10\*, 120.5, 119.4, 53.8, 53.6\*, 37.0, 36.9\*, 30.4, 30.3\*, 26.9, 25.6\*, 16.4, 15.8\*, 11.4, S40

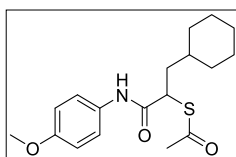
11.0\*. **132** was obtained as a diastereomeric mixture (52:48). The values labeled with \* belong to the second diastereomer. HRMS (ESI)  $m/z$  calculated for  $C_{14}H_{18}Cl_2NO_2S$   $[M+H]^+$  334.0435, found 334.0404.

**2-(Acetylthio)-N-(4'-methoxyphenyl)-3-methylpentanamide 133.** Compound **133** was synthesized



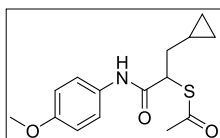
according to the general procedure **GP-5**, using compound **84** (100 mg, 0.391 mmol), potassium thioacetate (89 mg, 0.78 mmol) and acetone (5 mL). The reaction was stirred at room temperature overnight. The crude product was purified using column chromatography ( $CH_2Cl_2$ ) to give **133** as beige solid (50 mg, 43%). m.p. = 100 °C.  $^1H$  NMR (500 MHz,  $DMSO-d_6$ )  $\delta$  10.12 (s, 1H+1H\*), 7.48 (d,  $J = 8.5$  Hz, 2H+2H\*), 6.87 (d,  $J = 8.5$  Hz, 2H+2H\*), 4.17 (d,  $J = 7.5$  Hz, 1H), 4.11 (d,  $J = 8.0$  Hz, 1H\*), 3.71 (s, 3H+3H\*), 2.36 (s, 3H+3H\*), 1.96–1.76 (m, 1H+1H\*), 1.66–1.53 (m, 1H), 1.49–1.37 (m, 1H\*), 1.27–1.04 (m, 1H+1H\*), 0.95 (d,  $J = 6.5$  Hz, 3H), 0.91 (d,  $J = 6.5$  Hz, 3H\*), 0.90–0.82 (m, 3H+3H\*).  $^{13}C$  NMR (126 MHz,  $DMSO-d_6$ )  $\delta$  194.7, 194.6\*, 168.2, 168.1\*, 155.5, 155.4\*, 131.9, 131.8\*, 120.9, 113.9, 55.2, 53.8, 53.6\*, 37.3, 37.1\*, 30.4, 30.3\*, 26.8, 25.6\*, 16.3, 15.9\*, 11.4, 11.1\*. **133** was obtained as a diastereomeric mixture (50:50). The values labeled with \* belong to the second diastereomer. HRMS (ESI)  $m/z$  calculated for  $C_{15}H_{22}NO_3S$   $[M+H]^+$  296.1320, found 296.1289.

**2-S-(Acetylthio)-N-(4'-methoxyphenyl)-3-cyclohexylpentanamide 134.** Compound **134** was



synthesized according to the general procedure **GP-5**, using compound **85** (80 mg, 0.27 mmol), potassium thioacetate (62 mg, 0.54 mmol) and acetone (5 mL). The reaction was stirred at room temperature overnight. The crude product was purified using column chromatography ( $CH_2Cl_2$ ) to give **134** as white solid (63 mg, 70%). m.p. = 74 °C.  $^1H$  NMR (500 MHz,  $DMSO-d_6$ )  $\delta$  10.15 (s, 1H), 7.49 (d,  $J = 8.5$  Hz, 2H), 6.87 (d,  $J = 8.0$  Hz, 2H), 4.27 (t,  $J = 7.5$  Hz, 1H), 3.71 (s, 3H), 2.35 (s, 3H), 1.91–1.76 (m, 2H), 1.72–1.41 (m, 5H), 1.30–1.04 (m, 4H), 1.00–0.82 (m, 2H).  $^{13}C$  NMR (126 MHz,  $DMSO-d_6$ )  $\delta$  194.4, 168.3, 155.5, 131.9, 121.0, 113.9, 55.2, 45.8, 40.2, 40.1, 35.2, 32.7, 32.2, 30.3, 26.0, 25.6. HRMS (ESI)  $m/z$  calculated for  $C_{18}H_{26}NO_3S$   $[M+H]^+$  336.1633, found 336.1599.

**2-(Acetylthio)-N-(4'-methoxyphenyl)-3-cyclopropylpentanamide 135.** Compound **135** was



synthesized according to the general procedure **GP-5**, using compound **86** (109 mg, 0.430 mmol), potassium thioacetate (98 mg, 0.86 mmol) and acetone (3.5 mL). The reaction was stirred at room temperature overnight. The crude product was purified using reverse phase flash chromatography ( $CH_3CN$  (HCOOH 0.05%)/ $H_2O$  (HCOOH 0.05%) 5:95  $\rightarrow$  95:5) to give **135** as beige solid (47 mg, 37%).  $^1H$  NMR (500 MHz,  $CDCl_3$ )  $\delta$  8.00 (br, 1H), 7.42 (d,  $J = 8.2$  Hz, 2H), 6.84 (d,  $J = 8.2$  Hz, 2H), 4.12 (t,  $J = 7.4$  Hz, 1H), 3.77 (s, 3H), 2.39 (s, 3H), 2.07–1.99 (m, 1H), 1.61–1.53 (m, 1H), 0.88–0.78 (m, 1H), 0.53–0.43 (m, 2H), 0.19–0.12 (m, 2H).  $^{13}C$  NMR (126 MHz,  $CDCl_3$ )  $\delta$  197.6, 168.7, 156.4, 131.0, 121.4, 114.1, 55.5, 47.3, 34.8, 30.4, 9.1, 4.7, 4.6. MS (ESI $^+$ )  $m/z$  294.04  $[M+H]^+$ .



## Thioacetates as surrogates for ColH inhibition of thiols

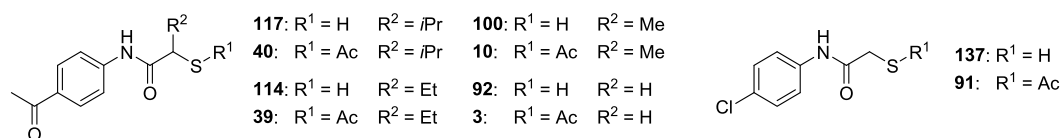


**Figure S1.** Structures of compounds that were tested for their ColH inhibitory activities both in their thiol and thioacetate forms.

**Table S2.** K<sub>i</sub> values of selected thiols and their corresponding thioacetates.

Cpd.	K <sub>i</sub> (μM) <sup>a</sup> ColH
<b>117</b>	0.0025 ± 0.0004
<b>40</b>	0.26 ± 0.01
<b>114</b>	0.0023 ± 0.0005
<b>39</b>	0.16 ± 0.01
<b>100</b>	0.0035 ± 0.0007
<b>10</b>	0.19 ± 0.02
<b>92</b>	0.020 ± 0.003
<b>3</b>	0.31 ± 0.01
<b>137</b>	0.21 ± 0.01
<b>91</b>	4.0 ± 0.3

<sup>a</sup>Means and SD of at least two independent experiments

Though the exact inhibition values of the thioacetates vary in the range of 20–100-fold of the inhibition of the free thiols, they follow the same pattern as their corresponding thiols. This means, in both thiols and thioacetate compounds, the 4-Ac compound with an ethyl residue (**114** and **39**) is the most potent among the 4-Ac compounds, and the 4-Cl compounds without a side chain (**137** and **91**) are by far less active than all 4-Ac compounds.

These values of the thioacetates can of course just be used to show relative tendencies. For exact inhibition data, the free thiol forms have to be used.

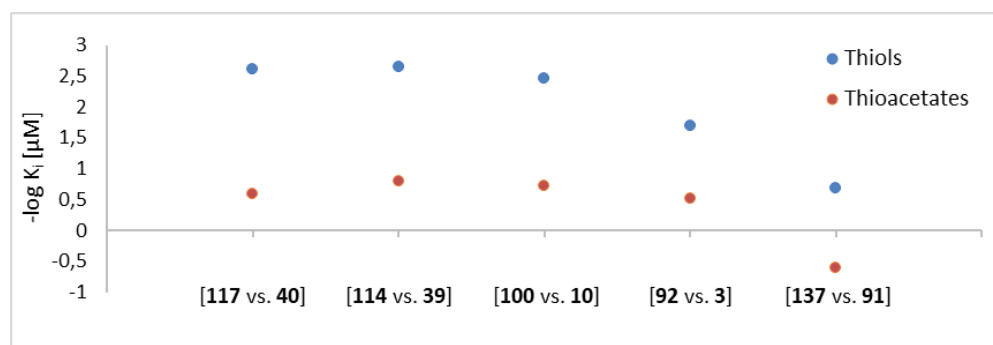


**Figure S2.** Graphical comparison of activities of the aforementioned compounds

## Inhibition [%] of ColH at 1 $\mu$ M concentration

**Table S3.** Inhibition values in % of tested compounds.  $K_i$  values of all compounds that exceeded 90% inhibition at 1  $\mu$ M were measured and can be found in the main paper, Table 5.

Cpd.	R <sup>1</sup>	R <sup>2</sup>	ColH inhibition [%] <sup>a</sup> at 1 $\mu$ M
<b>2</b>	4-OMe	H	94 $\pm$ 0
<b>7</b>	4-OMe	Me	100 $\pm$ 1
<b>10</b>	4-Ac	Me	97 $\pm$ 4
<b>6</b>	3,4-diCl	Me	69 $\pm$ 2
<b>23</b>	4-OMe	Et	96 $\pm$ 3
<b>39</b>	4-Ac	Et	97 $\pm$ 1
<b>18</b>	3,4-diCl	Et	85 $\pm$ 3
<b>24</b>	4-OMe	<i>i</i> Pr	99 $\pm$ 1
<b>40</b>	4-Ac	<i>i</i> Pr	97 $\pm$ 0
<b>19</b>	3,4-diCl	<i>i</i> Pr	85 $\pm$ 5
<b>13</b>	4-OMe	<i>n</i> Pr	100 $\pm$ 4
<b>12</b>	3,4-diCl	<i>n</i> Pr	94 $\pm$ 4
<b>14</b>	4-Me	<i>n</i> Pr	88 $\pm$ 3
<b>17</b>	H	<i>n</i> Pr	26 $\pm$ 1
<b>25</b>	4-OMe	<i>i</i> Bu	96 $\pm$ 1
<b>36</b>	4-Ac	<i>i</i> Bu	93 $\pm$ 2
<b>20</b>	3,4-diCl	<i>i</i> Bu	88 $\pm$ 1
<b>30</b>	3-OMe	<i>i</i> Bu	13 $\pm$ 6
<b>31</b>	2-OMe	<i>i</i> Bu	7 $\pm$ 5
<b>32</b>	2,4-di-OMe	<i>i</i> Bu	0 $\pm$ 12
<b>33</b>	3,4-di-OMe	<i>i</i> Bu	40 $\pm$ 5
<b>34</b>	4-OH	<i>i</i> Bu	78 $\pm$ 4
<b>35</b>	2-OH	<i>i</i> Bu	6 $\pm$ 5
<b>37</b>	4-Me	<i>i</i> Bu	98 $\pm$ 1
<b>38</b>	4-Cl	<i>i</i> Bu	94 $\pm$ 2
<b>26</b>	4-OMe	<i>n</i> Bu	104 $\pm$ 6
<b>21</b>	3,4-diCl	<i>n</i> Bu	83 $\pm$ 5
<b>27</b>	4-OMe	<i>s</i> Bu	94 $\pm$ 2
<b>22</b>	3,4-diCl	<i>s</i> Bu	64 $\pm$ 5
<b>29</b>	4-OMe	cyclohexylmethyl	95 $\pm$ 3
<b>28</b>	4-OMe	cyclopropylmethyl	99 $\pm$ 4

<sup>a</sup>Means and SD of at least two independent experiments

## Crystallographic data

### Co-crystal structures of LasB with 25 and 37 and ColH with 100

**Table S4.** Data collection and refinement statistics for LasB in complex with compounds **25** and **37** and ColH in complex with compound **100**<sup>a</sup>

PDB ID	LasB with compound <b>25</b>	LasB with compound <b>37</b>	ColH with compound <b>100</b>
	7NLK	7NLM	7BBK
<b>Data collection</b>			
Space group	P 1 2 <sub>1</sub> 1	P 1 2 <sub>1</sub> 1	P 2 <sub>1</sub> 2 <sub>1</sub> 2 <sub>1</sub>
Cell dimension			
<i>a</i> , <i>b</i> , <i>c</i> (Å)	40.70, 89.93, 41.24	43.77, 91.97, 67.08	51.43, 81.98, 102.95
$\alpha$ , $\beta$ , $\gamma$ (°)	90.0, 114.3, 90.0	90.0, 92.8, 90.0	90.00, 90.00, 90.00
Resolution	1.65 (1.68 – 1.65)	1.70 (1.73 – 1.70)	1.91 (1.978 – 1.91)
R <sub>sym</sub> or R <sub>merge</sub>	0.075 (0.36)	0.10 (0.46)	0.1058 (0.7499)
R <sub>pim</sub>	0.032 (0.15)	0.055 (0.238)	0.04427 (0.3076)
CC (1/2)	0.99 (0.96)	0.99 (0.88)	0.996 (0.889)
Mean (I) /sd (I)	19.3 (5.9)	8.7 (3.2)	10.58 (2.22)
Completeness (%)	97.8 (95.7)	99.7 (98.8)	99.49 (99.55)
Redundancy	6.3 (6.1)	4.7 (4.6)	6.7 (6.8)
Wilson B-factor	12.47	12.56	26.48
<b>Refinement</b>			
Resolution range (Å)	44.97 – 1.65	45.99 – 1.70	43.6 – 1.91
Total reflections	201,297 (9,275)	273,157 (14,204)	228,821 (22,978)
R <sub>work</sub> / R <sub>free</sub>	0.1853 (0.2129) / 0.2056 (0.2305)	0.1762 (0.2418) / 0.1996 (0.2568)	0.1987 (0.3443) / 0.2440 (0.4374)
No. of atoms	2588	5152	3370
Protein	2283	4618	3076
Ligands	19	36	15
Solvent	286	498	279
Protein residues	298	596	380
<i>B</i> -factors	17.56	18.72	33.34
Protein	16.04	17.48	33.35
Ligands	30.23	21.88	31.79
Water	28.81	29.98	33.32
Bond length (Å)	0.009	0.012	0.011
Bond angles (°)	1.18	1.34	1.03
MolProbity score	1.23	1.44	0.95
Ramachandran favored (%)	96.28	95.95	98.14
Ramachandran allowed (%)	3.38	3.71	1.86
Ramachandran outliers (%)	0.34	0.34	0.00

<sup>a</sup>Statistics for the highest-resolution shell are shown in parentheses.

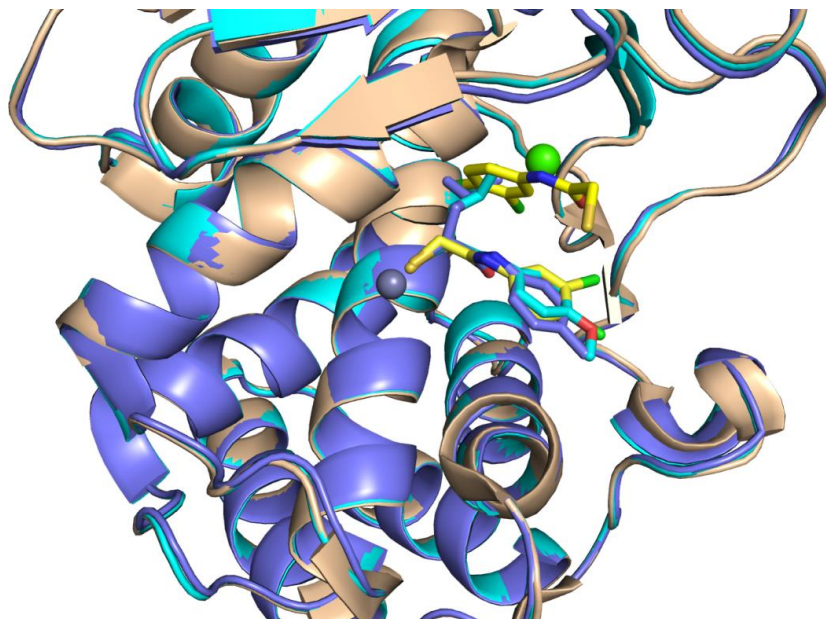


**Figure S3.** Comparison of the LasB complex structures with bound **25** (cyan), **37** (blue) and **1** (yellow, PDB 6F8B). The metal ions are depicted as spheres: Zn<sup>2+</sup> (gray) and Ca<sup>2+</sup> (green).

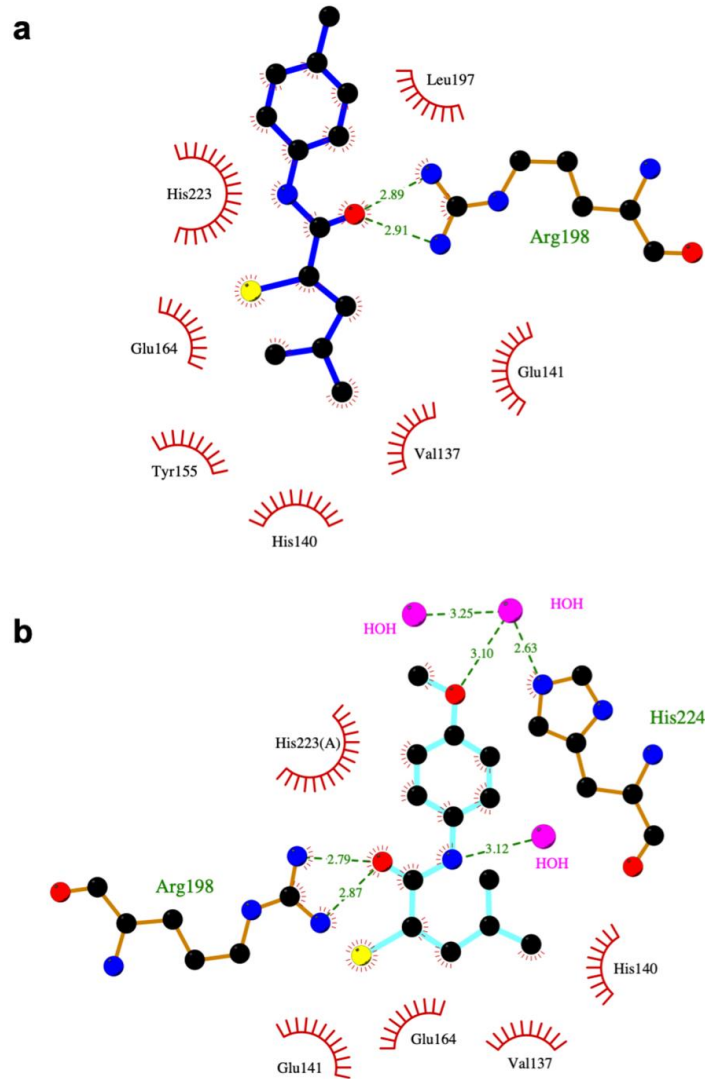


**Figure S4.** Ligplot diagram showing the interactions of **a) 37** and **b) 25** with LasB. Hydrogen bonds are shown as dashed green lines with distances given. Hydrophobic interactions are depicted as red spoked arcs.

## SafetyScreen44™ Panel

### Eurofins Cerep

#### In Vitro Pharmacology: Binding Assays (Figure S5)

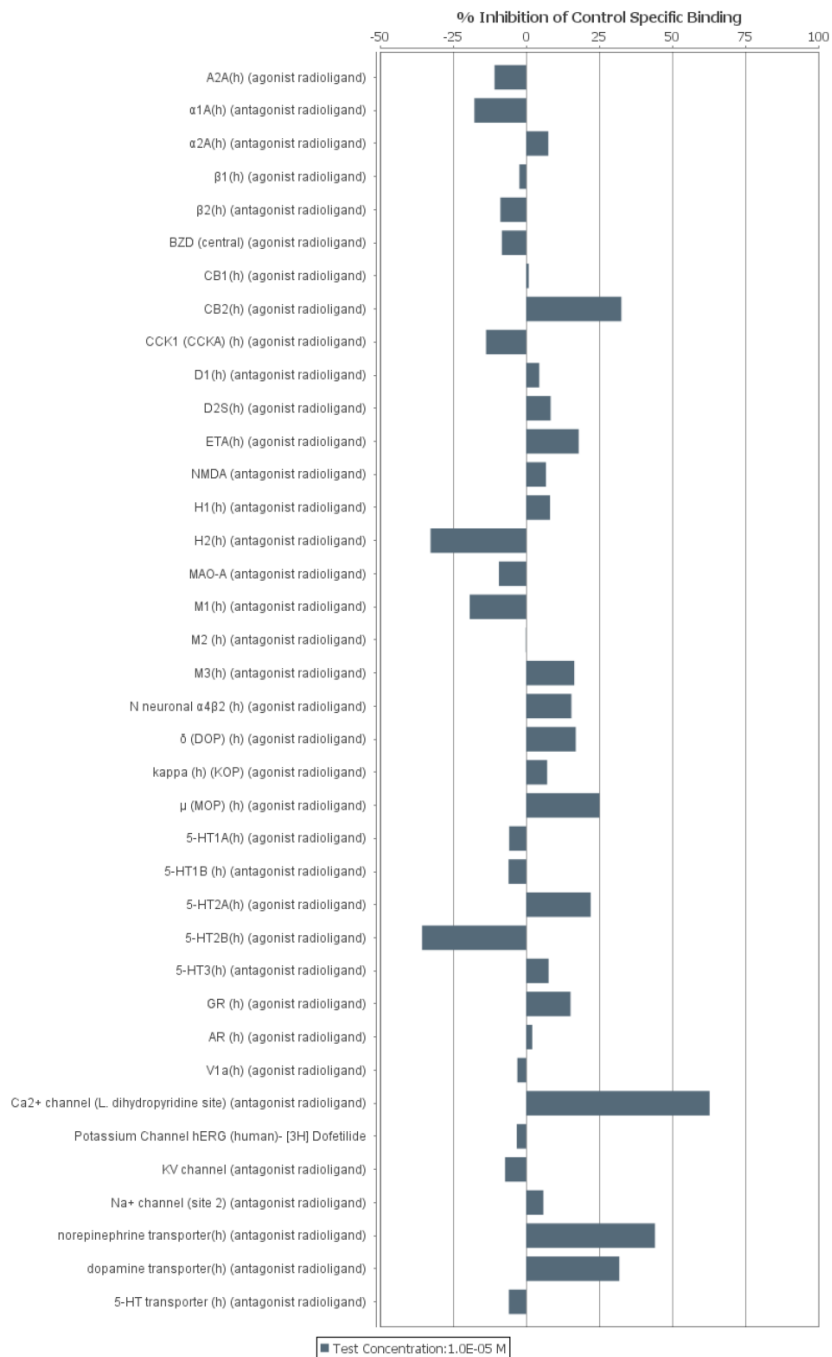


**Figure S5.** Inhibition of binding of 38 off-targets by 10 μM of compound **37**. These experiments were performed by the contract research organization Eurofins Cerep SA (Celle-L'Evescault, France).

S47

***In Vitro Pharmacology: Enzyme and Uptake Assays (Figure S6)***

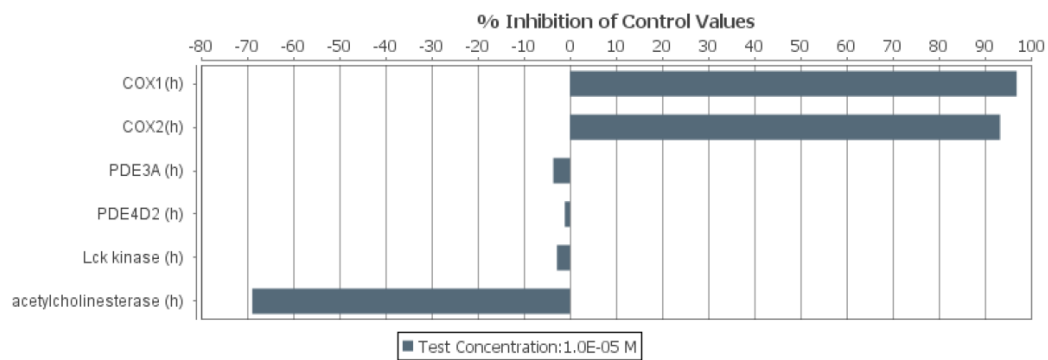


**Figure S6.** Inhibition of six off-targets in presence of compound **37** at 10  $\mu$ M in enzyme and uptake assays. These experiments were performed by the contract research organization Eurofins Cerep SA.

## Additional information on the *in vitro* lung and skin-cell assays

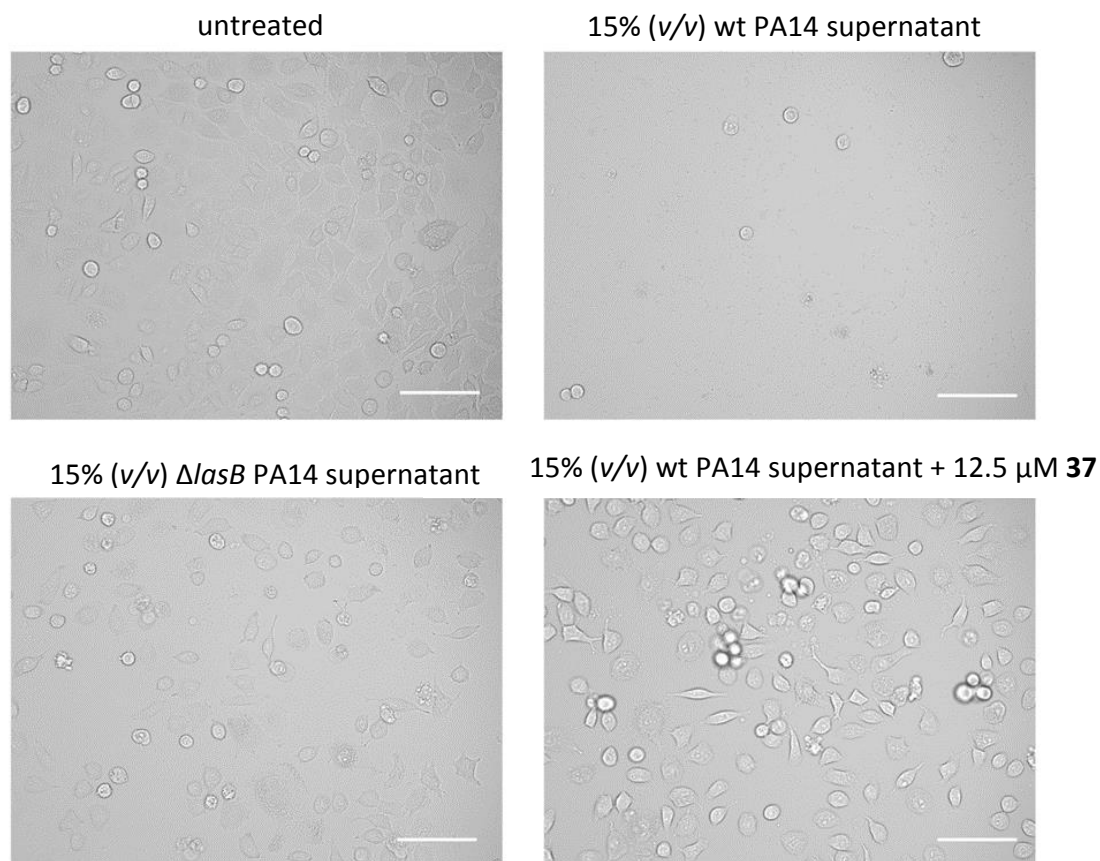


**Figure S7.** Bright-field signals of adenocarcinomic human alveolar basal epithelial (A549) cells untreated (top left), treated with 15% (v/v) wild-type (wt) PA14 culture supernatant (top right), 15% (v/v) LasB knockout ( $\Delta lasB$ ) PA14 supernatant (bottom left) and the deactivation of the LasB effect of PA14 supernatant with 12.5  $\mu\text{M}$  of compound **37** (bottom right). Compound **37** maintained the cell integrity and prevented the morphological changes (A549 cell has an epithelial shape) and cell rounding that could happen due to apoptosis. Images were generated with 20X objective by Leica Las X and modified with the software Fiji ImageJ. Scale bar = 100  $\mu\text{m}$ , PA14: *P. aeruginosa*.



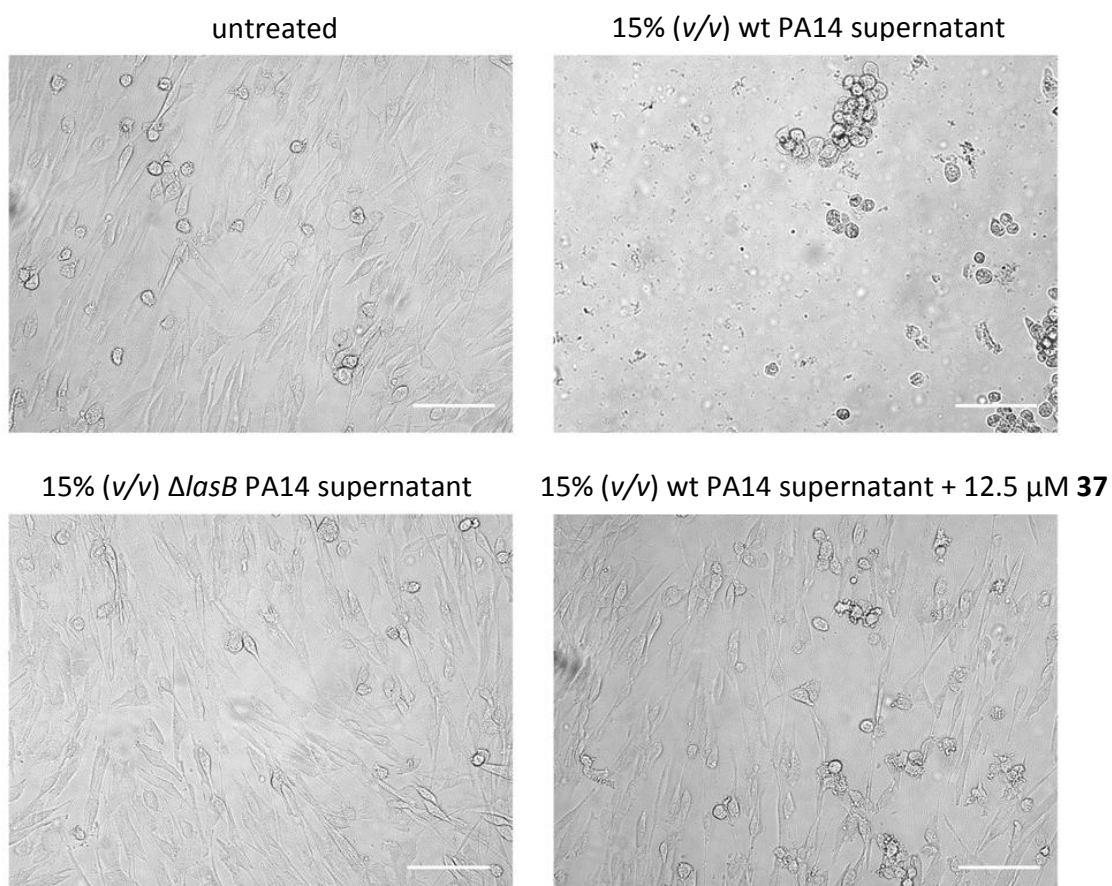


**Figure S8.** Bright-field signals of normal human dermal fibroblasts (NHDF) untreated (top left), treated with 15% (v/v) wild-type (wt) PA14 culture supernatant (top right), 15% (v/v) LasB knockout ( $\Delta lasB$ ) PA14 culture supernatant (bottom left) and the deactivation of the LasB effect of PA14 supernatant with 12.5  $\mu\text{M}$  of compound **37** (bottom right). Compound **37** maintained the cell integrity and prevented the morphological changes (NHDF cell has a spindle shape) and cell rounding that could happen due to apoptosis. Images were generated with 20X objective by Leica Las X and modified with the software Fiji ImageJ. Scale bar = 100  $\mu\text{m}$ , PA14: *P. aeruginosa*.

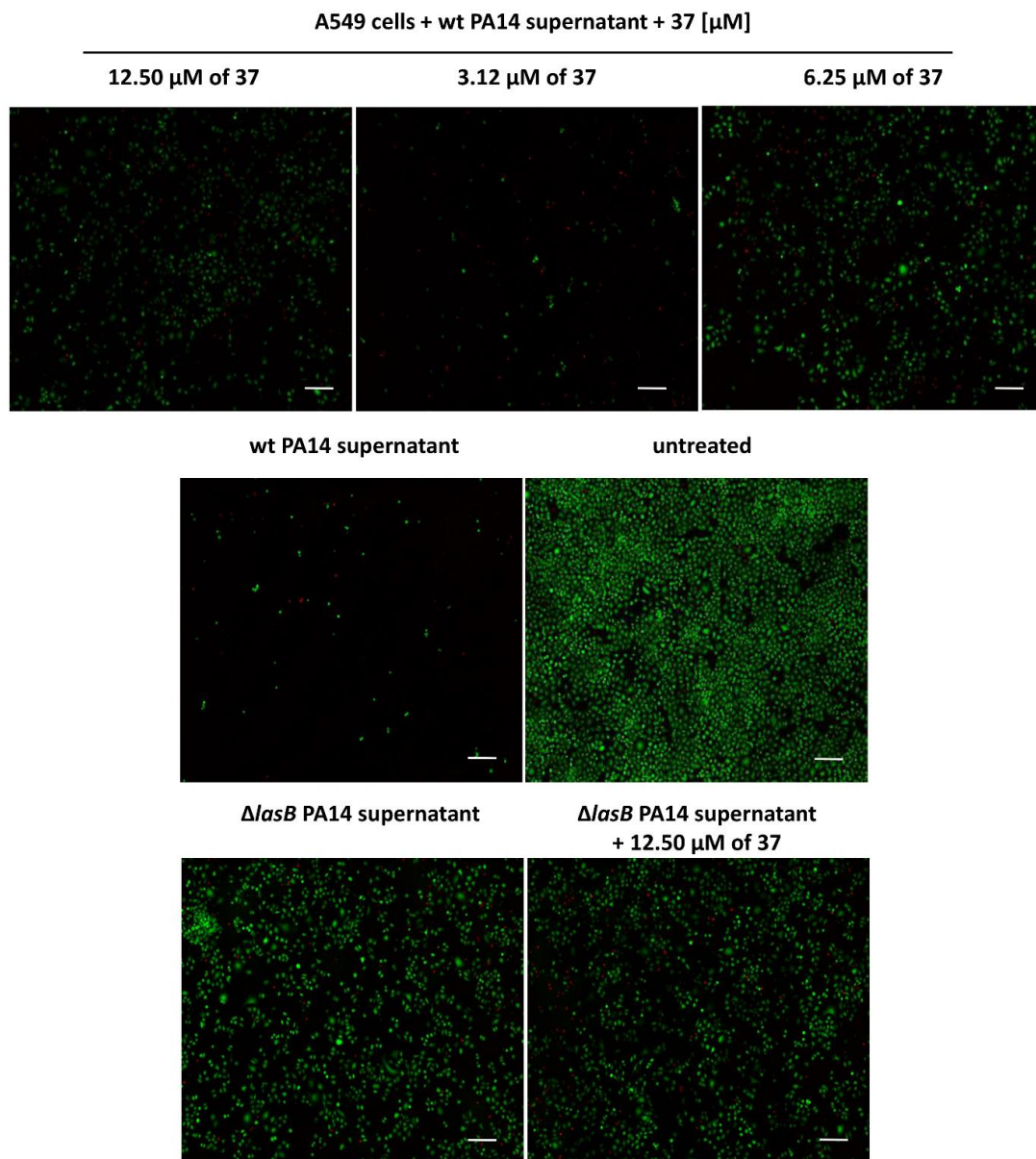


**Figure S9.** Live/dead imaging of adenocarcinomic human alveolar basal epithelial (A549) cells treated with 15% (v/v) wild-type (wt) PA14 or LasB knockout ( $\Delta\text{lasB}$ ) PA14 supernatants with varying amounts of compound **37** with an epifluorescence microscope. Scale bar = 200  $\mu\text{m}$ , PA14: *P. aeruginosa*.

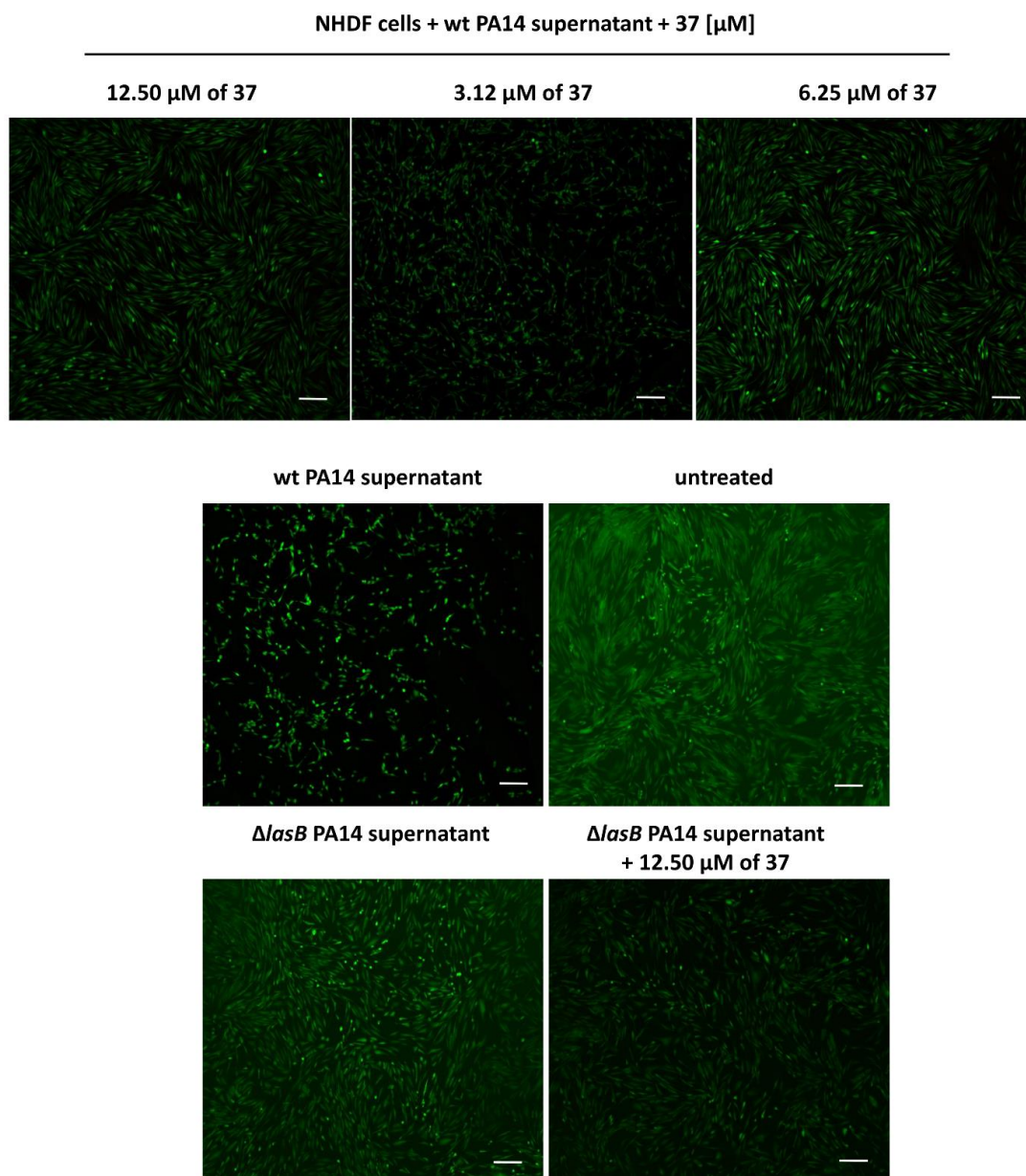


**Figure S10.** Live/dead imaging of normal human dermal fibroblasts (NHDF) cells treated with 15% (v/v) wild-type (wt) PA14 or LasB knockout ( $\Delta\text{lasB}$ ) PA14 supernatants with varying amounts of compound **37** with an epifluorescence microscope. Scale bar = 200  $\mu\text{m}$ , PA14: *P. aeruginosa*.

## *In vivo* pharmacokinetic studies

**Table S5.** PK parameters of compound **37** after 10 mg/kg i.v.

$C_0$ [ng/mL]	$256 \pm 69$
$t_{1/2}$ [min]	$1.1 \pm 0.2$
$CL_{obs}$ [mL/min/kg]	$505 \pm 119$
$AUC_{0-t}$ [ng/mL*h]	$241 \pm 23$
$V_{obs}$ [L/kg]	$46 \pm 3$

**Table S6.** Q1 and Q3 masses for caffeine and **37**.

ID	Q1 Mass [Da]	Q3 Mass [Da]	time [msec]	CE [volts]	CXP [volts]	DP [volts]
<b>37</b>	235.949	178.900	50.0	-26.0	-19.0	-85.0
		106.000	50.0	-38.0	-11.0	-85.0
<b>caffeine</b>	195.024	138.000	30.0	25.0	14.0	130.0
		110.000	30.0	31.0	18.0	130.0

## References

- (1) Kaya, C.; Walter, I.; Yahiaoui, S.; Sikandar, A.; Alhayek, A.; Konstantinović, J.; Kany, A. M.; Hauptenthal, J.; Köhnke, J.; Hartmann, R. W.; Hirsch, A. K. H. Substrate- inspired Fragment Merging and Growing Affords Efficacious LasB Inhibitors. *Angew. Chem. Int. Ed.* **2021**, *61*, e202112295. <https://doi.org/10.1002/anie.202112295>.
- (2) Kaya, C.; Walter, I.; Alhayek, A.; Shafiei, R.; Jézéquel, G.; Andreas, A.; Konstantinović, J.; Schönauer, E.; Sikandar, A.; Hauptenthal, J.; Müller, R.; Brandstetter, H.; Hartmann, R. W.; Hirsch, A. K. H. Structure-Based Design of  $\alpha$ -Substituted Mercaptoacetamides as Inhibitors of the Virulence Factor LasB from *Pseudomonas aeruginosa*. *ACS Infect. Dis.* **2022**, *in print*. <https://doi.org/10.1021/acsinfecdis.1c00628>.
- (3) Kany, A. M.; Sikandar, A.; Hauptenthal, J.; Yahiaoui, S.; Maurer, C. K.; Proschak, E.; Köhnke, J.; Hartmann, R. W. Binding Mode Characterization and Early *in Vivo* Evaluation of Fragment-Like Thiols as Inhibitors of the Virulence Factor LasB from *Pseudomonas aeruginosa*. *ACS Infect. Dis.* **2018**, *4* (6), 988–997. <https://doi.org/10.1021/acsinfecdis.8b00010>.
- (4) Yahiaoui, S.; Voos, K.; Hauptenthal, J.; Wichelhaus, T. A.; Frank, D.; Weizel, L.; Rotter, M.; Brunst, S.; Kramer, J. S.; Proschak, E.; Ducho, C.; Hirsch, A. K. H. *N*-Aryl Mercaptoacetamides as Potential Multi-Target Inhibitors of Metallo- $\beta$ -Lactamases (MBLs) and the Virulence Factor LasB from *Pseudomonas aeruginosa*. *RSC Med. Chem.* **2021**, *12* (10), 1698–1708. <https://doi.org/10.1039/D1MD00187F>.
- (5) Schönauer, E.; Kany, A. M.; Hauptenthal, J.; Hüsecken, K.; Hoppe, I. J.; Voos, K.; Yahiaoui, S.; Elsässer, B.; Ducho, C.; Brandstetter, H.; Hartmann, R. W. Discovery of a Potent Inhibitor Class with High Selectivity toward Clostridial Collagenases. *J. Am. Chem. Soc.* **2017**, *139* (36), 12696–12703. <https://doi.org/10.1021/jacs.7b06935>.

## A6. SUPPORTING INFORMATION TO CHAPTER F

**Optimized Phosphonate Derivatives as highly potent Inhibitors of *P. aeruginosa* Virulence Factor Elastase B (LasB) and *Clostridium* Virulence Factor Collagenase H (ColH).**

Katrin Voos, Jelena Konstantinović, Esther Schönauer, Katharina Rox, Anna K. H. Hirsch\* and Christian Ducho\*

\* corresponding authors

Please note that the following chapter is the supporting information of a manuscript in preparation.

## 1. General Procedures

**General procedure GP-3: Synthesis of 2-bromo-2-alkyl-*N*-aryl-acetamide derivatives (taken from Chapter E).** 2-Bromoalkanoic acid (1.2 eq) and EDC-HCl (1.2 eq) were added to a solution of the corresponding aniline (1.0 eq) in CH<sub>2</sub>Cl<sub>2</sub>. The resultant mixture was stirred overnight at room temperature. The reaction was stopped and CH<sub>2</sub>Cl<sub>2</sub> was added to the mixture. The obtained solution was washed with 1 M HCl and with saturated aqueous NaCl solution. The organic layer was dried over anhydrous Na<sub>2</sub>SO<sub>4</sub>, filtrated and concentrated under reduced pressure to afford the crude product. The obtained crude product was used for the next step without further purification or purified using column chromatography.

**General procedure GP-4: Synthesis of 2-chloro-2-alkyl-*N*-aryl-acetamide derivatives (taken from Chapter E).** Aniline (1.0 eq) and DIPEA (1.2 eq) were dissolved in dry CH<sub>2</sub>Cl<sub>2</sub> or THF and cooled on ice to 0 °C. To this solution, 2-chloroalkanoic acid chloride (1.2 eq) was added dropwise and the resulting mixture was stirred at 0 °C. The reaction mixture was quenched with 0.5 M NaHCO<sub>3</sub>. After dilution with CH<sub>2</sub>Cl<sub>2</sub>, the mixture was extracted thrice with 0.5 M NaHCO<sub>3</sub> and 0.5 M HCl, as well as once with saturated aqueous NaCl. The CH<sub>2</sub>Cl<sub>2</sub> layer was dried with anhydrous Na<sub>2</sub>SO<sub>4</sub> and concentrated under reduced pressure to give the titled compounds in clean form without any further purification.

**General Procedure GP-8: Synthesis of 2-diethylphosphono-2-alkyl-*N*-aryl-acetamide derivatives.** Alkyl halide (1 eq.) was suspended in triethylphosphite (5 – 20 eq.) and flushed with Ar. The mixture was heated to 150 – 170 °C and stirred at this temperature for 1 – 3 d until the TLC indicated complete transformation. The reaction mixture was concentrated in high vacuum to evaporate excessive triethylphosphite. The resulting oily residue was further purified using flash chromatography on high performance silica gel, to yield the named diethylphosphonates.

**General Procedure GP-9: Synthesis of 2-phosphono-2-alkyl-*N*-aryl-acetamide derivatives.** Diethylphosphonate (1.0 eq.) was dissolved in dry CH<sub>2</sub>Cl<sub>2</sub> (10 mL) then TMSBr (5 eq.) was added dropwise over 10 min and the reaction was stirred at RT overnight (15 – 20 h). On the next day, MeOH (10 mL) was added and stirred for another 1 2 h, then concentrated in vacuo until dryness. The resulting residue was further purified via HPLC. Compounds **35**, **33** and **34** were additionally transferred into their sodium forms using ion-exchange chromatography.

## 2. Compounds 16, 20, 22–31 (already published)

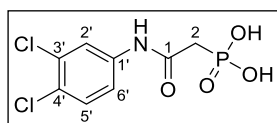
Compound **16** was synthesized by Katrin Voos and its synthesis is published in Chapter C. Original compound number in the paper<sup>194</sup> / Chapter B was “*compound 26*”. Therefore, the compound can be referenced as **B-26** or **16**.

Compound **20** was synthesized by Andreas Martin Kany at HIPS and its synthesis is published in Chapter A. Original compound number in the paper<sup>193</sup> / Chapter A was “*compound 3*”. Therefore, the compound can be referenced as **A-3** or **20**.

Compounds **22–31** were synthesized by Katrin Voos and their synthesis is published in Chapter B.

## 3. Synthesis of compounds 32–55

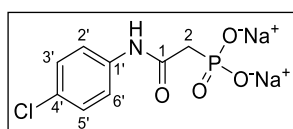
**(2-((3,4-Dichlorophenyl)amino)-2-oxoethyl)phosphonic acid 32**. Compound **32** was synthesized



according to **GP-9**, using intermediate **40** (540 mg, 1.59 mmol) and TMSBr (1.05 mL, 8.03 mmol) in dry CH<sub>2</sub>Cl<sub>2</sub> (10 mL). The reaction was stirred for 19 h at rt, then MeOH (10 mL) was added and stirred for another 1 h. After

concentration *in vacuo* and HPLC purification (method **HPLC-01**) **32** was obtained as white solid (348 mg, 77%). <sup>1</sup>H NMR (500 Hz, DMSO-*d*<sub>6</sub>) δ = 10.28 (s, 1H, NH), 8.00 (d, *J* = 2.4 Hz, 2'-H), 7.55 (d, *J* = 8.8 Hz, 5'-H), 7.45 (dd, *J* = 2.4, 8.8 Hz, 6'-H), 2.82 (d, *J* = 21.4 Hz, 2-H); <sup>13</sup>C NMR (126 MHz, DMSO-*d*<sub>6</sub>) δ = 165.01 (d, *J* = 6.3 Hz, 1-C), 139.36 (3'-C or 4'-C), 130.95 (3'-C or 4'-C), 130.70 (5'-C), 124.51 (1'-C), 120.13 (2'-C), 119.05 (6'-C), 38.69 (d, *J* = 160.0 Hz, 2-C); <sup>31</sup>P NMR (203 MHz, DMSO-*d*<sub>6</sub>) δ = 15.59; HRMS (ESI<sup>+</sup>) *m/z* calculated for C<sub>8</sub>H<sub>9</sub>Cl<sub>2</sub>NO<sub>4</sub>P 283.9641 [M+H]<sup>+</sup>, found 283.9637; HRMS (ESI<sup>-</sup>) *m/z* calculated for C<sub>8</sub>H<sub>7</sub>Cl<sub>2</sub>NO<sub>4</sub>P 281.9495 [M-H]<sup>-</sup>, found 281.9495; HPLC (method **HPLC-01**): *R*<sub>t</sub> = 11.5 min; λ<sub>max</sub> = 252 nm.

**Sodium (2-((4-chlorophenyl)amino)-2-oxoethyl)phosphonate 33**. Compound **33** was synthesized



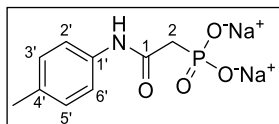
according to **GP-9**, using intermediate **41** (106 mg, 0.332 mmol) and TMSBr (230 μL, 1.76 mmol) in dry CH<sub>2</sub>Cl<sub>2</sub> (10 mL). The reaction was stirred for 22 h at rt, then MeOH (10 mL) was added and stirred for another

1 h. After concentration, HPLC purification (method **HPLC-02**) and ion exchange chromatography **33** was obtained as white solid (56 mg, 58%). MP > 300 °C; <sup>1</sup>H NMR (500 Hz, MeOD-*d*<sub>4</sub>) δ 7.62 (d, *J* = 8.9 Hz, aryl-H<sub>a</sub>), 7.29 (d, *J* = 8.9 Hz, aryl-H<sub>b</sub>), 2.69 (d, *J* = 18.0 Hz, 2H, 2-H); <sup>13</sup>C NMR (126 MHz, MeOD-*d*<sub>4</sub>) δ 162.77 (1-C), 129.81 (1'-C or 4'-C), 119.97 (aryl-C<sub>b</sub>), 119.65 (1'-C or 4'-C), 112.82 (aryl-C<sub>a</sub>), 31.83 (d, *J* = 112.1 Hz, 2-C); <sup>31</sup>P NMR (203 MHz, MeOD-*d*<sub>4</sub>) δ 11.91; HRMS (ESI<sup>+</sup>) *m/z* calculated for



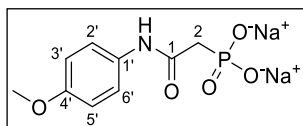
$C_8H_{10}ClNO_4P$  250.0030  $[M+H]^+$ , found 250.0028; HRMS (ESI-)  $m/z$  calculated for  $C_8H_8ClNO_4P$  247.9885  $[M-H]^-$ , found 247.9884; HPLC (method **HPLC-02**):  $R_t$  = 18.5 min;  $\lambda_{max}$  = 250 nm.

**Sodium (2-((4-methylphenyl)amino)-2-oxoethyl)phosphonate 34.** Compound **34** was



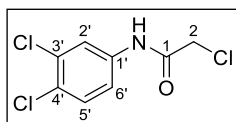
synthesized according to **GP-9**, using intermediate **42** (218 mg, 0.728 mmol) and TMSBr (500  $\mu$ L, 3.82 mmol) in dry  $CH_2Cl_2$  (10 mL). The reaction was stirred for 18 h at rt, then MeOH (10 mL) was added and stirred for another 1 h. After concentration, HPLC purification (method **HPLC-03**) and ion exchange chromatography **34** was obtained as white solid (51 mg, 26%). MP > 300  $^{\circ}C$ ;  $^1H$  NMR (500 Hz, MeOD- $d_4$ )  $\delta$  7.44 (d,  $J$  = 8.5 Hz, 3'-H, 5'-H), 7.09 (d,  $J$  = 8.1 Hz, 2'-H, 6'-H), 2.78 (d,  $J$  = 19.7 Hz, 2-H), 2.28 (s, 3H, 4'-CH<sub>3</sub>);  $^{13}C$  NMR (126 MHz, MeOD- $d_4$ )  $\delta$  169.37 (1-C), 157.76 (4'-C), 133.03 (1'-C), 122.91 (3'-C, 5'-C), 114.81 (2'-C, 6'-C), 55.82 (4'-CH<sub>3</sub>), 39.95 (d,  $J$  = 120.2 Hz, 2-C);  $^{31}P$  NMR (203 MHz, MeOD- $d_4$ )  $\delta$  = 13.22; HRMS (ESI+)  $m/z$  calculated for  $C_9H_{13}NO_4P$  230.0577  $[M+H]^+$ , found 230.0575; HRMS (ESI-)  $m/z$  calculated for  $C_9H_{11}NO_4P$  228.0431  $[M-H]^-$ , found 228.0430; HPLC (method **HPLC-03**):  $R_t$  = 19.0 min;  $\lambda_{max}$  = 246 nm.

**Sodium (2-((4-methoxyphenyl)amino)-2-oxoethyl)phosphonate 35.** Compound **35** was



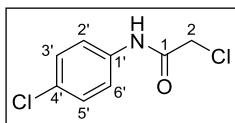
synthesized according to **GP-9**, using intermediate **43** (152 mg, 0.505 mmol) and TMSBr (330  $\mu$ L, 2.52 mmol) in dry  $CH_2Cl_2$  (10 mL). The reaction was stirred for 16 h at rt, then MeOH (10 mL) was added and stirred for another 1 h. After concentration, HPLC purification (method **HPLC-04**) and ion exchange chromatography **35** was obtained as white solid (71 mg, 49%). MP > 300  $^{\circ}C$ ;  $^1H$  NMR (500 Hz, MeOD- $d_4$ )  $\delta$  7.48 (d,  $J$  = 9.0 Hz, 2H, 3'-H, 5'-H), 6.86 (d,  $J$  = 9.0 Hz, 2H, 2'-H, 6'-H), 3.77 (s, 3H, 4'-OCH<sub>3</sub>), 2.79 (d,  $J$  = 19.9 Hz, 2H, 2-H);  $^{13}C$  NMR (126 MHz, MeOD- $d_4$ )  $\delta$  166.24 (1-C), 158.01 (4'-C), 132.78 (1'-C), 123.00 (3'-C, 5'-C), 114.89 (2'-C, 6'-C), 55.84 (4'-OCH<sub>3</sub>), 38.50 (d,  $J$  = 130.2 Hz, 2-C);  $^{31}P$  NMR (203 MHz, MeOD- $d_4$ )  $\delta$  13.35; HRMS (ESI+)  $m/z$  calculated for  $C_9H_{13}NO_5P$  246.0526  $[M+H]^+$ , found 246.0524; HRMS (ESI-)  $m/z$  calculated for  $C_9H_{11}NO_5P$  244.0380  $[M-H]^-$ , found 244.0380; HPLC (method **HPLC-04**):  $R_t$  = 21.5 min;  $\lambda_{max}$  = 250 nm.

**2-chloro-N-(3,4-dichlorophenyl)acetamide 36.** Compound **36** was synthesized according to **GP-4**,



using 3,4-dichloroaniline (4.00 g, 24.7 mmol), 2-chloroacetyl chloride (2.20 mL, 27.6 mmol) and DIPEA (8.70 mL, 50.0 mmol) in  $CH_2Cl_2$  (20 mL). The reaction was stirred for 1 h 30 min on ice at 0  $^{\circ}C$ . After extraction, **36** was obtained as brown solid without further purification (5.14 g, 87%).  $^1H$  NMR (300 Hz,  $CDCl_3$ )  $\delta$  = 8.24 (*br s*, 1H, NH), 7.79 (d,  $J$  = 2.0 Hz, 2'-H), 7.43-7.36 (m, 2H, 5'-H, 6'-H), 4.19 (s, 2H, 2-H);  $^{13}C$  NMR (75 MHz,  $CDCl_3$ )  $\delta$  = 164.04 (1-C), 136.21 (3'-C or 4'-C), 133.19 (3'-C or 4'-C), 130.81 (5'-C), 128.78 (1'-C), 121.92 (2'-C), 119.39 (6'-C), 42.89 (2-C)

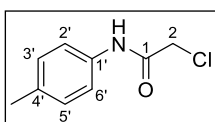
**2-chloro-*N*-(4-chlorophenyl)acetamide 37.** 4-Chloroaniline (143 mg, 1.13 mmol) and DIPEA



(220  $\mu$ L, 1.29 mmol) were dissolved in dry THF (8 mL) and cooled on ice bath to 0°C. Chloroacetyl chloride (110  $\mu$ L, 1.38 mmol) was added dropwise to the stirred solution over a period of 5 min. The mixture was stirred on ice for a total

of 1 h. The reaction mixture was diluted with EtOAc (200 mL), washed with water (3x 30 mL), saturated NaHCO<sub>3</sub> (1x 30 mL), diluted HCl (0.5 M, 1x 30 mL), and brine (1x 30 mL), dried over Na<sub>2</sub>SO<sub>4</sub>, filtered and concentrated *in vacuo* to give **37** as yellow solid (258 mg, quant.). <sup>1</sup>H NMR (500 Hz, CDCl<sub>3</sub>)  $\delta$  8.22 (br, 1 H, NH), 7.51 (d,  $J$  = 8.8 Hz, 2 H, 3'-H, 5'-H), 7.33 (d,  $J$  = 8.8 Hz, 2 H, 2'-C, 6'-C), 4.19 (s, 2 H, 2-H); <sup>13</sup>C NMR (126 Hz, CDCl<sub>3</sub>)  $\delta$  163.93 (1-C), 135.36 (1'-C or 4'-C), 130.50 (1'-C or 4'-C), 129.34 (2'-C, 6'-C), 121.46 (3'-C, 5'-C), 42.95 (2-H); HRMS (ESI)  $m/z$  calculated for C<sub>8</sub>H<sub>8</sub>Cl<sub>2</sub>NO 204.00 [M+H]<sup>+</sup>, found 204.00; TLC (CH<sub>2</sub>Cl<sub>2</sub> – MeOH, 9:1): R<sub>f</sub> = 0.35.

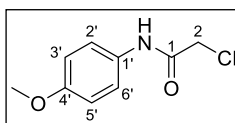
**2-chloro-*N*-(4-methylphenyl)acetamide 38.** Compound **38** was synthesized according to GP-4,



using *p*-toluidine (499 mg, 4.66 mmol), DIPEA (1.70 mL, 9.76 mmol) and chloroacetyl chloride (450  $\mu$ L, 5.65 mmol) in 10 mL of dry CH<sub>2</sub>Cl<sub>2</sub>. The reaction was stirred for 2 h 30 min at 0 °C. After extraction **38** was obtained as brown solid

without further purification (784 mg, 92%). <sup>1</sup>H NMR (500 Hz, CDCl<sub>3</sub>)  $\delta$  8.18 (br, 1 H, NH), 7.42 (d,  $J$  = 8.4 Hz, 2 H, aryl-H<sub>a</sub>), 7.16 (d,  $J$  = 8.3 Hz, 2 H, aryl-H<sub>b</sub>), 4.18 (s, 2 H, 2-H), 2.33 (s, 3 H, 4'-CH<sub>3</sub>); <sup>13</sup>C NMR (126 Hz, CDCl<sub>3</sub>)  $\delta$  163.84 (1-C), 135.15 (1'-C or 4'-C), 134.22 (1'-C or 4'-C), 129.77 (aryl-C<sub>b</sub>), 120.36 (aryl-C<sub>a</sub>), 43.01 (2-H), 21.05 (4'-CH<sub>3</sub>); HRMS (ESI)  $m/z$  calcd. for C<sub>9</sub>H<sub>11</sub>ClNO [M+H]<sup>+</sup> 184.0524, found: 184.0520; TLC (petroleum ether-EtOAc, 7:3): R<sub>f</sub> = 0.40.

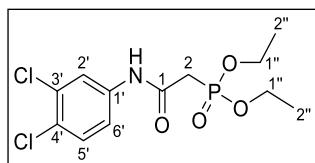
**2-chloro-*N*-(4-methoxyphenyl)acetamide 39.** Compound **39** was synthesized according to GP-4,



using 4-methoxyaniline (1.41 g, 11.5 mmol), DIPEA (4.00 mL, 23.0 mmol) and chloroacetyl chloride (1.00 mL, 12.56 mmol) in 15 mL of dry CH<sub>2</sub>Cl<sub>2</sub>. The reaction was stirred for 2 h 20 min at 0 °C. After extraction **39** was obtained as

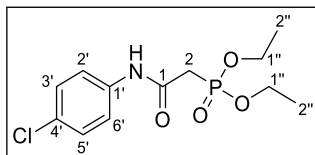
brown solid without further purification (1.83 g, 80%). <sup>1</sup>H NMR (500 Hz, CDCl<sub>3</sub>)  $\delta$  8.18 (br, 1 H, NH), 7.43 (d,  $J$  = 9.0 Hz, 2 H, 3'-H, 5'-H), 6.88 (d,  $J$  = 9.0 Hz, 2 H, 2'-C, 6'-C), 4.18 (s, 2 H, 2-H), 3.80 (s, 3 H, 4'-OCH<sub>3</sub>); <sup>13</sup>C NMR (126 Hz, CDCl<sub>3</sub>)  $\delta$  163.90 (1-C), 157.22 (4'-C), 129.78 (1'-C), 122.22 (3'-C, 5'-C), 114.38 (2'-C, 6'-C), 55.60 (4'-OCH<sub>3</sub>), 42.96 (2-C); HRMS (ESI)  $m/z$  calculated for C<sub>9</sub>H<sub>11</sub>ClNO<sub>2</sub> 200.0473 [M+H]<sup>+</sup>, found 200.0466; TLC (petroleum ether-EtOAc, 2:8): R<sub>f</sub> = 0.50.

**Diethyl 2-((3,4-dichlorophenyl)amino)-2-oxoethyl)phosphonate 40.** Compound **40** was



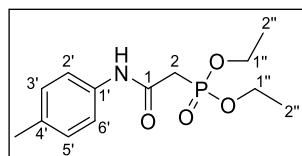
synthesized according to **GP-8**, using intermediate **36** (1.53 g, 6.42 mmol) and triethylphosphite (11.0 mL, 63.6 mmol). The reaction was stirred for 3 d at 150 °C. After concentration in high vacuum to evaporate excessive triethylphosphite, and column chromatography (petroleum ether – EtOAc – MeOH, 95:5:0 → 0:90:10) **40** was obtained as brown solid (0.55 g, 25%). <sup>1</sup>H NMR (500 Hz, CDCl<sub>3</sub>) δ = 9.58 (s, 1H, NH), 7.66 (d, *J* = 2.3 Hz, 2'-H), 7.31 (dd, *J* = 2.3, 8.8 Hz, 6'-H), 7.22 (d, *J* = 8.8 Hz, 5'-H), 4.21 (quint., *J* = 7.3 Hz, 4H, P-O-CH<sub>2</sub>CH<sub>3</sub>), 3.05 (d, *J* = 21.2 Hz, 2-H), 1.38 (t, *J* = 7.1 Hz, 6H, P-O-CH<sub>2</sub>CH<sub>3</sub>); <sup>13</sup>C NMR (126 MHz, CDCl<sub>3</sub>) δ = 162.40 (d, *J* = 4.0 Hz, 1-C), 137.64 (3'-C or 4'-C), 132.63 (3'-C or 4'-C), 130.32 (5'-C), 127.36 (1'-C), 121.19 (2'-C), 118.74 (6'-C), 63.38 (d, *J* = 6.6 Hz, P-O-CH<sub>2</sub>CH<sub>3</sub>), 36.39 (d, *J* = 129.4 Hz, 2-C), 16.51 (d, *J* = 6.0 Hz, P-O-CH<sub>2</sub>CH<sub>3</sub>); <sup>31</sup>P NMR (203 MHz, CDCl<sub>3</sub>) δ = 22.58; TLC (petroleum ether-EtOAc, 2:8): *R*<sub>f</sub> = 0.10.

**Diethyl 2-((4-chlorophenyl)amino)-2-oxoethyl)phosphonate 41.** Compound **41** was synthesized



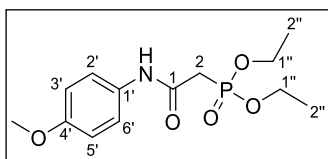
according to **GP-8**, using intermediate **37** (115 mg, 0.564 mmol) and triethylphosphite (2.00 mL, 11.6 mmol). The reaction was stirred for 22 h at 150 °C. After concentration in high vacuum to evaporate excessive triethylphosphite, and column chromatography (petroleum ether – EtOAc, 2:8) **41** was obtained as white solid (152 mg, 84%). <sup>1</sup>H NMR (500 Hz, CDCl<sub>3</sub>) δ 9.14 (s, 1H, NH), 7.44 (d, *J* = 8.9 Hz, aryl-H<sub>a</sub>), 7.21 (d, *J* = 8.9 Hz, aryl-H<sub>b</sub>), 4.21 – 4.15 (m, 4H, P-O-CH<sub>2</sub>CH<sub>3</sub>), 3.02 (d, *J* = 20.8 Hz, 2H, 2-H), 1.36 (t, *J* = 7.1 Hz, 3H, P-O-CH<sub>2</sub>CH<sub>3</sub>); <sup>13</sup>C NMR (126 MHz, CDCl<sub>3</sub>) δ 162.24 (d, *J* = 3.6 Hz, 1-C), 136.56, (1'-C or 4'-C) 129.41 (1'-C or 4'-C), 128.99 (aryl-C<sub>b</sub>), 121.07 (aryl-C<sub>a</sub>), 63.24 (d, *J* = 6.5 Hz, P-O-CH<sub>2</sub>CH<sub>3</sub>), 36.22 (d, *J* = 129.4 Hz, 2-C), 16.49 (d, *J* = 5.6 Hz, P-O-CH<sub>2</sub>CH<sub>3</sub>); <sup>31</sup>P NMR (203 MHz, CDCl<sub>3</sub>) δ 22.73; HRMS (ESI<sup>+</sup>) *m/z* calculated for C<sub>12</sub>H<sub>18</sub>ClNO<sub>4</sub>P 306.0656 [M+H]<sup>+</sup>, found 306.0645; TLC (petroleum ether – EtOAc, 2:8): *R*<sub>f</sub> = 0.20.

**Diethyl 2-((4-methylphenyl)amino)-2-oxoethyl)phosphonate 42.** Compound **42** was synthesized



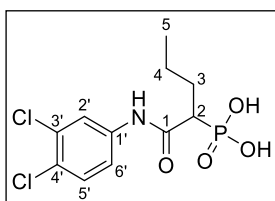
according to **GP-8**, using intermediate **38** (229 mg, 1.25 mmol) and triethylphosphite (4.50 mL, 26.0 mmol). The reaction was stirred for 18 h at 150 °C. After concentration in high vacuum to evaporate excessive triethylphosphite, and column chromatography (petroleum ether – EtOAc, 2:8) **42** was obtained as orange solid (276 mg, 74%). <sup>1</sup>H NMR (500 Hz, CDCl<sub>3</sub>) δ 8.76 (s, 1H, NH), 7.39 (d, *J* = 8.5 Hz, 3'-H, 5'-H), 7.10 (d, *J* = 8.2 Hz, 2'-H, 6'-H), 4.20 – 4.14 (m, 4H, P-O-CH<sub>2</sub>CH<sub>3</sub>), 2.99 (d, *J* = 20.6 Hz, 1H, 2-H), 2.30 (s, 3H, 4'-CH<sub>3</sub>), 1.35 (t, *J* = 7.1 Hz, 3H, P-O-CH<sub>2</sub>CH<sub>3</sub>); <sup>13</sup>C NMR (126 MHz, CDCl<sub>3</sub>) δ 162.01 (d, *J* = 3.5 Hz, 1-C), 135.32 (1'-C), 134.21 (4'-C), 129.56 (2'-C, 6'-C), 120.09 (3'-C, 5'-C), 63.12 (d, *J* = 6.7 Hz, P-O-CH<sub>2</sub>CH<sub>3</sub>), 36.19 (d, *J* = 129.6 Hz, 2-C), 20.99 (s, 4'-CH<sub>3</sub>), 16.49 (d, *J* = 6.0 Hz, P-O-CH<sub>2</sub>CH<sub>3</sub>); <sup>31</sup>P NMR (203 MHz, CDCl<sub>3</sub>) δ 22.90; HRMS (ESI<sup>+</sup>) *m/z* calculated for C<sub>13</sub>H<sub>21</sub>NO<sub>4</sub>P 286.1203 [M+H]<sup>+</sup>, found 286.1199; TLC (petroleum ether – EtOAc, 2:8): *R*<sub>f</sub> = 0.10.

**Diethyl (2-((4-methoxyphenyl)amino)-2-oxoethyl)phosphonate 43.** Compound **43** was



synthesized according to **GP-8**, using intermediate **39** (208 mg, 1.04 mmol) and triethylphosphite (3.50 mL, 20.2 mmol). The reaction was stirred for 21 h at 150 °C. After concentration in high vacuum to evaporate excessive triethylphosphite, and column chromatography (petroleum ether – EtOAc, 2:8) **43** was obtained as yellow solid (235 mg, 75%). <sup>1</sup>H NMR (500 Hz, CDCl<sub>3</sub>) δ 8.71 (s, 1H, NH), 7.42 (d, *J* = 9.0 Hz, 3'-H, 5'-H), 6.83 (d, *J* = 9.0 Hz, 2'-H, 6'-H), 4.20 – 4.14 (m, 4H, P-O-CH<sub>2</sub>CH<sub>3</sub>), 3.78 (s, 3H, 4'-OCH<sub>3</sub>), 2.99 (d, *J* = 20.6 Hz, 2H, 2-H), 1.35 (t, *J* = 7.1 Hz, 3H, P-O-CH<sub>2</sub>CH<sub>3</sub>); <sup>13</sup>C NMR (126 MHz, CDCl<sub>3</sub>) δ 161.96 (d, *J* = 3.3 Hz, 1-C), 156.63 (4'-C), 131.03 (1'-C), 121.83 (3'-C, 5'-C), 114.24 (2'-C, 6'-C), 63.13 (d, *J* = 6.2 Hz, P-O-CH<sub>2</sub>CH<sub>3</sub>), 55.60 (4'-OCH<sub>3</sub>), 36.03 (d, *J* = 129.9 Hz, 2-C), 16.50 (d, *J* = 6.2 Hz, P-O-CH<sub>2</sub>CH<sub>3</sub>); <sup>31</sup>P NMR (203 MHz, CDCl<sub>3</sub>) δ 22.97; HRMS (ESI<sup>+</sup>) *m/z* calculated for C<sub>13</sub>H<sub>21</sub>NO<sub>5</sub>P 302.1152 [M+H]<sup>+</sup>, found 302.1134; TLC (petroleum ether – EtOAc, 2:8): R<sub>f</sub> = 0.10.

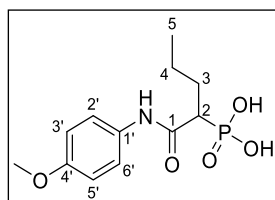
**(1-((3,4-Dichlorophenyl)amino)-1-oxopentan-2-yl)phosphonic acid 44.** Compound **44** was



synthesized according to **GP-9**, using intermediate **53** (494 mg, 1.29 mmol) and TMSBr (850 μL, 6.55 mmol) in dry CH<sub>2</sub>Cl<sub>2</sub> (6 mL). The reaction was stirred for 15 h at rt, then MeOH (10 mL) was added and stirred for another 1 h. After concentration *in vacuo* and HPLC purification (method **HPLC-05**) **45** was obtained as white solid (355 mg, 85%). MP = 226 °C; <sup>1</sup>H NMR

(500 Hz, DMSO-*d*<sub>6</sub>) δ = 10.27 (s, 1H, NH), 8.04 (d, *J* = 2.4 Hz, 2'-H), 7.54 (d, *J* = 8.8 Hz, 5'-H), 7.46 (dd, *J* = 2.5, 8.8 Hz, 6'-H), 2.85 (ddd, *J* = 3.3, 11.2, 22.0 Hz, 2-H), 1.97-1.87 (m, 1H, 3-H<sub>a</sub>), 1.66-1.57 (m, 1H, 3-H<sub>b</sub>), 1.35-1.25 (m, 1H, 4-H<sub>a</sub>), 1.24-1.15 (m, 1H, 4-H<sub>b</sub>), 0.86 (t, *J* = 7.4 Hz, 3H, 5-H); <sup>13</sup>C NMR (75 MHz, DMSO-*d*<sub>6</sub>) δ = 168.42 (d, *J* = 4.6 Hz, 1-C), 139.39 (3'-C or 4'-C), 130.91 (3'-C or 4'-C), 130.62 (5'-C), 124.39 (1'-C), 120.21 (2'-C), 119.08 (6'-C), 47.89 (d, *J* = 126.6 Hz, 2-C), 28.88 (d, *J* = 4.2 Hz, 3-C), 21.19 (d, *J* = 15.4 Hz, 4-C), 13.69 (5-C); <sup>31</sup>P NMR (162 MHz, DMSO-*d*<sub>6</sub>) δ = 18.81; HRMS (ESI<sup>+</sup>) *m/z* calculated for C<sub>11</sub>H<sub>15</sub>Cl<sub>2</sub>NO<sub>4</sub>P 326.0110 [M+H]<sup>+</sup>, found 326.0108; HRMS (ESI<sup>-</sup>) *m/z* calculated for C<sub>11</sub>H<sub>13</sub>Cl<sub>2</sub>NO<sub>4</sub>P 323.9965 [M-H]<sup>-</sup>, found 323.9967; HPLC (method **HPLC-05**): R<sub>t</sub> = 17.0 min; λ<sub>max</sub> = 253 nm.

**(1-((4-Methoxyphenyl)amino)-1-oxopentan-2-yl)phosphonic acid 45.** Compound **45** was

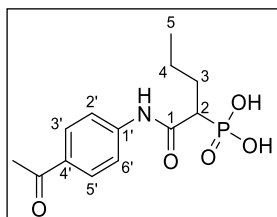


synthesized according to **GP-9**, using intermediate **54** (491 mg, 1.43 mmol) and TMSBr (940 μL, 7.18 mmol) in dry CH<sub>2</sub>Cl<sub>2</sub> (6 mL). The reaction was stirred for 15 h at rt, then MeOH (10 mL) was added and stirred for another 1 h. After concentration *in vacuo* and HPLC purification (method **HPLC-06**) **45** was obtained as white solid (360 mg, 88%). MP = 244 °C; <sup>1</sup>H NMR

(500 Hz, DMSO-*d*<sub>6</sub>) δ = 9.75 (s, 1H, NH), 7.50 (d, *J* = 9.1 Hz, 3'-H, 5'-H), 6.86 (d, *J* = 9.1 Hz, 2'-H, 6'-H), 3.71 (s, 3H, 4'-OCH<sub>3</sub>), 2.82 (ddd, *J* = 3.3, 11.2, 21.7 Hz, 1H, 2-H), 1.96-1.86 (m, 1H, 3-H<sub>a</sub>), 1.64-1.55 (m, 1H, 3-H<sub>b</sub>), 1.36-1.16 (m, 2H, 4-H), 0.86 (t, *J* = 7.3 Hz, 3H, 5-H); <sup>13</sup>C NMR (126 MHz, DMSO-*d*<sub>6</sub>): δ = 167.25

(d,  $J = 4.5$  Hz, 1-C), 155.01 (4'-C), 132.66 (1'-C), 120.54 (3'-C, 5'-C), 113.72 (2'-C, 6'-C), 55.16 (4'-OCH<sub>3</sub>), 47.48 (d,  $J = 127.8$  Hz, 2-C), 29.06 (d,  $J = 4.5$  Hz, 3-C), 21.19 (d,  $J = 15.7$  Hz, 4-C), 13.73 (5-C); <sup>31</sup>P NMR (203 MHz, DMSO-*d*<sub>6</sub>)  $\delta = 19.87$ ; HRMS (ESI<sup>+</sup>)  $m/z$  calculated for C<sub>12</sub>H<sub>19</sub>NO<sub>5</sub>P 288.0995 [M+H]<sup>+</sup>, found 288.0992; HRMS (ESI<sup>-</sup>)  $m/z$  calculated for C<sub>12</sub>H<sub>17</sub>NO<sub>5</sub>P 286.0850 [M-H]<sup>-</sup>, found 286.0850; HPLC (method **HPLC-06**):  $R_t = 16.5$  min;  $\lambda_{\max} = 251$  nm.

**(1-((4-Acetylphenyl)amino)-1-oxopentan-2-yl)phosphonic acid 46.** Compound **46** was



synthesized according to **GP-9**, using intermediate **55** (94 mg, 0.26 mmol) and TMSBr (190  $\mu$ L, 1.45 mmol) in dry CH<sub>2</sub>Cl<sub>2</sub> (5 mL). The reaction was stirred for 21 h at rt, then MeOH (10 mL) was added and stirred for another 1 h. After concentration *in vacuo* and HPLC purification (method **HPLC-07**)

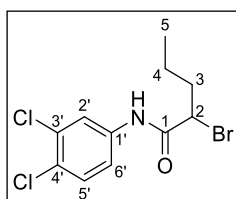
**46** was obtained as white solid (47 mg, 60%). <sup>1</sup>H NMR (500 Hz, DMSO-*d*<sub>6</sub>)  $\delta = 10.25$  (s, 1H, NH), 7.91 (d,  $J = 8.8$  Hz, 2H, 3'-H, 5'-H), 7.73 (d,  $J = 8.8$  Hz, 2H, 2'-H, 6'-H), 2.93 (ddd,  $J = 3.3, 11.0, 22.0$  Hz, 1H, 2-H), 2.52 (s, 3H, (CO)CH<sub>3</sub>), 2.02-1.86 (m, 1H, 3-H<sub>a</sub>), 1.70-1.56 (m, 1H, 3-H<sub>b</sub>), 1.38-1.16 (m, 1H, 4-H), 0.87 (t,  $J = 7.3$  Hz, 3H, 5-H); <sup>13</sup>C NMR (126 MHz, DMSO-*d*<sub>6</sub>)  $\delta = 196.47$  ((CO)CH<sub>3</sub>), 168.45 (d,  $J = 5.0$  Hz, 1-C), 143.64 (4'-C), 131.55 (1'-C), 129.41 (3'-C, 5'-C), 118.28 (2'-C, 6'-C), 47.84 (d,  $J = 126.6$  Hz, 2-C), 28.97 (d,  $J = 4.1$  Hz, 3-C), 26.40 ((CO)CH<sub>3</sub>), 21.18 (d,  $J = 15.5$  Hz, 4-C), 13.67 (5-C); <sup>31</sup>P NMR (203 MHz, DMSO-*d*<sub>6</sub>)  $\delta = 19.04$ ; HRMS (ESI<sup>-</sup>)  $m/z$  calculated for C<sub>13</sub>H<sub>17</sub>NO<sub>5</sub>P 298.0849 [M-H]<sup>-</sup>, found 298.0835; HPLC (method **HPLC-07**):  $R_t = 16.0$  min;  $\lambda_{\max} = 288$  nm.

**(1-((3,4-Dichlorophenyl)amino)-4-methyl-1-oxopentan-2-yl)phosphonic acid 47.** Compound **47** was synthesized by Jelena Konstantinović. It was published as compound nr. 64 in our patent application.<sup>1</sup>

**(1-((4-Methoxyphenyl)amino)-4-methyl-1-oxopentan-2-yl)phosphonic acid 48.** Compound **48** was synthesized by Jelena Konstantinović. It was published as compound nr. 66 in our patent application.<sup>1</sup>

**(1-((4-Acetylphenyl)amino)-4-methyl-1-oxopentan-2-yl)phosphonic acid 49.** Compound **49** was synthesized by Jelena Konstantinović. It was published as compound nr. 67 in our patent application.<sup>1</sup>

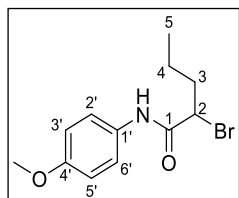
**N-(3,4-Dichlorophenyl)-2-bromopentanamide 50.** Compound **50** was synthesized according to **GP-**



**3**, using 3,4-dichloroaniline (1.60 g, 9.90 mmol), 2-bromopentanoic acid (1.50 mL, 11.4 mmol) and EDC·HCl (2.20 g, 11.5 mmol) in CH<sub>2</sub>Cl<sub>2</sub> (10 mL). The reaction was stirred for 19 h at rt. After extraction, **50** was obtained as white solid without further purification (3.06 g, 95%). <sup>1</sup>H NMR (300 Hz, CDCl<sub>3</sub>)  $\delta = 8.08$  (s, 1H, NH), 7.77 (d,  $J = 2.2$  Hz, 1H, 2'-H), 7.40 (d,  $J = 8.7$  Hz, 1H, 5'-H), 7.35

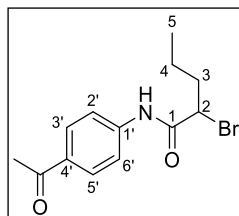
(dd,  $J = 2.3, 8.7$  Hz, 6'-H), 4.43 (dd,  $J = 5.3, 8.2$  Hz, 1H, 2-H), 2.24–2.00 (m, 2H, 3-H), 1.64–1.44 (m, 2H, 4-H), 0.98 (t,  $J = 7.4$  Hz, 3H, 5-H);  $^{13}\text{C}$  NMR (75 MHz,  $\text{CDCl}_3$ )  $\delta = 167.14$  (1-C), 136.72 (1'-C), 133.15 (3'-C or 4'-C), 130.78 (5'-C), 128.52 (3'-C or 4'-C), 121.87 (2'-C), 119.36 (6'-C), 51.78 (2-C), 37.92 (3-C), 20.72 (4-C), 13.38 (5-C); HRMS (ESI<sup>+</sup>)  $m/z$  calculated for  $\text{C}_{11}\text{H}_{13}\text{BrCl}_2\text{NO}$  323.9552 [M+H]<sup>+</sup>, found 323.9552; TLC (petroleum ether-EtOAc, 3:7):  $R_f = 0.70$ .

***N*-(4-Methoxyphenyl)-2-bromopentanamide 51.** Compound **51** was synthesized according to **GP-3**,



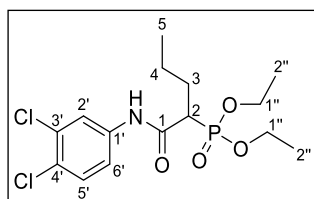
using 4-methoxyaniline (1.73 g, 14.1 mmol), 2-bromopentanoic acid (2.20 mL, 16.8 mmol) and EDC·HCl (3.21 g, 16.7 mmol) in  $\text{CH}_2\text{Cl}_2$  (10 mL). The reaction was stirred for 18 h at rt. After extraction, **51** was obtained as white solid without further purification (4.48 g, quant.).  $^1\text{H}$  NMR (300 MHz,  $\text{CDCl}_3$ )  $\delta = 7.99$  (s, 1H, NH), 7.43 (d,  $J = 9.0$  Hz, 2H, aryl-H<sub>a</sub>), 6.88 (d,  $J = 9.0$  Hz, 2H, aryl-H<sub>b</sub>), 4.43 (dd,  $J = 5.2, 8.2$  Hz, 1H, 2-H), 3.80 (s, 3H, 4'-OCH<sub>3</sub>), 2.25–1.97 (m, 2H, 3-H), 1.65–1.45 (m, 2H, 4-H), 0.98 (t,  $J = 7.3$  Hz, 3H, 5-H);  $^{13}\text{C}$  NMR (126 MHz,  $\text{CDCl}_3$ )  $\delta$  166.84 (1-C), 157.16 (4'-C), 130.36 (1'-C), 122.08 (aryl-C<sub>a</sub>), 114.41 (aryl-C<sub>b</sub>), 55.67 (4'-OCH<sub>3</sub>), 52.40 (2-C), 38.15 (3-C), 20.74 (4-C), 13.42 (5-C); HRMS (ESI<sup>+</sup>)  $m/z$  calculated for  $\text{C}_{12}\text{H}_{17}\text{BrNO}_2$  286.0438 [M+H]<sup>+</sup>, found 286.0427; TLC (petroleum ether-EtOAc, 3:7):  $R_f = 0.65$ .

***N*-(4-Acetylphenyl)-2-bromopentanamide 52.** Compound **52** was synthesized according to **GP-3**,



using 4-aminoacetophenone (300 mg, 2.22 mmol), 2-bromopentanoic acid (350  $\mu\text{L}$ , 2.55 mmol) and EDC·HCl (515 mg, 2.69 mmol) in 10 mL  $\text{CH}_2\text{Cl}_2$ . The reaction was stirred overnight at room temperature. After extraction, **52** was obtained as yellow oil without further purification (676 mg, quant.).  $^1\text{H}$  NMR (300 MHz,  $\text{CDCl}_3$ )  $\delta$  8.24 (*br s*, 1H), 7.97 (d,  $J = 8.7$  Hz, 2H), 7.66 (d,  $J = 8.7$  Hz, 2H), 4.46 (dd,  $J = 5.4, 8.1$  Hz, 1H), 2.59 (s, 3H), 2.26–2.02 (m, 2H), 1.66–1.45 (m, 1H), 0.98 (t,  $J = 7.4$  Hz, 3H);  $^{13}\text{C}$  NMR (75 MHz,  $\text{CDCl}_3$ )  $\delta$  197.01, 167.16, 141.53, 133.64, 129.88, 119.25, 51.83, 37.87, 26.63, 20.71, 13.36; HRMS (ESI)  $m/z$  calculated for  $\text{C}_{13}\text{H}_{17}\text{BrNO}_2$  298.0437 [M+H]<sup>+</sup>, found 298.0422; TLC (petroleum ether – EtOAc, 7:3):  $R_f = 0.30$ .

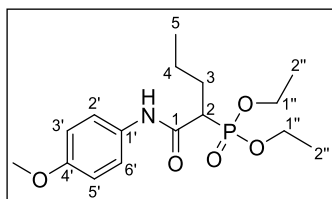
**Diethyl (1-((3,4-dichlorophenyl)amino)-1-oxopentan-2-yl)phosphonate 53.** Compound **53** was



synthesized according to **GP-8**, using intermediate **50** (1.22 g, 3.75 mmol) and triethylphosphite (6.0 mL, 34.7 mmol). The reaction was stirred for 3 d at 150 °C. After concentration in high vacuum to evaporate excessive triethylphosphite, and column chromatography (petroleum ether – EtOAc, 9:1 → 0:10) **53** was obtained as yellow wax-like solid (1.05 g, 73%).  $^1\text{H}$  NMR (500 Hz,  $\text{CDCl}_3$ )  $\delta = 9.83$  (s, 1H, NH), 7.63 (d,  $J = 2.3$  Hz, 2'-H), 7.31 (dd,  $J = 2.5, 8.8$  Hz, 6'-H), 7.12 (d,  $J = 8.8$  Hz, 5'-H), 4.34–4.08 (m, 4H, P-O-CH<sub>2</sub>CH<sub>3</sub>), 3.11 (ddd,  $J = 3.4, 10.9, 22.1$  Hz,

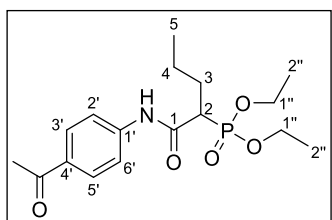
1H, 2-H), 2.17–2.02 (m, 1H, 3-H<sub>a</sub>), 1.80–1.65 (m, 1H, 3-H<sub>b</sub>), 1.53–1.21 (m, 2H, 4-H), 1.40 (t, *J* = 7.1 Hz, 3H, P-O-CH<sub>2</sub>CH<sub>3</sub><sub>a</sub>), 1.37 (t, *J* = 7.1 Hz, 3H, P-O-CH<sub>2</sub>CH<sub>3</sub><sub>b</sub>), 0.93 (t, *J* = 7.3 Hz, 3H, 5-H); <sup>13</sup>C NMR (75 MHz, CDCl<sub>3</sub>) δ = 166.36 (d, *J* = 4.4 Hz, 1-C), 138.02 (3'-C or 4'-C), 132.35 (3'-C or 4'-C), 130.05 (5'-C), 126.86 (1'-C), 120.98 (2'-C), 118.50 (6'-C), 64.16 (d, *J* = 6.2 Hz, P-O-C<sub>a</sub>H<sub>2</sub>CH<sub>3</sub>), 62.32 (d, *J* = 6.9 Hz, P-O-C<sub>b</sub>H<sub>2</sub>CH<sub>3</sub>), 47.14 (d, *J* = 129.9 Hz, 2-C), 29.28 (d, *J* = 5.4 Hz, 3-C), 21.58 (d, *J* = 15.1 Hz, 4-C), 16.56 (t, *J* = 5.7 Hz, P-O-CH<sub>2</sub>CH<sub>3</sub>), 13.76 (5-C); <sup>31</sup>P NMR (203 MHz, CDCl<sub>3</sub>) δ = 25.48; HRMS (ESI<sup>+</sup>) *m/z* calculated for C<sub>15</sub>H<sub>23</sub>Cl<sub>2</sub>NO<sub>4</sub>P 382.0736 [M+H]<sup>+</sup>, found 382.0734; TLC (petroleum ether-EtOAc, 4:6): R<sub>f</sub> = 0.10.

**Diethyl (1-((4-methoxyphenyl)amino)-1-oxopentan-2-yl)phosphonate 54.** Compound **54** was



synthesized according to **GP-8**, using intermediate **51** (1.25 g, 4.38 mmol) and triethylphosphite (7.0 mL, 40.4 mmol). The reaction was stirred for 3 d at 150 °C. After concentration in high vacuum to evaporate excessive triethylphosphite, and column chromatography (petroleum ether – EtOAc, 9:1 → 0:10) **54** was obtained as white solid (0.94 g, 62%). <sup>1</sup>H NMR (500 Hz, DMSO-*d*<sub>6</sub>) δ = 9.96 (s, 1H, NH), 7.47 (d, *J* = 9.0 Hz, 3'-H, 5'-H), 6.88 (d, *J* = 9.0 Hz, 2'-H, 6'-H), 4.10–3.95 (m, 4H, P-O-CH<sub>2</sub>CH<sub>3</sub>), 3.71 (s, 3H, 4'-OCH<sub>3</sub>), 3.05 (ddd, *J* = 3.5, 11.1, 21.6 Hz, 1H, 2-H), 1.97–1.87 (m, 1H, 3-H<sub>a</sub>), 1.63–1.55 (m, 1H, 3-H<sub>b</sub>), 1.36–1.23 (m, 2H, 4-H), 1.22 (t, *J* = 7.1 Hz, 3H, P-O-CH<sub>2</sub>CH<sub>3</sub><sub>a</sub>), 1.20 (t, *J* = 7.1 Hz, 3H, P-O-CH<sub>2</sub>CH<sub>3</sub><sub>b</sub>), 0.87 (t, *J* = 7.3 Hz, 3H, 5-H); <sup>13</sup>C NMR (126 MHz, DMSO-*d*<sub>6</sub>) δ = 165.90 (d, *J* = 4.4 Hz, 1-C), 155.34 (4'-C), 132.13 (1'-C), 120.67 (3'-C, 5'-C), 113.89 (2'-C, 6'-C), 61.91 (d, *J* = 6.2 Hz, P-O-C<sub>a</sub>H<sub>2</sub>CH<sub>3</sub>), 61.70 (d, *J* = 6.4 Hz, P-O-C<sub>b</sub>H<sub>2</sub>CH<sub>3</sub>), 55.18 (4'-OCH<sub>3</sub>), 45.90 (d, *J* = 131.01 Hz, 2-C), 28.78 (d, *J* = 5.1 Hz, 3-C), 20.92 (d, *J* = 16.1 Hz, 4-C), 16.32 (d, *J* = 5.6 Hz, P-O-CH<sub>2</sub>CH<sub>3</sub>), 13.56 (5-C); <sup>31</sup>P NMR (203 MHz, DMSO-*d*<sub>6</sub>) δ = 24.76; HRMS (ESI<sup>+</sup>) *m/z* calculated for C<sub>16</sub>H<sub>27</sub>NO<sub>5</sub>P 344.1621 [M+H]<sup>+</sup>, found 344.1617. TLC (petroleum ether-EtOAc, 2:8): R<sub>f</sub> = 0.20.

**Diethyl (1-((4-acetylphenyl)amino)-1-oxopentan-2-yl)phosphonate 55.** Compound **55** was



synthesized according to **GP-8**, using intermediate **52** (210 mg, 0.704 mmol) and triethylphosphite (2.50 mL, 14.4 mmol). The reaction was stirred for 22 h at 150 °C. After concentration in high vacuum to evaporate excessive triethylphosphite, and column chromatography (petroleum ether – EtOAc, 2:8) **55** was obtained as white solid (104 mg, 42%). <sup>1</sup>H NMR (500 Hz, CDCl<sub>3</sub>) δ 9.55 (s, 1H, NH), 7.73 (d, *J* = 8.8 Hz, 2'-H, 6'-H), 7.55 (d, *J* = 8.8 Hz, 3'-H, 5'-H), 4.29 – 4.13 (m, 4H, P-O-CH<sub>2</sub>CH<sub>3</sub>), 3.10 (ddd, *J* = 3.7, 10.7, 22.3 Hz, 1H, 2-H), 2.49 (s, 3H, 4'-COCH<sub>3</sub>), 2.14 – 2.04 (m, 1H, 3-H<sub>a</sub>), 1.82 – 1.73 (m, 1H, 3-H<sub>b</sub>), 1.56 – 1.46 (m, 1H, 4-H<sub>a</sub>), 1.39 – 1.34 (m, 7H, P-O-CH<sub>2</sub>CH<sub>3</sub>, 4-H<sub>b</sub>), 0.94 (t, *J* = 7.3 Hz, 3H, 5-H); <sup>13</sup>C NMR (126 MHz, CDCl<sub>3</sub>) δ 197.03 (4'-COCH<sub>3</sub>), 166.54 (d, *J* = 2.1 Hz, 1-C), 142.67 (1'-C), 132.60 (4'-C), 129.52 (2'-C, 6'-C), 118.86 (3'-C, 5'-C), 63.86 (d, *J* = 6.5 Hz, P-O-C<sub>a</sub>H<sub>2</sub>CH<sub>3</sub>), 62.58 (d, *J* = 6.8 Hz, P-O-C<sub>b</sub>H<sub>2</sub>CH<sub>3</sub>), 47.25 (d, *J* = 129.3 Hz, 2-C), 29.26 (d, *J* = 5.2 Hz, 3-C), 26.43 (4'-COCH<sub>3</sub>), 21.65 (d, *J* = 14.8 Hz, 4-C), 16.56 (d, *J* = 6.2 Hz, P-O-CH<sub>2</sub>CH<sub>3</sub>), 16.50 (d, *J* = 6.2 Hz, P-

## A6. Supporting Information to Chapter F

O-CH<sub>2</sub>C<sub>6</sub>H<sub>3</sub>), 13.81 (5-C); <sup>31</sup>P NMR (203 MHz, CDCl<sub>3</sub>) δ 25.50; HRMS (ESI<sup>+</sup>) *m/z* calculated for C<sub>17</sub>H<sub>27</sub>NO<sub>5</sub>P 356.1621 [M+H]<sup>+</sup>, found 356.1621. TLC (petroleum ether – EtOAc, 2:8): R<sub>f</sub> = 0.15.

### 4. HPLC procedures

Preparative column chromatography was done using an Agilent Technologies 1200 Series HPLC-system equipped with an Agilent 1100/1200 Quaternary Pump and a PDA detector.

**Eluent A:** Acetonitrile + 0.1% TFA

**Eluent B:** Water + 0.1% TFA

**Column:** Agilent Prep-C18 (10 μm, 30 x 100 mm)

**Flow rate:** 9.0 mL/min

**Detection:** PDA (200-400 nm)

Gradients used for purification can be found in the following tables with reference to the compounds purified.

**HPLC method 1.** Method HPLC-01 used for the purification of compound 32.

Time [min]	0	10	18	18.5	20.5	21	22
A%	45	82	82	100	100	45	45

**HPLC method 2.** Method HPLC-02 used for the purification of compound 33.

Time [min]	0	25	26	30	31	33
A%	35	35	100	100	35	35

**HPLC method 3.** Method HPLC-03 used for the purification of compound 34.

Time [min]	0	23	24	26	27	28
A%	30	45	100	100	30	30

**HPLC method 4.** Method HPLC-04 used for the purification of compound 35.

Time [min]	0	27	28	32	33	35
A%	20	30	100	100	20	20

**HPLC method 5.** Method HPLC-05 used for the purification of compound 44.

Time [min]	0	1	20	21	24	24.5	25
A%	45	45	801	100	100	45	45



**HPLC method 6.** Method **HPLC-06** used for the purification of compound **45**.

Time [min]	0	1	15	18.5	19	23	24	25
A%	30	30	62	62	100	100	30	30

**HPLC method 7.** Method **HPLC-07** used for the purification of compound **46**.

Time [min]	0	1	14	20	21	23	24	25
A%	30	30	56	56	100	100	30	30

## 5. PK Sample Preparation and Analysis

The PK determination was performed as described previously by the HZI in cooperation with Sartorius.<sup>198</sup> Groups of male CD1 mice (25-30 g, Charles River UK) were housed in groups of up to 6 and maintained under a 12 h light/dark cycle with free access to food and water. Temperature and humidity were controlled according to U.K. HO regulations. On the day of the study, mice were briefly anaesthetized with isoflurane before suspending the mouse by its upper incisors on a board held at an angle of approx. 45 degrees. Mice were then dosed intratracheally with compound 16 at the designated dose formulated in ethanol/tyloxapol/glycerol/phosphate-buffered saline (PBS) [10:1:5:84] in a 1 mL/kg dosing volume up to a maximum of 30  $\mu$ L per mouse. All samples were stored at -20  $^{\circ}$ C until sent for analysis on dry ice.

All PK plasma samples were analyzed via HPLC-MS/MS using an Agilent 1290 Infinity II HPLC system coupled to an AB Sciex QTrap 6500plus mass spectrometer. The lower limits of quantification are indicated in Table S5. Caffeine was used as internal standard.

HPLC conditions were as follows: column: Agilent Zorbax Eclipse Plus C18, 50x2.1 mm, 1.8  $\mu$ m; temperature: 30  $^{\circ}$ C; injection volume: 10  $\mu$ L; flow rate: 700  $\mu$ L/min; solvent A: water + 0.1% formic acid; solvent B: acetonitrile + 0.1% formic acid; gradient: 99% A at 0 min, 99% – 0% A from 0.1 min to 4.00 min, 0% A until 4.50 min, 0% – 99% A from 4.50 to 4.70 min. Mass spectrometric conditions were as follows: Scan type: MRM, positive mode; Q1 and Q3 masses for caffeine, 16 can be found in Table S6; peak areas of each sample and of the corresponding internal standard were analyzed using MultiQuant 3.0 software (AB Sciex). Peak areas of the respective sample of 16 were normalized to the internal standard peak area. Peaks of PK samples were quantified using the calibration curve. PK parameters were determined using a non-compartmental analysis with PKSolver.<sup>212</sup> ELF concentrations were calculated using equations (S3) and (S4).<sup>196</sup>

$$V_{ELF} = V_{BALF} \times \frac{Urea_{BALF}}{Urea_{plasma}} \quad (S3)$$

$$c_{ELF} = c_{BALF} \times \frac{V_{BALF}}{V_{ELF}} \quad (S4)$$

## A6. Supporting Information to Chapter F

**Table 1.** PK parameters in BALF and ELF.

	<b>BALF</b>	<b>ELF</b>
<b>T<sub>max</sub> [h]</b>	0.7 ± 0.3	0.8 ± 0.1
<b>C<sub>max</sub> [µg/ml]</b>	0.31 ± 0.14	38.6 ± 35.1
<b>AUC<sub>0-t</sub> [µg/ml*h]</b>	0.27 ± 0.09	33.6 ± 10.7
<b>Medium residence time (MRT) [h]</b>	1.4 ± 0.0	1.3 ± 0.4

## A7. SUPPORTING INFORMATION TO CHAPTER G

**Functionalized  $\alpha$ -Side chains as Booster for the Inhibitory Activity of *N*-Aryl mercaptoacetamides on *C. histolyticum* Virulence Factor ColH**

Katrin Voos, Esther Schönauer, Jelena Konstantinović, Sebastian Dahmen, Marcel Lutz, Selina Wolter, Anna K. H. Hirsch\* and Christian Ducho\*

\* corresponding authors

Please note that the following chapter is the supporting information of a manuscript in preparation.

## 1. General Procedures

**General procedure GP-1: Synthesis of 2-chloroalkanoic acids (taken from Chapter E).** Amino acid (1.0 eq) was dissolved in 6 M HCl (2 mL/mmol or until mostly dissolved) under nitrogen atmosphere and cooled to  $-5\text{ }^{\circ}\text{C}$ . Sodium nitrite (2.5 eq) was dissolved in water (0.3 mL/mmol amino acid) and added slowly dropwise. The reaction was stirred overnight while warming to room temperature. The reaction was extracted with EtOAc/THF. The combined organic extracts were washed with saturated aqueous NaCl solution and dried over anhydrous  $\text{Na}_2\text{SO}_4$  and filtered. The solvent was removed under reduced pressure to afford the crude product. The crude product obtained was used in the next step without further purification.

**General procedure GP-5: Synthesis of *N*-aryl-2-thioacetyl-2-alkylacetamide derivatives (taken from Chapter E).** *N*-aryl-2-halo-2-alkylacetamide derivative (1.0 eq) (purified or as crude) was dissolved in acetone, and potassium thioacetate (1–2 eq) was added to the solution. The resultant mixture was stirred at room temperature. After concentration under vacuum, the resultant residue was diluted with  $\text{H}_2\text{O}$  and extracted with EtOAc. The organic layer was washed with saturated aqueous NaCl solution, dried over anhydrous  $\text{Na}_2\text{SO}_4$ , filtered and evaporated under reduced pressure. The crude residue was purified using column chromatography.

**General procedure GP-6: Synthesis of 2-mercapto-*N*-aryl-2-alkylacetamide derivatives (taken from Chapter E).** NaOH (3–4 eq) was added to a solution of *N*-aryl-2-thioacetyl-2-alkylacetamide (1.0 eq) in MeOH under argon atmosphere. The reaction was stirred at room temperature. The reaction was acidified with 2 M HCl and extracted with EtOAc and 0.5 M HCl. The organic layer was washed with 0.5 M HCl and with saturated aqueous NaCl solution, dried over anhydrous  $\text{Na}_2\text{SO}_4$ , filtered and evaporated under reduced pressure. The product was obtained in pure form or purified using column chromatography or preparative HPLC.

**General procedure GP-10: Synthesis of  $\Omega$ -amine protected  $\alpha$ ,  $\Omega$ -diamino acids.**  $\alpha$ ,  $\Omega$ -Diamino acid hydrochloride (1.0 eq) and NaOH (1.1 eq) were dissolved in water. Ethyltrifluoroacetate (1.0 eq) was added to the solution and the reaction was stirred heavily for at least 2 h. White crystals were formed during the reaction. To improve precipitation, the solution was cooled to  $2\text{--}8^{\circ}\text{C}$  and left without stirring overnight. The formed crystals were filtered, washed with a small portion of cold water and used directly without further purification in the next reaction.

**General procedure GP-11: Synthesis of 2-bromoalkanoic acids.** ( $\Omega$ -protected)  $\alpha$ -Amino acid (1.0 eq) and KBr (1.5 eq) were dissolved in 2 M  $\text{H}_2\text{SO}_4$  (1 mL/mmol or until mostly dissolved) under nitrogen atmosphere and cooled to  $-5\text{ }^{\circ}\text{C}$ . Sodium nitrite (2.0 eq) was added slowly in small portions. The reaction was stirred overnight while warming to room temperature. The reaction was extracted with EtOAc/THF (3:1). The combined organic extracts were washed with saturated aqueous NaCl solution and dried over anhydrous  $\text{Na}_2\text{SO}_4$  and filtered. The solvent was removed under reduced pressure to afford the crude product. The crude product obtained was used in the next step without further purification.

**General procedure GP-12: Synthesis of 2-mercapto-*N*-aryl-2-aminoalkylacetamide derivatives with free  $\Omega$ -amine in the side chain.** Et<sub>3</sub>N (50  $\mu$ L/mL) and LiOH (50 mg/mL) were added to a solution of  $\Omega$ -(2'',2'',2''-trifluoroacetamido)-protected 2-mercapto-*N*-aryl-2-( $\Omega$ -amino)alkylacetamide derivatives (1.0 eq) in MeOH under argon atmosphere. The reaction was stirred at room temperature for 3-4 h with LCMS control. After complete deprotection, the reaction was acidified to  $\sim$ pH 1 with TFA, diluted with water and directly purified using preparative HPLC.

## 2. Compounds 66, 67 and 93–99

**Methyl 3-mercapto-4-((4'-methoxyphenyl)amino)-4-oxobutanoate 66.** Compound **66** was synthesized by Jelena Konstantinović. Its original compound number is **JMK142**.

**Methyl 3-mercapto-4-((3',4'-dichlorophenyl)amino)-4-oxobutanoate 67.** Compound **67** was synthesized by Jelena Konstantinović. Its original compound number is **JMK208**.

**2-Mercapto-*N*-(3',4'-dichlorophenyl)-5-(2,2,2-trifluoroacetamido)pentanamide 93.** Compound **93** was synthesized by Sebastian Dahmen during his Master's thesis.<sup>213</sup> Its original compound number is **SD23**.

**5-Amino-*N*-(3',4'-dichlorophenyl)-2-mercaptopentanamide (TFA salt) 94.** Compound **94** was synthesized by Sebastian Dahmen during his Master's thesis.<sup>213</sup> Its original compound number is **SD24**.

**2-Mercapto-*N*-(3',4'-dichlorophenyl)-6-(2,2,2-trifluoroacetamido)hexanamide 95.** Compound **95** was synthesized by Sebastian Dahmen during his Master's thesis.<sup>213</sup> Its original compound number is **SD16**.

**6-Amino-*N*-(3',4'-dichlorophenyl)-2-mercaptohexanamide (TFA salt) 96.** Compound **96** was synthesized by Sebastian Dahmen during his Master's thesis.<sup>213</sup> Its original compound number is **SD17**.

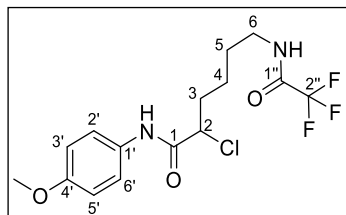
**2-Mercapto-*N*-(3',4'-dichlorophenyl)-4-(methylthio)butanamide 97.** Compound **97** was synthesized by Sebastian Dahmen during his Master's thesis.<sup>213</sup> Its original compound number is **SD05**.

**2-Mercapto-3-methoxy-*N*-(4'-methoxyphenyl)propenamide 98.** Compound **98** was synthesized by Jelena Konstantinović. Its original compound number is **JMK159**.

**2-Mercapto-3-methoxy-*N*-(3',4'-dichlorophenyl)propenamide 99.** Compound **99** was synthesized by Jelena Konstantinović. Its original compound number is **JMK175**.

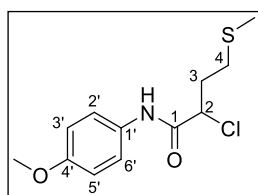
### 3. Synthesis of compounds 72–74, 77–92

#### 2-Chloro-6-(2'',2'',2''-trifluoroacetamido)-N-(4'-methoxyphenyl)hexanamide **72**.



was synthesized in 3 steps. The first step was performed according to **GP-10**, using DL-lysine hydrochloride (2.05 g, 11.2 mmol), NaOH (0.51 g, 12.8 mmol) and ethyltrifluoroacetate (1.40 mL, 11.8 mmol) in water (10 mL). The reaction was stirred vigorously for 25 h at rt. The resulting white crystals were filtered, washed with cold water, and used without further purification in the next step. (606 mg, max. 2.5 mmol, max. 22%). The named crystals were subjected to **GP-1**. Therefore, they were dissolved in 6 M HCl (5 mL) and cooled to  $-5\text{ }^{\circ}\text{C}$ .  $\text{NaNO}_2$  (0.44 g, 6.4 mmol) in  $\text{H}_2\text{O}$  (2 mL) was added dropwise over a period of 10 min. The reaction was stirred for 22 h at  $-5\text{ }^{\circ}\text{C}$ , which was allowed to slowly warm up to rt. The resulting mixture was extracted according to **GP-1** and the resulting crude yellow oil was used directly for the last step. In the last step, the named crude oil was reacted with 4-methoxyaniline (350 mg, 2.80 mmol) and EDC·HCl (607 mg, 3.17 mmol) in  $\text{CH}_2\text{Cl}_2$  (2 mL) according to **GP-3**. The reaction was stirred at rt for 17 h. Column chromatography (petroleum ether – EtOAc, 7:3) gave **72** as white solid (368 mg, 9% over 3 steps). MP =  $141\text{ }^{\circ}\text{C}$ ;  $^1\text{H NMR}$  (500 Hz,  $\text{DMSO}-d_6$ )  $\delta$  = 10.16 (s, 1H, 1-NH), 9.42 (t,  $J$  = 5.4 Hz, 1H, 5-NH), 7.50 (d,  $J$  = 9.1 Hz, 3'-H, 5'-H), 6.90 (d,  $J$  = 9.1 Hz, 2'-H, 6'-H), 4.47 (dd,  $J$  = 6.8, 7.6 Hz, 1H, 2-H), 3.72 (s, 3H, 4'-OCH<sub>3</sub>), 3.19 (q,  $J$  = 6.6 Hz, 2H, 6-H), 2.04–1.96 (m, 1H, 3-H<sub>a</sub>), 1.91–1.84 (m, 1H, 3-H<sub>b</sub>), 1.56–1.49 (m, 2H, 5-H), 1.46–1.37 (m, 1H, 4-H<sub>a</sub>), 1.35–1.26 (m, 1H, 4-H<sub>b</sub>);  $^{13}\text{C NMR}$  (126 MHz,  $\text{DMSO}-d_6$ )  $\delta$  = 166.26 (1-C), 156.17 (quart,  $J$  = 35.9 Hz,  $\text{NHCOCF}_3$ ), 155.69 (4'-C), 131.44 (1'-C), 121.04 (3'-C, 5'-C), 113.95 (2'-C, 6'-C), 59.13 (2-C), 55.17 (4'-OCH<sub>3</sub>), 38.89 (6-C), 33.81 (3-C), 27.63 (5-C), 22.98 (4-C);  $^{19}\text{F NMR}$  (376 MHz,  $\text{DMSO}-d_6$ )  $\delta$  =  $-74.37$ ; HRMS (ESI<sup>+</sup>)  $m/z$  calculated for  $\text{C}_{15}\text{H}_{19}\text{F}_3\text{N}_2\text{O}_3$  367.1031 [M+H]<sup>+</sup>, found 367.1022; TLC (petroleum ether – EtOAc, 1:1):  $R_f$  = 0.40.

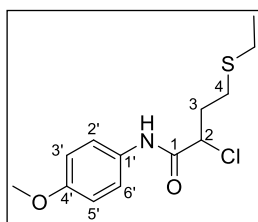
#### 2-Chloro-4-(methylthio)-N-(4'-methoxyphenyl)butanamide **73**.



2 steps. The first step was performed according to **GP-1**. Therefore, DL-methionine (5.02 g, 33.6 mmol) was dissolved in 6 M HCl (33 mL) and cooled to  $-5\text{ }^{\circ}\text{C}$ .  $\text{NaNO}_2$  (5.80 g, 84.1 mmol) was dissolved in  $\text{H}_2\text{O}$  (11 mL) and added dropwise over a period of 1 h 30 min. The reaction was stirred for 19 h at  $-5\text{ }^{\circ}\text{C}$ , which was allowed to slowly warm up to rt. The resulting mixture was extracted according to **GP-1** and the resulting crude yellow oil was used directly for the next step (4.21 g, max. 25.0 mmol, max. 74%). The named crude oil was reacted with 4-methoxyaniline (2.67 g, 21.7 mmol) and EDC·HCl (4.88 g, 25.5 mmol) in DMF (15 mL) according to **GP-3**. The reaction was stirred at rt for 18 h. Column chromatography (petroleum ether – EtOAc, 9:1), followed by HPLC purification (method **HPLC-08**) gave **73** as white solid (130 mg, 1% over 2 steps).  $^1\text{H NMR}$  (500 Hz,  $\text{DMSO}-d_6$ )  $\delta$  = 10.25 (s, 1H, NH), 7.52 (d,  $J$  = 9.1 Hz, 2H 3'-H, 5'-H), 6.91 (d,  $J$  = 9.1 Hz, 2H, 2'-H, 6'-H), 4.63 (dd,  $J$  = 5.8, 8.3 Hz, 1H, 2-H), 3.73 (s, 3H, 4'-OCH<sub>3</sub>), 2.65–2.51 (m, 2H, 4-H), 2.29–2.21 (m, 1H, 3-H<sub>a</sub>), 2.16–2.09 (m, 1H, 3-H<sub>b</sub>), 2.08 (s, 3H, SCH<sub>3</sub>);  $^{13}\text{C NMR}$  (126 MHz,  $\text{DMSO}-d_6$ )  $\delta$  = 165.93 (1-C), 155.72 (4'-C), 131.47 (1'-C), 121.03 (3'-C, 5'-C), 113.95 (2'-C, 6'-C), 57.98 (2-C), 55.18 (4'-OCH<sub>3</sub>), 33.32 (3-C), 29.65

(4-C), 14.57 (SCH<sub>3</sub>); LCMS (ESI<sup>+</sup>) *m/z* calculated for C<sub>12</sub>H<sub>17</sub>NO<sub>2</sub>S 274.07 [M+H]<sup>+</sup>, found 274.13; TLC (petroleum ether – EtOAc, 6:4): R<sub>f</sub> = 0.60; HPLC (method **HPLC-08**): R<sub>t</sub> = 26.0 min; λ<sub>max</sub> = 256 nm.

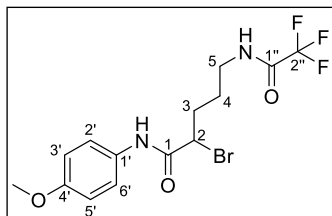
**2-Chloro-4-(ethylthio)-N-(4'-methoxyphenyl)butanamide 74.** Compound **74** was synthesized in 2



steps by Marcel Lutz during his project work. The first step was performed according to **GP-1**. Therefore, DL-ethionine (1.06 g, 6.48 mmol) was dissolved in 6 M HCl (3.5 mL) and cooled to -5 °C. NaNO<sub>2</sub> (1.19 g, 17.3 mmol) was dissolved in H<sub>2</sub>O (2 mL) and added dropwise over a period of 1 h. The reaction was stirred for 22 h at -5 °C, which was allowed to slowly warm up to rt. The

resulting mixture was extracted according to **GP-1** and the resulting crude yellow oil was used directly for the next step. The named crude oil was reacted with 4-methoxyaniline (1.02 g, 8.27 mmol) and EDC·HCl (1.91 g, 7.89 mmol) in CH<sub>2</sub>Cl<sub>2</sub> (10 mL) according to **GP-3**. The reaction was stirred at rt for 19 h. Column chromatography (petroleum ether – EtOAc, 9:1 → 7:3) gave **74** as brown solid (378 mg, 20% over 2 steps). <sup>1</sup>H NMR (300 Hz, DMSO-*d*<sub>6</sub>) δ = 10.25 (s, 1H, NH), 7.52 (d, *J* = 9.1 Hz, 2H 3'-H, 5'-H), 6.90 (d, *J* = 9.1 Hz, 2H, 2'-H, 6'-H), 4.64 (dd, *J* = 8.2, 5.9 Hz, 1H, 2-H), 3.73 (s, 3H, 4'-OCH<sub>3</sub>), 2.70–2.50 (m, 4H, 4-H, SCH<sub>2</sub>CH<sub>3</sub>), 2.29–2.05 (m, 2H, 3-H), 1.18 (t, *J* = 7.4 Hz, 3H, SCH<sub>2</sub>CH<sub>3</sub>); <sup>13</sup>C NMR (75 MHz, DMSO-*d*<sub>6</sub>) δ = 165.88 (1-C), 155.68 (4'-C), 131.46 (1'-C), 121.02 (3'-C, 5'-C), 113.94 (2'-C, 6'-C), 58.00 (2-H), 55.16 (4'-OCH<sub>3</sub>), 33.88 (3-C), 26.97 (4-C), 24.75 (SCH<sub>2</sub>CH<sub>3</sub>), 14.60 (SCH<sub>2</sub>CH<sub>3</sub>); LCMS (ESI<sup>+</sup>) *m/z* calculated for C<sub>13</sub>H<sub>19</sub>ClNO<sub>2</sub>S 288.08 [M+H]<sup>+</sup>, found 288.10; TLC (petroleum ether – EtOAc, 1:1): R<sub>f</sub> = 0.55.

**2-Bromo-5-(2'',2'',2''-trifluoroacetamido)-N-(4'-methoxyphenyl)pentanamide 77.** Compound

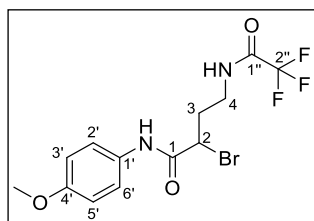


**77** was synthesized in 3 steps. The first step was performed according to **GP-10**, using DL-ornithine hydrochloride (2.85 g, 16.9 mmol), NaOH (0.70 g, 17.4 mmol) and ethyltrifluoroacetate (2.10 mL, 17.7 mmol) in water (10 mL). The reaction was stirred vigorously for 2 h at rt, then it was left to stand at 4 °C overnight. The resulting white crystals were

filtered, washed with cold water, and used without further purification in the next step. The named crystals were subjected to **GP-11**, using KBr (3.03 g, 25.5 mmol) and NaNO<sub>2</sub> (2.32 g, 33.6 mmol) in 2 M H<sub>2</sub>SO<sub>4</sub> (16 mL) at -5 °C. NaNO<sub>2</sub> was added in small portions over a period of 20 min. The reaction was stirred for 20 h at -5 °C, which was allowed to slowly warm up to rt. The resulting mixture was extracted according to **GP-11** and the resulting crude yellow oil was used directly for the last step. In the last step, the named crude oil was reacted with 4-methoxyaniline (2.47 g, 20.1 mmol) and EDC·HCl (3.81 g, 19.9 mmol) in DMF (10 mL) according to **GP-3**. The reaction was stirred at rt for 20 h. Column chromatography (petroleum ether – EtOAc, 7:3) gave **77** as slightly brown solid (236 mg, 4% over 3 steps). <sup>1</sup>H NMR (500 Hz, DMSO-*d*<sub>6</sub>) δ = 10.20 (s, 1H, 1-NH), 9.48 (t, *J* = 5.4 Hz, 1H, 5-NH), 7.51 (d, *J* = 9.1 Hz, 3'-H, 5'-H), 6.91 (d, *J* = 9.1 Hz, 2'-H, 6'-H), 4.50 (dd, *J* = 6.8, 7.5 Hz, 1H, 2-H), 3.72 (s, 3H, 4'-OCH<sub>3</sub>), 3.22 (q, *J* = 7.1 Hz, 2H, 5-H), 2.04–1.96 (m, 1H, 3-H<sub>a</sub>), 1.90–1.83 (m, 1H, 3-H<sub>b</sub>), 1.69–1.60 (m, 1H, 4-H<sub>a</sub>), 1.58–1.48 (m, 1H, 3-H<sub>a</sub>); <sup>13</sup>C NMR (126 MHz, DMSO-*d*<sub>6</sub>) δ = 166.14 (1-C), 156.41 & 156.13 (NHCOCF<sub>3</sub>), 155.72 (4'-C), 131.43 (1'-C), 121.04 (3'-C, 5'-C), 113.99 (2'-C, 6'-C), 58.90 (2-C), 55.20 (4'-

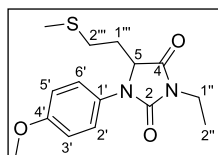
OCH<sub>3</sub>), 38.57 (5-C), 31.62 (3-C), 25.25 (4-C); <sup>19</sup>F NMR (376 MHz, DMSO-*d*<sub>6</sub>) δ = -74.37; TLC (petroleum ether-EtOAc, 1:1): R<sub>f</sub> = 0.45.

**2-Bromo-4-(2'',2'',2''-trifluoroacetamido)-N-(4'-methoxyphenyl)butanamide 78.** Compound **78**



was synthesized in 3 steps. The first step was performed according to **GP-10**, using DL-diaminobutyric acid dihydrochloride (5.10 g, 26.7 mmol), NaOH (2.11 g, 52.8 mmol) and ethyltrifluoroacetate (3.20 mL, 26.9 mmol) in water (15 mL). The reaction was stirred vigorously for 2 h at rt, then it was left to stand at 4 °C overnight. The resulting white crystals were filtered, washed with cold water, and used without further purification in the next step. The named crystals were subjected to **GP-11**, using KBr (4.76 g, 40.0 mmol) and NaNO<sub>2</sub> (3.68 g, 53.3 mmol) in 2 M H<sub>2</sub>SO<sub>4</sub> (27 mL) at -5 °C. NaNO<sub>2</sub> was added in small portions over a period of 30 min. The reaction was stirred for 23 h at -5 °C, which was allowed to slowly warm up to rt. The resulting mixture was extracted according to **GP-11** and the resulting crude yellow oil was used directly for the last step. In the last step, the named crude oil was reacted with 4-methoxyaniline (3.95 g, 32.0 mmol) and EDC·HCl (6.14 g, 32.0 mmol) in DMF (10 mL) according to **GP-3**. The reaction was stirred at rt for 25 h. Column chromatography (petroleum ether – EtOAc, 7:3), followed by HPLC purification (method **HPLC-09**) gave **78** as white solid (200 mg, 2% over 3 steps). <sup>1</sup>H NMR (500 Hz, DMSO-*d*<sub>6</sub>) δ = 10.24 (s, 1H, 1-NH), 9.51 (t, *J* = 5.3 Hz, 4-NH), 7.51 (d, *J* = 9.1 Hz, 3'-H, 5'-H), 6.91 (d, *J* = 9.0 Hz, 2'-H, 6'-H), 4.53 (dd, *J* = 5.6, 8.4 Hz, 2-H), 3.72 (s, 3H, 4'-OCH<sub>3</sub>), 3.40-3.30 (m, 2H, 4-H), 2.27 – 2.20 (m, 1H, 3-H<sub>a</sub>), 2.13 – 2.06 (m, 1H, 3-H<sub>b</sub>); <sup>13</sup>C NMR (126 MHz, DMSO-*d*<sub>6</sub>) δ = 165.75 (1-C), 155.73 (4'-C), 131.43 (1'-C), 121.07 (3'-C, 5'-C), 113.98 (2'-C, 6'-C), 56.73 (2-C), 55.20 (4'-OCH<sub>3</sub>), 36.30 (4-C), 32.96 (3-C); <sup>19</sup>F NMR (282 MHz, DMSO-*d*<sub>6</sub>) δ = -74.35; TLC (petroleum ether-EtOAc, 1:1): R<sub>f</sub> = 0.35; HPLC (method **HPLC-09**): R<sub>t</sub> = 24.7 min; λ<sub>max</sub> = 262 nm.

**1-(4'-Methoxyphenyl)-3-ethyl-5-(2''''-(methylthio)ethyl)imidazolidine-2,4-dione 79.** Compound



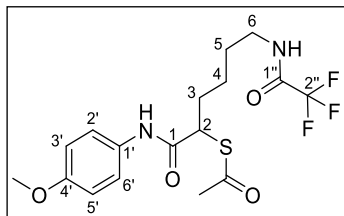
**79** was observed as sideproduct of the synthesis of **73**. It synthesized in 2 steps. The first step was performed according to **GP-1**. Therefore, DL-methionine (5.02 g, 33.6 mmol) was dissolved in 6 M HCl (33 mL) and cooled to -5 °C. NaNO<sub>2</sub> (5.80 g, 84.1 mmol) was dissolved in H<sub>2</sub>O (11 mL) and added dropwise over a

period of 1 h 30 min. The reaction was stirred for 19 h at -5 °C, which was allowed to slowly warm up to rt. The resulting mixture was extracted according to **GP-1** and the resulting crude yellow oil was used directly for the next step (4.21 g, max. 25.0 mmol, max. 74%). The named crude oil was reacted with 4-methoxyaniline (2.67 g, 21.7 mmol) and EDC·HCl (4.88 g, 25.5 mmol) in DMF (15 mL) according to **GP-3**. The reaction was stirred at rt for 18 h. Column chromatography (petroleum ether – EtOAc, 9:1), followed by HPLC purification (method **HPLC-08**) gave **79** as hygroscopic, instable, slightly yellow solid (186 mg, 2% over 2 steps). <sup>1</sup>H NMR (500 Hz, DMSO-*d*<sub>6</sub>) δ = 7.08 (d, *J* = 9.0 Hz, 2H, 3'-H, 5'-H), 6.86 (d, *J* = 9.0 Hz, 2H, 2'-H, 6'-H), 5.07 (dd, *J* = 7.2, 4.8 Hz, 1H, 5-H), 3.72 (s, 3H, 4'-OCH<sub>3</sub>), 3.58 (q, *J* = 7.2 Hz, 2H, 1''-H), 2.60-2.53 (m, 2H, 2'''-H), 2.16-2.02 (m, 2H, 1'''-H), 2.05 (s, 3H, SCH<sub>3</sub>), 1.20 (t, *J* = 7.2 Hz, 3H, 2''-H); <sup>13</sup>C NMR (126 MHz, DMSO-*d*<sub>6</sub>) δ = 171.47 (4-C), 155.41 (4'-C), 147.68 (2-C), 137.39 (1'-C), 124.37 (3'-C, 5'-C), 113.89 (2'-C, 6'-C), 78.12 (5-C), 55.10 (OCH<sub>3</sub>), 34.75 (1''-C), 29.86 (1'''-C), 28.04



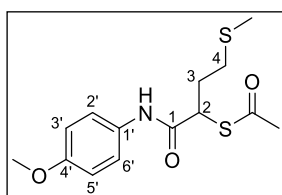
(2'''-C), 14.51 (SCH<sub>3</sub>), 12.34 (2''-C); LCMS (ESI<sup>+</sup>) *m/z* calculated for C<sub>15</sub>H<sub>21</sub>N<sub>2</sub>O<sub>3</sub>S 309.13 [M+H]<sup>+</sup>, found 309.15; TLC (petroleum ether – EtOAc, 6:4): R<sub>f</sub> = 0.60; HPLC (method **HPLC-08**): R<sub>t</sub> = 29.5 min; λ<sub>max</sub> = 263 nm.

**2-(Acetylthio)-6-(2'',2'',2'''-trifluoroacetamido)-N-(4'-methoxyphenyl)hexanamide 80.**



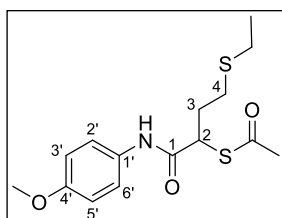
Compound **80** was synthesized according to **GP-5**, using intermediate **72** (261 mg, 0.712 mmol) and KSac (198 mg, 1.74 mmol) in acetone (5 mL). The reaction was stirred for 6 h at rt. Extraction and purification via column chromatography (petroleum ether – EtOAc, 8:2) gave **80** as colorless oil (179 mg, 62%). <sup>1</sup>H NMR (500 Hz, DMSO-*d*<sub>6</sub>) δ = 10.13 (s, 1H, 1-NH), 9.39 (t, *J* = 5.4 Hz, 1H, 5-NH), 7.48 (d, *J* = 9.1 Hz, 3'-H, 5'-H), 6.87 (d, *J* = 9.1 Hz, 2'-H, 6'-H), 4.19 (dd, *J* = 7.0, 8.1 Hz, 1H, 2-H), 3.71 (s, 3H, 4'-OCH<sub>3</sub>), 3.16 (dt, *J* = 6.2, 6.9 Hz, 2H, 6-H), 2.35 (s, 3H, SC(O)CH<sub>3</sub>), 1.93–1.86 (m, 1H, 3-H<sub>a</sub>), 1.70–1.63 (m, 1H, 3-H<sub>b</sub>), 1.55–1.48 (m, 2H, 5-H), 1.39–1.23 (m, 2H, 4-H); <sup>13</sup>C NMR (126 MHz, DMSO-*d*<sub>6</sub>) δ = 194.47 (S(O)C(O)CH<sub>3</sub>), 168.04 (1-C), 156.16 (quart., *J* = 36.7 Hz, NHCOCF<sub>3</sub>), 155.50 (4'-C), 131.78 (1'-C), 120.96 (3'-C, 5'-C), 113.85 (2'-C, 6'-C), 55.17 (4'-OCH<sub>3</sub>), 47.85 (2-C), 38.93 (6-C), 32.45 (3-C), 30.28 (SC(O)CH<sub>3</sub>), 27.81 (5-C), 23.86 (4-C); <sup>19</sup>F NMR (376 MHz, DMSO-*d*<sub>6</sub>) δ = -74.37; TLC (petroleum ether – EtOAc, 6:4): R<sub>f</sub> = 0.25.

**2-(Acetylthio)-4-(methylthio)-N-(4'-methoxyphenyl)butanamide 81.**



Compound **81** was synthesized according to **GP-5**, using intermediate **73** (110 mg, 0.402 mmol) and KSac (153 mg, 1.34 mmol) in acetone (5 mL). The reaction was stirred for 2 h 20 min at rt. Extraction and purification via column chromatography (petroleum ether – EtOAc, 9:1 → 0:10) gave **81** as slightly brown solid (89 mg, 71%). <sup>1</sup>H NMR (300 Hz, DMSO-*d*<sub>6</sub>) δ = 10.16 (s, 1H, 1-NH), 7.49 (d, *J* = 9.1 Hz, 2H 3'-H, 5'-H), 6.87 (d, *J* = 9.1 Hz, 2H, 2'-H, 6'-H), 4.30 (dd, *J* = 6.6, 7.9 Hz, 1H, 2-H), 3.71 (s, 3H, 4'-OCH<sub>3</sub>), 2.55–2.44 (m, 2H, 4-H), 2.37 (s, 3H, SC(O)CH<sub>3</sub>), 2.23–2.11 (m, 1H, 3-H<sub>a</sub>), 2.05 (s, 3H, SCH<sub>3</sub>), 1.97–1.85 (m, 1H, 3-H<sub>b</sub>); <sup>13</sup>C NMR (75 MHz, DMSO-*d*<sub>6</sub>) δ = 194.26 (S(O)C(O)CH<sub>3</sub>), 167.49 (1-C), 155.51 (4'-C), 131.73 (1'-C), 121.00 (3'-C, 5'-C), 113.83 (2'-C, 6'-C), 55.16 (4'-OCH<sub>3</sub>), 47.02 (2-C), 32.22 (3-C), 30.50 (4-C), 30.31 (SC(O)CH<sub>3</sub>), 14.54 (SCH<sub>3</sub>); LCMS (ESI<sup>+</sup>) *m/z* calculated for C<sub>14</sub>H<sub>20</sub>NO<sub>3</sub>S<sub>2</sub> 314.09 [M+H]<sup>+</sup>, found 314.08; TLC (petroleum ether – EtOAc, 6:4): R<sub>f</sub> = 0.35.

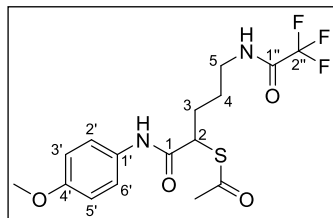
**2-(Acetylthio)-4-(ethylthio)-N-(4'-methoxyphenyl)butanamide 82.**



Compound **82** was synthesized by Marcel Lutz during his project work according to **GP-5**, using intermediate **74** (379 mg, 1.16 mmol) and KSac (320 mg, 2.80 mmol) in acetone (5 mL). The reaction was stirred for 3 h at rt. Extraction and purification via column chromatography (petroleum ether – EtOAc, 8:2 → 0:10) gave **82** as slightly yellow solid (80 mg, 19%). <sup>1</sup>H NMR (500 Hz, DMSO-*d*<sub>6</sub>) δ = 10.16 (s, 1H, NH), 7.50 (d, *J* = 9.1 Hz, 2H, 3'-H, 5'-H), 6.89 (d, *J* = 9.1 Hz, 2H, 2'-H, 6'-H), 4.32 (dd, *J* = 8.1, 6.4 Hz, 1H, 2-H), 3.73 (s, 3H, 4'-OCH<sub>3</sub>), 2.54–2.49 (m, 4H, 4-H, SCH<sub>2</sub>CH<sub>3</sub>), 2.37 (s, 3H, SC(O)CH<sub>3</sub>), 2.20–2.13 (m, 1H, 3-H<sub>a</sub>), 1.95–1.87 (m, 1H, 3-H<sub>b</sub>), 1.16 (t, *J* = 7.4 Hz, 3H, SCH<sub>2</sub>CH<sub>3</sub>); <sup>13</sup>C NMR (126 MHz, DMSO-*d*<sub>6</sub>) δ = 194.25 (S(O)C(O)CH<sub>3</sub>), 167.47 (1-C), 155.51 (4'-C), 131.72 (1'-C), 121.00 (3'-C, 5'-

C), 113.83 (2'-C, 6'-C), 55.14 (4'-OCH<sub>3</sub>), 47.11 (2-C), 32.75 (3-C), 30.29 (SCOCH<sub>3</sub>), 27.77 (4-C), 24.66 (SCH<sub>2</sub>CH<sub>3</sub>), 14.50 (SCH<sub>2</sub>CH<sub>3</sub>); HRMS (ESI<sup>+</sup>) *m/z* calculated for C<sub>15</sub>H<sub>20</sub>NO<sub>3</sub>S<sub>2</sub> 328.1036 [M+H]<sup>+</sup>, found 328.1018; TLC (petroleum ether – EtOAc, 8:2): R<sub>f</sub> = 0.10.

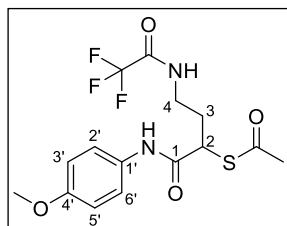
**2-(Acetylthio)-5-(2'',2'',2''-trifluoroacetamido)-N-(4'-methoxyphenyl)pentanamide 83.**



Compound **83** was synthesized according to **GP-5**, using intermediate **77** (223 mg, 0.561 mmol) and KSAc (137 mg, 1.19 mmol) in acetone (7 mL). The reaction was stirred for 4 h 30 min at rt. The mix was concentrated *in vacuo*, extracted, and purified by column chromatography (petroleum ether – EtOAc, 7:3) to give **83** as orange solid (220 mg, quant.).

<sup>1</sup>H NMR (300 Hz, DMSO-*d*<sub>6</sub>) δ = 10.14 (s, 1H, 1-NH), 9.42 (t, *J* = 5.3 Hz, 1H, 5-NH), 7.48 (d, *J* = 9.1 Hz, 3'-H, 5'-H), 6.88 (d, *J* = 9.1 Hz, 2'-H, 6'-H), 4.20 (dd, *J* = 6.5, 8.0 Hz, 1H, 2-H), 3.71 (s, 3H, 4'-OCH<sub>3</sub>), 3.20 (q, *J* = 6.5 Hz, 2H, 5-H), 2.36 (s, 3H, SCOCH<sub>3</sub>), 1.94-1.82 (m, 1H, 3-H<sub>a</sub>), 1.73-1.43 (m, 3H, 3-H<sub>b</sub>, 4-H<sub>a</sub>, 4-H<sub>b</sub>); <sup>13</sup>C NMR (75 MHz, DMSO-*d*<sub>6</sub>) δ = 194.46 (SCOCH<sub>3</sub>), 167.87 (1-C), 155.52 (4'-C), 131.72 (1'-C), 120.91 (3'-C, 5'-C), 113.88 (2'-C, 6'-C), 55.18 (2-C), 47.71 (4'-OCH<sub>3</sub>), 38.28 (5-C), 30.30 (SCOCH<sub>3</sub>), 30.21 (3-C), 26.05 (4-C); <sup>19</sup>F NMR (282 MHz, DMSO-*d*<sub>6</sub>) δ = -74.37; HRMS (ESI<sup>+</sup>) *m/z* calculated for C<sub>16</sub>H<sub>20</sub> F<sub>3</sub>N<sub>2</sub>O<sub>4</sub>S 393.1090 [M+H]<sup>+</sup>, found 393.1081; TLC (petroleum ether-EtOAc, 3:7): R<sub>f</sub> = 0.55.

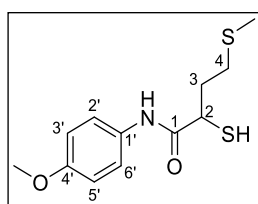
**2-(Acetylthio)-N-(4-methoxyphenyl)-4-(2'',2'',2''-trifluoroacetamido)butanamide 84.**



Compound **84** was synthesized according to **GP-5**, using intermediate **78** (148 mg, 0.386 mmol) and KSAc (140 mg, 1.23 mmol) in acetone (5 mL). The reaction was stirred for 2 h 30 min at rt. The reaction mixture was concentrated *in vacuo* and taken up with EtOAc (200 mL). The organic layer was washed with water (3x 50 mL) and brine (1x 10 mL), then dried over

Na<sub>2</sub>SO<sub>4</sub>, filtered and concentrated. **84** was obtained after column chromatography (PE/EtOAc 7/3) as clear wax-like solid (129 mg, 88%). <sup>1</sup>H NMR (500 Hz, DMSO-*d*<sub>6</sub>) δ = 10.17 (s, 1H, 1-NH), 9.44 (t, *J* = 5.5 Hz, 1H, 4-NH(COCF<sub>3</sub>)), 7.48 (d, *J* = 9.1 Hz, 2H, 3'-H & 5'-H), 6.88 (d, *J* = 9.1 Hz, 2H, 2'-H & 6'-H), 4.24 (dd, *J* = 6.7 Hz, 7.8 Hz, 1H, 2-H), 3.71 (s, 3H, 4'-OCH<sub>3</sub>), 3.24 (q, *J* = 6.9 Hz, 2H, 4-H), 2.37 (s, 3H, SCH<sub>3</sub>), 2.17 – 2.09 (m, 1H, 3-H<sub>a</sub>), 1.93 – 1.86 (m, 1H, 3-H<sub>b</sub>); <sup>13</sup>C NMR (126 MHz, DMSO-*d*<sub>6</sub>) δ = 194.25 (SCOCH<sub>3</sub>), 167.42 (1-C), 156.23 (d, 35.9 Hz, NCOCF<sub>3</sub>), 155.57 (4'-C), 131.69 (1'-C), 121.02 (3'-C, 5'-C), 113.89 (2'-C, 6'-C), 55.19 (4'-OCH<sub>3</sub>), 45.64 (2-C), 37.08 (SCOCH<sub>3</sub>), 31.65 (4-C), 30.33 (3-C); <sup>19</sup>F NMR (282 MHz, DMSO-*d*<sub>6</sub>) δ = -74.45; HRMS (ESI<sup>+</sup>) *m/z* calculated for C<sub>15</sub>H<sub>19</sub>F<sub>3</sub>N<sub>2</sub>O<sub>4</sub>S 379.0934 [M+H]<sup>+</sup>, found 379.0923; TLC (petroleum ether-EtOAc, 1:1): R<sub>f</sub> = 0.64.

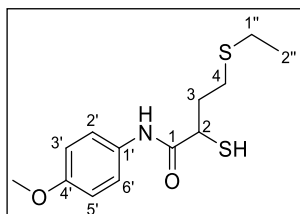
**2-mercapto-4-(methylthio)-N-(4'-methoxyphenyl)butanamide 85.** Compound **85** was



synthesized according to **GP-6**, using intermediate **81** (77 mg, 0.25 mmol) and NaOH (61 mg, 1.5 mmol) in MeOH (3 mL). The reaction was stirred for 1 h 30 min at rt. After HPLC purification (method **HPLC-10**) **85** was obtained as white solid (36 mg, 54%). MP = 75 °C; <sup>1</sup>H NMR (500 Hz, DMSO-*d*<sub>6</sub>) δ = 9.98 (s, 1H, 1-NH), 7.49 (d, *J* = 9.1 Hz, 2H 3'-H, 5'-H), 6.88 (d, *J* = 9.1 Hz, 2H, 2'-H, 6'-H),

3.71 (s, 3H, 4'-OCH<sub>3</sub>), 3.56 (dt,  $J = 7.3, 9.4$  Hz, 1H, 2-H), 3.03 (d,  $J = 9.5$  Hz, 1H, SH), 2.55-2.51 (m, 2H, 4-H), 2.17-2.10 (m, 1H, 3-H<sub>a</sub>), 2.05 (s, 3H, SCH<sub>3</sub>), 1.91-1.84 (m, 1H, 3-H<sub>b</sub>); <sup>13</sup>C NMR (126 MHz, DMSO-*d*<sub>6</sub>)  $\delta = 170.07$  (1-C), 155.36 (4'-C), 132.10 (1'-C), 120.76 (3'-C, 5'-C), 113.90 (2'-C, 6'-C), 55.18 (4'-OCH<sub>3</sub>), 40.78 (2-C), 34.48 (3-C), 30.83 (4-C), 14.61 (SCH<sub>3</sub>); HRMS (ESI<sup>-</sup>)  $m/z$  calculated for C<sub>12</sub>H<sub>16</sub>NO<sub>2</sub>S<sub>2</sub> 270.0628 [M-H]<sup>-</sup>, found 270.0616; HPLC (method **HPLC-10**):  $R_t = 17.0$  min;  $\lambda_{\max} = 255$  nm.

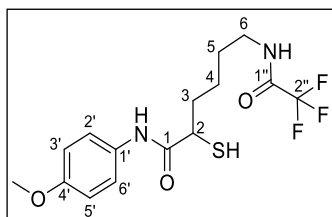
**2-mercapto-4-(ethylthio)-*N*-(4'-methoxyphenyl)butanamide 86.** Compound **86** was synthesized



according to **GP-6**, using intermediate **82** (49 mg, 0.15 mmol) and NaOH (20 mg, 0.50 mmol) in MeOH (1 mL). The reaction was stirred for 2 h at rt. After HPLC purification (method **HPLC-11**) **86** was obtained as white solid (18 mg, 42%). MP = 75 °C; <sup>1</sup>H NMR (300 Hz, DMSO-*d*<sub>6</sub>)  $\delta = 9.97$  (s, 1H, NH), 7.50 (d,  $J = 9.1$  Hz, 2H 3'-H, 5'-H), 6.88 (d,  $J = 9.1$  Hz, 2H, 2'-H, 6'-H), 3.72 (s,

3H, 4'-OCH<sub>3</sub>), 3.57 (dt,  $J = 7.3, 9.4$  Hz, 1H, 2-H), 3.03 (d,  $J = 9.5$  Hz, 1H, SH), 2.60-2.47 (m, 4H, 4-H, SCH<sub>2</sub>CH<sub>3</sub>), 2.18-2.06 (m, 1H, 3-H<sub>a</sub>), 1.92-1.81 (m, 1H, 3-H<sub>b</sub>), 1.17 (t,  $J = 7.4$  Hz, 3H, SCH<sub>2</sub>CH<sub>3</sub>); <sup>13</sup>C NMR (75 MHz, DMSO-*d*<sub>6</sub>)  $\delta = 170.02$  (1-C), 155.33 (4'-C), 132.07 (1'-C), 120.74 (3'-C, 5'-C), 113.87 (2'-C, 6'-C), 55.15 (4'-OCH<sub>3</sub>), 40.83 (2-C), 35.03 (3-C), 28.11 (4-C), 24.76 (SCH<sub>2</sub>CH<sub>3</sub>), 14.67 (SCH<sub>2</sub>CH<sub>3</sub>); HRMS (ESI<sup>-</sup>)  $m/z$  calculated for C<sub>13</sub>H<sub>18</sub>NO<sub>2</sub>S<sub>2</sub> 284.0784 [M-H]<sup>-</sup>, found 284.0772; HPLC (method **HPLC-11**):  $R_t = 18.5$  min;  $\lambda_{\max} = 255$  nm.

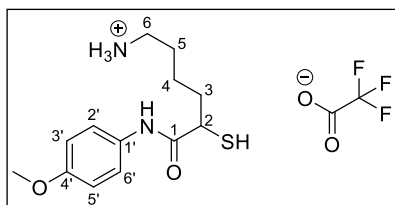
**2-mercapto-6-(2'',2'',2''-trifluoroacetamido)-*N*-(4'-methoxyphenyl)hexanamide 87.** Compound



**87** was synthesized according to **GP-6**, using intermediate **80** (114 mg, 0.280 mmol) and NaOH (50 mg, 1.25 mmol) in MeOH (3 mL). The reaction was stirred for 1 h 30 min at rt. After HPLC purification (method **HPLC-12**) **87** was obtained as white solid (16 mg, 16%). MP = 132 °C; <sup>1</sup>H NMR (500 Hz, DMSO-*d*<sub>6</sub>)  $\delta = 9.93$  (s, 1H, 1-NH), 9.42 (t,

$J = 5.5$  Hz, 1H, 5-NH), 7.49 (d,  $J = 9.1$  Hz, 3'-H, 5'-H), 6.88 (d,  $J = 9.1$  Hz, 2'-H, 6'-H), 3.71 (s, 3H, 4'-OCH<sub>3</sub>), 3.43-3.33 (m, 1H, 2-H), 3.19-3.14 (m, 2H, 6-H), 2.92 (d,  $J = 9.3$  Hz, 1H, SH), 1.90-1.82 (m, 1H, 3-H<sub>a</sub>), 1.67-1.60 (m, 1H, 3-H<sub>b</sub>), 1.50 (quint.,  $J = 7.4$  Hz, 2H, 5-H), 1.41-1.33 (m, 1H, 4-H<sub>a</sub>), 1.31-1.22 (m, 1H, 4-H<sub>b</sub>); <sup>13</sup>C NMR (126 MHz, DMSO-*d*<sub>6</sub>)  $\delta = 170.44$  (1-C), 156.30 & 156.02 (NHCOCF<sub>3</sub>), 155.35 (4'-C), 132.07 (1'-C), 120.77 (3'-C, 5'-C), 113.89 (2'-C, 6'-C), 55.17 (4'-OCH<sub>3</sub>), 41.84 (2-C), 35.17 (3-C), 27.87 (5-C), 24.24 (4-C); <sup>19</sup>F NMR (376 MHz, DMSO-*d*<sub>6</sub>)  $\delta = -74.38$ ; HRMS (ESI<sup>+</sup>)  $m/z$  calculated for C<sub>15</sub>H<sub>20</sub>F<sub>3</sub>N<sub>2</sub>O<sub>3</sub>S 365.1141 [M+H]<sup>+</sup>, found 365.1138; HRMS (ESI<sup>-</sup>)  $m/z$  calculated for C<sub>15</sub>H<sub>18</sub>F<sub>3</sub>N<sub>2</sub>O<sub>3</sub>S 363.0996 [M-H]<sup>-</sup>, found 363.0999; HPLC (method **HPLC-12**):  $R_t = 15.5$  min;  $\lambda_{\max} = 255$  nm.

**2-mercapto-*N*-(4-methoxyphenyl)-5-(amino)hexanamide (TFA salt) 88.** Compound **88** was

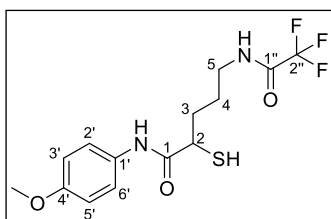


synthesized according to **GP-12**, using intermediate **87** (11 mg, 0.03 mmol), Et<sub>3</sub>N (100  $\mu$ L, 1.36 mmol) and LiOH (100 mg, 4.17 mmol) in MeOH (2 mL). The reaction was stirred for 4 h at rt. The mixture was acidified with TFA and diluted with water and directly purified via preparative HPLC (method **HPLC-13**). **88**

was obtained as colorless wax-like solid (6 mg, 52%). <sup>1</sup>H NMR (500 Hz, DMSO-*d*<sub>6</sub>)  $\delta = 9.97$  (s, 1H, 1-

NH), 7.65 (s, 3H, 5-NH<sub>3</sub><sup>+</sup>), 7.50 (d, *J* = 9.1 Hz, 2H, 3'-H & 5'-H), 6.89 (d, *J* = 9.1 Hz, 2H, 2'-H & 6'-H), 3.72 (s, 3H, 4'-OCH<sub>3</sub>), 3.44 – 3.39 (m, 1H, 2-H), 2.99 (d, *J* = 9.2 Hz, 1H, SH), 2.81 – 2.74 (m, 2H, 6-H), 1.92 – 1.84 (m, 1H, 3-H<sub>a</sub>), 1.68 – 1.61 (m, 1H, 3-H<sub>b</sub>), 1.56 – 1.50 (m, 2H, 5-H), 1.46 – 1.37 (m, 1H, 4-H<sub>a</sub>), 1.34 – 1.25 (m, 1H, 4-H<sub>b</sub>); <sup>13</sup>C NMR (126 MHz, DMSO-*d*<sub>6</sub>)  $\delta$  = 170.44 (1-C, HMBC), 155.42 (4'-C, HMBC), 132.17 (1'-C, HMBC), 120.71 (3'-C, 5'-C), 113.91 (2'-C, 6'-C), 55.19 (4'-OCH<sub>3</sub>), 41.77 (2-C), 38.72 (6-C, HSQC), 35.09 (3-C, HSQC), 26.81 (5-C, HSQC), 24.03 (4-C); <sup>19</sup>F NMR (282 MHz, DMSO-*d*<sub>6</sub>)  $\delta$  = -73.60; HRMS (ESI<sup>-</sup>) *m/z* calculated for C<sub>13</sub>H<sub>19</sub>N<sub>2</sub>O<sub>2</sub>S 267.1173 [M-H]<sup>-</sup>, found 267.1161; HPLC (method **HPLC-13**): R<sub>t</sub> = 10.8 min;  $\lambda_{\max}$  = 255 nm.

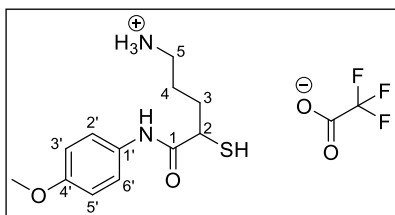
**2-mercapto-5-(2'',2'',2''-trifluoroacetamido)-N-(4'-methoxyphenyl)pentanamide 89.**



Compound **89** was synthesized according to GP-6, using intermediate **83** (150 mg, 0.382 mmol) and NaOH (50 mg, 1.25 mmol) in MeOH (2 mL). The reaction was stirred for 1.5 h at rt. The mixture was acidified with TFA and diluted with water and directly purified via preparative HPLC (method **HPLC-14**). **89** was obtained as white solid (30 mg, 22%).

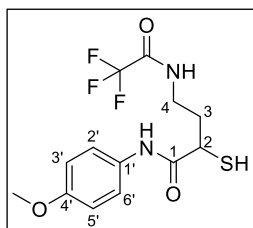
MP = 139 °C; <sup>1</sup>H NMR (500 Hz, DMSO-*d*<sub>6</sub>)  $\delta$  = 9.96 (s, 1H, 1-NH), 9.46 (t, *J* = 5.3 Hz, 1H, 5-NH), 7.50 (d, *J* = 9.1 Hz, 3'-H, 5'-H), 6.89 (d, *J* = 9.1 Hz, 2'-H, 6'-H), 3.72 (s, 3H, 4'-OCH<sub>3</sub>), 3.46-3.41 (m, 1H, 2-H), 3.19 (q, *J* = 6.5 Hz, 2H, 5-H), 3.00 (d, *J* = 9.3 Hz, 1H, SH), 1.90-1.82 (m, 1H, 3-H<sub>a</sub>), 1.67-1.55 (m, 2H, 3-H<sub>b</sub>, 4-H<sub>a</sub>), 1.53-1.44 (m, 1H, 4-H<sub>b</sub>); <sup>13</sup>C NMR (126 MHz, DMSO-*d*<sub>6</sub>)  $\delta$  = 170.64 (1-C, HMBC), 156.62 (NHCOCF<sub>3</sub>, HMBC), 155.7 (4'-C), 132.07 (1'-C, HMBC), 126.48 (NHCOCF<sub>3</sub>), 120.72 (3'-C, 5'-C), 113.91 (2'-C, 6'-C), 55.18 (2-C), 41.65 (4'-OCH<sub>3</sub>), 38.78 (5-C), 32.87 (3-C), 26.44 (4-C); <sup>19</sup>F NMR (282 MHz, DMSO-*d*<sub>6</sub>)  $\delta$  = -74.35; HRMS (ESI<sup>+</sup>) *m/z* calculated for C<sub>14</sub>H<sub>18</sub> F<sub>3</sub>N<sub>2</sub>O<sub>3</sub>S 351.0985 [M+H]<sup>+</sup>, found 351.0984; HPLC (method **HPLC-14**): R<sub>t</sub> = 20.5 min;  $\lambda_{\max}$  = 255 nm.

**2-Mercapto-N-(4-methoxyphenyl)-5-(amino)pentanamide (TFA salt) 90.** Compound **90** was

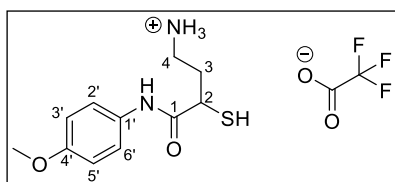


synthesized according to GP-12, using intermediate **89** (30 mg, 0.09 mmol), Et<sub>3</sub>N (100  $\mu$ L, 1.36 mmol) and LiOH (103 mg, 4.29 mmol) in MeOH (2 mL). The reaction was stirred for 3 h 30 min at rt. The mixture was acidified with TFA and diluted with water and directly purified via preparative HPLC (method

#HPLC\_R446). **90** was obtained as colorless wax-like solid (18 mg, 57%). <sup>1</sup>H NMR (500 Hz, DMSO-*d*<sub>6</sub>)  $\delta$  = 10.02 (s, 1H, 1-NH), 7.70 (s, 3H, 5-NH<sub>3</sub><sup>+</sup>), 7.51 (d, *J* = 9.1 Hz, 2H, 3'-H & 5'-H), 6.89 (d, *J* = 9.1 Hz, 2H, 2'-H & 6'-H), 3.72 (s, 3H, 4'-OCH<sub>3</sub>), 3.48 – 3.43 (m, 1H, 2-H), 3.03 (d, *J* = 9.3 Hz, 1H, SH), 2.83 – 2.76 (m, 2H, 5-H), 1.94 – 1.86 (m, 1H, 3-H<sub>a</sub>), 1.74 – 1.61 (m, 2H, 3-H<sub>b</sub> & 4-H<sub>a</sub>), 1.59 – 1.50 (m, 1H, 4-H<sub>b</sub>); <sup>13</sup>C NMR (126 MHz, DMSO-*d*<sub>6</sub>)  $\delta$  = 170.23 (1-C), 155.48 (4'-C), 132.03 (1'-C), 120.74 (3'-C, 5'-C), 113.94 (2'-C, 6'-C), 55.20 (4'-OCH<sub>3</sub>), 41.49 (2-C), 38.49 (5-C), 32.39 (3-C), 25.18 (4-C); <sup>19</sup>F NMR (282 MHz, DMSO-*d*<sub>6</sub>)  $\delta$  = -73.67; HRMS (ESI<sup>-</sup>) *m/z* calculated for C<sub>12</sub>H<sub>17</sub>N<sub>2</sub>O<sub>2</sub>S 253.1016 [M-H]<sup>-</sup>, found 253.1016; HPLC (method **HPLC-14**): R<sub>t</sub> = 12.5 min;  $\lambda_{\max}$  = 253 nm.

**2-Mercapto-*N*-(4-methoxyphenyl)-4-(2'',2'',2''-trifluoroacetamido)butanamide 91.** Compound

**91** was synthesized according to **GP-6**, using intermediate **84** (109 mg, 0.288 mmol) and NaOH (40 mg, 1.00 mmol) in MeOH (2 mL). The reaction was stirred for 1 h 10 min at rt. The mixture was acidified with TFA and diluted with water and directly purified via preparative HPLC (method **HPLC-15**). **91** was obtained as white solid (57 mg, 59%\*). \*Purity  $^1\text{H NMR}$  95%,  $^{19}\text{F NMR}$  shows 2 impurities, therefore purity is estimated to be ~90–95%.  $^1\text{H NMR}$  (500 Hz, DMSO- $d_6$ )  $\delta$  = 9.98 (s, 1H, 1-NH), 9.47 (t,  $J$  = 5.3 Hz, 1H, 4-NH(COCF $_3$ )), 7.49 (d,  $J$  = 9.1 Hz, 2H, 3'-H & 5'-H), 6.89 (d,  $J$  = 9.1 Hz, 2H, 2'-H & 6'-H), 3.72 (s, 3H, 4'-OCH $_3$ ), 3.47 (dt,  $J$  = 7.4, 9.3 Hz, 1H, 2-H), 3.30 (q,  $J$  = 6.5 Hz, 2H, 4-H), 3.10 (d,  $J$  = 9.4 Hz, 1H, SH), 2.15 – 2.08 (m, 1H, 3-H $_a$ ), 1.89 – 1.81 (m, 1H, 3-H $_b$ );  $^{13}\text{C NMR}$  (126 MHz, DMSO- $d_6$ )  $\delta$  = 169.93 (1-C), 155.38 (4'-C), 132.05 (1'-C), 121.13 (4'-NH(COCF $_3$ )), 120.79 (3'-C, 5'-C), 113.90 (2'-C, 6'-C), 55.18 (4'-OCH $_3$ ), 39.52 (2-C, HSQC), 37.25 (4-C), 34.02 (3-C);  $^{19}\text{F NMR}$  (282 MHz, DMSO- $d_6$ )  $\delta$  = -74.31; (2 impurities: -73.48, -74.37); HRMS (ESI $^-$ )  $m/z$  calculated for C $_{13}$ H $_{14}$ F $_3$ N $_2$ O $_3$ S 335.0683 [M-H] $^-$ , found 335.0685; HPLC (method **HPLC-15**):  $R_t$  = 13.0 min;  $\lambda_{\text{max}}$  = 255 nm.

**2-mercapto-*N*-(4-methoxyphenyl)-4-(amino)butanamide (TFA salt) 92.** Compound **92** was

synthesized according to **GP-12**, using intermediate **91** (27 mg, 0.08 mmol), Et $_3$ N (100  $\mu\text{L}$ , 1.36 mmol) and LiOH (100 mg, 4.17 mmol) in MeOH (2 mL). The reaction was stirred for 3.5 h at rt. The mixture was acidified with TFA and diluted with water and directly purified via preparative HPLC (method **HPLC-16**). **92** was obtained as colorless wax-like solid (21 mg, 74%).  $^1\text{H NMR}$  (500 Hz, DMSO- $d_6$ )  $\delta$  = 10.07 (s, 1H, 1-NH), 7.83 (s, 3H, 4-NH $_3^+$ ), 7.50 (d,  $J$  = 9.1 Hz, 2H, 3'-H & 5'-H), 6.90 (d,  $J$  = 9.1 Hz, 2H, 2'-H & 6'-H), 3.71 (s, 3H, 4'-OCH $_3$ ), 3.58 – 3.53 (m, 1H, 2-H), 3.26 (d,  $J$  = 9.3 Hz, 1H, SH), 2.98 – 2.90 (m, 1H, 4-H $_a$ ), 2.86 – 2.78 (m, 1H, 4-H $_b$ ), 2.17 – 2.10 (m, 1H, 3-H $_a$ ), 1.97 – 1.90 (m, 1H, 3-H $_b$ );  $^{13}\text{C NMR}$  (126 MHz, DMSO- $d_6$ )  $\delta$  = 169.66 (1-C), 155.46 (4'-C), 131.92 (1'-C), 120.83 (3'-C, 5'-C), 113.94 (2'-C, 6'-C), 55.20 (4'-OCH $_3$ ), 39.52 (2-C, HSQC), 36.96 (4-C), 32.83 (3-C);  $^{19}\text{F NMR}$  (282 MHz, DMSO- $d_6$ )  $\delta$  = -73.64; HRMS (ESI $^+$ )  $m/z$  calculated for C $_{11}$ H $_{17}$ N $_2$ O $_2$ S 241.1005 [M+H] $^+$ , found 241.1000; HRMS (ESI $^-$ )  $m/z$  calculated for C $_{11}$ H $_{15}$ N $_2$ O $_2$ S 239.0860 [M-H] $^-$ , found 239.0860; HPLC (method **HPLC-16**):  $R_t$  = 10.2 min;  $\lambda_{\text{max}}$  = 255 nm.

#### 4. HPLC procedures

Preparative column chromatography was done using an Agilent Technologies 1200 Series HPLC-system equipped with an Agilent 1100/1200 Quaternary Pump and a PDA detector.

**Eluent A:** Acetonitrile + 0.1% TFA

**Eluent B:** Water + 0.1% TFA

**Column:** Agilent Prep-C18 (10  $\mu$ m, 30 x 100 mm)

**Flow rate:** 9.0 mL/min

**Detection:** PDA (200-400 nm)

Gradients used for purification can be found in the following tables with reference to the compounds purified.

**HPLC method 8.** Method **HPLC-08** used for the purification of compounds **73** and **79**.

Time [min]	0	1	25	31	32	38	39	40
A%	50	50	84	84	100	100	50	50

**HPLC method 9.** Method **HPLC-09** used for the purification of compound **78**.

Time [min]	0	28	28.5	29.5	30	31
A%	55	55	100	100	55	55

**HPLC method 10.** Method **HPLC-10** used for the purification of compound **85**.

Time [min]	0	3	20	21	28	29	30
A%	70	70	90	100	100	70	70

**HPLC method 11.** Method **HPLC-11** used for the purification of compound **86**.

Time [min]	0	1	18	23	24	33	34	35
A%	70	70	90	90	100	100	70	70

**HPLC method 12.** Method **HPLC-12** used for the purification of compound **87**.

Time [min]	0	1	13.5	18	19	23	24	25
A%	70	70	85	85	100	100	70	70

**HPLC method 13.** Method **HPLC-13** used for the purification of compound **88**.

Time [min]	0	17	17.5	22	22.5	23
A%	25	55	100	100	25	25

## A7. Supporting Information to Chapter G

**HPLC method 14.** Method **HPLC-14** used for the purification of compound **89** and **90**.

Time [min]	0	1	16	21	21.5	23.5	24	25
A%	50	50	75	75	100	100	50	50

**HPLC method 15.** Method **HPLC-15** used for the purification of compound **91**.

Time [min]	0	1	16	19	19.5	20
A%	70	70	100	100	70	70

**HPLC method 16.** Method **HPLC-16** used for the purification of compound **92**.

Time [min]	0	12	13	15	15.5	16
A%	25	40	100	100	25	25

## DANKSAGUNG

An erster Stelle möchte ich mich bei meinem Doktorvater Prof. Christian Ducho für das interessante Promotionsthema, die stete Diskussionsbereitschaft und die Möglichkeit zur Teilnahme und der Präsentation von Ergebnissen auf verschiedenen Konferenzen bedanken.

Bei Herrn Prof. Dr. Rolf W. Hartmann bedanke ich mich für die Betreuung als wissenschaftlicher Begleiter während der Promotion.

Des Weiteren danke ich Frau Prof. Anna K. H. Hirsch für die Übernahme des Zweitgutachtens, sowie die Möglichkeit der Kooperation mit dem HIPS.

Ich danke allen Kooperationspartnern, für die stete Diskussionsbereitschaft und die Möglichkeit die gemeinsamen Ergebnisse publizieren zu können. Hier geht ein besonderer Dank vor allem an Esther Schönauer für die schnelle biologische *in vitro* Evaluationen gegen ColH meiner Compounds, sowie Messung einiger Co-Kristallstrukturen, an Alaa Alhayek für diverse *in vitro*, *ex vitro*, und *in vivo* Experimente zur weiteren biologischen Evaluation gegen ColH und LasB, Jelena Konstantinovic für die *in vitro* Evaluationen gegen LasB und die intensive Zusammenarbeit bei der Erstellung von Paper-Manuskripten, Jörg Hauptenthal für die zelltoxikologischen Untersuchungen, sowie Samir Yahiaoui für diverse Diskussionen und Gedankenanstöße.

Allen ehemaligen und aktuellen Mitarbeitern des AK Ducho danke ich für die gute Atmosphäre in der Arbeitsgruppe und den Zusammenhalt v.a. im ersten harten Corona-Lockdown. Besonders bedanken möchte ich mich bei meinen Bürokollegen Kristin Leyerer, Ole Schneemann und Stefan Koppermann für die gute Zeit und die hilfreichen Diskussionen. Ole, Melissa Wojtyniak, Marius Wirth, Anna Heib und Simone Rosinus danke ich zudem für die gute Laborzusammenarbeit in unseren beiden Laborreihen Reihen mit stimmungsvoller Musikuntermalung, mit der stressige oder lange Arbeitstage etwas besser auszuhalten waren.

Dem Instru-Team Dr. Stefan Boettcher, Ole und Sven Lauterbach danke ich für die für die gute Zusammenarbeit bei der Organisation und Betreuung dieses Praktikums.

Ich danke meiner Hiwine Lea Eschweiler, meinem Vertiefungspraktikanten Marcel Lutz, sowie unserem Masteranden Sebastian Dahmen für die gemeinsame Arbeit im Labor, sowie ihren Beiträgen zu dieser Doktorarbeit.

Stefan B. danke ich für die Hilfe bei diversen MS- oder HPLC-Fragen. Auch danke ich Stefan B. und Stefanie Weck für die Messung hochaufgelöster Massen an der Orbitrap.

Auch möchte ich mich herzlich bei Kristin, Simone, Anna, Janis und Andreas für das Korrekturlesen meiner Arbeit bedanken.

Dem Team des Sprachenzentrums der Universität des Saarlandes danke ich für das gute Kursangebot und die schnelle Umstellung während Corona auf Online-Angebote, sodass hier auch ein Ausgleich neben dem Promotionsalltag möglich war.



## Danksagung

Ein großer Dank gilt auch meinen Freunden und meinen neuen Arbeitskollegen. Hier Danke ich besonders Ljuba, Karina, Lisa, Luise, Julia, Laura und Myriam für die herzliche Aufnahme in Darmstadt. Weiterhin Danke ich auch meinem Freunden, die ich schon seit Kindertagen kenne, besonders Hannah und Michelle, für eine tolle Freundschaft seit über 20 Jahren. Zusätzlich danke ich Dan Hensel und Konstantin Kuznetsov vom Hochschulsport und Robert, Anne und Stefan vom TG Grün-Gold Saarbrücken, für die gemeinsamen Tanzstunden.

Janis danke ich für seine uneingeschränkte Unterstützung während der Doktorzeit und darüber hinaus. Danke für dein Verständnis, wenn es mal spät wurde, dein offenes Ohr, und die Versuche mich aufzumuntern, wenn ich mal schlecht gelaunt war. Dank dir ist mir auch während Corona nicht die Decke auf den Kopf gefallen. Danke, dass du mich ermutigst meinen eigenen Weg zu gehen.

Der größte Dank gilt meine Familie, meiner Mutter Stefanie, meinem Vater Artur, meinen Schwestern Lara und Julia, sowie meinem Bruder David. Ich danke euch für die Unterstützung während meines gesamten Studiums und den steten Rückhalt in schwierigen Zeiten. Danke, dass ihr stets an mich geglaubt habt und ich daher so werden konnte wie ich heute bin.